Natural Resources Canada | Ressources naturelles Canada

GEOLOGICAL SURVEY OF CANADA
OPEN FILE 7853

Targeted Geoscience Initiative 4: Contributions to the Understanding of Volcanogenic Massive Sulphide Deposit Genesis and Exploration Methods Development

J.M. Peter and P. Mercier-Langevin
(Editors)

2015

Canada

GEOLOGICAL SURVEY OF CANADA
OPEN FILE 7853

Targeted Geoscience Initiative 4: Contributions to the Understanding of Volcanogenic Massive Sulphide Deposit Genesis and Exploration Methods Development

J.M. Peter[1] **and P. Mercier-Langevin**[2]

[1]Geological Survey of Canada, Ottawa, Ontario
[2]Geological Survey of Canada, Québec, Quebec

2015

doi:10.4095/296540

This publication is available for free download through GEOSCAN (http://geoscan.nrcan.gc.ca/)

Recommended citation

Peter, J.M. and Mercier-Langevin, P. (ed.), 2015. Targeted Geoscience Initiative 4: Contributions to the Understanding of Volcanogenic Massive Sulphide Deposit Genesis and Exploration Methods Developmen; Geological Survey of Canada, Open File 7853, 214 p. doi:10.4095/296540

Publications in this series have not been edited; they are released as submitted by the author.

Contribution to the Geological Survey of Canada's Targeted Geoscience Initiative 4 (TGI-4) Program (2010-2015)

TABLE OF CONTENTS

GEOLOGICAL SURVEY OF CANADA
OPEN FILE 7853

Targeted Geoscience Initiative 4: Contributions to the Understanding of Volcanogenic Massive Sulphide Deposit Genesis and Exploration Methods Development

The Targeted Geoscience Initiative 4 contributions to the understanding of volcanogenic massive sulphide deposit genesis and exploration methods development: introduction and preface

Jan M. Peter[1] **and Patrick Mercier-Langevin**[2]

[1]Geological Survey of Canada, Ottawa, Ontario
[2]Geological Survey of Canada, Québec, Quebec

2015

This publication is available for free download through GEOSCAN (http://geoscan.nrcan.gc.ca/)

Recommended citation

Peter, J.M. and Mercier-Langevin, P., 2015. The Targeted Geoscience Initiative 4 contributions to the understanding of volcanogenic massive sulphide deposit genesis and exploration methods development: introduction and preface, *In:* Targeted Geoscience Initiative 4: Contributions to the Understanding of Volcanogenic Massive Sulphide Deposit Genesis and Exploration Methods Development, (ed.) J.M. Peter and P. Mercier-Langevin; Geological Survey of Canada, Open File 7853, p. 1–14.

Publications in this series have not been edited; they are released as submitted by the author.

Contribution to the Geological Survey of Canada's Targeted Geoscience Initiative 4 (TGI-4) Program (2010–2015)

TABLE OF CONTENTS

The Targeted Geoscience Initiative 4 contributions to the understanding of volcanogenic massive sulphide deposit genesis and exploration methods development: introduction and preface

Jan M. Peter[1]* and Patrick Mercier-Langevin[2]†

[1]Central Canada Division, Geological Survey of Canada, 601 Booth Street, Ottawa, Ontario K1A 0E8
[2]Québec Division, Geological Survey of Canada, 490 rue de la Couronne, Québec, Quebec G1K 9A9
*Corresponding author's e-mail: jan.peter@nrcan.gc.ca
†Corresponding author's e-mail: pmercier@nrcan.gc.ca

ABSTRACT

Research on topical aspects of the genesis of, and exploration for, volcanogenic massive sulphide (VMS) deposits was formulated and carried out under the auspices of the Volcanogenic Massive Sulphide Ore System of the Targeted Geoscience Initiative 4 Program. Research activities were focussed on addressing two main themes: 1) development of innovative, new, and unconventional detection and vectoring methodologies for VMS exploration; these studies were conducted at the Izok Lake deposit, Nunavut, and regionally throughout the Bathurst Mining Camp, northern New Brunswick, as well as at numerous VMS deposits and prospects regionally throughout the Slave Province, Nunavut and Northwest Territories; and 2) understand the controls on precious metal (gold, silver) endowment or enrichment in VMS deposits. These studies were conducted at several deposits: Lalor Mine, Manitoba; Lemarchant deposit, Newfoundland; Ming Mine, Newfoundland; and the Lemoine deposit, Quebec.

Detection and development of vectoring methods focussed on the application of optical reflectance spectrometry (airborne, ground, laboratory), oxygen isotope geochemistry, laser ablation inductively coupled plasma mass spectrometric analysis of volatile elements, multiple sulphur isotope geochemistry, till geochemistry and indicator minerals, and integration of rock properties and geophysics. Each of these research activities produced results that influence exploration strategies for VMS deposits in Canada and elsewhere.

Studies focussed on determining the controls on precious metal endowment or enrichment in VMS deposits employed geology, volcanology/volcanic architectural analysis, lithogeochemistry, chemostratigraphy, geodynamic setting analysis, geochronology, hydrothermal alteration systematics, petrography, mineralogy and mineral chemistry (mineralization, alteration, host rock), oxygen isotope geochemistry, sulphur isotope geochemistry, lead isotope geochemistry, and metallogenic considerations. Collectively these studies demonstrate that in all cases, gold enrichment was primary (not late/secondary; i.e., seafloor and aerial weathering, overprinted unrelated mineralizing systems) and was the result of one or more of the following processes: 1) magmatic input, as evidenced by the presence of complex mineral assemblages that include sulphosalts and native elements, anomalous trace element signatures (e.g. epithermal suite: Au-As-Sb-Ag-Hg; felsic magma-associated: Bi-W-Te-In-Sn); and 2) boiling in a shallow-water setting. Only minimal remobilization of gold occurred in deposits in response to greenschist- and amphibolite-facies metamorphism.

INTRODUCTION

The recently completed Targeted Geoscience Initiative 4 (TGI-4) Program (April 1, 2010 – March 31, 2015) was focussed on expanding geoscientific knowledge and developing new cutting-edge tools to increase industry's success in exploring for deep mineral deposits. The TGI-4 program was carried out in collaboration with territorial and provincial government geological survey organizations, industry, and academia. Seven ore deposit types (so-called "ore systems") were studied: lode gold, Ni-Cu-(PGE); volcanogenic massive sulphide, SEDEX, intrusion-related; uranium, and rare metals, together with exploration methods development.

Canada's base metal reserves and production largely reside within and come from volcanogenic massive sulphide (VMS) deposits. Various sources, including Natural Resources Canada's Minerals and Metals Sector data, indicate that 27% of Cu, 49% of Zn, 20% of Pb, 40% of Ag, and 3% of Au production in 2012 came from VMS deposits. Despite redoubled exploration efforts, reserves are steadily declining, mainly

Peter, J.M. and Mercier-Langevin, P., 2015. The Targeted Geoscience Initiative 4 contributions to the understanding of volcanogenic massive sulphide deposit genesis and exploration methods development: introduction and preface, *In:* Targeted Geoscience Initiative 4: Contributions to the Understanding of Volcanogenic Massive Sulphide Deposit Genesis and Exploration Methods Development, (ed.) J.M. Peter and P. Mercier-Langevin; Geological Survey of Canada, Open File 7853, p. 1–14.

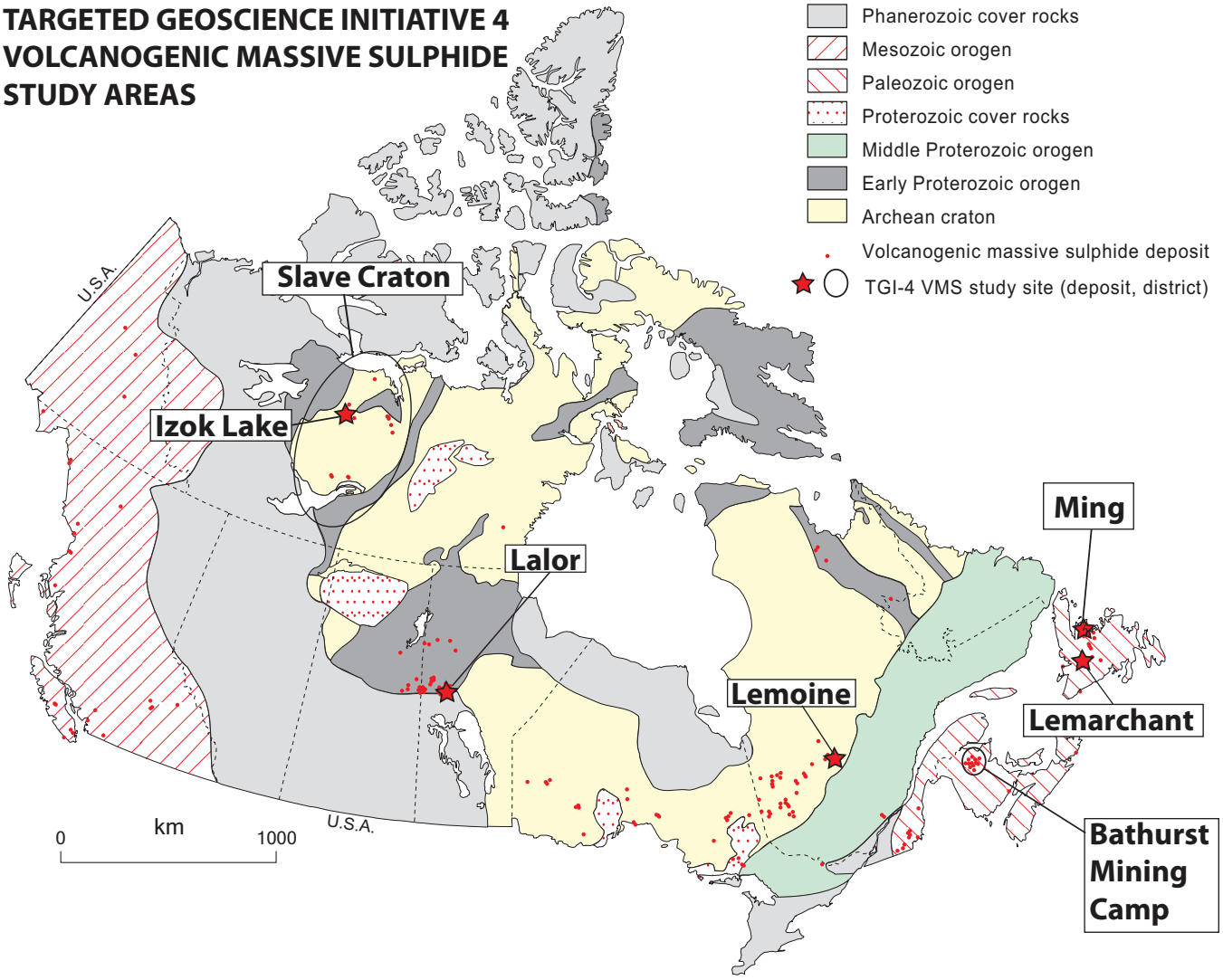

Figure 1. Map of Canada showing the locations of the volcanogenic massive sulphide deposits and mining/mineral deposit districts in which TGI-4 research was conducted.

because traditional exploration methods have discovered most of the deposits that are either exposed or shallowly buried.

In a concerted effort to reverse this trend, research activities at several sites (Fig. 1) were initiated to enhance exploration effectiveness centered on addressing two main premises:

1. New, unconventional, and innovative technologies that are not currently employed in VMS exploration combined with new tools and methodologies could be used to identify fertile VMS systems and vector (give directional and distance information) toward concealed, so-called "deeply buried" deposits. The TGI-4 program investigated technologies and methods that included a) a study of the efficacy of airborne and ground hyperspectral optical spectroscopy in the recognition of VMS-associated hydrothermal alteration at the Izok Lake deposit test site; b) a study of bulk rock oxygen isotope mapping at the Izok Lake deposit test site and its effectiveness in providing additional/ancillary lithogeochemical data to vector toward mineralization in areas with high metamorphic grades; c) a reconnaissance study to determine the applicability of multiple sulphur isotope analysis of VMS deposits across the Slave Province for fingerprinting fertile terrains or precious metal-rich terrains; d) a study of laser ablation inductively coupled plasma mass spectrometry of volatile trace elements (e.g. As, Cd, Hg, In, Sb, Tl) in pyrite, chlorite, and white mica from select polymetallic VMS deposits and host rocks in the Bathurst Mining Camp (BMC) to determine it's potential as a tool to vector toward mineralization; e) a synoptic review of surficial exploration methods for VMS deposits (including boulder tracing, till geochemical, and indicator mineral surveying); f) a study integrating deposit-specific rock property data with geophysi-

cal data using the BMC as a test site for the creation of more accurate predictive models and methodologies.

2. Precious metal-enriched (gold, silver) VMS deposits are a much more attractive exploration target than base metal-only deposits because gold and silver credits can significantly increase the value of the ore. Although VMS deposits are perhaps the best understood of all metallic mineral deposits (largely because of the discovery and study of modern seafloor massive sulphide analogues), the salient controls on the enrichment of Au and Ag remain poorly and incompletely understood. For this reason, particular focus was placed on the study of several VMS deposits across Canada with precious-metal enrichment (Lalor Mine, Snow Lake Camp, Manitoba; Lemarchant deposit, Tally Pond volcanic belt, Newfoundland; Ming Mine, Rambler and Ming Mining Camp, Newfoundland; and the Lemoine deposit, Abitibi greenstone belt, Quebec. Some site-specific research studies of the TGI-4 Lode Gold project gathered key knowledge about linkages between gold-rich VMS and synvolcanic gold deposits (Dubé et al., 2015, and references therein). Below, we provide a brief overview of the research themes outlined above, their rationales, methodologies, and salient conclusions.

VOLCANOGENIC MASSIVE SULPHIDE DEPOSIT DETECTION AND VECTORING RESEARCH ACTIVITIES

Hyperspectral Optical Reflectance Spectrometry in the Exploration for Volcanogenic Massive Sulphide Deposits

This research activity investigated the application of ground and airborne optical remote sensing methods for the detection of hydrothermal alteration zones associated with VMS deposits using the Archean Izok Lake polymetallic (Zn-Cu-Pb-Ag) deposit, Nunavut as a test site. The current resource is 15 Mt grading 13% Zn, 2.3% Cu, 1.4% Pb, and 73 g/t Ag (MMG Inc., 2013 Annual Report). The deposit is located in a subarctic environment where lichens are abundant on the rock outcrops. The rhyolitic host rocks to the deposit have been hydrothermally altered and contain white mica. White mica has an Al-OH absorption feature in the short-wave infrared (SWIR) wavelength region that shifts due to chemical compositional changes. In and around the Izok Lake deposit there are systematic trends in the wavelength of the Al-OH absorption feature that corresponds to distance from the massive sulphide lenses. Furthermore, these trends can be detected in whole-rock data of outcrop samples that have been collected throughout the area. Research results demonstrate the feasibility of using hyperspectral remotely sensed data to delineate metamorphosed VMS-associated hydrothermal alteration zones and determine alteration intensity in high-latitude regions. The study constitutes the first successful demonstration of the application of airborne hyperspectral mapping of metamorphosed hydrothermal alteration (white mica distribution and chemical variation) as a vectoring tool in northern Canada where rock-encrusting lichen is pervasive. The findings have been presented in this volume (Laakso et al., 2015a), a journal paper (Laakso et al., 2015b), a submitted manuscript, and in a recently completed Ph.D. thesis (Laakso, 2015). An ancillary project was also completed that demonstrated the successful application of airborne hyperspectral imaging in the detection of hydrothermal alteration associated with orogenic gold mineralization in the Hope Bay Belt (a subset of data over a known deposit was used), and this was reported in Yarra et al. (2014) and a B.Sc. Honours thesis (Yarra, 2013).

Oxygen Isotope Mapping in the Exploration for Volcanogenic Massive Sulphide Deposits

Mapping of the oxygen isotope compositions of bulk rocks has long been known to be useful in deciphering the hydrothermal fluid-flow patterns and the fluid-rock interactions in hydrothermal mineral deposit environments (e.g. Taylor, 1979). In VMS environments, oxygen isotope mapping studies have effectively delineated high-temperature altered rocks in the footwall (^{18}O depleted) from low-temperature altered rocks in the hanging wall (^{18}O enriched), and can be used to distinguish hydrothermal systems that formed a single deposit from those that formed multiple, stacked deposits (e.g. Cathles, 1993; Taylor and Holk, 1998; Holk et al., 2008). However, previous such studies (of VMS systems) commonly investigated rocks that have been metamorphosed to greenschist facies or lower, and there are even fewer case studies of rocks that have undergone amphibolite-facies grade or higher metamorphism. Furthermore, few (if any) studies have integrated optical reflectance data. To address this knowledge-gap, such research was conducted at the Izok Lake deposit in concert with the study of Laakso et al. (2015a) detailed above.

At the same time as outcrop samples were collected for determining spectral data in the vicinity of the deposit, samples were also collected of felsic rocks (host to mineralization) for determination of oxygen isotope compositions. In most instances, the samples for oxygen isotope studies were the same (subset of) as those used for the spectral measurement, or they were collected from the same outcrop. A few additional samples were collected for which no spectral measure-

ments were collected. The data show a distinct oxygen isotope zonation that is centred over the massive sulphide lenses, with high ^{18}O values (>10 per mil, ranging up to 14.7‰) around the mineralization (in hanging-wall rocks); further away to the south-southwest, ^{18}O values are lower (<10, down to below 6‰) in the footwall. This zonation is the product of water/rock interaction during the formation of the deposit, and the centring of this zonation over the massive sulphide lenses indicates that this paleohydrothermal system is relatively "up right" (i.e. top-down or plan view). The isotopic zonation broadly corresponds to a zone of bulk rock Na_2O depletion, and, to some extent, with a mapped distribution of the Ishikawa alteration index and short-wave infrared spectral mapping of white mica and biotite+chlorite-related absorption features; however, the pattern of oxygen isotope zonation provides a more focussed "target" and forms a hanging-wall "vector" to the buried sulphide lenses. The isotopic signatures have been retained despite subsequent amphibolite-facies metamorphism. This study contrasts with most of the other oxygen isotopic studies of VMS environments that describe ^{18}O-depleted upflow zones in the stratigraphic footwall (e.g. Mercier-Langevin et al., 2014a). Results of the study are documented in Taylor et al. (2015a), and a subset of the oxygen isotope data (together with X-ray diffractometry data) forms the basis of a B.Sc. Honours thesis (Davis, 2014).

Multi-Sulphur Isotope Fingerprinting of Volcanogenic Massive Sulphide Deposits

Sulphur isotopic analysis has long been used to study metallic mineral deposits, including VMS deposits (e.g. Ohmoto and Rye, 1979). These studies employed the isotopes of ^{34}S and ^{32}S. More recently, mass independent fractionation amongst the sulphur isotopes has been identified (Farquhar et al., 2000), and there is a growing awareness that this could be useful in deciphering the role of mantle (juvenile) and atmospherically cycled sulphur in VMS and other deposit types of Paleoproterozoic or older age (e.g. Bekker et al., 2009; Farquhar et al., 2010; Jamieson et al., 2013).

The typical mass-dependent fractionation (MDF) trend between ^{33}S and ^{34}S is linear ($\delta^{33}S = 0.515\ \delta^{34}S$: Farquhar et al., 2000). However, prior to 2.45 Ga, the distribution of sulphur isotopes was controlled by the production of anomalous amounts of ^{33}S through photolysis reactions in the atmosphere (e.g. Farquhar et al., 2001). This was facilitated by the low atmospheric oxygen concentrations that allowed the mass-independent fractionation (MIF) of the isotopes of sulphur. This fractionation resulted in deviations (both positive and negative) in $\Delta^{33}S$ ($\delta^{33}S_{MEASURED} - \delta^{33}S_{MDF\text{-}PREDICTED}$) from this linear trend (e.g. Farquhar and Wing, 2003) that can be used as a tracer of surface-processed sulphur. The sulphur produced by MIF is transported to the Earth's surface as sulphur ($S°$; $\Delta^{33}S > 0‰$) and sulphate (H_2SO_4; $\Delta^{33}S < 0‰$), and incorporated in sulphides via bacterial sulphate reduction (BSR) or thermal (TSR) sulphate reduction.

A study was initiated to assess the usefulness of multiple sulphur isotopic (^{32}S, ^{33}S, ^{34}S, and ^{36}S) analysis of VMS sulphides in Archean (pre-2.45 Ga) rocks in serving as a fingerprint of petrotectonic setting and/or mineralizing processes. A previous lead isotope study of samples from 30 Archean VMS deposits and occurrences throughout the Slave Province conducted by Thorpe et al. (1992) provided the ideal sample suite (and Pb isotope data for comparison). These galena, sphalerite, and pyrite separates reveal a variable contribution from Archean atmosphere-derived sulphur, as evidenced by variable $\Delta^{33}S$ values. The data indicate that bimodal-mafic type (bimodal rift setting) deposits have a restricted range of $\Delta^{33}S$ (-0.3 to 0.1‰), whereas bimodal-felsic type (arc-like settings) deposits exhibit a broad range of $\Delta^{33}S$ (-0.8 to 0.6‰). Mantle-derived (juvenile) sulphur is essentially the sole source of sulphur in bimodal-mafic type deposits; these deposits are also characterized by relatively low silver contents. Bimodal-felsic type deposits, typified by high silver contents, contain variable amounts of atmosphere-derived sulphur that was more readily available in arc-like settings. Thus, this study, presented in Taylor et al. (2015b), indicates that multiple sulphur isotopic analyses may be useful in discrimination between, and selection of, terranes for VMS exploration, particularly those that are precious metal-rich.

Volatile Element Vectoring for Volcanogenic Massive Sulphide Deposit Exploration

Mercury, a volatile element (i.e. possesses a high vapour pressure), in bulk rocks has long been used as a pathfinder element in VMS exploration (see Lentz, 2005, and references therein). Thallium, another volatile element, has also been shown (also in bulk rocks) to be useful as an exploration vector in VMS exploration (Large et al., 2001). The advent of inductively coupled plasma mass spectrometry (ICP-MS) provides for the facile quantitative analysis of these and other volatile elements at the ppm to ppb levels in geological materials. The coupling of ICP-MS with laser ablation (LA-ICP-MS) provides in situ, high-spatial-resolution sampling and allows discrete mineral phases to be analyzed (e.g. Danyushevsky et al., 2011).

The application of LA-ICP-MS volatile element (including As, Cd, Hg, In, Sb, Tl) analysis of pyrite, chlorite, and white mica from selected polymetallic Zn-Pb-Cu-Ag VMS deposits of the Bathurst Mining Camp (BMC), northern New Brunswick as a vectoring

tool in VMS exploration has been investigated. These minerals were selected because they are ubiquitously present within the mineralization and/or the hydrothermally altered host rocks to VMS mineralization and can accommodate a wide range of volatile trace elements. The data for the BMC indicate that pyrite, chlorite, and white mica contain significant abundances of volatile trace elements. In particular, pyrite grains typically contain As, Sb, Tl, Au, Hg, In, and Cd; white mica typically contains As, Sb, Tl, In, Hg, Cd, and Bi, and in comparison to white mica, chlorite is preferentially enriched in Cd and Bi. Volatile element contents of chlorite and white mica indicate that these elements are crystal lattice-bound.

Stratigraphic profiles of the examined deposits reveal distinct volatile trace element features. Pyrite in the footwall alteration zones typically displays systematically increasing volatile trace element contents with decreasing distance stratigraphically upward to the ore horizon. However, in the hanging-wall alteration zones, there are no consistent pyrite chemical compositional trends. Pyrite in the hanging wall of some deposits shows high As in the upper portions and, to a lesser extent, higher abundances of other volatile trace elements. The volatile trace element contents of chlorite and white mica in hanging wall- and footwall-altered rocks increase with decreasing distance toward mineralization. The study outlining these relationships is presented in Soltani Dehnavi et al. (2014, 2015), with the Ph.D. thesis research continuing after the end of the TGI-4 program. Results have shown that systematic trends in distribution of volatile trace element contents of pyrite, chlorite, and white mica can be used to vector toward VMS mineralization in the BMC. This methodology may be applicable in other areas where polymetallic deposits occur, and may complement other geochemical and geophysical exploration methods.

Boulder Tracing, Till Geochemistry, and Indicator Minerals in the Exploration for Volcanogenic Massive Sulphide Deposits

Given that most of Canada has been glaciated and is extensively covered by glacial drift, exploration methods employing surficial materials remain vitally important to VMS exploration. As such, a critical review and appraisal of best practises for drift prospecting for VMS, together with a review of selected case studies from different regions across Canada was completed under TGI-4. Focus was placed on boulder tracing, till geochemistry, and indicator minerals. Till sampling, appropriate size fractions of till to analyze, sample processing, and analytical techniques were all considered. As expected, Cu, Pb, and Zn are shown to be indicator elements of VMS deposits, and pathfinder elements include As, Ag, Au, Ba, Bi, Cd, Hg, In, Sb, Se, Sn, and Tl. Abundances of these elements should be determined in the <0.063 mm (silt + clay) fraction of till. Indicator minerals of VMS deposits should be recovered from the >3.2 specific gravity heavy mineral concentrate of till, and effect minerals include galena, sphalerite, chalcopyrite, pyrite, and pyrrhotite, native gold, electrum, cassiterite, cinnabar, and barite, and, in metamorphic terrain, metamorphosed minerals of mineralization, alteration, or exhalites, including sillimanite, andalusite, gahnite, staurolite, and spessartine. There has been much recent research on the application of the chemical composition of magnetite as a VMS exploration tool (Dupuis and Beaudoin, 2011; Makvandi et al., 2013), and this mineral may also be considered in exploration. The findings are presented in McClenaghan and Peter (2013), McClenaghan et al. (2015), and McClenaghan and Peter (in press). This work has identified avenues for future research of drift exploration methods for VMS deposits, including reducing sample size, lowering analytical costs, and identifying new indicator minerals and chemical discrimination criteria.

Integration of Rock Property and Geophysical Data for Volcanogenic Massive Sulphide Exploration

Geophysical modelling algorithms and methodologies are becoming increasingly more sophisticated and capable of providing realistic results. However, in order for these models to provide optimal results, actual rock property parameters must be used. Physical rock property information provides a direct link between the geophysical data and geological interpretations. Research into the better integration of rock property and geophysical data was conducted within TGI-4 with the aim of developing or refining selected methodologies or work-flow. The data-rich Bathurst Mining Camp (BMC), northern New Brunswick (the same site of the volatile element vectoring study described above), was used as the test site for this research. The study used an existing physical rock property (density and magnetic susceptibility measurements) database for host rocks and VMS mineralization that was then expanded by incorporating new measurements taken of in situ samples and drill cores.

Density data were used to reprocess existing ground gravity and airborne gravity gradiometry (AGG) survey data by applying a laterally variable Bouguer and terrain density correction linked to averaged, measured density values and mapped extents of the different tectonostratigraphic groups that make up the BMC. The results of this reprocessing changed the previously determined gravity and gradient anomaly patterns and allowed isolated anomalies to be more discretely

resolved, thus reducing the impact of the terrain-related signal in the AGG data. Helicopter-borne frequency domain electromagnetic (EM) data were inverted for magnetic susceptibility and forward modelled into a magnetic anomaly grid for a small test site in the BMC. Magnetic susceptibility values from the physical property database were used to validate the results of the inversion, and this computed near-surface magnetic anomaly grid was used as a reference to effectively filter measured total magnetic intensity data to represent solely near surface magnetic sources (i.e. potential VMS targets). Although petrophysical measurements in the BMC may differ from other locales, the various methodologies developed can be used elsewhere.

The research results are summarized in Tschirhart and Morris (2015), with individual research aspects covered in Tschirhart et al. (2014a,b, in press-a, in press-b), a submitted manuscript, and a recently completed M.Sc. thesis (Tschirhart, 2013).

PRECIOUS METAL-ENRICHMENT PROCESSES IN VOLCANOGENIC MASSIVE SULPHIDE DEPOSITS

Volcanogenic massive sulphide deposits can contain variable amounts of precious metals (Au, Ag), and the credits received from these metals during mining can significantly enhance the economic potential of these deposits such that they are highly desirable exploration targets. The currently understood spectrum of enrichment processes in these deposits ranges from one, or a combination of (e.g. Hannington and Scott, 1989; Huston, 2000; Dubé et al., 2007; Mercier-Langevin et al., 2011): 1) "fertile" Au- and/or Ag-enriched source rocks and fluids that originated in a specific geodynamic setting, or from magmatic input, respectively; 2) optimal ligand complexing and transport of the metals and/or their efficient deposition by processes such as boiling/phase separation and zone refining; 3) superposition of another (type of) mineralization style such as epithermal, intrusion-related, or orogenic; 4) supergene weathering on the seafloor or on land; and/or 5) metamorphic redistribution. In an effort to refine the genetic and exploration models for Au and/or Ag enriched VMS deposits, research was conducted at several precious metal-enriched VMS deposits across Canada (Lalor Mine, Snow Lake Camp, Manitoba; Lemarchant deposit, Tally Pond volcanic belt, Newfoundland; Ming Mine, Rambler, and Ming Mining Camp, Newfoundland; and the Lemoine deposit, Abitibi greenstone belt, Quebec.

Mercier-Langevin et al. (2015) provide a summary of these various enrichment processes and the TGI-4 research that addresses some of these processes. Key observations and circumstantial lines of evidence include the following: volcanogenic massive sulphide deposits in volcanic belts that formed in pericratonic settings or on older crust basement in the early stages of rifting are commonly slightly better endowed in precious metals than those formed in belts or settings with limited to no basement influence (see also the multi-sulphur isotope study of the Slave VMS deposits, which is outlined above, as well as in Taylor et al. (2015b), which presents a similar observation). Gold-rich and auriferous VMS are preferentially associated with calc-alkaline or transitional magmatic successions that display the full continuum of magmatic differentiation fractionation (andesite-dacite-rhyodacite-rhyolite) and with thick felsic volcanic packages. Evidence for a magmatic input includes i) the presence of complex mineral assemblages comprising sulphosalts, sulphides, native elements; and ii) anomalous trace element signatures (e.g. enrichment in the "epithermal suite" of elements Au-As-Sb-Ag-Hg and/or in felsic magma-associated elements Bi-W-Te-In-Sn) (e.g. Gill et al., 2015; Pilote et al., 2015; see below); and iii) a laterally extensive sericitic (phyllic) ±siliceous alteration halo or a zone of intense aluminous (argillic- to advanced argillic-style) alteration (e.g. Dubé et al., 2014). Deposition in response to boiling/phase separation (in a shallow water setting) is evidenced by i) bladed textures of certain minerals (e.g. Gill et al., 2015; see below); and ii) heterogeneous Au and Ag distributions and mineralogical residence sites within or near the sulphide bodies.

Lalor Volcanogenic Massive Sulphide Deposit

Characteristics and Gold-Enrichment Processes of the Lalor Deposit

Lalor is a Paleoproterozoic VMS deposit that contains 25.3 Mt of ore grading 2.9 g/t Au, 25 g/t Ag, 5 wt% Zn, and 0.79 wt% Cu, including 8.8 Mt at 4.6 g/t Au. Lalor is the largest deposit (and also most Au-rich) in the Snow Lake Camp, Manitoba; TGI-4 conducted two research projects here: 1) a Ph.D. study to understand the geological evolution of the deposit and the ore-forming hydrothermal system, including the controls on gold enrichment; and 2) a M.Sc. study of the mineralization styles in the deposit.

Major findings of the first study are 1) Lalor is within a complex volcanic package (Lalor volcanic succession) composed of mafic to felsic, tholeiitic to calc-alkaline, extrusive to intrusive volcanic rocks of the ca. 1.89 Ga Lower Chisel subsequence; 2) the ore is hosted in both mafic and felsic rocks; 3) the Lalor deposit is not situated at the top of the Lower Chisel subsequence as is typical of the other Zn-rich deposits of the Snow Lake district, but is at a slightly lower stratigraphic position; 4) the host rocks were affected by intense and laterally extensive hydrothermal alteration that occurred during ore deposition; 5) the altered

rocks and the deposit were subsequently subjected to syndeformational amphibolite-grade metamorphism that resulted in the development of distinct minerals and metamorphic mineral assemblages of varying composition from variably altered precursor lithologies; 6) Five distinct alteration and metasomatic chemical associations (K, K-Mg-Fe, Mg-Fe, Mg-Ca, and Ca) are recognized, based on mineralogical (mineral assemblages) and bulk geochemical compositions; 7) mineralization occurs within stratigraphically and structurally stacked Zn-rich, Au-rich, and Cu-Au-rich ore lenses; 8) the Zn-rich massive sulphide lenses are preferentially associated with the low- to high-temperature K and Mg-Ca alteration zones; 9) the Cu-Au-rich zones, which occur at depth, stratigraphically below the Zn-rich mineralization, are hosted in transposed, presumably originally discordant high-temperature Mg-Fe altered rocks; and 10) Au has been in part locally remobilized into low-strain sites that are not spatially associated with any particular chemical association. These conclusions are summarized from the following cadre of research conducted at Lalor: Caté et al. (2013, 2014a,b,c, 2015) and Mercier-Langevin et al. (2014a). The Ph.D. thesis research (Caté) is continuing beyond the conclusion of the TGI-4 program.

Two major findings for the second study are that there are four ore types at Lalor and that these types are associated with different host rocks.

Four Ore Types of the Lalor Deposit

Type 1 Fe-Zn massive sulphide ore is the most common ore type in 6 (of the 11) ore lenses and consists of massive coarse-grained pyrite and sphalerite with trace galena.

Type 2 Cu-Au mineralization consists of semi-massive and stockwork chalcopyrite and pyrrhotite.

Type 3 Au-Ag-Pb-Cu-rich ore consists of stringer and disseminated sulphides and sulphosalts. Galena is an important indicator of Au mineralization and occurs in this ore type as fine-grained blebs in a matrix of chlorite, dolomite, calcite, anthophyllite, Ca-plagioclase, and calc-silicate minerals (epidote, grossular, diopside, Ca- amphibole ± scapolite). Where abundant, the galena is associated with chalcopyrite, pyrite, and pyrrhotite, and with minor to trace sphalerite, Ag-Sb-Pb sulphosalts, electrum, and native gold.

Type 4 low-sulphide ore contains ≤10 vol% disseminated pyrite, and has variable Au grades. The sulphides and sulphosalts in ore types 3 and 4 are thought to have been remobilized from pre-existing disseminated mineralization during metamorphism.

Host Rocks of Mineralization at the Lalor Deposit

Type 1 mineralization occurs predominantly occurs in quartz-muscovite±kyanite-biotite schist (K-alteration association). Type 2 mineralization occurs in garnetiferous quartz- biotite±staurolite-amphibole-cordierite gneisses (footwall Mg-Fe alteration association). Type 3 mineralization mainly occurs in chlorite-carbonate-actinolite schist (Mg-Ca and Ca alteration associations). Type 4 mineralization occurs in quartz-biotite-anthophyllite gneiss, with minor chlorite, staurolite, and coarse almandine garnet.

Despite extensive recrystallization and local remobilization, type 1 and 2 ore are interpreted to represent typical (metamorphosed) low- and high-temperature VMS deposit ore assemblages, respectively. Significant Au was introduced first by high-temperature (>300°C) fluids responsible for the Type 2 Cu-Au mineralization. The Type 3 Au-Ag-Pb-Cu mineralization is thought to have formed in the subseafloor from late-stage, lower temperature (and possibly boiling) hydrothermal fluids (<300°C). Although all the ore types are extensively recrystallized and partly remobilized, Au enrichment at Lalor is thought to have been primary, and not secondary; this is supported by lead isotopic compositions of ore galena and whole-rock oxygen isotope compositions. Furthermore, the Au-rich assemblages are very similar to those in unmetamorphosed Au-rich VMS deposits.

The above research summary is detailed in Duff et al. (2013, 2015) and is the subject of a M.Sc. thesis that is still in progress (Duff).

Lemoine Au-Rich Volcanogenic Massive Sulphide Host Succession, Waconichi Formation, Abitibi

The Lemoine deposit, which is now mined out, was a small but exceptionally rich auriferous (0.76 Mt grading 4.2 wt % Cu, 9.6 wt % Zn, 4.2 g/t Au, and 83 g/t Ag) VMS deposit in the Chibougamau area of the Archean Abitibi greenstone belt (Mercier-Langevin et al., 2014b). The deposit was the second highest grade VMS deposit in Canada, and occurred in the predominantly tholeiitic Lower Lemoine Member of the Waconichi Formation, which is overlain by transitional basalt and transitional to calc-alkaline rhyolite of the Upper Lemoine Member. Research at Lemoine aimed to reconstruct the volcanic architecture immediately east of the deposit to elucidate whether this might have been a salient control responsible for the high base and precious metal grades. Field mapping, geochemical analyses, and detailed core logging of every accessible drillhole in the study area, east of the former mine, helped to refine the volcanic architecture of the Lower Lemoine Member subunits and identify their mode of emplacement. This work also identified previously unrecognized volcanic vents northeast of the Lemoine deposit, which may have been the site of paleohy-

drothermal fluid up-flow and may host additional mineralization. Furthermore, results show that many of the felsic-dominated host rocks to the Lemoine are shallow intrusive rocks that define a major thermal corridor over a large synvolcanic intrusion. This research, summarized above, is presented in Boulerice et al. (2015), and is the subject of a M.Sc. thesis that remains in progress (Boulerice).

Lemarchant Volcanogenic Massive Sulphide Deposit and Precious Metal-Enrichment Processes

Lemarchant, a Cambrian precious metal-enriched Zn-Pb-Ba-Ag-Au VMS deposit, is located in the bimodal felsic Tally Pond Group of the Central Mobile Belt, Newfoundland Appalachians. TGI-4 research aims here were to 1) characterize the ore facies and zonation of ore; 2) determine the paragenetic sequence of the ore minerals; 3) determine the siting of precious metals in the host rocks and ore assemblages; 4) determine the source(s) of mineralizing fluids; and 5) determine the causes of base and precious metal-enrichment. Research results show that the deposit was formed in three discrete stages: Stage 1: barite-rich, low-temperature (<250°C) VMS mineralization; Stage 2: 150 to 250°C intermediate- to high-sulphidation epithermal-style mineralization; and Stage 3: polymetallic, high-temperature (>300°C) VMS mineralization. Sulphur isotopes suggest that S is derived from three sources: thermochemically reduced seawater sulphate, leached igneous basement rock, and magmatic SO_2. Lead isotopes indicate that Pb is primarily derived from evolved crustal material, with some input from juvenile volcanic rocks (i.e. arc-rift). Precious metals associated with epithermal-style mineralization are consistent with a magmatic contribution to the hydrothermal fluid. Precious metals were precipitated from intermittently boiled fluids (evidenced by bladed barite), at relatively shallow (<1500 m) water depth. This summary is extracted from Gill et al. (2015), Gill and Piercey (2014), Gill et al. (2013), and a recently completed M.Sc. thesis (Gill, 2015).

Ming Volcanogenic Massive Sulphide Deposit and Gold-Enrichment Processes

Ming is a VMS deposit hosted by the Rambler rhyolite in the Rambler Camp, Baie Verte Peninsula, northwest Newfoundland. Research funded by TGI-4 aimed to reconstruct the architecture and morphology of the deposit and its Au-rich zones, and identify the hydrothermal alteration zoning and key associations. The deposit is hosted in Cambro-Ordovician intermediate to felsic rocks that are underlain by ca. 490 Ma ophiolite slivers of boninitic composition. The deposit consists of five elongated, moderately plunging, semi-massive to massive sulphide lenses that occur in the uppermost part of a calc-alkaline intermediate to felsic volcanic succession. The immediate hanging wall varies from mafic volcanic breccia to magnetite-rich volcanogenic siltstone. There are seven distinct alteration mineral assemblages (from proximal to distal from mineralization): quartz-pyrite, quartz-calcite-garnet, sericite-green mica-sulphide, sericite-quartz-pyrite, chlorite-amphibole-quartz, chlorite-sericite-quartz-sulphide, and chlorite-stringer zone. A chalcopyrite-pyrrhotite-pyrite stringer zone associated with the chlorite-stringer zone assemblage occurs 50–100 m stratigraphically below the Ming North and Ming South lenses, at what was the site of high-temperature fluid discharge from a hydrothermal system. Brueckner et al. (2014) showed that Au-enrichment was syngenetic, based on the complex assemblage of sulphide minerals (e.g. sulphosalts, Au-Ag-Hg-bearing phases), and not due to subsequent remobilization, as had been previously suggested. Research outlined above is summarized from Pilote et al. (2014, 2015), Pilote and Piercey (2013), and Ph.D. thesis (Pilote) research, which is continuing beyond the completion of the TGI-4 program.

IMPLICATIONS FOR EXPLORATION

The legacies of TGI-4-funded VMS research in the exploration for VMS deposits are myriad. There are a number of key findings and advances in the development of exploration and vectoring methods:

1. A test of the efficacy of airborne and ground hyperspectral optical spectroscopy for recognition of VMS-associated hydrothermal alteration at the Izok Lake deposit showed that chlorite and white mica alteration minerals possess spectral variability that relates to the chemical compositional variations in the altered rocks. This information can be used to vector toward mineralization and areas for further exploration in Canada's North, and has direct application to other hydrothermal ore deposits with similar alteration styles (e.g. orogenic lode gold deposits), and can serve as a first-pass "green" (i.e. no boots on the ground) method to define areas for follow-up work.
2. Bulk-rock oxygen isotope mapping at the Izok Lake VMS deposit identified a relatively "upright" paleohydrothermal system with a hanging-wall "cap" centred over the mineralization, as defined by high $\delta^{18}O$ values (up to 14.7‰). These results reaffirm that this method can be used to not only recognize high-temperature hydrothermally altered footwall rocks associated with mineralization, but also to determine the overall morphology and orientation (i.e. architecture) of a paleohydrothermal fluid flow system, as well as to vector toward the

concealed mineralization. Such isotopic "fingerprints" are retained in the rocks that have been metamorphosed, even up to high-grade conditions.

3. Multiple sulphur isotope analysis was undertaken on sulphide minerals from 30 VMS deposits across the Slave Province. The distribution of $\delta^{34}S$ and $\Delta^{33}S$ of sulphides across the Slave Craton does not reflect known variations in the crustal age or the origin of the crust, nor the metal content of the VMS; however, deposits formed in rift settings are characterized by a restricted range of $\Delta^{33}S$ values (from approximately -0.3 to 0.1‰), whereas deposits formed in arc-like settings exhibit a broad range in $\Delta^{33}S$ values (approximately -0.8 to 0.6‰), indicating atmospheric-derived sulphur was more readily available in the latter. The former group of deposits mostly have lower Ag contents than the latter.
4. Volatile trace element (e.g. As, Cd, Hg, In, Sb, Tl) contents of pyrite, chlorite, and white mica in selected polymetallic VMS deposits of the BMC, as determined by laser ablation inductively coupled plasma mass spectrometry, are shown to be a potential tool in vectoring toward mineralization. Pyrite in the footwall alteration zones typically displays systematically increasing volatile trace element contents with decreasing distance stratigraphically upward to the ore horizon. Chlorite and white mica show that volatile element contents in both hanging wall- and footwall-altered rocks increase with decreasing distance toward mineralization.
5. A review of surficial exploration methods for VMS mineralization included boulder tracing, till geochemical, and indicator mineral surveying. Best practices for till sampling and analyses have been identified. Geochemical indicators of mineralization include Cu, Pb, Zn, As, Ag, Au, Ba, Bi, Cd, Hg, In, Sb, Se, Sn, and Tl, all in the <63 µm (silt+clay) fraction. VMS indicator minerals recovered from the <3.2 specific gravity heavy mineral concentrate of till include the main ore minerals (galena, sphalerite, chalcopyrite, pyrite, and pyrrhotite), accessory minerals (native gold, electrum, cassiterite, cinnabar, and barite), and, in metamorphic terrain, metamorphosed minerals of mineralization, alteration, or exhalites, including sillimanite, andalusite, gahnite, staurolite, and spessartine.
6. Rock property (density and magnetic susceptibility) data were integrated with geophysical data (ground gravity, airborne gravity gradiometry, airborne magnetics and EM) in the Bathurst Mining Camp, which has led to the development of several new tools: a new laterally variable density correction procedure to produce more accurate geological maps, and a methodology to separate near-surface from deep-seated magnetic sources in frequency domain EM data; these methodologies have application elsewhere.

The studies that focussed on determining the controls on precious metal endowment or enrichment in VMS deposits resulted in several key implications:

1. In all the deposits that were studied, gold enrichment was primary, and was not due to secondary processes, such as seafloor and/or aerial weathering or overprinting by subsequent (non-VMS) mineralizing systems.
2. In several deposits studied (Lemarchant, Ming, Lemoine), gold enrichment was facilitated by magmatic input, as evidenced by the presence of complex mineral assemblages that include sulphosalts and native elements, with anomalous trace element signatures (e.g. epithermal suite: Au-As-Sb-Ag-Hg; felsic magma-associated: Bi-W-Te-In-Sn). Such mineralogical and metal relationships are strong prognostic indicators for potentially economic gold enrichment.
3. In several deposits studied (Lemarchant, Ming, and perhaps Lalor), boiling in a shallow-water setting is thought to have destabilized the gold complexes and produced gold-enriched mineralization. Exploration should be focussed on identifying shallow-water regimes (e.g. calderas and arc settings) in which seafloor hydrothermal activity may have taken place.
4. In the most highly metamorphosed and strongly deformed deposits studied (Lalor, Ming), there was only minimal remobilization during metamorphism and deformation subsequent to primary gold enrichment. Therefore, exploration for gold-enriched deposits should focus on primary permissive geological environments, and undue emphasis should not be placed on (high) metamorphic grade or on overprinting structural features (e.g. shear zones).

ACKNOWLEDGEMENTS

The various research activities completed under the TGI-4 project would not have been possible without the close cooperation and support of numerous partners from industry: Hudbay Minerals (C. Antoine, Sarah Bernauer, Brian Janser, Jason Levers, D. Smyth, Vicki Morrison, Craig Taylor), Votorantim Metals Canada (Chris Marmont), Rambler Metals & Mining PLC (Larry Pilgrim, George Ogilvie), Canadian Zinc Corporation (formerly Paragon Minerals; Christine Devine, Michael Vande Guchte), Minerals and Metals Group Ltd. (MMG) (Ian Neill, Dave Kelley, Kimberley

Bailey, Trish Toole), Bell Geospace (John Mims), Fugro Airborne Surveys (now CGG; Greg Hodges), ALS Minerals (Matthew Leybourne), Patterson, Grant & Watson Ltd. (Hernan Ugalde), and Cogitore Resources Inc. (now Yorbeau Resources) (Sylvain Lépine, Gérald Riverin); academia: Université du Québec-Institut national de la recherche scientifique (Pierre-Simon Ross, Antoine Caté, Alexandre Boulerice), University of Ottawa (Mark Hannington, Shamus Duff), University of Alberta (Benoit Rivard, Kati Laakso), McMaster University (Bill Morris, Peter Tschirhart), Memorial University of Newfoundland (Stephen Piercey, Jean-Luc Pilote, Shannon Gill), University of New Brunswick (David Lentz, Chris McFarlane, Azam Soltani-Dehnavi), Brock University (Frank Fueten, Raja Yarra), University of Waterloo (Brian Kendall, Cynthia Davis), McGill University (Boswell Wing), and Queen's University (Dan Layton-Matthews); and provincial and territorial government surveys: Manitoba Geological Survey (Simon Gagné, Ric Syme, Christian Böhm), New Brunswick Department of Energy and Mines (Jim Walker, Mike Parhill), Geological Survey of Newfoundland (John Hinchey, Andy Kerr), Ministère de l'Énergie et des Ressources naturelles – Géologie Québec (Francois Leclerc, Jean Goutier, Patrice Roy), and C.S. Lord Northern Geoscience Centre (Luke Ootes); and independent researchers: Gwendy Hall and Ingrid Kjarsgaard. We thank Valérie Bécu and Elizabeth Ambrose for editing and technical layout.

REFERENCES

Bekker, A., Barley, M. E., Fiorentini, M. L., Rouxel, O. J., Rumble, D., and Beresford, S. W., 2009. Atmospheric sulfur in Archean komatiite-hosted nickel deposits; Science, v. 326, p. 1086–1089.

Boulerice, A.R., Ross, P.-S., and Mercier-Langevin, P., 2015. Geological and geochemical characteristics of the Waconichi Formation east of the Lemoine auriferous volcanogenic massive sulphide deposit, Abitibi greenstone belt, Quebec, *In:* Targeted Geoscience Initiative 4: Contributions to the Understanding of Volcanogenic Massive Sulphide Deposit Genesis and Exploration Methods Development, (ed.) J.M. Peter and P. Mercier-Langevin; Geological Survey of Canada, Open File 7853, p. 171–182.

Brueckner, S., Piercey, S. J., Sylvester, P. J., Maloney, S., and Pilgrim, L., 2014. Evidence for syngenetic precious metal enrichment in an Appalachian volcanogenic massive sulfide system: the 1806 zone, Ming Mine, Newfoundland; Economic Geology, v. 109, p. 1611–1642.

Caté, A., Mercier-Langevin, P., Ross, P.S., Duff, S., Hannington, M., Dubé, B., and Gagné, S., 2013. Preliminary observations on the geological environment of the Paleoproterozoic auriferous volcanogenic massive sulphide deposit of Lalor, Snow Lake, Manitoba; Geological Survey of Canada, Open File 7372, 13 p.

Caté, A., Mercier-Langevin, P., Ross, P.-S., Duff, S., Hannington, M. D., Gagné, S., and Dubé, B., 2014a. Insight on the chemostratigraphy of the volcanic and intrusive rocks hosting the Lalor auriferous volcanogenic massive sulphide deposit host succession, Snow Lake, Manitoba; Geological Survey of Canada, Current Research 2014-6, 23 p.

Caté, A., Mercier-Langevin, P., Ross, P.-S., and Simms, D., 2014b. Structural controls on geometry and ore distribution in the Lalor auriferous VMS deposit, Snow Lake, west-central Manitoba (part of NTS 63K16): preliminary results from underground mapping, *In:* Report of Activities 2014; Manitoba Mineral Resources, Manitoba Geological Survey, p. 104–115.

Caté, A., Mercier-Langevin, P., Ross, P.S., Duff, S., Hannington, M.D., Dubé, B., and Gagné, S., 2014c. The Paleoproterozoic Lalor VMS deposit, Snow Lake, Manitoba: preliminary observations on the nature and architecture of the gold- and base metal-rich ore and alteration zones; Geological Survey of Canada, Open File 7483, 19 p.

Caté, A., Mercier-Langevin, P., Ross, P.-S., Duff, S., Hannington, M.D., Dubé, B., and Gagné, S., 2015. Geology and Au enrichment processes at the Paleoproterozoic Lalor auriferous volcanogenic massive sulphide deposit, Snow Lake, Manitoba, *In:* Targeted Geoscience Initiative 4: Contributions to the Understanding of Volcanogenic Massive Sulphide Deposit Genesis and Exploration Methods Development, (ed.) J.M. Peter and P. Mercier-Langevin; Geological Survey of Canada, Open File 7853, p. 131–145.

Cathles, L.M., 1993. Oxygen isotope alteration in the Noranda mining district, Abitibi greenstone belt, Quebec: Economic Geology, v. 88, p. 1483–1511.

Danyushevsky, L.V., Robinson, P., Gilbert, S., Norman, M., Large, R., McGoldrick, P., and Shelley, J.M.G., 2011. A technique for routine quantitative multi-element analysis of sulphide minerals by laser ablation ICP-MS; Geochemistry: Exploration, Environment, Analysis, v. 11, p. 51–60.

Davis, C., 2014. Integrated whole rock geochemical and oxygen isotope systematics of hydrothermal alteration associated with the Izok Lake volcanogenic massive sulphide (VMS) deposit, Nunavut, Canada; B.Sc. Honours thesis, University of Waterloo, Waterloo, Ontario.

Dubé, B., Gosselin, P., Mercier-Langevin, P., Hannington, M., and Galley, A., 2007. Gold-rich volcanogenic massive sulphide deposits, *In:* Mineral Deposits of Canada: A Synthesis of Major Deposit Types, District Metallogeny, the Evolution of Geological Provinces, and Exploration Methods, (ed.) W.D. Goodfellow; Geological Association of Canada, Mineral Deposits Division, Special Publication 5, p. 75–94.

Dubé, B., Mercier-Langevin, P., Kjarsgaard, I., Hannington, M., Bécu, V., Côté, J., Moorhead, J., Legault, M., and Bédard, N., 2014. The Bousquet 2-Dumagami world-class Archean Au-rich volcanogenic massive sulfide deposit, Abitibi, Quebec: metamorphosed submarine advanced argillic alteration footprint and genesis; Economic Geology, v. 109, p. 121–166.

Dubé, B., Mercier-Langevin, P., Castonguay, S., McNicoll, V.J., Bleeker, W., Lawley, C.J.M., De Souza, S., Jackson, S.E., Dupuis, C., Gao, J.-F., Bécu, V., Pilote, P., Goutier, J., Beakhouse, G.P., Yergeau, D., Oswald, W., Janvier, V., Fontaine, A., Pelletier, M., Beauchamp, A.-M., Katz, L.R., Kontak, D.J., Tóth, Z., Lafrance, B., Gourcerol, B., Thurston, P.C., Creaser, R.A., Enkin, R.J., El Goumi, N., Grunsky, E.C., and Lauzière, K, 2015. Precambrian lode gold deposits – a summary of TGI-4 contributions to the understanding of lode gold deposits, with an emphasis on implications for exploration, *In:* Targeted Geoscience Initiative 4: Contributions to the Understanding of Precambrian Lode Gold Deposits and Implications for Exploration, (ed.) B. Dubé and P. Mercier-Langevin; Geological Survey of Canada, Open File 7852, p. 1–24.

Duff, S., Hannington, M.D., Caté, A., Mercier-Langevin, P., Kjarsgaard, I., Dubé, B., and Gagné, S., 2013. Major ore types

of the Lalor gold-rich massive sulphide deposit, Snow Lake, *In:* Program with Abstracts; Geological Association of Canada – Mineralogical Association of Canada (GAC-MAC) Joint Annual Meeting, Winnipeg, Manitoba, May 22–24, 2013, Abstract Volume 36, p. 88.

Duff, S., Hannington, M.D., Caté, A., Mercier-Langevin, P., and Kjarsgaard, I.M., 2015. Major ore types of the Paleoproterozoic Lalor auriferous volcanogenic massive sulphide deposit, Snow Lake, Manitoba, *In:* Targeted Geoscience Initiative 4: Contributions to the Understanding of Volcanogenic Massive Sulphide Deposit Genesis and Exploration Methods Development, (ed.) J.M. Peter and P. Mercier-Langevin; Geological Survey of Canada, Open File 7853, p. 147–170.

Dupuis, C. and Beaudoin, G., 2011. Discriminant diagrams for iron oxide trace element fingerprinting of mineral deposit types; Mineralium Deposita, v. 46, p. 319–335.

Farquhar, J. and Wing, B.A., 2003. Multiple sulfur isotopes and the evolution of the atmosphere; Earth and Planetary Science Letters, v. 6707, p. 1–13.

Farquhar, J., Bao, H., and Thiemens, M., 2000. Atmospheric influence of Earth's earliest sulfur cycle; Science, v. 289, p. 756–758.

Farquhar, J., Savarino, J., Airieau, S., and Thiemens, M., 2001. Observation of wavelength-sensitive mass-independent sulfur isotope effects during SO_2 photolysis: Implications for the early atmosphere; Journal of Geophysical Research, v. 106, p. 32829–32839.

Farquhar, J., Wu, N., Canfield, E.D., and Oduro, H., 2010. Connections between sulfur cycle evolution, sulfur isotopes, sediments, and base metal sulfide deposits; Economic Geology, v. 105, p. 509–533.

Gill, S., 2015. Mineralogy, metal zoning, and genesis of the barite-rich Zn-Pb-Cu-Ag-Au Lemarchant volcanogenic massive sulfide (VMS) deposit; M.Sc. thesis, Memorial University of Newfoundland, St. John's, Newfoundland, 154 p.

Gill, S.B., and Piercey, S. J., 2014. Preliminary observations on styles of mineralization and sulphide-mineral zonation in the Cambrian Zn-Pb-Cu-Ag-Au Lemarchant volcanogenic massive-sulphide deposit, Newfoundland and Labrador; Geological Survey of Canada, Current Research 2014-5, 20 p.

Gill, S.B., Piercey, S.J., and Devine, C.A., 2013. Preliminary mineralogy of barite-associated sulphide mineralization in the Ordovician Zn-Pb-Cu-Ag-Au Lemarchant volcanogenic massive sulphide deposit, Newfoundland and Labrador; Geological Survey of Canada, Current Research 2013-17, 15 p.

Gill, S.B., Piercey, S.J., Layton-Matthews, D., Layne, G.D., and Piercey, G., 2015. Mineralogical, sulphur, and lead isotopic study of the Lemarchant Zn-Pb-Cu-Ag-Au-VMS deposit: Implications for precious-metal enrichment processes in the VMS environment, *In:* Targeted Geoscience Initiative 4: Contributions to the Understanding of Volcanogenic Massive Sulphide Deposit Genesis and Exploration Methods Development, (ed.) J.M. Peter and P. Mercier-Langevin; Geological Survey of Canada, Open File 7853, p. 183–195.

Hannington, M.D. and Scott, S.D., 1989. Gold mineralization in volcanic hosted massive sulfides: Implications of data from active hydrothermal vents on the modern sea floor, *In:* The Geology of Gold Deposits: The Perspective in 1988, (ed.) R.R. Keays, R.W.H. Ramsay, and D.I. Groves; Economic Geology, Monograph 6, p. 491–507.

Holk, G.J., Taylor, B.E., and Galley, A.G., 2008. Oxygen isotope mapping of the Archean Sturgeon Lake caldera complex, Northwestern Ontario, Canada; Mineralium Deposita, v. 43, p. 623–640.

Huston, D.L., 2000. Gold in volcanic-hosted massive sulfide deposits; distribution, genesis, and exploration, *In:* Gold in 2000, (ed.) S.G. Hagemann and P.E. Brown; Reviews in Economic Geology, v. 13, p. 401–426.

Jamieson, J.W., Wing, B.A., Farqhuar, J., and Hannington, M.D., 2013. Neoarchaean seawater sulphate concentrations from sulphur isotopes in massive sulphide ore; Nature Geoscience, v. 6, p. 61–64.

Laakso, K., 2015. Applying hyperspectral remote sensing Techniques for the detection of hydrothermal alteration zones and gossans in northern Canada; Ph.D. thesis, University of Alberta, Edmonton, Alberta, 210 p.

Laakso, K., Rivard, B., and Peter, J.M., 2015. Hyperspectral reflectance spectrometry in the exploration for VMS deposits using the Izok Lake Zn-Cu-Pb-Ag deposit, Nunavut as a test site, *In:* Targeted Geoscience Initiative 4: Contributions to the Understanding of Volcanogenic Massive Sulphide Deposit Genesis and Exploration Methods Development, (ed.) J.M. Peter and P. Mercier-Langevin; Geological Survey of Canada, Open File 7853, p. 15–25.

Laakso, K., Rivard, B., Peter, J.M., White, H.P., Maloley, M., Harris, J., and Rogge, D., 2015b. Application of airborne, laboratory and field hyperspectral methods to mineral exploration in the Canadian Arctic: recognition and characterization of volcanogenic massive sulfide-associated hydrothermal alteration in the Izok Lake deposit area, Nunavut, Canada; Economic Geology, v. 110, p. 925–941.

Large, R.R., Allen, R.L., Blake, M.D., and Herrmann, W., 2001. Hydrothermal alteration and volatile element halos for the Rosebery K Lens volcanic-hosted massive sulfide deposit, western Tasmania; Economic Geology, v. 96, p. 1055–1072.

Lentz, D.R., 2005. Mercury as a lithogeochemical exploration vectoring technique: a review of methodologies and applications, with selected VMS case histories, *In:* The Gangue; Geological Association of Canada, Mineral Deposits Division, v. 85, p. 1, 5–11.

Makvandi, S., Beaudoin, G., Ghasemzadeh-Barvarz, M., and McClenaghan, M.B., 2013. Fingerprinting volcanogenic massive sulfide deposits using magnetite chemistry: Application to till from Izok Lake, Nunavut, Canada, *In:* Proceedings; 12th Biennial SGA Meeting, Uppsala, Sweden, August 12-15, 2013, 4 p.

McClenaghan, M.B. and Peter, J.M., 2013. Till geochemical signatures of volcanogenic massive sulphide deposits in glaciated terra, *In:* a summary of Canadian examples; Geological Survey of Canada, Open File 7354, 36 p.

McClenaghan, M.B. and Peter, J.M., in press. Till geochemical signatures of volcanogenic massive sulphide deposits in glaciated terra*In:* an overview of Canadian examples; Geochemistry: Exploration, Environment, Analysis.

McClenaghan, M.B., Peter, J.M., and Layton-Matthews, D., 2015. Overview of VMS exploration in glaciated terrain using indicator minerals, till geochemistry, and boulder tracing: A Canadian perspective, *In:* Targeted Geoscience Initiative 4: Contributions to the Understanding of Volcanogenic Massive Sulphide Deposit Genesis and Exploration Methods Development, (ed.) J.M. Peter and P. Mercier-Langevin; Geological Survey of Canada, Open File 7853, p. 81–99.

Mercier-Langevin, P., Hannington, M.D., Dubé, B., and Bécu, V., 2011. The gold content of volcanogenic massive sulfide deposits; Mineralium Deposita, v. 46, p. 509–539.

Mercier-Langevin, P., Caté, A., and Ross, P.-S., 2014a. Whole-rock oxygen-isotope mapping of the footwall alteration zones at the Lalor auriferous VMS deposit, Snow Lake, west-central Manitoba (NTS 63K16), *In:* Report of Activities 2014; Manitoba Mineral Resources, Manitoba Geological Survey, p. 113–130.

Mercier-Langevin, P., Lafrance, B., Bécu, V., Dubé, B., Kjarsgaard, I., and Guha, J., 2014b. The Lemoine auriferous volcanogenic massive sulfide deposit, Chibougamau camp, Abitibi greenstone belt, Québec, Canada: geology and genesis; Economic Geology, v. 109, p. 231–269.

Mercier-Langevin, P., Hannington, M.D., Dubé, B., Piercey, S.J., Peter, J.M., and Pehrsson, S.J., 2015. Precious metal enrichment processes in volcanogenic massive sulphide deposits — A summary of key features, with an emphasis on TIGI-4 research contributions, *In:* Targeted Geoscience Initiative 4: Contributions to the Understanding of Volcanogenic Massive Sulphide Deposit Genesis and Exploration Methods Development, (ed.) J.M. Peter and P. Mercier-Langevin; Geological Survey of Canada, Open File 7853, p. 101–114.

Ohmoto, H. and Rye, R.O., 1979. Isotopes of sulfur and carbon, *In:* Geochemistry of hydrothermal ore deposits, 2nd edition, (ed.) H.L. Barnes; John Wiley and Sons, Toronto, Canada, p. 509–567.

Pilote, J.-L. and Piercey, S.J., 2013. Volcanostratigraphy of the 1807 zone of the Ming Cu-Au volcanogenic massive sulphide deposit, Baie Verte Peninsula, northern Newfoundland; Geological Survey of Canada, Current Research 2013-20, 13 p.

Pilote, J.-L., Piercey, S.J., and Mercier-Langevin, P., 2014. Stratigraphy and hydrothermal alteration of the Ming Cu-Au volcanogenic massive-sulphide deposit, Baie-Verte Peninsula, Newfoundland; Geological Survey of Canada, Current Research 2014-7, 18 p.

Pilote, J.-L., Piercey, S.J., and Mercier-Langevin, P., 2015. Volcanic architecture and alteration assemblages of the Ming Cu-Au-(Zn-Ag) VMS deposit, Baie Verte, Newfoundland: Implications for Au-enrichment processes and exploration, *In:* Targeted Geoscience Initiative 4: Contributions to the Understanding of Volcanogenic Massive Sulphide Deposit Genesis and Exploration Methods Development, (ed.) J.M. Peter and P. Mercier-Langevin; Geological Survey of Canada, Open File 7853, p. 197–210.

Soltani Dehnavi, A., McFarlane, C.R.M., McClenaghan, S.H., and Lentz, D.R., 2014. In situ LA ICP-MS of sulphide minerals in VMS deposits throughout the Bathurst Mining Camp, New Brunswick, Canada: volatile trace element contents and distribution with implications for their syngenetic to polyphase metamorphic history; Geological Survey of Canada, Open File 7537, 1 sheet, doi:10.4095/293681.

Soltani Dehnavi, A., Lentz, D.R., and McFarlane, C.R.M., 2015. LA-ICP-MS analysis of volatile trace elements in massive sulphides and host rocks of selected VMS deposits of the Bathurst Mining Camp, New Brunswick: methodology and application to exploration, *In:* Targeted Geoscience Initiative 4: Contributions to the Understanding of Volcanogenic Massive Sulphide Deposit Genesis and Exploration Methods Development, (ed.) J.M. Peter and P. Mercier-Langevin; Geological Survey of Canada, Open File 7853, p. 59–80.

Taylor, B. and Holk, G., 1998. Stable isotope applications in the exploration for volcanic-associated massive sulphide deposits: a preliminary summary, *In:* Database for CAMIRO Project 94E07: interrelationships between subvolcanic intrusions, large-scale alteration zones and VMS deposits, (ed.) A. Galley, A. Bailes, M. Hannington, G. Holk, J. Katsube, F. Paquette, S. Paradis, F. Santaguida, B. Taylor, and B. Hillary; Geological Survey of Canada, Open File 4431, p. 41–46.

Taylor, B.E., Peter, J.M., Laakso, K., and Rivard, B., 2015a. Oxygen isotope zonation about the Izok Ag-VMS deposit, Slave Province, Nunavut: hanging-wall vector to mineralization, *In:* Targeted Geoscience Initiative 4: Contributions to the Understanding of Volcanogenic Massive Sulphide Deposit Genesis and Exploration Methods Development, (ed.) J.M. Peter and P. Mercier-Langevin; Geological Survey of Canada, Open File 7853, p. 27–44.

Taylor, B.E., Peter, J.M., and Wing, B.A., 2015b. Multiple sulphur isotope reconnaissance of Slave Province volcanogenic massive sulphide deposits, *In:* Targeted Geoscience Initiative 4: Contributions to the Understanding of Volcanogenic Massive Sulphide Deposit Genesis and Exploration Methods Development, (ed.) J.M. Peter and P. Mercier-Langevin; Geological Survey of Canada, Open File 7583, p. 45–58.

Taylor, H.P., Jr., 1979. Oxygen and hydrogen isotope relationships in hydrothermal mineral deposits, *In:* Geochemistry of Hydrothermal Ore Deposits, (ed.) H. Barnes; John Wiley and Sons, New York, p. 236–277.

Thorpe, R.I., Cumming, G.L., and Mortensen, J.K., 1992. A significant Pb isotope boundary in the Slave Province and its probable relation to ancient basement in the western Slave Province, *In:* Project Summaries: Canada – Northwest Territories Mineral Development Subsidiary Agreement 1987-1991, (comp.) D.G. Richardson and M. Irving; Geological Survey of Canada, Open File Report 2484, p. 179–184.

Tschirhart, P., 2013. Geophysical processing and interpretation with geologic controls: examples from the Bathurst Mining Camp; M.Sc. thesis, McMaster University, Hamilton, Ontario, 129 p.

Tschirhart, P., Morris, W., and Hodges, G., 2014a. A new residual separation for magnetic datasets using susceptibility from frequency domain electromagnetic data; Geological Survey of Canada, Open File 7371, 1 sheet. doi:10.4095/293726

Tschirhart, P., Morris, W.A., and Hodges, G., 2014b. A new regional/residual separation for magnetic datasets using susceptibility from frequency domain electromagnetic data; Geophysics, v. 78, p. B351–B359.

Tschirhart, P.A. and Morris, W.A., 2015. Integration of rock properties and geophysics, Bathurst Mining Camp, *In:* Targeted Geoscience Initiative 4: Contributions to the Understanding of Volcanogenic Massive Sulphide Deposit Genesis and Exploration Methods Development, (ed.) J.M. Peter and P. Mercier-Langevin; Geological Survey of Canada, Open File 7853, p. 101–115.

Tschirhart, P. and Morris, W.A., in press-a. Analysis of petrophysical properties of rocks from the Bathurst Mining Camp: Constraints on gravity and magnetic modelling; Interpretation.

Tschirhart, P. and Morris, W.A., in press-b. Improved edge detection mapping through stacking and integration: A case study in the Bathurst Mining Camp; Geophysical Prospecting.

Yarra, D.R., Fueten, F., Peter, J.M., and Harris, J., 2014. Recognition of hydrothermal alteration using airborne hyperspectral imagery and gold favourability mapping in the Hope Bay volcanic belt, Nunavut; Geological Survey of Canada, Open File 7470, 1 sheet. doi:10.4095/293727

Yarra, R., 2013. Recognition of Hydrothermal alteration using airborne Hyperspectral Imagery and Gold Favourability Mapping in the Hope Bay Volcanic Belt, Nunavut; B.Sc. Honours thesis, Brock University, Saint Catharines, Ontario.

GEOLOGICAL SURVEY OF CANADA
OPEN FILE 7853

Targeted Geoscience Initiative 4: Contributions to the Understanding of Volcanogenic Massive Sulphide Deposit Genesis and Exploration Methods Development

Hyperspectral reflectance spectrometry in the exploration for VMS deposits using the Izok Lake Zn-Cu-Pb-Ag deposit, Nunavut as a test site

Kati Laakso[1], Benoit Rivard[1], and Jan M. Peter[2]

[1]University of Alberta, Edmonton, Alberta
[2]Geological Survey of Canada, Ottawa, Ontario

2015

This publication is available for free download through GEOSCAN (http://geoscan.nrcan.gc.ca/)

Recommended citation

Laakso, K., Rivard, B., and Peter, J.M., 2015. Hyperspectral reflectance spectrometry in the exploration for VMS deposits using the Izok Lake Zn-Cu-Pb-Ag deposit, Nunavut as a test site, *In:* Targeted Geoscience Initiative 4: Contributions to the Understanding of Volcanogenic Massive Sulphide Deposit Genesis and Exploration Methods Development, (ed.) J.M. Peter and P. Mercier-Langevin; Geological Survey of Canada, Open File 7853, p. 15–25.

Publications in this series have not been edited; they are released as submitted by the author.

Contribution to the Geological Survey of Canada's Targeted Geoscience Initiative 4 (TGI-4) Program (2010–2015)

TABLE OF CONTENTS

Hyperspectral reflectance spectrometry in the exploration for VMS deposits using the Izok Lake Zn-Cu-Pb-Ag deposit, Nunavut as a test site

Kati Laakso[1]*, Benoit Rivard[1], and Jan M. Peter[2]

[1]Centre for Earth Observation Sciences at the University of Alberta, Department of Earth and Atmospheric Sciences, University of Alberta, 1-26 Earth Sciences Building, University of Alberta, Edmonton, Alberta T6G 2E3
[2]Central Canada Division, Geological Survey of Canada, 601 Booth Street, Ottawa, Ontario K1A 0E8
*Corresponding author's e-mail: laakso@ualberta.ca

ABSTRACT

We have investigated the application of ground, laboratory and airborne optical remote sensing methods to the detection of hydrothermal alteration zones associated with volcanogenic massive sulphide (VMS) deposits using the Izok Lake Zn-Cu-Pb-Ag deposit, Nunavut as a test site. The deposit is located in a subarctic environment where lichens are abundant on the rock outcrops. The rhyolitic host rocks to the deposit have been hydrothermally altered and contain white mica and chlorite group minerals. These alteration minerals have Al-OH and Fe-OH absorption features in the short-wave infrared (SWIR) wavelength region. The absorption feature wavelength positions can shift as a function of chemical compositional changes within minerals. In and around the Izok Lake deposit there are systematic trends in the Al-OH and Fe-OH absorption feature wavelength positions with distance from the massive sulphide lenses. Furthermore, these trends can be detected in bulk rock lithogeochemical data. Our results demonstrate the feasibility of using hyperspectral remotely sensed data to delineate hydrothermal alteration zones and determine alteration intensity in high-latitude regions.

INTRODUCTION

Volcanogenic massive sulphide (VMS) deposits are economically important sources of metals (Gibson et al., 2007) formed on or near the seafloor from hydrothermal systems that are spatially and temporally associated with submarine magmatism and volcanism. Cold seawater is drawn into the upper parts of the crust, which results in the establishment of a convective cell of circulating hydrothermal fluids. As the fluid temperature increases, metals are leached from the host rocks. These dissolved metals are precipitated near the seafloor, resulting in the formation of massive sulphide lenses. A key geochemical reaction along the fluid flow path is the breakdown of feldspar minerals through interactions with acidic hydrothermal fluids, and the subsequent formation of white micas and chlorite (Barrett and MacLean, 1994). The temperature and chemical gradients induced by mixing of high-temperature hydrothermal fluids with cold seawater result in a range of chemical, mineralogical and textural changes in the host rocks and the precipitation of syngenetic and stratabound accumulations of massive to semi-massive sulphides. These phyllosilicates are typical hydrothermal alteration minerals. Generally, the stratigraphic footwall immediately beneath the massive sulphides is characterized by chloritic alteration, and the areas more distal from the massive sulphides by sericitic alteration.

The white mica group minerals formed during VMS-associated hydrothermal alteration can have variable chemical compositions that range from paragonite to muscovite to celadonite. Paragonite is favoured at high temperatures (Duke, 1994), but the chemical composition of the hydrothermal fluids and the water/rock ratio of the system may also simultaneously influence the composition (Kranidiotis and MacLean, 1987). The chemical composition of the phyllosilicate minerals may be governed through Tschermak substitution, in which tetrahedral Si substitution for Al is coupled with octahedral Mg-Fe substitution for Al. These substitutions can be observed as spectral shifts within the Al-OH absorption features near 2200 nm (Bishop et al., 2008). The wavelength position of this absorption feature shifts systematically toward shorter wavelengths as the Al content of the octahedral sites increases, and a systematic shift toward longer wavelengths takes place when the relative proportion of octahedral Mg and Fe increase (Duke, 1994). Similar changes take place in the chlorite group minerals that show a spectral shift of an Fe-OH absorption feature near 2250 nm

Laakso, K., Rivard, B., and Peter, J.M., 2015. Hyperspectral reflectance spectrometry in the exploration for VMS deposits using the Izok Lake Zn-Cu-Pb-Ag deposit, Nunavut as a test site, *In:* Targeted Geoscience Initiative 4: Contributions to the Understanding of Volcanogenic Massive Sulphide Deposit Genesis and Exploration Methods Development, (ed.) J.M. Peter and P. Mercier-Langevin; Geological Survey of Canada, Open File 7853, p. 15–25.

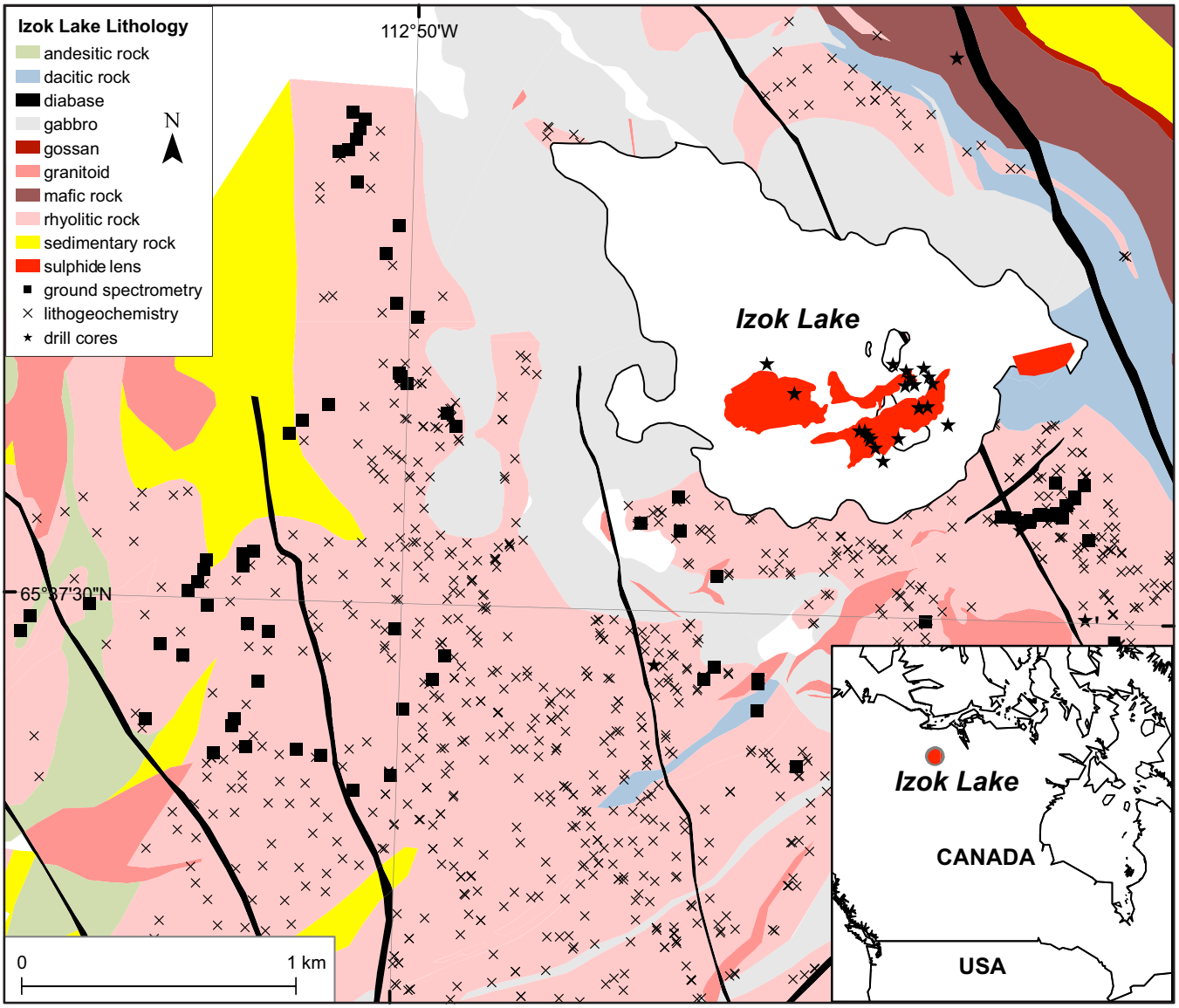

Figure 1. Locational (inset) and geological map of the study area showing the locations of the ground spectrometric data (black squares) and drill-core sites (stars). The airborne survey covers the whole study area. The geology, surface projections of sulphide lenses on islands and under Izok Lake and locations of lithogeochemical samples (x) are from MMG Ltd. (unpubl.).

toward shorter wavelengths with increasing Mg, and toward longer wavelengths with increasing Fe (McLeod et al., 1987).

Several hydrothermal alteration indices have been developed to determine alteration style and measure its intensity (e.g. Ishikawa et al., 1976; and references therein). These indices are calculated using elements that were added (numerator) and those that were lost (denominator) during alteration. The spatial distribution of the alteration index values can then be used to vector toward massive sulphide mineralization.

Our study area is the Izok Lake Zn-Cu-Pb-Ag VMS deposit which is located at 65°38'N, 112°48'W in the Point Lake greenstone belt, Nunavut (Fig. 1). The deposit is comprised of several massive sulphide lenses that are hosted by rhyolitic rocks. These rocks contain white mica and chlorite group minerals that result from hydrothermal alteration during massive sulphide formation (Morrison, 2004), and here we present spectral and bulk geochemical data for these rhyolitic rocks. The Izok Lake region is characterized by Arctic tundra vegetation that is dominated by shrubs, sedges, grasses and flowering herbs (Laidler et al., 2008), and many rock outcrops in the study area are covered by abundant lichens. These lichens mask the spectral characteristics of the rocks, potentially compromising the use of remote sensing data for geologic applications. A comprehensive description of the study area is given in Laakso et al. (in press).

The research objective was to assess the applicability of hyperspectral remote sensing to the detection and delineation of hydrothermal alteration zones associated

with the Izok Lake deposit. White micas, biotite and chlorite are the predominant phyllosilicate alteration minerals near the Izok Lake deposit, and for this reason, the Al-OH and Fe-OH absorption feature wavelengths positions were measured using ground, laboratory and airborne hyperspectral instruments. The ground data were also compared with hydrothermal alteration indices calculated from bulk lithogeochemical data to determine if the spectral data could serve as a proxy for mapping hydrothermal alteration.

SAMPLING AND METHODS

Ground Spectrometry

These data were acquired throughout the study area with the objective of mapping any outcropping hydrothermal alteration zones associated with the Izok Lake deposit. A total of 285 spectra were acquired from the areas in the vicinity of the massive sulphide mineralization. At each rock outcrop, one to eight spectral measurements, each with a 1 cm diameter circular outline, were collected from lichen-free weathered rock surfaces. The spectra were acquired with an ASD FieldSpec® Pro 3 spectrometer that records in the 350–2500 nm wavelength range with a spectral resolution of 10 nm in the short-wave infrared wavelength region. The spectrometer was equipped with a fore optic contact probe to ensure consistent illumination conditions during data acquisition. Radiance values were converted to reflectance values by means of a panel of pressed polytetrafluoroethylene, commercially known as Spectralon™ (Labsphere, New Hampshire, US). The geographic coordinates of the field sites were recorded with a handheld GPS.

The Al-OH and Fe-OH absorption feature wavelength positions of the spectra were extracted to discern any spectral shifts associated with the areas of hydrothermally altered rock. An average wavelength position was then computed from these spectra; this was achieved by conducting continuum removal and recording the minimum (the smallest hull quotient value) of each spectrum. Next, these values were averaged per rock outcrop, and this resulted in 98 Al-OH and 85 Fe-OH absorption feature wavelength position observations (Fig. 1). The inverse distance weighting (IDW: ArcGIS Desktop: Release 10, Environmental Systems Research Institute) interpolation technique was used to create a continuous surface of the Al-OH and Fe-OH wavelength positions. The results were clipped to a 200 m radius around each averaged ground spectrum to minimize extrapolation and to create a realistic representation of the spatial trends of the absorption feature wavelength positions of the study area.

In a separate analysis, the horizontal distance between each spectral result at the measurement locations and its nearest massive sulphide lens (see Fig. 1) was calculated to investigate the spectral trends as a function of distance from the massive sulphide lenses.

Laboratory Spectrometry

In order to establish the character and extent of the hydrothermal alteration zones of the Izok Lake deposit in the vertical dimension, spectrometric data were obtained from 28 drill cores (Fig. 1). Of the 781 spectral readings that were acquired with an ASD FieldSpec 3 spectrometer and a TerraSpec 4 hi-resolution mineral spectrometer, 624 spectra were from rhyolitic rocks. The measurements obtained from the rhyolitic rocks were calibrated to reflectance and the Al-OH and Fe-OH wavelength positions of each measurement were extracted as described above for ground spectral measurements.

The distance between each Al-OH and Fe-OH absorption feature observations of the drill cores and its spatially nearest massive sulphide lens was calculated to investigate changes in the spectral properties of the phyllosilicate minerals with distance to the mineralization. The locations and spatial dimensions of the massive sulphide lenses were extracted from the drill-core logs of MMG Ltd. Finally, the results obtained from the drill-core spectra were combined with the corresponding ground spectral results to obtain a three-dimensional model of the spatial variation of the Al-OH and Fe-OH absorption feature wavelength positions in the Izok Lake deposit.

Lithogeochemistry

A database of whole-rock major element oxide analyses of 2902 rock outcrop hand samples collected from the study area was provided by MMG Ltd. (Fig. 1). These samples are from areas proximal and distal to mineralization. The locations of the samples are shown in Figure 1. Whole-rock major oxide analyses were performed by ALS Minerals (North Vancouver, B.C.) using Inductively Coupled Plasma-Atomic Emission Spectroscopy (ICP-AES) on rock powders.

A subset of the database that encompasses 1241 rhyolitic rock samples was used to identify large-scale hydrothermal alteration trends across the study area. Hydrothermal alteration was assessed by means of the Ishikawa index (AI: Ishikawa et al., 1976):

$$AI = 100(K_2O+MgO)/(K_2O+MgO+Na_2O+CaO)$$

The IDW interpolation technique was used to create a continuous representation of the AI values across the study area.

The AI has two drawbacks for quantifying hydrothermal alteration. First, it does not take into account carbonate alteration that can be significant in some VMS deposits. Second, it does not differentiate

between sericitic and chloritic alteration. For these reasons, Large et al. (2001) introduced the Chlorite-Carbonate-Pyrite Index (CCPI):

$$CCPI=100(FeO+MgO)/(FeO+MgO+Na_2O+K_2O)$$

The Alteration Box Plot (Large et al., 2001) plots the AI values against the CCPI values to discern different alteration trends within VMS deposits. Here, we use the Alteration Box Plot to account for possibly distinct hydrothermal alteration zones in the study area and summarize the results (AI+CCPI) to determine the spatial distribution of these zones. Furthermore, the alteration intensity estimates are divided into four quartiles that each represent a fourth of the sampled population. The results were spatially joined with their nearest Al-OH wavelength position to assess the capability to infer alteration intensity estimates from hyperspectral remote sensing data.

Airborne Spectrometry

Airborne hyperspectral data were acquired over a 94 km^2 area comprising 58 flight lines within the Point Lake greenstone belt in August, 2010. The data were acquired by SpecTIR LLC (Reno, Nevada) using the ProSpecTIR® (AISA dual) sensor at a spatial resolution of 1 m. This sensor collects data in a nominal spectral resolution of 5 nm between 390 to 2500 nm. These data were resampled to a 6.3 nm interval, resulting in 360 spectral channels.

The airborne dataset was pre-processed by SpecTIR by first radiometrically calibrating the digital numbers of the raw data to radiance values using the preflight gains and offsets measured by the sensor manufacturer. Next, the radiance data was atmospherically corrected to reflectance data using the ATCOR-4® software package (Richter and Schläpfer, 2002). Finally, the dataset was geospatially corrected using the data extracted from a three-axis gyroscope attitude INS (Inertial Navigation System) that was positioned with a 12-channel GPS system.

The airborne data were analyzed and compared with the ground spectral dataset to investigate the accuracy of the Al-OH absorption feature wavelength positions extracted from the airborne dataset. First, pixels in the airborne data associated with vegetation were removed by means of the Normalized Difference Vegetation Index ($NDVI_{705}$; Gitelson and Merzlyak, 1994) to which a threshold was applied. Next, spectral endmembers were extracted from the remaining pixels using the Spatial-Spectral Endmember Extraction (SSEE) tool of Rogge et al. (2007). Of the 137 endmembers extracted, 22 were selected to represent rocks, vegetation and lichens, or mixtures of these. This endmember spectral database was then input into the linear spectral unmixing computer calculations. The resulting endmember images were investigated and a single endmember image was chosen to represent pixels of the rhyolitic rock outcrops with a minimal lichen cover. A threshold was extracted from this image and applied to the original hyperspectral image to retain rhyolitic rock outcrop pixels with sparse vegetation and the lowest degree of lichen cover.

Next, the wavelength position of the Al-OH absorption feature was calculated after hull removal from the 2188–2212 nm wavelength range. Wavelength positions at 2194 nm and 2212 nm were discarded because they are likely associated with vegetation rather than the rhyolitic rocks, and hence only the wavelengths at 2200 nm and 2206 nm were used in the airborne data analysis. At this stage, 261 pixels remained, representing <1% of the original amount of pixels associated with the rhyolitic rock outcrops in the airborne data. As with the ground spectral and lithogeochemical datasets, an interpolated surface was created from the result using the IDW tools of the ArcGIS software package. The result was cropped to a 200 m diameter buffer around each observation in order to minimize the effects of extrapolation to areas of no observations. This protocol was not repeated for the Fe-OH absorption features of biotite/chlorite because these minerals could not be reliably detected in the airborne hyperspectral dataset.

The results were then compared with the ground spectral dataset. This dataset was resampled from the sampling interval of the ground spectrometry (1 nm in the SWIR wavelength region) to the sampling interval of the airborne spectrometry (6.3 nm). The Al-OH absorption feature wavelength positions (n=261) of the airborne spectrometric dataset were then linked with their geographically nearest Al-OH absorption feature wavelength positions of the ground spectral dataset. The accuracy of the airborne result was assessed by calculating the differences between the Al-OH absorption feature wavelength positions of the airborne and ground spectral datasets.

RESULTS

Spatial Distribution of the Ground and Laboratory Absorption Feature Wavelength Positions

An Al-OH absorption feature is present in >90% of the rhyolitic rock outcrops, indicating that the mineral responsible for this spectral feature is ubiquitously abundant throughout the study area. The average wavelengths of the absorption features in these outcrops varies between 2194 and 2211 nm. The wide range of the absorption feature wavelengths results from spectral shifts, as is illustrated in Figure 2a and b. The spatial distribution of the Al-OH absorption features of the

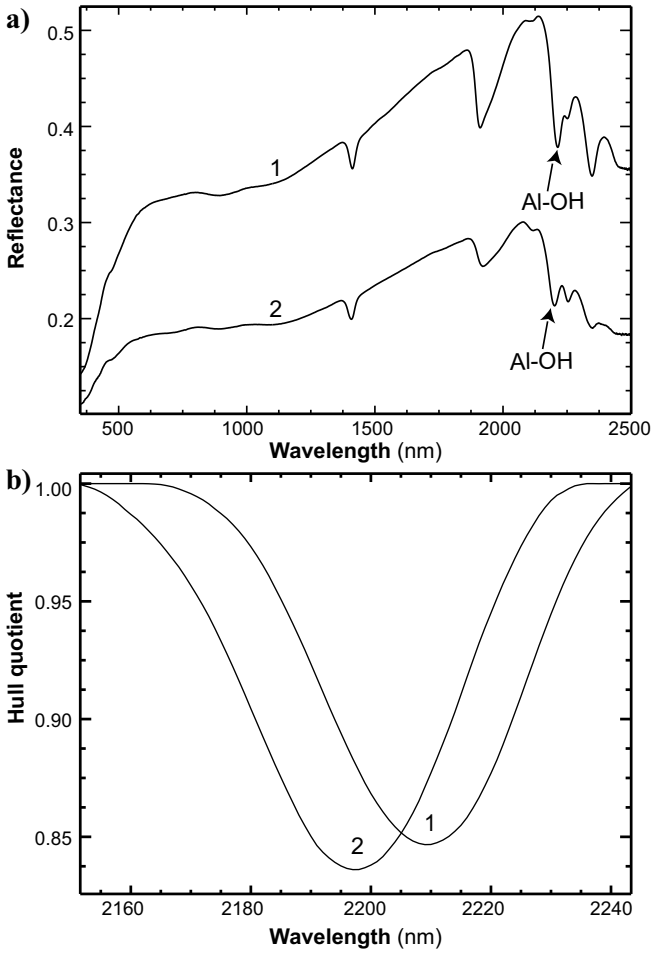

Figure 2. a) Ground reflectance spectra for measurement 313 (2211 nm, spectrum 1) and 134 (2197 nm, spectrum 2); **b)** hull quotient-corrected spectra 1 and 2 shown in (a).

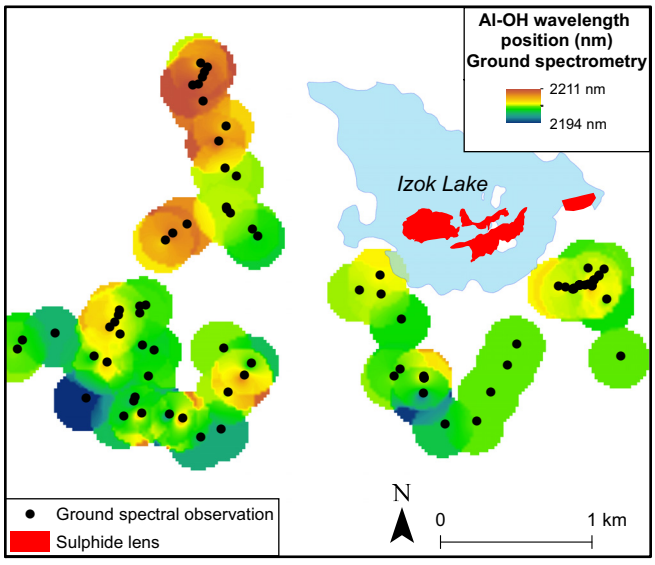

Figure 3. Colour ramp map of the interpolated Al-OH absorption feature wavelengths extracted from the ground spectrometry, the geographic data and surface projections of the sulphide lenses are from MMG Ltd. (unpubl.).

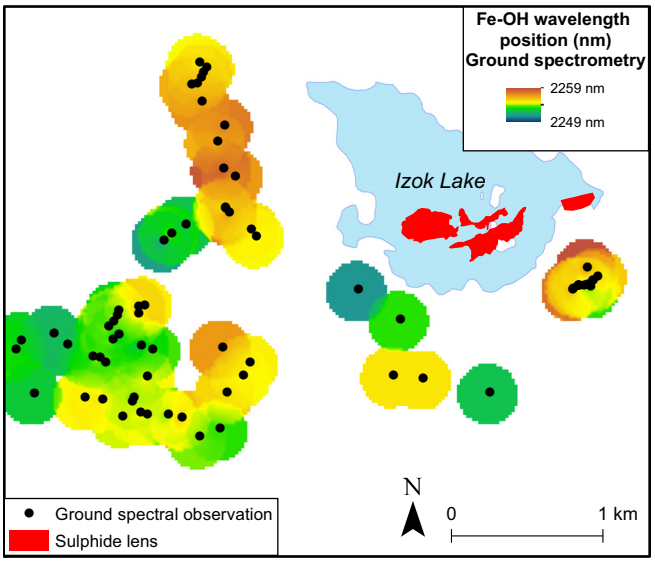

Figure 4. Colour ramp map of the interpolated Fe-OH absorption feature wavelengths extracted from the ground spectrometry; the geographic data and surface projections of the sulphide lenses are from MMG Ltd. (unpubl.).

ground spectral dataset, shown in Figure 3, suggests that the rocks surrounding the massive sulphide lenses contain relatively long Al-OH absorption feature wavelengths, with the highest Al-OH absorption features located northwest of the massive sulphide lenses.

An Fe-OH absorption was observed in 79% of the rock outcrops, indicating that this mineral group is less common than white micas in the study area. The average Fe-OH wavelengths of the rock outcrops range between 2249 and 2259 nm. The spatial distribution of the Fe-OH absorption features suggest that the longest Fe-OH absorption feature wavelength positions occur near the massive sulphide lenses (Fig. 4).

The spatial distributions of the Al-OH and Fe-OH absorption feature wavelength positions extracted from both the ground and drill-core spectra were further assessed by correlating them with their distance to the nearest massive sulphide mineralization. The results, shown in Figure 5a and b, indicate that rocks within 500 m of massive sulphide mineralization display considerable variation in the Al-OH and Fe-OH wavelength positions. Moreover, the shift toward longer Al-OH and Fe-OH absorption feature wavelength positions can be observed approximately 1000 to 2000 m from the massive sulphide lenses. It is notable that this trend is more evident in the Fe-OH absorption features than in the Al-OH absorption features that show weak or non-existent trends in the study area.

Alteration Intensity Variation Extracted from the Alteration Indices

Figure 6 show the spatial distribution of the AI and the Alteration Box plot values. This figure indicates that

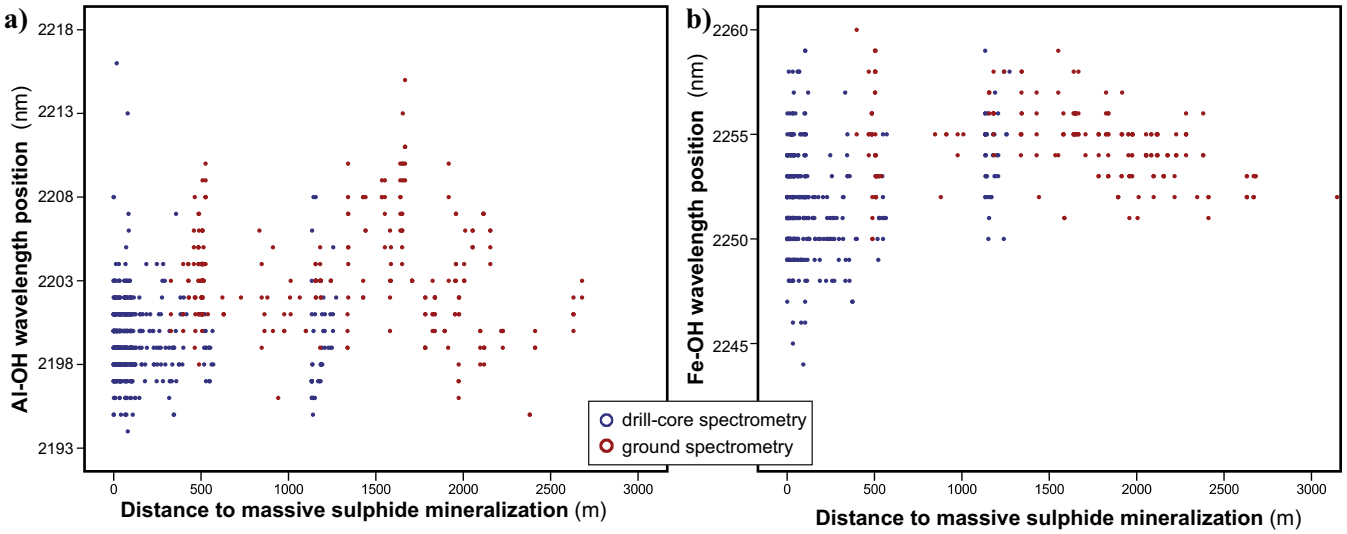

Figure 5. Bivariate plots of **(a)** Al-OH absorption feature wavelength positions of the ground and drill-core spectra versus distance from massive sulphide mineralization; and **(b)** Fe-OH absorption feature wavelength positions of the ground and drill-core spectra versus distance from massive sulphide mineralization. The results are shown for the intensely altered area within a 3000 m diameter distance of the deposit.

the rhyolitic rocks around the massive sulphide lenses have been intensely altered, as evidenced by high (99%) alteration intensity values. Moreover, both alteration intensity estimates show an area of intense hydrothermal alteration that spans up to 2.7 km southwest from the massive sulphide lenses (Fig. 6a,b). The high AI values of this area suggest near complete replacement of feldspars and glass by white mica and chlorite (Large et al., 2001).

The correlation between the alteration intensity and the Al-OH absorption feature in the ground spectra was investigated using Pearson product-moment correlation coefficient analysis. This was done by calculating the correlation coefficient between the Al-OH absorption feature wavelength positions of the ground spectral dataset and the Alteration Box Plot values subdivided into quartile ranges. The results (Fig. 6b) show a moderate, inverse correlation (r=-0.486, n=85, 99% confidence level, two-tailed) between these datasets, indicating that high alteration intensities are associated with a shift toward shorter Al-OH absorption feature wavelength positions.

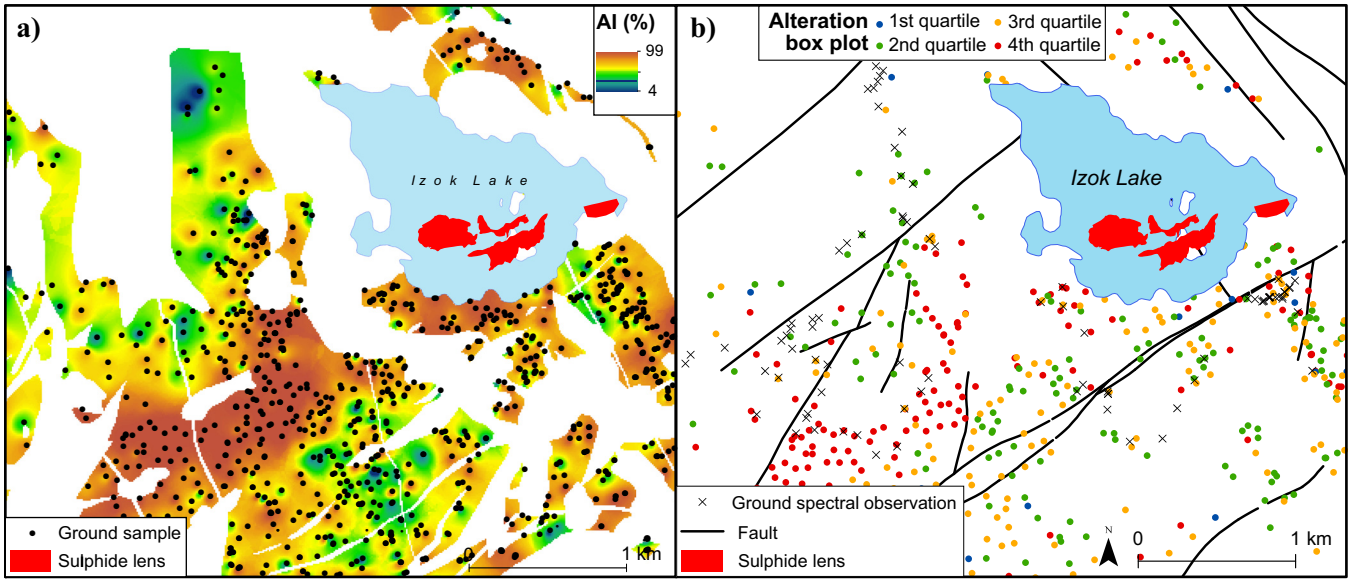

Figure 6. a) Colour ramp map of the AI content (%). **b)** Symbol map of the alteration box plot results, divided into four quartiles. Also shown are the measurement locations of the Al-OH absorption feature wavelength positions in the ground spectral dataset. The plot displays the AI and CCPI values of each lithogeochemical sample summarized and divided into four quartiles.

Airborne Spectrometric Absorption Feature Wavelengths

The Al-OH absorption feature wavelength positions of the airborne data (n=261) show a bimodal frequency distribution with absorption features at 2200 nm and at 2206 nm. A comparison between the ground and airborne spectral datasets reveals a relatively low accuracy of the airborne spectrometry as measured by the difference between the ground and airborne spectra: 65% of the Al-OH absorption feature wavelength positions of the airborne data (n=169) are within three nanometres of their spatially nearest airborne spectrometric value. However, in the vicinity of the massive sulphide lenses there is a zone of relatively long Al-OH absorption feature wavelength positions, spanning between 2200 and 2206 nm. This area coincides spatially with the relatively long Al-OH absorption feature wavelength positions in the ground spectrometric data that range between 2197 and 2211 nm. This area, located 800 to 1900 m west of the sulphide lenses coincides spatially with a high alteration intensity area (Figs. 6b, 7). Previous studies have suggested that phengitic white micas preferably develop in areas of high-temperature fluid flow (e.g. Hellyer VMS deposit; Yang et al., 2011).

DISCUSSION

There is considerable variation in the Al-OH absorption feature wavelength positions of white micas in the Izok Lake area indicative of variable effects of hydrothermal alteration processes. The Al-OH wavelength range of the ground spectral dataset (2194–2211 nm) suggests that the chemical composition of white micas ranges from paragonitic to muscovitic to slightly phengitic. Similarly, the Fe-OH wavelength range of biotite/chlorite (2249–2259 nm) indicates that these minerals have Mg-rich, intermediate and Fe-rich compositions in the study area. Iron enrichment is common in the highly altered areas of VMS deposits that typically contain Fe-rich chlorite (e.g. MacLean and Hoy, 1991) and hence iron enrichment near the massive sulphide lenses conforms to this idealized model. Both the white micas and biotite/chlorite show strongest variation in the Al-OH and Fe-OH absorption feature wavelength positions in the immediate vicinity (0–500 m) of the massive sulphide lenses (Fig. 5), indicative of strong temperature and geochemical gradients at the time of massive sulphide formation.

The alteration intensity variation of the Izok Lake area was estimated by means of the AI and the alteration box plot. Correlations between the alteration box plot and the Al-OH absorption feature wavelength positions reveal a relationship between high alteration intensity values and a shift toward shorter Al-OH absorption feature wavelength positions. Nevertheless,

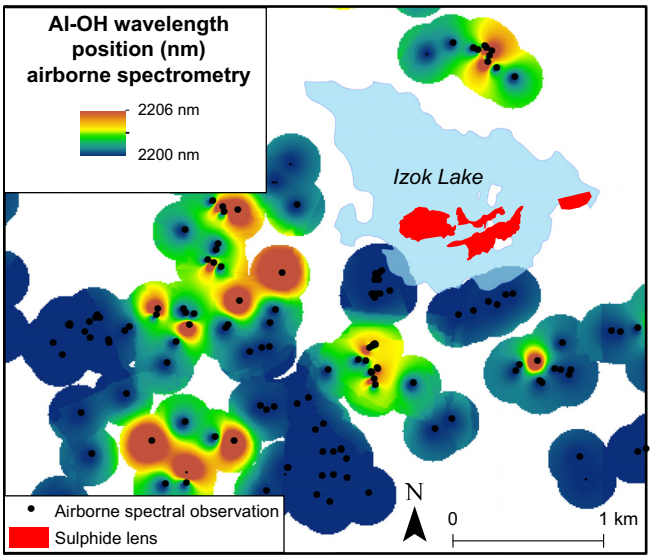

Figure 7. Colour ramp map of the interpolated Al-OH absorption feature wavelengths extracted from the airborne data; the surface projection of the sulphide lenses is from MMG Ltd. (unpubl.).

the area of high alteration intensities (800 to 1900 m from the massive sulphide lenses) is characterized by relatively long Al-OH absorption feature wavelength positions (up to 2211 nm), and hence the shift toward shorter wavelengths is relative. Also, there is no one-to-one correspondence between the hyperspectral datasets and the lithogeochemical data.

A comparison between the airborne and ground spectra reveals a detection accuracy of 65%. This low accuracy of the airborne spectrometric data may result from the abundant lichen cover that necessitated the masking out of 99% of the pixels associated with the rhyolitic rock outcrops. Contrary to the white mica group minerals, the Fe-OH absorption features of biotite/chlorite group minerals could not be detected in the airborne hyperspectral dataset. One factor that may have contributed to this result is the lower abundance of these minerals in the study area: white micas were observed in >90% of the rhyolitic rock outcrops, whereas biotite/chlorite group minerals were observed in only 79% of the rhyolitic rock outcrops.

Despite the relatively low detection accuracy of the airborne spectrometric data, the ability to detect an area of phengitic muscovite using both the ground and airborne datasets independently demonstrates the efficacy of airborne spectrometry for the recognition and delineation of zones of hydrothermally altered rocks in outcrops in the Izok Lake area.

IMPLICATIONS FOR EXPLORATION

Our results indicate that hydrothermal alteration zones associated with VMS deposits can be detected by ground and airborne hyperspectral remote sensing of

natural outcrops, despite the presence of abundant lichen cover. Given the similarity in alteration styles between VMS and orogenic gold deposits, the method has applicability to such deposits, and likely other styles of mineralization that have pronounced associated alteration zones.

Our study highlights the importance of careful selection of wavelengths for image analysis in environments where the spectral signatures are strongly influenced by spectral mixing between two or several elements. Two absorption feature wavelength positions (2194 nm and 2212 nm) were discarded from the airborne dataset due to the effects of spectral mixing of rocks and vegetation that could not be completely eliminated through spectral unmixing analysis.

Airborne surveying of prospective areas (e.g. greenstone belts) may provide a relatively low cost, "green" (i.e. no ground disturbance) mineral exploration method that can be utilized in conjunction with other traditional methods. Optical remote sensing methods are likely to be increasingly used in exploration in Canada's sparsely vegetated north given the impending availability of (albeit lower spatial resolution) commercial satellite and microsatellite hyperspectral sensors that are soon to be launched by several countries (see e.g. Staenz et al., 2013). The hyperspectral detection of hydrothermal alteration zones in remote, high-latitude regions of Canada (and elsewhere) that typically lack infrastructure may provide a facile and cost-effective exploration method to augment traditional geological, geochemical, and geophysical methods. Our study lends support for the development of future airborne and spaceborne hyperspectral sensors of higher spectral resolutions that would allow for better spectral unmixing and separation of cellulose and non-photosynthetic vegetation materials from white mica and chlorite group minerals. Unmanned Aerial Vehicles (UAVs) may also be a platform that can provide valuable high spatial resolution hyperspectral data at the regional scale.

ACKNOWLEDGMENTS

Funding came from the Research Affiliate Program and a grant from the Targeted Geoscience Initiative 4 (TGI-4) Program of the Earth Sciences Sector, Natural Resources Canada. The hyperspectral airborne data were acquired under the Strategic Investment in Northern Economic Development (SINED) Program of Indian and Northern Affairs Canada (now Aboriginal and Northern Affairs Canada), and we gratefully acknowledge the contributions of Donald James in facilitating the survey. We thank MMG Ltd., particularly Kimberley Bailey, Trish Toole, Ian Neill, and Dave Kelley, for logistical and field support in 2010 and 2013, and for geological discussions and access to company data. A review by Jeanne Percival (Geological Survey of Canada) helped to clarify the text.

REFERENCES

Barrett, T.J. and MacLean, W.H., 1994. Mass changes in hydrothermal alteration zones associated with VMS deposits of the Noranda area; Exploration and Mining Geology, v. 3, p. 131–160.

Bishop, J.L., Lane, M.D., Dyar, M.D., and Brown, A.J., 2008. Reflectance and emission spectroscopy study of four groups of phyllosilicates: smectites, kaolinite-serpentines, chlorites and micas; Clay Minerals, v. 43, p. 35–54.

Duke, E.F., 1994. Near infrared spectra of muscovite, Tschermak substitution, and metamorphic reaction progress: Implications for remote sensing; Geology, v. 22, p. 621–624.

Gibson, H.L., Allen, R.L., Riverin, G. and Lane, T.E., 2007. The VMS model: Advances and application to exploration geology, *In:* Proceedings of Exploration 07, (ed.) B. Milkereit; Fifth Decennial International Conference on Mineral Exploration, Toronto, September 9-12, 2007, p. 713–730.

Gitelson, A. and Merzlyak, M.N., 1994. Spectral reflectance changes associated with autumn senescence of *Aesculus hippocastanum* L. and *Acer platanoides* L. leaves. Spectral features and relation to chlorophyll estimation; Journal of Plant Physiology, v. 143, p. 286–292.

Ishikawa, Y., Sawaguchi, T., Iwaya, S.-I. and Horiuchi, M., 1976. Delineation of prospecting targets for Kuroko deposits based on modes of volcanism of underlying dacite and alteration haloe; Mining Geology, v. 26, p. 105–117.

Kranidiotis, P. and MacLean, W., 1987. Systematics of chlorite alteration at the Phelps Dodge massive sulfide deposit, Matagami, Quebec; Economic Geology, v. 82, p. 1898–1911.

Laakso, K., Rivard, B., Peter, J., White, H., Maloley, M., Harris, J. and Rogge, D., in press. Application of airborne, laboratory and field hyperspectral methods to mineral exploration in the Canadian Arctic: recognition and characterization of volcanogenic massive sulfide-associated hydrothermal alteration in the Izok Lake deposit area, Nunavut, Canada; Economic Geology.

Laidler, G.J., Treitz, P.M., and Atkinson, D.M., 2008. Remote sensing of Arctic vegetation: Relations between the NDVI, spatial resolution and vegetation cover on Boothia Peninsula, Nunavut; Arctic, v. 61, p. 1–13.

Large, R.R., Gemmell, J.B., Paulick, H., and Huston, D.L., 2001. The alteration box plot: A simple approach to understanding the relationship between alteration mineralogy and lithogeochemistry associated with volcanic-hosted massive sulfide deposits; Economic Geology, v. 96, p. 957–971.

MacLean, W. and Hoy, L.D. 1991. Geochemistry of hydrothermally altered rocks at the Horne Mine, Noranda, Quebec; Economic Geology, v. 86, p. 506–528.

McLeod, R.L., Gabell, A.R., Green, A.A., and Gardavsky, V., 1987. Chlorite infrared spectral data as proximity indicators of volcanogenic massive sulphide mineralisation, *In:* Proceedings; Pacific Rim Congress '87, Gold Coast, Australia, August 26-29, 1987, p. 321–324.

Morrison, I.R., 2004. Geology of the Izok massive sulfide deposit, Nunavut Territory, Canada; Exploration and Mining Geology, v. 13, p. 25–36.

Richter, R. and Schläpfer, D., 2002. Geo-atmospheric processing of airborne imaging spectrometry data. Part 2: Atmospheric/topographic correction; International Journal of Remote Sensing, v. 23, p. 2631–2649.

Rogge, D.M., Rivard, B., Zhang, J., Sanchez, A., Harris, J., and Feng, J., 2007. Integration of spatial-spectral information for the improved extraction of endmembers; Remote Sensing of Environment, v. 110, p. 287–303.

Staenz, K., Mueller, A., and Heiden, U., 2013. Overview of terrestrial imaging spectroscopy mission, In: Transactions of 2013 IEEE International; Geoscience and Remote Sensing Symposium (IGARSS), Melbourne, Australia, July 21-26, 2013, p. 3502–3505.

Yang, K., Huntington, J.F., Gemmell, J.B., and Scott, K.M., 2011. Variations in composition and abundance of white mica in the hydrothermal alteration system at Hellyer, Tasmania, as revealed by infrared reflectance spectroscopy; Journal of Geochemical Exploration, v. 108, p. 143–156.

GEOLOGICAL SURVEY OF CANADA
OPEN FILE 7853

Targeted Geoscience Initiative 4: Contributions to the Understanding of Volcanogenic Massive Sulphide Deposit Genesis and Exploration Methods Development

Oxygen isotope zonation about the Izok Ag-VMS deposit, Slave Province, Nunavut: hanging-wall vector to mineralization

Bruce E. Taylor[1], Jan M. Peter[1], Kati Laakso[2,3], and Benoit Rivard[2]

[1]Geological Survey of Canada, Ottawa, Ontario
[2]University of Alberta, Edmonton, Alberta
[3]Spectral Imaging Ltd., Oulu, Finland

2015

This publication is available for free download through GEOSCAN (http://geoscan.nrcan.gc.ca/)

Recommended citation

Taylor, B.E., Peter, J.M., Laakso, K., and Rivard, B., 2015. Oxygen isotope zonation about the Izok Ag-VMS deposit, Slave Province, Nunavut: hanging-wall vector to mineralization, *In:* Targeted Geoscience Initiative 4: Contributions to the Understanding of Volcanogenic Massive Sulphide Deposit Genesis and Exploration Methods Development, (ed.) J.M. Peter and P. Mercier-Langevin; Geological Survey of Canada, Open File 7853, p. 27–44.

Publications in this series have not been edited; they are released as submitted by the author.

Contribution to the Geological Survey of Canada's Targeted Geoscience Initiative 4 (TGI-4) Program (2010–2015)

TABLE OF CONTENTS

Oxygen isotope zonation about the Izok Ag-VMS deposit, Slave Province, Nunavut: hanging-wall vector to mineralization

Bruce E. Taylor[1]*, J.M. Peter[1], Kati Laakso[2,3], and Benoit Rivard[2]

[1]Central Canada Division, Geological Survey of Canada, 601 Booth Street, Ottawa, Ontario K1A 0E8
[2]Centre for Earth Observation Sciences at the University of Alberta, Department of Earth and Atmospheric Sciences, University of Alberta, 1-26 Earth Sciences Building, University of Alberta, Edmonton, Alberta T6G 2E3
[3]SPECIM, Spectral Imaging Ltd., Teknologiantie 18 A FI-90590 Oulu, Finland
*Corresponding author's e-mail: btaylor@nrcan-rncan.gc.ca

ABSTRACT

Oxygen isotope compositions were determined for 99 whole-rock samples of felsic host rocks collected in the vicinity of the Izok volcanogenic massive sulphide deposit. The results reveal a distinct pattern of oxygen isotope zonation spatially centred over the massive sulphide lenses produced by water/rock reaction in a hydrothermal system. The zonation indicates that this paleo-hydrothermal system is relatively 'up right', centered over the massive sulphide lenses. Analyzed samples are primarily from the hanging wall, and have $\delta^{18}O_{V\text{-}SMOW}$ values as high as 14.7‰. In contrast to isotopic studies describing ^{18}O-depleted footwall and upflow zones, the ^{18}O-enriched zoning pattern in the Izok Lake area illustrates a clear hanging-wall "vector" to the buried sulphide lenses. This isotopic 'fingerprint' of an Archean hydrothermal system has been retained in the rocks, despite subsequent amphibolite facies metamorphism. The isotopic zonation broadly corresponds to an isopleth indicating loss of Na_2O from the rocks, and, to some extent, with a mapped distribution of the Ishikawa alteration index and short-wave infrared spectral mapping of white-mica and biotite+chlorite-related absorption features. However, the pattern of oxygen isotope zonation provides a more focused 'target'.

INTRODUCTION

Submarine, magmatic-centred hydrothermal systems profoundly alter the isotopic, mineralogical, and chemical compositions of host igneous and sedimentary rocks. Subsequent metamorphism and deformation can modify the chemical and physical properties of the altered rocks further. Oxygen isotope techniques can be used to map the morphology of volcanogenic massive sulphide (VMS)-associated submarine hydrothermal systems and provide a robust, quantitative parameter with which to determine the paleo-architecture of the hydrothermal system, including flow paths and thermal gradients. Isotopic mapping of these features offers a 'fingerprint' that can be used as an exploration 'vector'. As established in other studies of VMS systems, oxygen isotope alteration and zoning survives metamorphic recrystallization and deformation, although the morphologies of the oxygen isotope zones may reflect associated strain (e.g. Sturgeon Lake: Holk et al., 2008; Snow Lake: Taylor and Timbal, 1998a; Bailes et al., in press). Herein we summarize the results of an oxygen isotope study of the Izok Lake paleo-hydrothermal system, host to a large, undeveloped Zn-Cu VMS deposit. The study reveals a zone of significant oxygen isotope enrichment in hanging-wall rocks that can serve as vector to the buried Zn-Cu-Pb-Ag volcanogenic massive sulphide ore bodies. Furthermore, the data provide a framework for comparison to other chemical, mineralogical and spectral rock properties of the hydrothermal alteration zones at Izok Lake that collectively can be used to construct more comprehensive exploration methods.

LOCATION AND GEOLOGICAL SETTING

The Izok deposit is located in southwestern Nunavut, and is hosted primarily by metamorphosed rhyolitic rocks Archean age and, to a lesser extent, by intermediate to mafic metavolcanic and metasedimentary rocks of the Point Lake greenstone belt within the Slave Craton (also referred to herein as the Slave Province; Fig. 1). Mortensen et al. (1988) determined an Archean U/Pb zircon age of 2623 Ma for rhyolite in the Izok Lake area. Bailey and Stubley (2013a,b) divided the assemblage of rhyolitic rocks into 7 units on the basis of lithogeochemistry, noting that the rocks largely represent reworked and re-sedimented volcanic and volcaniclastic detritus. The stratigraphically lowest rhyolitic unit (R1), hosts the Izok deposit.

Taylor, B.E., Peter, J.M., Laakso, K., and Rivard, B., 2015. Oxygen isotope zonation about the Izok Ag-VMS deposit, Slave Province, Nunavut: hanging-wall vector to mineralization, *In:* Targeted Geoscience Initiative 4: Contributions to the Understanding of Volcanogenic Massive Sulphide Deposit Genesis and Exploration Methods Development, (ed.) J.M. Peter and P. Mercier-Langevin; Geological Survey of Canada, Open File 7853, p. 27–44.

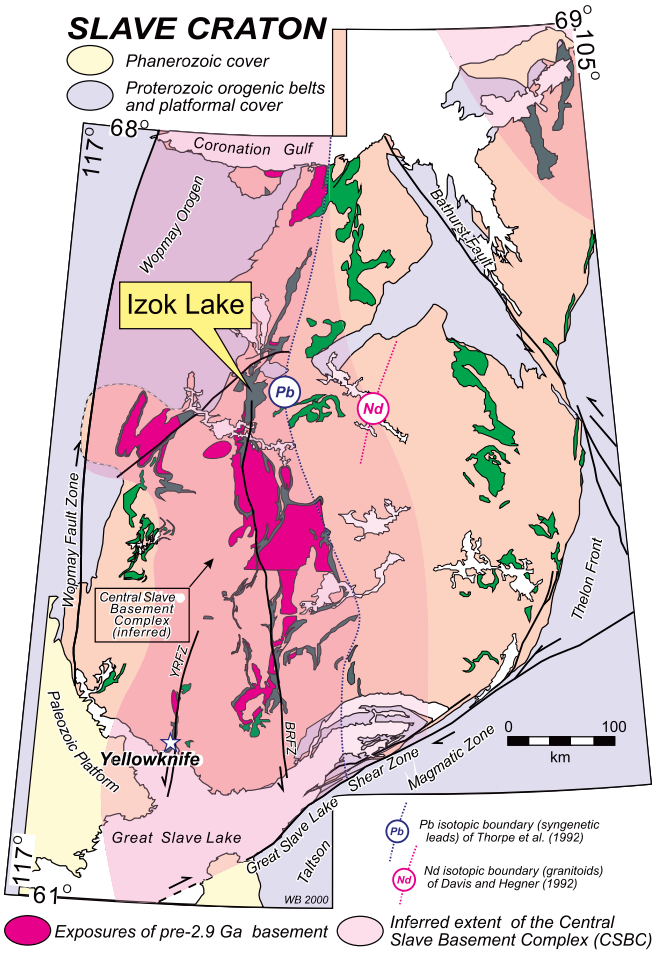

Figure 1. Geological map of the Slave craton (province; modified after Bleeker and Hall, 2007) showing the location of the Izok Zn-Cu-Pb-Ag VMS deposit (65°37.5'N; 112°48.0'W), in the Kitikmeot region of Nunavut. The deposit represents a resource of 15 Mt grading 13% Zn, 2.3% Cu, 1.4% Pb, and 73 g/t Ag (MMG, Inc., Annual Report 2013).

Massive sulphides were discovered at Izok Lake in 1974 by Texasgulf, Inc., intercepting massive sulphide in the first drill hole (Morrison, 2004). The name 'Izok' was derived from "Is OK" reference used by early explorationists (Morrsion, 2004). The deposit consists of five sulphide lenses comprising a current resource of 15 Mt grading 13% Zn, 2.3% Cu, 1.4% Pb, and 73 g/t Ag (MMG Inc., Annual Report 2013).

The simplified geological map of the Izok Lake Area, shown in Figure 2, illustrates the dominance of rhyolitic flows and volcaniclastic rocks. Four generations of folds have been interpreted of the area as the result of a complex deformational history (Stubley and Bailey, 2013); only the last two generations, F_3 and F_4, are represented in Figure 2. The F_3 antiform aligned with the massive sulphide lenses is subparallel to many, smaller F_2 folds. The axial planes of these folds are generally upright, to slightly northwest-tilted. The axis of a broad, arching fold at a high angle to the general trends of the F_2-F_3 folds represents the last episode of folding (Stubley and Bailey, 2013); the domical apex formed by the intersection the F_3 and F_4 folds is located in the vicinity of the massive sulphide lenses. Consequently, the F_3 fold axis is shown as doubly-plunging, although fold axes in the area are generally sub-horizontal to shallow dipping (Bailey and Stubley, person. comm.). A region of sillimanite- and garnet-bearing rocks (amphibolite-grade metamorphic equivalents of hydrothermally altered rocks) southwest of the sulphide lenses appears to be situated along the axis of the F_3 antiform (Fig. 2).

Only rhyolitic rocks throughout the area were analyzed for their oxygen isotope compositions in order to provide a sensitive means of mapping the VMS-related paleo-hydrothermal system. A typical outcrop exposure is shown in Figure 3a, which illustrates a well-developed, penetrative schistosity in hydrothermally altered rocks. Outcrops are typically densely covered with lichen. Figure 3b shows volcaniclastic textures in an outcrop that was power-washed to remove the lichen. Photographs in Figure 3c and 3d illustrate the porphyroblastic textures of garnet- and sillimanite-bearing mineral assemblages characteristic of metamorphosed hydrothermally altered rocks.

SAMPLE SELECTION AND METHODOLOGY

A total of 99 samples, consisting of 85 representative hand samples or chip collections from surface outcrops and 14 samples collected from selected drill core, were analyzed for their oxygen isotope compositions in this study. Surface samples were collected throughout much of the Izok Lake area, within 8 km of the VMS lenses (Fig. 2); however, samples from drill core were only collected in the immediate vicinity of the VMS lenses.

Analysis of aliquots of 5–15 mg of dried rock powder were carried out by standard fluorination methods employing ClF_3 (Borthwick and Harmon, 1982; Taylor, 2004). Oxygen isotope compositions are reported in the usual δ-notation, relative to V-SMOW (Vienna Standard Mean Ocean Water), and considered accurate to better than 0.2 per mil (‰, 1σ). Analyses were performed at the University of Western Ontario, London. Consistency among the data was monitored by analysis of common internal working standards, international reference materials, and blind duplicates.

The oxygen isotope data acquired in the present study were compared to spectral measurements from Laakso et al. (2015) made on the same samples or outcrops. Spectra were acquired in the field with a hand-held ASD FieldSpec® Pro 3 spectrometer (hereafter referred to as "ASD"). The ASD records spectra in the 350–2500 nanometres (nm) wavelength range with a spectral resolution of 10 nm in the short-wave infrared

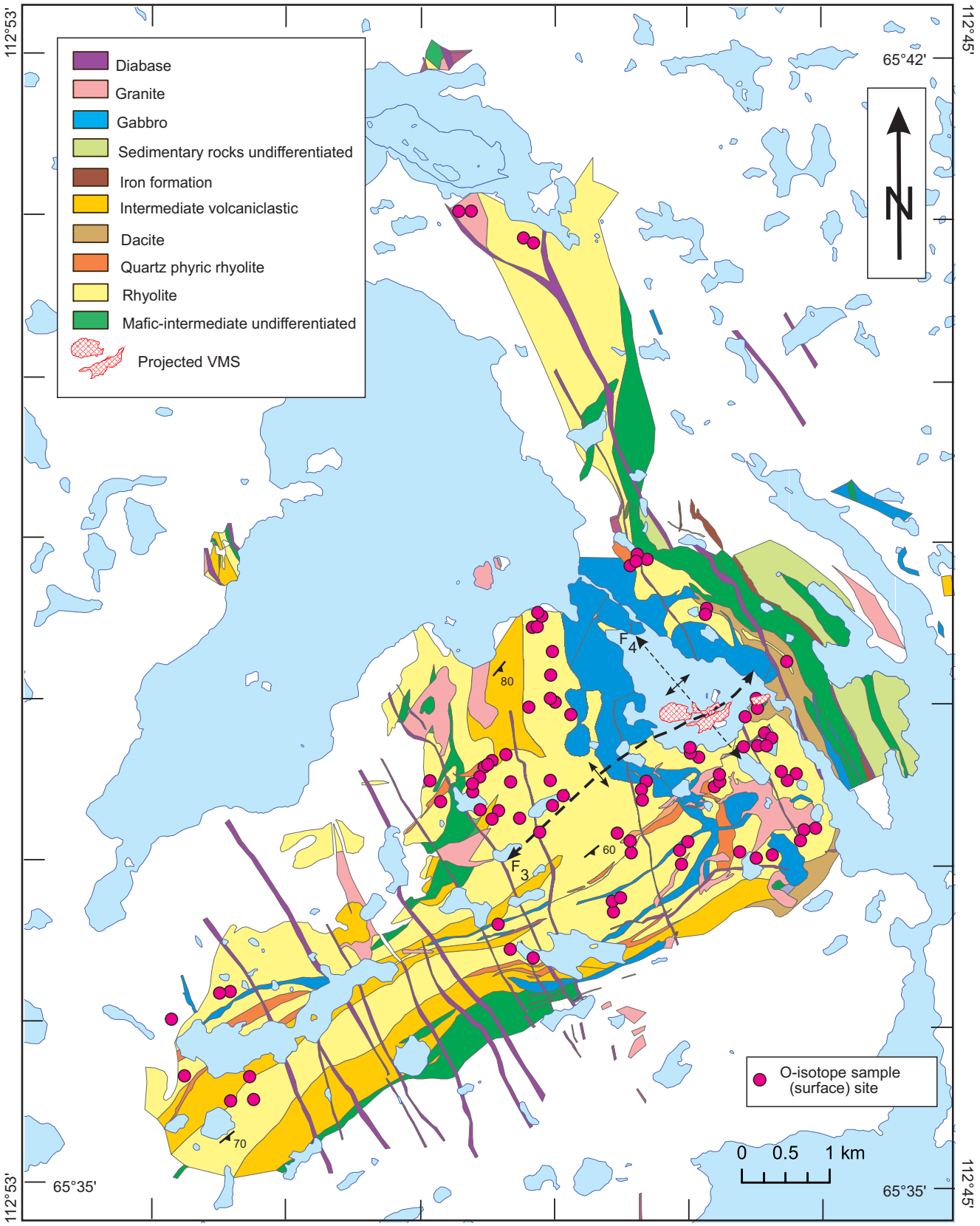

Figure 2. Simplified regional geological map of the Izok Lake area, Nunuavut (based on Stubley and Bailey, 2013, after Inmet, unpub.; Minerals and Metals Group, Ltd.), showing the locations of 99 surface-collected whole-rock samples from the hanging wall to the deposit, which were analysed in this study for their oxygen isotope compositions. An additional 14 samples were analyzed from drill core (see Fig. 9). The buried VMS bodies comprising the Izok deposits are represented by projection (Minerals and Metals Group, Ltd., unpub.). See text for discussion of F_3 and F_4 folds.

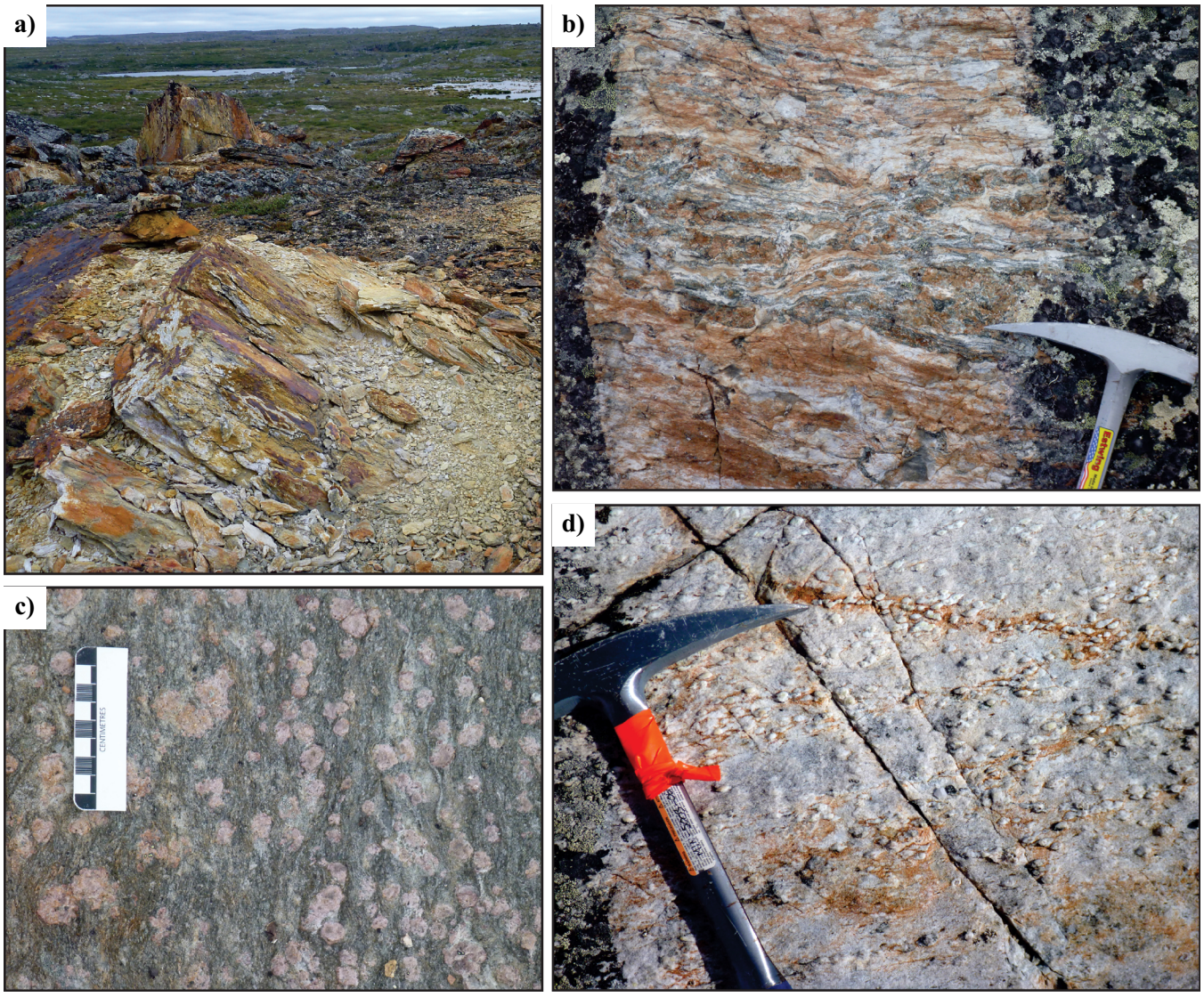

Figure 3. Outcrop photographs of rhyolitic rocks in the Izok Lake area. **a)** Rust-stained, sericite-altered, rhyolitic volcaniclastic rocks in outcrop with schistose parting. **b)** Power-washed exposure of foliated rhyolitic volcaniclastic rock with siliceous clasts in chlorite-bearing matrix. **c)** Garnet porphyroblasts decorate this power-washed exposure of foliated, chlorite-bearing rhyolite. **d)** Clots of sillimanite in muscovite-rich meta-rhyolite (some muscovite of retrograde origin envelopes sillimanite) attest to a high metamorphic grade.

wavelength region. The spectra were acquired with a fore optic contact probe. Radiance values were converted to reflectance values by means of a Spectralon™ (Labsphere, New Hampshire, U.S.A.) 99% panel. The geographic locations of the field sites were recorded with a handheld GPS.

RESULTS

The geographic distribution of isotopic compositions of the 85 analysed surface samples, grouped in 2‰ fashion, is shown in Figure 4. The $\delta^{18}O$ values of the surface samples vary from 5.8 to 14.7‰; only three samples have $\delta^{18}O$ values of <6‰ (Figs. 4, 5). As indicated in Figure 4, rocks having the lowest $\delta^{18}O$ values (<6‰, but only by a few tenths per mil; 5.8‰) are among the most distal from the VMS lenses, and represent fresh rhyolite. Typically, mantle-derived fresh, unaltered rhyolite has oxygen isotope compositions of ~6–7.5‰ (e.g. Taylor, 1968). Rhyolite that has values of $\delta^{18}O > 9$‰ (light- and dark-blue coded, and many of the green-coded samples in Fig. 4) are isotopically enriched relative to fresh, unaltered rhyolite as a result of hydrothermal alteration. The histogram shown in Figure 5 for surface samples and drill-core samples illustrates that the majority of samples analysed have $\delta^{18}O$ values > 9‰; indeed, the mean value of $\delta^{18}O$ is 10.16‰. Fourteen drill-core samples within the vicinity of Izok VMS lenses have a somewhat restricted range of $\delta^{18}O$ from 8.9 to 12.4‰, centred about the mean value for all samples. The significance of this distribution is discussed later.

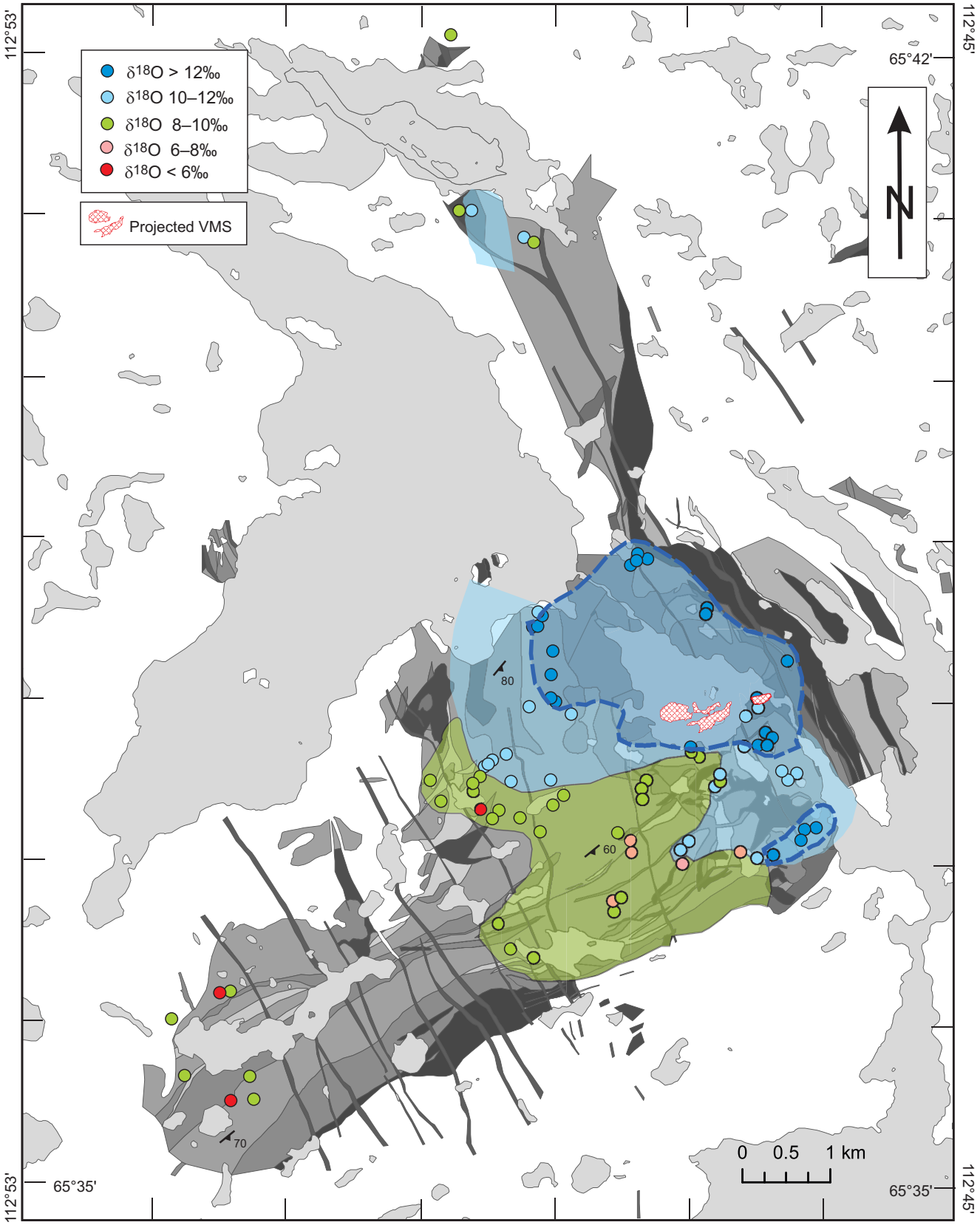

Figure 4. Geological map of Izok Lake area, showing site locations of analyzed rhyolite samples, colour-coded using 2‰ brackets to represent isotopic variation. See Figure 2 for a coloured version of the geological map. Note the increase in whole-rock $\delta^{18}O$ values as the VMS lenses (surface projections: MMG, Inc.) are approached.

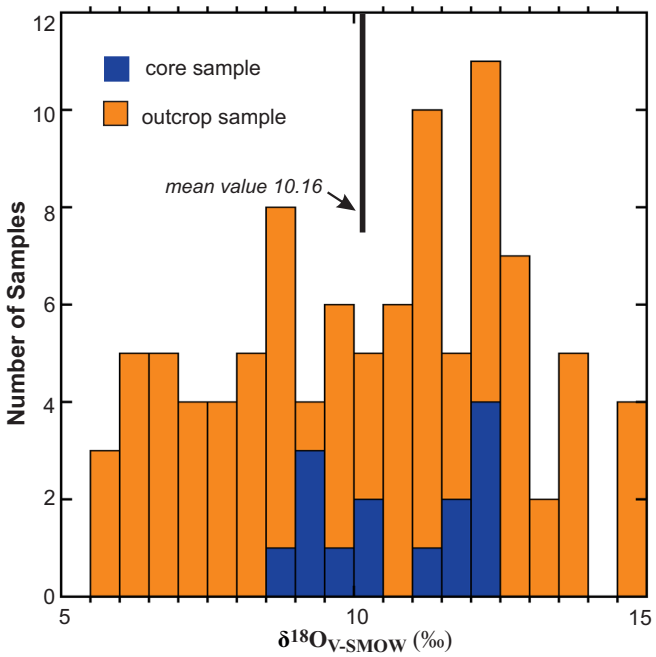

Figure 5. Histogram of whole-rock oxygen isotope compositions for rhyolite samples collected from surface outcrops (n=85) in the Izok Lake area and from drill core (n=14;) in the vicinity of the Izok massive sulphide lenses. The distribution represents a range of $\delta^{18}O$ = 5.8 to 14.7‰. Fresh rhyolite (and, permissibly, those slightly altered by seawater at moderate temperatures) typically has $\delta^{18}O$ values of ~6-7‰, whereas, rocks with heavier isotopic compositions, especially ≥ 9‰, have been hydrothermally altered at low to moderate temperatures (see text).

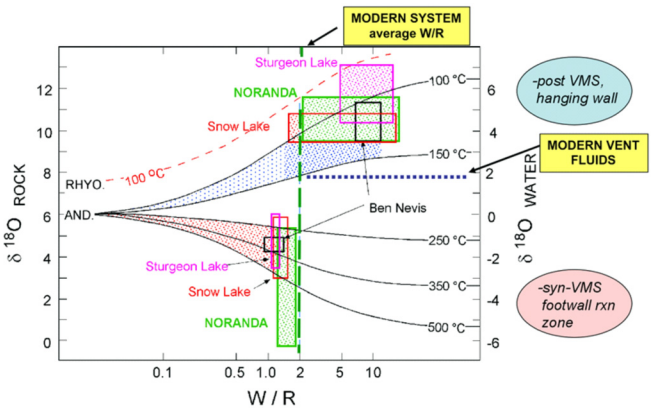

Figure 6. Plot of whole-rock oxygen isotope alteration (variation of $\delta^{18}O_{ROCK}$; RHYO.= rhyolite, AND.= andesite) and seawater hydrothermal fluid ($\delta^{18}O_{WATER}$) as a function of integrated water/rock ratio (W/R) during hydrothermal alteration. Rock alteration begins at the left side of the diagram, with the $\delta^{18}O_{ROCK}$ and $\delta^{18}O_{WATER}$ changing along the pathways shown as hydrothermal alteration occurs. At high temperatures, $\delta^{18}O_{ROCK}$ decreases, recording a measurable alteration signature in the footwall. Low-temperature alteration may be recorded in the hanging wall if the rocks are deposited before cessation of hydrothermal activity. Fields for whole-rock isotopic compositions (both high and low temperature) from several studied examples (see Holk et al., 2008; Taylor et al., 2009) and selected reference points from modern systems are shown.

DISCUSSION

Water-Rock Interaction

The effects of oxygen isotope exchange between hydrothermal fluids and volcanic and sedimentary rocks in seawater-dominated hydrothermal systems have been documented systematically over the last several decades. A brief review here of the systematics and several examples provides background essential to a discussion of the Izok Lake VMS hydrothermal system.

The progressive oxygen isotope exchange between seawater ($\delta^{18}O$ = 0‰) and fresh volcanic rocks (e.g. rhyolite and andesite; $\delta^{18}O \approx 6$ and 7.5‰, respectively; Taylor, 1968) is depicted in Figure 6 as a function of the integrated water/rock ratio (W/R). In this diagram the isotopic compositions of rhyolite and andesite are shown on the left ordinate, and seawater on the right ordinate. The change in composition of each (rocks and water) then varies as a function of temperature and cumulative isotopic exchange accompanying chemical and mineralogical changes to the rock during hydrothermal alteration. The oxygen isotope composition of unaltered rhyolite and andesite may vary slightly (generally 1–2‰) from that shown here as a function of source materials and tectonic setting (e.g. Sheppard and Taylor, 1986; Taylor, 1986). It is the mineralogical alteration of the rocks (particularly, glassy components) that promotes significant oxygen isotope exchange. The oxygen isotope composition of the whole-rock, determined by the mineralogical mode and the individual mineral-water oxygen isotope fractionation factors, is strongly influenced by the abundance of dominant alteration minerals such as chlorite or muscovite. Note that at low to moderate values of W/R, the whole-rock oxygen isotope composition remains within the general range of fresh, isotopically 'unaltered' rocks because feldspar-water fractionation factors (which can play a significant role in this scenario) are relatively small in the 200–250°C range. Several reference points are shown in Figure 6, including an average oxygen isotope composition of ≈ 2‰ for modern vent fluids (e.g. Shanks, 2001). Vent fluids have positive values of $\delta^{18}O$ because of water/rock interaction along the flow paths in the hydrothermal systems. Figure 6 can be used to estimate W/R ratios from comparison of the oxygen isotope compositions of fresh and altered rocks.

The results of comprehensive oxygen isotope studies of a number of felsic magmatic-centred mineralized and non-mineralized sea floor hydrothermal systems, plotted as fields for both high- and low-temperature zones (i.e. <6 and >9‰), are compared in Figure 6. In general terms, the size and distribution of the plotted zones illustrates the size and complexity of the individual hydrothermal systems and, with the exception of

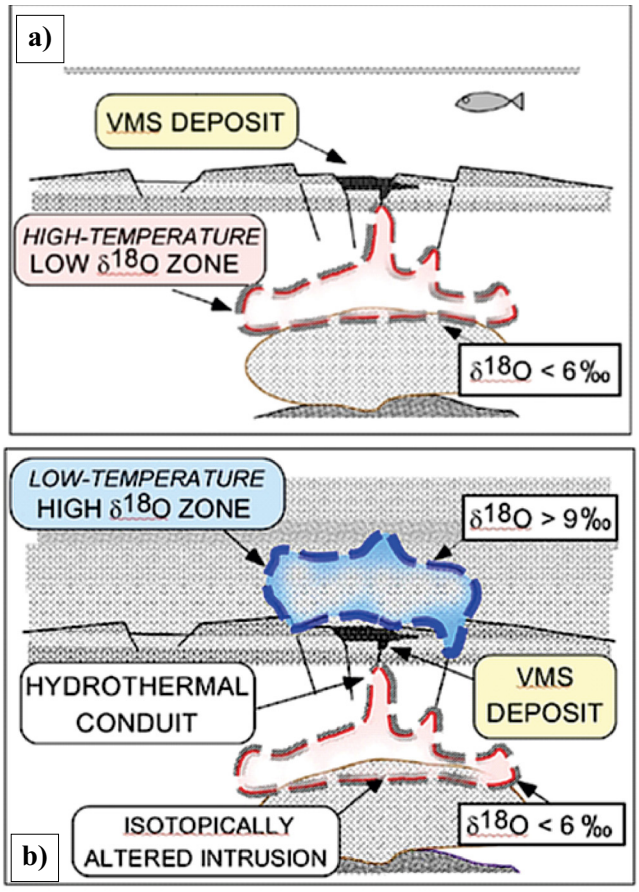

Figure 7. a) Schematic cross-section of the formation of a high-temperature reaction zone associated with a subvolcanic intrusion, characterized by a low $\delta^{18}O$ zone in a marine hydrothermal system (Taylor et al., 2009). Most unaltered volcanic rocks have $\delta^{18}O$ values of 6-9‰; high-temperature alteration is indicated by $\delta^{18}O$ < 6‰. Distribution of the high-temperature alteration zone records hydrothermal fluid flow. The zone may collapse on high-temperature heat source (e.g. synvolcanic pluton, locally crystallized and fractured), which may be up to 1–2 km beneath the seafloor (e.g. Galley et al., 2007). Synvolcanic faults that acted as hydrothermal conduits ("feeder zones") may be identified by lowered values of $\delta^{18}O$. **b)** Schematic cross-section of the formation of a low-temperature, high-$\delta^{18}O$ zone in a marine hydrothermal system. Lower temperature alteration is typically indicated by $\delta^{18}O_{WR}$ > 9‰. Note that volcanism and/or sedimentation must continue during the waning of the hydrothermal system to record lower-temperature alteration. A high-$\delta^{18}O$ "cap" may develop in the hanging wall, above the upflow zone in the footwall, providing a hanging-wall "vector" to guide exploration. Examples of high-$\delta^{18}O$ hanging-wall indicators of buried VMS may be found at Sturgeon Lake, Ontario (Holk et al., 2008), Flin Flon, Manitoba. (Ames et al., in press), and Snow Lake, Manitoba. (Taylor and Timbal, 1998b; Bailes et al., in press).

Noranda, represent single episode systems. High-temperature alteration is designated as a syn-VMS reaction zone in Figure 6 because it develops at depth as the VMS deposit(s) form at or near the sea floor in rocks that are, except along narrow fluid pathways, not significantly isotopically altered (Taylor and Holk, 1998). Low-temperature alteration zones are designated as 'post-VMS, hanging wall' and correspond to the hanging-wall zone depicted in Figure 7. In the case of Noranda, the extended, ^{18}O-depleted field represents the combined effects of at least four, superposed episodes of magmatism and hydrothermal activity (Taylor et al., 2009). Consequently, the temperature implied by Figure 6 for water/rock interaction well above 500°C is apparent only.

The Ben Nevis complex in the Noranda camp, shown in Figure 6, has small zones of associated high- and low-temperature alteration. It is an upright pluton, ca. 10 my younger than the Flavrian intrusive complex (Piercey et al., 2008). The orientation of the Ben Nevis paleo-hydrothermal system precluded study of the hanging wall and of any possible effects of volcanogenic mineralization (Taylor and Timbal, 1998a). Still, a small hydrothermal system driven by the heat of the cooling Ben Nevis pluton, produced similar, if restricted, isotopic alteration zones to the larger complexes represented.

Long-lived submarine hydrothermal systems centred on subvolcanic VMS-producing intrusive centres that fuelled long-lived hydrothermal systems can produce a high-$\delta^{18}O$ alteration zone in rocks deposited after most or all of the near surface VMS mineralization has been deposited (see Fig. 7b). This post-VMS hanging-wall feature, is characterized by a range of $\delta^{18}O$ values that, as shown, can be on the order of 9.0 to 13‰. Isotopic alteration at Sturgeon Lake (Holk et al., 2008) provides a particularly useful example of such a post-VMS, high-$\delta^{18}O$ zone in the hanging wall, with $\delta^{18}O$ values of up to 13‰. Continual, shallowing growth and eventual emergence of the volcanic edifice at Sturgeon Lake played an important role in the lower temperature ^{18}O enrichment of the hanging-wall volcanic rocks (Holk et al., 2008).

Oxygen Isotope Zonation in Marine Hydrothermal Systems

Much of the discussion in previously published oxygen isotope studies of VMS hydrothermal systems focussed on the high-temperature, ^{18}O-depleted reaction zones and hydrothermal pathways in the footwalls to deposits (e.g. Larson, 1984; Taylor and South, 1985; Cathles, 1993; Taylor et al., 2009, 2014). Although this is an important isotopic aspect of submarine hydrothermal alteration, it is the lower-temperature alteration systematics and resulting isotopic zoning patterns that are of particular interest in the Izok Lake area. Examples of previously documented high-^{18}O hanging-wall enrichment associated with VMS deposits include: Kuroko deposits, Hokuroku District, Japan (Green et al., 1983), Sturgeon Lake, Ontario (Holk et al, 2008), and LaRonde Penna, Noranda, Quebec (Beaudoin et al.,

2014). The mapping of the distribution of both the high-temperature, ^{18}O-depleted, and low-temperature, ^{18}O-enriched alteration zones can be used in exploration vectoring.

The schematic evolution of oxygen isotope zonation in a simple (i.e. one intrusion/intrusive episode) felsic magmatic-centred submarine hydrothermal system is shown in cross-section in Figure 7. This figure illustrates the spatial relationship of zones of oxygen isotope enrichment to the zone of massive sulphide formation observed in the Izok Lake area. The high-temperature zone of oxygen isotope depletion shown schematically in Figure 7a, as mapped in other paleo-hydrothermal systems, represents the cumulative high-temperature alteration during the life of the hydrothermal system. As such, as the system waxes and wanes, the boundaries can move, up and down, respectively; it may also 'collapse', moving downward, upon the intrusion that provides the thermal drive for hydrothermal circulation as the intrusion crystallizes and fractures at temperatures of ~350°C. In multi-stage, sub-volcanic intrusive complexes, magmatic pulses may invade previously hydrothermally altered portions of the hydrothermal system, stoping and disrupting altered rock.

Hydrothermal circulation will proceed as long as sufficient heat remains to provide the buoyancy to the fluids. In an area of active volcanism, continued volcanism and sedimentation may bury the VMS deposit shortly after (or during) its formation. Lower temperature hydrothermal alteration and, in particular, oxygen isotope alteration may accompany the protracted cooling of the heat source, leaving an imprint on the hanging-wall rocks of higher $\delta^{18}O$ values in areas above fluid upflow zones. As shown in Figure 7b, lower temperature alteration may also affect some rocks in the foot wall. The high-$\delta^{18}O$ zone, or 'cap' above the upflow zone, can provide a vector in the hanging-wall rocks to buried VMS.

The oxygen isotope zonation described above can be employed as an effective tool with which to map the architecture and orientation of a paleo-submarine hydrothermal system. The pattern of mapped oxygen isotope zones indicates the polarity of the system with respect to thermal gradients and fluid flow. The alteration patterns and the location of the VMS depositional zone shown schematically above are sufficiently reliable that the general architecture of paleo-hydrothermal systems may be understood even in the absence of a complete system in the area of interest, providing 'vectors' for exploration.

Oxygen Isotope Zonation at Izok Lake

Sampling and analysis of only rocks of rhyolitic composition in the Izok Lake area permitted use of a finer grouping (2‰) of oxygen isotope composition than the <6 and >9‰ divisions typically used for map contouring purposes (Fig. 8). This approach allowed comparison of the isotopic changes throughout the area of an (originally) isotopically similar rock. Isotopic differences due primarily to different rock compositions (e.g. basalt, andesite, etc.) were thereby eliminated. Consequently, an improved definition of the zone boundaries of oxygen isotope alteration resulted. Figure 9 displays the pattern of oxygen isotope alteration zones in the immediate vicinity of the Izok deposit based on analyses of drill core samples that encompass the projected extent of the buried sulphide lenses. The positions of the zone boundaries in both Figures 8 and 9 are necessarily strongly influenced by the distribution of available analyses; the locations of zone boundaries northeast of Izok Lake are uncertain. The boundaries are also influenced by the inferred folding along northeast-southwest axes, yet the pattern of zoning indicates a moderately upright, only slightly tilted to the northwest, top-down (i.e. plan) view of the paleo-hydrothermal system. We interpret the high-$\delta^{18}O$ zone that encompasses the vertical projections of VMS lenses beneath Izok Lake in Figure 8 to be the low-temperature alteration 'cap' above the upflow zone responsible for the sulphide mineralization (see Fig. 7b). Comparison of the detailed oxygen isotope zonation map (Fig. 9) with that shown in Figure 8 (note the inset outline of Fig. 9) provides the basis for this interpretation.

South of the locations of the projected VMS lenses in Figure 8, there are five samples with oxygen isotope compositions in the 6–8‰ interval, indicating a relatively small zone of isotopically 'normal' rocks. A small zone encompassing these five samples was not drawn for simplicity, although it, like other zones, would have a shape reflecting the northeast-southwest folding.

The three samples with $\delta^{18}O$ values < 6‰ (actually 5.8‰; see Fig. 5) are among the furthest from the VMS lenses. Rather than indicating high-temperature alteration, these samples have an isotopic composition close to that consistent with unaltered rhyolite, or those altered at moderate temperatures (i.e. ~200–250°C; see Fig. 6). Similarly, those sites colour-coded green in Figure 8 represent samples in this "unaltered" group. Collectively, the broad dispersal of 6–8‰ samples contrasts with the more restricted, high-$\delta^{18}O$ zone encircling Izok Lake.

Applying the same $\delta^{18}O$ interval of 2‰ defined as above, isotopic zonation in the immediate vicinity of the buried VMS lenses at the southwestern end of Izok Lake is shown in Figure 9. Whereas, the regional oxygen isotope zonation map in Figure 8 emphasizes the high-$\delta^{18}O$ zone encompassing Izok Lake, the close spacing of drill core samples near and adjacent to VMS lenses permits the definition of a 'central' zone of

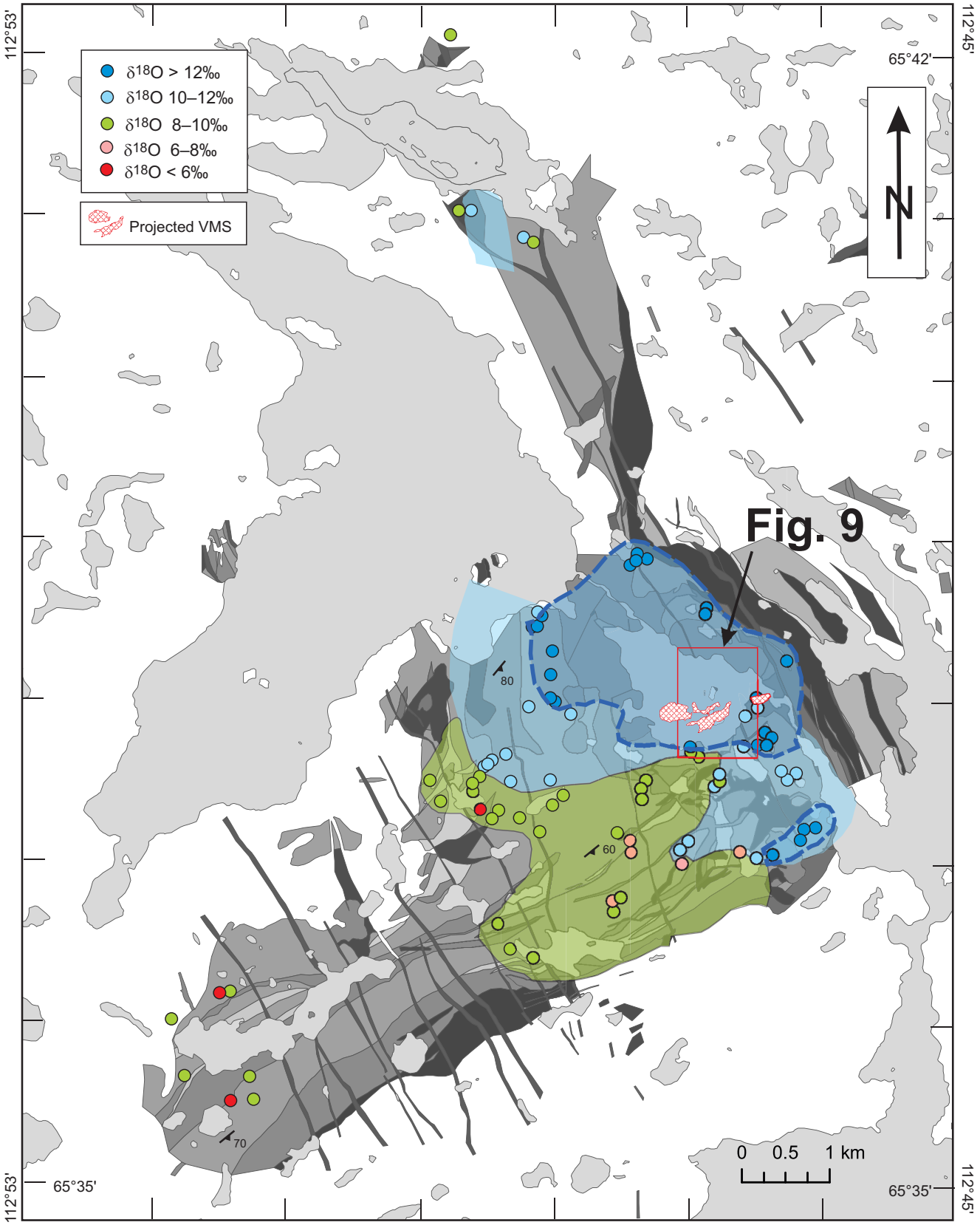

Figure 8. Map of oxygen isotope zonation in the hanging-wall rocks of the Izok Lake area, which encompasses the projections (Bailey and Stubley, 2013a,b) of buried VMS mineralization. The pattern of zoning shown in this figure characterizes a relatively upright hydrothermal system and is viewed from the "top" down (i.e. plan view). The high $\delta^{18}O$ (low-temperature) zone provides a hanging-wall target for exploration. A small area of isotopically "normal" rocks is indicated south of the projected VMS bodies; the corresponding zone boundaries are not shown for simplicity. Note the location of Figure 9.

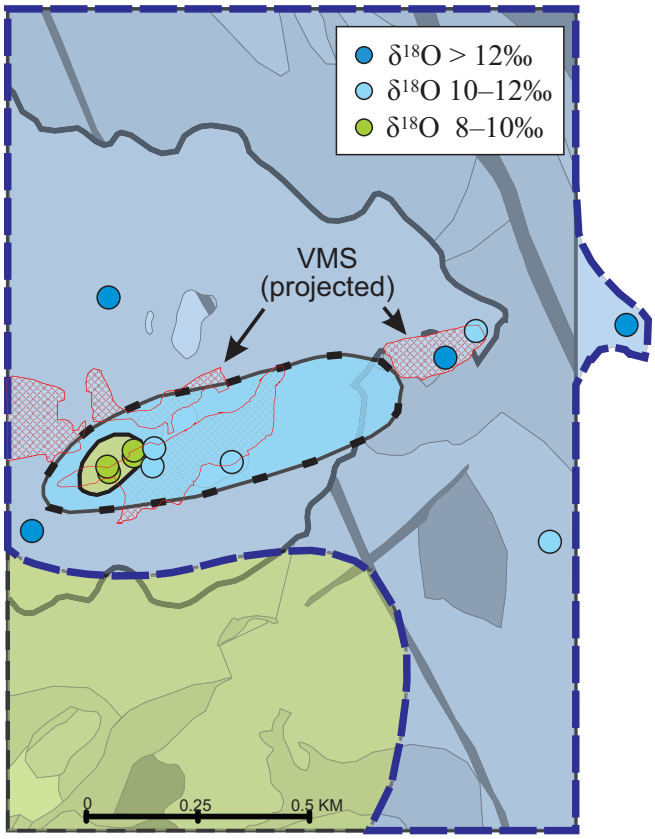

Figure 9. Oxygen isotope zonation in the vicinity of VMS bodies based on analyses of samples from drill core. The location of this area is indicated by an inset frame in Figure 8. A relative decrease in $\delta^{18}O_{WR}$ closely associated with the VMS, in an otherwise isotopically enriched zone, is likely located above a more deeply buried upflow zone. The drillholes shown were all less than 600 m in depth, limiting access to the footwall. In most cases, samples were collected within several hundred metres of mass sulphide.

relatively lower $\delta^{18}O$. The location of this 'central' zone suggests that it is situated above a footwall upflow zone. The locations of the projected outlines of the larger VMS lenses beneath Izok Lake coincide with the small zone of $\delta^{18}O$ = 8–10‰ shown in Figure 9.

Comparison with the Caldera-Hosted Sturgeon Lake VMS District

Oxygen isotope zonation of the Archean Sturgeon Lake caldera and VMS district in northwestern Ontario by Holk et al. (2008) is illustrated in Figure 10. Here, there are high-$\delta^{18}O$ zones in the hanging wall similar to those mapped at Izok Lake. The structural setting of the Sturgeon Lake caldera is such that the very steep, northward dips of the volcanic section provide a cross-section through the caldera.

A shallow, emergent volcanic complex above the Biedelman Bay intrusive complex, led to the development of an extensive, low-temperature, high-$\delta^{18}O$ alteration zone in the hanging wall above the Mattabi VMS deposit. Comparison of the isotopic composition and placement of the low-temperature oxygen isotope zonation at Sturgeon Lake and Izok Lake is instructive: Sturgeon Lake provides a cross-sectional view, whereas Izok Lake a top-down (plan) view of the high-$\delta^{18}O$, "capping" alteration zone. High-temperature, ^{18}O-depleted upflow zones are present beneath the level of the Mattabi VMS at Sturgeon Lake (Fig. 10). The top-down view of the paleo hydrothermal system at Izok Lake, and the limited deep drilling, limits the access to similar, low-$\delta^{18}O$ upflow zones which must lie deep beneath the Izok deposit. Morrison (2004) reports the occurrence of 'stringer zones' in the footwalls to several sulphide lenses.

An important feature of the Biedelman Bay intrusive complex is that the level of emplacement is very-late to post-hydrothermal. This is indicated by the lack of isotopic alteration of the intrusion at its upper contact, as evidenced by the presence of fresh rock in abrupt contact/juxtaposed with previously-altered, basaltic wallrocks. The Biedleman Bay intrusive complex is genetically related, however, to extrusive rocks deposited higher in the section (Holk et al., 2008).

Oxygen Isotope Zonation and Lithogeochemical Indicators of Alteration

The oxygen isotope zonation patterns, at Izok Lake can be compared with other geochemical, mineralogical, and mineral chemical indicators of hydrothermal alteration. Sodium depletion/removal in bulk rocks is due to the destruction of Na-Ca feldspars in VMS-bearing footwall successions and has long been used as a monitor of hydrothermal alteration (e.g. Franklin, 1997). The distribution of sodium in surface lithogeochemical samples of hanging-wall rhyolite (i.e. R2 rhyolite and younger; R1 rhyolite hosts the VMS lenses: Bailey and Stubley, 2013a,b), mapped as the isopleth of 1% Na_2O, in the Izok Lake area is shown in Figure 11. Rhyolitic rocks within the isopleth contain less than 1% Na_2O (Morrison, 2004). The marked coincidence of this Na depletion zone with the mapped oxygen isotope zones (the >12‰ zone in particular; see also Fig. 9) indicates the large size (several km in diameter) of the zone of rocks that were hydrothermally altered by the Izok VMS-forming hydrothermal system. However, the extensive nature of apparent sodium loss indicated in Figure 11 makes it a less spatially definitive vectoring tool relative to oxygen isotope mapping.

A potentially useful indicator of hydrothermal alteration is the Ishikawa Index (AI = $100(K_2O+MgO)/(K_2O+ MgO+Na_2O+CaO)$): Ishikawa et al., 1976), calculated from whole-rock chemical analyses. This index was mapped using lithogeochemical samples collected from outcrops on a regional scale in the Izok Lake area by Laakso et al. (2015) by interpolation of 1241 whole-rock chemical analyses using an inverse distance

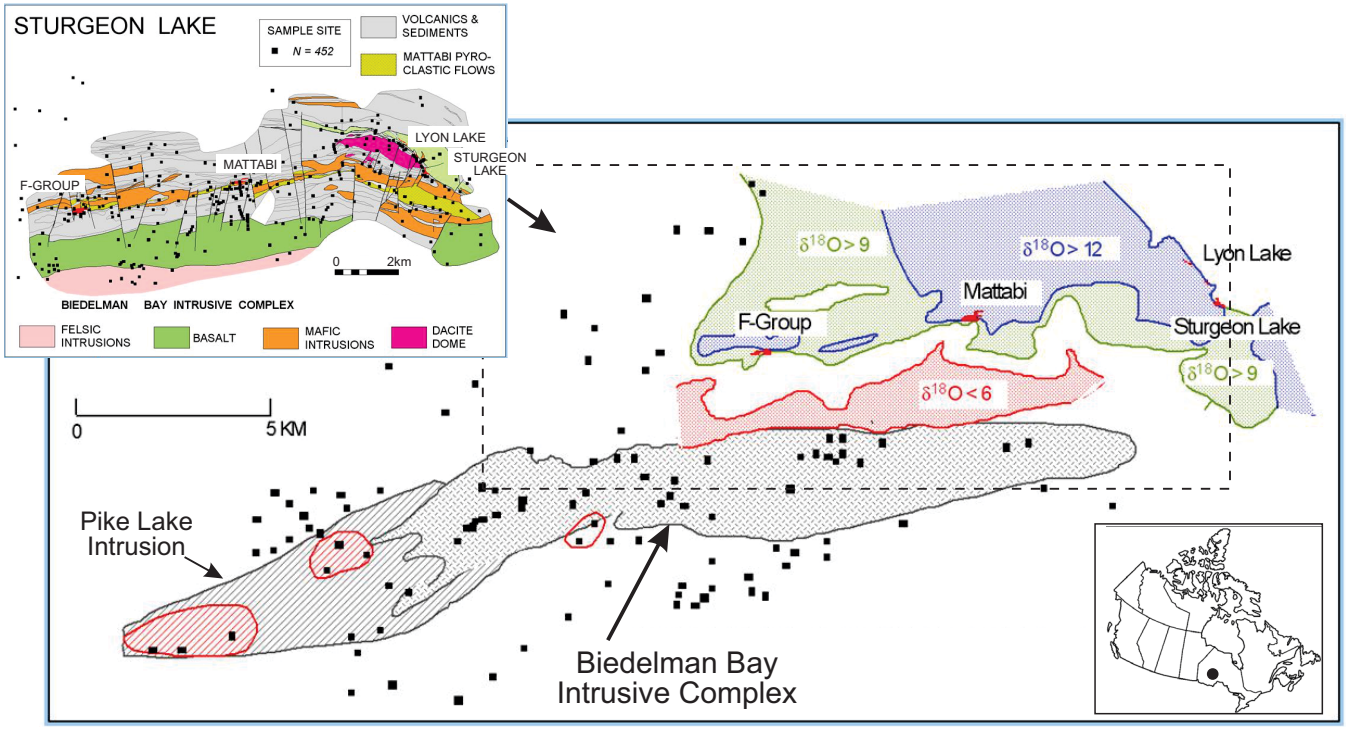

Figure 10. Oxygen isotope zonation above the Biedelman Bay intrusive complex, Sturgeon Lake, Ontario (Holk et al., 2008; geology modified from Franklin et al., 1975), provides an instructive comparison to Izok Lake. The dip of the layered volcanic rocks is nearly vertical; the inset geological map (simplified from Morton et al., 1999) and the map of oxygen isotope zoning are virtual cross-sections depicting both the high-temperature reaction zone and a later, low-temperature alteration of hanging-wall rocks. The geological and hydrothermal history of this caldera complex played an important role in the development of high values of $\delta^{18}O_{WR}$ in the hanging wall (see Holk et al., 2008).

weighting method (IDW; Fig. 11). There is a general correspondence between the region encompassed by the Na_2O depletion isopleth, the oxygen isotope zoning (see also Fig. 8) and the AI. Note, however, that the area suggested from the AI to be the most intensely altered appears to align with the general trend of fold axes and the distribution of VMS lenses. Although the AI map pattern appears to be structurally influenced, and the projected VMS lenses coincide with the intersection of the linear trend of maximum Ishikawa Index (AI) and the central area of high $\delta^{18}O$, the intense alteration (AI) indicated may have been somewhat broader prior to folding. Notably, this zone of high AI correlates spatially with a prominent occurrence of sillimanite-garnet-bearing rocks mapped by Stubley and Bailey (2013, unpub.) likely derived from metamorphism of muscovite-chlorite-bearing alteration assemblages. Whereas, the AI mapped in the Izok Lake area provides an indication of the broad extent of hydrothermal alteration, the more restricted oxygen isotope zonation pattern defines both the upright architecture (geometry) of the paleo-hydrothermal system and an effective 'vector' to mineralization in addition

Oxygen Isotope Zonation and Short-Wave Infrared Reflectance Spectrometry

Ground spectrometric data were acquired in the visible near infrared-short-wave infrared spectral region (VNIR-SWIR) by Laakso et al. (2015) to map the spectral properties of the phyllosilicate minerals in the rhyolitic rocks of the Izok Lake area. These authors focused on the spectral region of the Al-OH absorption feature near 2200 nm associated with white mica, and for the Fe-OH absorption feature (near 2250 nm) associated with biotite and chlorite. Up to eight spectra were measured at each selected outcrop, and averaged to yield a final ground spectral dataset of 285 measurements. A sub-set of these data is used here for comparison with oxygen isotope data for samples collected within 200 m of the same site.

Chlorite and white mica minerals are universally important components of hydrothermally altered of volcanic rocks associated with VMS deposits. Variation in the position of the absorption features for each of these minerals reflects a variation in their chemical composition (Duke, 1994). For example, a shift to longer wavelengths in the position of the Al-OH absorption feature is due to increasing substitution of Mg and Fe for Al (Duke, 1994; Bishop et al., 2008). A similar shift in the Fe-OH position is due to an increase in Fe in chlorite. Laakso et al. (2015) noted a concomitant change in the position on an Alteration Box Plot (Large et al., 2001; a bi-variate plot of AI versus Chlorite-Carbonate-Pyrite Index, or CCPI), with

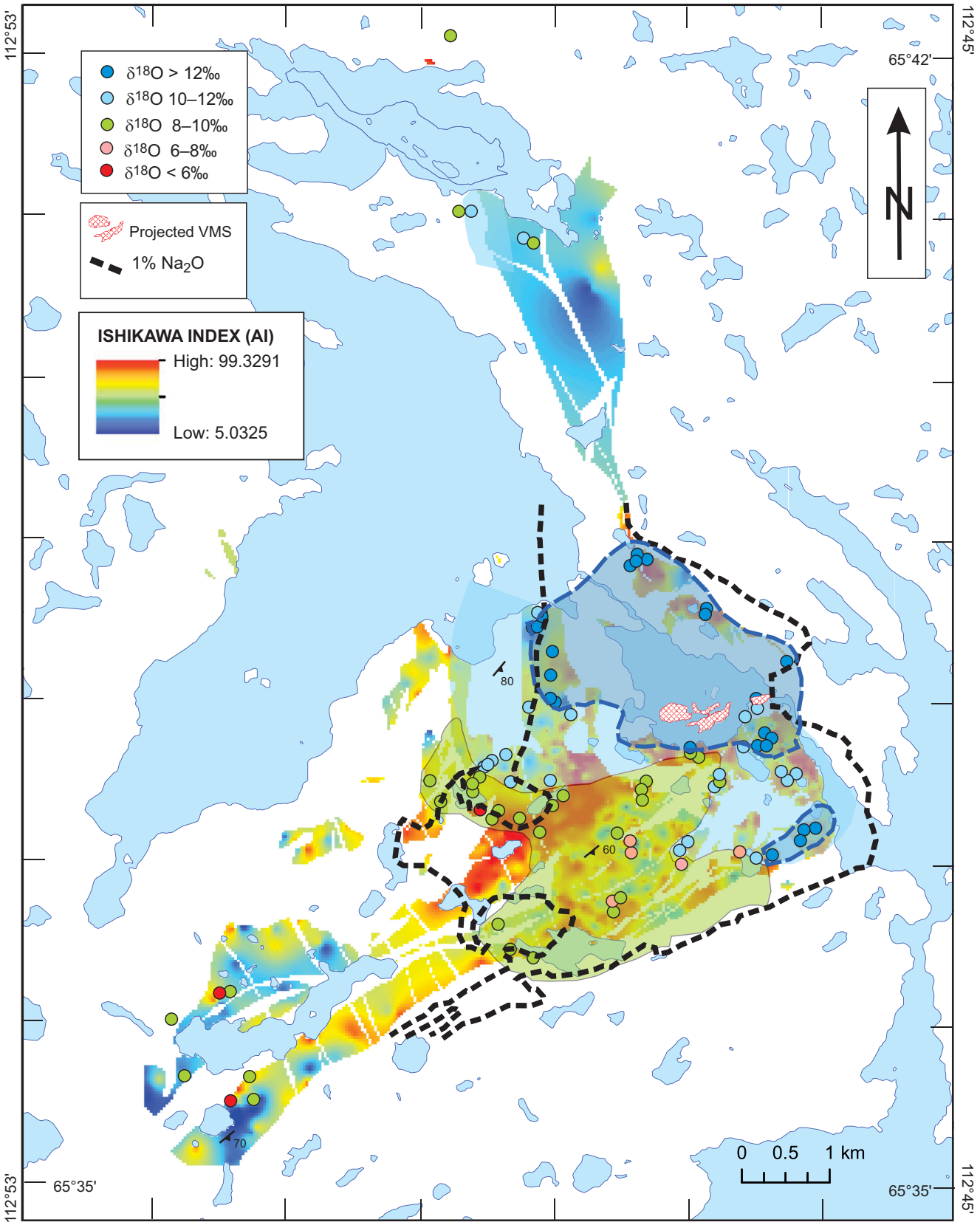

Figure 11. Map of the Izok Lake area comparing the oxygen isotope zonation to the location of a <1% Na_2O isopleth (Morrison, 2004) and to the variation in rock alteration based on the chemical Ishikawa Index (AI = 100(K_2O+MgO)/(K_2O+MgO+Na_2O +CaO).

increasing wavelength position of the Al-OH absorption feature.

Linear regression of the whole-rock values of $\delta^{18}O$ plotted in Figure 12a indicates a significant correlation with the spectral positions of the absorption features for Al-OH ($R^2 = 0.53$; due to white micas) and Fe-OH ($R^2 = 0.62$; due to chlorite). A shift towards shorter Al-OH absorption feature wavelengths, corresponding to an increase in the Al content of the white micas, was also documented in a biotite- to sillimanite-grade metamorphic progression in rocks from the Belt Supergroup by Duke and Lewis (2010). That is, the Al content increases with increasing temperature of crystallization. Similarly, a slight increase in Al-OH wavelength correlates with an increase in $\delta^{18}O$ (Fig. 12a), which may reflect a decrease in hydrothermal alteration temperature that has been preserved despite subsequent high-grade regional metamorphism. A shift towards longer Al-OH absorption feature wavelengths also appears to coincide with a decrease in alteration intensity (Laakso et al., 2015) in the ground spectral data. In some instances, the Al-OH wavelength/alteration intensity correlation has been inferred to indicate a low-temperature recharge zone (van Ruitenbeek et al., 2005). In the Izok Lake area, however, we do not favour such an interpretation to explain the relatively long Al-OH wavelengths in hanging-wall rocks. Rather, the high-Al-OH wavelengths variations may largely reflect distal, lower temperature waning discharge alteration mineral assemblages that were subsequently recrystallized during regional metamorphism.

The presence of abundant Fe chlorite in the footwall upflow zones (so-called "pipes") of VMS hydrothermal systems (e.g. Larson, 1984; MacLean and Hoy, 1991; Taylor et al., 2014) and high Fe contents of modern high-temperature vent fluids (e.g. Von Damm, 1995) are typically interpreted to be the product of high-temperature, "prograde" hydrothermal circulation and evolution (e.g. van Ruitenbeek et al., 2005). However, in the Izok Lake area, the increase in the wavelength of the Fe-OH absorption feature (indicating an increase in the Fe/(Fe+Mg) ratio of biotite and chlorite) correlates with an increase, rather than decrease, in whole-rock $\delta^{18}O$ (Fig. 12b). This indicates alteration occurred at lower, rather than higher temperatures. Moreover, Laakso et al. (2015) noted an increase in the wavelength of the Fe-OH absorptions of biotite and chlorite near the massive sulphide lenses at Izok Lake. However, in various hydrothermal settings, variations in the Fe/(Fe+Mg) of chlorite are interpreted to be controlled primarily by the composition of the hydrothermal fluid (e.g. Kuroko deposits: Shikazono and Kawahata, 1987; Matagami, Quebec: Kranidiotis and MacLean, 1987; modern geothermal sites: Cathelineau, 1988) and by physical properties of the system (e.g. temperature: Mercier-Langevin et al., 2014). For example, chlorite from low-temperature sericite-chlorite±carbonate assemblages developed near the seafloor (VMS-bearing zone, and immediate hanging wall) at the Lemoine Au-bearing VMS deposit are Fe-rich (Mercier-Langevin et al., 2014). A similar relationship at Izok Lake is consistent with the correlation between $\delta^{18}O$ and the Fe-OH wavelength shown in Figure 12.

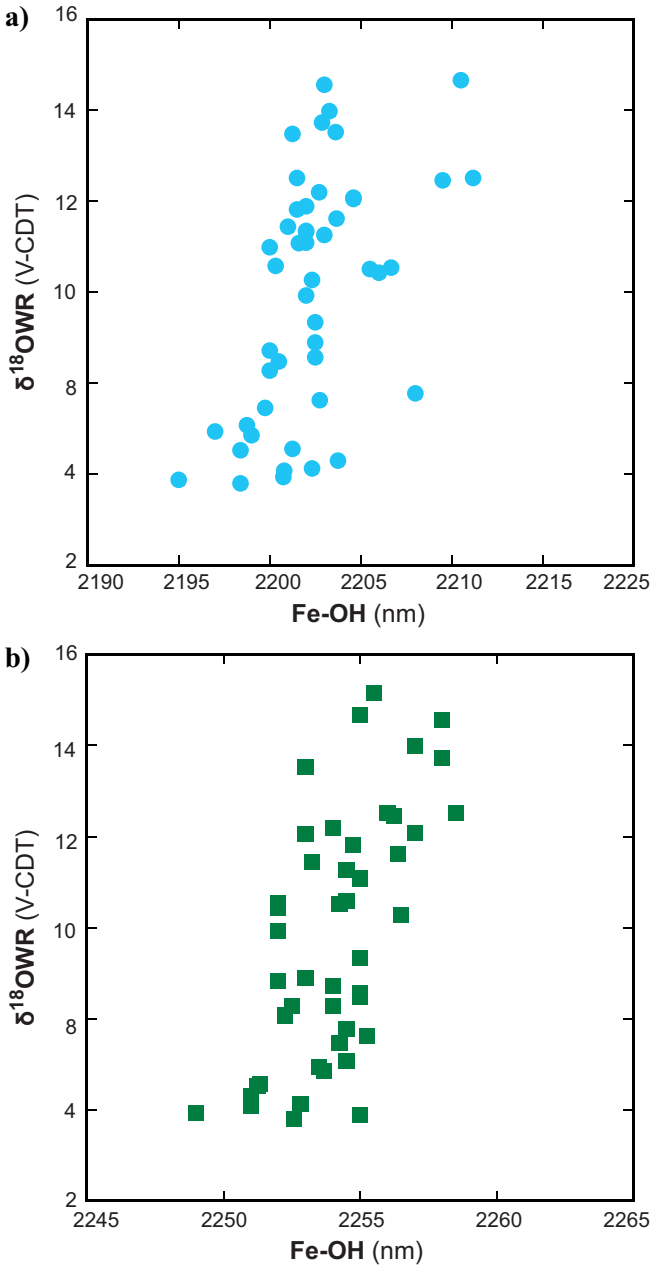

Figure 12. a) Plot of $\delta^{18}O_{WR}$ versus Al-OH absorption feature illustrates a correlation (linear fit, $R^2 = 0.53$) suggesting decreasing mineralogical alteration and increasing paragonite (Na+) substitution in white mica at lower water/rock interaction temperatures. **b)** Plot of $\delta^{18}O_{WR}$ versus Fe-OH absorption feature ($R^2 = 0.62$) implies, unexpectedly, an increase in alteration intensity at lower temperatures (increasing $\delta^{18}O_{WR}$), assuming a marine hydrothermal fluid (i.e. $\delta^{18}O_{H_2O}$ ~0‰).

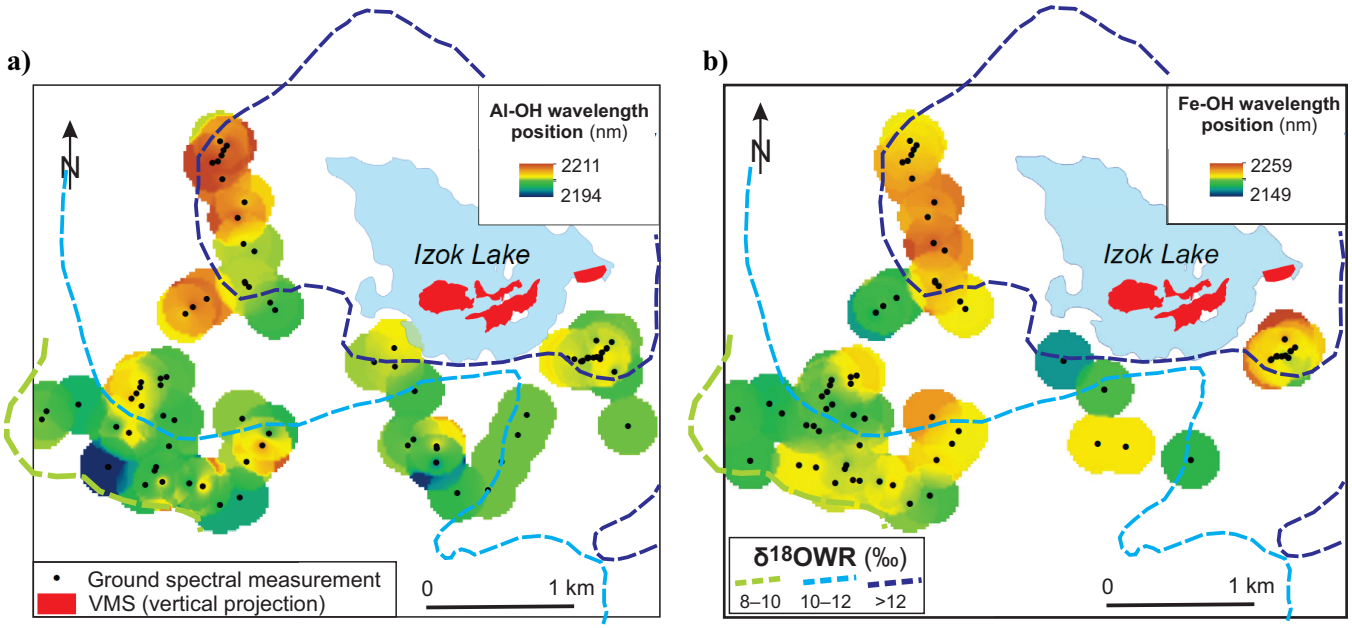

Figure 13. a) Alteration map based on a field-measured, short-wave infrared spectral feature for Al-OH absorption due to white mica. Boundaries of oxygen isotope zones (see Fig. 8) are shown for comparison. **b)** Alteration map based on a field-measured spectral feature for Fe-OH absorption due to chlorite. Increasing wavelength (in nm) is associated with an increase in the Chlorite-Carbonate-Pyrite Alteration Index; CCPI = 100 (FeO+MgO) /(FeO+MgO+Na_2O+K_2O).

A comparison between the spatial extent of the oxygen isotope zones and measured Al-OH and Fe-OH wavelength positions is shown in Figure 13a,b, respectively. Areas of the longest wavelengths for both Al-OH and Fe-OH absorption features are largely within the zone of highest $\delta^{18}O$. The areas of the longest Al-OH wavelength appear to be concentrated at the outer margins of the high-$\delta^{18}O$ zone, although this spatial relationship may result from the location of outcrops selected for measurement. In addition, there is only a slight correspondence between the areas of longest wavelength positions and the area of highest AI (compare Figs. 11 and 13a,b). However, the lack of correspondence may be only apparent, and biased by the distribution and density of measurement sites. A general correspondence between variation in positions of the absorption features and the pattern of oxygen isotope zonation is nevertheless apparent.

IMPLICATIONS FOR EXPLORATION

The paleo-hydrothermal system responsible for the Izok VMS deposit has been effectively mapped using whole-rock oxygen isotope analyses. The distribution of oxygen isotope alteration, mapped in the form of zones, describes a top-down (plan) view of a nearly upright hydrothermal system, with a ^{18}O-enriched 'cap' overlying the VMS deposit that provides a hanging-wall vector to subsurface mineralization. Oxygen isotope zonation based on analytical results for drill core samples collected near and just beneath the VMS deposit indicates the general location of an upflow zone in the footwall.

Because some subvolcanic centres that are prospective for VMS were active through several distinct magmatic episodes, and each could potentially be associated with VMS deposition, explorationists should be aware of the potential presence of multiple, vertically 'stacked' hydrothermal alteration systems and massive sulphide lenses, especially if the subvolcanic centre is large and long-lived. Although a discrete subvolcanic intrusion that would have provided the heat to drive the hydrothermal system in the Izok Lake area has not been identified, our oxygen isotope mapping indicates that the Izok deposit is situated at the top of the related hydrothermal system. On the basis of this study, the presence of a multiple, 'stacked' mineralization-alteration system, with additional sulphide bodies at depth, cannot be ruled out.

Despite subsequent amphibolite-facies metamorphism, the pattern of oxygen isotope alteration zonation remains undisturbed, emphasizing the value of the isotopic technique to exploration, and limited only by the availability and distribution of samples. The oxygen isotope effects of alteration in a seafloor VMS-related system is a robust 'fingerprint' that remains in the rock to the temperature of melting, disturbed only by deformation which will be reflected by the morphology of the oxygen isotope zoning. Therefore, oxygen isotope mapping is a viable tool to determine the location and architecture of a potentially VMS-bearing hydrothermal system. Furthermore, correlation of whole-rock $\delta^{18}O$ with spectral data reinforces the utility of a multi-faceted approach to alteration mapping.

ACKNOWLEDGEMENTS

This research has been supported by the Targeted Geoscience Initiative 4 (TGI-4) Program of the Earth Sciences Sector, Natural Resources Canada. MMG Limited, particularly Kimberley Bailey, Trish Toole, and Ian Neill, kindly provided needed sample material and assistance in the field. Discussions with Kimberley Bailey and Mike Stubley (Stubley Geoscience Inc.) were especially helpful. Beth McClenaghan (G.S.C.) kindly supplied several drill-core samples and descriptions. Oxygen isotope analyses were carried out under contract at the University of Western Ontario.

REFERENCES

Ames, D., Galley, A. G., Taylor, B.E., Kjarsgaard, I. M., and Tardif, N., in press. Hanging wall vectoring for buried VMS deposits, Paleoproterozoic Flin Flon mining camp, Manitoba, Canada; Economic Geology.

Bailes, A.H., Galley, A.G., Paradis, S., and Taylor, B.E., in press. Variations in large synvolcanic alteration zones at Snow Lake, Manitoba, Canada, with proximity to associated VMS deposits; Economic Geology.

Bailey, K. and Stubley, M., 2013a. The Izok volcanic-hosted massive sulphide deposit, Nunavut, Canada: A new interpretation of the rhyolitic stratigraphy and implications for exploration, *In:* Abstracts Volume; Society of Economic Geologists Annual Meeting, Whistler, September 24-27, 2013, p. 133 –139.

Bailey, K. and Stubley, M., 2013b. Izok volcanic-hosted massive sulphide deposit, Nunavut, Canada: A new interpretation of the rhyolitic stratigraphy and implications for exploration, *In:* Abstracts Volume Society of Economic Geologists Annual Meeting, Whistler, September 24-27, 2013, p. 44.

Beaudoin, G., Mercier-Langevin, P., Dube, B., and Taylor, B.E., 2014. Low-temperature alteration at the world-class LaRonde Penna Archean Au-rich volcanogenic massive sulfide deposit, Abitibi Subprovince, Quebec, Canada: evidence from whole-rock oxygen isotopes; Economic Geology, v. 109, p. 167–182.

Bishop, J.L., Lane, M.D., Dyar, M.D. and Brown, A.J., 2008. Reflectance and emission spectroscopy study of four groups of phyllosilicates: smectites, kaolinite-serpentines, chlorites and micas; Clay Minerals, v. 43, p. 35–54.

Bleeker, W. and Hall, B., 2007. The Slave Craton: Geological and metallogenic evolution, *In:* Mineral deposits of Canada: A Synthesis of Major Deposit Types, District Metallogeny, the Evolution of Geological Provinces, and Exploration Methods, (ed.) W.D. Goodfellow; Geological Association of Canada, Mineral Deposits Division, Special Publication 5, p. 849–879.

Borthwick, J. and Harmon, R.S., 1982. A note regarding ClF_3 as an alternative to BrF_5 for oxygen isotope analysis; Geochimica et Cosmochimica Acta, v. 46, p. 1665–1668.

Cathelineau, M., 1988. Cation site occupancy in chlorites and illites as a function of temperature; Clay Minerals, v. 23, p. 471–485.

Cathles, L.M., 1993. Oxygen isotope alteration in the Noranda mining district, Abitibi greenstone belt, Quebec; Economic Geology, v. 88, p. 1483–1511.

Davis, W.J. and Hegner, E., 1992. Neodymium isotopic evidence for the tectonic assembly of late Archean crust in the Slave Province, Northwest Canada; Contributions to Mineralogy and Petrology, v. 111, p. 493–504.

Duke, E.F., 1994. Near infrared spectra of muscovite, Tschermak substitution, and metamorphic reaction progress: Implications for remote sensing; Geology, v. 22, p. 621–624.

Duke, E.F. and Lewis, R.S., 2010. Near infrared spectra of white mica in the Belt Supergroup and implications for metamorphism; American Mineralogist, v. 95, p. 908–920.

Franklin, J.M., 1997. Lithogeochemical and mineralogical methods for base metal and gold exploration, *In:* Proceedings of Exploration 97, (ed) A.G. Gubins; Fourth Decennial International Conference on Mineral Exploration, Prospectors and Developers Association of Canada, p. 191–208.

Galley, A.G., Hannington, M.D., and Jonasson, I.R., 2007. Volcanogenic massive sulphide deposits, *In:* Mineral deposits of Canada: A Synthesis of Major Deposit Types, District Metallogeny, the Evolution of Geological Provinces, and Exploration Methods, (ed.) W.D. Goodfellow; Geological Association of Canada, Mineral Deposits Division, Special Publication 5, p. 141–161.

Green, G.R., Ohmoto, H., Date, J., and Takahashi, T., 1983. Whole-rock oxygen isotope distribution in the Fukazawa-Kosaka area, Hokuroku district, Japan; Economic Geology Monograph 5, p. 395−411.

Holk, G.J., Taylor, B.E., and Galley, A.G., 2008. Oxygen isotope mapping of the Archean Sturgeon Lake caldera complex and VMS-related hydrothermal system, Northwestern Ontario, Canada; Mineralium Deposita, v. 43, p. 623–640.

Ishikawa, Y., Sawaguchi, T., Iwaya, S., and Horiuchi, M., 1976. Delineation of prospecting targets for Kuroko deposits based on modes of volcanism of underlying dacite and alteration haloes; Mining Geology, v. 26, p. 105–117.

Kranidiotis, P. and MacLean, W., 1987. Systematics of chlorite alteration at the Phelps Dodge massive sulfide deposit, Matagami, Quebec; Economic Geology, v. 82, p. 1898–1911.

Laakso, K., Rivard, B., and Peter, J.M., 2015. Hyperspectral reflectance spectrometry in the exploration for VMS deposits using the Izok Lake Zn-Cu-Pb-Ag deposit, Nunavut as a test site, *In:* Targeted Geoscience Initiative 4: Contributions to the Understanding of Volcanogenic Massive Sulphide Deposit Genesis and Exploration Methods Development, (ed.) J.M. Peter and P. Mercier-Langevin; Geological Survey of Canada, Open File 7853, p. 15–25.

Large, R.R., Gemmell, J.B., Paulick, H. and Huston, D.L., 2001. The alteration box plot: A simple approach to understanding the relationship between alteration mineralogy and lithogeochemistry associated with volcanic-hosted massive sulfide deposits; Economic Geology, v. 96, p. 957–971.

Larson, P.B., 1984. Geochemistry of the alteration pipe at the Bruce Cu-Zn volcanogenic massive sulfide deposit, Arizona; Economic Geology, v. 79, p. 1880−1896.

MacLean, W. and Hoy, L.D., 1991. Geochemistry of hydrothermally altered rocks at the Horne Mine, Noranda, Quebec; Economic Geology, v. 86, p. 506–528.

Mercier-Langevin, P., Lafrance, B., Bécu, V., Dubé, B., Kjarsgaard, I., and Guha, J., 2014. The Lemoine auriferous volcanogenic massive sulfide deposit, Chibougamau camp, Abitibi, greenstone belt, Quebec, Canada: geology and genesis; Economic Geology, v. 109, p. 231–269.

Morrison, I. R., 2004. Geology of the Izok massive sulfide deposit, Nunavut Territory, Canada; Exploration Mining Geology, v. 13, p. 25–36.

Mortensen, J.K., Thorpe, R.I., Padgham, W.A., King, J.E., and Davis, W.J., 1988. U-Pb zircon ages for felsic volcanism in Slave Province, N.W.T., *In:* Radiogenic Age and Isotopic Studies: Report 2; Geological Survey of Canada, Paper 88-2, p. 85–95.

Piercey, S.J., Chaloux, E.C., Péloquin, A.S., Hamilton, M.A., and Creasar, R.A., 2008. Syn-volcanic and younger plutonic rocks from the Blake River Group: Implications for regional metallogenesis; Economic Geology, v. 103, p. 1243–1268.

Shanks, W.C. III, 2001. Stable isotopes in seafloor hydrothermal systems - Vent fluids, hydrothermal deposits, hydrothermal alteration, and microbial processes, *In:* Stable Isotope Geochemistry, (ed.) J.W. Valley and D.R. Cole; Reviews in Mineralogy and Geochemistry, v. 43, p. 469–525.

Sheppard, S.M.F. and Taylor, H.P. Jr., 1986. Igneous rocks: III. Isotopic case studies of Magmatism in Africa, Eurasia and Oceanic Islands *In:* Stable Isotopes in High-Temperature Geological Processes, (ed.) J. W. Valley, H.P. Jr Taylor, and J.R. O'Neil; Mineralogical Society of America, Reviews in Mineralogy, v. 16, p. 319–372.

Shikazono, N. and Kawahata, H., 1987. Compositional differences in chlorite from hydrothermally altered rocks and hydrothermal ore deposits; The Canadian Mineralogist, v. 25, p. 465–474.

Stubley, M. and Bailey, K., 2013. Bedrock geology of the southern Izok Lake area, West-central Slave Craton; Unpublished report, MMG Resources, Inc., 52 p.

Taylor, B.E., 2004. Fluorination methods in stable isotope analysis, Chapter 20, *In:* Handbook of Stable Isotope Analytical Techniques, Volume 1, (ed.) P.A. de Groot; Elsevier, Amsterdam, p. 400–472.

Taylor, B.E., de Kemp, E., Grunsky, E., Martin, L., Maxwell, G., Riggs, D., Goutier, J., Lauziere, K., and Dube, B., 2014. Three-dimensional visualization of the Archean Horne and Quemont hydrothermal systems, Blake River Group, Quebec; Economic Geology, v.109, p. 183–203.

Taylor, B. and Holk, G., 1998. Stable isotope applications in the exploration for volcanic-associated massive sulphide deposits: a preliminary summary, *In:* Database for CAMIRO Project 94E07: interrelationships between subvolcanic intrusions, large-scale alteration zones and VMS deposits (ed.) A. Galley, A. Bailes, M. Hannington, G. Holk, J. Katsube, F. Paquette, S. Paradis, F. Santiguida, and B. Taylor; Geological Survey of Canada, Open File 4431, p. 41–46.

Taylor, B.E., Holk, G., Dubé, B., and Galley, A., 2009 Oxygen isotope zoning in subvolcanic, intrusion-centered submarine hydrothermal systems as a guide to VMS exploration, *In:* Proceedings; 24th International Applied Geochemistry Society Meeting, Fredericton, June 1-4, 2009, p. 255–258.

Taylor, B.E. and South, B.C., 1985. Regional stable isotope systematics of hydrothermal alteration and massive sulfide deposition in the West Shasta district, California; Economic Geology, v. 80, p. 2149−2163.

Taylor, B.E. and Timbal, A., 1998a. Regional stable isotope studies in the Snow Lake area, *In:* Database for CAMIRO Project 94E07: interrelationships between subvolcanic intrusions, large-scale alteration zones and VMS deposits (ed.) A. Galley, A. Bailes, M. Hannington, G. Holk, J. Katsube, F. Paquette, S. Paradis, F. Santiguida, and B. Taylor; Geological Survey of Canada, Open File 4431, p. 271–280.

Taylor, B.E. and Timbal, A., 1998b. Regional stable isotope studies in the Noranda Volcanic Complex, *In:* Database for CAMIRO Project 94E07: interrelationships between subvolcanic intrusions, large-scale alteration zones and VMS deposits (ed.) A. Galley, A. Bailes, M. Hannington, G. Holk, J. Katsube, F. Paquette, S. Paradis, F. Santiguida, and B. Taylor; Geological Survey of Canada, Open File 4431, p. 243–252.

Taylor, H.P., Jr., 1968. The oxygen isotope geochemistry of igneous rocks; Contributions to Mineralogy and Petrology, v. 19, p. 1–71.

Taylor, H.P., Jr., 1986. Igneous rocks: II. Isotopic case studies of circumpacific magmatism, Chapter 9, *In:* Stable Isotopes in High-Temperature Geological Processes, (ed.) J.W. Valley, H.P. Taylor Jr., and J.R. O'Neil; Mineralogical Society of America, Reviews in Mineralogy, v. 16, p. 273–318.

Thorpe, R.I., Cumming, G.L., and Mortensen, J.K., 1992. A significant Pb isotope boundary in the Slave Province and its probable relation to ancient basement in the western Slave Province, *In:* Project Summaries, Canada-Northwest Territories Mineral Development Agreement 1987-91, (comps) D.G. Richardson and M. Irving; Geological Survey of Canada, Open File 2484, p. 179–184.

van Ruitenbeek, F.J.A., Cudahy, T., Hale, M., and van der Meer, F. D., 2005. Tracing fluid pathways in fossil hydrothermal systems with near-infrared spectroscopy; Geology, v. 33, p. 597–600.

Von Damm, K.L., 1995. Temporal and compositional diversity in seafloor hydrothermal fluids; Reviews in Geophysics, v. 33, Supplement Part 2, p. 1297–1305.

GEOLOGICAL SURVEY OF CANADA
OPEN FILE 7853

Targeted Geoscience Initiative 4: Contributions to the Understanding of Volcanogenic Massive Sulphide Deposit Genesis and Exploration Methods Development

Multiple sulphur isotope reconnaissance of Slave Province volcanogenic massive sulphide deposits

Bruce E. Taylor[1], Jan M. Peter[1], and Boswell A. Wing[2]

[1]Geological Survey of Canada, Ottawa, Ontario
[2]McGill University, Montreal, Quebec

2015

This publication is available for free download through GEOSCAN (http://geoscan.nrcan.gc.ca/)

Recommended citation

Taylor, B.E., Peter, J.M., and Wing, B.A., 2015. Multiple sulphur isotope reconnaissance of Slave Province volcanogenic massive sulphide deposits, *In:* Targeted Geoscience Initiative 4: Contributions to the Understanding of Volcanogenic Massive Sulphide Deposit Genesis and Exploration Methods Development, (ed.) J.M. Peter and P. Mercier-Langevin; Geological Survey of Canada, Open File 7853, p. 45–58.

Publications in this series have not been edited; they are released as submitted by the author.

Contribution to the Geological Survey of Canada's Targeted Geoscience Initiative 4 (TGI-4) Program (2010–2015)

TABLE OF CONTENTS

Figures

Multiple sulphur isotope reconnaissance of Slave Province volcanogenic massive sulphide deposits

Bruce E. Taylor[1]*, Jan M. Peter[1], and Boswell A. Wing[2]

[1]Central Canada Division, Geological Survey of Canada, 601 Booth Street, Ottawa, Ontario K1A 0E8
[2]Department of Earth and Planetary Sciences, McGill University, 3450 University Street, Montreal, Quebec H3A 2A7
*Corresponding author's e-mail: btaylor@nrcan-rncan.gc.ca

ABSTRACT

Multi-sulphur isotope (^{32}S, ^{33}S, ^{34}S, and ^{36}S) analysis of galena, sphalerite, and pyrite from 30 Archean volcanogenic massive sulphide deposits and occurrences from across the Slave Province reveals a variable contribution from Archean atmosphere-derived sulphur. Mass-independent fractionation of the sulphur isotopes produced anomalous abundances ($\Delta^{33}S$) of the sulphur isotopes that were incorporated to varying degrees in deposits that formed in different tectonic settings. Our data indicate that deposits of the bimodal-mafic type (bimodal rift setting) are characterized by a restricted range of $\Delta^{33}S$ from -0.3 to 0.1 per mil, whereas deposits of the bimodal-felsic type (arc-like settings) exhibit a broader range in $\Delta^{33}S$, from -0.8 to 0.6 per mil. Mantle-derived (juvenile) sulphur is essentially the sole source of sulphur in deposits of the bimodal-mafic type, whether derived directly by magmatic degassing, or indirectly by leaching of magmatic sulphides in the associated hydrothermal system; these deposits are also characterized by relatively low silver contents. Bimodal-felsic type deposits, typified by high silver contents, contain variable amounts of atmosphere-derived sulphur that was more readily available in arc-like settings.

INTRODUCTION

Herein we present the results of a reconnaissance study of the multiple sulphur isotope compositions of sulphides from 30 selected Archean volcanogenic massive sulphide (VMS) deposits or occurrences in the Slave Province (Fig. 1). Several of these VMS deposits (notably High Lake, Hackett River, and Izok Lake) have significant contents of precious metals, in particular Ag. Bleeker and Hall (2007 and references therein) described two major subdivisions of volcanism in the Slave Province: mafic, rift-related volcanism (ca. 2.73–2.70 Ga and 2.70–2.66 Ga) and transitional to calc-alkaline arc-like volcanism. Both occurred on an ancient basement complex, with crustal ages becoming younger to the east (Bleeker and Hall, 2007). These volcanic rocks were deposited in two different tectonic environmental settings, with the older (ca. 2.73–2.70 Ga) rocks in bi-modal rift settings, and the younger (post-2.70 Ga) rocks in arc-like settings, in which calc-alkaline volcanism occurred. VMS deposits occur in rocks of both these time periods. We conducted a reconnaissance multiple sulphur isotope investigation of sulphide minerals from VMS deposits throughout the Slave Province. In rocks older than ca. 2.2 Ga, and especially those older than 2.45 Ga, mass-independent fractionation (MIF) of sulphur provides a unique environmental tracer. Our goals were to ascertain whether the sulphur isotope compositions reflect these different ages of volcanism, and host-rock lithogeochemical and deposit metal contents.

BACKGROUND

Prior to ca. 2.45 Ga, the distribution of sulphur isotopes was characterized by production of anomalous amounts of ^{33}S through photolysis reactions in the atmosphere involving volcanic SO-SO_2 (Farquhar et al., 2000, 2001). The result of this process, which was able to proceed due to the absence of an ozone layer and to low pressures (concentrations) of atmospheric oxygen, was the mass-independent fractionation (MIF) of the isotopes of sulphur and the creation of a unique tracer of surface-processed sulphur (e.g. Farquhar and Wing, 2003). A brief discussion of the causes and effects of MIF follows in order to provide background for discussion of the data acquired in this study.

The typical mass-dependent fractionation (MDF) relationship between ^{33}S and ^{34}S is shown by the linear trend of values in Figure 2 and is contrasted with the trend for MIF, which is indicated by positive and negative values of $\Delta^{33}S$ (= $\delta^{33}S_{MEASURED} - \delta^{33}S_{MDF\text{-}PREDICTED}$; see Fig. 2), relative to MDF, which is defined by the equation $\delta^{33}S = 0.515\ \delta^{34}S$ (Farquhar et al., 2000). In the absence of the shielding effects of ozone during the Archean, MIF is thought to have been

Taylor, B.E., Peter, J.M., and Wing, B.A., 2015. Multiple sulphur isotope reconnaissance of Slave Province volcanogenic massive sulphide deposits, *In:* Targeted Geoscience Initiative 4: Contributions to the Understanding of Volcanogenic Massive Sulphide Deposit Genesis and Exploration Methods Development, (ed.) J.M. Peter and P. Mercier-Langevin; Geological Survey of Canada, Open File 7853, p. 45–58.

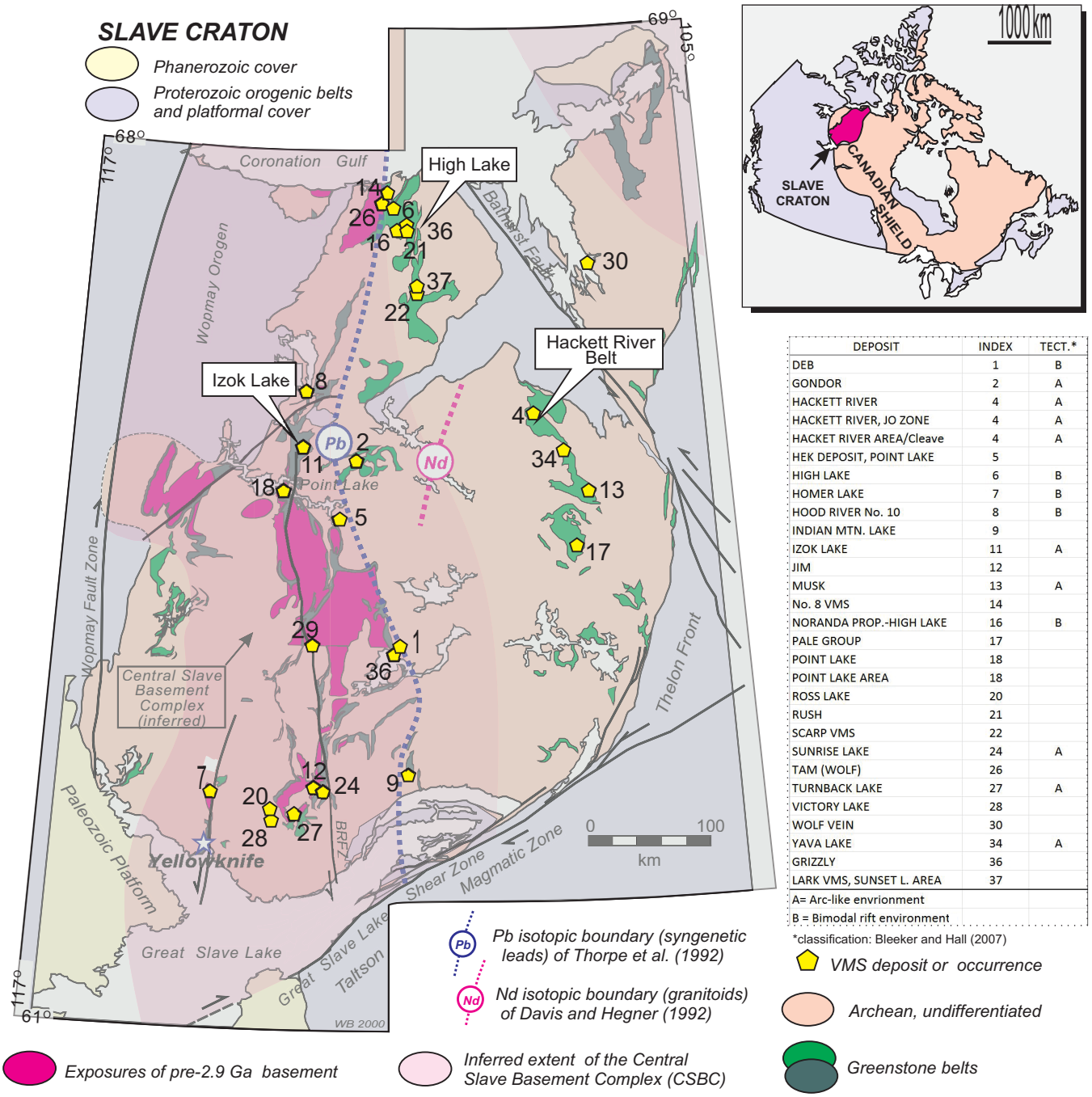

DEPOSIT	INDEX	TECT.*
DEB	1	B
GONDOR	2	A
HACKETT RIVER	4	A
HACKETT RIVER, JO ZONE	4	A
HACKET RIVER AREA/Cleave	4	A
HEK DEPOSIT, POINT LAKE	5	
HIGH LAKE	6	B
HOMER LAKE	7	B
HOOD RIVER No. 10	8	B
INDIAN MTN. LAKE	9	
IZOK LAKE	11	A
JIM	12	
MUSK	13	A
No. 8 VMS	14	
NORANDA PROP.-HIGH LAKE	16	B
PALE GROUP	17	
POINT LAKE	18	
POINT LAKE AREA	18	
ROSS LAKE	20	
RUSH	21	
SCARP VMS	22	
SUNRISE LAKE	24	A
TAM (WOLF)	26	
TURNBACK LAKE	27	A
VICTORY LAKE	28	
WOLF VEIN	30	
YAVA LAKE	34	A
GRIZZLY	36	
LARK VMS, SUNSET L. AREA	37	
A= Arc-like envrionment		
B = Bimodal rift environment		

*classification: Bleeker and Hall (2007)

Figure 1. Generalized geological map of the Slave Craton (Province) (after Bleeker and Hall, 2007), showing the locations of volcanogenic massive sulphide deposits included in this study (see index for deposit names, numbers, and tectonic environments). Undifferentiated Archean rocks include granitoid, gneiss, and turbidite sequences. Tholeiitic greenstone belts are indicated by the darker green colour. Exposures of pre-2.9 Ga basement, and boundaries based on Pb isotopes in deposits (Thorpe et al., 1992) and on Nd isotopes in granitoid rocks (Davis and Hegner, 1992) are shown for reference.

caused by UV photolysis of atmospheric SO_2-SO, resulting in an excess or depletion of ^{33}S relative to that produced by mass-dependent fractionation of sulphur among existing sulphur-bearing compounds (Farquhar et al., 2000). The resulting MIF sulphur is transported to the Earth's surface as native sulphur (S°; $\Delta^{33}S > 0$) or sulphate (H_2SO_4; $\Delta^{33}S < 0$), and incorporated in pyrite via bacterial (BSR) or thermal (TSR) sulphate reduction. These processes are schematically shown in the context of a seafloor hydrothermal system in Figure 3. MIF was a significant process prior to 2.45 Ga. Thus, non-zero $\Delta^{33}S$ values are a unique, chemically conservative tracer/signal of atmospheric sulphur that can be variably present in pre-2.45 Ga paleohydrothermal systems. This MIF signal cannot be modified or masked by MDF processes, but is susceptible to dilution.

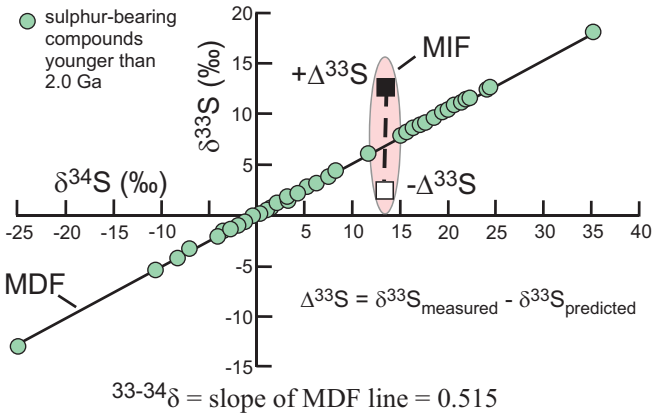

Figure 2. Plot of $\delta^{33}S$ versus $\delta^{34}S$ illustrating the mass-dependent fractionation (MDF; $\delta^{33}S = 0.515\ \delta^{34}S$) that has dominated S-isotope abundances since ca. 2.0 Ga (modified from Farquhar et al., 2001; Farquhar and Wing, 2003). Prior to that, an atmosphere depleted in ozone and oxygen facilitated photochemical fractionation of ^{33}S relative to ^{34}S from atmospheric SO–SO_2, resulting in mass-independent fractionation (MIF) of the sulphur isotopes ($\Delta^{33}S$), with reduced sulphur products enriched in ^{33}S (verified) and oxidized sulphur products depleted in ^{33}S sulphates (predicted, but not yet corroborated).

Archean oceans are generally thought to have been low in sulphate, with $\Delta^{33}S \approx 0$ (e.g. Jamieson et al., 2013), but details remain controversial.

The occurrence of the MIF signal in sulphides as a function of geological age is shown in Figure 4, where the abrupt presence of a marked MIF signal at ca. 2.45 Ga, and older, is apparent. The apparently sudden onset of a MIF signal (Fig. 4) has been attributed to a rapid oxygenation of the Earth's atmosphere and termed the "Great Oxidation Event" (GOE) (e.g. Holland, 2006). Although the onset of a MIF signal appears abrupt in this figure, the oxidation of the Earth's atmosphere was not sudden and linear, but gradual and punctuated (e.g. Ohmoto, et al., 2006; Pufahl and Hiatt, 2012; Planavsky et al, 2014). Since 2.0 Ga, however, sulphur isotope distribution has been controlled by the MDF processes, which have dominated over MIF processes.

SAMPLE SELECTION AND METHODOLOGY

Sulphide samples were selected from the archived collection of Ralph Thorpe (formerly, Geological Survey

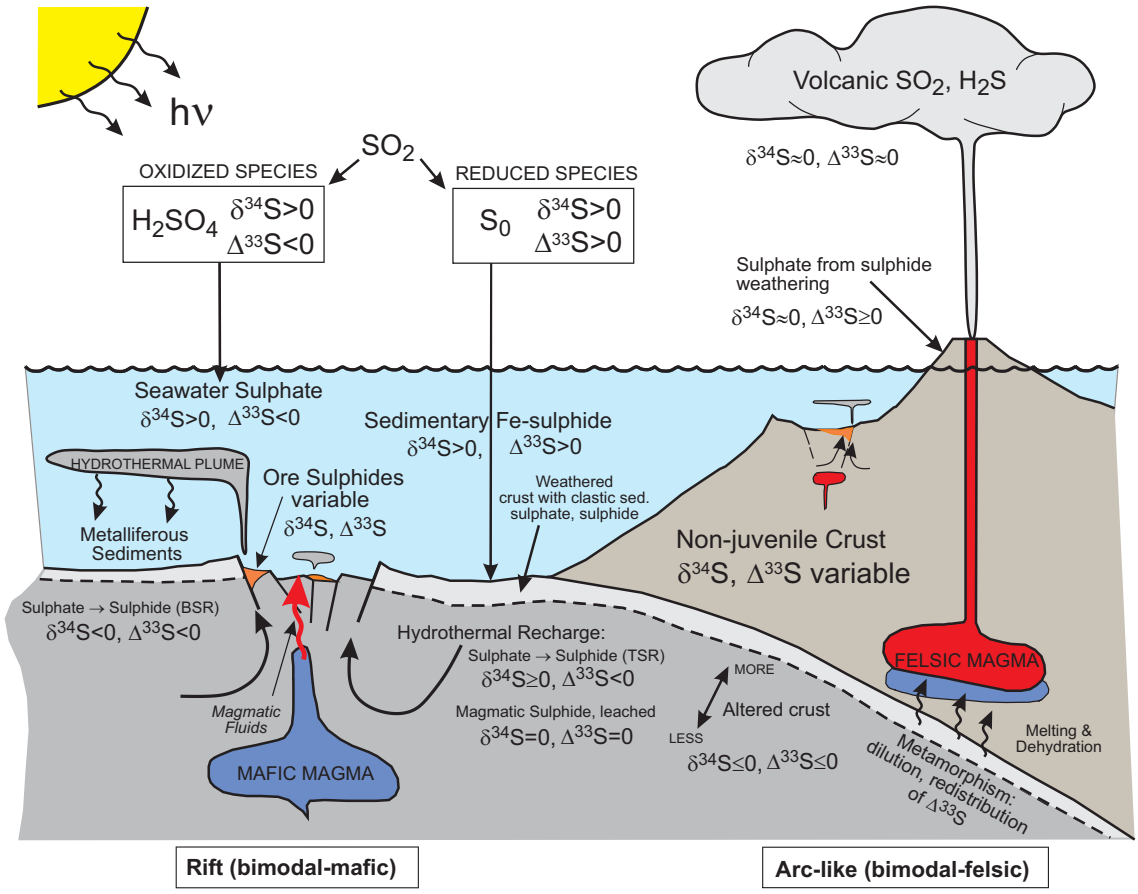

Figure 3. Schematic diagram of an Archean volcanogenic massive sulphide-producing submarine hydrothermal system illustrating sources, sinks, and general fractionation tendencies for sulphur isotopes in two principal tectonic settings (adapted, in part, from Farquhar and Wing, 2003 and Sharman et al., in press). The mass-independent fractionation (MIF) "signal" (i.e., $\Delta^{33}S \neq 0$) is thought to derive from photolysis reactions involving atmospheric (volcanic) SO_2. Microbial sulphate reduction (BSR) and hydrothermal sulphate reduction (TSR) forms sulphides with $\Delta^{33}S < 0$. Such sulphate-reduction systems were generally similar to those operating today. Mixing of sulphur sources may dilute the MIF signal in some crustal sinks.

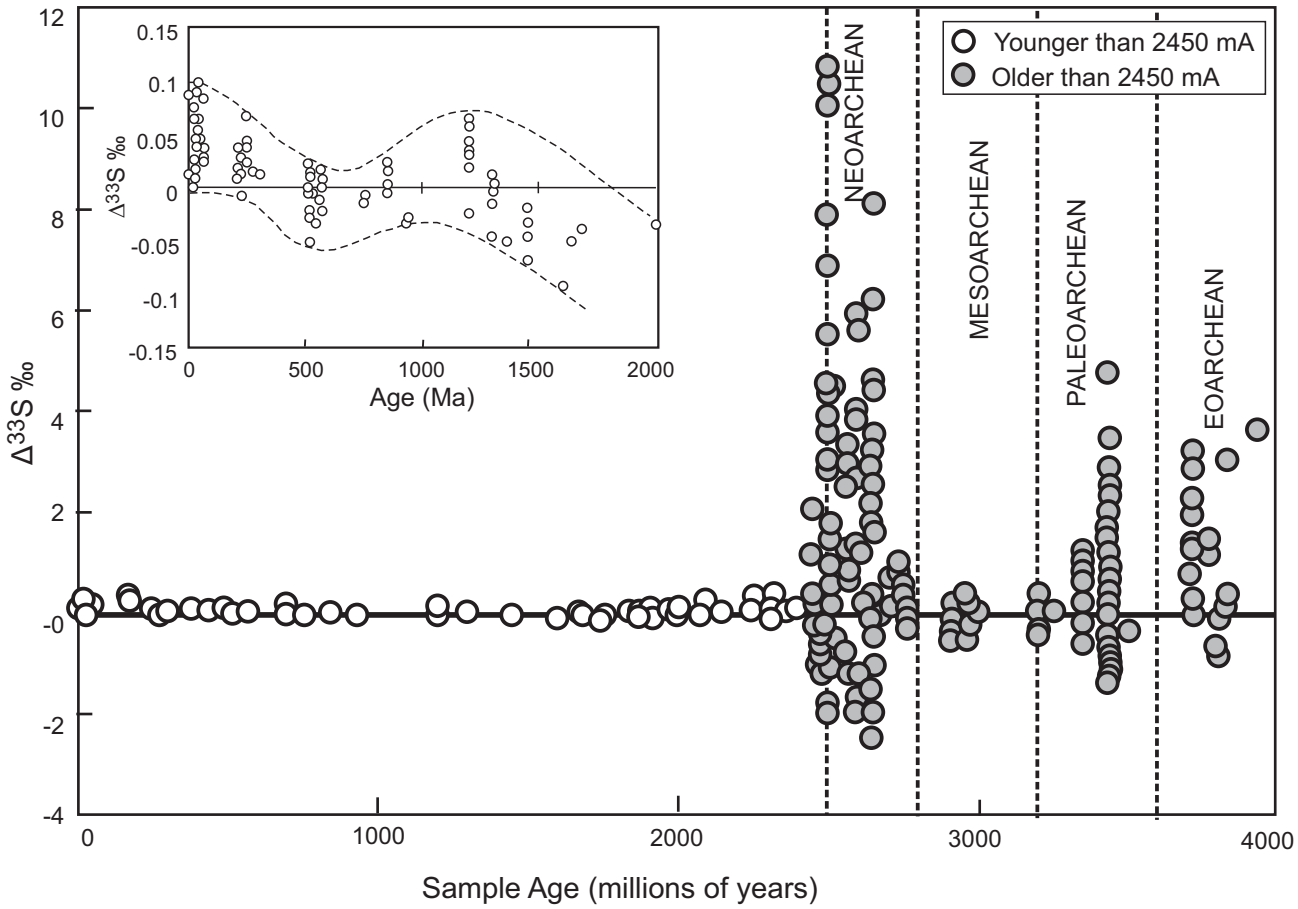

Figure 4. Plot of $\Delta^{33}S$ versus age for sulphides (from Farquhar et al., 2010) illustrates the presence of marked mass-independent fractionation (MIF) in the isotopic record prior to ca. 2.45 Ga. A subsequent, rapid increase in atmospheric oxygen is inferred to have occurred about 2.45 Ga, after which MDF dominated. Inset illustrates minor (± 0.1‰) variation in $\Delta^{33}S$ of marine sulphate since about 2.0 Ga.

of Canada) for Pb isotope analysis (see Thorpe, 2008) with the aim to select as geographically representative a set of samples as possible. In some cases the samples analyzed in this study were aliquots of the same galena concentrates previously analyzed for lead isotopes (Thorpe et al., 2008). In numerous cases, however, hand-picked separates of pure pyrite, sphalerite, or galena prepared from small chip samples of massive sulphide were used. In a few instances, the small grain size precluded efficient purification to 100%, and the analyzed samples also contained small amounts of silicate minerals and/or other sulphides.

Sulphide samples of 1 to 3 mg size were converted to SF_6 (generally <5 µmol total yield) by laser-assisted fluorination in an atmosphere of 100% pure F_2 using a micro-isotopic laser extraction system (MILES; Taylor, 2004), modified by the addition of a Stanford Research Institute® gas chromatograph (model 310), dedicated computer and control software, and associated high-vacuum line with gas chromatograph- (GC) multiport valves for injecting/collecting sample splits (Fig. 5). The SF_6 generated by the fluorination reaction was cryogenically separated from non-condensable by-product gases and excess F_2 at -192°C and then passed through a variable temperature trap at -135°C for additional purification before further on-line purification over two GC columns in series: Haysep Q (2 m length) and Molsieve 5A (2 m length) at 60°C by means of a pure He carrier gas at a rate of 25 mL/min. The SF_6 was isolated from contaminants and the carrier gas by means of a high-efficiency cold finger at -192°C (Taylor, 2004) and sealed in 6 mm glass tubes for subsequent analysis by mass spectrometry. The sealed gases were analyzed for the four stable isotopes of sulphur (^{32}S, ^{33}S, ^{34}S, ^{36}S) in a Thermo-Electron MAT 253 isotope ratio mass spectrometer in the Department of Earth and Planetary Sciences, McGill University, Montreal. The mass spectrometer was fitted with a dual inlet, micro-volume and a custom-built (B.E. Taylor) inlet manifold designed for use with micro samples.

Results are reported using the standard δ-notation, in per mil (‰) relative to V-CDT. Uncertainties in $\delta^{34}S$, as determined on duplicates, were typically <0.2‰ and <0.02‰ for $\Delta^{33}S$. However, the technical challenges of irregular intervals between sample extraction (Ottawa) and mass spectrometry (Montreal), may have added

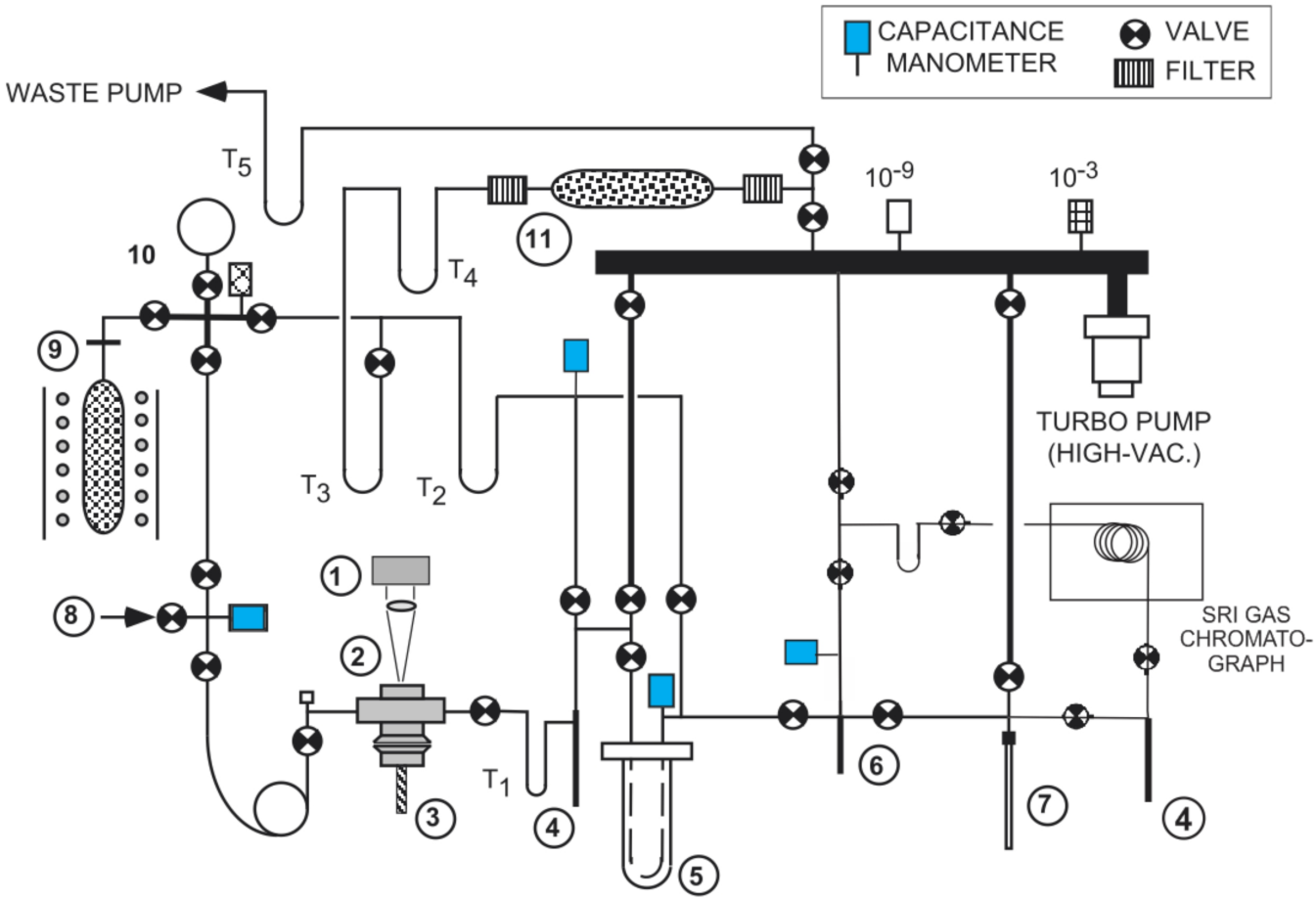

Figure 5. Schematic diagram of MILES+GC (Micro-Isotopic Laser Extraction System) plus Stanford Research Institute® gas chromatograph (Model 310). Components include (1) zoom stereo microscope; (2) Synrad® 25 watt CO_2 laser and beam delivery system; (3) small-volume sample chamber, with individual Ni crucibles (for grains), or flat stage (for in situ analysis), and cooling finger; (4) fritted P-trap (100% efficient separation of condensable sample from carrier gas; (5) variable temperature trap for cryogenic separations; (6) mini P-trap/manometer; and (7) 6 mm cracker tube (Pyrex® glass) for collection of purified SF6 sample. Associated GC valves and high-vacuum piping for sample injection onto GC columns (see text) not illustrated for simplicity (modified from Taylor, 2004).

slightly to the external uncertainty of each analysis due to the necessity of using multiple small aliquots of reference gas. Some gas chromatographic spectra of product gases from fluorination of sulphide samples containing trace to minor amounts of silicates yielded peaks of another gas (likely SOF_2) in addition to SF_6. Although this appears to have had little effect on the $\delta^{34}S$ values in sulphide-silicate mixtures up to 1:1 (B.E. Taylor, unpub.), potential effects on other isotopes are unknown.

RESULTS

Figure 6a plots the 72 $\delta^{34}S$ values (‰, V-CDT) of pure and mixed sulphides (i.e. concentrates of pyrite, sphalerite, and/or galena, with traces of other sulphides or silicates in a few samples) from VMS deposits in the Slave Province obtained in this study that exhibit a distribution of approximately -2 /+4‰ about a mean $\delta^{34}S$ value of 0.77‰; range: -2.5 to 3.9‰, with two outliers. The mean value and small range of $\delta^{34}S$ values are indicative of mantle-dominated Archean sulphur. The distribution of $\Delta^{33}S$ values for pure and mixed sulphides (defined as in Fig. 6a) from Slave Province VMS deposits shown in Figure 6b indicates a slight predominance of negative $\Delta^{33}S$ values (mean value = -0.08‰; range: -1.03 to 1.53‰) that indicates the involvement of sulphur generated by MIF processes.

DISCUSSION

The incorporation of ^{33}S in abundances that deviate from those determined by mass-dependent fractionation (i.e. $\delta^{33}S = 0.515\ \delta^{34}S$) in sulphides from Archean VMS deposits signifies that mass-independent fraction (MIF) signatures resulting from photolysis of atmospheric SO_2 are preserved in hydrothermal systems (Farquhar and Wing, 2003). The deviation from the MDF equation for sulphur isotopes (Fig. 2) provides a unique tracer of the involvement of surface processed (atmospheric-derived) sulphur in VMS deposits older than 2.45 Ga (e.g. Farquhar et al., 2010).

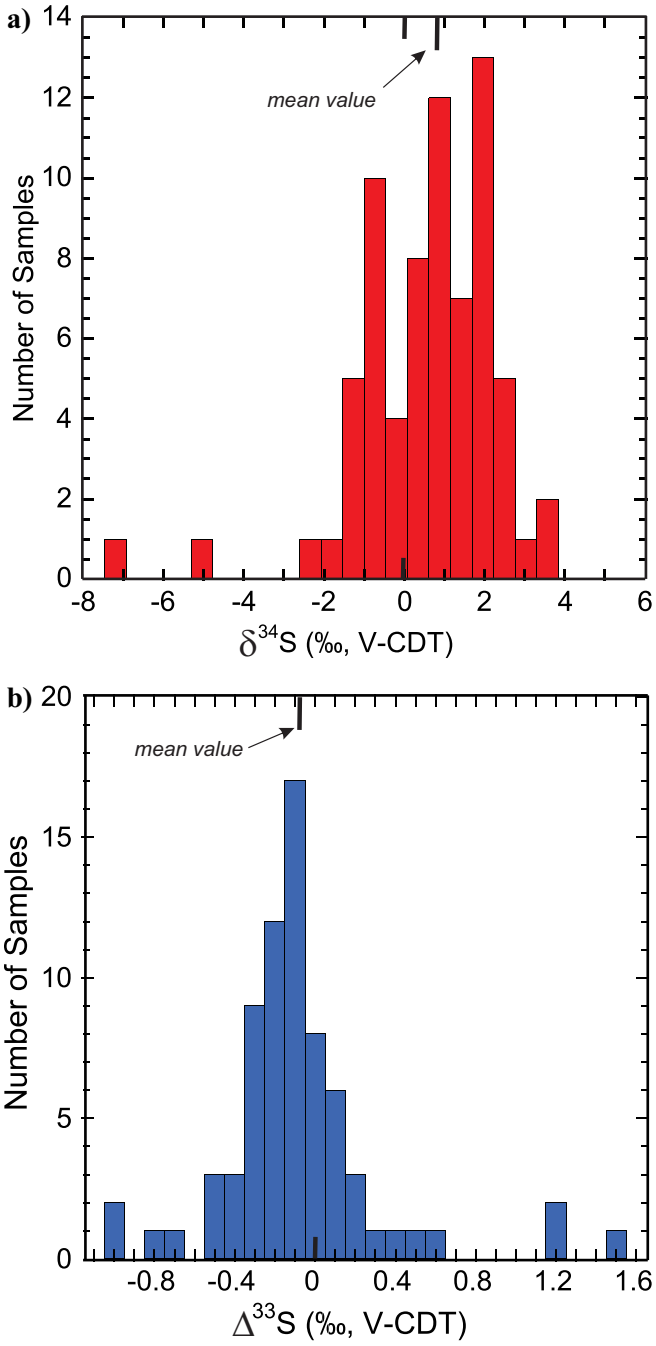

Figure 6. a) Histogram of $\delta^{34}S$ values (‰, V-CDT; n=72) of pure and mixed sulphide (a concentrate of pyrite, sphalerite, and/or galena; traces of other sulphides, or silicate possible in some samples) from volcanogenic massive sulphide (VMS) deposits in the Slave Province (this study). The mean $\delta^{34}S$ value (0.77‰) and range of $\delta^{34}S$ values are indicative of a dominance of mantle-dominated Archean sulphur. **b)** Histogram of Δ33S values (‰, V-CDT; n=72) of pure and mixed sulphide samples (as in Fig. 6a) from Slave Province VMS deposits depicts a normal distribution with a mean value of -0.08‰, and a range typical of rocks older than ca. 2.45 Ga (e.g. ± 1.0‰). Although the primitive mantle value ($\Delta^{33}S = 0$) dominates, incorporation of surface-derived sulphur (indicated by $\Delta 33S \neq 0$) is apparent in a significant number of the samples.

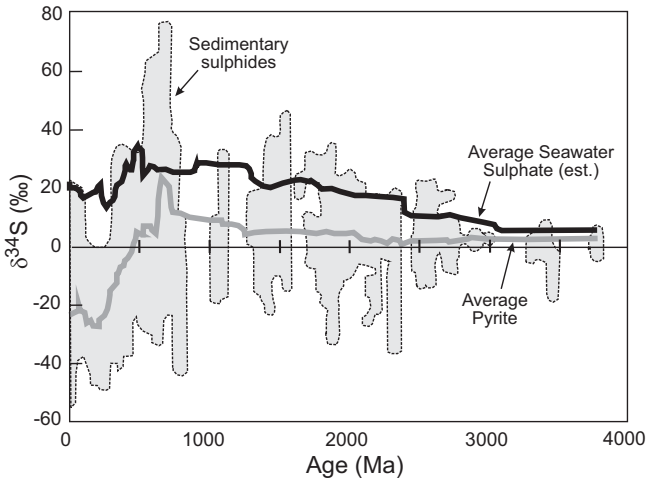

Figure 7. Plot of $\delta^{34}S$ versus age for both sulphides and sulphates. A running average composition of sulphide is shown by the gray curve, and for that of sulphate by the black curve (modified after Farquhar et al, 2010).

Archean seawater sulphate is thought to be characterized by rather homogeneous, negative values of $\Delta^{33}S$ (approximately -2‰; Zhelezinskaia et al., 2014), due to the low sulphate contents of Archean seawater, limited BSR, and mass balance considerations upon SO_2 photolysis (Farquar et al., 2000; Fig. 7). However, recent investigations of trace sulphate contained in marine carbonate (so-called carbonate-associated sulphate; CAS), have reported positive values of $\Delta^{33}S$ up to ~10‰ (Paris et al., 2014). Moreover, the apparent absence of large sulphur-isotope fractionations between sulphide and sulphate in Archean rocks has been accepted as an indication of limited microbial sulphate reduction (Zhelezinskaia et al., 2014).

Zhelezinskaia et al. (2014) report large negative values of $\delta^{34}S$ to approximately -40‰, with uniform negative values of $\Delta^{33}S$ in one carbonate unit, determined using secondary ion mass spectrometry (SIMS) that indicates marked bacterial sulphate reduction (BSR), despite very low aqueous sulphate levels. However, neither SO_2- nor SF_6-based techniques have yielded such negative $\delta^{34}S$ values for these same samples (lower limit of approximately -17‰), and this implies that there is high isotopic variability at the microscopic scale; SIMS and SF_6-based analyses are in good agreement for $\Delta^{33}S$ (Zhelezinskaia et al., 2014). The implications of this new finding are not yet fully understood. Although the incorporation in Archean sulphides of ^{33}S by MIF provides a clear atmospheric signal, the Archean sulphur cycle remains incompletely understood, including the preservation of an atmospheric $\Delta^{33}S$ signal during subsequent MDF processes.

All of the VMS deposits in the Slave Province sampled for this study (Fig. 1) satisfy the age criterion for

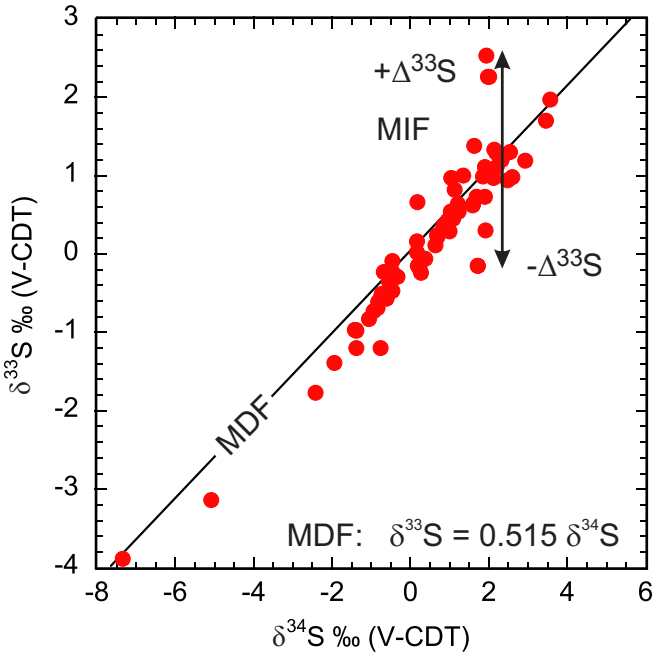

Figure 8. Plot of $\delta^{33}S$ versus $\delta^{34}S$ for pure pyrite, galena, sphalerite, or mixtures dominated by one of these minerals. Line for mass-dependent fractionation (MDF; $\Delta^{33}S = 0.515\ \delta^{34}S$) is shown for reference. Deviation from the MDF trend due to mass-independent fractionation (MIF) indicates variable, significant contributions of surficial (surface-processed) sulphur. Symbol size is approximately ten times larger than the uncertainty.

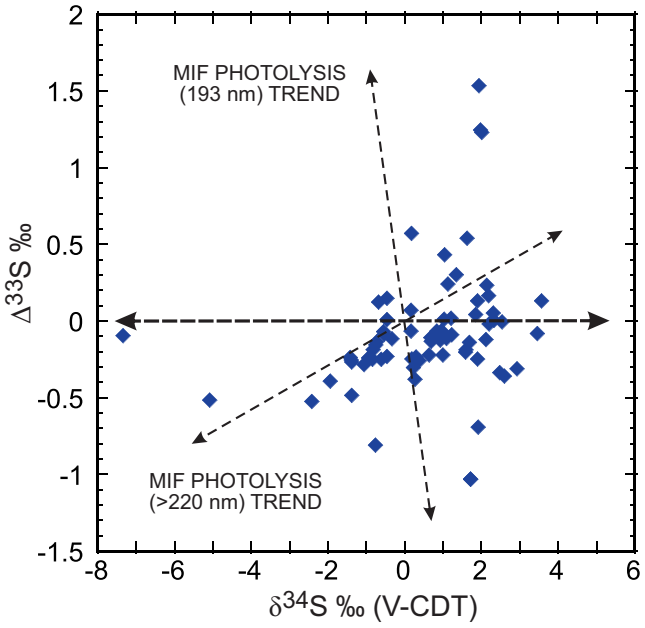

Figure 9. Plot of $\Delta^{33}S$ vs $\delta^{34}S$ for pure and mixed sulphides from Slave Province volcanogenic massive sulphide deposits analyzed in this study; the data indicate marked mass-independent fractionation (MIF), and mimic trends of experimental arrays based on photolysis experiments (after Farquhar and Wing, 2003). MIF trends for photolysis reactions in experiments using 193 nm wavelength and >220 nm wavelength light sources under low pressures of CO and O; other arrays are discussed in the text. The correspondence between the arrays and the Slave Province results is consistent with photolysis of Archean atmospheric SO_2 to explain the marked MIF.

effective use of $\Delta^{33}S$ to detect surficially processed sulphur. Our intent was to document any differences in $\delta^{34}S$ and $\Delta^{33}S$ among the deposits sampled, and if present, determine whether they correlate with isotopic markers of crustal age and provenance: Nd isotope line of Davis and Hegner (1992); Pb isotope line of Thorpe et al. (1992) (see Fig. 1). In addition, we investigated whether our data would have implications for the origin of VMS deposits in the Slave Province with regard to either their tectonic environments or their Ag contents.

Evidence and Assessment of Mass-Independent Fractionation in Slave Volcanogenic Massive Sulphide Deposits

Deviation of isotopic compositions from the MDF relationship ($\delta^{33}S = 0.515\ \delta^{34}S$) provides the criterion for MIF (see Fig. 8). Samples cover a broad range of $\delta^{33}S$ and $\delta^{34}S$, and some correspond to the above equation. However, both positive and negative deviations from the MDF equation, indicated by $+\Delta^{33}S$ and by $-\Delta^{33}S$, respectively, shown in Figure 8, demonstrate the clear presence of MIF in many samples. Zhelezinskaia et al. (2014) suggest that VMS deposits with $-\Delta^{33}S$ are likely an important sink for atmospheric sulphate. Complete thermal sulphate reduction (TSR) of dissolved marine sulphate with a $-\Delta^{33}S$ signature in the flow paths of circulating hydrothermal seawater fluids (Fig. 3) would result in reduced sulphur with negative $\Delta^{33}S$ values. When combined with magmatic sulphur (leached and/or degassed), the resulting VMS sulphides would have values of $\Delta^{33}S \leq 0‰$. Our data for sulphides from Slave VMS deposits (Fig. 8) are consistent with such a scenario for most samples. Galena from the Jo Zone at Hackett River is the most negative $\Delta^{33}S$ value (-0.810‰) recorded in our study.

Details regarding the origin of MIF of sulphur isotopes are still a matter of some debate. Photolysis experiments on SO_2 using ultraviolet light, particularly the 193 nm wavelength (Farquhar et al., 2001), demonstrate striking MIF effects, although other wavelengths may also be important (Farquhar and Wing, 2003; Paris et al., 2014). Reaction products include S° with lower $\delta^{34}S$ and higher $\Delta^{33}S$ than the initial SO_2; residual SO_2 and product sulphate have higher values of $\delta^{34}S$ and lower values of $\Delta^{33}S$. Comparison of $\Delta^{33}S$ and $\delta^{34}S$ for Slave Province VMS sulphides with experimentally determined fractionation trends for photolysis-induced MIF suggests a general agreement with a UV-photolysis origin (Fig. 9).

Sulphur Sources in Archean Volcanogenic Massive Sulphide Deposits of the Slave Province

The similarity in the topologies of the curves for the mean $\delta^{34}S$ values of sulphides in VMS deposits and marine sulphate versus age has influenced the variation (from greatest to least) inferred for role of seawater sulphate in VMS deposits in three different hypotheses: (1) incorporation by bacterial sulphate reduction by BSR (Sangster, 1968); (2) partial reduction of seawater sulphate by TSR, plus leaching of wall-rock sulphide (Sasaki, 1970); and (3) partial reduction of sulphate to sulphide, plus leaching of wall-rock sulphide during water/rock interaction in the "anhydrite buffer model" (Ohmoto et al., 1983). In the Archean, MIF sulphur isotope abundances in VMS deposits (i.e. $\Delta^{33}S \neq 0$) similarly provide seemingly incontrovertible evidence for incorporation of some surficial sulphur, despite estimates of the low concentration of sulphate in seawater (e.g. <80 ppm, or µmol/litre: Jamieson et al., 2013; <1000 ppm: Zhelezinskaia et al., 2014). Estimates of the amount of seawater sulphate incorporated in Archean VMS based on $\Delta^{33}S$ are low (≤3%: Jamieson et al., 2013; ≤25%: Sharman et al., in press; see also Ono et al., 2007), despite the assertion of Zhelezinskaia et al. (2014) that VMS deposits should constitute a significant sink for atmospheric sulphate.

Jamieson et al. (2013) document a maximum of 3% seawater sulphate in the giant Neoarchean Kidd Creek deposit based on multi-sulphur isotope data. Detailed multi-sulphur isotope analyses of VMS deposits in the ca. 2.7 Ga Noranda complex (Abitibi subprovince) by Sharman et al. (in press) concluded that both magmatic sulphur (directly contributed or leached) and surface-processed sulphur were incorporated in the sulphide mineralization. Magmatic sulphur is interpreted to have been the dominant sulphur source for the central Noranda camp VMS deposits, with the contribution of surficial sulphur increasing during evolution of the Noranda caldera. Deposits formed on the margin of the caldera contain <5% sulphur originating from seawater sulphate, whereas sulphide deposits that formed later in the caldera's evolution contain up to 25% (Sharman et al., in press). For comparison, Ono et al. (2007) used high-precision multi-sulphur isotope analysis to conclude that seawater sulphate contributes 11 to 27% of the sulphur comprising vent sulphides in the modern day TAG (Trans-Atlantic Geotraverse) hydrothermal field. The maximum estimated present-day seawater sulphate contribution (27%; Ono et al., 2007) is in good agreement with the maximum contribution (≤25%) estimated for VMS deposits in the Noranda caldera by Sharman et al. (in press), and consistent with the estimate of Jamieson et al. (2013) for the Archean Kidd Creek deposit. From this we infer that the dominant source of sulphur in the Slave Province VMS deposits is of magmatic (mantle) origin (i.e. $\delta^{34}S \approx 0$; $\Delta^{33}S \approx 0$). Although consistent with a direct magmatic origin (i.e. by magmatic degassing), Ono et al. (2007) demonstrated that 73 to 89% of the sulphur in the modern seafloor VMS system at TAG was derived by leaching from the underlying basalt during hydrothermal alteration. Derivation of all or the majority of sulphur in VMS from reduction of seawater sulphate is, thus, not required. Contributions of ~10 to 30% sulphur derived from seawater sulphate to VMS are sufficient to explain the topological similarity of the age versus $\delta^{34}S$ curves for both sulphur in VMS deposits (see Huston, 1999 and references therein) and seawater sulphate (Claypool, et al., 1980). Below, we consider the implications of variation in the contribution of seawater sulphate to Slave VMS deposits for their environment of formation.

Slave Province-Wide Variations in $\delta^{34}S$ and $\Delta^{33}S$

The values of $\delta^{34}S$ determined for VMS samples from the Slave Province are plotted on a geological base map of the province in Figure 10, which shows the age of basement rocks, geographic locations of greenstone belts, and , for reference, Pb- and Nd-isotope divisions/boundaries of the Slave crust. No correlations with any of these features are apparent. Figure 11 plots the $\Delta^{33}S$ ranges for sulphides from VMS deposits across the Slave Province on the same geological base map as in Figure 10. At the province-wide scale, there are no correlations apparent with the same features outlined above; however, any correlations would be complicated by the relatively narrow range of $\Delta^{33}S$ involved, the reconnaissance nature (possible non-representativeness) of our database, the relatively limited number of samples from each sample site, and the comparison of sulphide concentrates with pure minerals.

The lack of correlations of the ranges of $\delta^{34}S$ and $\Delta^{33}S$ with geographic location or geology indicates that processes and sulphur sources were similar in the formation of all of the Slave VMS deposits.

Relationships between $\delta^{34}S$ and $\Delta^{33}S$, Tectonic Setting, and Silver Contents in Selected Volcanogenic Massive Sulphide Deposits in the Slave Province

Two different tectonic settings were suggested by Bleeker and Hall (2007) for several of the VMS deposits analyzed in this study: an arc-like environment and a bimodal-rift environment (see Figs. 1 and 3). The tectonic styles and settings of Archean greenstone belts in general (and the VMS-hosting Slave greenstone belts specifically) remains a matter of some debate and uncertainty (e.g. Cawood et al., 2006). For most of the deposits discussed below and shown in

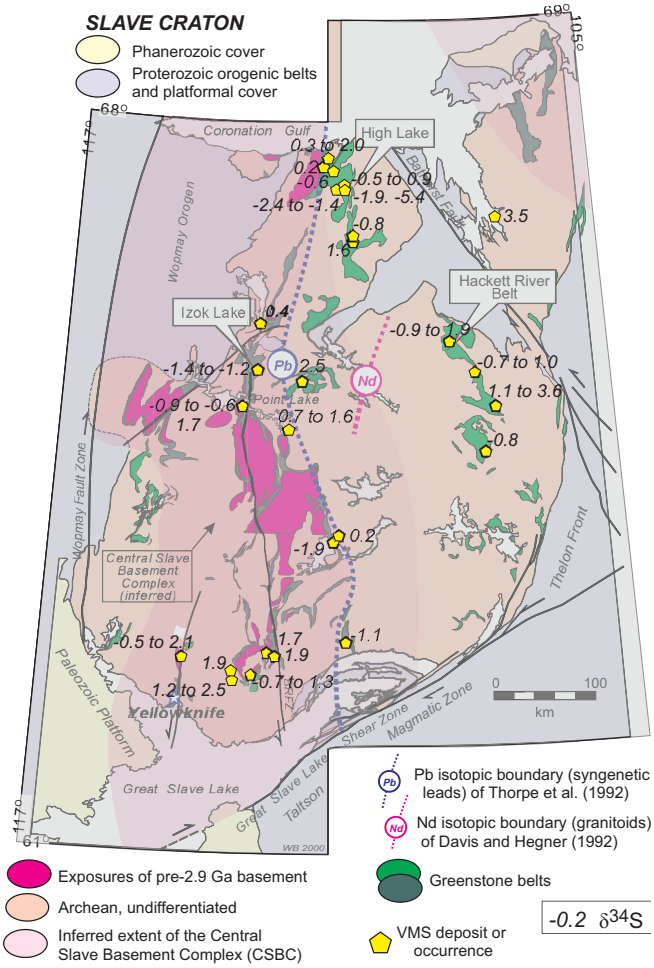

Figure 10. Map showing the distribution and, in some cases, range, of $\delta^{34}S$ values for pure and mixed sulphide samples from volcanogenic massive sulphide deposits in the Slave Craton. Although both mass-dependent fractionation (MDF) and mass-independent fractionation (MIF) processes played an important role in determining the $\delta^{34}S$ values plotted in this figure, a correlation between $\delta^{34}S$ and the age of crust, Pb isotope (Thorpe et al., 1992), and Nd isotope (Davis and Hegner, 1992) lines is not apparent. See Figure 1 for additional legend information.

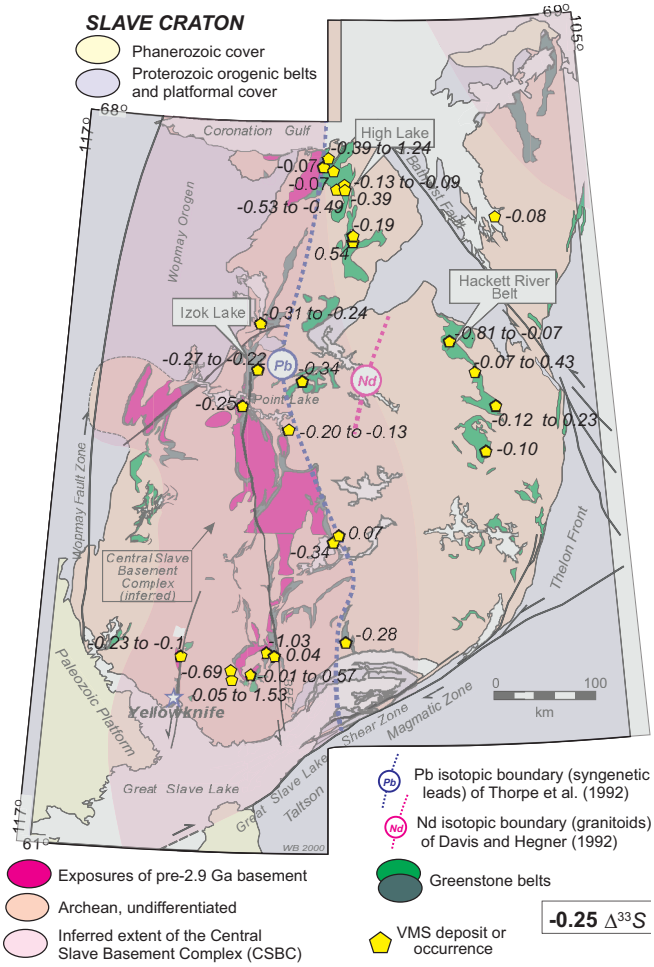

Figure 11. Map showing the distribution and (where applicable) range of $\Delta^{33}S$ for pure and mixed sulphide samples from VMS deposits in the Slave Craton. Correlations between $\Delta^{33}S$ and older crust, Pb isotope (Thorpe et al., 1992), and Nd isotope (Davis and Hegner, 1992) lines are not apparent. However, variations in $\Delta^{33}S$ may correlate with tectonic environment (see Fig. 12). See Figure 1 for additional legend information.

Figure 12, the "bimodal rift environment" of Bleeker and Hall (2007) corresponds with the 'bimodal-mafic" VMS deposit type of Franklin et al. (2005a,b), and the "arc-like" setting to their 'bimodal-felsic" VMS deposit type. The Gondor deposit (Bubar and Heslop, 1985) is the single exception to this general association among the deposits represented in Figure 12. The deposit is hosted by felsic pyroclastic and volcaniclastic rocks, and is situated ~1 km above a presumed heat-providing, felsic subvolcanic porphyry intrusion (Bubar and Heslop, 1985; Fig. 3). Bubar and Heslop (1985) suggested that a felsic caldera developed in response to extension and subsidence in the underlying mafic (oceanic) crust. The thickness of this mafic crust evidently prompted the deposit-type classification of bimodal-mafic (Franklin et al., 2005a,b).

Although the multiple sulphur isotope systematics of VMS deposits constituted our principal focus, we sought correlations with other significant characteristics of the deposits; silver was selected. In Figure 12, the contrasting silver grades of the deposits appear to broadly correspond to the classifications of "bimodal rift" (or bimodal-mafic) and "arc-like" (or bimodal felsic). VMS deposits from "arc-like" settings have grades of >100 g/t Ag; deposits include Hackett River (160–231 g/t), Musk (343 g/t), Sunrise Lake (172 g/t), and Turnback Lake (XL; 102 g/t), Indian Mountain (116.6 g/t), and Yava Lake (102 g/t) (Franklin et al., 2005b; Campbell, 2007). The Gondor and Izok Lake deposits are exceptions, with silver grades of 46 and 73 g/t, respectively (Franklin et al., 2005b; MMG Ltd., 2013). In contrast to most deposits in the "arc-like"

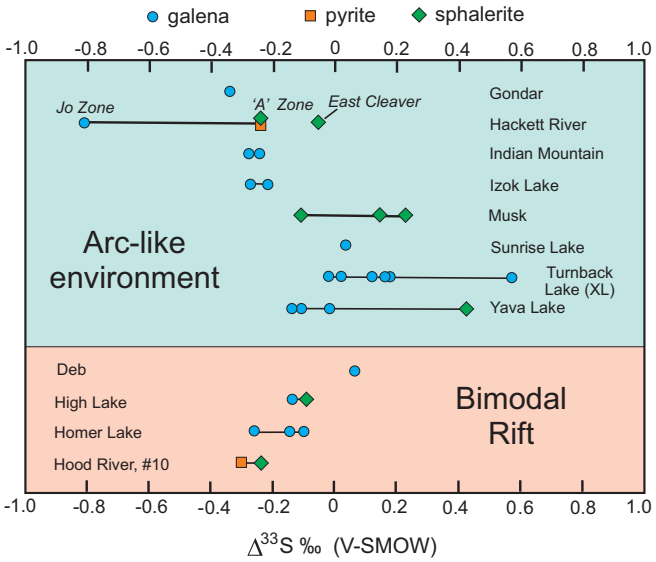

Figure 12. Comparison of $\Delta^{33}S$ values from selected VMS deposits, grouped according to their interpreted tectonic environment, as classified by Bleeker and Hall (2007). Deposits formed in arc-like environments (see sample location and index in Fig. 1) may be associated with a larger range of $\Delta^{33}S$ than observed for deposits formed in a bimodal-rift environment where mantle-derived sulphur appears to dominate. The large negative value of $\Delta^{33}S$ for the Jo zone at Hackett River is interpreted to be due to greater contributions of sulphur from reduced seawater sulphate.

environment, deposits in the "bimodal rift" category all have silver grades of <100 g/t. These include Deb (21.9 g/t), High Lake (75 g/t), Homer Lake (69.3 g/t), and Hood #10 (34 g/t) (Franklin et al., 2005b; TerraX, 2015). Thus, the two general tectonic settings distinguished in Figure 12 typically also correspond to contrasts in silver grades and magmatic association (bimodal-mafic versus bimodal-felsic), which may suggest a connection with magma genesis (e.g. juvenile character) and evolution (e.g. fractional crystallization versus crustal melt). Nevertheless, the tectonic environments in which these VMS deposits formed (and associated host rock/magma compositions), also have influenced the sulphur isotope systematics of the deposits.

Our limited database shows that VMS deposits in the bimodal rift (bimodal-mafic) environment display a restricted range of $\Delta^{33}S$, primarily -0.2 to 0‰ (Fig. 12). In contrast, VMS deposits in "arc-like" tectonic environments display a broader range of $\Delta^{33}S$ values, spanning -0.8 to 0.6‰. Although our study is reconnaissance in nature, and additional information regarding the tectonic settings of all of the deposits analyzed is needed, the relationship in Figure 12 suggests that there may be differences in factors influencing the involvement of atmosphere-derived sulphur in these two tectonic environments. For example, VMS deposits formed in bimodal rift/bimodal-mafic rift environments may represent deeper water settings associated with high-temperature mafic magmatism. The values of $\Delta^{33}S$ plotted in Figure 12 suggest minimal sulphur contributions from other than mantle sources, whether directly (i.e. magmatic degassing) or indirectly (e.g. leached from mantle rocks during alteration processes). However, VMS deposits in arc-like settings appear to have a larger range of $\Delta^{33}S$, including both positive and negative values, indicating the incorporation of some atmosphere-derived sulphur. These environments could include slightly younger, and more evolved magmatism in the arc-like setting (see Bleeker and Hall, 2007), increased diversity of (more-evolved) host rocks, and shallow-water (perhaps even subaerial) volcanism and settings. The arc-like (bimodal-felsic) environment evidently facilitated the increased incorporation of MIF sulphur, potentially involving additional surface sources as well as crustal (via hydrothermal recycling; see Fig. 3). Note, however, that the correspondence of higher Ag contents with greater contributions of MIF sulphur is only apparent (and due to geological association) and not causative. Nevertheless, the recognition of VMS mineralization with relatively greater amounts of atmospheric sulphur through multi-sulphur isotope analysis may prove useful in paleotectonic setting and volcanic environment determination and terrain assessment in greenfields VMS exploration.

IMPLICATIONS FOR EXPLORATION

The potential correlation between environment and factors promoting precious metal enrichment (e.g. redox conditions) suggests that further study and application of multi-sulphur isotope analysis will broaden our understanding of important aspects of deposit genesis. Although detection (and quantification) of MIF sulphur is not likely to constitute a camp-scale "vector", it may assist in comparison and selection of potential precious metal-rich VMS environments for further exploration.

SUMMARY AND CONCLUSIONS

Volcanogenic massive sulphide deposits throughout the Slave Province contain variable contributions of atmosphere-derived (i.e. surface-processed) sulphur based on the values and ranges of $\Delta^{33}S$ determined in this study. Moreover, the contrast in two principal tectonic environments hosting VMS deposits appears to be also reflected by both the silver grades of the deposits and their sulphur isotope systematics, particularly the contributions of atmospheric sulphur. Assessment of paleotectonic settings and volcanic environments and mineralization processes can benefit from multi-sulphur isotope studies.

FUTURE WORK

Comparison with multi-sulphur isotope studies elsewhere, a broader assessment of metal and Pb isotope ratios, and analysis of the tectonic environments of each deposit remain as goals for this study. The unique significance of $\Delta^{33}S$ as a definitive tracer of Archean atmospheric sulphur demands a detailed study of one or several selected deposits in the Slave Province. Such a study would provide a better understanding of (1) the timing of acquisition of $\Delta^{33}S$ anomalies, (2) a better assessment of the balance of magmatic versus environmental sulphur sources, and (3) improved assessment of the apparent association of MIF with tectonic environment. The study of Sharman et al. (in press) in Noranda, Quebec suggests that small shifts in $\Delta^{33}S$ are controlled by the local geological environment and may be associated with the precious metal (gold) contents. The use of $\Delta^{33}S$ as a potential tracer in Archean VMS studies can also be applied to younger VMS deposits in comparable settings, but requires exceptionally high-precision techniques (Ono et al., 2007). The unique tracing capabilities due to MIF sulphur in the Archean makes detailed studies of Archean VMS deposits by the techniques employed in this study more tractable. Constraints and processes determined by studies of ancient deposits would apply to younger examples.

ACKNOWLEDGEMENTS

This study could not have been completed without the legacy collections of Ralph Thorpe, which were carefully archived by the Geological Survey of Canada. Anne Theriault kindly facilitated their access. Andre Pellerin and Thi Hao Bu are thanked for assisting with various technical aspects of this study, especially in testing of the gas chromatograph-based sample purification line added to MILES. We thank J. Jamieson for a review of this contribution.

REFERENCES

Bleeker, W. and Hall, B., 2007. The Slave Craton: geological and metamorphic evolution, *In:* Mineral Deposits of Canada: A Synthesis of Major Deposit Types, District Metallogeny, the Evolution of Geological Provinces, and Exploration Methods, (ed.) W.D. Goodfellow; Geological Association of Canada, Mineral Deposits Division, Special Publication 5, p. 849–879.

Bubar, D.S. and Heslop, J.B., 1985. Geology of the Gondor volcanogenic massive sulphide deposit, Slave Province, NWT; Canadian Institute of Mining and Metallurgy Bulletin, v. 78, p. 52–60.

Campbell, C. (ed.), 2007. A guide to mineral deposits of the Northwest Territories; Department of Industry, Tourism and Investment, 206 p.

Cawood P.A., Kröner A., and Pisarevsky S., 2006. Precambrian plate tectonics: Criteria and evidence; GSA Today, v. 16, p. 4–11.

Claypool, G.E., Holser, W.T., Kaplan, I.R., Sakai, H., and Zak, I., 1980. The age curve of sulphur and oxygen isotopes in marine sulfate and their mutual interpretation; Chemical Geology, v. 28, p. 199–260.

Davis, W.J. and Hegner, E., 1992. Neodymium isotopic evidence for the tectonic assembly of late Archean crust in the Slave Province, Northwest Canada; Contributions to Mineralogy and Petrology, v. 111, p. 493–504.

Farquhar, J., Bao, H., and Thiemens, M., 2000. Atmospheric influence of Earth's earliest sulfur cycle; Science, v. 289, p. 756–758.

Farquhar, J., Savarino, J., Airieau, S., and Thiemens, M., 2001. Observation of wavelength-sensitive mass-independent sulfur isotope effects during SO_2 photolysis: Implications for the early atmosphere; Journal of Geophysical Research, v. 106, p. 32829–32839.

Farquhar, J. and Wing, B.A., 2003. Multiple sulfur isotopes and the evolution of the atmosphere; Earth and Planetary Science Letters, v. 6707, p. 1–13.

Farquhar, J., Wu, N., Canfield, E.D., and Oduro, H., 2010. Connections between sulfur cycle evolution, sulfur isotopes, sediments, and base metal sulfide deposits: Economic Geology, v. 105, p. 509–533.

Franklin, J.M., Gibson, H.L., Jonasson, I.R., and Galley, A.G., 2005a. Volcanogenic massive sulfide deposits, *In:* Economic Geology 100th Anniversary Volume, (ed.) J.W. Hedenquist, J.F.H. Thompson, R.J. Goldfarb, and J.P. Richards; Society of Economic Geologists, Littleton, Colorado, p. 523–560.

Franklin, J.M., Gibson, H.L., Jonasson, I.R., and Galley, A.G., 2005b. Volcanogenic massive sulfide deposits, *In:* Economic Geology 100th Anniversary Volume, (ed.) J.W. Hedenquist, J.F.H. Thompson, R.J. Goldfarb, and J.P. Richards; Society of Economic Geologists, Littleton, Colorado, p. 1-45.

Holland, H.D., 2006. The oxygenation of the atmosphere and oceans; Philosophical Transactions of the Royal Society B: Biological Sciences, v. 361, p. 903–915.

Huston, D.L., 1999. Stable isotopes and their significance for understanding the genesis of volcanic-hosted massive sulfide deposits, *In:* Volcanic-Associated Massive Sulfide Deposits: Processes and Examples in Modern and Ancient Settings, (ed.) C.T. Barrie and M.D. Hannington; Reviews in Economic Geology, v. 8, p. 157–179.

Jamieson, J.W., Wing, B.A., Farqhuar, J., and Hannington, M.D., 2013. Neoarchaean seawater sulphate concentrations from sulphur isotopes in massive sulphide ore; Nature Geoscience, v. 6, p. 61–64.

MMG Ltd., 2013. Annual Report, 164 p. http://www.mmg.com/en/Investors-and-Media/Reports-and-Presentations/Annual-Reports.aspx

Ohmoto, H., Mizukami, M., Drummond, S.E., Eldridge, C.S., Pisutha-Arnond, V., and Lenaugh, T.C., 1983. Chemical processes in Kuroko formation, *In:* The Kuroko and Related Volcanogenic Massive Sulfide Deposits, (ed.) H. Ohmoto and B.J. Skinner; Economic Geology, Monograph 5, p. 570–604.

Ohmoto, H., Watanabe, Y., Ikema, H., Poulson, S.R., and Taylor, B.E., 2006. Sulphur isotope evidence for an oxic Archaean atmosphere; Nature, v. 442, p. 908–911.

Ono, S., Shanks, W.C., III, Rouxel, O.J., and Rumble, D., 2007. S33 constraints on the seawater sulfate contribution in modern seafloor hydrothermal vent sulfides; Geochimica et Cosmochimica Acta, v. 71, p. 1170–1182.

Paris, G., Adkins, J.F., Sessions, A.L., Webb, S.M., and Fischer, W.W., 2014. Neoarchean carbonate-associated sulfate records positive anomalies; Science, v. 346, p. 739–741.

Planavsky, N.J., Asael, D., Hofmann, A., Reinhard, C.T., Lalonde, S.V., Knudsen, A., Wang, X., Ossa, F.O., Pecoits, E., Smith, A.B.J., Beukes, N.J., Bekker, A., Johnson, T. M., Konhauser, K.O., Lyons, T.W., and Rouxel, O.J., 2014. Evidence for oxy-

genic photosynthesis half a billion years before the Great Oxidation Event; Nature Geoscience v. 7, p. 283–286.

Pufahl, P.K. and Hiatt, E.E., 2012. Oxygenation of the Earth's atmosphere-ocean system: A review of physical and chemical sedimentological responses; Marine and Petroleum Geology, v. 32, p. 1–20.

Sasaki, A., 1970. Seawater sulfate as a possible determinant for sulfur isotopic compositions of some strata-bound sulfide ores; Geochemical Journal, v. 4, p. 41–51.

Sangster, D.F., 1968. Relative sulphur isotope abundances of ancient seas and strata-bound sulphide deposits, *In:* Proceedings; Geological Association of Canada, v. 19, p. 79–91.

Sharman, E.R., Taylor, B.E., Minarik, W.G., Dubé, B., and Wing, B.W., in press. Sulfur isotope and trace element data from ore sulfides in the Noranda district (Abitibi, Canada): implications for volcanogenic massive sulfide deposit genesis; Mineralium Deposita.

Taylor, B.E., 2004. Fluorination methods in stable isotope analysis, Chapter 20 *In:* Handbook of Stable Isotope Analytical Techniques, Volume 1, (ed.) P.A. de Groot; Elsevier Science, p. 400–472.

Terra X, 2015. prospectus, available at http://www.terraxminerals.com/s/Home.asp

Thorpe, R.I., 2008. Release of lead isotope data in 4 databases: Canadian, Western Superior, foreign, and whole rock and feldspar; Geological Survey of Canada, Open File 5664, 42 p.

Thorpe, R.I., Cumming, G.L., and Mortensen, J.K., 1992. A significant Pb isotope boundary in the Slave Province and its probable relation to ancient basement in the western Slave Province; Geological Survey of Canada, Open File Report 2484, p. 179–184.

Zhelezinskaia, I., Kaufman, A.J., Farquhar, J., and Cliff, J., 2014. Large sulfur isotope fractionations associated with Neoarchean microbial sulfate reduction; Science, v. 346, p. 742–744.

GEOLOGICAL SURVEY OF CANADA
OPEN FILE 7853

Targeted Geoscience Initiative 4: Contributions to the Understanding of Volcanogenic Massive Sulphide Deposit Genesis and Exploration Methods Development

LA-ICP-MS analysis of volatile trace elements in massive sulphides and host rocks of selected VMS deposits of the Bathurst Mining Camp, New Brunswick: methodology and application to exploration

Azam Soltani Dehnavi, David R. Lentz, and Christopher R.M. McFarlane

[1]University of New Brunswick, Fredericton, New Brunswick

2015

Recommended citation

Soltani Dehnavi, A., Lentz, D.R., and McFarlane, C.R.M., 2015. LA-ICP-MS analysis of volatile trace elements in massive sulphides and host rocks of selected VMS deposits of the Bathurst Mining Camp, New Brunswick: methodology and application to exploration, *In:* Targeted Geoscience Initiative 4: Contributions to the Understanding of Volcanogenic Massive Sulphide Deposit Genesis and Exploration Methods Development, (ed.) J.M. Peter and P. Mercier-Langevin; Geological Survey of Canada, Open File 7853, p. 59–80.

Publications in this series have not been edited; they are released as submitted by the author.

Contribution to the Geological Survey of Canada's Targeted Geoscience Initiative 4 (TGI-4) Program (2010–2015)

TABLE OF CONTENTS

Tables

LA-ICP-MS analysis of volatile trace elements in massive sulphides and host rocks of selected VMS deposits of the Bathurst Mining Camp, New Brunswick: methodology and application to exploration

Azam Soltani Dehnavi*, David R. Lentz†, and Christopher R.M. McFarlane‡

Department of Earth Sciences, University of New Brunswick, Fredericton, New Brunswick E3B 5A3
*Author's e-mail: azam.soltani@unb.ca
†Author's e-mail: dlentz@unb.ca
‡Author's e-mail: crmm@unb.ca

ABSTRACT

The application of volatile trace element contents of pyrite, chlorite, and white mica in selected polymetallic Zn-Pb-Cu-Ag volcanogenic massive sulphide (VMS) deposits of the Bathurst Mining Camp, northern New Brunswick (Armstrong A, Brunswick No. 12, Canoe Landing Lake, Halfmile Lake Deep Zone, Key Anacon, Louvicourt, and Restigouche) as a vectoring tool in VMS exploration has been investigated. In situ volatile trace element contents (As, Cd, Hg, In, Sb, Tl, etc.) were determined by laser ablation inductively coupled plasma mass spectrometry (LA-ICP-MS). Pyrite is a ubiquitous sulphide in altered host rocks to VMS mineralization and can accommodate a wide range of volatile trace elements. Most analyzed pyrite grains are arsenian with As contents up to 7.3 wt%, Sb (up to 2910 ppm), Tl (up to 4110 ppm), Au (up to 73.2 ppm), Hg (up to 220 ppm), In (up to 49 ppm), and Cd (up to 270 ppm). Variations in the spot chemical compositions of pyrite in stratigraphic profiles of the examined deposits reveal distinct volatile trace element features. Pyrite in the footwall alteration zones typically displays systematically increasing volatile trace element contents with decreasing distance stratigraphically upward to the ore horizon. However, in the hanging-wall alteration zones, there are no consistent pyrite chemical compositional trends. Pyrite in the hanging wall of some deposits, such as Brunswick No. 12, Canoe Landing Lake, Restigouche, and Key Anacon, show high As in the upper portions and, to a lesser extent, higher abundances of other volatile trace elements. Volatile element contents of chlorite and white mica (muscovitic to phengitic in composition) indicate that these elements are crystal lattice-bound. White mica typically contains As (up to 1.01 wt%), Sb (up to 4750 ppm), Tl (up to 698 ppm), In (up to 563 ppm), Hg (up to 67 ppm), Cd (up to 83 ppm), and Bi (up to 185 ppm). In comparison to white mica, chlorite is preferentially enriched in Cd (0.07–420 ppm) and Bi (0.02–185 ppm). The spot LA-ICP-MS analyses of chlorite and white mica demonstrate that volatile trace element contents of hanging-wall- and footwall-altered rocks increase with decreasing distance toward mineralization.

Our data indicate that pyrite, chlorite, and white mica are the residence sites of significant abundances of volatile trace elements, in particular As, Sb, Tl, Bi, and to lesser extent Cd, In, and Hg. Therefore, these minerals can serve as the primary widespread dispersal proxies for volatile elements in the studied drillholes. Systematic trends in volatile trace element distribution patterns in pyrite, chlorite, and white mica can be used to vector toward VMS mineralization in the Bathurst Mining Camp. This methodology may be applicable in other areas where polymetallic deposits occur, and may complement other geochemical and geophysical exploration methods.

INTRODUCTION

The world-class Zn-Pb-Cu-Ag volcanogenic massive sulphide (VMS) deposits of the Bathurst Mining Camp (BMC), northern New Brunswick, are hosted by Middle Ordovician bimodal volcanic and sedimentary rocks, which have undergone complex polyphase deformation and associated lower- to upper-greenschist- and locally blueschist-facies regional metamorphism. Deformation and metamorphism occurred primarily during closure of the Tetagouche-Exploits back-arc basin in the Late Ordovician to Early Silurian (Salinic Orogeny) and Late Silurian Acadian Orogeny (Goodfellow and McCutcheon, 2003).

The volatile trace elements of interest in this study belong to the siderophile element group (As, Sb, Tl, and Bi) and the chalcophile element group (Cd, Hg,

Soltani Dehnavi, A., Lentz, D.R., and McFarlane, C.R.M., 2015. LA-ICP-MS analysis of volatile trace elements in massive sulphides and host rocks of selected VMS deposits of the Bathurst Mining Camp, New Brunswick: methodology and application to exploration, *In:* Targeted Geoscience Initiative 4: Contributions to the Understanding of Volcanogenic Massive Sulphide Deposit Genesis and Exploration Methods Development, (ed.) J.M. Peter and P. Mercier-Langevin; Geological Survey of Canada, Open File 7853, p. 59–80.

and In). The volatile trace elements, particularly Hg, are potential pathfinders (lithogeochemical vectors within bounding host rocks) in geochemical prospecting for a wide variety of base- and precious-metal deposits. Primary and secondary dispersion haloes of volatile trace elements can be used for detecting buried mineralization (Ryall, 1981; Carr et al., 1986). The distributions of some volatile trace elements in VMS deposits of the BMC deposits have been reported previously (Goodfellow, 1975; Chen, 1978; Jambor, 1979, 1981; Luff et al., 1992; Lentz and Goodfellow, 1993, 1996; Lentz et al., 1997; Goodfellow and McCutcheon, 2003; McClenaghan et al., 2003, 2004, 2006, 2009; Peter et al., 2003a,b; McLellan et al., 2006; Walker and Lentz, 2006). The contents of these elements have been shown to be highly variable among the four time-stratigraphic ore horizons (Stratmat, Brunswick, Caribou, and Chester) in the BMC (Goodfellow and McCutcheon, 2003). The whole-rock analyses of Louvicourt samples exhibit atypically high contents of volatile elements Sb, Hg, and Tl (McClenaghan et al., 2006). The contents of some volatile trace elements in sulphides from the Brunswick No. 12 deposit have been previously determined by laser ablation inductively coupled plasma mass spectrometry (LA-ICP-MS) (McClenaghan et al., 2009). The volatile element contents of sedimentary rocks in the BMC have also previously been reported (Peter et al., 2003a,b). To date, however, there has been no comprehensive volatile trace element assessment of sulphide and silicate minerals in the BMC.

Herein we present a synopsis of the volatile trace element characterization of representative major deposits of the BMC (Armstrong, Brunswick No. 6 and No. 12, Caribou, Canoe Landing Lake, Halfmile Lake deep zone, Heath Steele B zone, Key Anacon, Louvicourt, and Restigouche). The deposits were selected based on their geological and exploration significance and because they have been previously well sampled and described. The volatile element composition of pyrite (the most abundant disseminated sulphide mineral in the stratigraphic footwall and hanging wall of the deposits), chlorite and white mica (muscovitic to phengitic in composition) were analyzed by LA-ICP-MS. This technique provides in situ measurement capabilities, high spatial resolution sampling, low detection limits, use of standard polished thin sections (no special sample preparation required), and cost efficiency (hundreds of analyses per day). The methodology development included an assessment of optimized ablation conditions, choice of external and internal standards, and data-reduction strategies.

The main objectives of this study are (1) to present the optimal methodology for analyzing volatile trace element contents of pyrite, chlorite, and white mica by LA-ICP-MS; (2) to characterize hydrothermal up-flow zones in studied drillholes in order to discriminate samples that are proximal to the sulphide horizons from those more distal (i.e. dispersion haloes); (3) to present mineral (sulphides and silicates) geochemical exploration vectoring tools that can be applied specifically to the BMC and to present approaches that can be used elsewhere.

METHODOLOGY

Optical Microscopy

Detailed optical microscopic (reflected and transmitted light) examination of polished thin sections is a prerequisite to in situ LA-ICP-MS analysis of pyrite and phyllosilicate minerals. Since LA-ICP-MS is a destructive technique, imaging of the samples prior to analysis is required. The fine-grained nature of the samples that were investigated in this study necessitated documentation of mineral textures and their relationship with coexisting phases. In order to yield meaningful results, sampling points (ablation spots) were selected to preclude sampling multiple phases simultaneously or phases with visible inclusions. Although inclusions may occur in subsurface at the micro- to nano-scale within the volume of material ablated, the former is readily detectable in the laser ablation time-series and can subsequently be omitted from the integrated spectra.

Laser Ablation Inductively Coupled Plasma Mass Spectrometry

The analyses were performed in the Department of Earth Sciences, University of New Brunswick, using a Resonetics Resolution™ M-50 193 nm ArF (excimer) laser system connected to an Agilent 7700X quadrupole inductively coupled plasma mass spectrometer (Q-ICP-MS) equipped with dual external rotary pumps. The instruments have a dedicated high-capacity (up to 20 L/min) Hg trap on all of the gas lines that enter the laser and ICP-MS. This allowed background ^{202}Hg gas to remain <1200 count per second (cps) under the highest sensitivity conditions. Modifications to standard analytical protocols were required in this study, and this included an assessment of optimized ablation conditions (laser sampling and energy density), choice of external and internal standards, and data-reduction strategies.

Analyses of pyrite were carried out in spot mode, and laser crater diameters of 17, 24, and 33 μm were selected on the basis of textural criteria, thickness of the polished sections, and necessary analytical precision and detection limits. The laser was operated at a repetition rate of 3 or 4 Hz, with the laser fluence held at ~1 J/cm^2 (see Table 1 for more information about the instrument operating conditions). Standard-sample

Table 1. Operating conditions for the LA-ICP-MS instrumentation used in this study.

ICP MS Agilent 7700x tuning	
RF power	1550 W
Torch depth	5.0 mm
Oxide production	ThO^+/Th^+ <0.3%
Double-charged production	$^{22}M^{++}/44Ca^+$ <0.3%
Ionization efficiency	$^{238}U^+/^{232}Th^+$ ~1.05

Laser ablation Resonetics S-155	
Type	193 nm excimer (20 ns pulse)
	LA condition for sulphides
Crater diameter	17-24-33 µm
Repetition rate	4-3 Hz
Fluence	~1 J/cm^2
Background time	40–120 s
Ablation time	40 s
Total time per spot	1.3–2.7 min
In-cell gas carrier	350 mL/min He and 960 mL/min Ar
N_2	2.0 mL/min
Type	LA condition for silicate
Crater diameter	66 µm
Repetition rate	4 Hz
Fluence	~1 J/cm^2
Background time	40 s
Ablation time	40 s
Total time per spot	80 s
In-cell gas carrier	325 mL/min He 960 mL/min Ar
N_2	2.0 mL/min

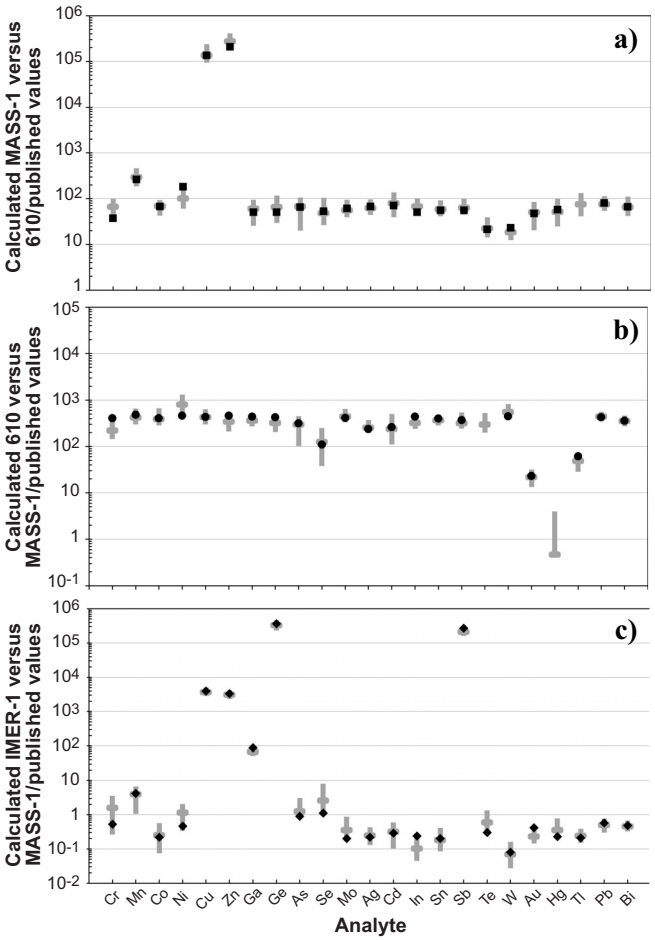

Figure 1. Assessment of the accuracy of data obtained from calculation of standards (MASS-1, NIST610, and IMER-1) analyzed along with pyrite samples. The average calculated values are compared to the published values for each standard. Plots show similar values for most of the elements. Internal standardization was obtained from the data published for the MASS-1, NIST610 (Fe), and IMER-1 (S) standards. Grey bars show the range of the examined elements (minimum and maximum).

bracketing and external calibration was performed using USGS MASS-1 (Wilson et al., 2002). For quantification of pyrite, Fe was selected as the internal standard (stoichiometric value). Data deconvolution was done offline using the Iolite™ 2.5 trace element data reduction scheme (Paton et al., 2011). Iolite has the ability to visualize the ion beam intensities against time and select portions of ablated signals to avoid transient signals related to inclusions or other heterogeneities. We also demonstrated that matrix-mismatching effects, such as using NIST610 (a Ca-Na-Si glass) as a standard to calculate element contents in MASS-1, were not a significant problem.

The MASS-1 standard was analyzed over 300 times over the course of one year and its calibration against NIST610 glass, using Fe as the internal standard, yielded average values that are close to the published values (Fig. 1a; Table 2). By analogy, under the same analytical conditions, the average contents obtained for NIST610 standardized against MASS-1, again using Fe as the internal standard, displayed very close correspondence to the reported values (Fig. 1b; Table 2). By using this approach, a wider calibration range is attained, and elements for which no certified values exist (such as Hg and Te in NIST610 glass, and Tl in MASS-1) can be rigorously assessed (Table 3). The informational values were added to the standard definitions (Soltani Dehnavi et al., 2014e).

The fine-grained nature of the chlorite and white mica and the presence of fine-grained quartz and pyrite, especially in association with white mica, made selection of ablation spots critically important (Fig. 2). One of the important features of LA-ICP-MS analysis is the ability to determine whether the elements occur in the mineral lattice or within micro-inclusions of other minerals. Lattice substitution of volatile trace elements in chlorite and white mica is indicated by the presence of a flat profile in the single-spot LA-ICP-MS data (Fig. 3). A beam diameter of 66 µm was used for spot analyses of chlorite and white mica. Silicon (stoichiometric values) was selected as the internal standard for quantification of white mica and chlorite. Data were corrected using NIST610 as an external standard. There are no certified Hg and Te values reported for

Table 2. Summary of obtained compositional variations of MASS-1, NIST 610, and IMER-1 in this study (ppm).

	Calculated NIST 610_Fe (n>300)				**Calculated MASS-1_Fe** (n>300)				**Calculated IMER-1 vs. MASS1_S** (n=60)			
Analyte	Min	Mean	Max	Published	Min	Mean	Max	Published	Min	Mean	Max	Suggested
Cr	165	224	380	405	41.9	67.3	89	37	0.31	1.62	3	0.53
Mn	337	423	580	485	212	298	405	260	1.25	4.05	5.6	4.20
Co	325	394	590	405	48	69.3	82.7	67	0.09	0.26	0.48	0.22
Ni	640	806	1160	459	68.4	102	125	180	0.4	1.16	1.73	0.46
Cu	338	428	560	430	107100	137102	209000	134000	3349	3695	4310	3930
Zn	241	346	429	456	202000	278297	361800	207383	2755	3150	3540	3328
Ga	310	361	465	438	29.1	60.7	83.1	50	60.6	68.4	82	87.8
Ge	232	324	430	426	33.7	66.0	102	50	276900	337552	383900	365500
As	115	300	396	317	22.8	67.9	93	65	BDL	1.25	2.6	0.90
Se	43	126	220	109	30	48.6	92	53	BDL	2.63	6.8	1.12
Mo	375	444	570	410	44.6	56.7	83	61	BDL	0.36	0.74	0.20
Ag	221	257	328	239	50.1	63.3	85	67	0.15	0.25	0.36	0.22
Cd	125	242	440	259	44.7	80.7	120	70	0.12	0.33	0.50	0.29
In	270	323	377	441	53.6	68.3	87.1	50	0.05	0.10	0.16	0.24
Sn	321	371	429	396	47.1	59.0	81	55	0.1	0.19	0.35	0.20
Sb	276	318	480	369	50.5	64.4	89.2	55	189600	216600	257200	269200
Te	224	302	460		16.4	22.4	34.5	21	BDL	0.60	1.12	0.30
W	468	552	720	445	14.2	18.6	22.7	23	0.03	0.07	0.14	0.08
Au	15.1	21.9	28.2	23	23.0	51.1	74	47	0.17	0.24	0.29	0.42
Hg	BDL	0.47	3.5		28.1	52.0	89	57	BDL	0.36	0.67	0.23
Tl	32.4	49.2	60.1	61	46.7	76.2	116		0.18	0.25	0.33	0.21
Pb	405	449	494	426	61.5	76.4	99.7	80	0.36	0.51	0.64	0.58
Bi	310	359	409	358	47.3	66.3	98	66	0.39	0.47	0.56	0.48

NOTE: BDL = below detection limit

NIST610; therefore, as described above, the informational values of NIST610 established as part of this study were used (Table 3) Table 1 contains additional information about the operating conditions of the instrument (Soltani Dehnavi et al., 2014f).

Accuracy and Precision

To evaluate the accuracy of the analyses, the element contents of each standard and pyrite were analyzed, the data reduced, and the results were compared to the published values; MASS-1 was calibrated against the external standard NIST610 and vice versa (Table 2). Iron was selected as an internal standard based on published values for each standard ($Fe_{MASS\text{-}1}$=15.6 wt% and $Fe_{NIST610}$=0.045 wt%). The average values obtained are in good agreement with the published data (Fig. 1a,b). In order to assess the reproducibility of this methodology, results obtained for IMER-1 (as consistency standard) were compared to the suggested values (see Ding et al., 2011). Element values for IMER-1 were then calculated against MASS-1 using S as the internal standard. The results demonstrate an acceptable degree of consistency and reproducibility with a range of accuracy and precision of less than 10% for most elements (Fig. 1c, Table 2). The relationships between the calculated values for standards and published values are shown in binary plots in Figure 4, with the best agreement for IMER-1 and MASS-1, whereas the poorest agreement is with NIST610.

Data quality monitoring for phyllosilicate minerals was conducted using the approach described above. NIST610 was calibrated against the external standard

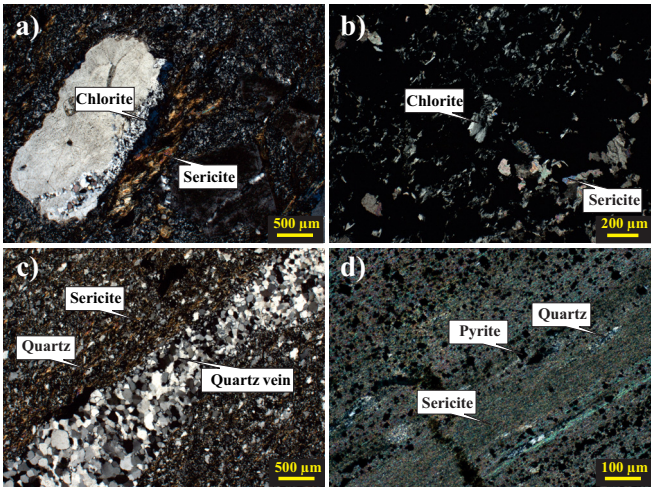

Figure 2. Photomicrographs (crossed-polars) of representative host-rock samples from the BMC. **a)** Fe-chlorite (chlorite) and white mica (sericite) (drillhole HN-119 @ 308': Halfmile Lake Deep Zone deposit); **b)** Mg-chlorite (chlorite) and white mica (sericite) together with sulphides (black colour) in a semi-massive sulphide sample (drillhole KA 93-42 @ 423 m: Key Anacon deposit); **c)** Fine-grained matrix composed of white mica (sericite) and quartz (drillhole HN-119 @ 617': Deep Zone, Halfmile Lake deposit); and **d)** white mica (sericite) band with disseminated fine-grained pyrite (sample from drillhole LGF-6 @ 210': Louvicourt deposit).

Table 3. Informational values for unreported elements that are calculated in this study for standards MASS-1 and NIST 610.

	Standards (ppm)	
Element	MASS-1	NIAT 610
Hg		0.47
Te		297
Tl	68.3	

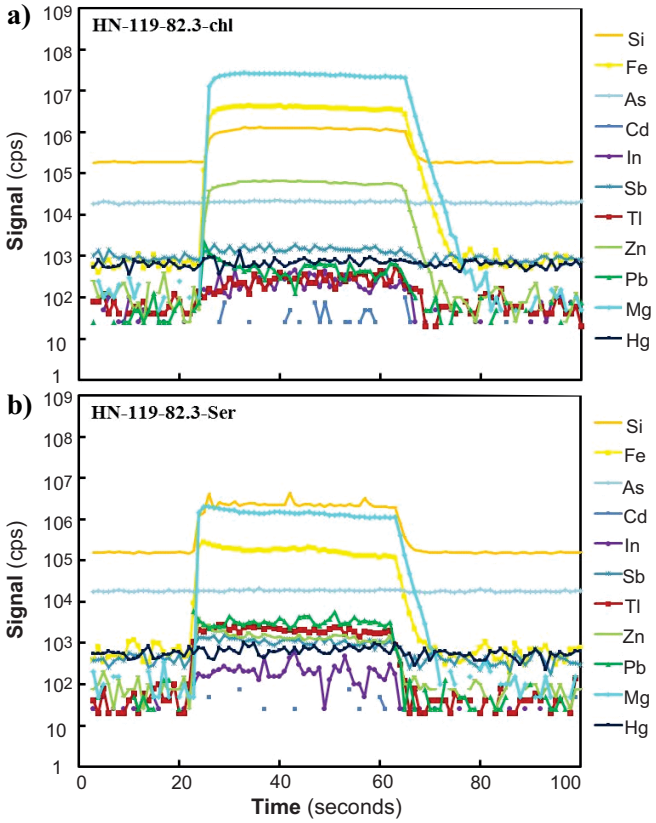

Figure 3. Raw count data (counts per seconds) for selected elements plotted as a function of time for a single-spot LA-ICP-MS for **(a)** chlorite and **(b)** white mica from the Halfmile Lake Deep Zone deposit, Bathurst Mining Camp.

NIST612 and vice versa, using published values for Si as the internal standard ($Si_{NIST610}$=32.7 wt% and $Si_{NIST612}$=33.6 wt%) (Table 4). The results demonstrate a good agreement between the values obtained in this study and data published for the standards (Fig. 5).

RESULTS

Laser Ablation Inductively Coupled Plasma Mass Spectrometry Pyrite Analyses

Summary statistics for LA-ICP-MS analyses of pyrite from the selected deposits in the BMC are presented in Table 5. Chemical compositions of pyrite are the average of 3 or 4 spot analyses. As demonstrated in previous studies, the measured trace element contents of pyrite are extremely variable (McClenaghan et al. (2004) using EMPA; McClenaghan et al. (2009) using LA-ICP-MS). LA-ICP-MS data presented in this study show that most pyrite in the BMC is arsenian, with As contents ranging from below the lower limit of detection (BDL) to 7.3 wt% (Soltani Dehnavi et al., 2012, 2013a,b, 2014a,b,c,d). In the samples analyzed, As is the most prevalent substitution in the pyrite structure. Arsenian pyrite also contains Sb (up to 2910 ppm), Tl (up to 4110 ppm), Au (up to 73.2 ppm), Hg (up to 220

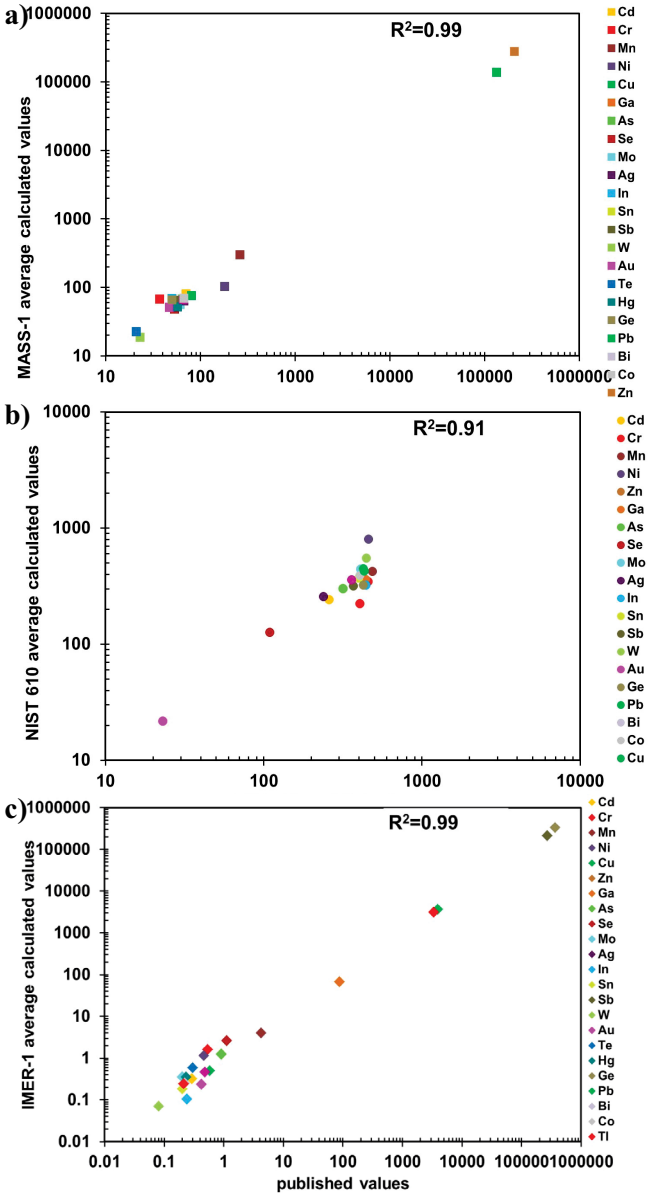

Figure 4. Binary plots comparing LA-ICP-MS results calculated by this study for elemental contents of standards MASS-1, NIST610, and IMER-1 to the published values for each standard. The strong correlation between the values is established for MASS-1 and IMER-1 and in slightly lower degree for NIST610.

ppm), In (up to 49 ppm), and Cd (up to 270 ppm) (Table 5, Fig. 6). There is a strong positive correlation between Sb and Tl, with the highest values in the Louvicourt deposit (Fig. 6a). Likewise, moderate correlations of both Sb and Tl with As show the highest values in the Louvicourt deposit (Fig. 6b,c). Antimony and Hg display a statistically poor positive correlation, with highest Hg values in the Louvicourt deposit (Fig. 6d). Indium and Cd are typically only present in low abundances (Fig. 6e). Contents of Bi exhibit positive correlation with Cu in all of the deposits except Louvicourt (Fig. 6f).

Table 4. Summary of obtained compositional variations of NIST 610, 612, and MASS-1 in this study (ppm).

	Calculated NIST 612_Si (n>150)				Calculated NIST 610_Si (n>100)				Calculated MASS-1 vs. NIST 610_Fe (n>100)			
Analyte	Min	Mean	Max	Published	Min	Mean	Max	Published	Min	Mean	Max	Suggested
Li	38.9	41.6	45.8	42	460	489	510	485	0.13	0.94	24.3	
Na	97750	100518	102750	103858	100820	102583	105090	99415	28310	36745	55300	25080
Mg	59.2	61.1	64	77	566	586	602	465	31.4	38.7	74	
Al	10959	11184	11420	11167	10560	10768	11080	10797	13.3	20.7	133	
Cl	100	172	247	131	180	359	627	438	2609	5302	13400	
K	60.3	63.7	66.3	66.3	489	506	535	486	34.6	48.2	100	
Ca	83210	84805	87700	85002	80050	82255	84760	82144	11.7	52.6	945	
Ti	35.8	38.9	45.7	44	436	493	526	434	2.04	6.8	28.2	
Cr	31	35.1	38.7	36	381	412	439	405	60.5	67.5	78.7	37
Mn	38.3	41.3	42.38	38	437	447	496	485	260	312	427	260
Fe	44.7	71.5	95.4	51	301	353	525	458				156000
Co	33.4	34.2	35.1	35	404	415	424	405	61.2	74.9	103	67
Ni	36.3	38.3	39.8	38.8	454	464	479	459	89.2	115	153	180
Cu	30.2	37.0	42.2	37	386	434	522	430	107600	153734	211600	134000
Zn	36.6	37.9	39.4	38	441	457	478	456	225500	297115	406000	207383
As	30.6	35.6	43.3	37	256	330	382	317	63	75	88	65
Rb	30.7	31.5	32.2	31.4	416	425	438	426	0.02	0.12	4.19	
Sr	71.3	76.8	79.4	78.4	509	527	578	516	0.38	0.62	11.9	
Cd	23.8	27.4	29.9	28.3	240	267	304	259	59.4	96.4	140	70
In	34.0	36.2	37.5	43	508	525	562	441	56.4	71.4	105	50
Sn	33.2	34.2	34.9	38	432	441	449	396	BDL	61.3	94.4	55
Sb	29.8	31.0	32.2	38	437	451	469	369	55.9	70.4	107	55
Cs	38.4	40.7	42.4	42	357	373	401	361	BDL	0.04	1.90	
Ba	36.6	37.7	39.0	39.7	446	459	469	435	0.64	3.05	83	
Hg	0.1	0.20	0.54		0.24	0.71	1.6		26.5	60.5	87.6	57
Tl	9.1	16.1	29.3	15.1	31	60.3	98.3	61	67.2	85.9	141	68.32
Pb	35.9	37.9	39.3	38.6	413	433	462	426	62.5	82.0	131	80
Bi	29.0	30.8	32.4	30	332	350	379	358	54.2	70.4	113	66

NOTE: BDL = below detection limit

Laser Ablation Inductively Coupled Plasma Mass Spectrometry Phyllosilicate Analyses

Summary statistics for LA-ICP-MS analyses of chlorite and white mica from representative major deposits of the BMC are presented in Table 6. McClenaghan (2011) reported that the compositions for white mica compositions in the BMC show a compositional variation between muscovite and phengite end-members. In addition, chlorite in the BMC is typically Fe-rich, although Mg-rich varieties also present (Peter et al., 2003a,b; McClenaghan, 2011). Our LA-ICP-MS data show that white mica typically contains As (below detection limit, 10100 ppm), Sb (BDL 4750 ppm), Tl (BDL 698 ppm), Hg (BDL 67 ppm), Cd (BDL 8.9 ppm), and Bi (BDL 15.7 ppm); however, Cd (BDL 83 ppm) and Bi (BDL 185 ppm) are preferentially more enriched in chlorite than in white mica (Fig. 7).

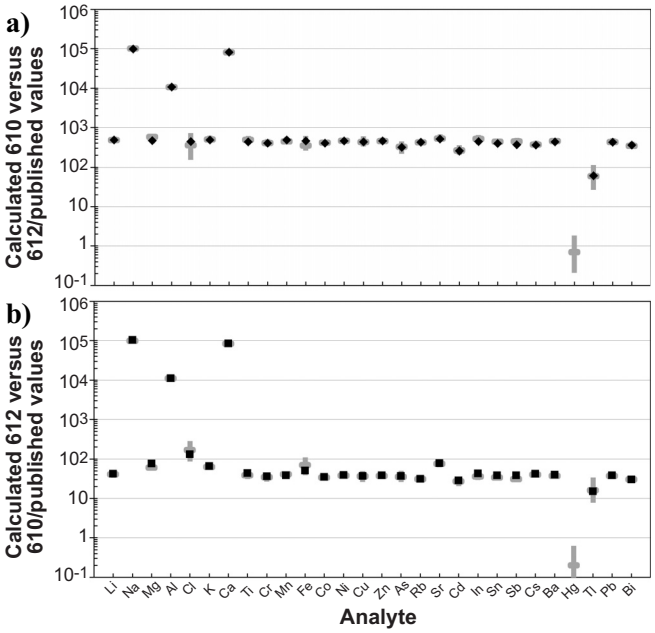

Figure 5. Assessment of the accuracy of data obtained from the calculation of standards NIST610 and NIST612, which were analyzed together with silicate samples. The average calculated values are compared to the published values for each standard. The plots show similar values for most of the elements. Internal standardization was obtained from the data published for these standards (Si). Grey bars show the range (minimum and maximum) of the elements that were examined.

DISCUSSION

Volatile Trace Element Dispersion Haloes

Volatile trace elements are potential pathfinders in geochemical prospecting for a wide variety of base- and precious-metal deposits. The characteristics of volatile trace elements that make them potential vectors is their presence in mineralizing fluids, their relatively high

Table 5. Summary of compositional variations of pyrite (LA-ICP-MS) for representative massive sulphide deposits of the Bathurst Mining Camp, New Brunswick (values in ppm).

Deposit		Drillhole	n	Fe	S	Cr	Mn	Co	Ni	Cu	Zn	Ga	Ge	As	Se	Mo	Ag	Cd	In
	MDL		792	24.65	1668	0.45	1.49	0.46	3.66	0.51	1.66	0.49	2.07	0.99	2.50	0.61	0.19	0.53	0.03
Armstrong A	Max	A-14		561000	569000	5.60	2600	750	540	5700	3600	42.1	8.90	6880	37.4	142.7	36	30.6	12.3
	Mean		54	498630	502944	1.17	206	83.5	28.3	555	186	1.57	BDL	2111	7.44	8.25	6.89	1.64	0.55
	Min			434000	446000	BDL	BDL	BDL	BDL	0.66	BDL	BDL	BDL	19.5	BDL	BDL	BDL	BDL	BDL
Brunswick No. 6	Max	B-259		657000	582000	1.56	207	1850	960	1750	50000	4.30	BDL	5690	43.9	12.8	82.0	98.0	45.3
	Mean		47	514872	491647	0.59	21.6	306	72.3	171	1461	BDL	BDL	1511	5.57	1.31	11.8	2.92	3.03
	Min			420000	382000	BDL	BDL	BDL	BDL	BDL	BDL	BDL	BDL	4.00	BDL	BDL	BDL	BDL	BDL
Caribou	Max	62-55		636000	549000	9.80	1770	915	1170	10470	243000	13.4	7	29700	710	29.8	117	260	49
	Mean		52	539135	466438	1.22	117	146	102	727	7331	1.14	BDL	1856	25.2	1.95	16.2	11.8	1.90
	Min			440000	405000	BDL	BDL	BDL	BDL	BDL	BDL	BDL	BDL	BDL	BDL	BDL	BDL	BDL	BDL
Halfmile Lake	Max	HN-119		571000	547000	19.2	4500	2620	41600	2070	8500	16.9	3.18	5800	604	9.80	50.3	21.8	14
	Mean		47	518362	481338	1.65	170	400	1485	192	392	1.00	BDL	1047	51.2	0.98	6.73	1.09	0.77
	Min			469000	431000	BDL	BDL	2.22	BDL	BDL	BDL	BDL	BDL	BDL	BDL	BDL	BDL	BDL	BDL
Restigouche	Max	CP-39		594000	540000	3.01	876	2210	1080	4950	107000	0.55	21.9	18700	720	38.2	183	135	43.9
	Mean		51	543137	465922	0.87	102	101	89.7	578	2701	BDL	2.98	1491	24.7	1.59	18.1	4.85	0.95
	Min			462000	412000	BDL	BDL	BDL	BDL	BDL	BDL	BDL	BDL	2.39	BDL	BDL	BDL	BDL	BDL
Heath Steele	Max	B-3409		602000	553000	2.20	16.5	12700	858	1900	10.2	2.32	2.70	7970	251	1.43	5.80	BDL	0.31
	Mean		29	542759	461034	0.95	1.53	858	129	116	BDL	BDL	BDL	1320	45.6	0.27	1.28	BDL	0.04
	Min			470000	400000	BDL	BDL	BDL	BDL	0.80	BDL	BDL	BDL	2.46	BDL	BDL	BDL	BDL	BDL
Canoe Landing Lake	Max	CL-94		782000	7000000	650	13840	19900	20200	564000	8000	1180	900	73000	5600	1390	1010	270	21.6
	Mean		159	572919	483824	11.8	452	792	1236	20179	351	10.7	9.50	3012	74.1	15.7	24.5	3.90	0.55
	Min			41200	318000	BDL	BDL	BDL	BDL	BDL	BDL	BDL	BDL	BDL	BDL	BDL	BDL	BDL	BDL
Key Anacon	Max	KA-93-42		719000	550000	4.9	2070	12200	5890	2750	3000	1.31	3.4	8150	293	15.2	70.0	8.20	2.90
	Mean		64	562844	457209	0.86	70.7	658	479	171	57.1	BDL	BDL	1474	32.4	0.69	4.30	BDL	0.10
	Min			447000	352000	BDL	BDL	BDL	BDL	BDL	BDL	BDL	BDL	BDL	BDL	BDL	BDL	BDL	BDL
Brunswick No. 12	Max	A1		707000	624000	7.00	2590	5740	23490	6800	26200	11.0	3.60	16200	52.3	39.7	313	57.0	19.2
	Mean		203	531756	479107	1.23	50.0	590	428	140	218	0.52	BDL	2038	5.35	1.61	11.3	0.68	0.17
	Min			403000	357000	BDL	BDL	BDL	BDL	BDL	BDL	BDL	BDL	BDL	BDL	BDL	BDL	BDL	BDL
Louvicourt	Max	LGF-6		746000	627000	2.45	2310	1300	1660	563000	4200	120	4.23	31300	26.0	94.0	2710	12.2	3.32
	Mean		86	633547	397523	0.71	117	111	144	13334	100	1.96	BDL	5497	3.30	8.26	78.9	0.77	0.13
	Min			381000	338000	BDL	BDL	BDL	BDL	BDL	BDL	BDL	BDL	BDL	BDL	BDL	BDL	BDL	BDL

NOTE: BDL = below detection limit

Table 5 continued.

Deposit		Drillhole	Sn	Sb	Te	W	Au	Hg	Tl	Pb	Bi	Fe	S	Cr	Mn	Co	Ni	Cu
	MDL		0.15	0.29	0.99	0.04	0.04	0.39	0.13	0.11	0.04	24.65	1668	0.45	1.49	0.46	3.66	0.51
Armstrong A	Max	A-14	2600	1744	2.68	13.2	0.49	24.5	217	9200	239	561000	569000	5.60	2600	750	540	5700
	Mean		58.6	145	BDL	0.78	0.11	1.65	29.7	820	36.3	498630	502944	1.17	206	83.5	28.3	555
	Min		BDL	BDL	BDL	BDL	BDL	BDL	BDL	2.29	BDL	434000	446000	BDL	BDL	BDL	BDL	0.66
Brunswick No. 6	Max	B-259	15200	1448	1.45	11.9	2.01	15.1	178	22700	319	657000	582000	1.56	207	1850	960	1750
	Mean		398	112	BDL	1.06	0.18	0.70	22.2	1695	45.2	514872	491647	0.59	21.6	306	72.3	171
	Min		BDL	BDL	BDL	BDL	BDL	BDL	BDL	BDL	BDL	420000	382000	BDL	BDL	BDL	BDL	BDL
Caribou	Max	62-55	11100	1012	10.1	6.70	7.47	17.4	280	450000	890	636000	549000	9.80	1770	915	1170	10470
	Mean		237	112	1.12	0.29	0.83	1.11	8.64	11215	109	539135	466438	1.22	117	146	102	727
	Min		BDL	BDL	BDL	BDL	BDL	BDL	BDL	0.15	BDL	440000	405000	BDL	BDL	BDL	BDL	BDL
Halfmile Lake	Max	HN-119	4800	1880	15.3	2.35	2.11	1.96	233	18600	321	571000	547000	19.2	4500	2620	41600	2070
	Mean		105	169	1.45	0.11	0.27	BDL	12.4	979	45.3	518362	481338	1.65	170	400	1485	192
	Min		BDL	BDL	BDL	BDL	BDL	BDL	BDL	0.17	BDL	469000	431000	BDL	BDL	2.22	BDL	BDL
Restigouche	Max	CP-39	137	830	22.3	10.1	9.60	2.74	250	50900	0.78	594000	540000	3.01	876	2210	1080	4950
	Mean		4.10	85.2	BDL	1.22	0.57	0.41	9.52	3301	0.14	543137	465922	0.87	102	101	89.7	578
	Min		BDL	BDL	BDL	BDL	BDL	BDL	BDL	0.10	BDL	462000	412000	BDL	BDL	BDL	BDL	BDL
Heath Steele	Max	B-3409	9.91	229	55.4	0.92	7.90	BDL	8.25	1140	108	602000	553000	2.20	16.5	12700	858	1900
	Mean		0.72	20.6	4.33	0.13	0.35	BDL	0.93	118	31.1	542759	461034	0.95	1.53	858	129	116
	Min		BDL	BDL	BDL	BDL	BDL	BDL	BDL	BDL	BDL	470000	400000	BDL	BDL	BDL	BDL	0.80
Canoe Landing Lake	Max	CL-94	2600	2473	141	25100	13.3	140	1660	84900	293	782000	7000000	650	13840	19900	20200	564000
	Mean		35.8	228	5.23	160	0.74	3.53	18.5	3376	28.5	572919	483824	11.8	452	792	1236	20179
	Min		BDL	BDL	BDL	BDL	BDL	BDL	BDL	BDL	BDL	41200	318000	BDL	BDL	BDL	BDL	BDL
Key Anacon	Max	KA-93-42	460	249	66.4	14.3	0.51	7.28	1336	39000	169	719000	550000	4.9	2070	12200	5890	2750
	Mean		9.63	24.7	2.97	0.74	0.08	BDL	25.7	1847	19.5	562844	457209	0.86	70.7	658	479	171
	Min		BDL	BDL	BDL	BDL	BDL	BDL	BDL	BDL	BDL	447000	352000	BDL	BDL	BDL	BDL	BDL
Brunswick No. 12	Max	A1	88.0	2910	96.4	3.02	5.20	4.47	208	6900	790	707000	624000	7.00	2590	5740	23490	6800
	Mean		1.82	117	2.54	0.25	0.34	BDL	7.10	403	49.7	531756	479107	1.23	50.0	590	428	140
	Min		BDL	BDL	BDL	BDL	BDL	BDL	BDL	BDL	BDL	403000	357000	BDL	BDL	BDL	BDL	BDL
Louvicourt	Max	LGF-6	7.60	2800	10.1	9.90	73.2	220	4110	48000	87.0	746000	627000	2.45	2310	1300	1660	563000
	Mean		0.27	359	1.02	0.40	1.86	8.91	197	3682	4.64	633547	397523	0.71	117	111	144	13334
	Min		BDL	BDL	BDL	BDL	BDL	BDL	BDL	0.38	0.04	381000	338000	BDL	BDL	BDL	BDL	BDL

NOTE: BDL = below detection limit

Table 5 continued.

Deposit		Drillhole	Zn	Ga	Ge	As	Se	Mo	Ag	Cd	In	Sn	Sb	Te	W	Au	Hg	Tl	Pb	Bi
	MDL		1.66	0.49	2.07	0.99	2.50	0.61	0.19	0.53	0.03	0.15	0.29	0.99	0.04	0.04	0.39	0.13	0.11	0.04
Armstrong A	Max	A-14	3600	42.1	8.90	6880	37.4	142.7	36	30.6	12.3	2600	1744	2.68	13.2	0.49	24.5	217	9200	239
	Mean		186	1.57	BDL	2111	7.44	8.25	6.89	1.64	0.55	58.6	145	BDL	0.78	0.11	1.65	29.7	820	36.3
	Min		BDL	BDL	BDL	19.5	BDL	BDL	BDL	BDL	BDL	BDL	BDL	BDL	BDL	BDL	BDL	BDL	2.29	BDL
Brunswick No. 6	Max	B-259	50000	4.30	BDL	5690	43.9	12.8	82.0	98.0	45.3	15200	1448	1.45	11.9	2.01	15.1	178	22700	319
	Mean		1461	BDL	BDL	1511	5.57	1.31	11.8	2.92	3.03	398	112	BDL	1.06	0.18	0.70	22.2	1695	45.2
	Min		BDL	BDL	BDL	4.00	BDL	BDL	BDL	BDL	BDL	BDL	BDL	BDL	BDL	BDL	BDL	BDL	BDL	BDL
Caribou	Max	62-55	243000	13.4	7	29700	710	29.8	117	260	49	11100	1012	10.1	6.70	7.47	17.4	280	450000	890
	Mean		7331	1.14	BDL	1856	25.2	1.95	16.2	11.8	1.90	237	112	1.12	0.29	0.83	1.11	8.64	11215	109
	Min		BDL	BDL	BDL	BDL	BDL	BDL	BDL	BDL	BDL	BDL	BDL	BDL	BDL	BDL	BDL	BDL	0.15	BDL
Halfmile Lake	Max	HN-119	8500	16.9	3.18	5800	604	9.80	50.3	21.8	14	4800	1880	15.3	2.35	2.11	1.96	233	18600	321
	Mean		392	1.00	BDL	1047	51.2	0.98	6.73	1.09	0.77	105	169	1.45	0.11	0.27	BDL	12.4	979	45.3
	Min		BDL	BDL	BDL	BDL	BDL	BDL	BDL	BDL	BDL	BDL	BDL	BDL	BDL	BDL	BDL	BDL	0.17	BDL
Restigouche	Max	CP-39	107000	0.55	21.9	18700	720	38.2	183	135	43.9	137	830	22.3	10.1	9.60	2.74	250	50900	0.78
	Mean		2701	BDL	2.98	1491	24.7	1.59	18.1	4.85	0.95	4.10	85.2	BDL	1.22	0.57	0.41	9.52	3301	0.14
	Min		BDL	BDL	BDL	2.39	BDL	BDL	BDL	BDL	BDL	BDL	BDL	BDL	BDL	BDL	BDL	BDL	0.10	BDL
Heath Steele	Max	B-3409	10.2	2.32	2.70	7970	251	1.43	5.80	BDL	0.31	9.91	229	55.4	0.92	7.90	BDL	8.25	1140	108
	Mean		BDL	BDL	BDL	1320	45.6	0.27	1.28	BDL	0.04	0.72	20.6	4.33	0.13	0.35	BDL	0.93	118	31.1
	Min		BDL	BDL	BDL	2.46	BDL	BDL	BDL	BDL	BDL	BDL	BDL	BDL	BDL	BDL	BDL	BDL	BDL	BDL
Canoe Landing Lake	Max	CL-94	8000	1180	900	73000	5600	1390	1010	270	21.6	2600	2473	141	25100	13.3	140	1660	84900	293
	Mean		351	10.7	9.50	3012	74.1	15.7	24.5	3.90	0.55	35.8	228	5.23	160	0.74	3.53	18.5	3376	28.5
	Min		BDL	BDL	BDL	BDL	BDL	BDL	BDL	BDL	BDL	BDL	BDL	BDL	BDL	BDL	BDL	BDL	BDL	BDL
Key Anacon	Max	KA-93-42	3000	1.31	3.4	8150	293	15.2	70.0	8.20	2.90	460	249	66.4	14.3	0.51	7.28	1336	39000	169
	Mean		57.1	BDL	BDL	1474	32.4	0.69	4.30	BDL	0.10	9.63	24.7	2.97	0.74	0.08	BDL	25.7	1847	19.5
	Min		BDL	BDL	BDL	BDL	BDL	BDL	BDL	BDL	BDL	BDL	BDL	BDL	BDL	BDL	BDL	BDL	BDL	BDL
Brunswick No. 12	Max	A1	26200	11.0	3.60	16200	52.3	39.7	313	57.0	19.2	88.0	2910	96.4	3.02	5.20	4.47	208	6900	790
	Mean		218	0.52	BDL	2038	5.35	1.61	11.3	0.68	0.17	1.82	117	2.54	0.25	0.34	BDL	7.10	403	49.7
	Min		BDL	BDL	BDL	BDL	BDL	BDL	BDL	BDL	BDL	BDL	BDL	BDL	BDL	BDL	BDL	BDL	BDL	BDL
Louvicourt	Max	LGF-6	4200	120	4.23	31300	26.0	94.0	2710	12.2	3.32	7.60	2800	10.1	9.90	73.2	220	4110	48000	87.0
	Mean		100	1.96	BDL	5497	3.30	8.26	78.9	0.77	0.13	0.27	359	1.02	0.40	1.86	8.91	197	3682	4.64
	Min		BDL	BDL	BDL	BDL	BDL	BDL	BDL	BDL	BDL	BDL	BDL	BDL	BDL	BDL	BDL	BDL	0.38	0.04

NOTE: BDL = below detection limit

Table 6. Summary of compositional variations of phyllosilicate minerals (LA-ICP-MS) for representative massive sulphide deposits of the Bathurst Mining Camp, New Brunswick (values in ppm).

Deposit	Halfmile	Drillhole	Mineral	n	Li	Na	Mg	Al	Cl	K	Ca	Ti	Cr	Mn	Fe	Co	Ni	Cu
	MDL			512	1.83	6.39	0.40	1.35	64.6	4.76	59.9	2.23	2.84	1.79	10.6	0.12	0.76	0.24
Halfmile Lake	Max	HN-119	White mica		110.30	57560	175100	218600	2090	104630	34610	25400	297	13484	389000	156	59	33
	Mean			81	21.61	3213	23215	147096	260	82253	1265	2350	67.3	910	56693	7.50	9.43	3.00
	Min				2.13	28.7	3960	16500	BDL	43	BDL	169	BDL	33.7	1278	0.15	BDL	BDL
Halfmile Lake	Max	HN-119	Chlorite		65.40	29580	87010	121200	1190	48170	8470	27400	431	6810	315000	96	169	88
	Mean			127	23.50	1144	53087	93197	132	7333	364	696	37.8	2987	154575	13.1	18.0	2.10
	Min				BDL	BDL	497	26200	BDL	BDL	BDL	38.1	BDL	7.2	840	BDL	BDL	BDL
Heath Steele	Max	B-3409	White mica		93.80	19040	48800	204400	3300	108760	23400	15800	250	4800	244000	65	169	23600
	Mean			117	29.15	2631	15986	150039	197	88503	598	2291	39.1	686	40559	4.80	7.18	205
	Min				4.20	126	4718	22900	BDL	7000	BDL	137	BDL	64.6	11330	0.65	BDL	BDL
Heath Steele	Max	B-3409	Chlorite		131.20	19900	92500	122300	3700	54700	145000	33200	297	20930	289800	188	222	10.4
	Mean			91	26.55	1797	34812	76278	271	8530	5426	1048	23.3	3546	128908	18.2	16.5	0.93
	Min				BDL	BDL	1412	2020	BDL	4.7	BDL	3.9	BDL	8.80	820	0.16	BDL	BDL
Louvicourt	Max	LGF-6	White mica		65.10	1232	37080	175800	7300	108160	52800	12900	353	24300	306000	142	124.1	13530
	Mean			47	42.80	818	18255	147907	761	94919	1820	2985	51.1	1265	47741	10.9	27.3	351
	Min				18.50	293	8360	59400	BDL	37200	BDL	65.8	3	190	7390	BDL	BDL	BDL
Louvicourt	Max	LGF-6	Chlorite		85.80	391	105800	105700	1700	52750	72800	4500	953	21200	372000	150	498	208
	Mean			31	42.91	80	61350	86978	284	7248	3354	868	40.3	4777	157764	61.1	210	7.59
	Min				10.50	BDL	8048	28600	11.1	11.2	15.9	70	0.53	151	19640	0.14	7.09	BDL

Table 6 continued.

Deposit	Halfmile	Drillhole	Mineral	Zn	As	Se	Rb	Sr	Cd	In	Sn	Sb	Te	Cs	Ba	Hg	Tl	Pb	Bi
	MDL			0.56	3.36	2.50	0.17	0.01	0.13	0.02	0.07	0.17	0.69	0.07	0.12	0.13	0.02	0.03	0.04
Halfmile Lake	Max	HN-119	White mica	1466	700	41.3	587	63.1	0.31	3.1	253	5.4	0.96	16.1	2337	2.89	43.5	129	15.7
	Mean			93.3	26.1	BDL	353	17.2	BDL	0.45	29.4	1.30	BDL	4.82	992	0.87	3.79	4.54	0.46
	Min			2.71	BDL	BDL	0.22	0.75	BDL	0.15	0.54	BDL	BDL	0.11	0.22	BDL	BDL	0.43	BDL
Halfmile Lake	Max	HN-119	Chlorite	83500	1110	109	222	45.7	83.2	42.2	104	4.3	0.97	15.5	741	3.84	13.23	39000	10.1
	Mean			2036	17.7	BDL	31.2	4.39	1.79	1.16	3.68	0.32	0.26	1.07	81.4	0.51	0.58	315	0.29
	Min			2.87	BDL	BDL	BDL	0.07	BDL	BDL	BDL	BDL	BDL	BDL	BDL	0.06	BDL	BDL	BDL
Heath Steele	Max	B-3409	White mica	402	23	57	664	185	0.84	21.6	359	7.3	0.96	22.4	10130	1.93	15.0	28.2	10.8
	Mean			93.5	5.96	BDL	427	27.4	BDL	0.64	24.8	1.33	BDL	6.44	1539	0.82	4.17	4.46	0.15
	Min			8.81	BDL	BDL	32.5	2.21	BDL	0.12	0.77	BDL	BDL	0.36	74.3	BDL	0.54	0.35	BDL
Heath Steele	Max	B-3409	Chlorite	1161	192	8.8	229	423	9.5	1.1	22.9	51.1	3.60	10.1	1728	1.13	5.21	285000	185
	Mean			317	14.0	BDL	34.8	15.8	0.19	0.19	2.42	2.63	BDL	1.03	162	0.41	0.60	3374	2.90
	Min			1.47	BDL	BDL	BDL	0.07	BDL	BDL	BDL	BDL	BDL	BDL	BDL	BDL	BDL	BDL	BDL
Louvicourt	Max	LGF-6	White mica	2332	10100	7.4	465	2795	8.19	511	981	4750	1.5	7.36	250200	67.1	698	4680	1.32
	Mean			453	250	2.70	367	120	0.43	30.7	75.4	117	BDL	4.53	26315	4.43	186	478	0.15
	Min			71.3	BDL	BDL	143	3.03	BDL	0.05	2.59	1.17	BDL	1.86	5650	0.36	49.7	0.87	BDL
Louvicourt	Max	LGF-6	Chlorite	6400	17.2	2.81	189	1210	0.85	384	983	2.06	0.50	2.41	115000	14.1	50.1	9900	1.88
	Mean			2046	7.32	BDL	26.6	153	0.12	51.9	99.6	0.75	0.27	0.49	12756	1.91	9.41	418	0.09
	Min			99.9	BDL	BDL	BDL	0.33	BDL	0.02	BDL	BDL	BDL	BDL	2.27	0.02	0.05	0.12	BDL

NOTE: BDL = below detection limit

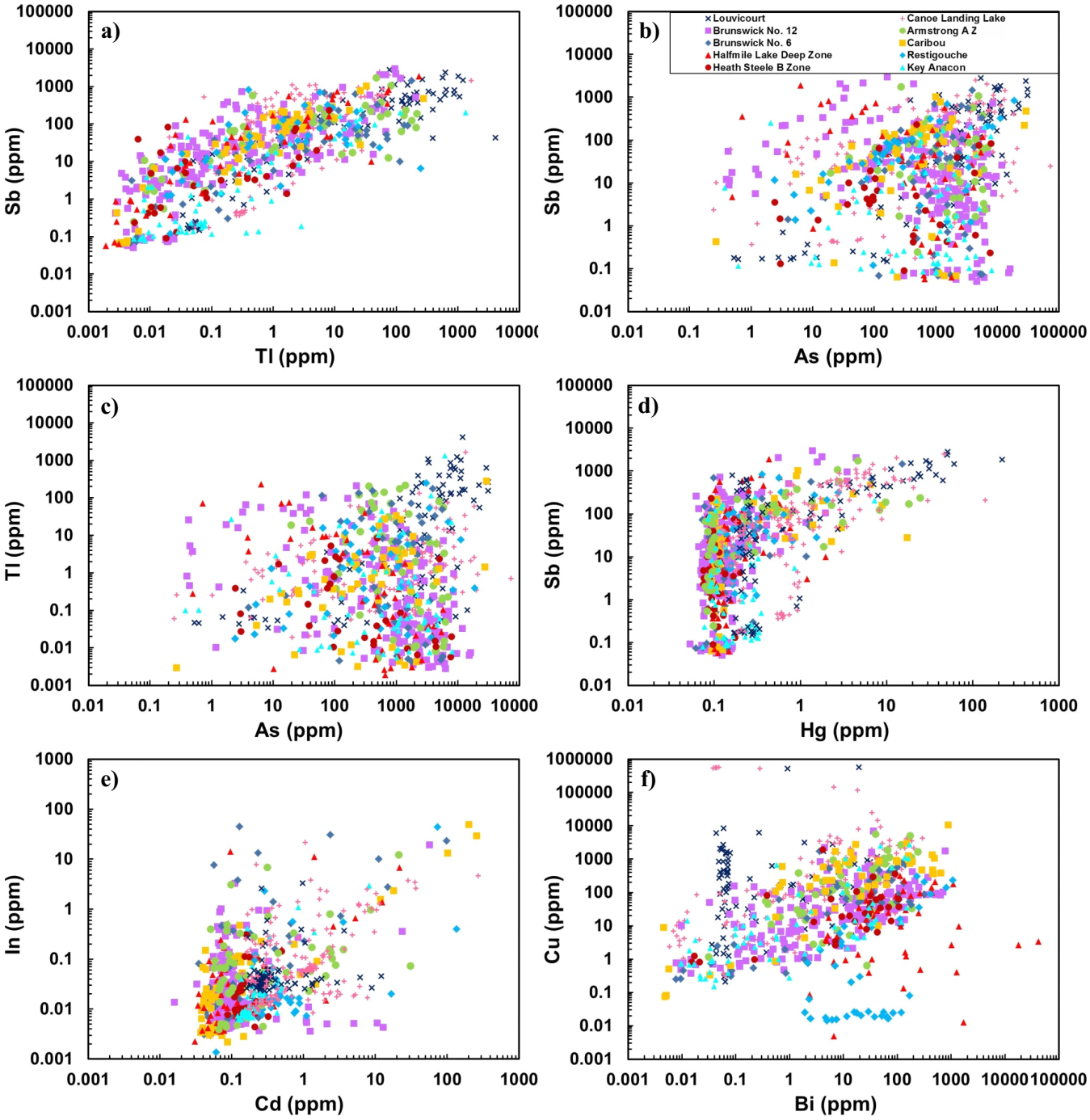

Figure 6. Binary plots of LA-ICP-MS analyses for selected volatile trace elements in pyrite from representative massive sulphide deposits of the Bathurst Mining Camp.

vapour pressure characteristics, and their role as transporting agents of metals during the mineralizing process (Ryall, 1981, and references therein; Carr et al., 1986). The volatile trace elements whose behaviour has previously been systematically and comprehensively studied in a VMS environment are Hg, Tl, and Sb (Boldy, 1963, 1979; Ryall, 1981 and references therein; Carr et al., 1986; Lentz and Goodfellow, 1993; Lentz et al., 1997; Large et al., 2001 and references therein).

A distinct primary Hg dispersion halo was documented in the hanging-wall rocks of the Norbec deposit, Noranda district, Quebec, and was considered to be a prospective exploration vector toward deeply buried and blind sulphide deposits (Boldy, 1963, 1979). Lentz and Goodfellow (1993), who studied core from the discovery drillhole (A1) at the Brunswick No. 12 deposit in the BMC, found that the distribution of hydrothermal elements displayed distinctive enrichments for Hg, Sb, and to lesser extent Tl, in the hanging wall of the deposit. Lentz et al. (1997) studied

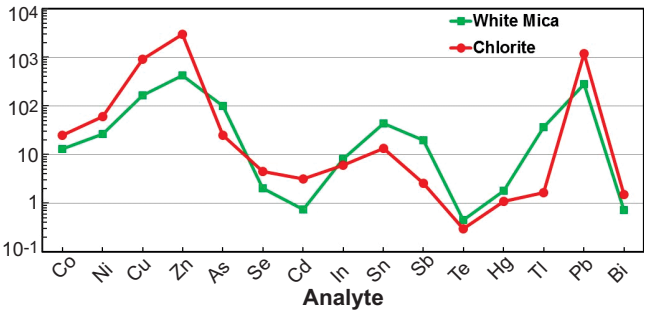

Figure 7. Comparision of average element values of chlorite and white mica obtained by LA-ICP-MS throughout the BMC, showing the relative distribution of volatile trace elements in these minerals.

whole-rock data for drillhole HSB 3409 from the Heath Steele B Zone and found increasing trends of some volatile elements, such as Hg, As, and Sb toward the ore horizon. Large et al. (2001) examined the distributions of Tl and Sb in the host-rock sequence to the Rosebery VMS deposit, Australia, and reported clearly defined, well developed, and widespread halo around the ore lenses.

In the present study, the composition of pyrite, chlorite, and white mica were examined from drillholes throughout selected deposits to identify the key residence sites of volatile trace elements. Though disseminated and vein sulphides are typically only prevalent proximal to mineralization in the BMC (Lentz et al., 1997), pyrite, which is the most widespread disseminated sulphide mineral in the footwall and hanging-wall sequences of VMS deposits can occur far (hundreds of metres) from massive sulphide mineralization (Corbett, 2001). In addition, pyrite compositions can be easily determined using LA-ICP-MS analyses and data reduction using the stoichiometric value of Fe, which can then be used as an internal standard to obtain reliable data. Finally, pyrite can contain significant contents of volatile trace elements, allowing it to be used as a potential volatile element vectoring mineral.

Chlorite and white mica are the most abundant phyllosilicate VMS-related hydrothermal alteration minerals in the BMC. Chlorite commonly occurs together with the massive sulphides (also with disseminated to semi-massive sulphides) and exhalative sedimentary rocks along mineralized horizons. White mica is ubiquitous in quartzo-feldspathic volcaniclastic rocks, siliciclastic, and exhalative sedimentary rocks. Moreover, variations in the chemical composition of chlorite and white mica can serve as a tool in discovering mineralization at depth. To demonstrate the applicability of these proposed vectoring minerals, integrated LA-ICP-MS volatile trace element data for pyrite and phyllosilicates have been plotted on drillhole stratigraphic logs (Figs. 8, 9).

Volatile Element Vectoring using Pyrite

The chemical variability of pyrite in alteration zones (massive sulphides and epithermal gold veins) from hanging wall to footwall has been shown to be an indicator of mineralization processes that can potentially be used in exploration (Roberts, 1982; Baker et al., 2006). Rogers et al. (2014) successfully used the trace element compositions of pyrite to identify high-temperature, VMS-related hydrothermal up-flow zones in the vicinity of the Hébécourt VMS prospect, Abitibi greenstone belt.

Figure 8 presents stratigraphic logs of pyrite volatile element profiles for selected deposits in the BMC that were determined in the current study. The abundance of pyrite systematically increases towards the ore horizon of the studied deposits in both the hanging wall and footwall. Pyrite in the altered footwall units typically displays systematically increasing volatile trace elements with decreasing distance to the ore horizon, particularly in the Restigouche (up to 150 m), Canoe Landing Lake (about 100 m), Armstrong (about 30 m), and Heath Steele B Zone (over 150 m) deposits. However, in the hanging-wall alteration zones, there is no consistent trend in the volatile element contents of pyrite. The Brunswick No. 12, Canoe Landing Lake, Restigouche, and Key Anacon deposits show that pyrite in the upper portions of the hanging wall has distinct As enrichment together with some other volatile trace elements, such as Sb, Tl, and Bi (Fig. 8). Therefore, systematic variations in the volatile trace element compositions of pyrite from alteration zones can serve as a potential vector to mineralization in the BMC. Below is a summary of pyrite volatile trace element systematics for the different deposits that were examined.

Restigouche Deposit – CP-39

The Restigouche deposit is hosted within feldspar crystal-rich and crystal-poor sequences of the Mount Brittain Formation. The footwall to the Restigouche deposit consists of silicified and chloritic, aphyric to sparsely feldspar-phyric rhyolite flows and hyaloclastite. The hanging wall comprises hyalotuff, chert, and feldspar crystal lithic tuff containing feldspar-crystal lithic tuff interlayered with thin beds of rhyolite tuff. Pyrite is the only sulphide mineral present in the altered felsic rocks of Restigouche deposit. Volatile trace elements are enriched in pyrite in the upper portion of the hanging wall and decrease in abundance toward the bedded sulphide horizon. Pyrite from the footwall has systematically increasing In, Cd, Hg, Sb, Bi, and Tl contents (up to 150 m) toward the ore horizon, and systematically decreasing As content (Fig. 8a).

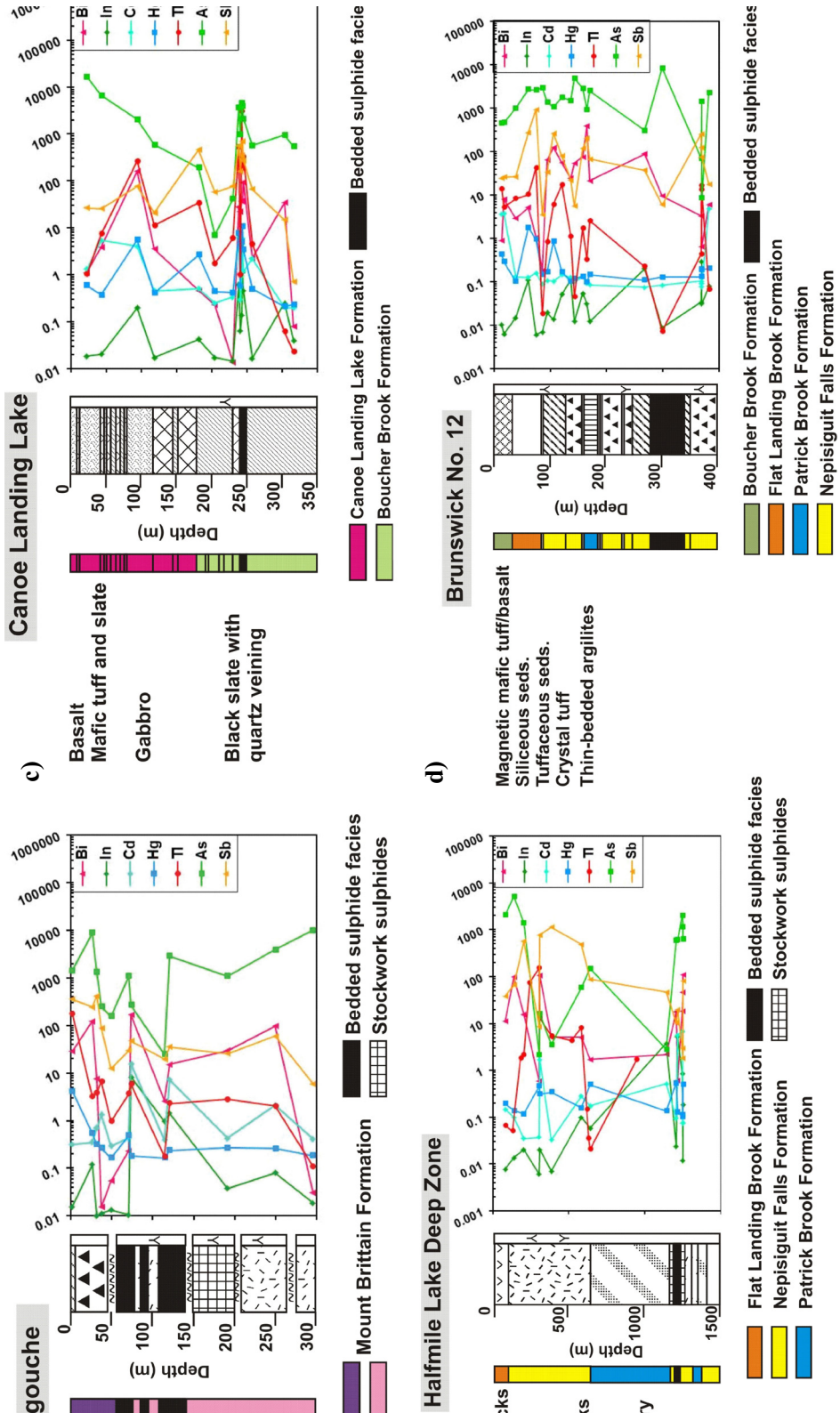

Figure 8. LA-ICP-MS geochemical data profiles illustrating volatile trace elements of pyrite plotted on the stratigraphic profiles of **a)** Restigouche deposit (CP-39); **b)** Halfmile Lake Deep Zone deposit (HN-119); **c)** Canoe Landing Lake deposit (CL-94-2); **d)** Brunswick No. 12 deposit (A-1).

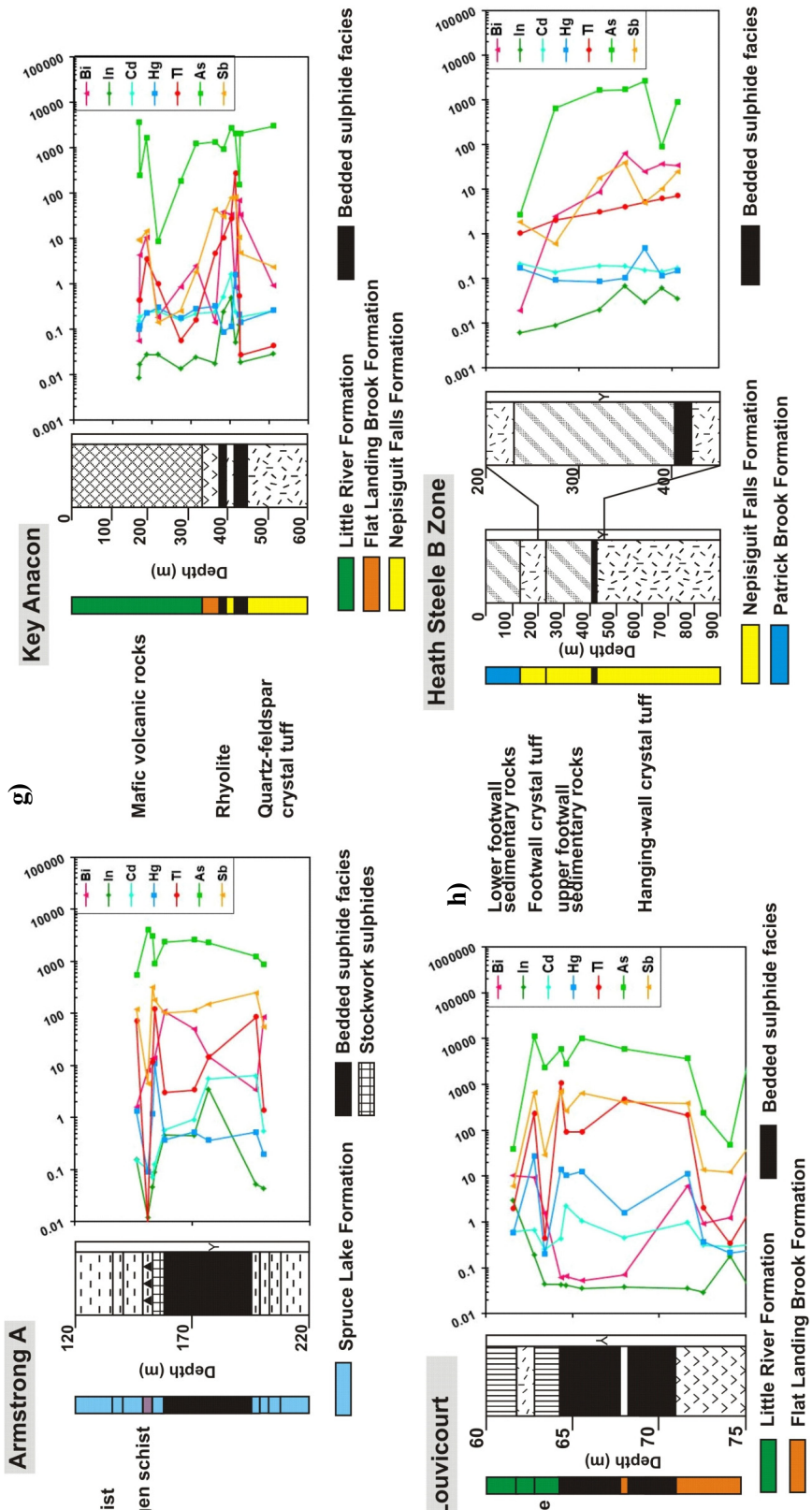

Figure 8 continued. LA-ICP-MS geochemical data profiles illustrating volatile trace elements of pyrite plotted on the stratigraphic profiles of **e)** Armstrong A Zone (A-14); **f)** Louvicourt deposit (LGF-6); **g)** Key Anacon deposit (93-42); and **h)** Heath Steele B Zone (HSB 3409).

Halfmile Lake Deep Zone – HN-119

The Halfmile Lake Deep zone is hosted within quartz-feldspar crystal tuff and volcaniclastic rocks of the Nepisiguit Falls Formation and is overlain by the sedimentary rocks of the Patrick Brook Formation. The Nepisiguit Falls Formation is within the upward-facing limb of the Halfmile Lake anticline. The Patrick Brook Formation lies below the Nepisiguit Falls Formation, and has been hydrothermally altered to a high degree (Mireku and Stanley, 2007; Walker and McCutcheon, 2010). Drillhole HN-119 of the Halfmile Lake Deep Zone contains over 1200 m of disseminated pyrite within the structural hanging wall of the deposit. The volatile trace elements of pyrite are variably enriched in the hanging-wall crystal tuff and volcaniclastic rocks of the Nepisiguit Falls Formation (Fig. 8b).

Canoe Landing Lake – CL-94-2

The deposit is hosted by thinly bedded slate, greywacke, phyllite, hyaloclastite, epiclastic rocks and pillowed flows of the Canoe Landing Lake Formation. This package is unconformably overlain by slate, intraformational conglomerate (mélange or olistostrome), and mafic volcanic rocks of the Boucher Brook Formation. Mafic tuff and basalt of the hanging wall in drillhole CL-94-2 contain disseminated pyrite; black to grey-green slate contains pyrite as nodules and laminations. Pyrite in the hanging wall of the deposit is As-rich over an interval of 150 m, particularly within mafic tuff and basalt; As contents significantly decrease in the slate with decreasing distance toward the ore horizon. Thallium and Sb also display a subtle trend of increasing abundances with decreasing distance to the ore horizon (Fig. 8c).

Brunswick No. 12 – A-1

The Brunswick horizon occurs near the top of the Nepisiguit Falls formation within the Tetagouche Group. Rocks hosting the Brunswick No. 12 deposit have been divided into four formations. From oldest to youngest, these are the Patrick Brook, Nepisiguit Falls, Flat Landing Brook, and Little River formations. Pyrite in the hanging-wall rocks of drillhole 12-A1 are enriched in As and Sb, and to a lesser extent, Tl and Hg; pyrite of the footwall sequence does not contain significant abundances of volatile elements (Fig. 8d).

Armstrong A – A-14

The Armstrong A deposit is hosted within chloritic to sericitic quartz-feldspar augen schist and phyllite of the Spruce Lake Formation. Two samples of host rock from the hanging wall show trends of increasing volatile trace element contents in pyrite with decreasing distance to the ore horizon. Pyrite from the stockwork of the deposit displays enrichment of volatile elements, especially As and Sb (Fig. 8e).

Louvicourt – LGF-6

The Louvicourt deposit is hosted within rhyolitic tuff, argillite, and basalt of the Flat Landing Brook Formation. It has been folded into anticlinal and synformal structures plunging 80° to the west, and are in thrust contact with basalt of the Little River Formation (Rose and Johnson, 1990). Pyrite in altered rhyolite of the footwall in drillhole LGF-6 from the Louvicourt deposit displays trends of increasing abundances for almost all of the volatile trace elements with decreasing distance toward the ore horizon. Pyrite in hanging-wall samples shows trends of increasing As, Sb, Tl, and Hg, whereas Bi and In decrease with decreasing distance to the ore horizon (Fig. 8f).

Key Anacon – KA 93-42

Key Anacon is hosted by felsic and mafic volcanic rocks and related sedimentary rocks of the Tetagouche Group. The volatile trace element contents of pyrite in the upper portion of the mafic volcanic rocks of the hanging wall are enriched, and show trends of increasing contents with decreasing distance towards the ore horizon (Fig. 8g).

Heath Steele B Zone – HSB 3409

The Heath Steele B zone is hosted in crystal-rich felsic volcaniclastic rocks and associated tuffaceous sedimentary rocks of the Nepisiguit Falls Formation. Pyrite occurs only in the upper footwall sedimentary rocks. Volatile trace elements increase with decreasing distance towards the ore horizon (Fig. 8h).

Volatile Element Vectoring using Phyllosilicate Minerals

The chemical compositions of phyllosilicate minerals are commonly used to vector toward VMS mineralization (i.e. proximal versus distal haloes) (Yang et al., 2011). LA-ICP-MS data for chlorite and muscovitic to phengitic white mica plotted on stratigraphic logs demonstrate that volatile trace element contents in the Halfmile Lake (over 1200 m in the hanging wall), Heath Steele B Zone (over 400 m in the hanging wall and footwall), and Louvicourt (~5 m in both the hanging wall and footwall) deposits increase in both the hanging-wall and footwall units with decreasing distance to the ore horizon (Fig. 9). The increase in volatile trace element contents towards the upper stratigraphic sections of the drillholes shows that the volatile element contents of phyllosilicate minerals can be used to vector toward mineralization within the VMS systems of the BMC. Below is a summary of phyllosilicate volatile trace element systematics for the deposits that have been examined to date.

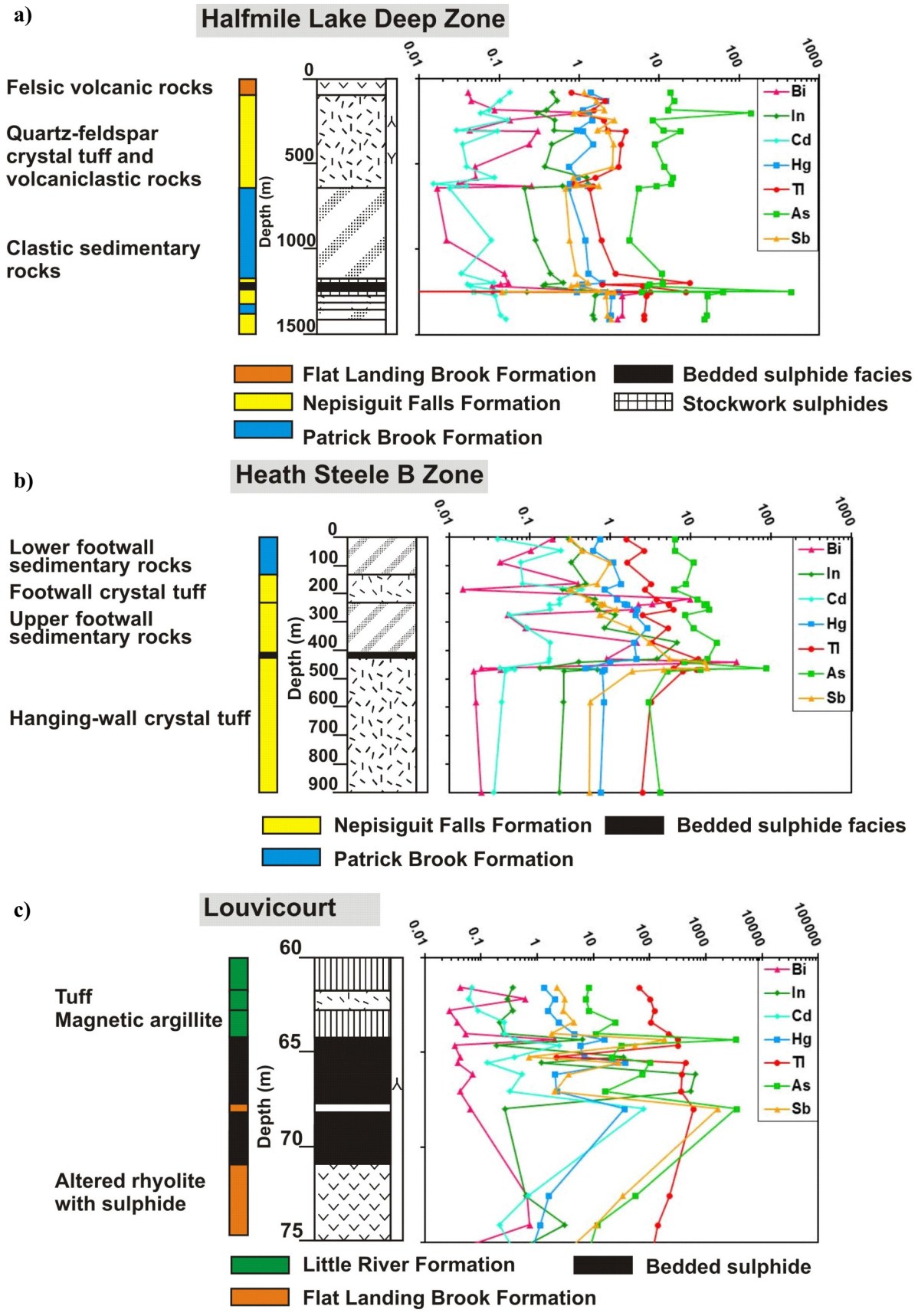

Figure 9. LA-ICP-MS geochemical data profiles illustrating volatile trace element contents of chlorite and white mica plotted on the stratigraphic profiles of **a)** Halfmile Lake Deep Zone (HN-119); **b)** Heath Steele B Zone (HSB 3409); and **c)** Louvicourt deposit (LGF-6) deposits.

Halfmile Lake Deep Zone – HN-119

Drillhole HN-119 shows higher abundances of volatile trace elements in chlorite and white mica in the crystal tuff and volcaniclastic rocks of the Nepisiguit Falls Formation than the clastic sedimentary rocks of the Patrick Brook Formation. The volatile trace elements subtly increase with decreasing distance toward the ore horizon (Fig. 9a).

Heath Steele B Zone – HSB 3409

The proportion of the K-mica and Fe-chlorite increases in the stratigraphic footwall rocks with decreasing distance to the ore horizon. This is coincident with distinctly increasing trends of volatile trace elements, in particular As, Tl, Hg, and In. (Fig. 9b).

Louvicourt – LGF-6

Chlorite and white mica within the tuffaceous argillite and chloritic iron formation in the hanging wall of the deposit have higher contents of Tl and to a lesser extent As and Sb, which systematically increase with decreasing distance towards the ore horizon. Concomitantly, the abundances of phyllosilicate minerals in the altered rhyolite in the footwall also increase with decreasing distance toward the ore horizon (Fig. 9c).

IMPLICATIONS FOR EXPLORATION

The methodology presented herein is shown to be effective in the BMC, but may also be applicable to polymetallic VMS environments elsewhere. The use of pyrite, chlorite, and white mica volatile element contents to vector toward VMS mineralization could be used as a complementary technique to field-based and other conventional exploration vectoring techniques.

FUTURE WORK

The promising results from this initial work on chlorite and white mica from a limited number of deposits will be expanded to include other deposits in the BMC. Particular focus will be placed on white mica from hydrothermal alteration zones. This will allow us to determine whether white mica volatile element compositions can serve as an indicator of proximal VMS-related hydrothermal activity, and if the volatile element data can be used to vector toward concealed mineralization.

ACKNOWLEDGEMENTS

This project is supported by funding from the Earth Science Sector, Natural Resources Canada Targeted Geoscience Initiative 4 program. We also appreciate colleagues at the Geological Survey of Canada, particularly Jan Peter (VMS Ore System Science Leader) and the New Brunswick Department of Energy and Mines in Bathurst, especially Jim Walker and Sean McClenaghan, for assistance in locating legacy datasets and samples. Allen Pring and Benjamin Wade (University of Adelaide, Australia) provided the sulphide standard (IMER-1) that was used, and Douglas Hall assisted with the micro-analytical analysis at UNB. We thank Jim Walker, Patrick Mercier-Langevin, and Jan Peter for reviews and Jan Peter for technical editing.

REFERENCES

Baker, T., Mustard, R., Brown, V., Pearson, N., Stanley, C.R., Radford, N.W., and Butler, I., 2006. Textural and chemical zonation of pyrite at Pajingo: a potential vector to epithermal gold veins; Geochemistry Exploration, Environment, Analysis, v. 6, p. 283–293.

Boldy, J., 1963. Mercury dispersion haloes as exploration targets; Falconbridge Ltd. internal report.

Boldy, J., 1979. Exploration discoveries, Noranda district, Quebec (Case History of a Mining Camp); Geological Survey of Canada, Economic Geology Report 31, p. 593– 603.

Carr, G.R., Wilmshurst, J.R., and Ryall, W.R., 1986. Evaluation of mercury pathfinder techniques: base metal and uranium deposits; Journal of Geochemical Exploration, v. 26, p. 1–117.

Chen, T.T., 1978. Colloform and framboidal pyrite from the Caribou deposit, New Brunswick; Canadian Mineralogist, v. 16, p. 9–15.

Corbett, K.D., 2001. New mapping and interpretations of the Mount Lyell mining district, Tasmania — a large hybrid Cu-Au system with an exhalative Pb-Zn top; Economic Geology, v. 96, p. 1089–1122.

Ding, L., Yang, G., Xia, F., Lenehan, C.E., Gujie Qian, G., McFadden, A., Brugger, J., Zhang, X., Chen, G., and Pring, A., 2011. A LA-ICP-MS sulphide calibration standard based on a chalcogenide glass; Mineralogical Magazine, v. 75, p. 279–287.

Goodfellow, W.D., 1975. Major and minor element haloes in volcanic rocks at Brunswick No. 12 sulphide deposit, N.B., Canada, *In:* Geochemical Exploration 1974, (ed.) I.L Elliot and W.K. Fletcher; Elsevier, Amsterdam, p. 279–295.

Goodfellow, W.D. and McCutcheon, S.R., 2003. Geologic and genetic attributes of volcanic sediment-hosted massive sulfide deposits of the Bathurst Mining Camp, northern New Brunswick–a synthesis, *In:* Massive sulfide deposits of the Bathurst mining camp, New Brunswick, and northern Maine, (ed.) W.D. Goodfellow, S.R McCutcheon, and J.M. Peter; Society of Economic Geologists, Economic Geology Monograph 11, p. 245–302.

Jambor, J.L., 1979, Mineralogical evolution of proximal distal features in New Brunswick massive sulphide deposits; Canadian Mineralogist, v. 17, p. 79–87.

Jambor, J.L., 1981, Mineralogy of Caribou massive sulphide deposit, Bathurst area, New Brunswick, Canada; Natural Resources Canada, CANMET Report 81-8E, 65 p.

Large, R.R., Allen, R.L., Blake, M.D., and Herrmann, W., 2001. Hydrothermal alteration and volatile element haloes for the Rosebery K lens volcanic-hosted massive sulfide deposit, western Tasmania; Economic Geology, v. 96, p. 1055–1072.

Lentz, D.R. and Goodfellow, W.D., 1993. Petrology and mass balance constraints on the origin of quartz augen schist associated with the Brunswick massive sulphide deposits, Bathurst, New Brunswick; Canadian Mineralogist, v. 31, p. 877–903.

Lentz, D.R. and Goodfellow, W.D., 1996. Intense silicification of footwall sedimentary rocks in the sulphide stringer zone beneath the Brunswick No. 12 massive sulphide deposit,

Bathurst, New Brunswick; Canadian Journal of Earth Sciences, v. 33, p. 284–302.

Lentz, D.R., Hall, D.C., and Hoy, L.D., 1997. Chemostratigraphic, alteration, and oxygen isotope trends in a profile through the stratigraphic sequence hosting the Heath Steele B zone massive sulphide deposit, New Brunswick; Canadian Mineralogist, v. 35, p. 841–874.

Luff, W., Goodfellow, W.D., and Juras, S., 1992. Evidence for a feeder pipe and associated alteration at the Brunswick No. 12 massive sulfide deposit; Exploration and Mining Geology, v. 1, p. 167–185.

MacLellan, K.L., Lentz, D.R., and McClenaghan, S.H., 2006. Petrology, geochemistry, and genesis of the copper zone at the Brunswick No. 6 volcanogenic massive sulfide deposit, Bathurst Mining Camp, New Brunswick, Canada; Exploration and Mining Geology, v. 15, p. 53–76.

McClenaghan, S.H., Goodfellow, W.D., and Lentz, D.R., 2003. Gold in massive sulfide deposits, Bathurst Mining Camp: distribution and genesis, *In:* Massive sulfide deposits of the Bathurst mining camp, New Brunswick, and northern Maine, (ed.) W.D. Goodfellow, S.R McCutcheon, and J.M. Peter; Society of Economic Geologists, Economic Geology Monograph 11, p. 303–326.

McClenaghan, S.H., Lentz, D.R., and Cabri, L.J., 2004. Abundance and speciation of gold in massive sulphides of the Bathurst Mining Camp, New Brunswick, Canada; Canadian Mineralogist, v. 42, p. 851–871.

McClenaghan, S.H., Lentz, D.R., and Beaumont-Smith, C.J., 2006. The gold-rich Louvicourt volcanogenic massive sulfide deposit, New Brunswick: a Kuroko analogue in the Bathurst Mining Camp, *In:* Volcanic-Hosted Massive Sulfide Deposits and their Geological Settings in the Bathurst Mining Camp, New Brunswick, (ed.) D.R. Lentz; Exploration and Mining Geology, v. 15, p. 127–154.

McClenaghan, S.H., Lentz, D.R., Martin, J., and Diegor, J., 2009. Gold in the Brunswick No. 12 volcanogenic massive sulfide deposit, Bathurst Mining Camp, Canada: Evidence from bulk-ore analysis and laser ablation ICP-MS data on sulfide phases; Mineralium Deposita, v. 44, p. 523–557.

McClenaghan, S.H., 2011. Trace-element systematics of volcanogenic massive sulphide deposits in the Bathurst Mining Camp, New Brunswick, Canada: Exploration to petrogenetic implications; Ph.D. thesis, University of New Brunswick, Fredericton, New Brunswick, 664 p.

McLellan, K.L., Lentz, D.R., and McClenaghan, S.H., 2006. Petrology, geochemistry, and genesis of the copper zone at the Brunswick No. 6 volcanogenic massive sulphide deposit, Bathurst Mining Camp, New Brunswick, Canada; Exploration and Mining Geology, v. 15, p. 53–76.

Mireku, L.K. and Stanley, C.R., 2007. Lithogeochemistry and hydrothermal alteration at the Halfmile Lake South Deep Zone, a volcanic-hosted massive sulfide deposit, Bathurst Mining Camp, New Brunswick; Exploration and Mining Geology, v. 15, p. 177–199.

Paton, C., Hellstrom, J.C., Paul, B., Woodhead, J.D., and Hergt, J.M., 2011. Iolite: Freeware for the visualisation and processing of mass spectrometric data; Journal of Analytical Atomic Spectrometry, v. 26, p. 2508–2518.

Peter, J.M., Kjarsgaard, I.M., Goodfellow, W.D., 2003a. Hydrothermal sedimentary rocks of the Heath Steele Belt, Bathurst Mining Camp, New Brunswick: Part 1. Mineralogy and mineral chemistry, *In:* Massive sulfide deposits of the Bathurst mining camp, New Brunswick, and northern Maine, (ed.) W.D. Goodfellow, S.R McCutcheon, and J.M. Peter; Society of Economic Geologists, Economic Geology Monograph 11, p. 361–390.

Peter, J.M., Goodfellow, W.D., Doherty, W., 2003b. Hydrothermal sedimentary rocks of the Heath Steele Belt, Bathurst Mining Camp, New Brunswick: Part 2. Bulk and rare earth element geochemistry and implications for origin, *In:* Massive sulfide deposits of the Bathurst mining camp, New Brunswick, and northern Maine, (ed.) W.D. Goodfellow, S.R McCutcheon, and J.M. Peter; Society of Economic Geologists, Economic Geology Monograph 11, p. 391–416.

Roberts, F.I., 1982. Trace element chemistry of pyrite: a useful guide to the occurrence of sulfide base metal mineralization; Journal of Geochemical Exploration, v. 17, p. 49–62.

Rogers, R., Ross, P.S., Goutier, J., and Mercier-Langevin, P., 2014. Using physical volcanology, chemical stratigraphy, and pyrite geochemistry for volcanogenic massive sulfide exploration: an example from the Blake River Group, Abitibi Greenstone Belt; Economic Geology, v. 109, p. 61–88.

Rose, D.G. and Johnson, S.C., 1990. New Brunswick computerized mineral occurrence database; New Brunswick Department of Natural Resources and Energy, Mineral Resources Division, internal report.

Ryall, W.R., 1981. The forms of mercury in some Australian stratiform Pb-Zn-Ag deposits of different regional metamorphic grades; Mineralium Deposita, v. 16, p. 425–435.

Soltani Dehnavi, A., Lentz, D.R., and McFarlane, C., 2012. New insight into the massive sulfide deposits in the Bathurst Mining Camp, New Brunswick: implication for volatile element signatures like Cd, Sb, Tl, As, and Hg elements in massive sulphide, *In:* Abstracts; Exploration, Mining and Petroleum New Brunswick conference, Fredericton, New Brunswick, November 4–6, 2012.

Soltani Dehnavi, A., McFarlane, C.R.M., McClenaghan, S.H., and Lentz, D.R., 2013a. In situ LA-ICP-MS of sulfide minerals in VMS deposits throughout the Bathurst Mining Camp, New Brunswick, Canada: volatile trace element contents and distribution with implications for their syngenetic to polyphase metamorphic history, *In:* Conference Program and Abstracts volume; Society of Economic Geologists Geoscience for Discovery 2013, Whistler, September 24–27, 2013.

Soltani Dehnavi, A., McFarlane, and Lentz, D.R., 2013b. Sulfide mineral chemistry from the massive sulfide deposits of Bathurst Mining Camp, Canada: implication for volatile trace-elements distribution and developing the trace-element exploration vectoring tool, *In:* Abstracts; Exploration, Mining and Petroleum New Brunswick conference, Fredericton, NB, November 2013.

Soltani Dehnavi, A., Lentz, D.R., McFarlane, C.R.M., and McClenaghan, S.H., 2014a. LA-ICP-MS trace-element study of pyrite from massive sulfide deposits of the Bathurst Mining Camp, Canada: Determination of volatile trace-element contents in pyrite and its application as a vectoring tool for the exploration of VMS deposits, *In:* Program with Abstracts; Geological Association of Canada-Mineralogical Association of Canada Annual Meeting, Fredericton, May 20–22, 2014, p. 260.

Soltani Dehnavi, A., McFarlane, C.R.M., Lentz, D.R., and McClenaghan, S.H., 2014b, Variation in sulphide mineral chemistry in massive sulfide deposits, Bathurst Mining Camp, Canada: Implication for measuring volatile trace-elements by LA-ICP-MS and its application as a vectoring tool for the exploration of VMS deposits, *In:* Program with Abstracts; Geological Association of Canada-Mineralogical Association of Canada Annual Meeting, Fredericton, May 20–22, 2014, p. 259–260.

Soltani Dehnavi, A., Lentz, D.R., and McFarlane, C.R.M., 2014c. Interpreting volatile trace-element signatures in volcanogenic massive sulphide deposits of the Bathurst Mining Camp,

Canada: Evidence from a LA-ICP-MS study on sulfide minerals, *In:* Abstracts; Goldschmidt conference, Sacramento, June 8–13, 2014, p. 2347.

Soltani Dehnavi, A., McFarlane, C.R.M., McClenaghan, S.H., and Lentz, D.R., 2014d. In situ LA ICP-MS of sulphide minerals in VMS deposits throughout the Bathurst Mining Camp, New Brunswick, Canada: volatile trace element contents and distribution with implications for their syngenetic to polyphase metamorphic history; Geological Survey of Canada, Open File 7537. doi:10.4095/293681

Soltani Dehnavi, A., Lentz, D.R., McFarlane, C.R.M., and McClenaghan, S.H., 2014e. In situ LA-ICP-MS systematics for quantitative volatile trace-element measurement in sulfide minerals: from developing methodology to its application in the case study of massive sulfide deposits of the Bathurst Mining Camp, Canada, *In:* Conference Program and Abstracts volume; Exploration, Mining and Petroleum New Brunswick conference, Fredericton, November 2-4, 2014, p. 91.

Soltani Dehnavi, A., McFarlane, C.R.M., Lentz, D.R., and McClenaghan, S.H., 2014f. Variations in phyllosilicate mineral chemistry from the massive sulfide deposits of the Bathurst Mining Camp, Canada: LA-ICP-MS systematics and its application in determination of volatile trace-element suite applicable in VMS exploration, *In:* Conference Program and Abstracts volume; Exploration, Mining and Petroleum New Brunswick conference, Fredericton, November 2-4, 2014, p. 93.

Walker, J.A. and Lentz, D.R., 2006. The Flat Landing Brook Zn-Pb-Ag massive sulfide deposit, Bathurst Mining Camp, New Brunswick, Canada, *In:* Volcanic-hosted Massive Sulfide Deposits and their Geological Settings in the Bathurst Mining Camp, New Brunswick, (ed.) D.R. Lentz; Exploration and Mining Geology, v. 15, p. 99–126.

Walker, J.A. and McCutcheon, S.R., 2011. A chemostratigraphic assessment of core from the discovery hole of the Halfmile Lake Deep VMS Zone, Bathurst Mining Camp, northeastern New Brunswick, *In:* Geological Investigations in New Brunswick for 2010, (ed.) G.L. Martin; New Brunswick Department of Natural Resources, Lands, Minerals and Petroleum Division, Mineral Resource Report 2011-2, p. 1–49.

Wilson, S.A., Ridley, W.I., and Koenig, A.E., 2002. Development of sulfide calibration standards for the laser ablation inductively-coupled plasma mass spectrometry technique; Journal of Analytical Atomic Spectrometry, v. 17, p. 406–409.

Yang, K., Huntington, J. F., Gemmell, J. B., Scott, K. M., 2011. Variations in composition and abundance of white mica in the hydrothermal alteration system at Hellyer, Tasmania, as revealed by infrared reflectance spectroscopy; Journal of Geochemical Exploration, v. 108, p. 143–156.

GEOLOGICAL SURVEY OF CANADA
OPEN FILE 7853

Targeted Geoscience Initiative 4: Contributions to the Understanding of Volcanogenic Massive Sulphide Deposit Genesis and Exploration Methods Development

Overview of VMS exploration in glaciated terrain using indicator minerals, till geochemistry, and boulder tracing: A Canadian perspective

M. Beth McClenaghan[1], Jan M. Peter[1], and Daniel Layton-Matthews[2]

[1]Geological Survey of Canada, Ottawa, Ontario
[2]Queen's University, Kingston, Ontario

2015

Recommended citation

McClenaghan, M.B., Peter, J.M., and Layton-Matthews, D., 2015. Overview of VMS exploration in glaciated terrain using indicator minerals, till geochemistry, and boulder tracing: A Canadian perspective, *In:* Targeted Geoscience Initiative 4: Contributions to the Understanding of Volcanogenic Massive Sulphide Deposit Genesis and Exploration Methods Development, (ed.) J.M. Peter and P. Mercier-Langevin; Geological Survey of Canada, Open File 7853, p. 81–99.

Publications in this series have not been edited; they are released as submitted by the author.

Contribution to the Geological Survey of Canada's Targeted Geoscience Initiative 4 (TGI-4) Program (2010–2015)

TABLE OF CONTENTS

Tables

Overview of VMS exploration in glaciated terrain using indicator minerals, till geochemistry, and boulder tracing: A Canadian perspective

M. Beth McClenaghan[1]*, Jan M. Peter[2], and Daniel Layton-Matthews[3]

[1]Northern Canada Division, Geological Survey of Canada, 601 Booth Street, Ottawa, Ontario K1A 0E8
[2]Central Canada Division, Geological Survey of Canada, 601 Booth Street, Ottawa, Ontario K1A 0E8
[3]Department of Geological Sciences and Geological Engineering, Queen's University, Kingston, Ontario K7L 3N6
*Corresponding author's e-mail: beth.mcclenaghan@nrcan.gc.ca

ABSTRACT

During the Quaternary, most of Canada's landmass was covered by ice sheets that eroded and dispersed metal-rich debris from volcanogenic massive sulphide (VMS) deposits across the landscape together with a blanket of unconsolidated debris. Therefore, boulder tracing, till geochemistry, and indicator minerals are important exploration methods for VMS deposits in Canada. This paper provides an overview of the development and application of these methods, including till sampling, appropriate size fractions of till to analyze, sample processing, and analytical techniques. Selected case histories from different regions across Canada are also presented.

Copper, Pb, and Zn are indicator elements of VMS deposits, and pathfinder elements include As, Ag, Au, Ba, Bi, Cd, Hg, In, Sb, Se, Sn, and Tl. Abundances of these elements are most commonly determined in the <0.063 mm (silt + clay) fraction of till. Indicator minerals of VMS deposits are recovered from the >3.2 specific gravity heavy mineral concentrate of till and include the main ore minerals (galena, sphalerite, chalcopyrite, pyrite, and pyrrhotite), accessory minerals (native gold, electrum, cassiterite, cinnabar, and barite), and, in metamorphic terrain, metamorphosed minerals of mineralization, alteration, or exhalites, including sillimanite, andalusite, gahnite, staurolite, and spessartine. Magnetite and its chemical composition may also be a useful VMS exploration tool. Ongoing and future research of drift exploration methods for VMS deposits will focus on reducing sample size, lowering analytical costs, and identifying new indicator minerals and chemical discrimination criteria.

INTRODUCTION

Most of Canada's landmass was glaciated during the Quaternary. Ice sheets eroded and dispersed sulphide-rich debris from volcanogenic massive sulphide (VMS) deposits and deposited a blanket of unconsolidated sediments over the mineral deposits. Thus, drift prospecting using till geochemistry and indicator minerals is an important exploration method for VMS deposits in Canada. The application of till geochemical methods to VMS exploration in Canada has a long history, starting with boulder tracing and till geochemistry studies (e.g. Dreimanis, 1958, 1960; Fortescue and Hornbrook, 1969; Shilts, 1975; Hoffman and Woods, 1991; Kaszycki et al., 1996; Parkhill and Doiron, 2003; McClenaghan and Peter, 2013). In the past 15 years, indicator mineral methods, routinely used for gold and diamond exploration, have been expanded to include a suite of VMS indicator minerals for exploration in glaciated terrain.

As part of the GSC's Targeted Geoscience Initiative 4 (TGI-4) VMS project (2010-2015), a small research activity was funded to compile information about the historical and current application of indicator minerals and till geochemistry to VMS exploration in the glaciated terrain of Canada. Herein we provide an overview of this history, VMS pathfinder elements and indicator minerals, and outline best practices for sampling, appropriate size fractions of till to analyze, sample processing, and analytical techniques. Case histories from different regions across Canada (Fig. 1) are also discussed. Some of the information about VMS till geochemical methods summarized here is derived from a detailed review of the application of till geochemical methods to VMS exploration in GSC Open File 7354 by McClenaghan and Peter (2013).

SAMPLE MEDIA

Boulders

Boulder tracing is one of the oldest exploration methods in glaciated terrain (e.g. Grip, 1953; Dreimanis, 1958; Lee, 1971; Hyvarinen et al., 1973). Since the late

McClenaghan, M.B., Peter, J.M., and Layton-Matthews, D., 2015. Overview of VMS exploration in glaciated terrain using indicator minerals, till geochemistry, and boulder tracing: A Canadian perspective, *In:* Targeted Geoscience Initiative 4: Contributions to the Understanding of Volcanogenic Massive Sulphide Deposit Genesis and Exploration Methods Development, (ed.) J.M. Peter and P. Mercier-Langevin; Geological Survey of Canada, Open File 7853, p. 81–99.

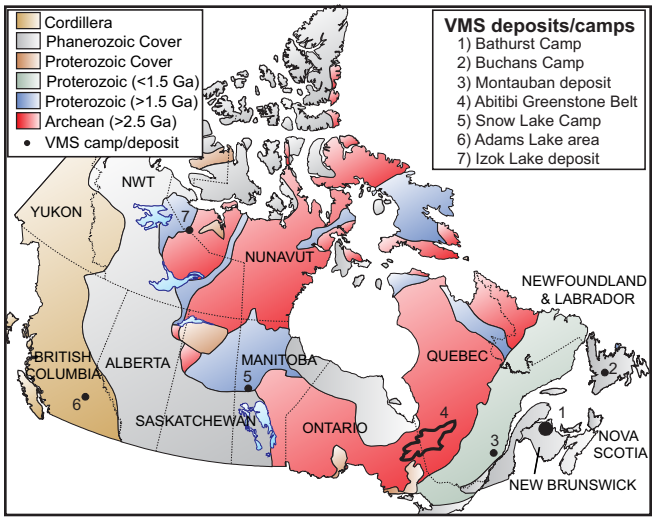

Figure 1. Location map of the volcanogenic massive sulphide camps and deposits that are discussed in this paper.

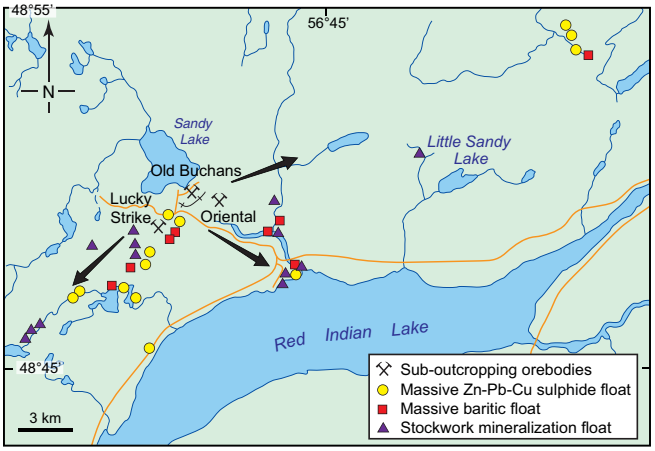

Figure 2. Map showing locations of surface float (boulders, cobbles) of massive sulphide, massive barite, and stockwork mineralization around the Buchans VMS deposits, Newfoundland. Black arrows indicate generalized known ice-flow directions (modified from James and Perkins, 1981).

1800s, mapping the distribution of mineralized massive sulphide boulders and cobbles has provided clues to the presence of concealed VMS mineralization in the glaciated terrain of Canada. Prospecting for massive sulphide boulders has contributed to the discoveries of the Orvan Brook, Anaconda, Rocky Turn, and Armstrong Brook VMS deposits in the Bathurst Mining Camp (BMC) (Dreimanis 1958; Lee, 1971), the Mogador VMS deposit in the Val d'Or Mining Camp in the Abitibi Greenstone Belt (AGB) (Dreimanis, 1958), and the Izok Lake VMS deposit, Nunavut (Money and Helsop, 1976) James and Perkins (1981) documented the presence of mineralized float down-ice of the Buchans VMS Mining District, Newfoundland that reflects the net result of ice flows to the southwest, southeast, and east-northeast (Fig. 2).

Till versus Soil Sampling

Some of the earliest VMS case studies and exploration programs in Canada were based on the traditional "soil" sampling approach (e.g. Bischoff, 1954; Byers, 1956; Ermengen, 1957; Morris, 1966; Govett, 1973; Miller, 1979; Telford and Becker, 1979; James and Perkins, 1981) adapted from use in areas of residual overburden and designed to avoid/ignore the effects of glaciation (Shilts, 1984). Soil formation through weathering destroys labile minerals such as sulphides. Thus, the geochemical signatures in soils formed on till are the combined result of clastic glacial dispersal and subsequent aqueous and gaseous dispersal (e.g. Cameron, 1977). Therefore, base metal contents may be lower in soil than in unweathered till, and geometry of glacial dispersal trains may be more difficult to interpret and trace up-ice to the source (e.g. Hoffman and Woods, 1991; Kaszycki et al., 1996; Paulen, 2001; Lett and Jackaman, 2002; Hall et al., 2003). In glaciated terrain, soil may be developed on a variety of sediment types in addition to till, including glaciofluvial, glaciolacustrine, eolian, colluvium, or weathered bedrock. Each of these can have very different transport and deposition mechanisms that can complicate the interpretation of soil geochemical data.

Dreimanis (1960) recognized early on that the optimal approach to mineral exploration in glaciated terrain would be to sample till — material eroded, transported, and deposited directly by glaciers — and that metal-rich debris within till is a product of mechanical dispersal. Since the late 1970s, most VMS case studies and regional geochemical surveys have sampled till (McClenaghan and Peter, 2013). Till sampling strategies for mineral exploration in the glaciated terrain of Canada have been summarized by Plouffe (1995), Levson (2001a,b), McMartin and McClenaghan (2001), McMartin and Campbell (2009), Paulen (2009), Spirito et al. (2011), Plouffe et al. (2013), and McClenaghan et al. (2013).

METHODS

Till Geochemical Analysis

Till and soil geochemical studies conducted from the 1950s through the 1980s typically determined only the main economic base metals (Cu, Pb and Zn) in VMS deposits, as these could be readily and cost-effectively analyzed. The earliest base metal-content determinations of till relied on "cold-extraction" techniques (abbreviated as cx, cx-THM, CxCu) that determine the content of readily soluble metal, or metals present as free ions or loosely bound ions on the surface of grains (Rose et al., 1979; Levinson, 1980). Cold extractions typically use buffer solutions and dilute acids, such as nitric, hydrochloric, acetic, or ethylenediaminetetraacetic (EDTA), and are commonly analyzed by

colourimetric methods. Cold extraction can be readily performed in the field because no preliminary sample treatment, such as drying or sieving, is required. "Hot extraction" techniques involve the use of one or more acid solutions at temperatures >100°C and are performed in an analytical laboratory. The sample is dried and sieved prior to analysis. The main advantage of using hot acids is that more of the total metals, such as those bound to non-silicates, are extracted than with cold-extraction techniques.

A major advance in VMS exploration was facilitated in the 1980s and 1990s by the development of inductively coupled plasma-mass spectrometry (ICP-MS) analytical instruments as this allowed for the determination of a broad suite of trace elements in rocks, mineralization, and surficial media (Piercey, 2010) that can be used to document and delineate multi-element signatures in till down-ice of VMS deposits. An extensive suite of VMS pathfinder elements (Cu, Pb, Zn, Ag, Au, Se, Sb, Bi, Ba, As, Cd, Hg, Sn, Ga, In, and Tl) can now be determined in the till matrix and can be used to indicate if the eroded VMS mineralization is Ag-rich or Au-rich, and if a deposit is enriched in deleterious trace elements, such as Se.

Most current exploration programs and government surveys that utilize till geochemistry employ a strong partial digestion, such as aqua regia, to determine the contents of the major ore elements Cu, Pb, and Zn, as well as the pathfinder elements As, Ag, Bi, Cd, Hg, In, Sb, Se, and Tl (McClenaghan et al., 2013). "Total" digestions, such as borate fusion or 4-acid digestion, and analysis by ICP-MS or instrumental neutron activation analysis (INAA) are used to determine the contents of Sn and Ba. Optimal methods to determine total gold content are fire assay/ICP-MS or INAA using a 30 g aliquot.

Size Fractions for Geochemical Analysis

The main VMS "ore" minerals chalcopyrite, galena, and sphalerite are relatively soft (hardness <4) and therefore are readily comminuted during glacial transport to the finest fraction of till (silt + clay) over short distances (Kauranne, 1959; Salminen, 1980; Nikarrinen et al., 1984; Nevalainen, 1989). Therefore, the geochemical analysis of either the silt + clay -250 mesh (<0.063 mm or 63 µm) or the centrifuged clay (<0.002 mm or 2 µm) fraction of till is ideal for detecting glacial dispersal from VMS deposits. The advantage of geochemically analyzing the <0.002 mm fraction of till is the high contrast between background and anomalously high metal contents (e.g. Shilts, 1975, 1995, 1996). There are also disadvantages of using the <0.002 mm fraction: 1) the clay separation process required to isolate the <0.002 mm fraction is costly and time-consuming and a large volume of material (~1 kg) is needed to recover sufficient clay-sized material for analysis (Lindsay and Shilts, 1995; Klassen, 2003); 2) the typical Canadian shield-derived tills have a low (<2 %) clay content; and 3) the clay-size fraction can adsorb and bind metal ions onto clay particle surfaces which can, in some cases, produce false anomalies from hydromorphic dispersion of metals not necessarily related to VMS mineralization (Pronk, 1987).

The <0.063 mm fraction of till is presently the most commonly analyzed size fraction for base metal exploration for a number of reasons: 1) it is readily and quickly recovered by sieving, especially in till samples with only minor (<2 %) clay and is thus inexpensive to prepare; 2) it provides reasonable contrast between background and anomalous metal contents; and 3) it is less susceptible to hydromorphic dispersion effects (Pronk, 1987).

Geochemical analysis of a coarser size fraction of till, such as the -80 mesh fraction (<0.177 mm or 177 µm), is not recommended because this size fraction contains a significant component of fine sand-sized material. The fine-sand component of till contains abundant detrital quartz and feldspar (Dreimanis and Vagners, 1972; Klassen, 2003) that dilutes metal contents in the finer silt- and clay-sized fractions and thus decreases the intensity of (i.e. mutes) the geochemical signature of a nearby VMS deposit (Nikkarinen et al., 1984).

Less commonly, a split of the heavy mineral concentrate (HMC) of large (5 to 10 kg) till samples with a specific gravity (SG) of >2.9 or >3.3 can be geochemically analyzed for base metals (e.g. Garrett, 1971; Gleeson and Cormier, 1971; Telford and Becker, 1979; Smith, 1992) and has been shown to enhance the contrast between background and anomalous values. Historically, till HMCs were pulverized and geochemically analyzed because there was no commercially available service to visually examine and identify indicator minerals for VMS and other base metal deposits (e.g. sedimentary exhalative (SEDEX), magmatic Cu-Ni-PGE). Currently, if geochemical analysis of the HMC is warranted, it is carried out on a split of the <0.25 mm -60 mesh (250 µm) HMC in order to preserve the coarser fraction (0.25–2.0 mm or 250–2000 µm) for visual examination and identification of VMS indicator minerals.

Field Portable X-Ray Fluorescence Analysis

Portable x-ray fluorescence spectrometry (pXRF) is increasingly being used in the field to actively guide till sampling programs and to follow-up geochemical anomalies in the same field season (e.g. Peter et al., 2010; Hall and McClenaghan, 2013; Kjarsgaard et al., 2014). Metal contents of unprocessed dry till samples (in open-ended pXRF cups covered by 4.0 µm

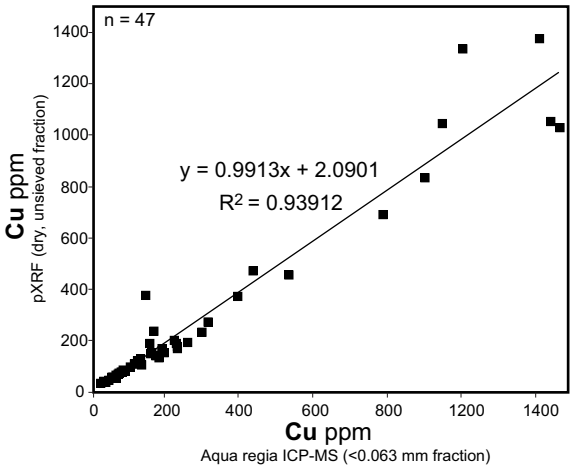

Figure 3. Bivariate plot of Cu (ppm) content in till as determined by portable XRF (pXRF) (InnovX Delta with Ta tube) on dry, unseived till versus Cu (ppm) content in till as determined by aqua regia ICP-MS on dry, sieved (<0.063 mm) till from the Halfmile Lake VMS deposit (unpublished GSC data).

Prolene® thin-film) can also be determined by pXRF after the samples have been collected to prioritize till samples for lab-based geochemical analysis. The good agreement of pXRF analytical values obtained in this manner with laboratory ICP-MS analyses of aqua regia digestions of the <0.063 mm fraction of base metal-rich till from the Halfmile Lake VMS deposit, BMC (Fig. 3) illustrates the utility of pXRF analysis for quantitative determination of metal contents of till.

Indicator Mineral Methods

Sulphide minerals have been recognized as useful indicator minerals of massive sulphide mineralization since till geochemical methods were first used for VMS exploration. Initially, only the HMC of selected till samples with anomalous Pb, Zn, or Cu contents were examined to determine the mineralogical residence site(s) (e.g. galena, sphalerite, chalcopyrite, pyrrhotite, bornite) of the anomalies (e.g. Dreimanis, 1958; Gleeson and Cormier, 1971; Cameron, 1977). The suite of indicator minerals for VMS deposits that can be recovered from till gradually expanded over time to include other ore minerals and alteration minerals (Averill, 2001). Today the suite includes sulphide ore minerals and native gold, as well as more physically and chemically robust oxide and silicate minerals, such as sillimanite, andalusite, gahnite, staurolite, spessartine (Table 1), which are indicative of metamorphosed massive sulphide mineralization, associated hydrothermal alteration, or exhalite zones.

VMS indicator minerals are most commonly visually identified and counted in the sand-sized (0.25–2.0 mm) HMC fraction of till (e.g. Averill, 2001; Budulan et al., 2012; Hicken et al., 2013; Paulen et al., 2013; McClenaghan et al., in press). The main advantage of using indicator minerals to explore for VMS deposits is that the indicator mineral grains are visible and identifiable using standard low-magnification optical microscopy, and this provides (1) physical evidence of the presence of mineralization or alteration; (2) information about the source that traditional geochemical methods cannot, including nature of the ore, alteration, and proximity to source; (3) extreme sensitivity and ability to detect only a few grains, equivalent to ppb-level indicator mineral abundances, even in regions where rocks dilute concentrates with non-indicator heavy minerals; and (4) the ability to visually identify and remove anthropogenic contamination (i.e. material from previous exploration, mining, or smelting activity).

Photographs of some of these minerals as they appear in a till HMC are shown in Figure 4. Volcanogenic massive sulphide indicator minerals are recovered from large (>10 kg) till samples after processing to concentrate the heavy (SG >3.2) minerals. Common processing methods used to concentrate heavy minerals and recover indicator minerals from till are described and illustrated in McClenaghan (2011). In Canada, the most widely used method to recover VMS indicator minerals from till is a combination of tabling and heavy liquid separation (e.g. McClenaghan, 2011; McClenaghan et al., 2012a,b,c; Layton-Matthews et al., 2014). Methods for collecting large till samples suitable for indicator mineral recovery are summarized in McMartin and McClenaghan (2001), McMartin and Campbell (2009), Paulen (2009), Spirito et al. (2011), and Plouffe et al. (2013). Once recovered from the HMC, indicator minerals can be further characterized and classified using microanalytical techniques, such as scanning electron microprobe (SEM), electron microprobe (EMP), and rapid SEM scanning, such as Quantitative Evaluation of Minerals by Scanning Electron Microscopy (QEMSCAN) and Mineral Liberation Analysis (MLA), to confirm their visual identification and provide insights into bedrock source and assess fertility. Layton-Matthews et al. (2014) provide a recent review of all these methods for indicator mineral characterization.

Gahnite

Gahnite ($ZnAl_2O_4$) is a zincian spinel that occurs around or within metamorphosed VMS deposits (Money and Heslop, 1976; Spry 1982; Sheridan and Ray, 1984; Spry and Scott, 1986; Bernier et al., 1987; Heimann et al. 2005; Ghosh and Praveen, 2008; Spry and Teale, 2009; Heimann et al., 2013). It is a useful indicator mineral of VMS deposits in surficial sediments because it is physically robust (hardness=8) and chemically stable in oxidizing environments (Morris et. al., 1997) and thus it can be recovered from glacial sediments (Stendal and Theobald, 1994; Morris et al.,

Table 1. Common indicator minerals of hydrothermal alteration zones associated with metamorphosed VMS deposits in glaciated terrain (modified from Averill, 2001).

Indicator Mineral	Zone	Chemical Composition	Specific Gravity	Hardness (Mohs)
Sillimanite	metmorphosed alteration	Al_2SiO_5	3.24	7.0
Kyanite	metamorphosed alteration	Al_2SiO_5	3.56–3.67	4.0–7.0
Corundum	metamorphosed alteration/alteration	Al_2O_3	4.0–4.1	9.0
Andalusite	metamorphosed alteration/alteration	Al_2SiO_5	3.15	6.5–7
Mg–Spinel	metamorphosed alteration	$MgAl_2O_4$	3.64	8.0
Staurolite	metamorphosed alteration	$(Fe,Mg,Zn)_2Al9(Si,Al)_4O_{22}(OH)_2$	3.65–3.77	7.0–7.5
Topaz	metamorphosed alteration	$Al_2SiO_4(F,OH)_2$	3.5–3.6	8.0
Mn–Epidote	alteration	$Ca_2(Al,Fe,Mn)_3Si_3O_{12}(OH)$	3.3–3.6	6.0–7.0
Anthophyllite	metamorphosed alteration/exhalite	$(Mg,Fe)_7Si_8O_{22}(OH)_2$	2.85–3.57	5.0–6.0
Orthopyroxene	metamorphosed alteration/exhalite	$(Mg,Fe)_2Si_2O_6$	3.4	5.0–6.0
Tourmaline	alteration/exhalite	$(Na,Ca)(Mg,Fe)_3Al_6(BO_3)_3(Si_6O_{18})(OH)_4$	3.06	7.0–7.5
Spessartine	alteration/exhalite	$Mn_3Al_2Si_3O_{12}$	4.18	6.5–7.5
Magnetite	gangue/exhalite	Fe_3O_4	5.15	5.5–6.0
Barite	gangue	$BaSO_4$	4.48	3.0–3.5
Franklinite	metamorphosed mineralization/exhalite	$(Zn, Mn,Fe)(Fe,Mn)_2O_4$	5.14	5.5–6.0
Willemite	metamorphosed mineralization	Zn_2SiO_4	3.9–4.2	5.5
Gahnite	metamorphosed mineralization	$ZnAl_2O_4$	4.0–4.6	7.5–8.0
Cinnabar	mineralization	HgS	8.1	2.0–2.5
Loellingite	mineralization	$FeAs_2$	7.1–7.7	5.0–5.5
Chalcopyrite	mineralization	$CuFeS_2$	4.1–4.3	3.5
Pyrite	mineralization	FeS_2	5–5.02	6.5
Galena	mineralization	PbS	7.2–7.6	2.5
Sphalerite	mineralization	(Zn,Fe)S	3.9–4.2	3.5–4.0
Native Gold	mineralization	Au	16.0–19.3	2.5–3.0
Electrum	mineralization	AuAg	16.0–19.3	2.5–3.0
Pyrrhotite	mineralization	$Fe_{(1-x)}S$	4.58–4.65	3.5–4
Cassiterite	mineralization	SnO_2	6.8–7.0	6–7
Beudantite	gossan (preglacial oxidation of mineralization)	$PbFe_3(AsO_4)(SO_4)(OH)_6$	4.1–4.3	4.0
Jarosite	gossan (preglacial oxidation of mineralization)	$KFe_3(SO_4)_2(OH)_6$	2.9–3.3	2.5–3.5
Goethite	gossan (preglacial oxidation of mineralization)	FeO(OH)	3.3–4.3	5.5

1997; Averill, 2001). Gahnite is readily concentrated in the heavy mineral fraction of glacial sediments because of its high specific gravity (SG 4-4.6) and can be easily visually identified because of its distinctive bluish green colour (Fig. 4).

Toverud (1977) and Peuraniemi (1990) were among the first to document the presence of gahnite in till down-ice of known VMS mineralization. Subsequently, Lalonde et al. (1994) reported gahnite in till up to 5 km down-ice of the Montauban VMS deposit in Quebec. McClenaghan et al. (2012c) reported the presence of gahnite in till around the Halfmile Lake VMS deposit in the BMC (Fig. 1). Most recently, a detailed study of the glacial dispersal of gahnite was conducted around the Izok Lake VMS deposit, Nunavut (Fig. 1) (Hicken et al., 2012; Paulen et al., 2013; McClenaghan et al., in press).

The major-element composition of gahnite can be used to distinguish prospective rocks (e.g. Spry, 1982, 1987; Spry and Scott, 1986; Spry and Teale, 2009). An example of a gahnite-composition discrimination plot developed by Heimann et al. (2005) is shown in Figure 5. The compositional range of gahnite from the Izok Lake VMS deposit and local till plots mainly in the field for metamorphosed massive sulphide deposits in Fe-Al metasedimentary and metavolcanic rocks. This plot is useful for evaluating gahnite grains in till where the bedrock source is unknown. Recently, O'Brien et al. (2014) have shown that the trace element composition of gahnite can aid in discriminating between gahnite originating from VMS deposits and that originating from Sedex and BHT deposits.

Magnetite

Magnetite (Fe_3O_4) is a major accessory mineral in many types of mineral deposits and igneous, metamorphic, and sedimentary rocks; it is extremely common in many VMS deposits (e.g. Ansil, Noranda, Quebec: Galley et al., 1995; Heath Steele B, New Brunswick: Lusk, 1969), but may be entirely absent in others (e.g. Iso, QC: Telford and Becker, 1979). In some deposits, magnetite tends to be concentrated in the core of the stockwork and central, basal part of the overlying sulphide lens. Factors that control its presence or absence

Figure 4. Photographs of selected VMS indicator minerals as they appear in heavy mineral concentrates of till from around VMS deposits.

are temperature, sulphur content, and redox of the mineralizing fluid (e.g. Large, 1977; Sharp and Gemmell, 2002) and/or the subsequent metamorphic fluids (Nesbitt and Kelley, 1980). The chemical composition of magnetite can be used to discriminate between a magmatic or hydrothermal origin (e.g. Dupuis and Beaudoin, 2011; Dare et al., 2012; Galicki et al., 2012; Nadoll et al., 2012; Sappin et al., 2014). Magnetite is an ideal indicator mineral in surficial sediments because it is physically robust (hardness=5.5–6.0) and resistive to chemical alteration during glacial transport and burial in sediments (e.g. Whiting and Faure, 1991). Magnetite in surficial sediments is readily concentrated into a heavy mineral fraction because of its high specific gravity (SG 5.1–5.2) and ferromagnetic character, which allows further separation in a magnetic fraction.

Dupuis and Beaudoin (2011) identified discrimination criteria to distinguish magnetite in VMS and Zn-Pb SEDEX deposits from other deposit types using a Cu/(Si+Ca) versus Al/(Zn+Ca) diagram (Fig. 6). They noted that magnetite in VMS deposits is enriched in Si, Zn, and Ca, and depleted in Al, compared to other deposit types. Makvandi et al. (2013) have reported on detailed studies of magnetite chemical compositions from two VMS deposits. In addition to mineral chemical composition, magnetite grain size, shape, surface texture, and mineral associations can also be used to discriminate different types of magnetite, identify the nature of the host rocks, and recognize transport mechanisms (glacial versus glaciofluvial) (Mandolla and Brooks, 2010; Makvandi et al., 2015).

Lead Isotope Fingerprinting of Galena in Till and Bulk Till

Lead is present in many VMS deposits where it is resident in galena, and less commonly as various sulphosalts and other minerals (e.g. in pyrite). Since galena contains no U, there is no growth of radiogenic lead subsequent to its formation. Thus, the Pb isotopic composition of galena reflects the Pb isotopic composition of the fluid from which the mineral was precipitated. Typically, galena in VMS deposits is distinctly more primitive (less radiogenic) than the Pb isotopic composition(s) of the host rocks (e.g. Sangster et al., 2000). The recognition of galena with such primitive isotopic compositions can be used to identify (and vector toward) VMS mineralization by following it up-ice.

Bell and Franklin (1993) first reported Pb isotopic analyses of till matrix (<0.063 mm) around VMS deposits down-ice of the Chisel Lake, Lost, and Ghost VMS deposits in the Snow Lake Camp, Manitoba (Fig. 1). Subsequent Pb isotopic studies by Bell and Murton (1995) and Simonetti et al. (1996) in the Snow Lake Camp confirmed that Pb isotopic analyses can be used to trace the glacial dispersal of Pb in till. Other examples of the application of Pb isotopes to till geochemistry include that of Bell and Murton (1995) for VMS deposits at Buchans, Newfoundland (Fig. 1) and Hussein et al. (2003) for the Halfmile Lake VMS deposit, BMC (Fig. 1). At the time these studies were published, Pb isotopic analyses of the till fine-fraction were conducted by thermal ionization mass spectrometry; the application was then predicted to be a "new" approach to mineral exploration for massive sulphide deposits (VMS) in glaciated terrain. Since then, there has been much progress in the application of ICP-MS for Pb isotopic analysis (e.g. Meffre et al., 2008), including the ability to analyze single galena grains from till (e.g. Paulen et al., 2011; Oviatt et al., 2013) as

1	Marble
2	Metamorphosed massive sulphide deposits and S-poor rocks in Mg-Ca-Al alteration zones
3	Metamorphosed massive sulphide deposits in Fe-Al metasedimentary and metavolcanic rocks
4	Metabauxite
5	Pegmatite
6	Unaltered and hydrothermally altered Fe-Al-rich metasedimentary and metavolcanic rocks
7	Al-rich granulite

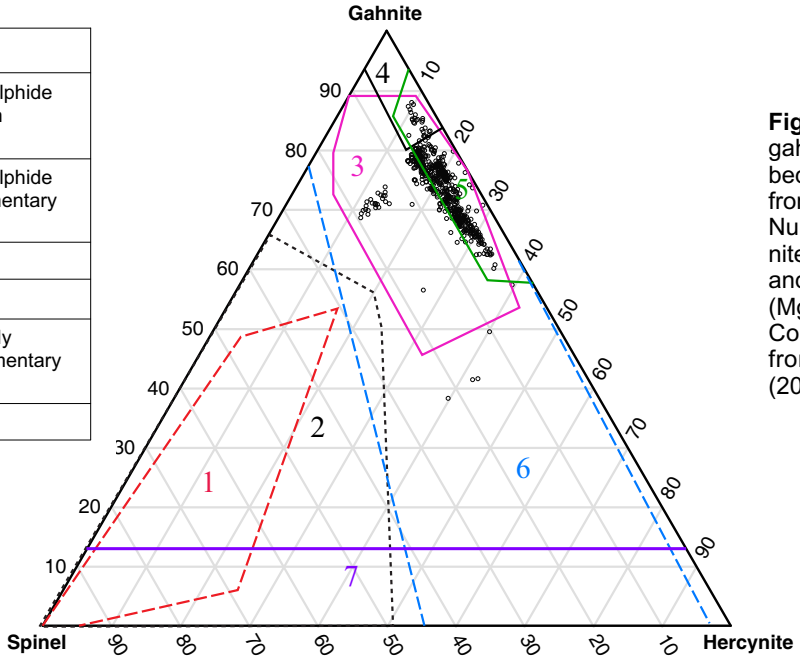

Figure 5. Ternary plot of gahnite composition from bedrock and till samples from the Izok Lake VMS, Nunavut deposit with gahnite (Zn), hercynite (Fe), and spinel sensu stricto (Mg) spinel end-members. Compositional fields are from Heimann et al. (2005).

well as other minerals such as gahnite (Layton-Matthews et al., 2014).

SELECTED CASE STUDIES

Noranda Camp, Abitibi Greenstone Belt

The Horne Cu-Au VMS deposit, discovered in 1923 in the Noranda Camp, central Abitibi Greenstone Belt (AGB) (Fig. 1), is the second largest VMS deposit (after Kidd Creek) and one of the largest Au deposits in the AGB (Galley et al., 2007). Using extensive surface till sampling and mapping of the locations of mineralized pebbles and cobbles down-ice (south to southwest) of the Horne deposit (Fig. 7), Dreimanis (1958, 1960) demonstrated that the deposit has a well defined glacial dispersal train that extends at least 2.4 km down-ice and that till geochemical sampling and analysis (Cu and Zn) is an effective VMS exploration tool in the region. In a second case study carried out at the MacDonald (Gallen) Cu-Zn-Au VMS deposit, located 6 km to the northeast of the Horne deposit, Dreimanis (1958, 1960) documented the presence of Cu- and Zn-rich till and clasts up to 0.9 km down-ice. In these early studies, Dreimanis (1958, 1960) concluded that since Canada is a glaciated landscape, the application of till geochemical and boulder tracing methods, in combination with geophysical and other prospecting methods, would lead to new discoveries of ore deposits.

Snow Lake Camp, Central Canadian Shield

In the Snow Lake Camp (Fig. 1), 70 km east of Flin Flon, detailed till sampling was used to outline south-southwest-trending glacial dispersal fans defined by Cu and Zn (Fig. 8) in two fractions of till around the Chisel Lake, Lost, and Ghost VMS deposits (Kaszycki et al., 1996). The contrast between background and anomalous Cu and Zn contents is greater for the <0.002 mm fraction of till than the <0.063 mm fraction. Glacial dispersal of these metals is detectable up to 1 km down-ice from the deposit. Areas of anomalous metal contents in the B-horizon developed on till are smaller in areal extent, indicating that the B-horizon contains less metals than the C-horizon in this area. Kaszycki et al. (1996) also identified a Cu, Hg, Pb, As, Au, and Sb multi-element anomaly in till north of the Chisel Lake deposit, an area where the Photo Lake VMS deposit was subsequently discovered. In addition to documenting the multi-element signatures of VMS deposits in

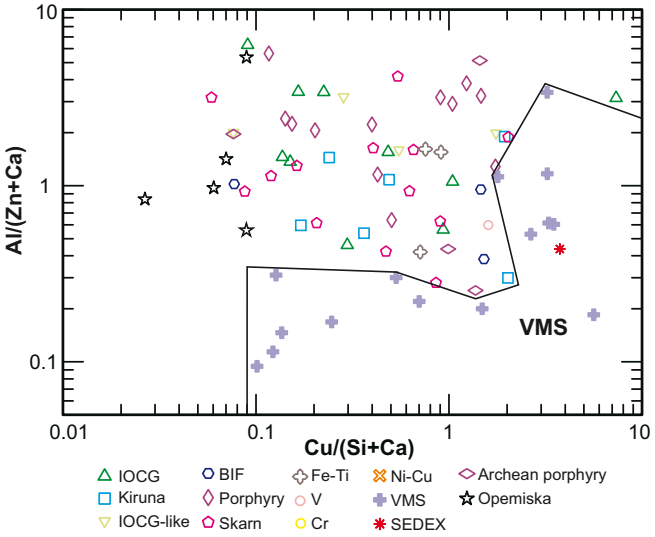

Figure 6. Cu/(Si+Ca) versus Al/(Zn+Ca) discriminant diagram for magnetite from various deposit types. Samples from VMS deposits are marked as purple crosses (modified from Dupuis and Beaudoin, 2011).

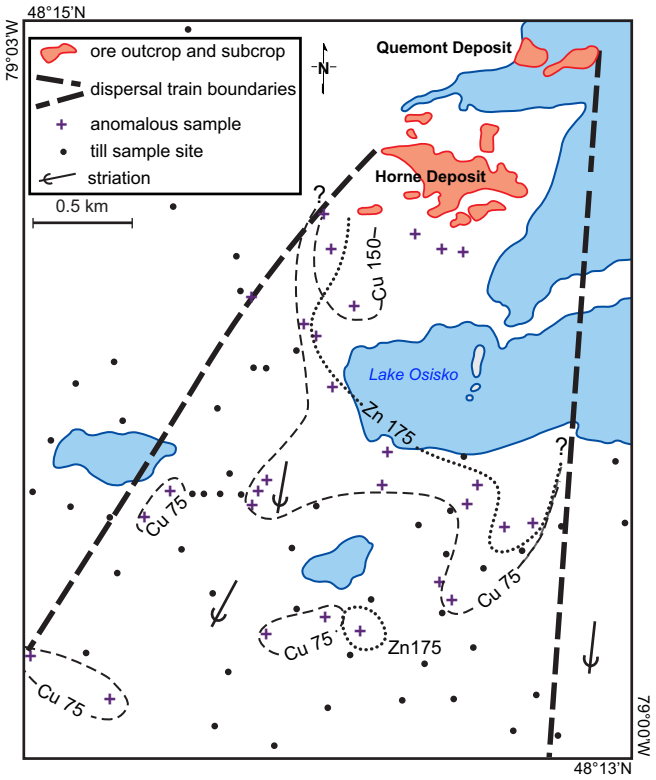

Figure 7. Map of the glacial dispersal train of mineralized clasts and metal-rich till down-ice (south to southwest) of the Horne and Quémont Cu-Zn-Au VMS deposits in Noranda, Quebec, in the central part of the Abitibi Greenstone Belt, Quebec. Contour lines indicate Cu and Zn contents in ppm (modified from Dreimanis, 1958).

till, Kaszycki et al. (1996) compared Cu/Zn ratios in till to those of underlying source rocks. They found that high Cu/Zn ratios in till closely match those in underlying felsic rocks that host Cu-rich VMS deposits, and that high Zn/Cu ratios in till closely reflect ratios in VMS deposits hosted in mafic rocks in the area.

Adams Lake Area, Cordillera

Deposit-scale till, soil, and vegetation sampling carried out around the Samatosum and Rea Ag-Pb-Zn-Cu VMS deposits, 80 km north of Kamloops in the Adams Lake area of south-central British Columbia (Fig. 1), has been reported by Lett et al. (1998), Paulen (2001), and Lett (2001). These relatively small (each <1 Mt) deposits occur in highly deformed and metamorphosed mafic volcanic and argillaceous sedimentary rocks of the Eagle Bay Assemblage (Bailey et al., 2000). Till and B-horizon soil developed on till around and down-ice of the deposits have anomalous Pb, Ag, As, Hg (Fig. 9), Sb, Au, and Zn contents in the <0.063 mm fraction (Paulen, 2001; Lett, 2001). Maximum metal contents of till occur 1.8 km down-ice (southeast); however, the surface till anomalies can be traced up to 10 km down-ice (Bobrowsky et al., 1997).

Halfmile Lake VMS Deposit, Appalachians

The Halfmile Lake Zn-Pb-Cu VMS deposit, in the westernmost part of the BMC in northern New

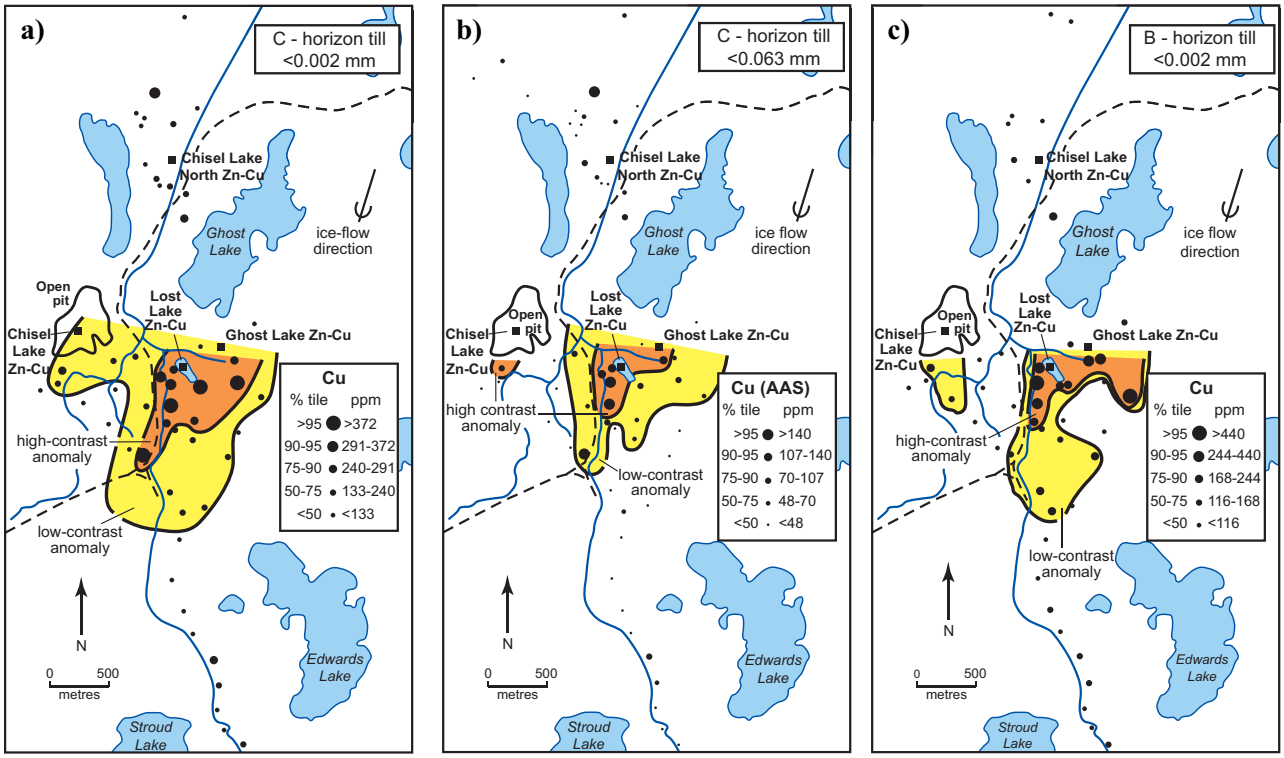

Figure 8. Distribution maps of Cu (ppm) in surface till around the Chisel Lake, Lost Lake, and Ghost Lake Zn-Cu VMS deposits in the Snow Lake Camp: **a)** <0.002 mm fraction of C-horizon soil developed on till; **b)** <0.063 mm fraction of C-horizon soil developed on till; and **c)** <0.002 mm fraction of B-horizon soil developed on till (modified from Kaszycki et al., 1996).

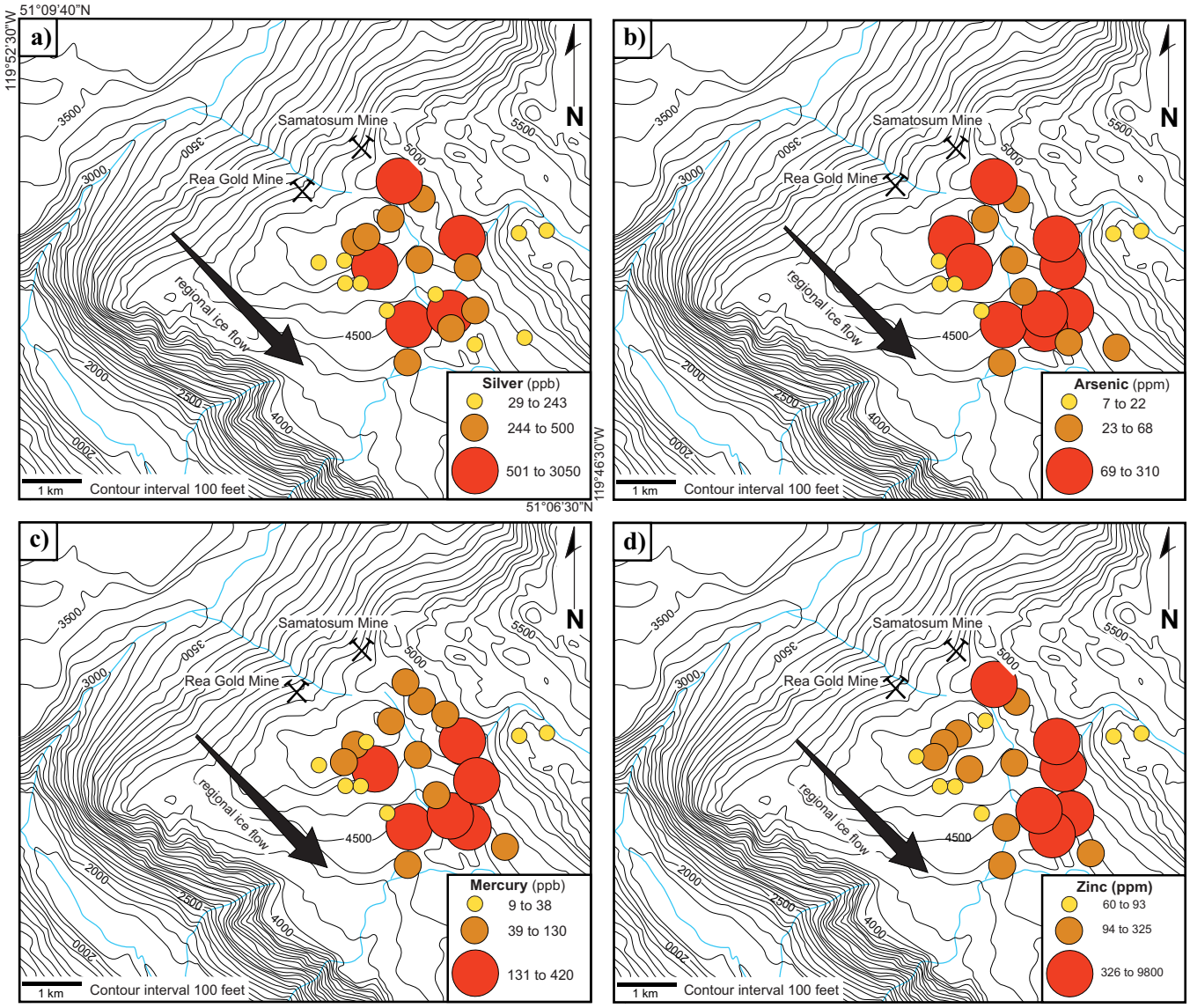

Figure 9. Maps of the distribution of **(a)** Ag, **(b)** As, **(c)** Hg, and **(d)** Zn in the <0.063 mm fraction of till down-ice (southeast) of the Rea Gold and Samatosum VMS deposits, British Columbia (modified from Paulen, 2001).

Brunswick (Fig. 1), was discovered in 1952 using soil geochemical and geophysical surveys (Adair, 1992; Parkhill and Doiron, 2003). The deposit is capped by a preglacial massive sulphide gossan that contains Pb, Cu, In, Au, Ag, Sn, As, Sb, Bi, and Se (Boyle, 2003). A well developed, ribbon-shaped glacial dispersal train (Fig. 10), extending at least 1 km down-ice (east-northeast to east-southeast), is best defined by Cu, Pb, In, Ag, As, Au, Sb, Bi, Hg, Sb, Se, and Sn in the <0.063 mm till fraction (Parkhill and Doiron, 2003; Budulan et al., 2012). Although Zn is the most abundant base metal in the deposit, it is not a pathfinder element in till immediately down-ice, likely due to Zn depletion in the gossan cap (Parkhill and Doiron, 2003). The broad multi-element signature in till around the Halfmile Lake deposit demonstrates significant glacial dispersal of mineralization from this VMS deposit.

Indicators minerals of the Halfmile Lake sulphide mineralization include chalcopyrite, galena, sphalerite, pyrite, pyrrhotite, and goethite. Indicator minerals of the preglacial gossan cap include gold, beudantite ($PbFe_3(AsO_4)(SO_4)(OH)_6$), jarosite ($KFe_3(SO4)_2(OH)_6$), and goethite (McClenaghan et al., 2012c; Budulan et al., 2015). Chalcopyrite and gold are the most useful of the indicator minerals identified as they have survived glacial transport and post-glacial weathering of the till. This case study is one of the first to demonstrate the recovery and usefulness of the secondary minerals jarosite and beudantite in till.

Izok Lake VMS Deposit, Arctic Permafrost

The Izok Lake Zn-Cu-Pb-Ag VMS deposit, located 360 km north of Yellowknife (Fig. 1), is one of the largest undeveloped Zn-Cu resources in North America

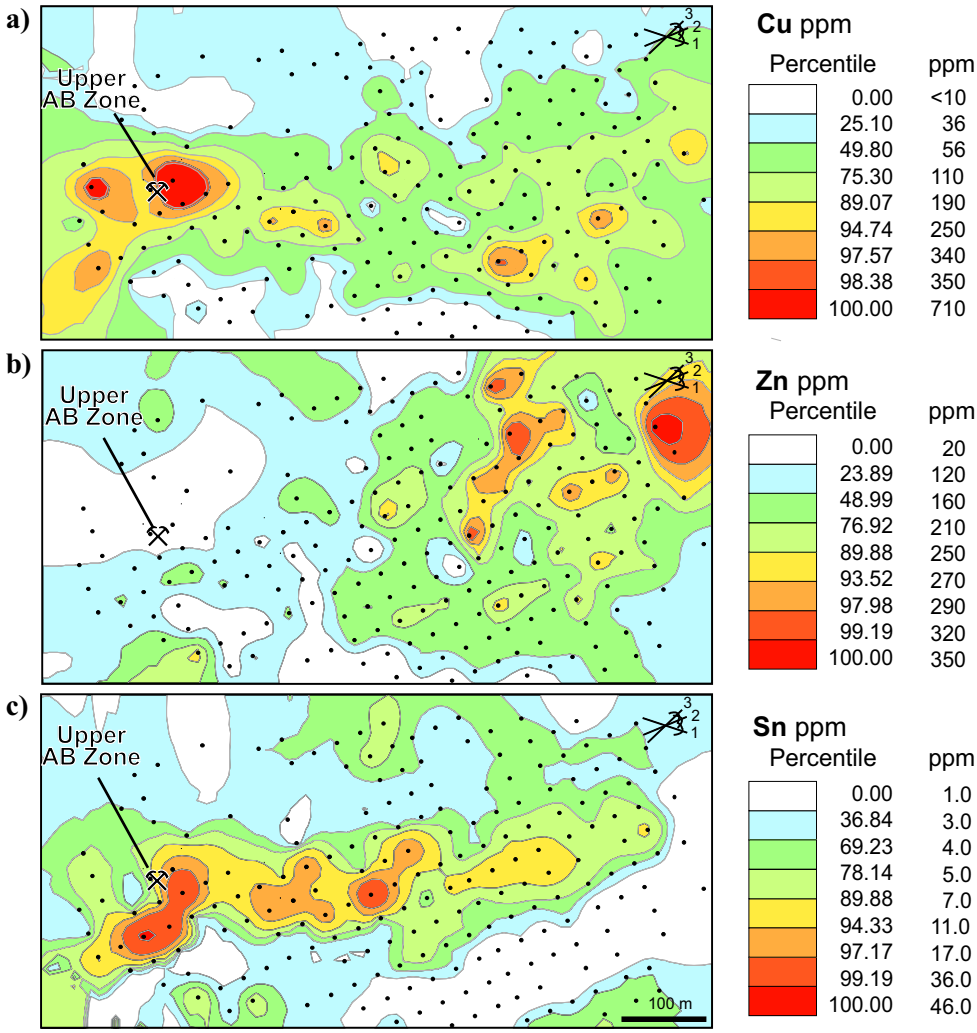

Figure 10. Distribution maps of **(a)** Cu, **(b)** Zn, and **(c)** Sn in the <0.063 mm fraction of till around the Halfmile Lake VMS deposit, Bathurst Mining Camp, New Brunswick, showing a well developed west-northwest-trending glacial dispersal train (modified from Parkhill and Doiron, 2003).

(Morrison, 2004). The deposit was discovered in the 1970s by following mineralized boulders along the west shore of Izok Lake. Till sampling in this region utilized mudboils in the permafrost terrain. Pathfinder elements of the deposit in till include Zn, Cu, Pb, Ag, Cd, and Bi and to a lesser extent Sb, Hg, Se, In, and Tl in the <0.063 mm fraction. Dispersed mineralization can be detected up to 1.3 km down-ice (northwest) from the deposit (Fig. 11a) (Hicken et al., 2012; McClenaghan et al., in press).

Gahnite is the most useful indicator of glacial dispersal from this deposit (Hicken et al., 2013; Paulen et al., 2013; McClenaghan et al., in press) because it is abundant in the deposit as well as in till down-ice. Immediately down-ice of the deposit, till contains thousands of gahnite grains per 10 kg sample. The compositions of gahnite in the local till (Fig. 5) are consistent with a bedrock source that is a metamorphosed massive sulphide deposit in Fe-Al metasedimentary and metavolcanic rocks. Chalcopyrite, sphalerite, galena, loellingite, and pyrite are also useful indicator minerals in till down-ice, but they are much less abundant (10s to 100s of grains).

At Izok Lake, debris from the VMS deposit has been glacially dispersed by two main ice-flow phases, an older flow to the southwest and a younger flow to the northwest, producing a fan-shaped train (Fig. 11b). The gahnite dispersal fan can be detected at least 40 km down-ice (McClenaghan et al., 2012a). At source, gahnite grains are intergrown with quartz, muscovite, and other minerals (Fig. 12). As the glacial transport distance down-ice increases, the proportion of quartz-gahnite and muscovite-gahnite intergrown grains decreases, the number of gahnite grains decreases, and the gahnite grain-size decreases (McClenaghan et al., 2014, in press).

CONCLUSIONS

Boulder tracing and till geochemical methods have been used for more than 50 years to explore for VMS deposits in glaciated terrain. Indicator minerals are a newer exploration tool that is now widely used in concert with till geochemistry and boulder tracing. Recent case studies at the Halfmile Lake and Izok Lake VMS deposits demonstrate the effectiveness of modern analytical and indicator mineral methods now being used

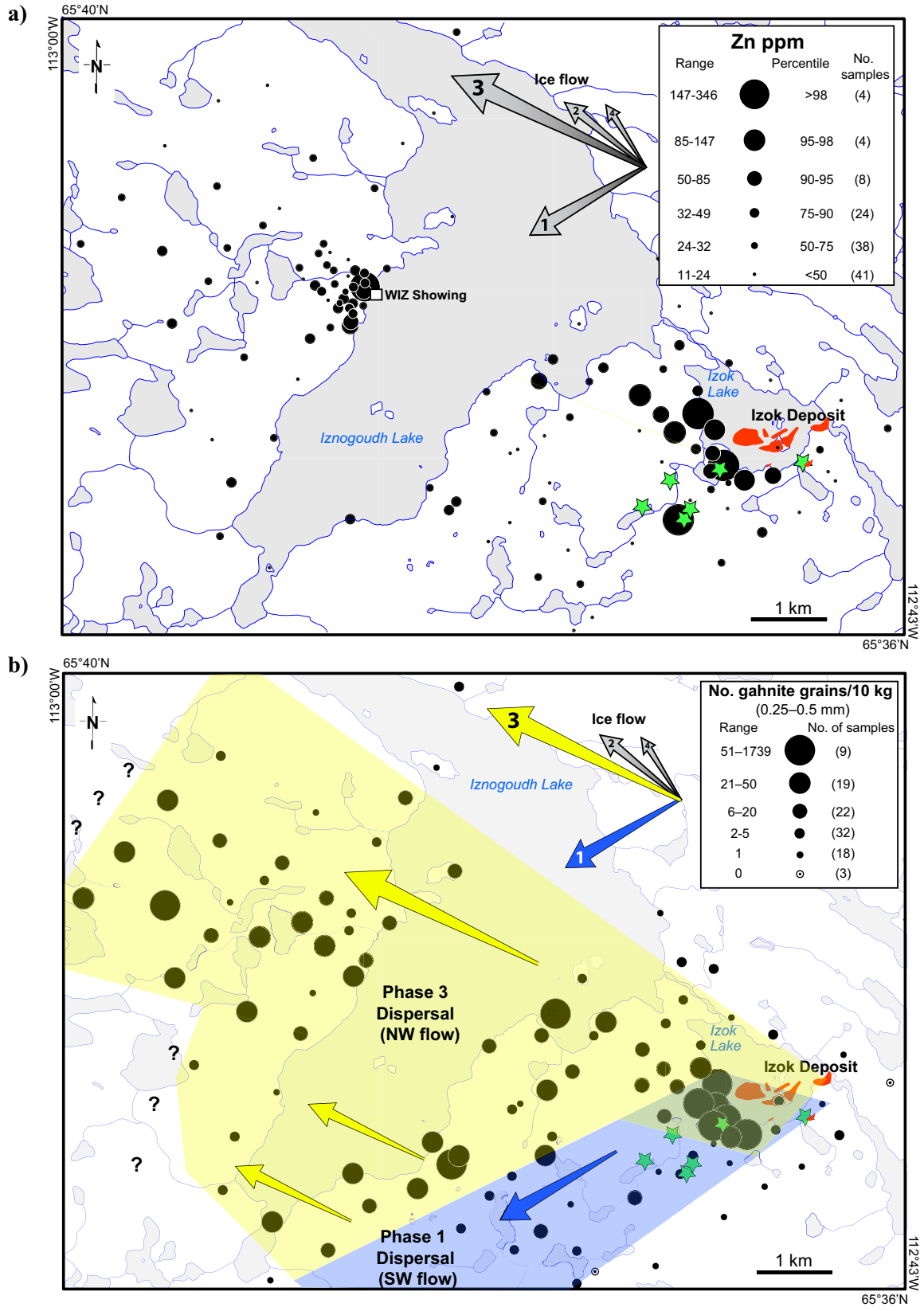

Figure 11. Distribution maps of **(a)** Zn in the <0.063 mm fraction of till, and **(b)** gahnite in the 0.25–0.5 mm non-ferromagnetic heavy mineral fraction of till around the Izok Lake VMS deposit, Nunavut. Arrows indicate relative ice-flow chronology (1 = oldest) and vigor (arrow size) of flow events. Blue-shaded polygon represents dispersal by the southwest (Phase 1) ice flow and yellow-shaded polygon represents dispersal by northwest (Phase 3) ice flows. Locations of gahnite-bearing rocks indicated by green stars and location of massive sulphide indicated by solid red polygons (unpublished data, MMG). Modified from McClenaghan et al. (in press).

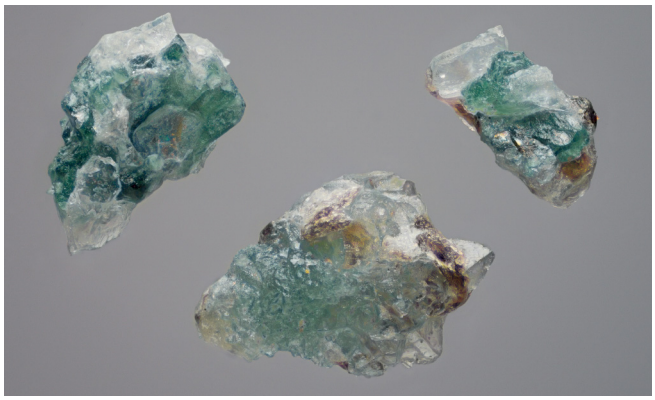

Figure 12. Macro photograph of 0.25–0.5 mm grains of gahnite (blue-green) intergrown with quartz (white) from till sample 12-MPB-913, collected 800 m down-ice (southwest) of the Izok Lake deposit, Nunavut. Field of view: 2.3 x 1.5 mm. Photograph taken by Michael J. Bainbridge Photography.

to explore for VMS deposits in Canada. Indicator elements of VMS deposits include Cu, Pb, and Zn, and pathfinder elements include As, Ag, Au, Ba, Bi, Cd, Hg, In, Sb, Se, Sn, and Tl. The <0.063 mm (silt + clay) fraction of till is the most commonly used medium in which to determine these elements. Indicator minerals of VMS deposits are recovered from the HMC (>3.2 SG) fraction of till and include the main ore minerals galena, sphalerite, chalcopyrite, pyrite, and pyrrhotite, as well as accessory minerals native gold, electrum, cassiterite, cinnabar, and barite. Where VMS deposits and their host rocks are metamorphosed, the indicator mineral suite includes physically and chemically robust oxide and silicate minerals indicative of metamorphosed mineralization, alteration, or exhalite zones, which includes sillimanite, andalusite, gahnite, staurolite, and spessartine. The recognition of magnetite and its chemical composition may also be useful for VMS exploration. Where VMS mineralization has undergone preglacial oxidation, secondary minerals, such as beudantite, jarosite, and goethite, may also be useful indicator minerals in till.

TECHNOLOGY TRANSFER

Education and dissemination of information about the application of indicator mineral and geochemical methods to mineral exploration have been a particular focus of this TGI-4 research activity, with special emphasis on VMS exploration. Overviews of indicator mineral methods have been presented at numerous workshops and short courses (Table 2).

Table 2. List of indicator mineral short course and workshop presentations given as part of the TGI-4 VMS research project.

Workshop/Short Course	Date	Topic
Laurentian University, Modular Course in Exploration Geochemistry	December 2010	Indicator mineral and till geochemical methods for mineral exploration, including VMS deposits
Association of Applied Geochemists Short Course: Indicator Mineral Methods in Mineral Exploration	August 21, 2011	Modern techniques for the recovery of indicator minerals from surficial sediments
PDAC Student-Industry Mineral Exploration Workshop (S-IMEW)	May 11, 2012	Indicator mineral and till geochemical methods for mineral exploration, including VMS deposits
Laurentian University, Modular Course in Exploration Geochemistry	December 2012	Indicator mineral and till geochemical methods for mineral exploration, including VMS deposits
Association for Mineral Exploration British Columbia short course:Exploring Through Cover - What Works, What Doesn't and Why	January 26, 2013	Indicator mineral and till geochemical methods for mineral exploration, including VMS deposits
PDAC Short Course: New Frontiers for Exploration in Glaciated Terrain	March 1, 2013	Indicator mineral and till geochemical methods for exploration for VMS deposits
PDAC Short Course: New Frontiers for Exploration in Glaciated Terrain	March 1, 2013	Fe oxide indicator rmineral chemistry in mineral exploration, including VMS deposits
PDAC Workshop: New Frontiers for Exploration in Glaciated Terrain	March 1, 2013	Quality assuranace and quality control measures for indicator mineral mineral programs
PDAC Student-Industry Mineral Exploration Workshop (S-IMEW)	May 10, 2013	Indicator mineral and till geochemical methods for mineral exploration, including VMS deposits
Geological Survey of Finland, Green Mining Project Workshop	September 11, 2013	Application of indicator mineral methods to mineral exploration in Canada
Association of Applied Geochemists Short Course: Application of Indicator Mineral Methods to Mineral Exploration	November 17, 2013	Modern techniques for indicator mineral chemistry
Association for Mineral Exploration British Columbia short course: Surficial Geology and Exploration Geochemistry – Know What You Are Sampling & Why	January 24, 2014	Indicator mineral and till geochemical methods for mineral exploration, including VMS deposits
PDAC Student-Industry Mineral Exploration Workshop (S-IMEW)	May 7, 2014	Indicator mineral and till geochemical methods for mineral exploration, including VMS deposits
Canadian Institute of Mining and Metallurgy Short Course: Prospecting Under Cover	November 5, 2014	Indicator mineral and till geochemical methods for mineral exploration, including VMS deposits
Laurentian University, Modular Course in Exploration Geochemistry	December 2014	Indicator mineral and till geochemical methods for mineral exploration, including VMS deposits

FUTURE DIRECTIONS

New indicator mineral recovery and chemical characterization methods are currently being developed to reduce sample size and analytical costs. Ongoing and future research will focus on smaller size fractions of till that currently are not examined (i.e. <0.063 mm) and the applications of new and more accessible analytical instruments to indicator mineral studies (e.g. hyperspectral, MLA express; Layton-Matthews et al., 2014, laser-induced breakdown spectroscopy (LIBS)). These developments will ultimately lead to the identification of new and/or improved indicator mineral methods of VMS deposits and increased exploration success.

ACKNOWLEDGEMENTS

This synoptic compilation of drift exploration methods for VMS deposits in glaciated terrain is an output of the GSC's Targeted Geoscience Initiative 4 (TGI-4) VMS Project. The Izok Lake VMS case study was funded by the GSC's Geo-Mapping for Energy and Minerals Program (GEM-1) (2008-2013). The Halfmile Lake case studies were funded by the GSC's EXTECH II (1994-1999) and Targeted Geoscience Initiative 3 (TGI-3) (2005-2010) projects. Figures from older publications were prepared by T. Barry (GSC). Roger Paulen (GSC) is thanked for his review of the manuscript.

REFERENCES

Adair, R.N., 1992. Stratigraphy, structure, and geochemistry of the Halfmile Lake massive-sulfide deposit, New Brunswick; Exploration and Mining Geology, v. 1, p. 151–166.

Averill, S.A., 2001. The application of heavy indicator mineralogy in mineral exploration, *In:* Drift Exploration in Glaciated Terrain, (ed.) M.B. McClenaghan, P.T. Bobrowsky, G.E.M. Hall, and S. Cook; Geological Society of London, Special Publication 185, p. 69–81.

Bailey, S.L., Paradis, S. and Johnston, S., 2000. Geological setting of the Samatosum and Rea massive-sulphide deposits, Eagle Bay assemblage, south central British Columbia; Geological Survey of Canada, Current Research 2000-A15, 10 p.

Bell, K. and Franklin, J.M., 1993. Application of Pb isotopes to mineral exploration in glacial terrains; Geology, v. 21, p. 1143–1146.

Bell, K. and Murton, J.B., 1995. A new indicator of glacial dispersal: lead isotopes; Quaternary Science Reviews, v. 14, p. 275–287.

Bernier, L., Pouliot, G. and MacLean, W.H., 1987. Geology and metamorphism of the Montauban North Gold Zone: a metamorphosed polymetallic exhalative deposit, Grenville Province, Quebec; Economic Geology, v. 82, p. 2076–2090.

Bischoff, C.T., 1954. Testing for copper and zinc in Canadian glacial soils; Transactions of the American Institute of Mining and Metallurgical Engineers, v. 199, p. 57–61.

Bobrowsky, P.T., Leboe, E.R., Dixon-Warren, A., Ledwon, A., MacDougall, D. and Sibbick, S.J., 1997. Till geochemistry of the Adams Plateau-North Barriere Lake area (82M/4 and 5); British Columbia Ministry of Employment and Investment, Open File 1997-9, 26 p.

Boyle, D. R., 2003. Preglacial weathering of massive sulphide deposits in the Bathurst Mining Camp, economic geology, geochemistry and exploration applications, *In:* Massive Sulfide Deposits of the Bathurst Mining Camp, New Brunswick, and Northern Maine (ed.) W.D. Goodfellow, S.R. McCutcheon, and J.M. Peter; Society of Economic Geologists, Economic Geology Monograph 11, p. 689–721.

Budulan, G., McClenaghan, M.B., Parkhill, M.A., Layton-Matthews, D. and Pyne, M., 2013. Till Geochemical signatures of the Halfmile Lake Zn-Pb-Cu volcanogenic Massive sulphide deposit, Bathurst Mining Camp, New Brunswick; Geological Survey of Canada, Open File 7174, 122 p.

Budulan, G., McClenaghan, M.B., Layton-Matthews, D., Crabtree, D., Pyne, M. and McClenaghan, S., 2015. Indicator mineral signatures of the Halfmile Lake Zn-Pb-Cu volcanogenic massive sulphide deposit, Bathurst Mining Camp, New Brunswick: Part 1-bedrock data; Geological Survey of Canada, Open File 7644, 75 p.

Byers, A.R., 1956. Geochemical investigations in the Flin Flon area; Canadian Mining Journal, v. 77, p. 83–86.

Cameron, E.M., 1977. Geochemical dispersion in mineralized soils of a permafrost environment; Journal of Geochemical Exploration, v. 7, p. 301–326.

Dare, S.A.S., Barnes, S.-J. and Beaudoin, G., 2012. Variation in trace element content of magnetite crystallized from a fractionating sulfide liquid, Sudbury, Canada: Implications for provenance discrimination; Geochimica et Cosmochimica Acta, v. 88, p. 27–50.

Dreimanis, A., 1958. Tracing ore boulders as a prospecting method; Canadian Institute of Mining and Metallurgy Bulletin, v. 5, p. 73–80.

Dreimanis, A., 1960. Geochemical Prospecting for Cu, Pb and Zn in glaciated areas, eastern Canada; International Geological Congress XXI Session, Part II, p. 7–19.

Dreimanis, A. and Vagners, U.J., 1972. The effect of lithology upon the texture of till, *In:* Research Methods in Pleistocene Geomorphology, (ed.) E. Yatsu and A. Falconer; Proceedings of Second Guelph Symposium on Geomorphology 1971, p. 66–82.

Dupuis, C. and Beaudoin, G., 2011. Discriminant diagrams for iron oxide trace element fingerprinting of mineral deposit types; Mineralium Deposita, v. 46, p. 319–335.

Ermengen, S.V., 1957. Geochemical prospecting in Chibougamau; Canadian Mining Journal, v. 4, p. 99–104.

Fortescue, J.A.C. and Hornbrook, E.H.W., 1969. Two quick projects, one at a massive sulphide orebody near Timmins, Ontario and the other at a copper deposit in Gaspé Park, Quebec; Geological Survey of Canada, Paper 67-23, Part II, p. 39–63.

Galicki, M., Marshall, D., Staples, R, Thorkelson, D., Downie, C., Gallagher, C., Enkin, R. and Davis, W., 2012. Iron oxide ± Cu ± Au deposits in the Iron Range, Purcell Basin, southeastern British Columbia; Economic Geology, v. 107, p. 1293–1301.

Galley, A. G., Watkinson, D. H., Jonasson, I. R. and Riverin, G., 1995. The subsea-floor formation of volcanic-hosted massive sulfide: evidence from the Ansil deposit, Rouyn-Noranda, Canada; Economic Geology, v. 90, p. 2006–2017.

Galley, A.G., Hannington, M.D. and Jonasson, I.R., 2007. Volcanogenic massive sulphide deposits, *In:* Mineral Deposits of Canada: A Synthesis of Major Deposit-Types, District Metallogeny, the Evolution of Geological Provinces, and Exploration Methods, (ed.) W.D. Goodfellow; Geological Association of Canada, Special Publication No. 5, p. 141–161.

Garrett, R.G., 1971. The dispersion of copper and zinc in glacial overburden at the Louvem deposit, Val d'Or, Quebec, *In:* Geochemical Exploration; Canadian Institute of Mining and Metallurgy, Special Volume 11, p. 157–158.

Ghosh, B. and Praveen, M.N., 2008. Indicator minerals as guides to base metal sulphide mineralization in Betul Belt, central India; Journal of Earth System Sciences, v. 117, p. 521–536.

Gleeson, C.F. and Cormier, R., 1971. Evaluation by geochemistry of geophysical anomalies and geological targets using overburden sampling at depth, *In:* Geochemical Exploration; Canadian Institute of Mining an Metallurgy, Special Volume 11, p. 159–165.

Govett, G.J.S., 1973. Geochemical exploration studies in glaciated terrain, New Brunswick, Canada, *In:* Prospecting in Areas of Glaciated Terrain-1973, (ed.) M.J. Jones; Institute of Mining and Metallurgy, p. 11–24.

Grip, E., 1953. Tracing of glacial boulders as an aid to ore prospecting in Sweden; Economic Geology, v. 48, p. 715–725.

Hall, G.E.M., Parkhill, M.A. and Bonham-Carter, G.F., 2003. Conventional and selective leach geochemical exploration methods applied to humus and B horizon soil overlying the Restigouche VMS deposit, Bathurst Mining Camp, New Brunswick, *In:* Massive Sulfide Deposits of the Bathurst Mining Camp, New Brunswick, and Northern Maine, (ed.) W.D. Goodfellow, S.R. McCutcheon, and J.M. Peter; Society of Economic Geologists, Economic Geology Monograph 11, p. 763–782.

Hall, G.E.M. and McClenaghan, M.B., 2013. Field portable XRF in exploration and mining, *In:* New Frontiers for Exploration in Glaciated Terrain, (ed.) R.C. Paulen and M.B. McClenaghan; Geological Survey of Canada, Open File 7374, p. 75–81.

Heimann, A., Spry, P.G. and Teale, G., 2005. Zincian spinel associated with metamorphosed Proterozoic base metal sulphide occurrences, Colorado: A re-evaluation of gahnite composition as a guide in exploration; Canadian Mineralogist, v. 43, p.601–622.

Heimann, A., Spry, P.G., Teale, G.S., Leyh, W.R., Conor, C.H.H., Mora, G. and O'Brien, J. J., 2013. Geochemistry and genesis of low-grade metasediment-hosted Zn-Pb-Ag mineralization, southern Proterozoic Curnamona Province, Australia; Journal of Geochemical Exploration, v. 128, p. 97–116.

Hicken, A.K., McClenaghan, M.B., Paulen, R.C. and Layton-Matthews, D., 2012. Till geochemical signatures of the Izok Lake Zn-Cu-Pb-Ag VMS deposit, Nunavut; Geological Survey of Canada, Open File 7046, 118 p.

Hicken, A.K., McClenaghan, M.B., Paulen, R.C., Layton-Matthews, D., Averill, S.A. and Crabtree, D., 2013. Indicator mineral signatures of the Izok Lake Zn-Cu-Pb-Ag VMS deposit, Nunavut: part 2 till; Geological Survey of Canada, Open File 7343, 48 p.

Hoffman, S.J. and Woods, G.A., 1991. Multidisciplinary exploration of the BOG volcanogenic massive-sulphide prospect, Bathurst, New Brunswick, Canada; Journal of Geochemical Exploration, v. 41, p.85–101.

Hussein, A.A., Lochner, C. and Bell, K., 2003. Application of Pb isotopes to mineral exploration in the Halfmile Lake area, Bathurst, New Brunswick, *In:* Massive Sulfide Deposits of the Bathurst Mining Camp, New Brunswick, and Northern Maine, (ed.) W.D. Goodfellow, S.R. McCutcheon, and J.M. Peter; Society of Economic Geologists, Economic Geology, Monograph 11, p. 679–688.

Hyvarinen, L., Kauranne, K. and Yletyinen, V., 1973. Modern boulder tracing in prospecting, *In:*Prospecting in Areas of Glaciated terrain-1973, (ed.) M.J. Jones; Institute of Mining and Metallurgy, p. 87–95.

James, L.D. and Perkins, E.W., 1981. Glacial dispersion from sulphide mineralization, Buchans area, Newfoundland, *In:* The Buchans Orebodies: Fifty Years of Geology and Mining, (ed.) E.A. Swanson, D.F. Strong, and J.G. Thurlow; Geological Association of Canada, Special Paper 22, p. 269–283.

Kaszycki, C.A., Nielsen, E. and Gobert, G., 1996. Surficial geochemistry and response to volcanic-hosted massive sulphide mineralization in the Snow Lake region, *In:* EXTECH I: A Multidisciplinary approach to massive sulphide research in the Rusty Lake-Snow Lake greenstone belts, Manitoba, (ed.) G.F. Bonham-Carter, A.G. Galley, and G.E.M. Hall; Geological Survey of Canada, Bulletin 426, p.139–154.

Kauranne, K., 1959. Pedogeochemical prospecting in glaciated terrain; Geological Survey of Finland, Bulletin 184, p. 1–10.

Kjarsgaard, B.A., Knight, R.D., Plourde, A.P. and Reynen, A.M.G., 2014. Portable XRF spectrometry of surficial sediment samples in the region of East Arm, Great Slave Lake, Northwest Territories, Canada; Geological Survey of Canada, Open File 7607, 38 p.

Klassen, R.A., 2003. The geochemical and physical properties of till, Bathurst Mining Camp, New Brunswick, Canada, *In:* Massive sulfide deposits of the Bathurst Mining Camp, New Brunswick and northern Maine, (ed.) W.D. Goodfellow, S. McCutcheon, R., and J.M. Peter; Society of Economic Geologists, Monograph 11, p. 763–782.

Lalonde, J.P., Bernier, L., Choinier, J. and Hebert, C., 1994. Dispersion of gahnite from the Montauban and Lac Dussault polymetallic deposits, Portneuf Township, Quebec; Ministère des Ressources naturelles du Québec, Secteur des Mines, p. 39.

Large, R. R., 1977. Chemical evolution and zonation of massive sulfide deposits in volcanic terrains; Economic Geology, v. 72, p. 549–572.

Layton-Matthews, D., Hamilton, C. and McClenaghan, B., 2014. Mineral chemistry: modern techniques and applications to exploration; in Application of Indicator Mineral Methods to Mineral Exploration, (ed.) M.B. McClenaghan, A. Plouffe, and D. Layton-Matthews; Geological Survey of Canada, Open File 7553, p. 9–18.

Lee, H.A., 1971. Mineral discovery in the Canadian Shield using the physical aspects of overburden; The Canadian Institute of Mining, Bulletin 64, No. 715, November 1971, p. 32–36.

Lett, R.E., 2001. Geochemical signatures around massive sulphide deposits in southern British Columbia, Canada, *In:* Drift Exploration in Glaciated Terrain, (ed.) M.B. McClenaghan, P.T. Bobrowsky, G.E.M. Hall, and S. Cook; Geological Society of London, Special Publication 185, p. 301–321.

Lett, R.E. and Jackaman, W., 2002. Geochemical exploration models, Volume 1. VMS deposits in south-central British Columbia (NTS 82L/13, L/14, 82M/4. M/5, M/6 and 92P/1E); British Columbia Ministry of Energy, Mines and Petroleum Resources, Open File 2000-31, 34 p.

Lett, R.E., Bobrowsky, P., Cathro, M. and Yeow, A., 1998. Geochemical pathfinders for massive sulphide deposits in the Southern Kootenay Terrane; British Columbia Geological Survey, Geological Fieldwork 1997, Paper 1998-1, p. 15-1 – 15-10.

Levinson, A. A., 1980. Introduction to Exploration Geochemistry, 2nd edition; Applied Publishing Ltd., Wilmette, Illinois, United States, 892 p.

Levson, V.M., 2001a, Till geochemistry and sampling techniques in the Canadian Cordillera, *In:* Drift Exploration in Glaciated Terrain, (ed.) M.B. McClenaghan, P.T. Bobrowsky, G.E.M. Hall, and S. Cook; Geological Society of London, Special Publication 185, p. 45–67.

Levson, V.M., 2001b, Regional till geochemical surveys in the Canadian Cordillera: sample media, methods and anomaly evaluation, *In:* Drift Exploration in Glaciated Terrain, (ed.) M.B. McClenaghan, P.T. Bobrowsky, G.E.M. Hall, and S. Cook; Geological Society of London, Special Publication 185, p. 67–76.

Lindsay, P.J. and Shilts, W.W., 1995. A standard laboratory procedure for separating clay-sized detritus from unconsolidated glacial sediments and their derivatives, *In:* Drift Exploration in the Canadian Cordillera, (ed.) P.T. Bobrowsky, S.J. Sibbick, J.M.

Newell, and P.F. Matysek; British Columbia Ministry of Energy, Mines and Petroleum Resources, Paper 1995-2, p. 149–163.

Lusk, J., 1969. Base metal zoning in the Heath Steele B-1 orebody, New Brunswick, Canada; Economic Geology, v. 64, p. 509–518.

Makvandi, S., Beaudoin, G., Barvarz, M.G. and McClenaghan, B., 2013. Developing indicator mineral methods; Application of iron oxides in discovery of VMS deposits, *In:* Program with Abstracts; Geological Association of Canada-Mineralogical Association of Canada joint annual meeting, Winnipeg 2013, v.36, p. 136.

Makvandi, S., Beaudoin, G., McClenaghan, B. and Layton-Matthews, D., 2015. The surface texture and morphology of magnetite from the Izok Lake volcanogenic massive sulfide deposit and local glacial sediments, Nunavut, Canada: application to mineral exploration; Journal of Geochemical Exploration, on-line version htttp://dx.doi.org/10.1016/j.gexplo.2014.12.13

Mandolla, S. and Brook, M.S., 2010. A preliminary scanning electron microscope (SEM) study of magnetite surface microtextures from the Wahianoa moraines, Mt Ruapehu, New Zealand; Geoscience, A working Paper Series in Physical Geography, Massey University, New Zealand, p. 1–9.

McClenaghan, M.B., 2011. Overview of common processing methods for recovery of indicator minerals from sediment and bedrock in mineral exploration; Geochemistry: Exploration, Environment, Analysis, v. 11, p. 265–278.

McClenaghan, M.B. and Peter, J.M., 2013. Till geochemical signatures of Canadian volcanogenic massive sulphide deposits in glaciated terrain; Geological Survey of Canada, Open File 7354, 36 p.

McClenaghan, M.B., Hicken, A.K., Paulen, R.C. and Layton-Matthews, D., 2012a. Indicator mineral counts for regional till samples around the Izok Lake Zn-Cu-Pb-Ag VMS deposit, Nunavut; Geological Survey of Canada, Open File 7029, 13 p., 1 CD-ROM.

McClenaghan, M.B., Hicken, A.K., Averill, S.A., Paulen, R.C. and Layton-Matthews, D., 2012b. Indicator mineral abundance data for bedrock and till samples from the Izok Lake Zn-Cu-Pb-Ag volcanogenic massive sulphide deposit, Nunavut; Geological Survey of Canada, Open File 7075, 11 p., 1 CD-ROM.

McClenaghan, M.B., Budulan, G., Averill, S.A., Layton-Matthews, D. and Parkhill, M.A., 2012c. Indicator mineral abundance data for bedrock and till samples from the Halfmile Lake Zn-Pb-Cu volcanogenic massive sulphide deposit, Bathurst Mining Camp, New Brunswick; Geological Survey of Canada, Open File 7076, 10 p.

McClenaghan, M.B., Plouffe, A., McMartin, I., Campbell, J.E., Spirito, W., Paulen, R.C., Garrett, R.G. and Hall, G.E.M., 2013. Till sampling and geochemical analytical protocols used by the Geological Survey of Canada; Geochemistry: Exploration, Environment, Analysis, v. 13, p. 285–301.

McClenaghan, M.B., Holmes, D.R.S., Averill, S.A., Paulen, R.C. and Layton-Matthews, D., 2014. Physical features indicating the glacial transport distance of gahnite from the Izok Lake Cu-Zn-Pb-Ag VMS deposit, Nunavut; Geological Survey of Canada, Open File 7603, 15 p.

McClenaghan, M.B., Paulen, R.C., Layton-Matthews, D., Hicken, A.K. and Averill, S.A., in press. Geochemical and indicator mineral signatures of the Izok Lake Zn-Cu-Pb-Ag VMS deposit in the glaciated terrain of northern Canada; Geochemistry: Exploration, Environment, Analysis.

McMartin, I. and McClenaghan, M.B., 2001. Till geochemistry and sampling techniques in glaciated Shield terrain, *In:* Drift Exploration in Glaciated Terrain, (ed.) M.B. McClenaghan, P.T. Bobrowsky, G.E.M. Hall, and S. Cook; Geological Society of London, Special Publication 185, p. 19–43.

McMartin, I. and Campbell, J.E., 2009. Near-surface till sampling protocols in shield terrain, with examples from western and northern Canada, *In:* Application of Till and Stream Sediment Heavy Mineral and Geochemical Methods to Mineral Exploration in Western and Northern Canada, (ed.) R.C. Paulen and I. McMartin; Geological Association of Canada, Short Course Notes 18, 75–95.

Meffre, S., Large, R., Scott, R., Woodhead, J., Chang, Z., Gilbert, S., Danyushevsky, L., Maslennikov, V. and Hergt, J., 2008. Age and pyrite Pb-isotopic composition of the giant Sukhoi Log sediment-hosted gold deposit, Russia; Geochimica et Cosmochimica Acta, v. 72, p. 2377–2391.

Miller, J.K., 1979. Geochemical dispersion over massive sulphides within the continuous permafrost zone, Bathurst Noresemines, Canada; Prospecting in Areas of Glaciated Terrain-1979, Institution of Mining and Metallurgy, London, p. 101-110.

Money, P.L. and Heslop, J.B., 1976. Geology of the Izok Lake massive sulphide deposit; Canadian Mining Journal, v. 97, p. 24–28.

Morris, H.C., 1966. Four geochemical exploration case-histories from Eastern Canada, *In:* Proceedings, Symposium on Geochemical Prospecting; Geological Survey of Canada, Paper 66-54, p. 273–274.

Morris, T.F., Breaks, F.W., Averill, S.A., Crabtree, D.C. and McDonald, A., 1997. Gahnite composition: Implications for base metal and rare-element exploration; Exploration and Mining Geology, v. 6, p. 253–260.

Morrison, I.R., 2004. Geology of the Izok Lake Massive Sulphide Deposit, Nunavut Territory, Canada; Exploration and Mining Geology, v. 13, p.25–36.

Nadoll, P., Mauk, J.L., Hayes, T.S., Koenig, A.E. and Box, S.E., 2012. Chemistry of magnetite from hydrothermal ore deposits and host rocks of the Mesoproterozoic Belt Supergroup, United States; Economic Geology, v. 107, p. 1275–1292.

Nesbitt, B. E. and Kelly, W. C., 1980. Metamorphic zonation of sulfides, oxides, and graphite in and around the orebodies at Ducktown, Tennessee; Economic Geology, v. 75, p. 1010–1021.

Nevalainen, R., 1989. Lithology of fine till fractions in the Kuhmo Greenstone Belt area, eastern Finland; Geological Survey of Finland, Special Paper 7, p. 59–65.

Nikkarinen, M., Kallio, E., Lestinen, P. and Äyräs, M. 1984. Mode of occurrence of copper and zinc in till over three mineralized areas in Finland; Journal of Geochemical Exploration, v. 21, p. 239–247.

O'Brien, J.J., Spry, P.G., Teale, G.S., Jackson, S. and Rogers, D., 2014. Major-trace element chemistry of gahnite in metamorphosed massive sulfide deposits: The use of discrimination diagrams to determine provenance, *In:* Application of indicator mineral methods to mineral exploration, (ed.) M.B. McClenaghan and D. Layton-Matthews; Geological Survey of Canada, Open File 7553, p. 29–33.

Oviatt, N.M., McClenaghan, M.B., Paulen, R.C., Gleeson, S.A., Averill, S.A. and Paradis, S., 2013. Indicator minerals in till and bedrock samples from the Pine Point Mississippi Valley-type District, Northwest Territories; Geological Survey of Canada, Open File 7423, 87 p.

Parkhill, M.A. and Doiron, A., 2003. Quaternary geology of the Bathurst Mining Camp and implications for base metal exploration using drift prospecting, *In:* Massive Sulfide Deposits of the Bathurst Mining Camp, New Brunswick, and Northern Maine, (ed.) W.D. Goodfellow, S.R. McCutcheon, and J.M. Peter; Society of Economic Geologists, Economic Geology Monograph 11, p. 631–660.

Paulen, R.C., 2001. Glacial transport and secondary hydromorphic metal mobilization: examples from the southern interior of British Columbia, Canada, *In:* Drift Exploration in Glaciated Terrain, (ed.) M.B. McClenaghan, P.T. Bobrowsky, G.E.M. Hall, and S. Cook; Geological Society of London, Special Publication 185, p. 323–337.

Paulen, R.C., 2009. Sampling techniques in the Western Canada Sedimentary Basin and the Cordillera, *In:* Application of till and stream sediment heavy mineral and geochemical methods to mineral exploration in western and northern Canada, (ed.) R.C. Paulen, and I. McMartin, I.; Geological Association of Canada, Short Course Notes 18, p. 49–74.

Paulen, R.C., Paradis, S., Plouffe, A. and Smith, I.R., 2011. Pb and S isotopic composition of indicator minerals in glacial sediments from NW Alberta. Canada: implications for Zn-Pb base metal exploration; Geochemistry: Exploration, Environment, Analysis, v. 11, p. 309–320.

Paulen, R.C., McClenaghan, M.B. and Hicken, A.K., 2013. Regional and local ice-flow history in the vicinity of the Izok Lake Zn-Cu-Pb-Ag VMS deposit, Nunavut; Canadian Journal of Earth Sciences, v. 50, p. 1209–1222.

Peter, J. M., Chapman, J. B., Mercier-Langevin, P., Layton-Matthews, D., Thiessen, E. and McClenaghan, M. B., 2010. Use of portable x-ray fluorescence spectrometry in vectoring for base metal sulfide exploration; Program and Abstracts Volume, Targeted Geoscience Initiative 3 Workshop: public geoscience in support of base metal exploration, , Vancouver, B.C. p. 3–6.

Peuraniemi, V., 1990. Heavy mineral geochemistry in the search for zinc ores, *In:* Proceedings, (ed.) F. Mrna; Exploration Geochemistry 1990, Third International Joint Symposium of the International Association of Geochemistry and Cosmochemistry and the Association of Exploration Geochemists, Prague, Czechoslovakia 1990, p. 291–294.

Plouffe, A. 1995. Drift-prospecting sampling methods; in Drift Exploration in the Canadian Cordillera, (ed.) P.T. Bobrowsky, S.J. Sibbick, J.M. Newell, P.F. Matysek; British Columbia Geological Survey, Paper 1995-2, p. 43–52.

Plouffe, A., McClenaghan, M. B., Paulen, R. C., McMartin, I., Campbell, J. E. and Spirito, W., 2013. Processing of glacial sediments for the recovery of indicator minerals: protocols used at the Geological Survey of Canada; Geochemistry: Exploration, Environment, Analysis, v. 13, p. 303–316.

Piercey, S.J., 2010. An overview of petrochemistry in the regional exploration for volcanogenic massive sulphide (VMS) deposits; Geochemistry: Exploration, Environment, Analysis, v. 10, p. 119–136.

Pronk, A.G., 1987. Pleistocene glacial dispersal and history in Buttle Valley, Vancouver Island, British Columbia: a feasibility study for alpine drift prospecting; Discussion: Canadian Journal of Earth Sciences, v. 24, p. 1504–1505.

Rose, A. W., Hawkes, H. E. and Webb, J. S., 1979. Geochemistry in Mineral Exploration, 2nd edition; Academic Press, London, United Kingdom, 635 p.

Salminen, R., 1980. On the geochemistry of copper in the Quaternary deposits in the Kiihtelysvaara, area, north Karelia, Finland; Geological Survey of Finland, Bulletin 309, 48 p.

Sangster, D. F., Outridge, P. M. and Davis, W. J., 2000. Stable lead isotope characteristics of lead ore deposits of environmental significance; Environmental Reviews, v. 8, p. 115–147.

Sappin, A.-A., Dupuis, C., Beaudoin, G., Pozza, M., McMartin, I. and McClenaghan, M.B., 2014. Optimal ferromagnetic fraction representative in till samples along ice-flow paths: case studies from the Sue-Dianne IOCG and Thompson deposits, Canada; Geochemistry: Exploration, Environment, Analysis, v. 14, p. 315–329.

Sharpe, R. and Gemmell, J. B., 2002. The Archean Cu-Zn magnetite-rich gossan hill volcanic-hosted massive sulfide deposit, Western Australia: genesis of a multistage hydrothermal system; Economic Geology, v. 97, p. 517–539.

Sheridan, D.M. and Ray, W.H., 1984. Precambrian deposits of zinc-copper-lead sulphides and zinc spinel (gahnite) in Colorado; U.S. Geological Survey, Bulletin 1550, 31 p.

Shilts, W.W., 1975. Principles of geochemical exploration for sulphide deposits using shallow samples of glacial drift; Canadian Institute of Mining and Metallurgy Bulletin, v. 68, p. 73–80.

Shilts, W.W., 1984. Till geochemistry in Finland and Canada; Journal of Geochemical Exploration, v. 21, p. 95–117.

Shilts, W.W., 1995. Geochemical portioning in till, *In:* Drift Exploration in the Canadian Cordillera, (ed.) P.T. Bobrowsky, S.J. Sibbick, J.M. Newell, P.F. Matysek; British Columbia Geological Survey, Paper 1995-2, p. 149–163.

Shilts, W.W., 1996. Drift exploration, *In:* Glacial Environments, Sediment Forms and Techniques, (ed.) J. Menzies; Butterworth Heinemann Ltd., Toronto, Ontario, Canada, p. 411–439.

Simonetti, A., Bell, K., and Hall, G.E.M., 1996. Pb isotopic ratios and elemental abundances for selective leachates from near-surface till: implications for mineral exploration; Applied Geochemistry, v. 11, p. 721–734.

Smith, S.L., 1992. Quaternary stratigraphic drilling transect, Timmins to the Moose River Basin, Ontario; Geological Survey of Canada, Bulletin 415, 100 p.

Spirito,W.A., McClenaghan, M.B., Plouffe, A., McMartin, I., Campbell, J.E., Garrett, R.G. and Hall, G.E.M., 2011. Till sampling and analytical protocols for GEM Projects: from field to archive; Geological Survey of Canada, Open File 6850, 83 p.

Spry, P.G., 1982. An unusual gahnite-forming reaction, Geco base-metal deposit, Manitouwadge, Ontario; Canadian Mineralogist, v. 20, p. 549–553.

Spry, P.G., 1987. The chemistry and origin of zincian spinel associated with the Aggeneys Cu-Pb-Zn-Ag deposits, Namaqualand, South Africa; Mineralium Deposita, v. 22, p. 262–268.

Spry, P.G. and Scott, S.D., 1986. The stability of zincian spinels in sulfide systems and their potential as exploration guides for metamorphosed massive sulfide deposits; Economic Geology, v. 81, p. 1446–1463.

Spry, P.G. and Teale, G.S., 2009. Gahnite composition as a guide in the search for metamorphosed massive sulfide deposits, *In:* International Association of Applied Geochemists, Indicator Mineral Workshop B, Fredericton, New Brunswick, May 2009, p. 27–34.

Stendal, H. and Theobald, P.K., 1994. Heavy-mineral concentrates in geochemical exploration; in Drainage Geochemistry, Handbook of Exploration Geochemistry, Volume 6, (ed.) M. Hale and J.A. Plant; Elsevier, Amsterdam, p. 185–225.

Telford, W. M. and Becker, A., 1979. Exploration case histories of the Iso and New Insco orebodies, *In:* Geophysics and geochemistry in the search for metallic ores, (ed.) P.J. Hood; Geological Survey of Canada, Economic Geology Report 31, p. 605–629.

Toverud, Ö., 1977. Geochemical and mineralogical aspects of some geochemical anomalies in glacial drift and peat in northern Sweden; Sveriges Geologiska Undersökning, Serie C NR 729, Årsbok 71, NR 4, 37 p.

Whiting, K.S. and Faure, G., 1991. Transport of magnetite and ilmenite by glaciers in the Adirondack Mountains of New York; Journal of Geology, v. 99, p. 482–492.

GEOLOGICAL SURVEY OF CANADA
OPEN FILE 7853

Targeted Geoscience Initiative 4: Contributions to the Understanding of Volcanogenic Massive Sulphide Deposit Genesis and Exploration Methods Development

Integration of rock properties and geophysics, Bathurst Mining Camp

Peter A. Tschirhart[1,2] **and William A. Morris**[1]

[1]McMaster University, Hamilton, Ontario
[2]Sander Geophysics Ltd., Ottawa, Ontario

2015

This publication is available for free download through GEOSCAN (http://geoscan.nrcan.gc.ca/)

Recommended citation

Tschirhart, P.A. and Morris, W.A., 2015. Integration of rock properties and geophysics, Bathurst Mining Camp, *In:* Targeted Geoscience Initiative 4: Contributions to the Understanding of Volcanogenic Massive Sulphide Deposit Genesis and Exploration Methods Development, (ed.) J.M. Peter and P. Mercier-Langevin; Geological Survey of Canada, Open File 7853, p. 101–115.

Publications in this series have not been edited; they are released as submitted by the author.

Contribution to the Geological Survey of Canada's Targeted Geoscience Initiative 4 (TGI-4) Program (2010–2015)

TABLE OF CONTENTS

Integration of rock properties and geophysics, Bathurst Mining Camp

Peter A. Tschirhart[1,2]* and William A. Morris[1]

[1]School of Geography & Earth Sciences, McMaster University, 1280 Main Street West, Hamilton, Ontario L8S 4K1
[2]Present Address: Sander Geophysics Ltd., 260 Hunt Club Road, Ottawa, Ontario K1V 1C1
*Corresponding author's e-mail: ptschirhart@sgl.com

ABSTRACT

Physical rock property information is an important aspect of geophysical processing and interpretation as it provides a direct link between geophysical data and geological interpretations. Herein, the existing physical rock property (density and magnetic susceptibility measurements) database for host rocks and volcanogenic massive sulphide (VMS) mineralization in the Bathurst Mining Camp (BMC), northern New Brunswick, is expanded by incorporating new measurements taken on *in situ* samples and drill cores from throughout the BMC. Descriptive statistics are calculated and presented, and density-magnetic susceptibility bivariate plots are used to illustrate patterns indicative of changes in the abundances of paramagnetic versus ferrimagnetic mineral phases. A discrete object magnetic inversion, solving for the remanent magnetization vector of the Armstrong B anomaly, is computed. The inversion is constrained geometrically by geological mapping at surface and diamond drilling at depth. Magnetic susceptibility values for the country rock and mineralization are from the physical property database. Results of the inversion suggest that the remanent vector was acquired sometime between 470 and 420 Ma, likely during the Salinic orogeny. Density information is used to reprocess ground gravity and airborne gravity gradiometry (AGG) data by applying a laterally variable Bouguer and terrain density correction linked to averaged, measured density values and mapped extents of the different tectonostratigraphic groups that make up the BMC. The results of this reprocessing subtly change the gravity and gravity-gradient anomaly patterns allowing for isolated anomalies to be more discretely resolved and reduce the impact of the terrain-related signal in the AGG data. Finally, helicopter-borne frequency domain electromagnetic data for a small test site within the BMC are inverted for magnetic susceptibility and forward modelled into a magnetic anomaly grid. Magnetic susceptibility values from the physical property database are used to validate the results of the inversion. This computed near-surface magnetic anomaly grid is then used as a reference to effectively filter measured total magnetic intensity data to represent solely near-surface magnetic sources. Although petrophysical measurements in the BMC may not apply elsewhere, the various methodologies presented are appropriate wherever the geological and geophysical requirements of the method are met.

INTRODUCTION

Physical properties of rocks are controlled by their chemical and mineralogical composition, which in turn reflects the geological processes involved in the initial formation of the rock and any subsequent metamorphism, alteration, erosion, and weathering. Evaluation of systematic patterns of physical property variations is important in the synthesis of geological and geophysical data for mineral exploration. Lithological classifications are based on mineralogy and textures, with rock silica content being an import classification characteristic of many types of lithology. Geophysical data, however, typically reflect the spatial distribution of accessory minerals (e.g. presence of magnetic or conductive minerals) not commonly used as the defining criteria for geological classifications. A complete understanding of the relationship between the geological and geophysical physical properties allows for the extraction of additional information, creation of more accurate, constrained geophysical and geological models, refinements to data processing methodologies, and ground truths for new geophysical methods.

In the Bathurst Mining Camp (BMC), northeastern New Brunswick (Fig. 1), Mwenifumbo et al. (2003) performed multi-sensor downhole logging at the Stratmat, Halfmile Lake, and Restigouche deposits and compiled and presented these data. Thomas (2003) also presented density information for drill-core samples from the Brunswick 12, Canoe Landing Lake, Heath Steele, Key Anacon, and Willet deposits. The integration of disparate individual datasets, however, may not be straightforward. Commonly, tools used for borehole logging are not cross-calibrated with tools used for core logging. Apparent differences in physical property values can also arise from factors, such as variations in borehole diameter, changes in sensor frequency, and

Tschirhart, P.A. and Morris, W.A., 2015. Integration of rock properties and geophysics, Bathurst Mining Camp, *In:* Targeted Geoscience Initiative 4: Contributions to the Understanding of Volcanogenic Massive Sulphide Deposit Genesis and Exploration Methods Development, (ed.) J.M. Peter and P. Mercier-Langevin; Geological Survey of Canada, Open File 7853, p. 101–115.

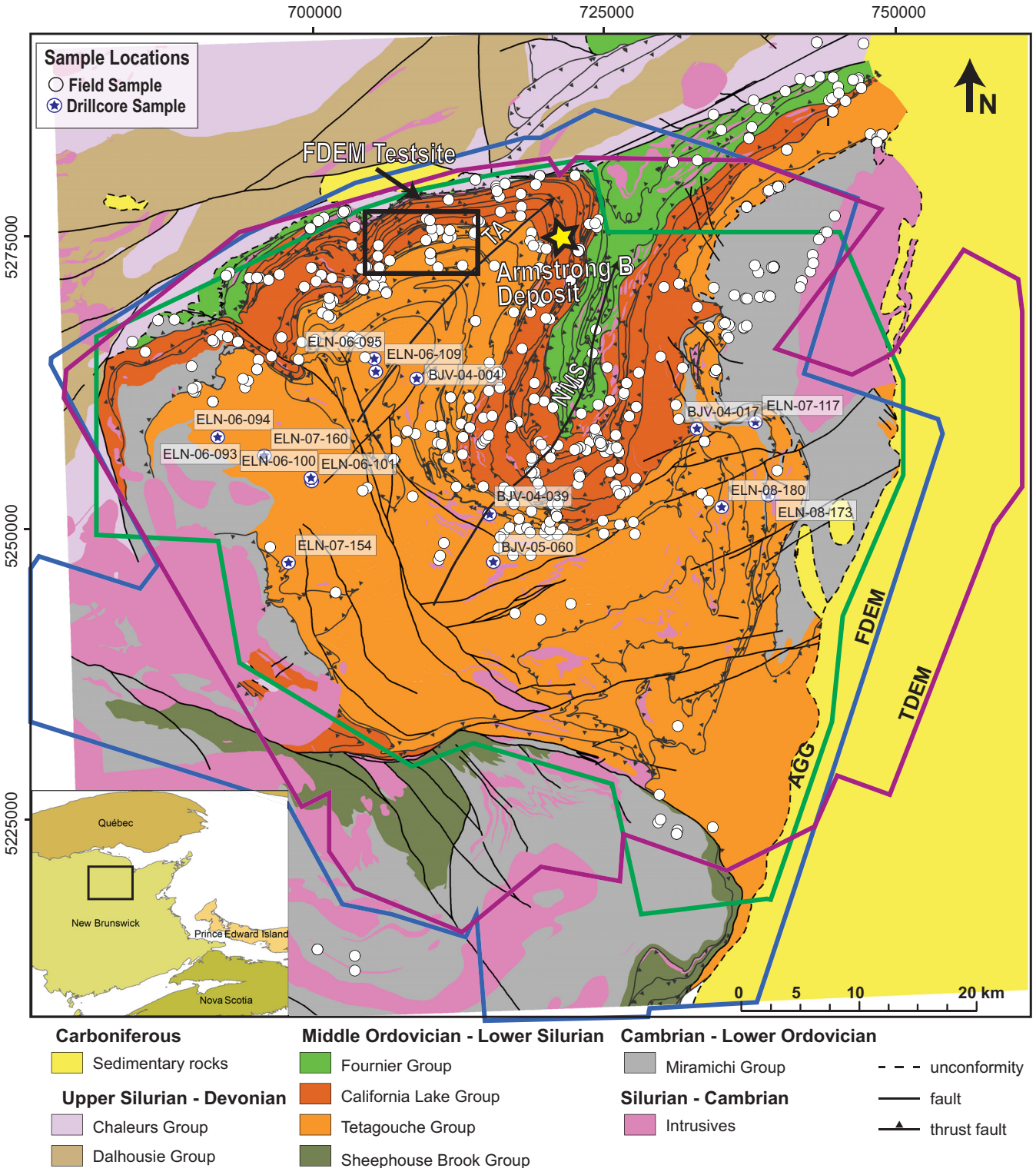

Figure 1. Tectonostratigraphic map of the Bathurst Mining Camp (modified from van Staal et al., 2003). Abbreviations: Airborne geophysical survey boundaries identified: AGG = Airborne gravity gradiometry survey; FDEM = frequency domain electromagnetic survey; NMS = Nine Mile Synform; TA = Tetagouche Antiform; TDEM = time domain electromagnetic survey. Rock property sample locations are shown as white circles.

measurement procedure. Borehole and core rock property datasets are best considered independently unless it can be shown that they are statistically equivalent. The initial objective of our study was to expand the physical property database presented in Thomas (2003) by incorporating new density and magnetic susceptibility information collected for drill-core samples and *in situ* field stations throughout the BMC. The density measurements were obtained using Archimedes' submersion approach and magnetic susceptibility were calculated by averaging three measurements taken on each sample. Descriptive statistics of the newly compiled density and magnetic susceptibility measurements are presented in tables and subjected to bivariate analyses to extract additional geological information.

The magnetic susceptibility data are then used as a constraint for a 3-D magnetic inversion model of the Armstrong B deposit to solve for the direction and intensity of the remanent vector associated with the magnetic anomaly of the deposit. The density data are used to develop a new Bouguer and terrain correction factor for ground gravity and airborne gravity gradiometry (AGG) by using a spatially variable density averaged from density measurements and linked to the geological map expression. Finally, a subset of the magnetic susceptibility measurements are used to ground-truth magnetic susceptibility values obtained from inversion of frequency domain airborne electromagnetic data (FDEM). The inverted magnetic susceptibility values are then used to forward model the total magnetic intensity and develop a new near-surface magnetic residual map for a small area northwest of the Tetagouche Antiform in the BMC (Fig. 1).

GEOLOGY

The BMC encompasses a semi-circular area of approximately 70 km in diameter in the Miramichi Highlands of northern New Brunswick (Fig. 1). Part of the larger Brunswick subduction complex (BSC), the BMC records the Late Ordovician – Silurian development, closure, and subduction of the Tetagouche-Exploits back-arc basin (van Staal et al., 2003). Felsic to mafic back-arc volcanogenic rocks with coeval sedimentary rocks of the California Lake, Tetagouche, Fournier, and Sheephouse Brook tectonic blocks diachronously developed in separate subbasins, sharing a common tectonic environment along the margin of the Laurentia continent (Rogers et al., 2003). The Tetagouche, Sheephouse Brook, and at least part of the California Lake blocks are underlain by rocks of the Miramichi Group that form the stratigraphic basement and are the oldest exposed sedimentary and volcanic rocks of the Bathurst Supergroup (van Staal et al., 2003). During the Late Ordovician – Late Silurian, these adjacent terranes were incorporated into the BSC during the Salinic orogeny (van Staal et al., 2008). Multiple phases of felsic through mafic intrusions were emplaced throughout the BMC during Ordovician, Silurian, and Devonian times. Sedimentary cover sequences, including the Silurian Chaleur and Kingsclear groups, Devonian Dalhousie Group, and Carboniferous Clifton Formation, occupy the edges of the BMC map region. A thorough discussion of the geology and tectonostratigraphy of each tectonic block is given in van Staal et al. (2003) and van Staal et al. (2008).

Deformation in the BMC was polyphase and long-lived, forming complex structures and tectonostratigraphic relationships. From the Ordovician through to the Early Silurian, ongoing subduction resulted in a series of tectonic blocks that were structurally juxtaposed and imbricated into a series of nappes. D_1 and D_2 thrusting created older over younger relationships both locally within individual nappes, and regionally across tectonic blocks (van Staal et al., 2003). Regional high-pressure, low-temperature penetrative deformation followed closure of the complex. D_3 and D_4 structures overprint D_1 and D_2 during unroofing and exhumation of the BMC.

D_1 thrust-related deformation is recognized as causing M_1 conditions (350–400°C, 5.5–5.8 kbar) across the BMC during the Ashgillian to Llandoverian (Currie et al., 2003). Assembly and steepening of the BMC nappes (with contained deposits) was likely complete by this time. Later metamorphism (M_2) has been recognized elsewhere in the BSC but its effect on the rocks of the BMC is minimal or absent (van Staal, et al., 2008).

RESULTS

Statistical Analysis

Statistical analysis of the expanded rock property database is presented in Tschirhart and Morris (2014). Physical property measurements made on the drill-core rock samples were divided into subpopulations based on their lithological classification. Statistical parameters (mean ($\overline{x}$), standard deviation (s), 25th, 50th (median), and 75th quartiles (Q_1, Q_2, and Q_3, respectively) were calculated from the density and magnetic susceptibility measurements and are listed in Tables 1 and 2, respectively. Henkel (1994) published a graphical template based on a comparison of magnetic susceptibility and density data that permits the discrimination between paramagnetic minerals (principally weakly magnetic biotite, amphibole, and pyroxene) and ferrimagnetic minerals (strongly magnetic magnetite and pyrrhotite) (Fig. 2a). Using this template it is possible to identify data trends (reduced susceptibility and density) indicative of the change in physical rock properties that may arise from the progressive effects

Table 1. Density statistics. $\overline{x}$ = mean; s = standard deviation, Q_1, Q_2, and Q_3 = 25th, 50th, and 75th quartiles, respectively.

Rock Type (N=1271)	**Density** (g/cm³)					
	N	$\overline{x}$	s	Q_1	Q_2	Q_3
Mafic *(N=165)*						
Basalt	105	2.85	0.11	2.77	2.86	2.93
Blueschist	9	2.88	0.08	2.84	2.86	2.92
Diabase	7	2.91	0.08	2.86	2.88	2.94
Gabbro	36	2.90	0.11	2.82	2.87	2.99
Mafic dyke	8	2.91	0.07	2.93	2.93	2.94
Sedimentary *(N=240)*						
Argillite	37	2.79	0.04	2.76	2.78	2.82
Graphitic argillite	11	2.76	0.04	2.73	2.75	2.78
Chert	8	2.68	0.08	2.65	2.69	2.72
Phyilite	8	2.78	0.10	2.72	2.76	2.84
Phylonite	2	2.73	0.06	2.71	2.73	2.75
Quartzite	11	2.68	0.05	2.64	2.68	2.71
Sericite-chlorite-altered sedimentary rocks	12	2.81	0.04	2.79	2.80	2.83
Shale	30	2.72	0.10	2.66	2.72	2.77
Siltstone	16	2.65	0.09	2.63	2.68	2.69
Siltstone and shale*	107	2.74	0.09	2.68	2.74	2.79
Slate	8	2.73	0.09	2.67	2.70	2.75
Tuffaceous sedimentary rocks	21	2.83	0.08	2.77	2.81	2.87
Turbidite	5	2.73	0.15	2.64	2.67	2.76
Iron Formation *(N=10)*						
Iron formation	10	3.00	0.15	2.93	2.97	3.02
Felsic-Intermediate *(N=806)*						
Granite	5	2.62	0.07	2.57	2.58	2.68
Ash tuff	30	2.71	0.05	2.68	2.71	2.73
Crystal tuff	193	2.73	0.05	2.70	2.73	2.75
Dacite	4	2.68	0.01	2.66	2.68	2.69
Felsic tuff	82	2.74	0.07	2.70	2.74	2.78
Quartz feldspar augen schist	11	2.69	0.08	2.67	2.68	2.76
Quartz feldspar porphyry	163	2.69	0.07	2.65	2.70	2.72
Rhyolite	225	2.71	0.07	2.67	2.71	2.74
Rhyolite agglomerate	22	2.69	0.03	2.66	2.68	2.71
Rhyolite tuff	45	2.72	0.10	2.64	2.72	2.75
Volcaniclastic	30	2.70	0.10	2.64	2.70	2.74
Sulphide *(N=50)*						
Massive	17	3.74	0.94	3.20	3.73	4.21
Semi-massive	13	3.04	0.21	2.90	3.08	3.10
Disseminated	20	2.94	0.89	2.88	2.93	3.00

*Uses 30 shale and 16 siltstone samples listed plus 61 additional samples that were not classified as either lithology

of hydrothermal alteration. To apply this approach to the many lithological units present in the BMC, the measurements were divided into a small number of rock classification subdivisions (felsic, mafic, sedimentary, iron formation, and sulphide), which are more appropriate for regional-scale investigations.

Perhaps the most important conclusion from this exercise is that none of the various lithological types can be fully represented by a tight (restricted) density or susceptibility range. Rather, the Henkel plots show that each rock type exhibits some variation in density and susceptibility values (Fig. 2a,b,c). These physical property variations are likely related to the effects of localized alteration or regional-scale metamorphic effects. However, without comparing results from several adjacent boreholes, it is not possible to outline any such patterns. Hydrothermal alteration influences the physical properties in two ways. The most common effect detected in sedimentary, tuffaceous, and some of the mafic volcanic rock samples is progressively increasing density values with a moderate increase in magnetic susceptibility. The hydrothermal alteration process imparts a progressive change in the abundance of paramagnetic minerals accompanied by an increase in density, perhaps as a result of porosity reduction during alteration. The second effect, best exhibited by the sedimentary rocks, is a much larger change in the magnetic susceptibility accompanied by a smaller change in density (Fig. 2b). The prevailing hypothesis is that during hydrothermal alteration, ferrimagnetic minerals within the host rock are altered to weakly magnetic paramagnetic minerals (Mwenifumbo et al., 2003). This hypothesis partly implies that density is systematically affected (reduced) by the alteration process, as the data show. Henkel's (1994) template defines separate trends for ferromagnetic- and paramagnetic-bearing rocks. Although most of the measurements of mafic volcanic samples plot in the paramagnetic mineral grouping, there are also a lesser number of samples that form a distinct cluster in the ferrimagnetic mineral grouping. In particular it should be noted that measurements of basalt samples (Fig. 2c) plot in both groups, suggesting that geophysical modelling must consider both weakly and strongly magnetic basalt. Sulphide samples were subdivided into three classes: massive (>75 vol% sulphides), semi-massive (25–75 vol% sulphides), and disseminated (sulphide grains not interconnected, typically with 25–75 vol% sulphides). The massive sulphide samples all plot in a region of high density and ferrimagnetic susceptibility (Fig. 2d), as expected. However, the density of the massive samples is quite variable. Gravity surveys are most effective in directly detecting sulphide bodies that are massive and of uniformly high density in a low-density country rock. Samples of disseminated and semi-massive sulphides plot in a well defined trend of increasing susceptibility with moderate increase in density (Fig. 2d). This trend reflects high contents of pyrrhotite and magnetite. The massive sulphide samples all plot within the region where ferrimagnetism predominates, except for one outlier with an anomalously low susceptibility. This relationship suggests that volcanogenic massive sulphide (VMS) mineralization may be associated with aeromagnetic anomalies that are controlled by remanent magnetism.

Table 2. Magnetic susceptibility statistics. $\bar{x}$ = mean; s = standard deviation, Q_1, Q_2, and Q_3 = 25th, 50th, and 75th quartiles, respectively.

		Susceptibility (SI)				
	N	$\bar{x}$	s	Q_1	Q_2	Q_3
Rock Type (1271)		*(SI x 10-3)*	*(SI x 10-6)*	*(SI x 10-3)*	*(SI x 10-3)*	*(SI x 10-3)*
Mafic *(N=165)*						
Basalt	105	0.48	4.90	0.24	0.36	0.54
Blueschist	9	2.66	6.60	0.42	2.13	10.35
Diabase	7	0.47	6.00	0.22	0.30	0.38
Gabbro	36	0.37	3.10	0.24	0.38	0.48
Mafic dyke	8	0.81	5.50	0.30	0.54	0.85
Sedimentary *(N=240)*						
Argillite	37	0.25	2.34	0.15	0.24	0.34
Graphitic argillite	11	0.23	4.63	0.11	0.18	0.11
Chert	8	0.40	7.30	0.15	0.28	0.52
Phyilite	8	0.23	1.72	0.16	0.22	0.34
Phylonite	2	0.14	1.69	0.12	0.14	0.17
Quartzite	11	0.05	3.00	0.02	0.06	0.10
Sericite-chlorite-altered sediments	12	0.26	1.64	0.18	0.31	0.36
Shale	30	0.21	5.95	0.10	0.18	0.36
Siltstone	16	0.09	5.29	0.04	0.08	0.14
Siltstone and shale*	107	0.20	5.14	0.09	0.19	0.51
Slate	8	0.19	2.47	0.13	0.19	0.29
Tuffaceous sedimentary rocks	21	1.08	4.84	0.41	0.79	2.60
Turbidite	5	0.22	1.70	0.18	0.20	0.38
Iron Formation *(N=10)*						
Iron formation	10	4.59	4.73	1.17	3.53	17.81
Felsic-Intermediate *(N=806)*						
Granite	2	0.05	2.50	0.03	0.05	0.08
Ash tuff	30	0.11	2.10	0.06	0.10	0.18
Crystal tuff	193	0.09	2.80	0.05	0.11	0.18
Dacite	3	0.05	4.00	0.03	0.05	0.09
Felsic tuff	82	0.11	3.00	0.06	0.12	0.24
Quartz feldspar augen schist	11	0.11	2.30	0.05	0.16	0.20
Quartz feldspar porphyry	163	0.05	3.30	0.02	0.05	0.12
Rhyolite	225	0.08	3.60	0.05	0.09	0.18
Rhyolite agglomerate	22	0.04	3.30	0.01	0.04	0.09
Rhyolite tuff	45	0.08	4.00	0.03	0.08	0.18
Volcaniclastic	30	0.05	3.90	0.01	0.05	0.14
Sulphide *(N=50)*						
Massive	17	5.99	8.67	2.05	8.87	26.18
Semi-massive	13	1.02	9.84	0.13	0.49	7.02
Disseminated	20	1.48	7.78	0.44	0.67	8.10

*Uses 30 shale and 16 siltstone sample listed plus 61 additional samples that were not classified as either lithology.

Samples of iron formation, an important ore equivalent (time-stratigraphic) marker horizon and exploration vector in the BMC (Peter et al., 2003), plot in two distinct populations; a higher susceptibility, lower density population, and a lower susceptibility, higher density population (Fig. 2e). These two populations are believed to correspond to the two distinct types of iron formation that are encountered in the camp; a Llanvirn-hematite rich (type 1) and an Aregian-magnetite rich (type 2). The distinction is significant as type 2 iron formation is more commonly associated with sulphide mineralization (Goodfellow and McCutcheon, 2003).

Constrained 3-D Geophysical Modelling

The Armstrong B deposit is located on the east limb of the Tetagouche Antiform (TA) (Fig. 1). The deposit consists of disseminated to massive sulphides hosted in a mixed sequence of ash, feldspar-crystal, and lithic-lapilli tuff of the Spruce Lake Formation (SLF) (Thomas et al., 2000). Due to the presence of abundant magnetically susceptible pyrrhotite, the lens-shaped deposit generates a 50 nT anomaly with the surround-

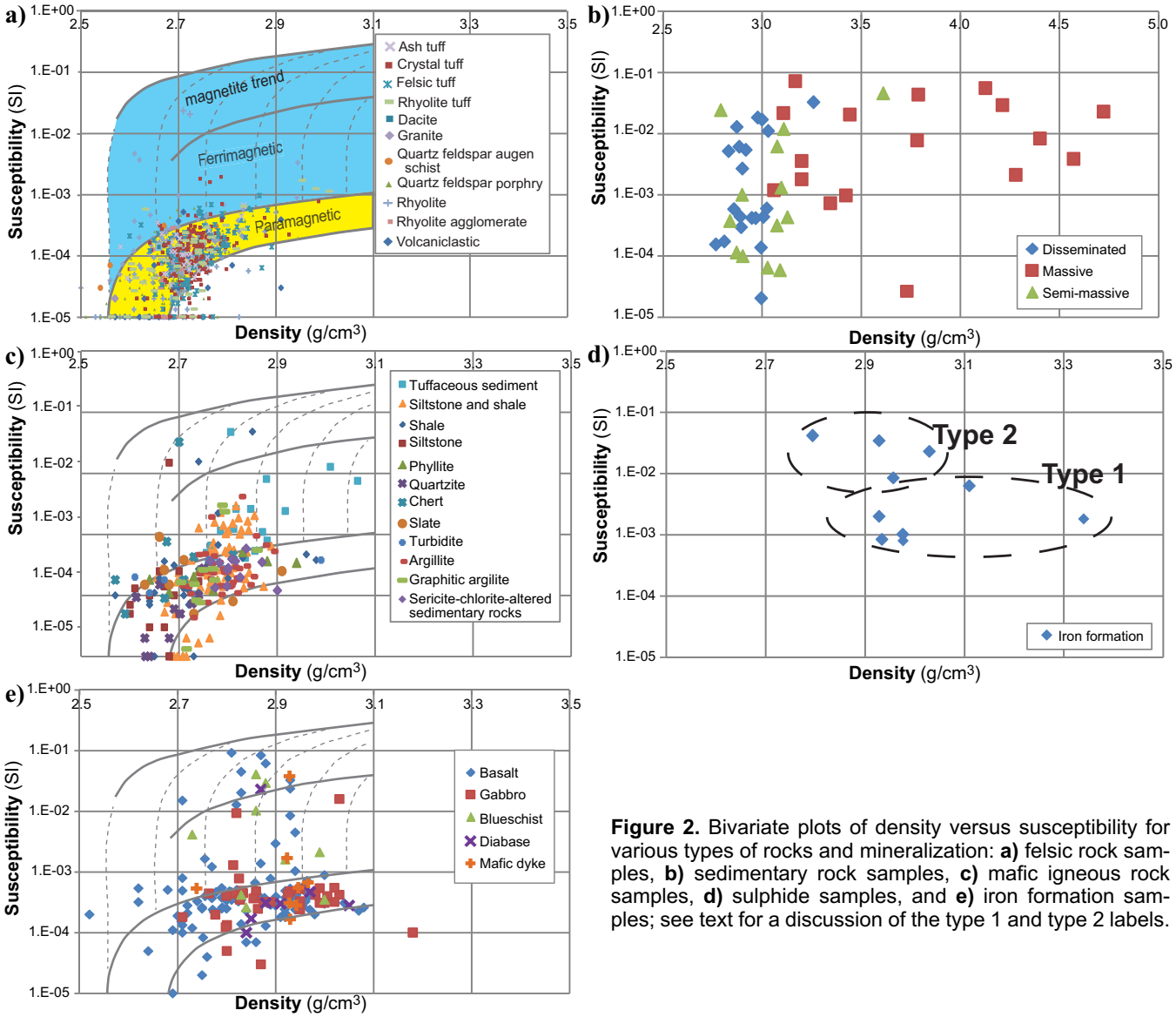

Figure 2. Bivariate plots of density versus susceptibility for various types of rocks and mineralization: **a)** felsic rock samples, **b)** sedimentary rock samples, **c)** mafic igneous rock samples, **d)** sulphide samples, and **e)** iron formation samples; see text for a discussion of the type 1 and type 2 labels.

ing magnetically weak felsic tuffs of the SLF (Fig. 3a). We applied a discrete object inversion approach using *pb*Encom Modelvision® software in which we fixed source body position, inducing field, strike length, and magnetization, and inverted for the residual total magnetization, body width, and body depth extent. The location and geometry of the deposit is well defined by several drillholes that intersect mineralization. This information, together with our petrophysical property measurements, was used to forward model the deposit as a steeply dipping (65°), northerly striking (15°) tabular body of 244 m length with an average magnetic susceptibility of 6 × 10^{-3} SI. The hosting SLF was assigned a magnetic susceptibility of 0.1 × 10^{-3} SI. The starting model is shown in Figure 3b.

The result of the inversion is shown in Figure 3c and 3d for the magnetic anomaly and geometric model, respectively. The root-mean-square error (RMSE) between the observed field (Fig. 3a) and the modelled field (Fig. 3c) is 2.8 nT (<1% of total signal) and closely matches the observed field. The misfit between the observed and calculated anomalies can be attributed mainly to an interfering magnetic anomaly associated with adjacent sources to the southwest and along the eastern edge of the study area. During the inversion computation, the estimated width of the magnetic source body increased from 25 to 165 m. This may be due to a resolution limitation imposed by the height of the magnetic sensor above the ground and the sampling rate of the sensor. Also, it is possible that the model is describing the orebody and its alteration halo, which may contain sufficient pyrrhotite to also register as a magnetic anomaly. The depth extent is also increased from 183 to 343 m, which can be attributed to the inaccurate depth extent determinations commonly inherent in geophysical inversion models (Spicer, 2010).

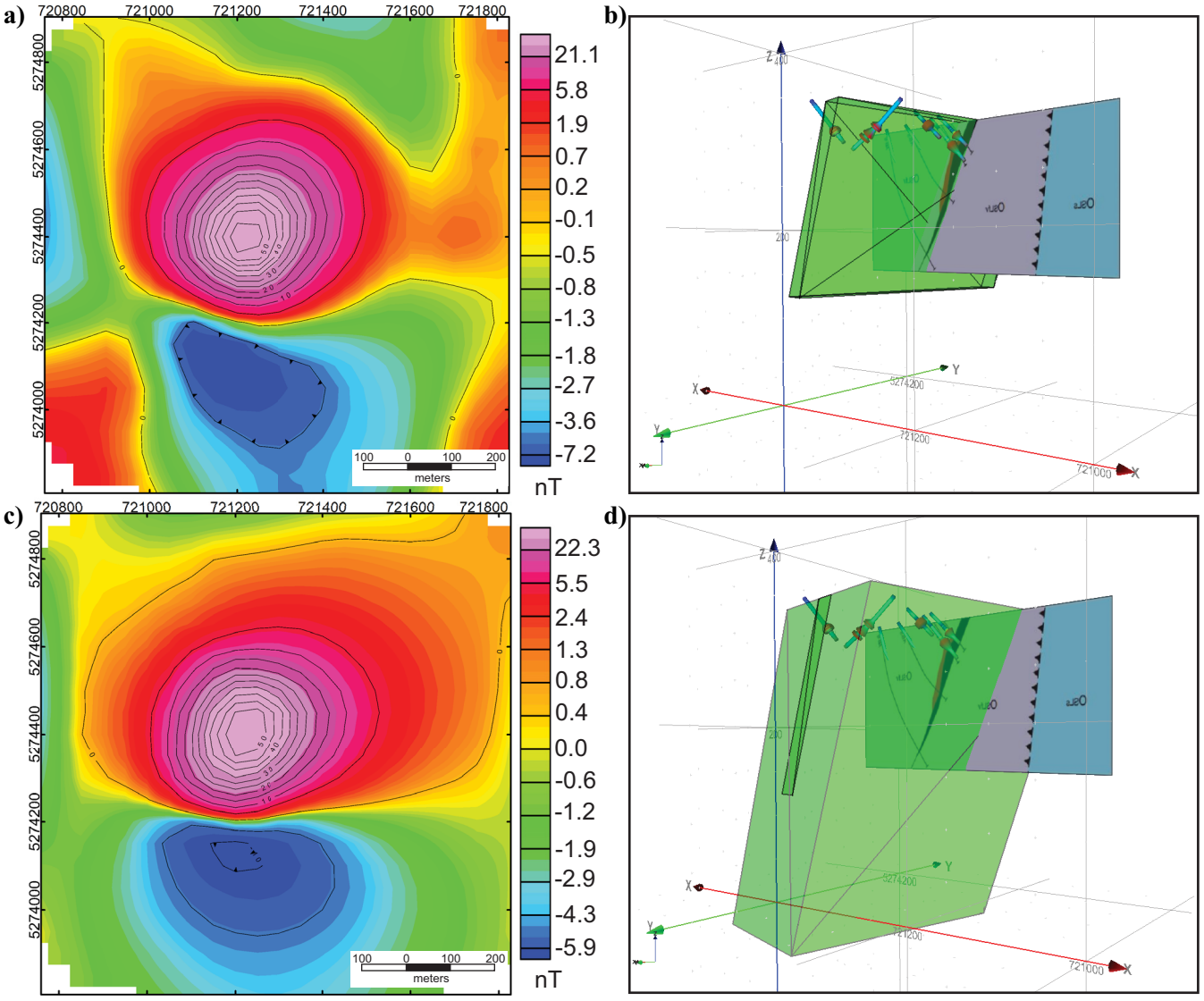

Figure 3. Starting model and solution of the Armstrong B deposit anomaly discrete object magnetic-inversion: **a)** observed magnetic anomaly; **b)** input 3-D discrete body geophysical model; **c)** calculated magnetic anomaly from inversion; and **d)** resultant discrete body model.

Acquisition or blocking of remanence is always linked to a geological event, whether it is primary deposition, later thermochemical recrystallization, or fluid flow associated with peak metamorphism or deformation. The upper age bound for remanence acquisition is the depositional age of the hosting SLF; 471 Ma (New Brunswick Dept. of Energy and Mines, 2013), whereas the lower age limit compatible with the geological evidence is the end of the Salinic orogenic episode ca. 418 Ma (van Staal et al., 2008). We speculate that the remanence most likely was imparted during D_1 or D_2 deformation when the sulphides were recrystallized (Goodfellow and McCutcheon, 2003). Using the Phanerozoic Apparent Polar Wander Path (APWP) published by Torsvik et al. (2012) for the Laurentian supercontinent, the expected remanence directions for the location of the Armstrong B deposit during the time period from 470 to 420 Ma can be estimated. The Koenigsberger (Q) ratio solved from the inversion is 1.4, implying that the remanent magnetization is of a higher magnitude than the inducing field. The remanent inclination and declination estimated by the inversion are I = -7° and D = 172°, respectively. Paleomagnetic results reported by Liss et al. (1993) from pillow basalts of the Tetagouche Group, sampled to the east of the Armstrong B deposit, give a mean *in situ* remanence direction of I = -6°, D = 140° that is not grossly dissimilar to the direction determined by modelling and inversion.

The remanence direction computed through the inversion differs from the APWP-derived remanence direction by slightly more than 30°. Most of this difference is attributed to the inclination of the computed remanence vector. This may be due to either (1) the

computed direction containing some portion of the present Earth's field that is the Koenigsberger ratio is higher than estimated or (2) the rocks have been tectonically rotated (tilted) subsequent to acquisition of the remanence direction. If (1) is valid, then the model remanence vector should fall on a great circle path between the present Earth's field direction and the expected remanence direction. Alternatively, if (2) is correct, then the difference between the model remanence direction and the expected remanence direction should fall on a small circle path with the axis of the small circle describing the strike of the fold axis. Based on the evidence provided by this study, it is not possible to definitively differentiate between the two options; however, (1) does outline a simple great circle path that intersects the apparent polar direction path within the time period 430 to 420 Ma. This time span coincides with the estimated peak of the Salinic orogeny: 430–423 Ma (van Staal et al., 2008). In contrast, (2) requires a tilt of approximately 30°, but the strike of this tilt rotation axis is perpendicular to the current strike of the Armstrong B deposit, and on this basis, (2) can be discounted. In summary, the Armstrong B deposit is has a strong remanent magnetization signal. Acquisition of this remanence occurred when the metamorphic temperatures cooled sufficiently to block the magnetization. The extant conclusion (1) also suggests that the orebody has been subject to only limited tectonic rotation since remanence acquisition.

Laterally Variable Density Correction

A detailed understanding of the physical rock properties is not only useful for petrophysical analysis and geophysical modelling, but also for improving the correction factors that are commonly applied to some geophysical data. Bouguer and terrain corrections in ground gravity calculations both require input of a density value that is reflective of the near-surface density. Airborne gravity gradiometer surveys measure the gravity gradient at some height above the topographic surface. As such, the primary signal recorded by an AGG survey is dominated by the density contrast between the topography and the air. To derive geologically meaningful information from these data it is necessary to apply a terrain correction, which requires a density estimate. Most commonly, a constant density of 2.67 g/cm^3 is used for these data corrections, as this value is considered to be the average density of crystalline, continental crust of granitic composition (Hinze, 2003). In many areas, including the BMC, universal application of this single correction value may introduce error into the reduced dataset. If the density of the near-surface rocks is higher (or lower) than the average density value, then elements of the topographic signal will be retained in the resulting data grid image. In areas where the geology comprises a series of lithologically distinct tectonic slices separated by thrust boundaries (such as in the BMC), it is possible (even likely) that the average surface density of each tectonic slice could be significantly different (Vajk, 1956). Tschirhart et al., (submitted) address this issue and propose application of a spatially variable density for Bouguer and terrain correction for ground gravity and terrain correction for airborne gravity gradiometry data. The correction factor used is determined using the mapped geology and measured density values. Briefly, a local average density that is reflective of a specific tectonostratigraphic group in the BMC is calculated from the measured physical property information. This local average density is then only applied to measurements taken within that area, as mapped by van Staal et al., (2003). With all measurements processed accordingly, the corrected data are combined and gridded.

Original ground gravity data reduced using a constant density of 2.67 g/cm^3 for the Bouguer and terrain correction are shown in Figure 4a. Ground gravity data reprocessed using a variable density for the Bouguer and terrain corrections are shown in Figure 4b. The difference between the constant and laterally variable density corrections is shown in Figure 4c. For the AGG data, the terrain correction was originally preformed using a variety of terrain correction densities ranging from 2.40 to 3.00 g/cm^3; for brevity only AGG G_{zz} (vertical gravity gradient) data corrected with a terrain density of 2.70 g/cm^3 are presented in Figure 4d. The G_{zz} component of the reprocessed AGG data using the laterally variable density correction are presented in Figure 4e, and the difference between the G_{zz} components of the constant (2.70 g/cm^3) and the laterally variable terrain correction is shown in Figure 4e. The differences in the final results using the constant correction and the spatially variable correction are subtle. For ground gravity, the overall shapes and trends of the major anomalies are unchanged by the reprocessing (Fig. 4c); however, the exact extents and amplitudes of these anomalies are altered. The major central gravity high, caused by the ophiolitic Fournier Group (Fig. 4a) and mafic volcanic rocks of the California Lake Group, is extended slightly to the east by tens of metres and is reduced in amplitude by a maximum of 2.1 mGal (Fig. 4c). Along the Tetagouche – California Lake contact, a small isolated body of dense Flat Landing Brook mafic volcanic rocks adjacent to the dense California Lake Group mafic volcanic rocks to the north is better resolved using the variable density method (Fig. 4c). By using a variable density method, a lower density correction value is applied to the Tetagouche Group than to the California Lake Group. A larger correction is applied to the groups containing higher density rock

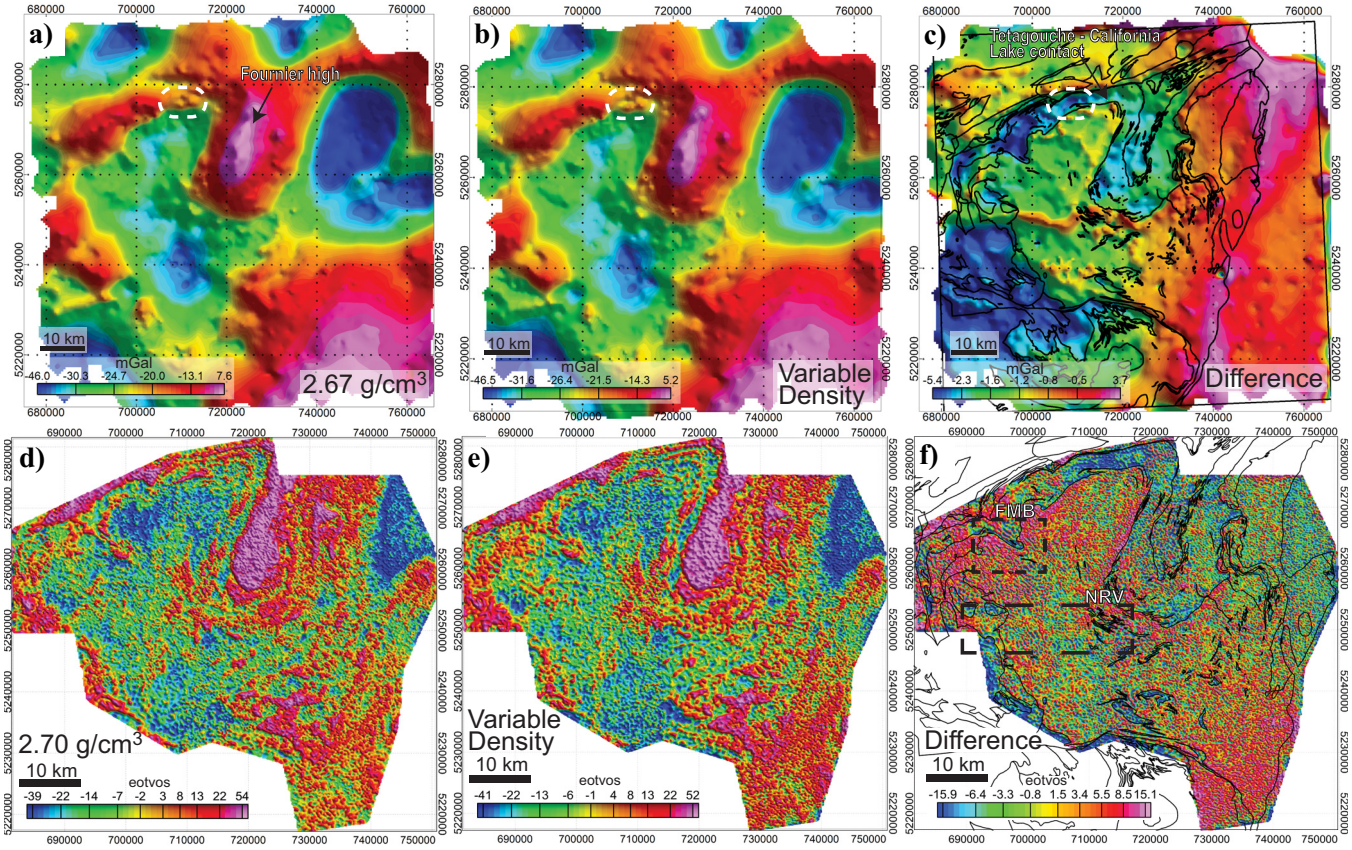

Figure 4. Constant density-corrected and laterally variable density-corrected gravity and gravity gradiometry (G_{zz}) maps and difference grids: **a)** ground gravity data map corrected using 2.67 g/cm^3; **b)** laterally variable density-corrected ground gravity map; **c)** difference between constant and laterally variable density-corrected ground gravity maps; **d)** Gzz component map corrected using 2.70 g/cm^3; **e)** laterally variable density-corrected G_{zz} component map; and **f)** difference between constant and laterally variable density corrected G_{zz} components. Circled area in (a) and (c) is discussed in the text. Abbreviations: FMB = Forty Mile Brook drainage basin; NRV = Nepisiguit River Valley.

units, and a smaller correction to those groups containing less dense rocks; thus, anomalously dense bodies within the less dense group become more pronounced/evident near more dense groups.

For AGG data, the difference between the constant density (Fig. 4d) and laterally variable density terrain corrected grid (Fig. 4e) is also subtle (Fig. 4f). The differences become much more apparent upon comparison of the end members of the constant terrain correction grids (i.e. 2.40 and 3.00 g/cm^3; Tschirhart et al., submitted). Locally, where the geological density matches the correction value, this incremental method may be appropriate. However, across larger areas, where near-surface density variations are complex due to structural and stratigraphic controls, this introduces considerable error. This applies for all tensor components, but for brevity is only shown for G_{zz} (Tschirhart, 2013). The influence of the Nepiguit River Valley (NRV), for example, appears to interfere with the true G_{zz} anomaly, producing false positives and negatives; however, this is minimized within the variable density grid by implying a correct reduction value (Fig. 4e).

Nettleton (1939) proposed that it is possible to determine the density of a topographic feature by iteratively searching for the minimum variance in a gravity signal profile after applying all appropriate terrain corrections. Exactly the same concept can be applied to gravity and topographic grids. Using two examples where there are marked differences in the gradient anomaly using different terrain correction values (NRV and part of the Forty Mile Brook (FMB) drainage basin) it is possible to determine the relationship of topography to the G_{zz} anomaly by plotting the covariance between G_{zz} and the topography against different density correction values (FitzGerald et al., 2011; Tschirhart et al., submitted). Covariance is a measure of the similarity between the morphology of the topographic and gravity image surfaces. The slope of the line of best fit between covariance and density reflects the importance of topography, with a steeper slope indicating greater importance. At the x-intercept, where covariance is zero, the G_{zz} anomaly should have no correlation with topography, and an optimum density correction value can be found. As shown in Table 3, the density correction values used in the variable density correction grid

Table 3. Lateral density correction values and terrain correction densities calculated using covariance.

Tectonostratigraphic Group	Average Density (g/cm³)	Terrain Correction Density NRV area (g/cm³)	FMB area (g/cm³)
Miramichi	2.75	2.83	*
Sheephouse Brook	2.81	*	*
Tetagouche	2.72	2.73	2.70
California Lake	2.82	2.82	2.82
Fournier	2.83	*	*
Kingsclear	2.75	*	*
Chaleurs	2.73	*	*
Dalhousie	2.72	*	*
Carboniferous sedimentary rock	2.73	*	*
Intrusives	2.75	2.40	*

* Group not present in test area

are very close to the "optimum" correction density values derived from the best-fit slope computation; however, rather than cross-referencing several grids (as in the case of the incremental terrain correction) all the information is presented in a single image (Fig. 4e). It is important to note that this method performs better in areas of rugged relief with uniform density, and it is much more difficult to apply in regions of extreme relief with multiple formations of different densities.

Magnetic Susceptibility Constraint for Frequency Domain Electromagnetic Data Inversion

Measured in-situ, magnetic susceptibly (MS_m) values were used to verify magnetic susceptibility values calculated through inversion of frequency domain electromagnetic (FDEM) data (MS_i) for a small test area north of the Tetagouche Anitform's hinge line (area bounded by rectangle shown in Figs. 1, 5a). These MS_i values are then used to forward model the local near-surface anomalous magnetic field to produce an optimal near-surface residual (Tschirhart et al., 2013). Magnetic susceptibility is recorded as a negative in-phase component by FDEM systems. Although the susceptibility signal is independent of frequency, it is most easily detected with low-frequency EM signals because at these wavelengths, conductivity, which is frequency dependent, is less dominant (Fraser, 1981; Hodges, 2004; Fig. 5b). Apparent resistivity is solved from the coplanar in-phase frequencies using a singular value decomposition inversion developed by Huang and Fraser (2000). Results of the inversion are then compared with *in situ* magnetic susceptibility values measured on 25 samples collected within the area (Fig. 5c). At four sample locations, negative MS_i values were

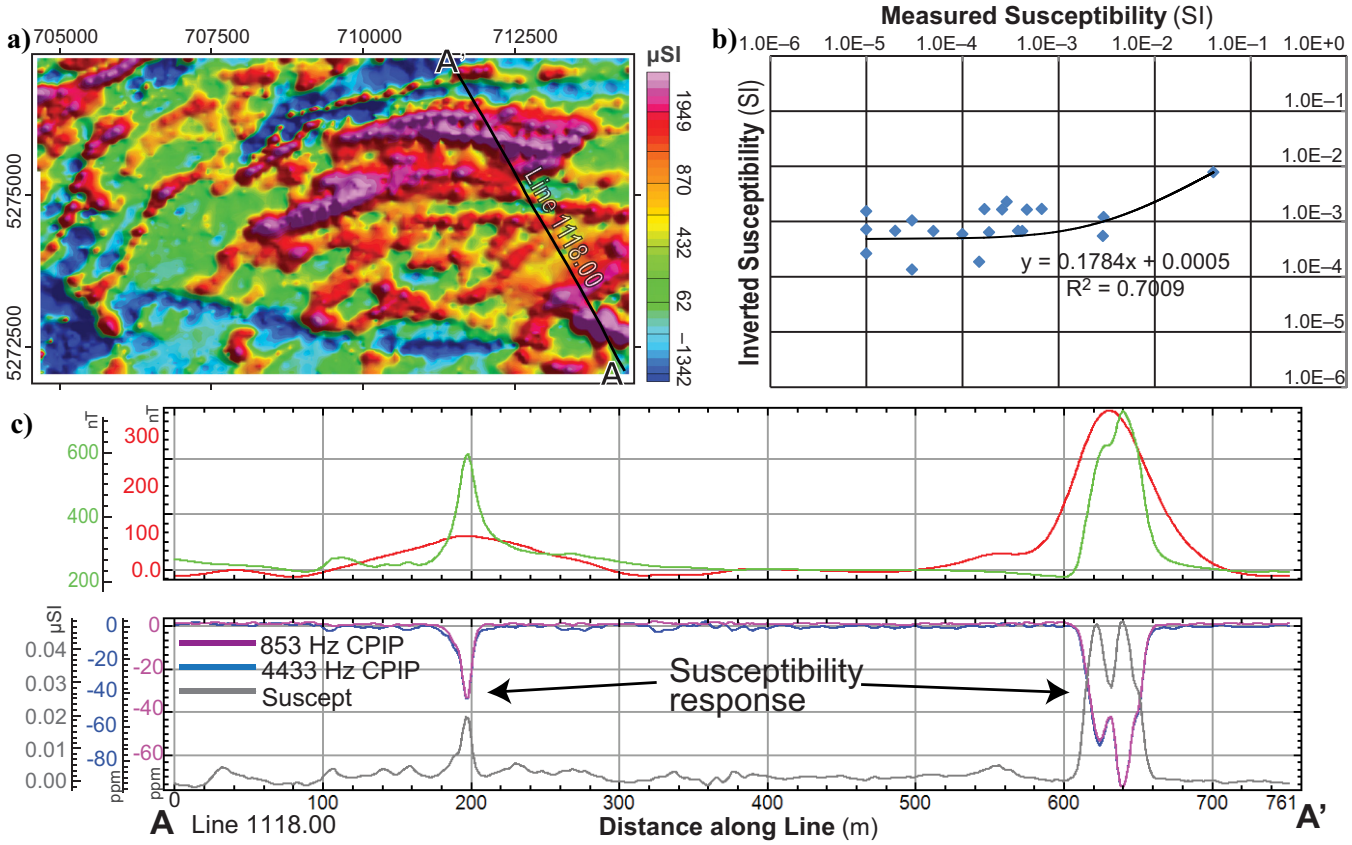

Figure 5. Apparent magnetic susceptibility inverted from frequency domain electromagnetic data: **a)** apparent magnetic susceptibility map of the test area (see Fig. 1 for location); **b)** results from Line 1118, comparing modelled and measured magnetic intensity (top) and the relationship between low- and mid-frequency coplanar in-phase response to inverted susceptibility (bottom); and **c)** bivariate plot of the inverted magnetic susceptibility value versus the measured magnetic susceptibility.

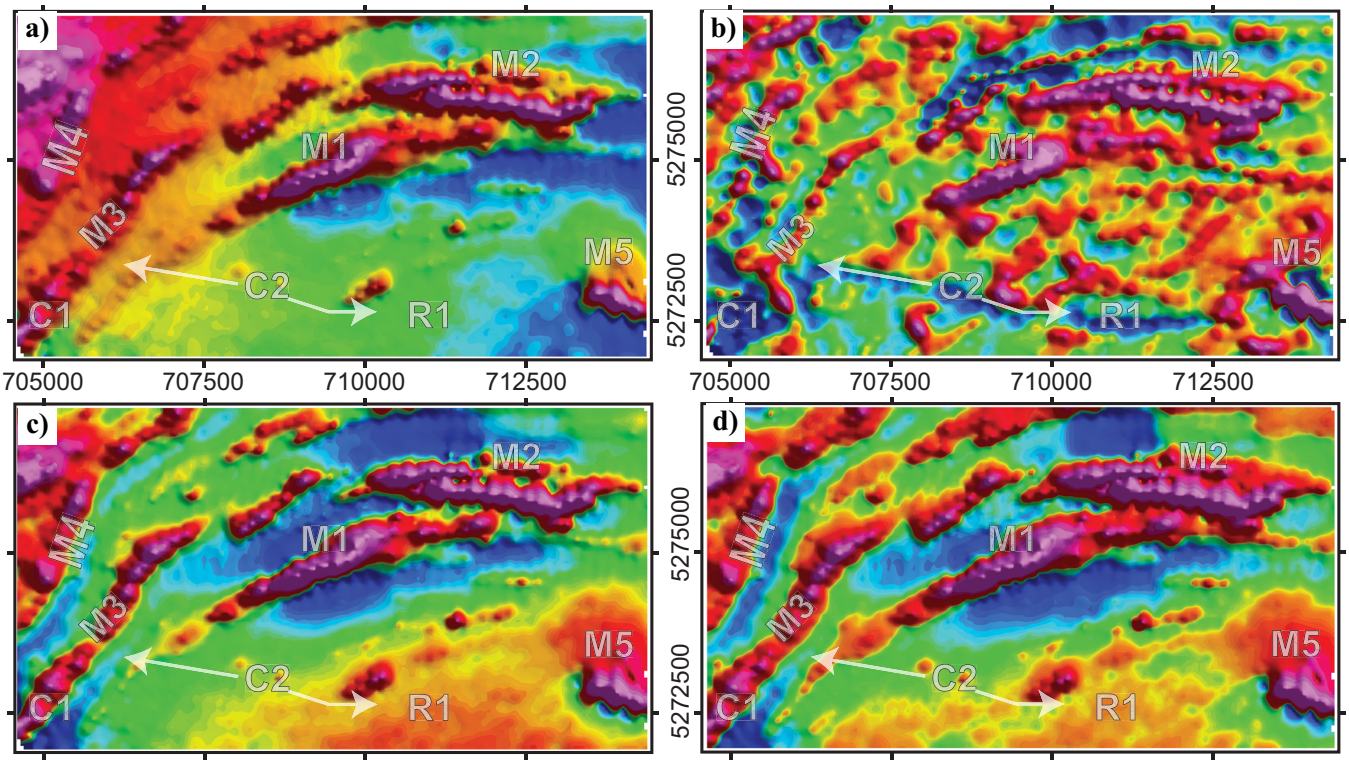

Figure 6. Plots showing the **(a)** pole-reduced total magnetic intensity map, **(b)** forward-modelled magnetic anomaly grid, **(c)** magnetic residual map constructed by removing an 800 m upward continued regional magnetic field, and **(d)** the magnetic residual map constructed by removing an 800 m non-linear filter regional magnetic field. M1 to M5 denotes prominent magnetic anomalies. R1 marks a remanent magnetic field. C1 and C2 mark conductivity anomalies.

calculated, and this arises when the EM response is dominated by surficial conductivity fluctuations. Of 21 positive MS_i values, a linear trend can be fitted between the calculated and measured magnetic susceptibilities (Fig. 5c). Discrepancies between MS_i and MS_m may be explained by the measured susceptibilities representing a single point source, whereas the inverted values represent an average of an area limited by the grid resolution, in this case: 50 x 50 m. It is also possible there may be a consistent bias in the EM signal response, producing a systematic shift in the computed susceptibility.

In order to generate an accurate near-surface magnetic anomaly map (residual) and effectively remove any deeper sourced (regional) signal, the MS_i data are forward-modelled to produce an anomalous magnetic field map (AMF_i). This map is then compared with the observed magnetic anomaly map and a suite of residual magnetic maps to select an optimal product that most closely matches the AMF_i. Figure 6 shows the total field magnetic anomaly (Fig. 6a), forward-modelled magnetic anomaly grid AMF_i (Fig. 6b), residual magnetic field that does not closely resemble the AMF_i (Fig. 6c), and a residual magnetic field that does closely resembles the AMF_i (Fig. 6d). Central to this method is that FDEM has a limited depth of penetration that is dependent upon the resistivity of the rock and frequency of the transmitting coil. Most FDEM systems have well defined effective depths of penetration, which in all cases are limited to within a couple of hundred metres below the surface. In Figure 6b, AMF_i identifies 5 prominent magnetic anomalies (annotated M1–M5) within the test area. The regional trend on this area is flat, and a proper residual must match this. Figure 6c shows a magnetic residual obtained using an 800 m upward continuation filter to model the regional field. As well, a magnetic residual produced using an 800 m non-linear filter (NLF) (Keating and Pinet, 2011) to model the regional field is shown in Figure 6d. The NLF residual generates an overall flat response, whereas the upward continuation method creates a gentle gradient in the centre of the study area (R1 area). The NLF also is superior in removing regional contributions in the northwest of the study area, which according to the AMF_i only contains thin, near-surface magnetic beds. There are some areas where the inversion poorly calculates the apparent magnetic susceptibility and subsequently incorrectly reproduces the anomalous magnetic field at these locations. Two such locations are identified in Figure 6 and labelled as C1 and C2. At location C1, there is a naturally conductive body that produces a dominant conductivity response that impedes the susceptibility response. Magnetic susceptibly is therefore not accurately recovered in the

inversion. Likewise, at location C2 a cultural source (power lines) creates a conductivity anomaly large enough to impede the susceptibility response. This therefore limits the applicability of this methodology to areas where conductivity is low. Another added benefit is that MS_i, and therefore TMI_i, are not affected by remanent magnetization and thus provide a means of mapping remanent source bodies and their relative remanent vector direction, positive or negative (Tschirhart et al., 2013).

IMPLICATIONS FOR EXPLORATION

The research reported herein has several implications for exploration. First and foremost, a comprehensive physical property database reduces the ambiguity associated with geophysical interpretation and provides ancillary information for the integration of geological and geophysical datasets. More accurate geophysical models and interpretations can therefore be developed at various scales because the physical rock property distributions are better understood. Large-scale geophysical modelling across the BMC has led to a better understanding of the deep structure of the major litho-stratigraphic units (Tschirhart and Morris, 2014). Small-scale 3-D inversions have shown the important effect of remanence within the BMC at a deposit-scale, and this method has been used to provide another independent age for mineralization in the Armstrong B deposit. This study has demonstrated that it is possible to derive regional magnetic susceptibility patterns from both aeromagnetic and frequency domain electromagnetic surveys. A pixel-by-pixel comparison of the susceptibility estimates derived from the two methods over a map area provides a method for locating regions where remanent magnetization is dominant. A density versus magnetic susceptibility bivariate plot using a Henkel (1994) template as a background serves to emphasize the presence of two geophysical manifestations of the effects of hydrothermal alteration: a) increased abundance of weakly magnetic paramagnetic minerals associated with a large density increase, and b) creation, or destruction of strongly magnetic ferrimagnetic minerals associated with a limited density increase.

Although the physical property information compiled here is specific to the BMC, the various methods developed can be applied elsewhere. Application of a variable density correction to ground and/or airborne gravity/gravity gradiometry is possible in any survey location. Similarly, the magnetic susceptibility inversion from FDEM data and its constraint to near-surface magnetic mapping is universally applicable.

ACKNOWLEDGEMENTS

The authors are grateful for the encouragement and support of Jan Peter throughout the duration of this project. Reviewers by J. Peter and V. Tschirhart greatly improved the content and clarity of this work.

REFERENCES

Currie, K.L., van Staal, C.R., Peter, J.M., and Rogers, N., 2003. Conditions of metamorphism of the main massive sulphide deposits and surrounding rocks in the Bathurst Mining Camp, *In:* Massive Sulfide Deposits of the Bathurst Mining Camp, New Brunswick, and Northern Maine, (ed.) W.D. Goodfellow, S.R. McCutcheon, and J.M. Peter; Society of Economic Geologist, Monograph 11, p. 65–78.

FitzGerald, D.J., Paterson, R., and Christensen, A.N., 2011. Decorrelating measured airborne gravity gradiometry data with topography; Geosynthesis Conference Abstract, Capetown.

Fraser, D.C., 1981. Magnetite mapping with a multi-coil airborne electromagnetic system; Geophysics, v. 46, p. 1579–1593.

Goodfellow, W.D. and McCutcheon, S.R., 2003. Geologic and genetic attributes of volcanic sediment-hosted massive sulfide deposits of the Bathurst Mining Camp, Northern New Brunswick, *In:* Massive Sulfide Deposits of the Bathurst Mining Camp, New Brunswick, and Northern Maine, (ed.) W.D. Goodfellow, S.R. McCutcheon, and J.M. Peter; Society of Economic Geologist, Monograph 11, p. 245–302.

Henkel, H., 1994. Standard diagrams of magnetic properties and density — A tool for understanding magnetic petrology; Journal of Applied Geophysics, v. 32, p. 43–53.

Hinze, W.J., 2003. Bouguer reduction density, why 2.67?; Geophysics, v. 68, p. 1559–1560.

Hodges, G., 2004. Mapping conductivity, magnetic susceptibility, and dielectric permittivity with helicopter electromagnetic data, *In:* Proceedings; Society of Exploration Geophysicists International Exposition and 74th Annual Meeting, Denver, Colorado, October 10-15, 2004, p. 660–663.

Huang, H. and Fraser, D.C., 2000. Airborne resistivity and susceptibility mapping in magnetically polarizable areas; Geophysics, v. 65, p. 502–511.

Keating, P. and Pinet, N., 2011. Use of non-linear filtering for the regional-residual separation of potential field data; Journal of Applied Geophysics, v. 73, p. 315–322.

Liss, M. J., van der Pluijm, B. A., and Van der Voo, R., 1993, Avalonian proximity of the Ordovician Miramichi Terrane, northern New Brunswick, northern Appalachians: Paleomagnetic evidence for rifting and back-arc basin formation at the southern margin of Iapetus; Tectonophysics, v. 227, p. 17–30.

Mwenifumbo, C.J., Elliot, B.E., and Street, P., 2003. Borehole geophysical characteristics of massive sulfide deposits in the Bathurst Mining Camp, *In:* Massive Sulfide Deposits of the Bathurst Mining Camp, New Brunswick, and Northern Maine, (ed.) W.D. Goodfellow, S.R. McCutcheon, and J.M. Peter; Society of Economic Geologist, Monograph 11, p. 841–860.

New Brunswick Department of Energy and Mines, 2013. New Brunswick Bedrock Lexicon, Spruce Lake Formation. http://dnr-mrn.gnb.ca/Lexicon/Lexicon/Lexicon_View.aspx. June 19, 2013

Nettleton, L.L., 1939. Determination of density for reduction of gravimeter observations; Geophysics, v. 4, p. 176–183.

Peter, J.M., Kjarsgaard, I.M., and Goodfellow, W.D., 2003. Hydrothermal sedimentary rocks of the Heath Steele Belt, Bathurst Mining Camp, New Brunswick: Part 1. Mineralogy and mineral chemistry, *In:* Massive Sulfide Deposits of the Bathurst Mining Camp, New Brunswick, and Northern Maine, (ed.) W.D. Goodfellow, S.R. McCutcheon, and J.M. Peter; Society of Economic Geologist, Monograph 11, p. 391– 416.

Rogers, N., van Staal, C.R., Winchester, J.A., and Fyffe, L.R., 2003. Provenance and chemical stratigraphy of the sedimentary rocks of the Miramichi, Tetagouche, California Lake, and Fourier Groups, Northern New Brunswick, *In:* Massive Sulfide Deposits of the Bathurst Mining Camp, New Brunswick, and Northern Maine, (ed.) W.D. Goodfellow, S.R. McCutcheon, and J.M. Peter; Society of Economic Geologist, Monograph 11, p. 111–128.

Spicer, W., 2010. Geologically Constrained Geophysical Modeling of magnetics and Gravity - the Baie Verte Peninsula, Newfoundland; M.Sc. thesis, McMaster University, Hamilton, Ontario, 166 p.

Thomas, M.D., 2003. Gravity signatures of massive sulfide deposits, Bathurst Mining Camp, New Brunswick, *In:* Massive Sulfide Deposits of the Bathurst Mining Camp, New Brunswick, and Northern Maine, (ed.) W.D. Goodfellow, S.R. McCutcheon, and J.M. Peter; Society of Economic Geologist, Monograph 11, p. 799–817.

Thomas, M.D., Walker, J.A., Keating, P., Shives, R., Kiss, F., and Goodfellow, W.D., 2000. Geophysical atlas of massive sulphide signatures, Bathurst mining camp, New Brunswick; Geological Survey of Canada, Open File 3887 (also New Brunswick Department of Natural Resources and Energy, Minerals and Energy Division, Open File 2000-4), 105 p.

Torsvik, T. H., Van der Voo, R., Preeden, U., Mac Niocaill, C., Steinberger, B., Doubrovine, P. V., van Hinsbergen, D.J.J., Domeier, M., Gaina, C., Tovher, E., Meert, J.G., McCausland, P.J., and Cocks, L.R.M., 2012. Phanerozoic polar wander, paleogeography and dynamics; Earth-Science Reviews, v. 114, p. 325–368.

Tschirhart, P.A., 2013. Geophysical processing and interpretation with geologic controls: Examples for the Bathurst Mining Camp; M.Sc. thesis, McMaster University, Hamilton, Ontario, 143 p.

Tschirhart, P.A. and Morris, W.A., 2014. Analysis of petrophysical properties of rocks from the Bathurst Mining Camp: Constraints on gravity and magnetic modelling; Interpretation, v. 2, p. SJ133–SJ150.

Tschirhart, P.A., Morris, W.A., and Hodges, G., 2013. A new regional/residual separation for magnetic data sets using susceptibility from frequency-domain electromagnetic data; Geophysics, v. 78, p. B351-B359.

Vajk, R., 1956. Bouguer corrections with varying surface density; Geophysics, v. 21, 1004–1020.

van Staal, C.R., Wilson, R.A., Rogers, N., Fyffe, L.R., Langton, J.P., McCutcheon, S.R., McNicoll, V., and Ravenhurst, C.E., 2003. Geologic and tectonic history of the Bathurst Supergroup, Bathurst Mining Camp, and its relationship to coeval rocks in Southwestern New Brunswick and adjacent Maine - A synthesis, *In:* Massive Sulfide Deposits of the Bathurst Mining Camp, New Brunswick, and Northern Maine, (ed.) W.D. Goodfellow, S.R. McCutcheon, and J.M. Peter; Society of Economic Geologist, Monograph 11, p. 37–60.

van Staal, C.R., Currie, K.L., Rowbotham, G., Goodfellow, W., and Rogers, N., 2008. Pressure-temperature paths and exhumation of Late Ordovician-Early Silurian blueschists and associated metamorphic nappes of the Salinic Brunswick subduction complex, northern Appalachians; Geological Society of America Bulletin, v. 120, p. 1455–1477.

GEOLOGICAL SURVEY OF CANADA
OPEN FILE 7853

Targeted Geoscience Initiative 4: Contributions to the Understanding of Volcanogenic Massive Sulphide Deposit Genesis and Exploration Methods Development

Precious metal enrichment processes in volcanogenic massive sulphide deposits — A summary of key features, with an emphasis on TGI-4 research contributions

Patrick Mercier-Langevin[1], Mark D. Hannington[2], Benoît Dubé[1], Stephen J. Piercey[3], Jan M. Peter[4], and Sally J. Pehrsson[4]

[1]Geological Survey of Canada, Québec, Quebec
[2]University of Ottawa, Ottawa, Ontario
[3]Memorial University of Newfoundland, St. John's, Newfoundland and Labrador
[4]Geological Survey of Canada, Ottawa, Ontario

2015

Recommended citation

Mercier-Langevin, P., Hannington, M.D., Dubé, B., Piercey, S.J., Peter, J.M., and Pehrsson, S.J., 2015. Precious metal enrichment processes in volcanogenic massive sulphide deposits — A summary of key features, with an emphasis on TIGI-4 research contributions, *In:* Targeted Geoscience Initiative 4: Contributions to the Understanding of Volcanogenic Massive Sulphide Deposit Genesis and Exploration Methods Development, (ed.) J.M. Peter and P. Mercier-Langevin; Geological Survey of Canada, Open File 7853, p. 117–130.

TABLE OF CONTENTS

Precious metal enrichment processes in volcanogenic massive sulphide deposits — A summary of key features, with an emphasis on TGI-4 research contributions

Patrick Mercier-Langevin[1*], Mark D. Hannington[2], Benoît Dubé[1], Stephen J. Piercey[3], Jan M. Peter[4], and Sally J. Pehrsson[4]

[1]Geological Survey of Canada, 490 rue de la Couronne, Québec, Quebec G1K 9A9
[2]Department of Earth Sciences, University of Ottawa, 140 Louis Pasteur, Ottawa, Ontario K1N 6N5
[3]Department of Earth Sciences, Memorial University of Newfoundland, St. John's, Newfoundland and Labrador A1B 3X5
[4]Geological Survey of Canada, 601 Booth Street, Ottawa, Ontario K1A 0E9
*Corresponding author's e-mail: pmercier@nrcan.gc.ca

ABSTRACT

Volcanogenic massive sulphide deposits contain precious metals (Au, Ag) that can be present in high to low grades and total amounts; depending on tonnage and/or precious metal grade, such deposits can represent desirable exploration targets. Globally, deposits with >3.46 g/t Au are considered "auriferous", those with ≥31 t of contained Au are "anomalous", and those with both large tonnage (≥31 t Au) and high gold grade (>3.46 g/t Au) are considered "Au-rich". There are still no clear statistical criteria to determine thresholds that would define "anomalous" Ag grades and/or total amount of Ag in volcanogenic massive sulphide deposits, as grades vary widely depending on the nature of the host succession.

Two general requisites may explain anomalous primary precious metal budgets in volcanogenic massive sulphide deposits: 1) inherently Au- and/or Ag-enriched source rocks and fluids due to a specific geodynamic setting or heritage and/or to magmatic input, and 2) efficient transport (favourable ligands) and precipitation (e.g. boiling/phase separation, zone refining). These two requisites, which are of different scales, may or may not be mutually exclusive. Late or "secondary" Au- and/or Ag-enrichment in volcanogenic massive sulphide deposits can be due to the superposition of mineralizing systems of a different style (e.g. epithermal, intrusion-related, orogenic, etc.). Weathering processes (e.g. supergene enrichment) on the seafloor or on land can also significantly modify the distributions of precious metals in a volcanogenic massive sulphide deposit.

Volcanogenic massive sulphide deposits in volcanic belts that formed in pericratonic settings or on older crust basement in the early stages of rifting are commonly slightly better endowed in precious metals than those formed in belts or settings with no or limited basement influence. Gold-rich and auriferous VMS are preferentially associated with calc-alkaline or transitional magmatic successions, with andesite-dacite-rhyodacite-rhyolite magmatic suites and with thick (10s to 100s of m) felsic volcanic packages. Evidence for a magmatic input and of deposition in response to boiling/phase separation include the presence of complex mineral assemblages comprising sulphosalts, sulphides, native elements, and anomalous trace element signatures (e.g. enrichment in the "epithermal suite" of elements Au-As-Sb-Ag-Hg and/or in felsic magma-associated elements Bi-W-Te-In-Sn). A laterally extensive sericitic (phyllic) ±siliceous alteration halo, a zone of intense aluminous (argillic to advanced argillic-style) alteration, and heterogeneous Au and Ag distributions and mineralogical residence sites within or near the sulphide bodies are also indicators of a possible magmatic contribution of Au, Ag, and other metals, such as Te and Bi, or metal deposition due to boiling in VMS systems.

INTRODUCTION

Volcanogenic massive sulphide (VMS) deposits contain variable amounts of precious metals, both in average grade and total contained metals. Gold and/or Ag-rich VMS deposits are attractive exploration targets as their precious metal content contributes significantly to their total value and their polymetallic nature makes them less vulnerable to metal price fluctuations. In order to objectively identify truly anomalous Au grades and contents in VMS deposits and help identify the geological parameters that may be responsible for atypical Au enrichments in VMS systems, Mercier-Langevin et al. (2011a) completed a statistical analysis of the global VMS grades and tonnages, resulting in several findings. 1) VMS deposits that contain more than 3.46 g/t Au are auriferous, regardless of their base

Mercier-Langevin, P., Hannington, M.D., Dubé, B., Piercey, S.J., Peter, J.M., and Pehrsson, S.J., 2015. Precious metal enrichment processes in volcanogenic massive sulphide deposits — A summary of key features, with an emphasis on TIGI-4 research contributions, *In:* Targeted Geoscience Initiative 4: Contributions to the Understanding of Volcanogenic Massive Sulphide Deposit Genesis and Exploration Methods Development, (ed.) J.M. Peter and P. Mercier-Langevin; Geological Survey of Canada, Open File 7853, p. 117–130.

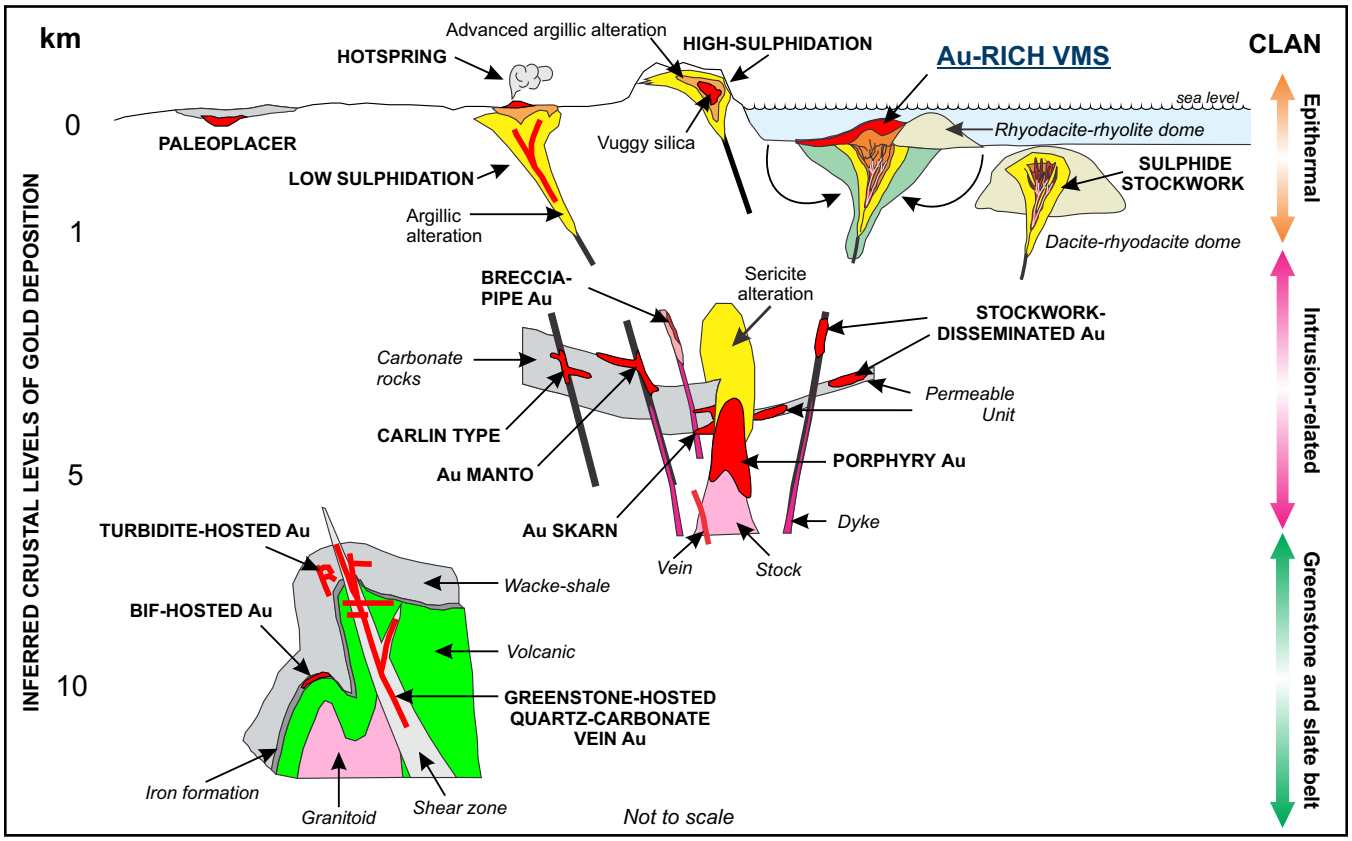

Figure 1. Schematic illustration of the various types of gold deposits, including Au-rich volcanogenic massive sulphide, shown at their inferred crustal level of formation (modified from Hannington et al. (1999), Poulsen et al. (2000), and Dubé et al. (2007a)).

metal content. Many of these deposits have gold grades (in g/t) higher than the combined content of base metals in weight percent, as previously noted by Poulsen and Hannington (1995), and are also considered to be auriferous. 2) Deposits with 31 t of Au or more (~1 Moz) exceed the geometric mean plus one geometric standard deviation and are clearly anomalous. 3) Deposits with a grade of more than 3.46 g/t Au and 31 t Au or more are considered Au-rich. Consideration of the geometric mean for smaller populations, such as VMS deposits in individual districts or mining camps, can also help to identify those deposits with statistically significant Au enrichments, even if they have Au grades that are far below the global mean value. There are still no clear statistical criteria to determine thresholds that would define "anomalous" Ag grades and/or total amount of Ag in volcanogenic massive sulphide deposits, as Ag grades vary significantly depending on the nature of the host succession. Deposits hosted in felsic-dominated successions are significantly richer in Ag than VMS deposits hosted in bimodal-mafic and mafic-dominated successions (25 g/t vs. 9.5 and 6.3 g/t, respectively, at the 50th percentile: Mosier et al. (2009); 93 g/t vs. 37 and 20 g/t, respectively, on average: Barrie and Hannington (1999); 56 g/t vs. 21 and 11 g/t, respectively, geometric mean: Franklin et al. (2005)). Globally, Canadian VMS deposits are characterized by average and median Ag grades of 63 and 37 g/t, respectively (Galley et al., 2007), indicating a right-skewed grade distribution due to a small number of very high-grade deposits. Therefore, in the absence of objective criteria, deposits with Ag grades above the average grade of their inferred group (e.g. felsic-dominated vs. mafic-dominated) or of the other deposits of their host district are considered to be Ag-rich.

Gold-rich and auriferous VMS deposits are considered to be subtypes of both VMS and lode gold deposits (Fig. 1), with some VMS deposits hosting world-class Au mines (Poulsen et al., 2000; Dubé et al., 2007a) and some considered to be hybrids of VMS and epithermal systems (e.g. Sillitoe et al., 1996; Galley et al., 2007). Although Au and Ag are commonly co-sited at the mineral-grain scale, and with only a few exceptions (e.g. Greens Creek, Alaska and Eskay Creek, British Columbia), Au-rich VMS deposits are not Ag-rich, and Ag-rich deposits are not Au-rich. This suggests distinct enrichment/transport mechanisms and/or variably endowed source rocks.

The geological characteristics, mechanisms of Au concentration, and genetic models for auriferous VMS deposits have been previously reviewed for both

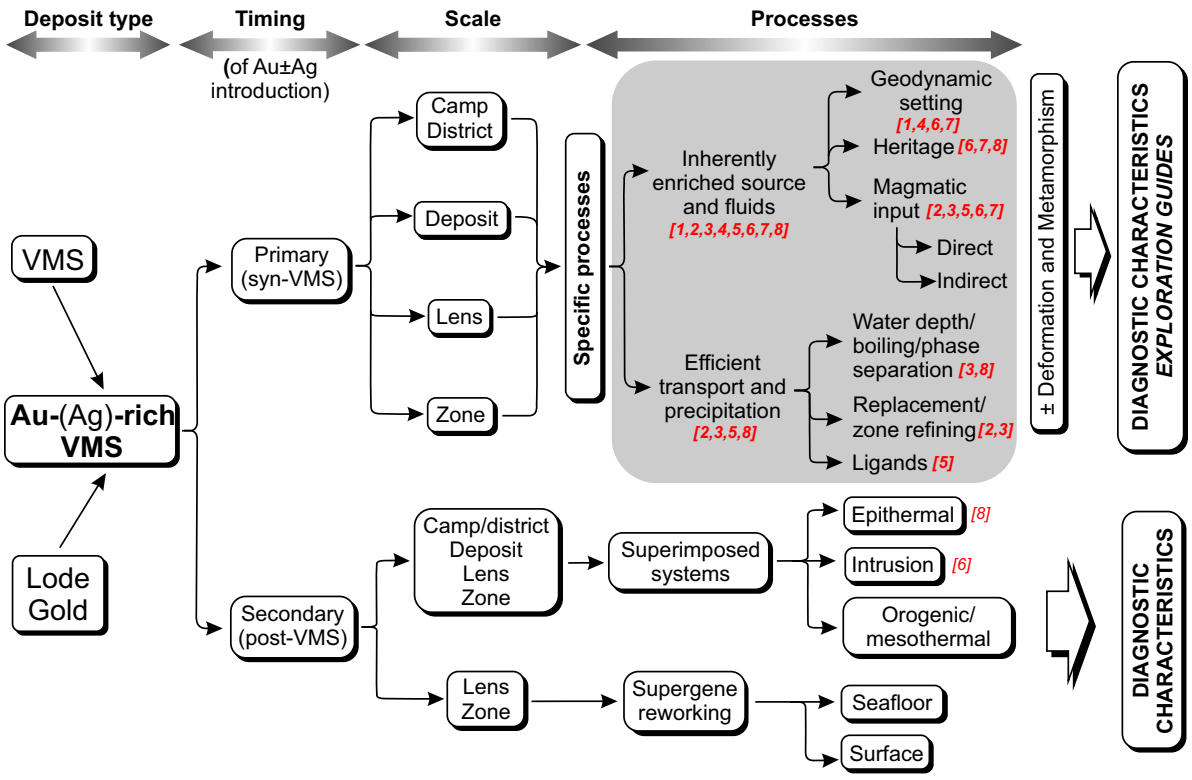

Figure 2. Graphic summary of the many different possible controls on Au- and Ag-enrichment in volcanogenic massive sulphide systems that operate on different spatial and temporal scales. The numbers in brackets refer to the deposits studied through the TGI-4 program and whether the specific mechanisms were documented or inferred. 1 = Lalor (Manitoba), 2 = Ming (Newfoundland), 3 = Lemarchant (Newfoundland), 4 = Boliden (Sweden), 5 = Lemoine (Quebec), 6 = Westwood (Quebec), 7 = Bousquet 2-Dumagami and LaRonde Penna (Quebec), 8 = Nurukawa (Japan).

ancient and modern settings (e.g. Hannington et al., 1986, 1999; Hannington and Scott, 1989; Huston and Large, 1989; Large et al., 1989; Large, 1992; Poulsen and Hannington, 1995; Sillitoe et al., 1996; Huston, 2000; Dubé et al., 2007a; Mercier-Langevin et al., 2011a), but controversies remain, especially concerning the source(s) of the precious metals. Ongoing research on ancient precious metal-rich deposits, including studies conducted under the auspices of the Targeted Geoscience Initiative 4 (TGI-4) Program VMS Ore System led by the Geological Survey of Canada, and those on modern seafloor hydrothermal systems (e.g. Hannington et al., 2005; de Ronde et al., 2011, 2012, 2014 and references therein) brings a wealth of new information that can be used to formulate and refine genetic and exploration models for such deposits and define exploration criteria.

Several different Au- and Ag-rich VMS deposits and districts were studied under the VMS (Peter and Mercier-Langevin, 2015) and Lode Gold Ore Systems projects of the TGI-4 program, building on work initiated during previous programs at Natural Resources Canada. The aim is to better understand precious metal-enrichment processes in VMS deposits and apply this information to improve genetic and exploration models. The deposits studied range from Archean to Miocene and from small (<1 Mt) to very large (50–100 Mt) in size. Furthermore, they occur as isolated deposits or parts of clusters, perfectly preserved to intensely deformed and metamorphosed, and vary markedly in Au and/or Ag grade. Only some examples are discussed here, with the aim of highlighting specific processes that are thought to play a critical role in precious metal enrichment of VMS, with an emphasis on Au. Readers are referred to Boulerice et al. (2015), Caté et al. (2015), Duff et al. (2015), Gill et al. (2015), Pilote et al. (2015) and Yergeau et al. (2015) for TGI-4 site-specific studies.

PRECIOUS METAL-RICH VMS SYSTEMS

Timing and Scale of Precious Metal Enrichment

Precious metals, and more particularly Au, can be introduced in VMS deposits during the lifetime of the VMS-forming hydrothermal system (so-called "primary" enrichment; Fig. 2) or they can be introduced and/or redistributed after the cessation of hydrothermal activity (so-called "secondary" enrichment; Fig. 2). The siting and scale of the enrichment processes can vary significantly. Some districts (or mining camps) are characterized by numerous Au-rich VMS deposits (e.g. Doyon-Bousquet-LaRonde mining camp,

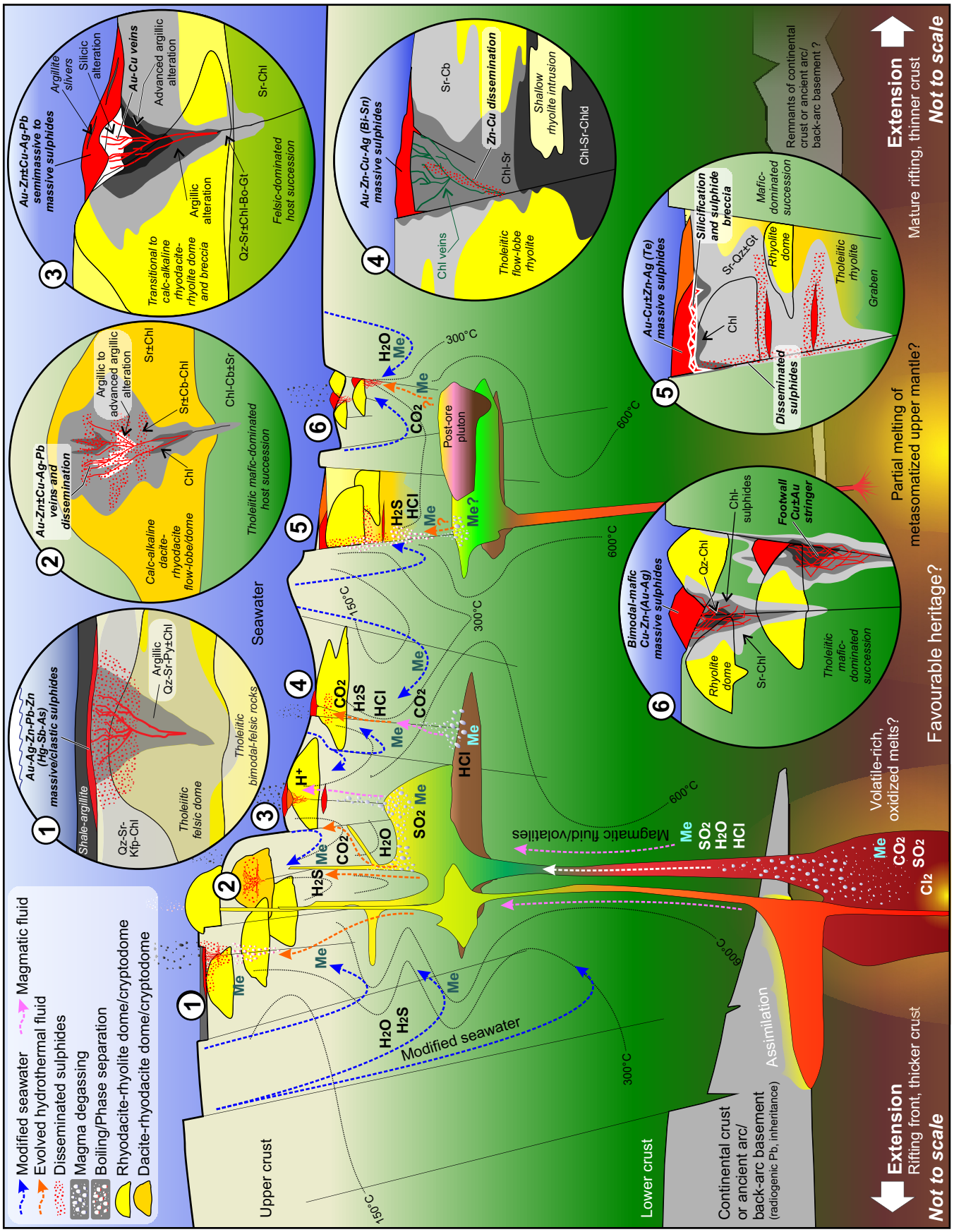
Modified seawater
Evolved hydrothermal fluid
Disseminated sulphides
Magma degassing
Boiling/Phase separation
Rhyodacite-rhyolite dome/cryptodome
Dacite-rhyodacite dome/cryptodome
Magmatic fluid
Au-Ag-Zn-Pb-Zn (Hg-Sb-As) massive/clastic sulphides
Shale-argillite
Qz-Sr-Kfp-Chl
Tholeiitic felsic dome
Argillic Qz-Sr-Py±Chl
Tholeiitic bimodal-felsic rocks
Au-Zn±Cu-Ag-Pb veins and dissemination
Calc-alkaline dacite-rhyodacite flow-lobe/dome
Argillic to advanced argillic alteration
Chl
Sr±Chl
Sr±Cb-Chl
Chl-Cb±Sr
Tholeiitic mafic-dominated host succession
Au-Zn±Cu-Ag-Pb semimassive to massive sulphides
Argillite slivers
Silicic alteration
Au-Cu veins
Advanced argillic alteration
Transitional to calc-alkaline rhyodacite-rhyolite dome and breccia
Argillic alteration
Qz-Sr±Chl-Bo-Gt
Felsic-dominated host succession
Sr-Chl
Au-Zn-Cu-Ag (Bi-Sn) massive sulphides
Chl veins
Sr-Cb
Zn-Cu dissemination
Chl-Sr
Shallow rhyolite intrusion
Tholeiitic flow-lobe rhyolite
Chl-Sr-Chld
Au-Cu±Zn-Ag (Te) massive sulphides
Disseminated sulphides
Chl
Silicification and sulphide breccia
Sr-Qz±Gt
Rhyolite dome
Mafic-dominated succession
Tholeiitic rhyolite
Graben
Bimodal-mafic Cu-Zn-(Au-Ag) massive sulphides
Rhyolite dome
Qz-Chl
Sr-Chl
Chl-sulphides
Footwall Cu±Au stringer
Tholeiitic mafic-dominated succession
Seawater
Modified seawater
Magmatic fluid/volatiles
Post-ore pluton
Me?
Upper crust
Lower crust
Continental crust or ancient arc/ back-arc basement
(radiogenic Pb, inheritance)
Assimilation
Volatile-rich, oxidized melts?
Partial melting of metasomatized upper mantle?
Remnants of continental crust or ancient arc/ back-arc basement ?
Favourable heritage?
Extension
Rifting front, thicker crust
Not to scale
Extension
Mature rifting, thinner crust
Not to scale
300°C
150°C
600°C
H2O
H2S
HCl
CO2
SO2
Me
H+
Cl2

Quebec: Dubé et al., 2007a, 2014; Mercier-Langevin et al., 2007a, 2011b) or by consistently anomalous high background Au (e.g. Mount Read Volcanics, Tasmania: Corbett, 1992). This illustrates the provinciality of some Au- and/or Ag-rich VMS deposits (Hannington et al., 1999; Huston, 2000) and strongly suggests large-scale geological controls on the enrichment of precious metals. Other districts might contain only one or two isolated auriferous VMS deposits (e.g. Nurukawa deposit, Hokuroku district, Japan: Yamada et al., 1987) or significantly "above district average" deposits (e.g. Caribou and Louvicourt deposits, Bathurst Mining Camp, New Brunswick: McClenaghan et al., 2003; Mercier-Langevin et al., 2011a). Many VMS deposits are characterized by lenses or zones that are significantly enriched in Au relative to the entire deposit (e.g. 1806 Zone, Ming deposit, Newfoundland: Pilote et al. (2014a, b, 2015), Brueckner et al. (2014); Brunswick 12 North End Zone: McClenaghan et al. (2009)). These different scales of Au (and Ag) enrichment indicate that local primary or secondary processes also play a major role in the precious metal budget of VMS systems.

Precious Metal Enrichment Processes

Anomalous primary precious metals budgets of VMS deposits can result from (1) inherently enriched source rocks and deep-seated fluids, and/or (2) efficient transport (in aqueous fluid and/or vapour) and precipitation. These two conditions are not necessarily mutually exclusive, and different processes can be active at the same time and/or at the same site but at different scales (Figs. 2 and 3). Secondary enrichment can be due to the superposition of younger mineralizing systems and weathering can significantly modify the distribution of precious metals.

In ancient, deformed and metamorphosed terranes and/or belts, it may be difficult to establish the absolute timing of the precious metal enrichment in a VMS deposit. For example, in the 1980s Au was first thought to be synvolcanic in the Au-rich VMS deposits of the Doyon-Bousquet-LaRonde mining camp, then in the 1990s a syntectonic overprint was proposed, and more recently the Au has been confirmed to be part of the VMS-forming systems (Dubé et al., 2007b, 2014; Mercier-Langevin et al., 2007a, b, 2009, 2011b, c; Wright-Holfeld, 2011; Yergeau, 2015; Yergeau et al., 2013, 2015, and references therein).

Among the more robust indications of a synvolcanic timing for Au are (1) the presence of auriferous sulphide clast-bearing units associated with the ore; (2) spatial correlation between Au and base metals, at the scale of the deposit or lens; (3) spatial association of Au with a VMS-associated alteration halo; (4) the presence of auriferous mineralization that is cut by synvolcanic dykes; (5) stacking of auriferous sulphide lenses in the volcanic sequence; and (6) gold-bearing late structural features that are devoid of Au outside the limits of the VMS orebody. The absence of isotopic (e.g. O, S, Pb) disturbance due to overprinting metasomatism associated with deformation and/or metamorphism is considered indirect evidence for syngenetic Au introduction, especially when supported by field evidence.

Primary (syn-VMS) Enrichment Processes

Inherently enriched source and fluids: An inherently enriched source (magma or host sequence) and/or fluids, as suggested by the strong provinciality of Au- and Ag-rich VMS deposits, can explain why some VMS deposits are enriched in precious metals. Enrichment in the source can be related to a specific geodynamic setting or heritage, as explained below, and is commonly thought to be associated with a direct magmatic input of Au- and/or Ag-bearing (and other metals) fluids and/or vapour into the ore-forming system (Figs. 2 and 3).

The geodynamic setting strongly influences not only the type of VMS deposits (and other deposit types, such as orogenic Au) that will be formed but also the metal budget of the deposits. For example, the Paleoproterozoic deposits of the Flin Flon-Snow Lake belt (Manitoba) and Skellefte District (Sweden) are, on average, slightly richer in Au than deposits in most major VMS-bearing belts, and include both Au-rich

Figure 3 (opposite page). Schematic diagram illustrating various settings and styles of precious metal-rich volcanogenic massive sulphide (VMS) deposits. Note that the diagram is not to scale, and some systems are much larger than others. The (relative) water depth as depicted may not be representative of the water depth at the time the deposits were formed. Metamorphic grade is not taken into account. Inset 1 depicts a system having features similar to those at Eskay Creek, with which Lemarchant may share some similarities. Inset 2 depicts a sub-seafloor mineralization similar to the Rainy River synvolcanic Au deposit. Inset 3 depicts Au-rich VMS-type systems such as Bousquet 2-Dumagami or LaRonde Penna. The Boliden and Nurukawa deposits are largely similar to this type of Au-rich VMS deposit. The Ming deposit also has some features common to this type of deposit. Inset 4 represents systems such as Lemoine. The Lalor deposit may have shared similarities with this type of system prior to intense deformation and metamorphism. Inset 5 depicts Horne- and Quemont-style Au-rich VMS systems. Inset 6 shows a typical Noranda-type VMS deposit in which Au typically occurs in the footwall stringer veins. This may have been the case at Lalor prior to deformation and metamorphism. See text for discussion. Based on Poulsen and Hannington (1995), Hannington et al. (1999), Huston (2000), Dubé et al. (2007a, 2014), Galley et al. (2007), Mercier-Langevin et al. (2007c, 2014b). Abbreviations: Bo= biotite, Cb= carbonate, Chl= chlorite, Chld= chloritoid, Gt= manganese garnet, Kfp= potassium feldspar, Me= metals, Py= pyrite, Qz= quartz, Sr= sericite.

(e.g. Skellefte: Boliden, Holmtjarn, and Petiknas North) and auriferous (e.g. Flin Flon-Snow Lake belt: Lalor) deposits. Although a number of processes active at various scales have been shown to be responsible for Au enrichment in these deposits, their particular setting (i.e. mature submarine arc and arc–back-arc rift systems constructed on older crust) appears to have influenced the overall Au budget of the deposits (Mercier-Langevin and Pehrsson, 2014; Fig. 3). This probably applies to some Archean and Phanerozoic VMS districts formed in similar settings. The crustal setting may be important for Ag enrichment, as suggested by the provinciality of "Ag-rich" versus "conventional" VMS deposits in the Slave Province, which may correlate with a tectonic setting ("arc-like environment" versus "bimodal rift" classification: Bleeker and Hall, 2007). Many of the VMS deposits enriched in Ag occur in "arc-like environments", and sulphides from these deposits display a larger range of $\Delta^{33}S$ compared to deposits from bimodal rift environments with a smaller range and primarily negative values of $\Delta^{33}S$; these characteristics suggest the incorporation of crustal sulphur (and, by inference, Ag and other metals) in the former group of deposits (Taylor et al., 2015). A common feature of belts such as Skellefte and Flin Flon-Snow Lake that host Au-enriched deposits is their crustally contaminated Pb-isotope signature and their association with felsic rocks showing evidence of contamination (e.g. inherited zircons, evolved Nd-isotope signature).

Another common characteristic of these Au-rich VMS-bearing belts and districts is a preferential association of Au-rich VMS deposits with rifted arc and back-arc settings characterized by transitional to calc-alkaline andesite-dacite-rhyodacite-rhyolite suites, comprising thick (10s to 100s of m) sequences of felsic volcanic rocks (Hannington et al., 1999; Dubé et al., 2007a; Mercier-Langevin et al., 2007c, d, 2011a; Fig. 3). Early rifting and extension-subsidence in an arc–back-arc-style environment is considered to be an important prerequisite in the genesis of the Au-rich VMS deposits of the Blake River Group in the southern Abitibi, where 6 of 11 of the richest and largest Au-rich VMS deposits are located (Mercier-Langevin et al., 2011a). The Au-rich VMS deposits of the Blake River Group occur in distinctly different volcanic and structural settings from other "conventional" VMS deposits in the district. The Horne and Quemont Au-rich deposits are separated in time and space from the Noranda Mine Sequence bimodal-mafic Cu-Zn VMS deposits; both of these former deposits are located in the southern part of the Noranda camp in fault-bounded structural blocks separated from the slightly younger Cu-Zn deposits (Mercier-Langevin et al., 2011a, b, c; McNicoll et al., 2014). The Bousquet Formation, which hosts the Au-rich VMS deposits of the Doyon-Bousquet-LaRonde mining camp, is coeval with the volcanic rocks that host the Cu-Zn VMS of the Noranda Mine Sequence, but is distinguished from them by its transitional to calc-alkaline affinity and dominantly felsic composition. The Bousquet Formation and its deposits were formed in a volcanic complex at the periphery of the central part of the Blake River Group, possibly in an area characterized by thicker basement, and therefore it is postulated to have been spatially more proximal to an arc (immature or early arc-rift stage). Recent dating in the Noranda and Doyon-Bousquet-LaRonde mining camps indicates that Horne and Quemont also formed during an episode of early extension-subsidence and thick transitional to felsic volcanism at Noranda (Monecke et al., 2008) at 2702–2701 Ma (McNicoll et al., 2014). Extension, VMS-related hydrothermal activity and transitional to calc-alkaline volcanism had migrated eastward to the Doyon-Bousquet-LaRonde mining camp by 2698–2697 Ma, at which time Horne and Quemont had already formed and the Cu-Zn deposits of the Noranda Mine Sequence were being deposited in the more mature, tholeiitic to transitional, mafic-dominated extensional setting (Monecke et al. 2008; Mercier-Langevin et al., 2011a, c).

A favourable heritage, or predisposition of certain areas of the upper mantle and lower crust to preconcentrate Au, has been proposed for Phanerozoic belts where ore-forming processes tap the same enriched lithospheric mantle source for a prolonged period of time with the recurrent generation of Au deposits, perhaps related to favourable geodynamic conditions that fertilize the upper mantle and lower crust and link them to the upper crust (Sillitoe, 2008; Hronsky et al., 2012; Fig. 3). Such favourable predisposition in the lower crust and/or upper mantle has been proposed to explain the strong provinciality of Au-rich VMS and orogenic Au deposits in the southern Abitibi belt (Dubé et al., 2007a; Mercier-Langevin et al., 2012). This uniquely endowed portion of the greenstone belt contains more than 85% of the Au in the entire belt (all deposit types) and more than 90% of the VMS-hosted Au (Mercier-Langevin et al., 2011a, 2014a).

A magmatic input of Au, either directly through degassing and/or fluid exsolution or indirectly through leaching of crystallized magma bodies at depth, is a plausible mechanism to explain precious metal-enrichment in some VMS deposits and districts, as indicated by research on active systems (e.g. Hannington et al., 1999; de Ronde et al., 2005; Fig. 3) and some ancient deposits (e.g. the Doyon-Bousquet-LaRonde mining camp: Dubé et al. (2007a, b, 2014), Mercier-Langevin et al. (2007a, c, d), Yergeau et al. (2015); the Lemoine deposit, northeastern Abitibi: Mercier-Langevin et al.

(2014b), and the Ming deposit, Newfoundland: Brueckner et al. (2014), Pilote et al. (2015)). The evidence for a direct magmatic input of Au can be circumstantial, but the involvement of magmatic fluids can be readily inferred in many ancient Au-rich VMS systems. The presence of extensive zones of aluminous alteration (metamorphosed advanced argillic alteration) at Bousquet 2-Dumagami and LaRonde Penna, for example, has been interpreted as evidence for a magmatic input into the hydrothermal system (Dubé et al., 2007b, 2014), and similar inferences have been made for Lemoine (Mercier-Langevin et al., 2014b), Boliden (Mercier-Langevin et al., 2013) and Nurukawa (Ishiyama et al., 2001). Such aluminous alteration zones develop in response to condensation of H_2S vapour or disproportionation of magmatically derived SO_2 that produce very low-pH, acidic, and oxidizing fluids, which leach most elements in the rock except for Al and Si. Although not diagnostic evidence for a magmatic input (e.g. Huston et al., 2011), the presence of a synvolcanic intrusion near the deposits is thought to be a prognostic indicator of this process. At the Westwood Mine, Au-rich VMS lenses are located above a synvolcanic intrusion that hosts part of the 5 Moz Au Doyon intrusion-related deposit, the latter being associated with local zones of aluminous alteration (Mercier-Langevin et al., 2009; Wright-Holfeld et al., 2010, 2011; Yergeau et al., 2013, 2015; Galley and Lafrance, 2014). The Horne (53.7 Mt at 6.06 g/t Au) and Quemont (13.8 Mt at 5.49 g/t Au: Mercier-Langevin et al., 2011b) deposits, located in the central Blake River Group, lack aluminous alteration, but, based on O isotopic evidence, are thought to have formed from long-lived hydrothermal systems that were related to synvolcanic magmatism (Taylor et al., 2014). According to Beaudoin et al. (2014), a heavy (6.5–22‰) $\delta^{18}O$ whole-rock composition also supports a magmatic input in the LaRonde Penna ore-forming hydrothermal system. Moreover, at both Horne and LaRonde Penna, there is no isotopic evidence for later magmatic activity or hydrothermal overprint, which supports synvolcanic Au introduction and is in agreement with field evidence.

At Lemoine, intense leaching of light rare earth elements in the high-temperature footwall alteration zones is considered to indicate acidic conditions in the presence of both CO_2 and HCl-bearing fluids sourced from the underlying Doré Lake synvolcanic intrusive complex. The presence of high Bi contents in the Au-rich ore is also considered to be evidence of a magmatic input (Mercier-Langevin et al., 2014b), which may have been facilitated by the relative abundance of shallow felsic intrusive rocks in the deposit host succession (Boulerice et al., 2015).

Specific element suites, such as In, Te, and Bi in high-temperature Cu-rich ores and As, Sb, Hg, and Ag (the "epithermal suite") and complex sulphosalt assemblages in low-temperature Zn-rich ore, also have been linked to a direct magmatic contribution of metals into the ore-forming hydrothermal system (Hannington et al., 1999; Huston et al., 2011); both associations have been documented at Ming (Brueckner et al., 2014; Pilote et al., 2015) and at Lemarchant in central Newfoundland (Gill et al., 2013, 2015).

Efficient transport and precipitation mechanisms: Whereas some districts contain VMS deposits that are uniformly enriched in Au and/or Ag, some districts/camps contain VMS deposits that are much more enriched than others in the same district (e.g. Horne and Quemont, Noranda district). This implies that local processes were involved in precious metal enrichment, including boiling/phase separation, optimal zone refining, availability of favourable ligands for aqueous- or vapour-phase transport, and the presence of elements acting as sinks for precious metals (e.g. Bi at Lemoine: Mercier-Langevin et al., 2014b) (Fig. 2). These processes govern which metals (including precious metals) were transported and deposited, and where in the system this occurred. The role of boiling/phase separation, which is largely controlled by the water depth, but also by the initial composition of the fluids, and the role of different ligands has been discussed in detail by Hannington et al. (1999), Huston (2000), and others, and readers are referred to these papers for in-depth discussions. Boiling is considered to have been a major factor for precious and other trace metal enrichment at Lemarchant in central Newfoundland (Gill et al., 2013, 2015; Gill and Piercey, 2014; Piercey et al., 2014; Gill, 2015). At the same time, evolving conditions in a VMS-forming hydrothermal system can have caused major redistribution of metals through zone refining (see Ohmoto, 1996), for example, concentrating precious metals in some specific areas, lenses, or zones in a VMS deposit (e.g. Large et al., 1989; Huston, 2000). This process is considered to be a key element in controlling the Au endowment of the 1806 zone at Ming relative to the other lenses of the deposit (Brueckner et al., 2014; Pilote et al., 2015).

Secondary (Post-Magmatic) Enrichment Processes

Secondary enrichment processes have affected the precious metal content and distribution in many deposits, and although not discussed in detail here, they include (1) superimposed mineralization of a different style; and (2) later reworking (Fig. 2). Supergene reworking can have occurred on the seafloor as the deposit was being formed or soon thereafter (e.g. Herzig et al., 1991; Galley and Koski, 1999; Maslennikov et al., 2012), or much later, as the deposits were exposed to

weathering on land (e.g. Boyle, 1979). Although supergene modification can have locally increased the grade of metals in near-surface gossans (e.g. Boyle, 2003), this mechanism most likely did not provide a significant new input of base and precious metals in VMS deposits, in contrast to overprinting systems (Fig. 2). A VMS deposit also can have been overprinted by a younger hydrothermal system (e.g. epithermal, intrusion-related, and orogenic) that added metals and/or influenced precious and base metal distribution. It is interesting to note however that VMS systems, which formed at or very near the seafloor, can have overprinted other styles of mineralization, commonly in response to major subsidence (e.g. VMS overprinting epithermal-style mineralization; Nurukawa deposit, Japan: Mercier-Langevin et al., unpubl. data).

In high-grade metamorphic belts, Au in VMS deposits is commonly preferentially located in structural sites (folds, high-strain zones, etc.) but in many cases this spatial relationship has been interpreted to reflect local remobilization of synvolcanic Au during deformation and metamorphism (e.g. Lalor, Snow Lake, Manitoba: Caté et al., 2013a, b, 2014a, b, 2015; Duff et al., 2015). Small-scale, local Au-Ag remobilization is documented in most deformed and metamorphosed VMS deposits, where Au-Ag is restricted to the immediate ore zones or deposit area, but does not extend into the structures outside the deposit; this indicates that there was no input of metals from an external source. At Lalor, for example, where (synvolcanic) Au, Ag, and Pb were remobilized and overprinted the footwall VMS-related alteration assemblages, the lead isotopic compositions of galena in the ore and whole-rock oxygen isotopic compositions of altered rocks show no evidence of post-magmatic disturbance, which would be expected if Au had been introduced during metamorphism (e.g. as in the nearby orogenic gold deposits: Mercier-Langevin et al., 2014c; Duff et al., 2015).

IMPLICATIONS FOR EXPLORATION

The TGI-4 program has made a number of key contributions to the current understanding of the mechanisms for precious metals enrichment in VMS deposits. However, evidence of the causative processes commonly is not observable in the field; therefore, exploration must focus on the visual evidence of the enrichment process(es) (or diagnostic features) that can be mapped at a range of different scales, as summarized in Figure 3. VMS deposits in mature and rifted arc sequences formed on older crust or ancient arc–back-arc basement in the early stages of rifting, which may be evidenced by tracer isotopes (e.g. Pb-Pb, Nd-Sm), high-resolution U-Pb geochronology (e.g. presence of inherited zircons), and whole-rock lithogeochemistry, appear to be slightly better endowed in precious metals, and Au-rich and auriferous VMS deposits tend to occur in clusters within those belts (provinciality). Gold-rich deposits are preferentially associated with calc-alkaline or transitional magmatic successions with andesite-dacite-rhyodacite-rhyolite magmatic suites and with thick (10s of 100s of metres) felsic volcanic rock packages or centres. A direct magmatic contribution (fluids and metals including Au and Ag) can be inferred in some Au-rich and auriferous VMS deposits, as evidenced by a spatial and temporal association with felsic synvolcanic intrusions, enrichment in the "epithermal suite" of elements (As-Sb-Ag-Bi-Hg-Te) and associated complex mineral assemblages, atypically extensive areas of sericitic (phyllic), siliceous, and especially metamorphosed argillic- to advanced argillic-style alteration.

A number of the characteristics enumerated above and their associated processes are also common to some magmatic-hydrothermal deposits, such as high-sulphidation deposits formed in subaerial to shallow submarine volcanic arc settings, supporting the inferred magmatic contribution of Au and/or Ag to precious metal-rich VMS systems (e.g. Lydon, 1996; Sillitoe et al., 1996; Hannington et al., 1999). Some Au deposits thought to have formed in the VMS environment at or near the seafloor from a magmatic-hydrothermal system may be hybrid (Hannington et al., 1999; Large et al., 2001; Galley et al., 2007), or they may lack some of the diagnostic characteristics of their deposit type, which may hinder a complete understanding of their genesis, and consequently decrease the effectiveness of exploration models. The Boliden deposit was originally considered to be an epithermal deposit (e.g. Bergman-Weihed et al., 1996) prior to the current interpretation that it is a VMS deposit (e.g. Allen et al., 1996; Mercier-Langevin et al., 2013, unpubl. data). The Archean Rainy River Au deposit in the Wabigoon Subprovince of northwestern Ontario may also be a good example of such a synvolcanic Au deposit that cannot readily be classified as a typical VMS or as an epithermal deposit; Wartman (2011) interprets the Rainy River deposit as having low-sulphidation-style mineralization, whereas Pelletier et al. (2014, 2015) recognize a number of diagnostic features typical of VMS deposits in their study of this deposit. Although the exact relationship between VMS, shallow-water hydrothermal systems, and epithermal deposits continues to be debated, exploration models for precious metal-rich VMS may have to take into account both the VMS and epithermal models.

On a more local scale, boiling/phase separation, zone refining, and the availability and/or stability of favourable ligands also can explain higher than average precious metals contents in some deposits or parts thereof. Deposits in which this occurred may possess

features such as bladed minerals, and complex or irregular Au and Ag distribution and mineralogical associations (e.g. Monecke et al., 2014).

In summary, from our work at Bousquet 2-Dumagami, LaRonde Penna, Westwood and Lemoine (Québec), Lalor (Manitoba), Ming and Lemarchant (Newfoundland), Boliden (Sweden), Nurukawa (Japan), Slave Province (Nunavut), and Rainy River (Ontario), TGI-4 research contributions to precious metal enrichment processes in VMS deposits indicate that primary enrichment in precious metals, and more particularly Au, can occur in deposits of all ages, and that a number of conditions and mechanisms are active at the same time and/or at the same site, but at different scales.

ACKNOWLEDGEMENTS

We express our sincerest thanks to numerous colleagues from the federal and provincial surveys, academia, and the industry, and to students for sharing their knowledge of VMS and Au deposits and belts, and for access to the study sites and material. This paper benefitted from a review by S. McClenaghan.

REFERENCES

Allen, R.L., Weihed, P., and Svensson, S.A., 1996. Setting of Zn-Cu-Au-Ag massive sulfide deposits in the evolution and facies architecture of a 1.9 Ga marine volcanic arc, Skellefte district, Sweden; Economic Geology, v. 91, p. 1022–1053.

Barrie, C.T. and Hannington, M.D., 1999. Classification of volcanic-associated massive sulfide deposits based on host-rock composition, *In:* Volcanic-Associated Massive Sulfide Deposits: Processes and Examples in Modern and Ancient Settings, (ed.) C. Tucker Barrie and M.D. Hannington; Reviews in Economic Geology, v. 8, p. 1–11.

Beaudoin, G., Mercier-Langevin, P., Dubé, B., and Taylor, B.E., 2014. Low-temperature alteration at the world-class LaRonde Penna Archean Au-rich volcanogenic massive sulfide deposit, Abitibi Subprovince, Quebec, Canada: Evidence from whole-rock oxygen isotopes; Economic Geology, v. 109, p. 167–182.

Bergman Weihed, J., Bergstrom, U., Billstrom, K., and Weihed, P., 1996. Geology, tectonic setting and origin of the Paleoproterozoic Boliden Au-Cu-As deposit, Skellefte district, Northern Sweden; Economic Geology, v. 91, p. 1073–1097.

Bleeker, W. and Hall, B., 2007. The Slave Craton: geological and metamorphic evolution, *In:* Mineral Deposits of Canada: A Synthesis of Major Deposit Types, District Metallogeny, the Evolution of Geological Provinces, and Exploration Methods, (ed.) W.D. Goodfellow; Geological Association of Canada, Mineral Deposits Division, Special Publication 5, p. 849–879.

Boulerice, A.R., Ross, P.-S., and Mercier-Langevin, P., 2015. Geological and geochemical characteristics of the Waconichi Formation east of the Lemoine auriferous volcanogenic massive sulphide deposit, Abitibi greenstone belt, Quebec, *In:* Targeted Geoscience Initiative 4: Contributions to the Understanding of Volcanogenic Massive Sulphide Deposit Genesis and Exploration Methods Development, (ed.) J.M. Peter and P. Mercier-Langevin; Geological Survey of Canada, Open File 7853, p. 171–182.

Boyle, D.R., 2003. Preglacial weathering of massive sulfide deposits in the Bathurst mining camp: economic geology, geochemistry, and exploration implications; Society of Economic Geologists, Monograph 11, p. 689–721.

Boyle, R.W., 1979. The geochemistry of gold and its deposits (together with a chapter on geochemical prospecting for the element); Geological Survey of Canada, Bulletin 280, 584 p.

Brueckner, S.M., Piercey, S.J., Sylvester, P.J., Maloney, S., and Pilgrim, L., 2014. Evidence for syngenetic precious metal enrichment in an Appalachian volcanogenic massive sulfide system: the 1806 zone, Ming mine, Newfoundland, Canada; Economic Geology, v. 109, 1611–1642.

Caté, A., Mercier-Langevin, P., Ross, P.-S., Duff, S., Hannington, M.D., Dubé, B., and Gagné, S., 2013a. The Paleoproterozoic Lalor VMS deposit, Snow Lake, Manitoba: preliminary observations on the nature and architecture of the gold- and base metal-rich ore and alteration zones; Geological Survey of Canada, Open File 7483, 19 p.

Caté, A., Mercier-Langevin, P., Ross, P.-S., Duff, S., Hannington, M.D., Dubé, B., and Gagné, S., 2013b. Preliminary observations on the geological environment of the Paleoproterozoic auriferous volcanogenic massive sulphide deposit of Lalor, Snow Lake, Manitoba; Geological Survey of Canada, Open File 7372, 13 p.

Caté, A., Mercier-Langevin, P., Ross, P.-S., and Simms, D., 2014a. GS-8 Structural controls on geometry and ore distribution in the Lalor auriferous VMS deposit, Snow Lake, west-central Manitoba (part of NTS 63K16): preliminary results from underground mapping, *In:* Report of Activities 2014; Manitoba Mineral Resources, Manitoba Geological Survey, p. 104–115.

Caté, A., Mercier-Langevin, P., Ross, P.-S., Duff, S., Hannington, M., Gagné, S., and Dubé, 2014b. Insights on the chemostratigraphy of the volcanic and intrusive rocks of the Lalor auriferous volcanogenic massive-sulphide deposit host succession, Snow Lake, Manitoba; Geological Survey of Canada, Current Research 2014-6, 20 p.

Caté, A., Mercier-Langevin, P., Ross, P.-S., Duff, S., Hannington, M.D., Dubé, B., and Gagné, S., 2015. Geology and Au enrichment processes at the Paleoproterozoic Lalor auriferous volcanogenic massive sulphide deposit, Snow Lake, Manitoba, *In:* Targeted Geoscience Initiative 4: Contributions to the Understanding of Volcanogenic Massive Sulphide Deposit Genesis and Exploration Methods Development, (ed.) J.M. Peter and P. Mercier-Langevin; Geological Survey of Canada, Open File 7853, p. 131–145.

Corbett, K.D., 1992. Stratigraphic-volcanic setting of massive sulfide deposits in the Cambrian Mount Read Volcanics, Tasmania; Economic Geology, v. 87, p. 564–586.

de Ronde, C.E.J., Hannington, M.D., Stoffers, P., Wright, I.C., Ditchburn, R.G., Reyes, A.G., Baker, E.T., Massoth, G.J., Lupton, J.E., Walker, S.L., Greene, R.R., Soong, C.W.R., Ishibashi, J., Lebon, G.T., Bray, C.J., and Resing, J.A., 2005. Evolution of a submarine magmatic-hydrothermal system: Brothers Volcano, southern Kermadec arc, New Zealand; Economic Geology, v. 100, p. 1097–1133.

de Ronde, C.E.J., Massoth, G.J., Butterfield, D.A., Christenson, B.W., Ishibashi, J., Ditchburn, R.G., Hannington, M.D., Brathwaite, R.L., Lupton, J.E., Kamenetsky, V.S., Graham, I.J., Zellmer, G.F., Dziak, R.P., Embley, R.W., Dekov, V.M., Munnik, F., Lahr, J., Evans, L.J., and Takai, K., 2011. Submarine hydrothermal activity and gold-rich mineralization at Brothers Volcano, Kermadec arc, New Zealand; Mineralium Deposita, v. 46, p. 541–584.

de Ronde, C.E.J., Butterfield, D.A., and Leybourne, M.I., 2012. Metallogenesis and mineralization of intraoceanic arcs I: Kermadec arc – Introduction; Economic Geology, v. 107, p. 1521–1525.

de Ronde, C.E.J., Hein, J.R., and Butterfield, D.A., 2014. Metallogenesis and mineralization of intraoceanic arcs II: the Aeolian, Izu-Bonin, Mariana, and Kermadec arcs, and the Manus backarc basin – Introduction; Economic Geology, v. 109, p. 2073–2077.

Dubé, B., Gosselin, P., Mercier-Langevin, P., Hannington, M.D., and Galley, A., 2007a. Gold-rich volcanogenic massive sulphide deposits, *In:* Mineral Deposits of Canada: A Synthesis of Major Deposit Types, District Metallogeny, the Evolution of Geological Provinces, and Exploration Methods, (ed.) W.D. Goodfellow; Geological Association of Canada, Mineral Deposits Division, Special Publication 5, p. 75–94.

Dubé, B., Mercier-Langevin, P., Hannington, M.D., Lafrance, B., Gosselin, P., and Gosselin, G., 2007b. The LaRonde Penna giant gold-rich volcanogenic massive sulfide deposit, Abitibi, Quebec: alteration footprint, genesis and implications for exploration; Economic Geology, v. 102, p. 633–666.

Dubé, B., Mercier-Langevin, P., Kjarsgaard, I., Hannington, M., Bécu, V., Côté, J., Moorhead, J., Legault, M., and Bédard, N., 2014. The Bousquet 2-Dumagami world-class Archean Au-rich volcanogenic massive sulfide deposit, Abitibi, Quebec: metamorphosed submarine advanced argillic alteration footprint and genesis; Economic Geology, v. 109, p. 121–166.

Duff, S., Hannington, M.D., Caté, A., Mercier-Langevin, and Kjarsgaard, I.M., 2015. Major ore types of the Paleoproterozoic Lalor auriferous volcanogenic massive sulphide deposit, Snow Lake, Manitoba, *In:* Targeted Geoscience Initiative 4: Contributions to the Understanding of Volcanogenic Massive Sulphide Deposit Genesis and Exploration Methods Development, (ed.) J.M. Peter and P. Mercier-Langevin; Geological Survey of Canada, Open File 7853, p. 147–170.

Franklin, J.M., Gibson, H.L., Jonasson, I.R., and Galley, A.G., 2005. Volcanogenic massive sulfide deposits, *In:* Economic Geology 100th Anniversary Volume, (ed.) J.W. Hedenquist, J.F.H. Thompson, R.J. Goldfarb, and J.P. Richards; Society of Economic Geologists, Littleton, Colorado, p. 523–560.

Galley, A.G. and Koski, R.A., 1999. Setting and characteristics of ophiolite-hosted volcanogenic massive sulfide deposits, *In:* Volcanic-Associated Massive Sulfide Deposits: Processes and Examples in Modern and Ancient Settings, (ed.) C. Tucker Barrie and M.D. Hannington; Reviews in Economic Geology, v. 8, p. 215–236.

Galley, A.G. and Lafrance, B., 2014. Setting and evolution of the Archean synvolcanic Mooshla Intrusive Complex, Doyon-Bousquet-LaRonde mining camp, Abitibi greenstone belt: emplacement history, petrogenesis, and implications for Au metallogenesis; Economic Geology, v. 109, p. 205–229.

Galley, A.G., Hannington, M.D., and Jonasson, I.R., 2007. Volcanogenic massive sulphide deposits, *In:* Mineral Deposits of Canada: A Synthesis of Major Deposit Types, District Metallogeny, the Evolution of Geological Provinces, and Exploration Methods, (ed.) W.D. Goodfellow; Geological Association of Canada, Mineral Deposits Division, Special Publication 5, p. 141–161.

Gill, S.B., 2015. Mineralogy, metal-zoning, and genesis of the Cambrian Zn-Pb-Cu-Ag-Au Lemarchant volcanogenic massive sulfide (VMS) deposit; M.Sc. thesis, Memorial University, St. John's, Newfoundland, 154 p.

Gill, S.B. and Piercey, S.J., 2014. Preliminary observations on styles of mineralization and sulphide-mineral zonation in the Cambrian Zn-Pb-Cu-Ag-Au Lemarchant volcanogenic massive-sulphide deposit, Newfoundland and Labrador; Geological Survey of Canada, Current Research 2014-5, 17 p.

Gill, S.B., Piercey, S.J., and Devine, C.A., 2013. Preliminary mineralogy of barite-associated sulphide mineralization in the Ordovician Zn-Pb-Cu-Ag-Au Lemarchant volcanogenic massive sulphide deposit, Newfoundland and Labrador; Geological Survey of Canada, Current Research 2013-17, 15 p.

Gill, S.B., Piercey, S.J., Layton-Matthews, D., Layne, G.D., and Piercey, G., 2015. Mineralogical, sulphur, and lead isotopic study of the Lemarchant Zn-Pb-Cu-Ag-Au-VMS deposit: Implications for precious-metal enrichment processes in the VMS environment, *In:* Targeted Geoscience Initiative 4: Contributions to the Understanding of Volcanogenic Massive Sulphide Deposit Genesis and Exploration Methods Development, (ed.) J.M. Peter and P. Mercier-Langevin; Geological Survey of Canada, Open File 7853, p. 183-195.

Hannington, M.D. and Scott, S.D., 1989. Gold mineralization in volcanogenic massive sulfides: Implications of data from active hydrothermal vents on the modern sea floor; Society of Economic Geologists, Monograph 6, p. 491–507.

Hannington, M.D., Peter, J.M., and Scott, S.D., 1986. Gold in sea-floor polymetallic sulfides; Economic Geology, v. 81, p. 1867–1883.

Hannington, M.D., Poulsen, K.H., Thompson, J.F.H., and Sillitoe, R.H., 1999. Volcanogenic gold in the massive sulfide environment, *In:* Volcanic-Associated Massive Sulfide Deposits: Processes and Examples in Modern and Ancient Settings, (ed.) C. Tucker Barrie and M.D. Hannington; Reviews in Economic Geology, v. 8, p. 325–356.

Hannington, M.D., de Ronde, C.E.J., and Petersen, S., 2005. Sea-floor tectonics and submarine hydrothermal systems, *In:* Economic Geology 100th Anniversary Volume; Society of Economic Geologists, Littleton, Colorado, p. 111–141.

Herzig, P.M., Hannington, M.D., Scott, S.D., Maliotis, G., Rona, P.A., and Thompson, G., 1991. Gold-rich seafloor gossans in the Troodos ophiolite and on the Mid-Atlantic ridge; Economic Geology, v. 86, p. 1747–1755.

Hronsky, J.M.A., Groves, D.I., Loucks, R.R., and Begg, G.S., 2012. A unified model for gold mineralization in accretionary orogens and implications for regional-scale exploration targeting methods; Mineralium Deposita, v. 47, p. 339–358.

Huston, D.L., 2000. Gold in volcanic-hosted massive sulfide deposits: distribution, genesis, and exploration, *In:* Gold in 2000, (ed.) S.G. Hagemann and P.E. Brown; Reviews in Economic Geology, v. 13, p. 400–426.

Huston, D.L. and Large, R.R., 1989. A chemical model for the concentration of gold in volcanogenic massive sulphide deposits; Ore Geology Reviews, v. 4, p. 171–200.

Huston, D.L., Relvas, J.M.R.S., Gemmell, J.B., and Drieberg, S., 2011. The role of granites in volcanogenic massive sulfide deposits; Mineralium Deposita, v. 46, p. 473–507.

Ishiyama, D., Hirose, K., Mizuta, T., Matsubaya, O., and Ishikawa, Y., 2001. The characteristics and genesis of the kaolinite-bearing gold-rich Nurukawa kuroko deposit, Aomori prefecture, Japan, In Water-rock interaction, (ed.) R. Cidu; Proceedings of the Tenth International Symposium on Water-Rock Interaction, Villasimius, Italia, 10–15 July 2001, p. 717–720.

Large, R.R., 1992. Evaluation of the source-rock control on precious metal grades in volcanic-hosted massive sulphide deposits from western Tasmania; Economic Geology, v. 87, p. 720–738.

Large, R.R., Huston, D.L., McGoldrick, P.J., Ruxton, P.A., and McArthur, G., 1989. Gold distribution and genesis in Australian volcanogenic massive sulfide deposits and their significance for gold transport models; Society of Economic Geologists, Monograph 6, p. 520–535.

Large, R.R., McPhie, J., Gemmell, J.B., Herrmann, W., and Davidson, G.J., 2001. The spectrum of ore deposit types, volcanic environments, alteration halos, and related exploration vectors in submarine volcanic successions: Some examples from Australia; Economic Geology, v. 96, p. 913–938.

Lydon, J.W., 1996. Characteristics of volcanogenic massive sulphide deposits: interpretations in terms of hydrothermal convection systems and magmatic hydrothermal systems; Boletin Geologico y Minera, v. 107, p. 215–264.

Maslennikov, V.V., Ayupova, N.R., Herrington, R.J., Danyushevskiy, L.V., and Large, R. R., 2012. Ferruginous and manganiferous haloes around massive sulphide deposits of the Urals; Ore Geology Reviews, v. 47, p. 5–41.

McClenaghan, S.H., Goodfellow, W.D., and Lentz, D.R., 2003. Gold in massive sulfide deposits, Bathurst mining camp: distribution and genesis, *In:* Massive Sulfide Deposits of the Bathurst Mining Camp, New Brunswick, and Northern Maine, (ed.) W.D. Goodfellow, S.R. McCutcheon, and J.M. Peter; Society of Economic Geologists, Monograph 11, p. 303–326.

McClenaghan, S.H., Lentz, D.R., Martin, J., and Diegor, W.G., 2009. Gold in the Brunswick No. 12 volcanogenic massive sulfide deposit, Bathurst Mining Camp, Canada: Evidence from bulk ore analysis and laser ablation ICP-MS data on sulfide phases; Mineralium Deposita, v.44, p.523–557.

McNicoll, V., Goutier, J., Dubé, B., Mercier-Langevin, P., Ross, P.-S., Dion, C., Monecke, T., Legault, M., Percival, J., and Gibson, H., 2014. New U-Pb geochronology from the Blake River Group, Abitibi Subprovince, Québec: implications for geological interpretations and base metal exploration; Economic Geology, v. 109, p. 27–59.

Mercier-Langevin, P. and Pehrsson, S., 2014. Paleoproterozoic auriferous VMS belts and deposits – key aspects and implications for exploration; Manitoba Mining and Minerals Convention 2014, Winnipeg, Manitoba, November 21–24, 2014.

Mercier-Langevin, P., Dubé, B., Lafrance, B., Hannington, M., Galley, A., Moorhead, J., and Gosselin, P., 2007a. Metallogeny of the Doyon-Bousquet-LaRonde mining camp, Abitibi greenstone belt, Quebec, *In:* Mineral Deposits of Canada: A Synthesis of Major Deposit Types, District Metallogeny, the Evolution of Geological Provinces, and Exploration Methods, (ed.) W.D. Goodfellow; Geological Association of Canada, Mineral Deposits Division, Special Publication 5, p. 673–701.

Mercier-Langevin, P., Dubé, B., Hannington, M.D., Lafrance, B., Galley, A.G., and Moorhead, J., 2007b. A group of papers devoted to the LaRonde Penna Au-rich volcanogenic massive sulfide deposit, eastern Blake River Group, Abitibi greenstone belt, Quebec – Preface; Economic Geology, v. 102, p. 577–583.

Mercier-Langevin, P., Dubé, B., Hannington, M.D., Richer-Laflèche, M., and Gosselin, G., 2007c. The LaRonde Penna Au-rich volcanogenic massive sulfide deposit, Abitibi greenstone belt, Quebec: Part II. Lithogeochemistry and paleotectonic setting; Economic Geology, v. 102, p. 611–631.

Mercier-Langevin, P., Dubé, B., Hannington, M.D., Davis, D., Lafrance, B., and Gosselin, G., 2007d. The LaRonde Penna Au-rich volcanogenic massive sulfide deposit, Abitibi greenstone belt, Quebec: Part I. Geology and geochronology; Economic Geology, v. 102, p. 585–609.

Mercier-Langevin, P., Wright-Holfeld, A., Dubé, B., Bernier, C., Houle, N., Savoie, A., and Simard, P., 2009. Stratigraphic setting of the Westwood-Warrenmac ore zones, Westwood Project, Doyon-Bousquet-LaRonde mining camp, Abitibi, Quebec; Geological Survey of Canada, Current Research 2009-03, 20 p.

Mercier-Langevin, P., Hannington, M.D., Dubé, B., Bécu, V., 2011a. The gold content of volcanogenic massive sulphide deposits; Mineralium Deposita, v. 46, p. 509–539.

Mercier-Langevin, P., Goutier, J., Ross, P.-S., McNicoll, V., Monecke, T., Dion, C., Dubé, B., Thurston, P., Bécu, V., Gibson, H., Hannington, M., and Galley, A., 2011b. The Blake River Group of the Abitibi greenstone belt and its unique VMS and gold-rich VMS endowment; GAC-MAC-SEG-SGA Joint Annual Meeting 2011, Ottawa, Field Trip 02B guidebook; Geological Survey of Canada, Open File 6869, 61 p.

Mercier-Langevin, P., Hannington, M., Dubé, B., McNicoll, V., Goutier, J., and Monecke, T., 2011c. Geodynamic influences on the genesis of Archean world-class gold-rich VMS deposits: examples from the Blake River Group, Abitibi greenstone belt, Canada; Proceedings of the Eleventh Biennial meeting of the Society for Geology Applied to Mineral Deposits, p. 85–87.

Mercier-Langevin, P., Houlé, M.G., Dubé, B., Monecke, T., Hannington, M.D., Gibson, H.L., and Goutier, J., 2012. A special issue on Archean magmatism, volcanism and ore deposits: Part 1. Komatiite-associated Ni-Cu-(PGE) sulfide and greenstone-hosted Au deposits – Preface; Economic Geology, v. 107, p. 745–753.

Mercier-Langevin, P., McNicoll, V., Allen, R., Blight, J., and Dubé, B., 2013. The Boliden gold-rich volcanogenic massive sulfide deposit, Skellefte District, Sweden: new U-Pb age constraints and implications at deposit and district scale; Mineralium Deposita, v. 48, p. 485–504.

Mercier-Langevin, P., Gibson, H.L., Hannington, M.D., Goutier, J., Monecke, T., Dubé, B., and Houlé, M.G., 2014a. A special issue on Archean magmatism, volcanism and ore deposits: Part 2. Volcanogenic massive sulfide deposits – Preface; Economic Geology, v. 109, p. 1–9.

Mercier-Langevin, P., Lafrance, B., Bécu, V., Dubé, B., Kjarsgaard, I., and Guha, J., 2014b. The Lemoine auriferous volcanogenic massive sulfide deposit, Chibougamau camp, Abitibi greenstone belt, Québec, Canada: geology and genesis; Economic Geology, v. 109, p. 231–269.

Mercier-Langevin, P., Caté, A., and Ross, P.-S., 2014c. GS-7 Whole-rock oxygen-isotope mapping of the footwall alteration zones at the Lalor auriferous VMS deposit, Snow Lake, west-central Manitoba (NTS 63K16), *In:* Report of Activities 2014; Manitoba Mineral Resources, Manitoba Geological Survey, p. 94–103.

Monecke, T., Gibson, H., Dubé, B., Laurin, J., Hannington, M., and Martin, L., 2008. Geology and volcanic setting of the Horne deposit, Rouyn-Noranda, Quebec; Initial results of a new research project; Geological Survey of Canada, Current Research 2008-9, 16 p.

Monecke, T., Petersen, S., and Hannington, M.D., 2014. Constraints on water depth of massive sulphide formation: evidence from modern seafloor hydrothermal systems in arc-related settings; Economic Geology, v. 109, p. 2079–2101.

Mosier, D.L., Berger, V.I., and Singer, D.A., 2009. Volcanogenic massive sulfide deposits of the World – Database and grade and tonnage models; United States Geological Survey, Open-File report 2009-1034, 46 p.

Ohmoto, H., 1996. Formation of volcanogenic massive sulfide deposits; the Kuroko perspective; Ore Geology Reviews, v. 10, p. 135–177.

Pelletier, M., Mercier-Langevin, P., Crick, D., Tolman, J., Beakhouse, G.P., and Dubé, B., 2014. 41. Targeted Geoscience Initiative 4. Lode gold deposits in ancient and deformed terranes: preliminary observations on the nature and distribution of the deformed and metamorphosed hydrothermal alteration associated with the Archean Rainy River gold deposit, northwestern Ontario, 2104, *In:* Summary of Field and other Activities; Ontario Geological Survey, Open File Report 6300, p. 41-1 to 41-10.

Pelletier, M., Mercier-Langevin, P., Dubé, B., Crick, D., Tolman J., McNicoll, V.J., Jackson, S.E., and Beakhouse, G.P., 2015. The Rainy River "atypical" Archean Au deposit, western Wabigoon Subprovince, Ontario, *In:* Targeted Geoscience Initiative 4: Contributions to the Understanding of Precambrian Lode Gold Deposits and Implications for Exploration (ed.) B. Dubé and

P. Mercier-Langevin; Geological Survey of Canada: Open File 7852, p. 193–207.

Peter, J.M. and Mercier-Langevin, P., 2015. The Targeted Geoscience Initiative 4 contributions to the understanding of volcanogenic massive sulphide deposit genesis and exploration methods development: introduction and preface, *In:* Targeted Geoscience Initiative 4: Contributions to the Understanding of Volcanogenic Massive Sulphide Deposit Genesis and Exploration Methods Development, (ed.) J.M. Peter and P. Mercier-Langevin; Geological Survey of Canada, Open File 7853, p. 1–14.

Piercey, S.J., Brueckner, S., Cloutier, J., Gill, S., Lode, S., Mercier-Langevin, P., and Pilote, J.-L., 2014. Precious metal-bearing volcanogenic massive sulphide (VMS) deposits: geological setting, styles, and lessons learned from the TGI-4 VMS project; Manitoba Mining and Minerals Convention 2014, Winnipeg, Manitoba, November 21–24, 2014.

Pilote, J.-L., Piercey, S., and Mercier-Langevin, P., 2014a. Stratigraphy and hydrothermal alteration of the Ming Cu-Au volcanogenic massive-sulphide deposit, Baie-Verte Peninsula, Newfoundland; Geological Survey of Canada, Current Research 2014-7, 18 p.

Pilote, J.-L., Piercey, S.J., and Mercier-Langevin, P., 2014b, Geological environment and formational controls of auriferous massive sulfide deposits: an example from the Cambro-Ordovician Cu-Au Ming VMS deposit in the Newfoundland Appalachians; Geological Survey of Canada, Open File 7731, 1 sheet.

Pilote, J.-L., Piercey, S.J., and Mercier-Langevin, P., 2015. Volcanic architecture and alteration assemblages of the Ming Cu-Au-(Zn-Ag) VMS deposit, Baie Verte, Newfoundland and Labrador: Implications for Au-enrichment processes and exploration, *In:* Targeted Geoscience Initiative 4: Contributions to the Understanding of Volcanogenic Massive Sulphide Deposit Genesis and Exploration Methods Development, (ed.) J.M. Peter and P. Mercier-Langevin; Geological Survey of Canada, Open File 7853, p. 197–210.

Poulsen, K.H. and Hannington, M.D., 1995. Volcanic-associated massive sulphide gold, *In:* Geology of Canadian Mineral Deposit Types, (ed.) O.R. Eckstrand, W.D. Sinclair, and R.I. Thorpe; Geological Survey of Canada, Geology of Canada Series no. 8, p. 183–196. doi:10.4095/207944

Poulsen, K.H., Robert, F., and Dubé, B., 2000. Geological classification of Canadian gold deposits; Geological Survey of Canada, Bulletin 540, 106 p.

Sillitoe, R.H., 2008. Special paper: Major gold deposits and belts of the North and South America Cordillera: Distribution, tectonomagmatic settings, and metallogenic considerations; Economic Geology, v. 103, p. 663–687.

Sillitoe, R.H., Hannington M.D., and Thompson J.F.H., 1996. High sulfidation deposits in the volcanogenic massive sulfide environment; Economic Geology, v. 91, p. 204–212.

Taylor, B.E., de Kemp, E., Grunsky, E., Martin, L., Maxwell, G., Rigg, D., Goutier, J., Lauzière, K., and Dubé, B., 2014. Three-dimensional visualization of the Archean Horne and Quemont Au-bearing volcanogenic massive sulfide hydrothermal systems, Blake River Group, Quebec; Economic Geology, v. 109, p. 183–203.

Taylor, B.E., Peter, J.M., and Wing, B.A., 2015. Multi-sulphur isotope reconnaissance of Slave Province volcanogenic massive sulphide deposits, *In:* Targeted Geoscience Initiative 4: Contributions to the Understanding of Volcanogenic Massive Sulphide Deposit Genesis and Exploration Methods Development, (ed.) J.M. Peter and P. Mercier-Langevin; Geological Survey of Canada, Open File 7583, p. 45–58.

Wartman, J.M., 2011. Physical volcanology and hydrothermal alteration of the Rainy River Gold Project, northwest Ontario; M.Sc. thesis, University of Minnesota, Duluth, Minnesota, 163 p.

Wright-Holfeld, A., 2011. The geology and geochemistry of the world-class Westwood deposit, Abitibi Subprovince, Québec; MSc thesis, Institut national de la Recherche Scientifique, Québec, Québec, 165 p.

Wright-Holfeld, A., Mercier-Langevin, P., and Dubé, B., 2010. Contrasting alteration mineral assemblages associated with the Westwood deposit ore zones, Doyon-Bousquet-LaRonde mining camp, Abitibi, Quebec; Geological Survey of Canada, Current Research 2010-9, 24 p.

Wright-Holfeld, A., Mercier-Langevin, P., and Dubé, B., 2011. Mass changes and element mobility associated with the Westwood deposit ore zones, Doyon-Bousquet-LaRonde mining camp, Abitibi, Quebec; Geological Survey of Canada, Current Research 2011-8, 15 p.

Yamada, R., Suyama, T., and Ogushi, O., 1987. Gold-bearing siliceous ore of the Nurukawa deposits, Akita Prefecture, Japan; Mining Geology, v. 37, p. 109–118.

Yergeau, D., 2015. Géologie du gisement synvolcanique aurifère atypique Westwood, Abitibi, Québec; Ph.D. thesis, Institut national de la Recherche Scientifique, Québec, Quebec, 682 p.

Yergeau, D., Mercier-Langevin, P., Dubé, B., Malo, M., Bernier, C., Savoie, A., and Simard, P., 2013. Synvolcanic Au-Cu±Ag-Zn-Pb massive sulphides, veins and disseminations of the Westwood deposit, Abitibi greenstone belt, Québec; Geological Survey of Canada, Open File 7482, 54 p.

Yergeau, D., Mercier-Langevin, P., Dubé, B., Malo, M., McNicoll, V.J., Jackson, S.E., Savoie, A., and La Rochelle, F., 2015. The Archean Westwood Au deposit, southern Abitibi: telescoped Au-rich VMS and intrusion-related Au systems, *In:* Targeted Geoscience Initiative 4: Contributions to the Understanding of Precambrian Lode Gold Deposits and Implications for Exploration (ed.) B. Dubé and P. Mercier-Langevin; Geological Survey of Canada: Open File 7852, p. 177–191.

GEOLOGICAL SURVEY OF CANADA
OPEN FILE 7853

Targeted Geoscience Initiative 4: Contributions to the Understanding of Volcanogenic Massive Sulphide Deposit Genesis and Exploration Methods Development

Geology and Au enrichment processes at the Paleoproterozoic Lalor auriferous volcanogenic massive sulphide deposit, Snow Lake, Manitoba

Antoine Caté[1], Patrick Mercier-Langevin[2], Pierre-Simon Ross[1], Shamus Duff[3], Mark D. Hannington[3], Benoît Dubé[2], and Simon Gagné[4]

[1]Institut national de la recherche scientifique – Centre Eau Terre Environnement, Québec, Quebec
[2]Geological Survey of Canada, Québec, Quebec
[3]University of Ottawa, Ottawa, Ontario
[4]Manitoba Geological Survey, Winnipeg, Manitoba

2015

This publication is available for free download through GEOSCAN (http://geoscan.nrcan.gc.ca/)

Recommended citation

Caté, A., Mercier-Langevin, P., Ross, P.-S., Duff, S., Hannington, M.D., Dubé, B., and Gagné, S., 2015. Geology and Au enrichment processes at the Paleoproterozoic Lalor auriferous volcanogenic massive sulphide deposit, Snow Lake, Manitoba, *In:* Targeted Geoscience Initiative 4: Contributions to the Understanding of Volcanogenic Massive Sulphide Deposit Genesis and Exploration Methods Development, (ed.) J.M. Peter and P. Mercier-Langevin; Geological Survey of Canada, Open File 7853, p. 131–145.

Publications in this series have not been edited; they are released as submitted by the author.

Contribution to the Geological Survey of Canada's Targeted Geoscience Initiative 4 (TGI-4) Program (2010–2015)

TABLE OF CONTENTS

Figures

Geology and Au enrichment processes at the Paleoproterozoic Lalor auriferous volcanogenic massive sulphide deposit, Snow Lake Manitoba

Antoine Caté[1,*], Patrick Mercier-Langevin[2†], Pierre-Simon Ross[1], Shamus Duff[3], Mark D. Hannington[3], Benoît Dubé[2], and Simon Gagné[4]

[1]Institut national de la recherche scientifique – Centre Eau Terre Environnement, 490 rue de la Couronne, Québec, Quebec, G1K 9A9
[2]Geological Survey of Canada, 490 rue de la Couronne, Québec, Quebec G1K 9A9
[3]Department of Earth Sciences, University of Ottawa, 140 Louis Pasteur, Ottawa, Ontario K1N 6N5
[4]Manitoba Geological Survey, Unit 360, 1395 Ellice Avenue, Winnipeg, Manitoba R3G 3P2
*Corresponding author's e-mail: antoine.cate@ete.inrs.ca
†Corresponding author's e-mail: pmercier@nrcan.gc.ca

ABSTRACT

The Paleoproterozoic Lalor auriferous volcanogenic massive sulphide deposit, located in the Snow Lake mining camp, Manitoba, is hosted in a complex volcanic package referred to as the Lalor volcanic succession. The deposit consists of stratigraphically and structurally stacked Zn-rich, Au-rich, and Cu-Au-rich ore lenses. The host volcanic succession comprises mafic to felsic tholeiitic to calc-alkaline extrusive to intrusive volcanic rocks of the ca. 1.89 Ga Lower Chisel subsequence, and the ore is hosted in both mafic and felsic rocks. Atypical of the other Zn-rich deposits of the Snow Lake district, the Lalor deposit is not situated at the top of the Lower Chisel subsequence, but is at a slightly lower stratigraphic position.

The volcanic rocks that host the deposit were affected by intense and laterally extensive ore-related hydrothermal alteration. These altered rocks were subsequently subjected to syndeformational amphibolite-grade metamorphism that resulted in the development of distinct minerals and metamorphic mineral assemblages of varying composition from variably altered precursor lithologies. Five distinct alteration- and metasomatism-related chemical associations (K, K-Mg-Fe, Mg-Fe, Mg-Ca, and Ca) are recognized based on mineralogical (mineral assemblages) and bulk geochemical compositions. Mapping of the host volcanic rocks and ore-related mineral assemblages and chemical associations at Lalor indicates the following: 1) the Zn-rich massive sulphide lenses are preferentially associated with the low- to high-temperature K and Mg-Ca alteration zones; 2) the Cu-Au-rich zones, which occur at depth, stratigraphically below the Zn-rich mineralization, are hosted in transposed, presumably originally discordant high-temperature Mg-Fe altered rocks; and 3) Au has been in part locally remobilized into low-strain sites that are not now spatially associated with any particular chemical association.

The Lalor volcanic succession is affected by polyphase deformation that has strongly influenced the geometry of the Lalor deposit. Pre-D_2 (synvolcanic?) deformation is evidenced by the abrupt termination of the intensely altered Lalor volcanic succession to the southwest and the presence of chemically distinctive and unaltered volcanic rocks of the Western succession. The present geometry of the deposit is largely controlled by D_2 deformational structures with important stretching (L_2), flattening (S_2), and structural staking (F_2 folding and syn- to late-D_2 transposition and shearing). The D_2 deformation and associated peak metamorphic conditions are thought to be responsible for the local remobilization of Au sulphosalts and some sulphides.

INTRODUCTION

The Paleoproterozoic Lalor auriferous volcanogenic massive sulphide (VMS) deposit, located in the Snow Lake mining camp of northern Manitoba, is currently being mined by owner and operator HudBay Minerals Inc. Combined reserves and resources are estimated at 25.3 Mt averaging 5 wt% Zn, 0.79 wt% Cu, 2.9 g/t Au, and 25 g/t Ag (HudBay Minerals Inc., 2014), including 8.8 Mt at 4.6 g/t Au, making it the largest and richest VMS deposit of the Snow Lake camp (Mercier-Langevin et al., 2014). Based on the grade and tonnage data, Lalor belongs to a subgroup of large, Au-enriched VMS deposits termed "anomalous", with over 31 t Au (c.f. Mercier-Langevin et al., 2011). However, with 8.8

Caté, A., Mercier-Langevin, P., Ross, P.-S., Duff, S., Hannington, M.D., Dubé, B., and Gagné, S., 2015. Geology and Au enrichment processes at the Paleoproterozoic Lalor auriferous volcanogenic massive sulphide deposit, Snow Lake, Manitoba, *In:* Targeted Geoscience Initiative 4: Contributions to the Understanding of Volcanogenic Massive Sulphide Deposit Genesis and Exploration Methods Development, (ed.) J.M. Peter and P. Mercier-Langevin; Geological Survey of Canada, Open File 7853, p. 131–145.

Mt of ore at 4.6 g/t, the Au and Au-Cu zones at Lalor exceed the 3.46 g/t Au and 31 t Au thresholds defining Au-rich VMS. Such deposits are challenging exploration targets because the Au-enrichment processes and their diagnostic characteristics are complex and variable, and can be masked by superimposed deformational and metamorphic effects that have modified or obliterated primary geological and mineralogical relationships.

The Geological Survey of Canada, in collaboration with the Manitoba Geological Survey, HudBay Minerals Inc., the Institut national de la recherche scientifique, and the University of Ottawa, conducted research at Lalor under the auspices of the VMS Ore System project of NRCan's Targeted Geoscientific Initiative 4 program. This project is largely based on extensive drill-core logging, underground mapping, 3-D modelling, and bulk geochemical, oxygen isotopic and mineral chemical analyses. The salient aims are to determine the geological and structural setting of the deformed and metamorphosed Lalor VMS deposit, its hydrothermal signature, the relative timing of volcanic, mineralizing, deformational, and metamorphic events, and to elucidate the genesis of the precious and base metal mineralization. This report summarizes some of the key aspects of the deposit geology and evolution determined so far, but our research at Lalor is ongoing.

GEOLOGICAL SETTING

The Lalor deposit is hosted in the Lalor volcanic succession (Caté et al., 2014a), which is part of the Chisel mature arc sequence of the Paleoproterozoic Snow Lake arc assemblage (Fig. 1; Bailes and Galley, 1999). The ca. 1.89 Ga Snow Lake arc assemblage occurs in the easternmost part of the Paleoproterozoic Flin Flon greenstone belt (Galley et al., 2007). The Chisel mature arc sequence consists of intercalated, geochemically fractionated, intermediate to mafic flows, volcaniclastic to volcanosedimentary units, and discrete felsic flow complexes and related subvolcanic intrusive phases. The volcanic sequence is cut by the Richards Lake synvolcanic pluton and the Chisel mafic intrusion. Zinc-rich, bimodal felsic-type VMS deposits are located at the contact between the lower and upper parts of the Chisel sequence (Bailes and Galley, 1999; Galley et al., 2007). The Chisel, Chisel North, Ghost, and Lost deposits are spatially and temporally associated with rhyolite domes and are located at the contact between the footwall Powderhouse dacite and the hanging-wall Threehouse basalt and volcaniclastic rocks (Galley et al., 2007), which marks the transition between the lower and upper parts of the Chisel sequence (Bailes and Galley, 1996; Engelbert et al., 2014).

Four discrete episodes of folding are recognized in the Snow Lake area (David et al., 1996; Kraus and Williams, 1999). D_1 and D_2 events produced tight, isoclinal, south-verging folds, shallowly dipping thrusts, and imparted the main foliation (Kraus and Williams, 1999; Bailes et al., 2013). These structures are refolded by NNE-SSW-trending F_3 folds and an associated S_3 crenulation cleavage (Martin, 1966; Kraus and Williams, 1999). F_4 folds with east-west-trending axes locally overprint F_3 folds (Kraus and Williams, 1999).

GEOLOGY OF THE LALOR DEPOSIT

The Lalor deposit consists of at least twelve stratigraphically and structurally stacked Zn-rich massive sulphide lenses, sulphide-poor Au-rich lenses, and transposed Cu- and Au-rich semi-massive to disseminated sulphide footwall stringer zones (Caté et al., 2013; Duff et al., 2013). The mineralized lenses are strongly transposed into the main foliation in the uppermost section of the Lalor volcanic succession, which has been intensely hydrothermally altered in the deposit footwall (Caté et al., 2014b; Mercier-Langevin et al., 2014).

Volcanic Stratigraphy

The Lalor volcanic succession is in contact with the Balloch volcanic succession ("Lalor-Chisel contact": Fig. 2). The VMS-hosting succession is truncated to the west by the Lalor West fault, and is in contact with a weakly altered volcanic package referred to herein as the Western volcanic succession (Fig. 2; Caté et al., 2014a). Mafic, intermediate, and felsic volcanic and intrusive rocks are present in the Lalor volcanic succession. However, because most of the rocks located in the stratigraphic footwall of the deposit have been affected by intense alteration, deformation, and metamorphism, there has been nearly complete destruction of the primary volcanic textures and it is generally not possible to determine protoliths by visual inspection. Thus, immobile element geochemistry is essential in mapping the units and reconstructing the volcanic stratigraphy of the intensely altered and deformed Lalor volcanic succession (Caté et al., 2014a).

Nine units were defined based on their spatial distribution and geochemical characteristics. These chemostratigraphic units are mafic (M), intermediate (I), and felsic (F) and have a tholeiitic to calc-alkaline affinity (Fig. 3; Caté et al., 2014a).

Unit F1

Unit F1 is rhyolitic to rhyodacitic, transitional to calc-alkaline, and is spatially located in the footwall of the Zn-rich massive-sulphide ore lenses. The unit could occur as dykes, sills or form small extrusive bodies, as evidenced by the presence of unit F1 geochemical signatures intercalated with other chemostratigraphic units (Figs. 2, 3). Relatively weakly altered intervals of unit F1 consist of massive aphyric rhyolite.

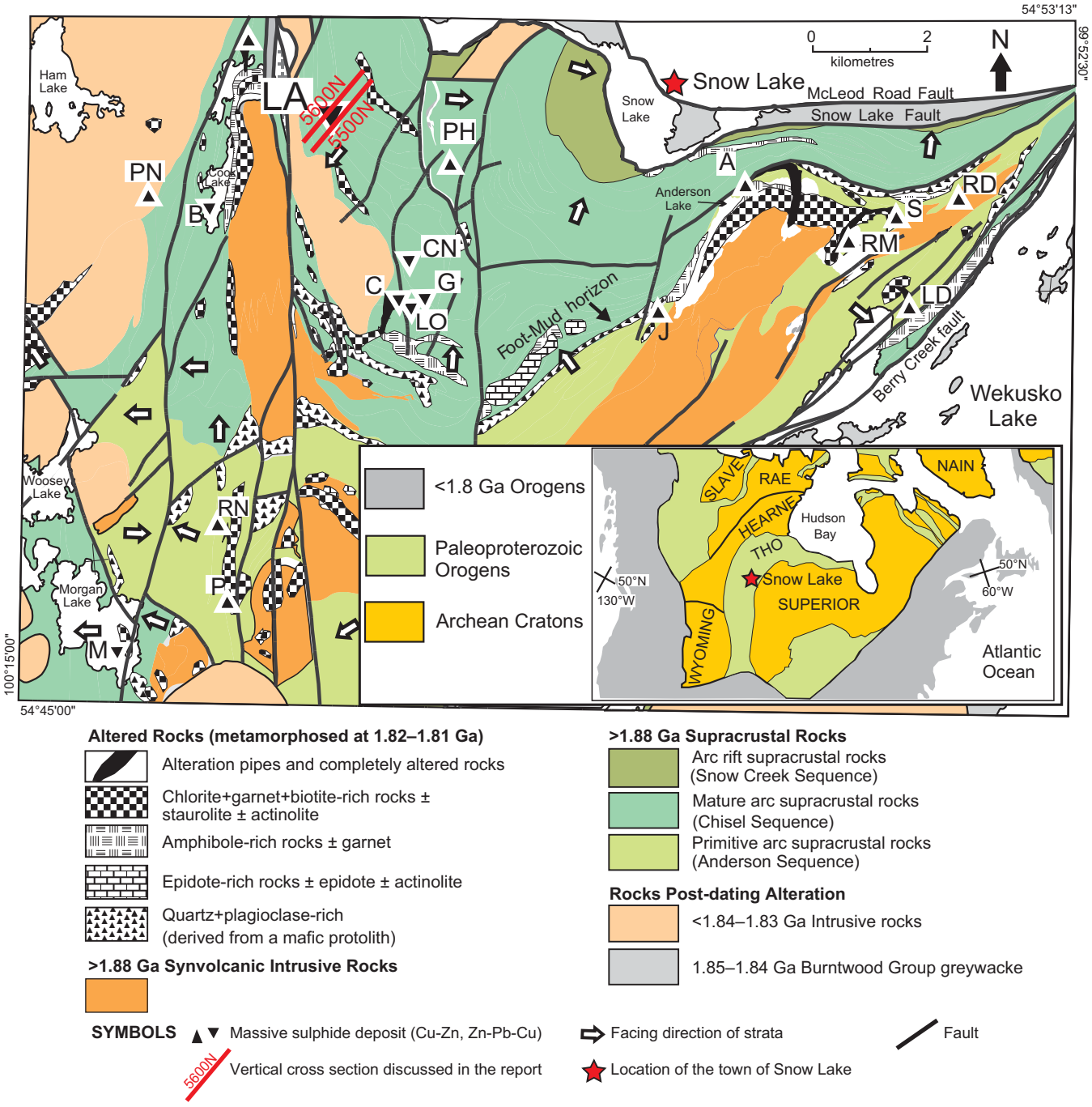

Figure 1. Simplified geological map of the Snow Lake area (from Galley et al., 2007), showing major alteration zones and VMS deposits, including the Lalor deposit (LA). Other deposits: A = Anderson; B = Bomber zone; C = Chisel Lake; CN = Chisel North; G = Ghost; J = Joannie zone; LO = Lost; LD = Linda zone; M = Morgan Lake zone; P = Pot Lake zone; PH = Photo Lake; PN = Pen zone; RD = Rod; RM = Ram zone; RN = Raindrop zone; S = Stall Lake. The location of the Snow Lake area is shown in the inset map.

Unit F2

Unit F2 is rhyolitic to rhyodacitic, transitional to calc-alkaline (Fig. 3) and forms a continuous, <50 m-thick unit (Fig. 2) that hosts the lowermost Zn-rich massive sulphide lenses (lens 20 and its underlying lenses). No primary volcanic textures are preserved. The trace element signature of unit F2 is similar to that of the Powderhouse dacite (Caté et al., 2014a) present in the footwall of the Chisel deposit southeast of Lalor (Bailes and Galley, 1996).

Unit F3

Unit F3 is felsic and of calc-alkaline affinity (Fig. 3) and is generally intercalated with unit F2. Unit F3 is intensely altered and no primary textures are preserved.

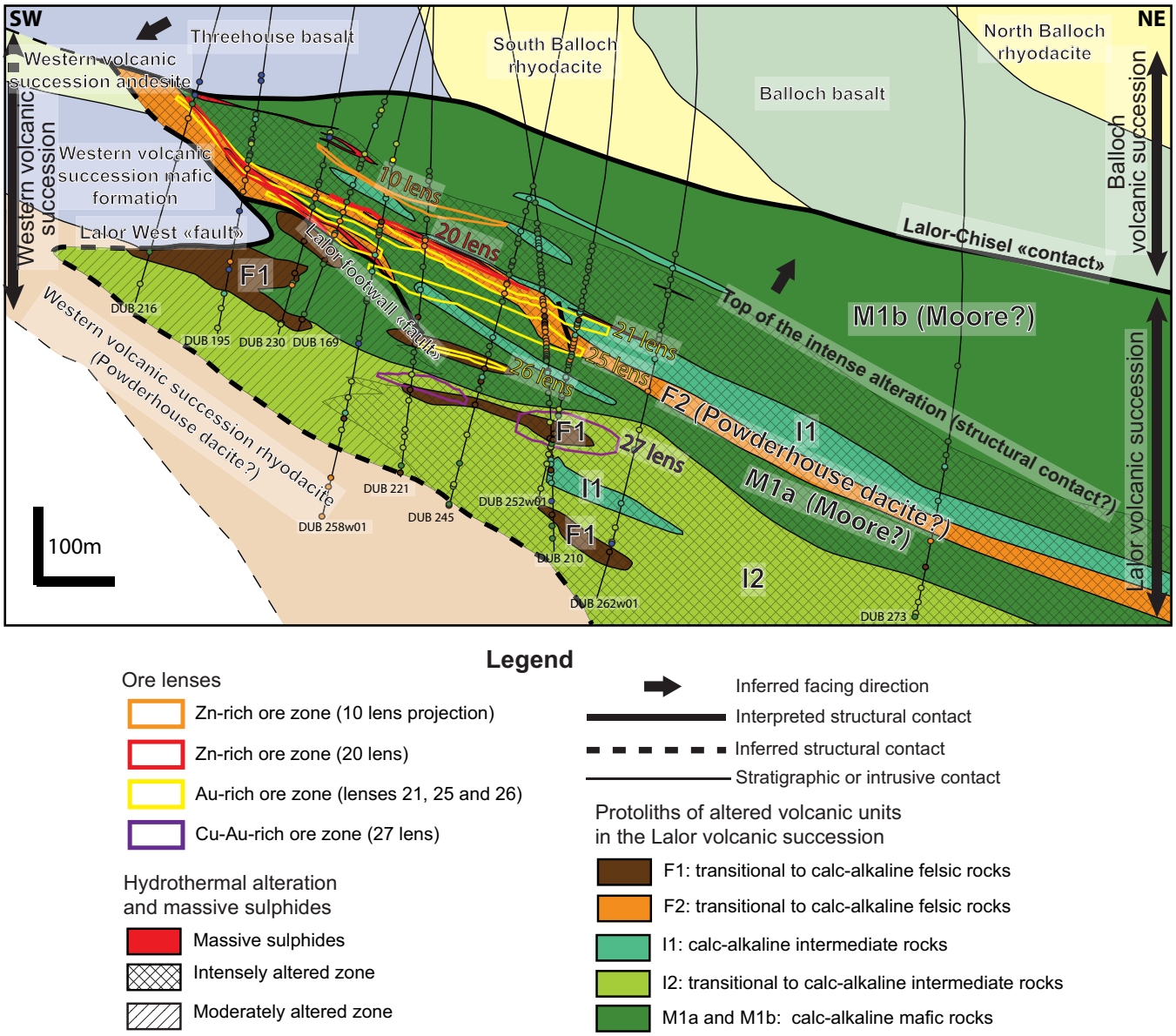

Figure 2. Simplified geological cross-section 5600 N (looking northwest) constructed subparallel to L_2 plunge and including the chemostratigraphic units of the Lalor volcanic succession (from Caté et al., 2014a). The top of the cross-section is at 600 m below surface. The Balloch and Western volcanic succession are in muted colours and the Lalor volcanic succession in brighter colours. Drillholes and samples (unit-colour filled circles along drillholes traces) are shown, together with the distribution of the interpreted units. Ore-zone morphologies are from Hudbay Minerals; 10 lens is projected from section 5500 N. Chemostratigraphic units F3, M2, and M3 are not depicted, as they are only present in narrow intervals and in minor amounts. Unit names of the Balloch volcanic succession are from Bailes (2008).

Unit I1

Unit I1 is a calc-alkaline andesite that forms discontinuous intervals throughout the entire Lalor volcanic succession (Fig. 2). Most of the least altered samples of unit I1 are aphyric to feldspar-phyric dykes that are up to 25 m thick, although some altered volcaniclastic rocks are also considered to be part of chemostratigraphic unit I1, based on their similar geochemical signature.

Unit I2

Unit I2 is a transitional to calc-alkaline andesite that forms a 150 m-thick interval at the base of the exposed Lalor volcanic succession (Fig. 2). Least altered samples consist of biotite-rich tuff, lapilli tuff, and tuff breccia.

Units M1a and M1b

Units M1a and M1b have similar immobile element signatures, but they are located at two different stratigraphic levels (Fig. 2). Unit M1a is present in the footwall of the lowermost Zn-rich massive sulphide lenses (20 lens and lower), and unit M1b hosts the uppermost Zn-rich massive sulphide lenses (10 and 11 lenses).

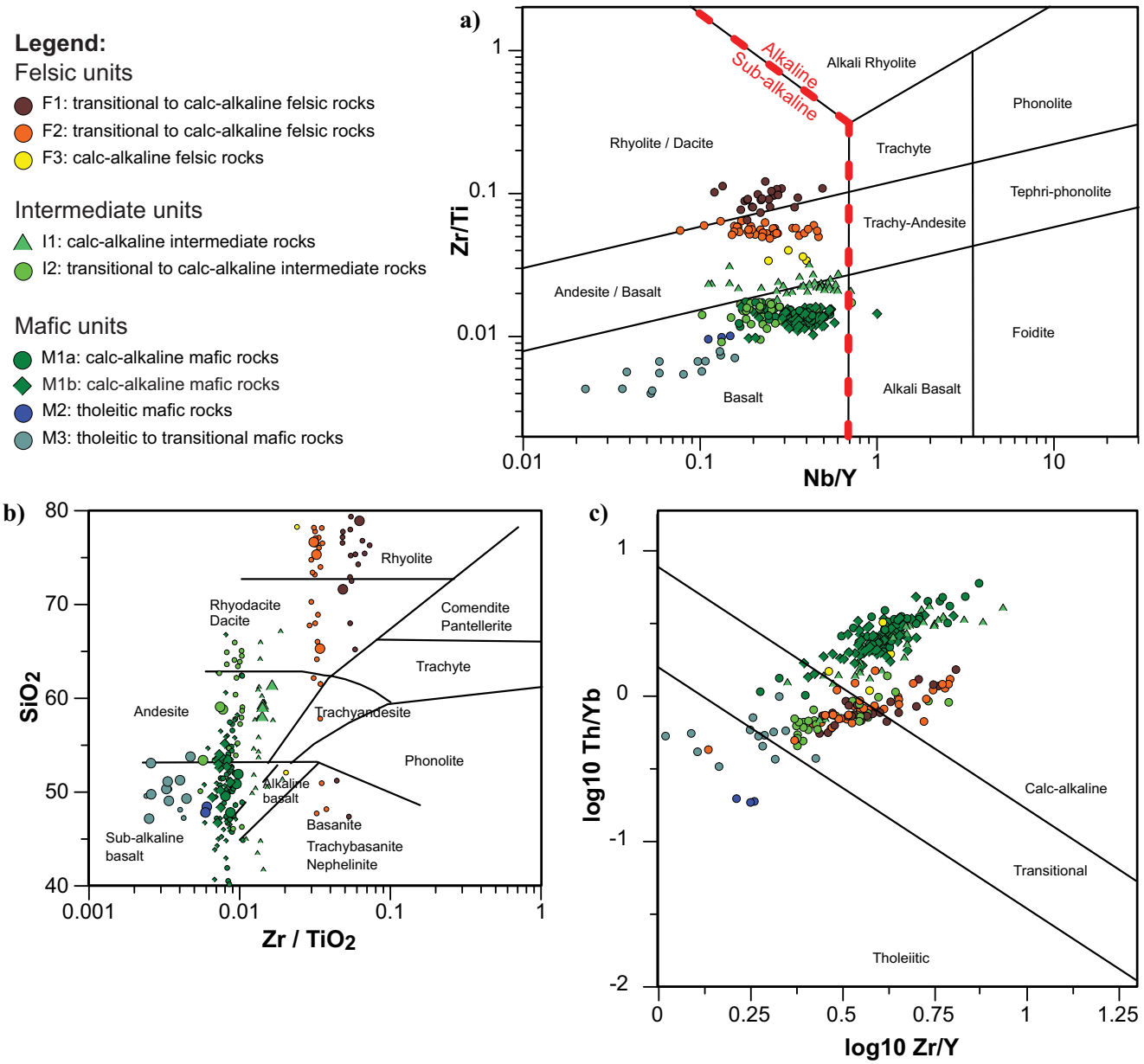

Figure 3. Discriminant geochemical diagrams of the Lalor-succession volcanic (± intrusive) rocks sampled from selected drillholes along section 5600 N (Fig. 2) and two least altered samples from DUB223. **a)** Pearce (1996) classification diagram modified after Winchester and Floyd (1977). **b)** Winchester and Floyd (1977) classification diagram. Thirty-six samples with <40 wt% SiO_2 and 9 samples with >80 wt% SiO_2 have been excluded as they fall out of the diagram range. As SiO_2 has been strongly affected by VMS alteration and vertically spreads the samples, only the SiO_2 content of the less altered samples (larger symbols, with 20<AI<60; AI = 100*($MgO+K_2O$)/($MgO+K_2O+Na_2O+CaO$), S<1 wt%, CO_2<1 wt%, Na_2O>0.5 wt%, LOI<2 wt% and unaltered-appearing texture and mineralogy) is used in this report to determine the fractionation of the units. **c)** Magmatic affinity diagram of Ross and Bédard (2009).

The upper part of the M1b unit (lenses 10 and 11 hanging wall) has not been intensely altered by the VMS hydrothermal system and is truncated by the Lalor-Chisel contact. Both units consist of calc-alkaline basalt to basaltic andesite and are very similar geochemically and texturally to the Moore basalt (Caté et al., 2014a) located in the footwall of the Chisel deposit (Bailes and Galley, 1996). Least altered samples of unit M1b are massive volcanic rock with some coarse mafic lapilli tuff.

Unit M2

Unit M2 is a tholeiitic basalt that forms post-VMS aphyric dykes that locally can be up to a few m thick.

Unit M3

Unit M3 consists of post-VMS aphyric, feldspar-phyric, and feldspar- and pyroxene-phyric dykes of tholeiitic to transitional affinity that have similar trace element signatures to that of the Treehouse basalt (Caté

et al., 2014a), which is located in the hanging wall of the Chisel deposit (Bailes and Galley, 1996).

Hydrothermal Alteration and Syn-Metamorphic Metasomatism

The host rocks at Lalor have been intensely hydrothermally altered over a large area extending to more than 350 m spatially below the ore horizon, and this alteration has modified the bulk geochemical composition and mineralogy of the volcanic rocks and obliterated most primary volcanic textures. Syn- to late D_2 peak amphibolite-grade metamorphism (Menard and Gordon, 1997) has significantly modified the VMS-related alteration mineralogy, with only minimal modification of the bulk geochemical composition of the rocks (Tinkham, 2013; Caté et al., 2014c), with the exception of some minor effects that are discussed below. Metamorphosed hydrothermally altered rocks generally contain variable proportions of coarse-grained quartz, muscovite, biotite, chlorite, Mg-Fe–amphibole, cordierite, garnet, staurolite, kyanite, sillimanite, Ca-amphibole, diopside, carbonate minerals, anhydrite, gahnite, sulphides, magnetite, and other trace minerals. The metamorphosed mineral assemblages and the relative abundance and composition of specific minerals within these assemblages can be correlated with bulk rock geochemical compositions to identify specific chemical associations and determine alteration zonation. Four distinct chemical associations (K, K-Mg-Fe, Mg-Fe, Ca-Mg) that correlate with the presence and relative abundance of key minerals have been documented in the altered rocks at Lalor (Caté et al., 2014c). A fifth chemical association (Ca) results from syndeformation and metamorphism metasomatism in the Lalor area. Dehydration and decarbonation reactions have locally modified the mineralogy, mineral textures, and bulk compositions of the hydrothermally altered rocks in the deposit footwall (Tinkham, 2013). Thus, the chemical associations are the collective result of multiple processes dominated by polyphase hydrothermal fluid flow, and localized syn-metamorphic metasomatism superimposed on volcanic rocks of varying composition.

K Chemical Association

The K chemical association occurs in muscovite-bearing (>5 vol% muscovite) rocks (Fig. 4a). Quartz, pyrite, biotite, kyanite, and sillimanite are also present in varying abundances. Minor (<5 vol%) relic plagioclase is locally preserved. The K chemical association occurs mainly in the wallrocks of the upper part of the deposit, proximal to the Zn-rich massive sulphide lenses (Fig. 5; Caté et al., 2014c). The abundance of pyrite increases toward the massive sulphide lenses up to a maximum of 40 vol%. Minor gahnite and sphalerite occur in the wallrocks immediately adjacent to massive sulphides. Bulk geochemical compositions and alteration indices indicate that the K chemical association corresponds to metamorphosed sericitic alteration (Fig. 6). Whole-rock oxygen isotope values indicate low- to moderate (~200–250°C) alteration temperatures (Mercier-Langevin et al., 2014).

K-Mg-Fe Chemical Association

The K-Mg-Fe chemical association occurs in biotite-bearing rocks that contain no muscovite, chlorite, Mg-Fe amphibole (anthophyllite, cummingtonite-grunerite, and gedrite series), cordierite and/or Ca amphibole (actinolite, hornblende, and tschermakite series) (Fig. 4b). Feldspar is minor or absent. These biotite-bearing rocks contain abundant Al-rich minerals (kyanite, sillimanite, staurolite, and/or garnet) and quartz. Pyrite increases in abundance toward massive sulphides, up to a maximum of 40 vol.%. The K-Mg-Fe chemical association is transitional between the K and the Mg-Fe chemical associations (Fig. 5). It is present both proximal to the uppermost Zn-rich sulphide lenses in the upper part of the deposit and in the deep footwall of the deposit. Bulk geochemical compositions and alteration indices indicate that the K-Mg-Fe chemical association corresponds to a metamorphosed chlorite-sericite alteration style (Fig. 5). Whole-rock oxygen isotope values suggest moderate (~250°C) alteration temperatures (Mercier-Langevin et al., 2014).

Mg-Fe Chemical Association

The Mg-Fe chemical association occurs in rocks that contain chlorite, Mg-Fe amphibole, and/or cordierite (Fig. 4c). These rocks also contain variable amounts of biotite, quartz, garnet, and staurolite, with rare feldspar. Muscovite is absent in rocks of this chemical association. Talc is locally abundant, especially close to Mg-Ca-altered rocks (see below). The abundance of biotite in the Mg-Fe chemical association increases near K-Mg-Fe-altered rocks. Gahnite is locally present, commonly in sulphide veinlets. The Mg-Fe chemical association affects a very large volume of rocks in the deposit footwall (Fig. 5). The Cu-Au mineralization (transposed footwall stringer zones) and minor portions of the Au-rich sulphide-poor lenses are hosted in the Mg-Fe-altered rocks. The Mg-Fe-altered rocks represent a high-temperature (~200–350°C), metamorphosed chlorite-dominated alteration zone, as indicated by bulk geochemical and oxygen isotope compositions (Mercier-Langevin et al., 2014) (Fig. 6).

Mg-Ca Chemical Association

The Mg-Ca chemical association corresponds to rocks that are mainly composed of variable amounts of Mg-chlorite, Ca-amphibole (mainly actinolite series),

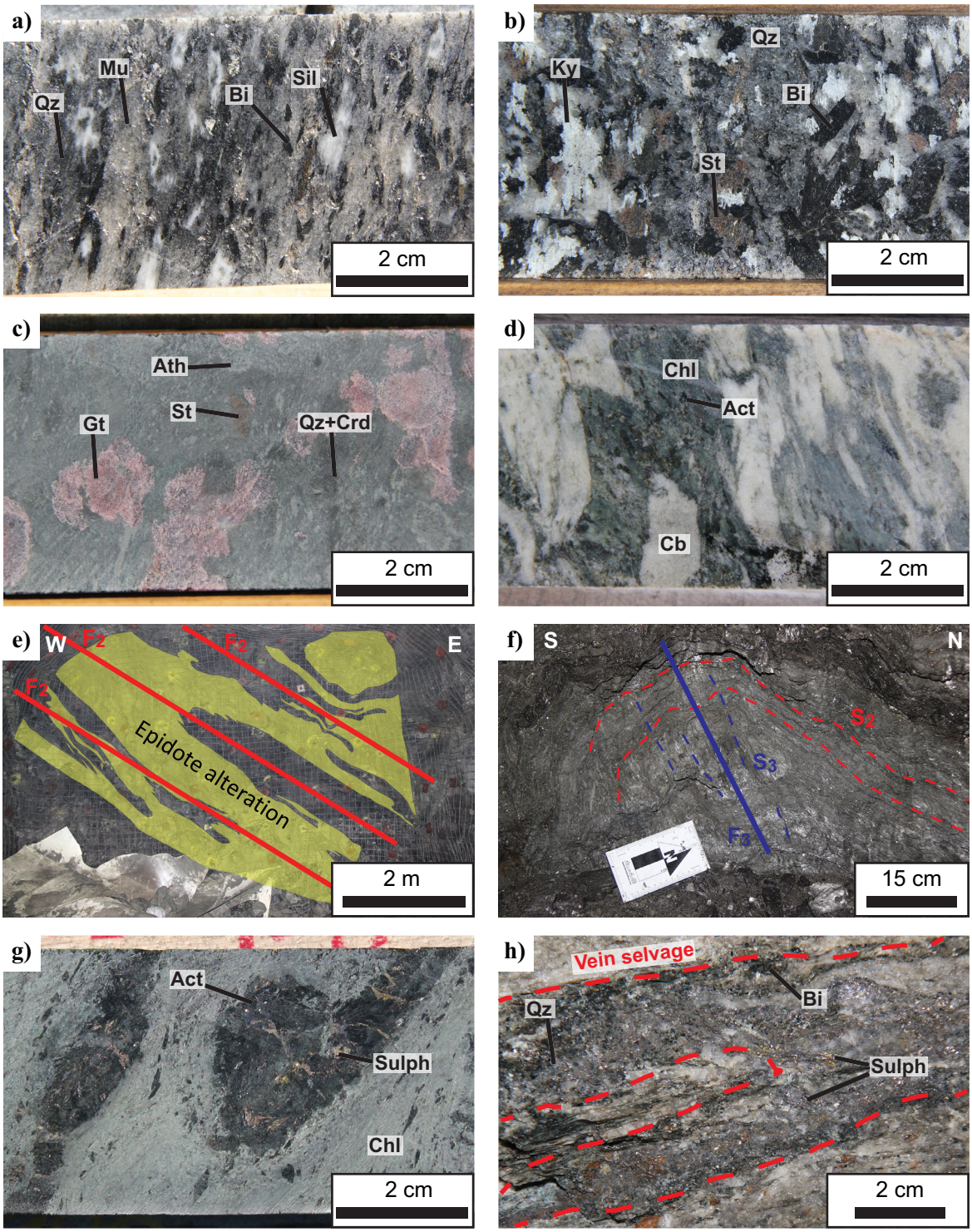

Figure 4. a) Metamorphic mineral assemblage of the K chemical association, with biotite, muscovite, and sillimanite porphyroblasts in a quartz-muscovite-biotite matrix. **b)** Metamorphic mineral assemblage of the K-Mg-Fe chemical association, with biotite, kyanite, and staurolite porphyroblasts in a quartz-biotite matrix**. c)** Metamorphic mineral assemblage of the Mg-Fe chemical association, with garnet, staurolite, and Mg-Fe amphibole porphyroblasts in a quartz-Mg-Fe amphibole-cordierite matrix. **d)** Metamorphic mineral assemblage of the Mg-Ca chemical association, with deformed carbonate spheroids and actinolite porphyroblasts in Mg-chlorite matrix. **e)** F_2-folded epidote-rich alteration layers in moderately altered andesite. **f)** S_3-crenulated S_2foliation affected by a F_3 fold in muscovite schist. **g)** S_2-perpendicular sulphide-filled fractures in F_2-folded actinolite layers in a chlorite matrix. Sulphides are pyrrhotite, chalcopyrite, and trace galena. This mineralization is part of the Au-rich 21 ore lens. **h)** Quartz-sulphide-biotite vein in a quartz-phlogopite-Mg-Fe amphibole mineral assemblage. Sulphides are sphalerite, pyrite, pyrrhotite, galena, and chalcopyrite. This mineralization is located in the 25 ore lens. Abbreviations: Act = actinolite, Ath = Mg-Fe amphibole, Bi = biotite, Cb = carbonate minerals (calcite and/or dolomite), Chl = chlorite, Crd = cordierite, Gt = garnet, Ky = Kyanite, Mu = muscovite, Qz = quartz, Sil = sillimanite, St = staurolite, Sulph = sulphides.

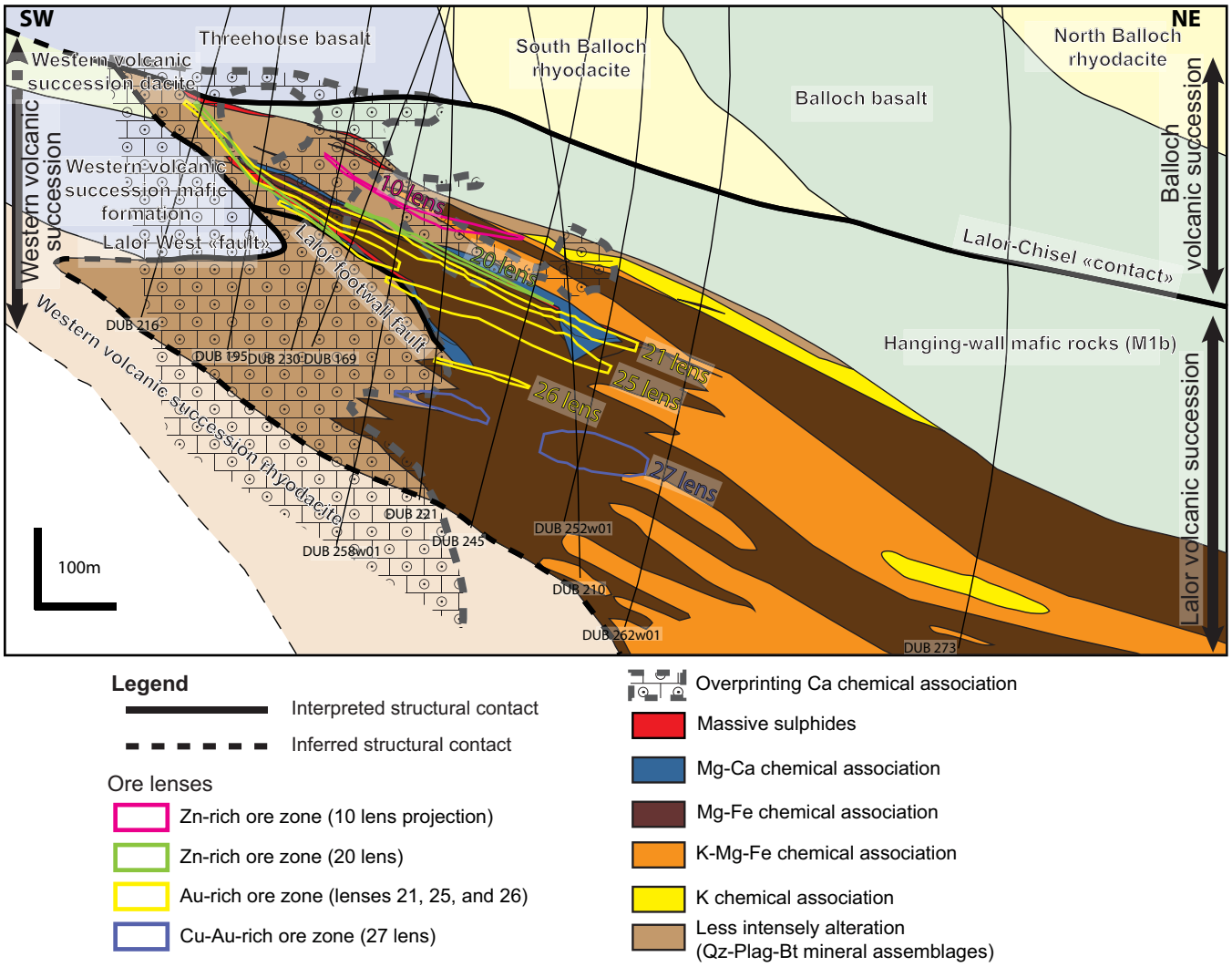

Figure 5. Simplified geological cross-section 5600 N (looking northwest) constructed subparallel to L_2 plunge with metamorphic mineral assemblages of altered volcanic rocks grouped according to chemical associations. The top of the cross-section is at 600 m below surface. Least altered volcanic rocks are in muted colours and the altered rocks of the Lalor volcanic succession in brighter colours. Traces of drillholes that have been used to interpret this section are shown. Ore-zone morphologies from Hudbay Minerals; 10 lens is projected from section 5500 N. Unit names in the Balloch volcanic succession are from Bailes (2008). Abbreviations: Bt = biotite, Plag = plagioclase, Qz = quartz.

and/or carbonate (calcite and/or dolomite) (Fig. 4d). Quartz, anorthite, biotite, talc, titanite, grossular, and anhydrite are common constituents. Diopside can be a major (>20 vol.%) component very locally. Crosscutting relationships indicate that layers (5 cm- to >1 m-thick sheet-like zones) of actinolite-rich mineral assemblages overprint the chlorite-rich and the carbonate-rich assemblages. The actinolite layers were folded during D_2, but they also overprint S_2 in a few places. Moreover, similar actinolite-rich layers overprint the other chemical associations (K, K-Mg-Fe, and Mg-Fe) proximal to Mg-Ca-altered rocks. Tinkham (2013) concluded that hydrous and carbonic metasomatism occurred by fluid circulation in the Mg-Ca-altered rocks during amphibolite-grade metamorphism. The Mg-Ca chemical association is mostly developed around the lowermost Zn-rich massive sulphide lenses and the sulphide-poor Au-rich zones, especially in the western part of the deposit (Fig. 5). The Mg-Ca chemical association corresponds to intense chlorite-carbonate alteration prior to amphibolite-grade metamorphism (Caté et al., 2014c). The Mg-Ca chemical association is characterized by bulk-rock $\delta^{18}O$ values similar to those of the Mg-Fe chemical association. This indicates that the Mg-Ca chemical association is the result of hydrothermal alteration at moderate to high temperatures (~200–300°C: Mercier-Langevin et al., 2014).

Ca Chemical Association

The Ca chemical association represents rocks that were metasomatized after VMS formation (pre- to post-peak D_2: Caté et al., 2014b). This metasomatism overprinted altered and unaltered rocks of the Lalor volcanic suc-

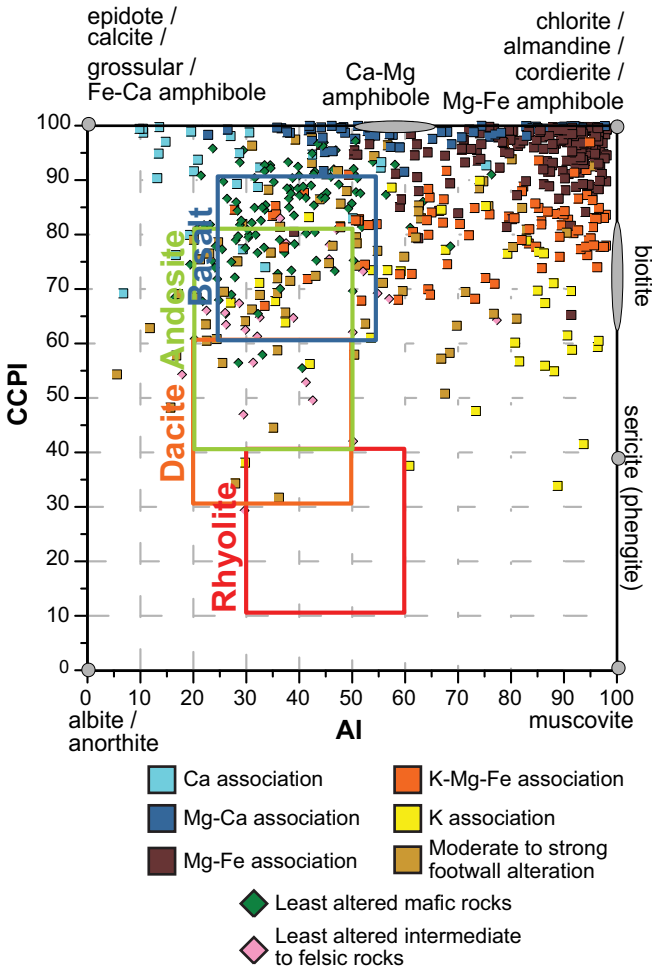

Figure 6. Box plot diagram (Large et al., 2001) with 699 samples of altered rocks classified by chemical association and least altered rocks. Classification of the samples has been done by macroscopic observation of the mineral assemblages. Fields of fresh volcanic rocks are from Gifkins et al. (2005). Main metamorphic minerals present at Lalor have been plotted. Abbreviation: CCPI = chlorite-carbonate-pyrite index (100*(MgO+FeO)/(MgO+FeO+Na_2O +K_2O)).

cession as well as post-VMS dykes and rocks of the Western and Balloch volcanic successions. The Ca chemical association is evidenced by pervasive layers of epidote and quartz with a halo rich in Ca-amphibole (hornblende to tschermakite series) that is generally developed after biotite. Veins of grossular, epidote, quartz, diopside, anhydrite, and/or calcite can be present in the centre of diffuse bands of Ca-rich alteration. The Ca-metasomatism tends to lower the alteration index (AI = 100∗(MgO+K_2O)/(MgO+K_2O+Na_2O+CaO)) and increase the chlorite-carbonate-pyrite index (CCPI = 100(Mg+FeO)/(MgO+FeO+Na_2O+K_2O)) of affected rocks (Fig. 6), and it can be differentiated from the other VMS-related alteration styles on this basis.

Although intensely altered rocks largely predominate in the Lalor footwall, weakly to moderately altered rocks are locally present. They typically have preserved volcanic textures, such as feldspar phenocrysts or phenoclasts. West of the deposit, these rocks are composed of quartz, feldspar, and biotite with variable abundances of muscovite, kyanite, and sillimanite. Tschermakite-series amphibole is present in mafic rocks; felsic rocks are richer in quartz. Despite moderate to strong alteration effects, in the deep footwall of the deposit, quartz-biotite-garnet-feldspar-altered rocks contain preserved textures of the primary volcanic rocks, such as volcanic lithic fragments.

Deformation and Metamorphism

The Lalor deposit has been affected by polyphase deformation (Kraus and Williams, 1999) and metamorphism up to amphibolite-grade (Menard and Gordon, 1997), which have had a major effect on the distribution, geometry, mineralogy, and textures of the ore zones and their host rocks (Caté et al., 2014a,b).

Main Structural Features and Structural Controls on the Geometry of the Ore Lenses and the Associated Footwall Alteration Zones

The Lalor volcanic succession is bounded at its top and to the west by structural contacts that probably formed early in the deformation history (pre-D_2; Caté et al., 2014b). The Lalor-Chisel contact is overprinted by the main S_2 foliation. The contact truncates the unaltered mafic volcaniclastic rocks at the top of the Lalor volcanic succession and cuts the units of the Balloch volcanic succession at a high angle (Fig. 5). The host deposit succession is bounded to the west by the Lalor West fault. This structural contact is folded by F_2 folds (Figs. 2 and 5), and displays evidence of further syn- to late-D_2 ductile shearing along the F_2 fold limbs (Caté et al., 2014b). The Lalor West fault is a sharp contact between strongly to intensely altered volcanic rocks of the Lalor volcanic succession and least (weakly) altered rocks of the Western volcanic succession. These major contacts predate main deformation (D_2, see below) and may result from syn-D_1 fold-and-thrust-style deformation, from an early (maybe synvolcanic) extension episode, or from the combination of both deformation styles.

Structural features associated with the D_1 deformation have been largely obliterated by the subsequent deformation events (Kraus and Williams, 1999; Caté et al., 2014b). Preserved structures (S_1 foliation and F_1 folds) are generally transposed into the S_2 fabric, forming a composite $S_{1\text{-}2}$ fabric, except in some F_2 fold hinge areas (Caté et al., 2014b).

The main deformation event in the Lalor deposit area is D_2. Tight to isoclinal, southwest-verging, inclined F_2 folds are common (Fig. 4e). A penetrative S_2 foliation (Fig. 4f) has developed everywhere and affects most of the phyllosilicate minerals (biotite, muscovite, and chlorite). A mineral and stretching lin-

eation (L_2) is associated with S_2 and affects the phyllosilicate and some of the amphibole minerals. Shear zones have been mapped underground (Caté et al., 2014b), and they appear to be syn- to late-D_2, but their kinematics and exact timing within D_2 remain unclear. Ore zones have been folded during D_2 deformation, transposed parallel to the S_2 foliation, and stretched parallel to the L_2 lineation (Caté et al., 2014b). Some base metal ore lenses are probably the result of structural dismemberment and stacking during F_2 folding and syn- to late-D_2 shearing/transposition.

The D_3 deformation event produced large open to locally tight upright folds (F_3) that locally affect the orientation of older features (Fig. 4f) without having a major effect at the deposit scale. An axial planar S_3 crenulation cleavage is developed in some muscovite or chlorite schists (Fig. 4f). The ore lenses are affected by broad, open F_3 folds (Caté et al., 2014b). Regional D_4 deformational effects have not been recorded in the rocks of the Lalor area.

Ore Remobilization during Metamorphism

As presented above, the geometry of ore lenses is structurally controlled by the D_2 and D_3 deformation events. The ductile behaviour of many sulphides during deformation (Kelly and Clark, 1975 and references therein) resulted in the local mechanical remobilization of sphalerite, chalcopyrite, and pyrrhotite in piercement structures, necks of boudinaged dykes, or fold hinges (Caté et al., 2014b,d). Sulphide-poor Au-Ag-Pb-Cu mineralization occurs in unaltered rocks close to massive sulphide mineralization (mafic dykes that crosscut the massive sulphides and least altered basalt in structural contact with massive sulphides). This mineralization comprises galena, chalcopyrite, pyrrhotite, pyrite, sulphosalts, and local minor arsenopyrite; it occurs in S_2-folded veinlets and in microfractures that crosscut the S_2 foliation, or in fractures in porphyroblasts (e.g. amphibole, Fig. 4g; Caté et al., 2014d). The sulphide-poor Au-rich ore zones are characterized by a similar Au-Ag-Pb-Cu association (Duff et al., 2015) and mineralization is preferentially located in narrow (<3 mm) fractures in more competent amphibole-rich mineral assemblages or in syn- to late-D_2 quartz veins, actinolite layers, and Ca-rich metasomatized rocks (Fig. 4g,h).

DISCUSSION

Stratigraphic Setting of the Lalor Deposit

The Lalor volcanic succession comprises numerous volcanic and subvolcanic units with mafic to felsic compositions and tholeiitic to calc-alkaline affinities (Fig. 3; Caté et al., 2014a). The bulk of the intensely hydrothermally altered rocks are located below the Zn-rich sulphide lenses, and this altered volume of rocks is the discordant footwall feeder pipe of the VMS system; whereas the Zn-rich ore lenses are the massive sulphide mineralization deposited at or below the seafloor. This overall geometry indicates that the Lalor volcanic succession, as a whole, is not overturned (Caté et al., 2014a), although there is likely structural complexity within the package and elucidating this is the subject of ongoing study. The lowermost Zn-rich massive-sulphide ore lenses (e.g. 20, 31, 32, and 40 lenses) are hosted in the felsic unit F2, whereas the uppermost lenses (e.g. 10 and 11 lenses) are hosted in the overlying mafic unit M1b. These massive sulphide bodies were most probably emplaced at or very near the paleo-seafloor. Thus, the formation of the Lalor deposit resulted either from two (or more) successive mineralizing events or more likely from protracted VMS-related hydrothermal activity that ceased during unit M1b (Caté et al., 2014a).

The trace element signatures of the various units of the Lalor volcanic succession are similar to those of units in the Lower Chisel subsequence (Caté et al., 2014a), and chemostratigraphic units M1 (a and b) and F2 may correspond to the Moore basalt and associated mafic volcaniclastic rocks, and to the Powderhouse dacite, respectively. Both the Moore basalt and Powderhouse dacite are present in the footwall of most of the other VMS deposits of the Chisel sequence (Bailes and Galley, 1996). Contrary to the Chisel, Chisel North, Ghost, and Lost VMS deposits host succession, there is no equivalent to the Threehouse mafic volcaniclastic rocks that conformably overlie the Lalor deposit. However, Threehouse-like dykes cut the Lalor volcanic succession, which suggests the presence of the Threehouse unit higher in the now truncated volcanic succession (Caté et al., 2014a). Therefore, the Lalor deposit is thought to be within the Lower Chisel subsequence (Caté et al., 2014a), and not at the contact between the Lower and Upper Chisel subsequences (i.e. at a slightly lower stratigraphic position than the other VMS deposits of the Chisel sequence).

Hydrothermal Setting of the Lalor Deposit

The Lalor deposit formed from hydrothermal fluids that circulated in the host volcanic pile and deposited massive sulphides at or very near the paleo-seafloor. The VMS-associated hydrothermal alteration was subsequently metamorphosed during deformation, resulting in the development of metamorphic mineral assemblages that largely reflect the bulk geochemical compositions of the initial alteration styles (Caté et al., 2014c). The wide variety of metamorphic mineral assemblages and their associated bulk geochemical compositions can be translated into, and mapped as, chemical associations to determine the primary alteration styles and their zonation (Caté et al., 2014c); this

allows for a better understanding of the primary geometry of the ore-forming system.

The uppermost Zn-rich massive-sulphide lenses (10 lens; Fig. 5) are mainly associated with the low-temperature K chemical association, whereas the lowermost massive-sulphide lenses (20 lens; Fig. 5) are dominantly associated with the high-temperature Mg-Ca and Mg-Fe chemical associations. The different alteration styles of the two groups of Zn-rich massive-sulphide lenses may indicate that these Zn-rich ore lenses formed in distinct hydrothermal environments and that they are stratigraphically (i.e. not structurally) stacked.

The Au-rich sulphide-poor ore lenses are dominantly associated with rocks attributed to the Mg-Ca chemical association, and to a lesser extent to rocks attributed to the Mg-Fe chemical association (Fig. 5), or to rocks unaffected by the VMS alteration but which are proximal to massive sulphide lenses. This could imply (1) the Au-rich ore lenses are syn-VMS and formed in primary alteration zones corresponding to the Mg-Ca chemical association (together with some syn-metamorphic remobilization) or (2) the rocks of the Mg-Ca chemical association are chemically and/or rheologically favourable host rocks for Au-rich mineralization emplaced during metamorphism by remobilization of metals present in the syn-VMS sulphide-rich ore lenses (Caté et al., 2014c).

The Cu-Au ore lenses occur in rocks of the high-temperature Mg-Fe chemical association (Fig. 5). These rocks correspond to a metamorphosed intense chloritic alteration that is generally present in the footwall alteration pipe of most VMS deposits. Thus, we interpret the Cu-Au mineralization to be the deformed equivalent of the high-temperature stringer zone located in the footwall of VMS deposits (Franklin, 1993).

The presence of actinolite-rich layers (part of the Mg-Ca chemical association) that overprint the Mg-Ca and less commonly the K, K-Mg-Fe, and Mg-Fe chemical associations, and Ca-rich metasomatism during deformation and metamorphism shows that, despite an overall preservation of the pre-metamorphism bulk-rock geochemical compositions, syn-metamorphic metasomatism locally occurred and led to changes in the bulk geochemical compositions and textures of the metamorphosed altered rocks. Moreover, the circulation of H_2O- and CO_2-rich fluids during metamorphism (Tinkham, 2013) may have remobilized Au along with minor amounts of Pb, Cu, Zn, and Ag.

Remobilization of Au and Formation of Au-rich Ore Lenses

Gold-rich sulphide-poor mineralization at Lalor occurs dominantly in rocks of the Mg-Ca chemical association. However, several Au-rich mineralization occurrences are situated in rocks of the Mg-Fe chemical association and rocks unaffected by the VMS-related alteration, including post-VMS mafic dykes that crosscut the sulphide lenses. Moreover, Au-rich mineralization preferentially occurs in competent amphibole-rich rocks, and ore textures suggest that the timing of this mineralization is late- to post-D_2. Collectively this indicates that the Au-rich, sulphide-poor mineralization was formed, at least in part, by the remobilization of Au along with minor amounts of Ag, Zn, Cu, and Pb during deformation and metamorphism. The scale of this remobilization remains unresolved, but it may have been in the range of centimetres to tens of metres. Importantly, Au-rich, sulphide-poor ore zones are always located in close proximity (within tens of metres) to VMS mineralization, and are entirely enclosed in the intensely altered footwall halo, which suggests that the Au was introduced into the rocks as part of the VMS-forming hydrothermal system. The Au-rich sulphide-poor ore zones may be the result of a pre-deformation, epithermal-style overprint on the VMS system, but most of the diagnostic characteristics of epithermal systems are lacking. The confinement of the Au mineralization within the VMS system also indicates that the bulk of the Au input probably occurred during the formation of the VMS deposit and not during metamorphism.

Various processes can lead to the remobilization of Au during metamorphism (Tomkins, 2007). At Lalor, Au-rich sulphide-poor mineralization is characterized by a specific metallic association (Duff et al., 2013, 2015). Specific mineral assemblages attributed to syn-deformation metamorphic metasomatism are commonly associated with Au mineralization (actinolite-rich layers of the Mg-Ca chemical association or Ca-rich metasomatism; Caté et al., 2014b,c); however, this association is not systematic (universal) and this could be due to the more competent nature of these amphibole-rich mineral assemblages. Moreover, the presence of sulphosalts in the Au mineralization indicates that the remobilization may have (partly or wholly) occurred during sulphide anatexis (Frost et al., 2002; Tomkins et al., 2006). However, hydrothermal remobilization may also have been important, and further work is needed to assess the contribution of the various remobilization processes.

IMPLICATIONS FOR EXPLORATION

The results presented here have various implications for mineral exploration at the deposit to regional scales, not only at Lalor but also elsewhere in metamorphosed volcanic belts. Prospectivity in the Chisel sequence is not limited to the Lower – Upper Chisel subsequences contact (Caté et al., 2014a). As in other districts (e.g.

Blake River Group: McNicoll et al., 2014), VMS deposits can occur at multiple stratigraphic levels in the Snow Lake camp. Volcanogenic massive sulphide deposits in the Chisel sequence are not necessarily preferentially associated with felsic volcanic rocks (e.g. Chisel, Chisel North, Ghost, Lost, and Photo deposits and Lalor lowermost lenses; Bailes and Galley, 1996; Caté et al., 2014a), but can be associated with mafic volcanic rocks (Lalor uppermost lenses; Caté et al., 2014a).

The bulk geochemical compositions of hydrothermally altered rocks have undergone only minor and local changes during post-ore deformation and metamorphism, and exploration vectors adapted from less metamorphosed rocks can be applied to deposits metamorphosed at amphibolite grade (e.g. Caté et al., 2014c). Moreover, the $\delta^{18}O$ signature of the hydrothermally altered rocks has been preserved through metamorphism and can be used as an exploration vector toward high-temperature reaction zones (Mercier-Langevin et al., 2014).

The presence of atypical metamorphic mineral assemblages (metamorphosed hydrothermally altered volcanic rocks), and changes in the nature and relative abundance of metamorphic minerals can be used to vector toward mineralization (Caté et al., 2014c). The wide variety of mineral assemblages and their coarse-grained nature allows for a better identification of the variations in primary alteration styles and paleo-hydrothermal alteration pathways in the field (Galley et al., 1993). The use of geochemistry and mineralogy (chemical association) can further help navigate within paleo-hydrothermal systems.

The present-day geometry of the Lalor deposit is dominantly structurally controlled by the D_2 deformation (Caté et al., 2014b,d), and the local D_2 foliation and stretching lineation must be taken into account at all scales. Moreover, local mechanical remobilization of ductile ore minerals (e.g. sphalerite and chalcopyrite) occurred, and led to the formation of structurally controlled mineralization at various scales.

The Au-rich zones result predominantly from local metamorphic remobilization of Au, most likely from the primary VMS mineralization (Caté et al., 2014d). The silicate gangue minerals are probably not genetically associated with the Au mineralization but likely served as a competent trap for locally remobilized Au. Exploration for Au-rich ore zones in VMS deposits affected by high-grade metamorphism should not be restricted to rocks affected by intense hydrothermal alteration, and drilling should be extended around the main massive sulphide bodies as shown by the presence of Au-rich sulphide-poor zones at Lalor.

FUTURE WORK

Results presented here are part of an ongoing Ph.D. thesis project by the senior author. Current and future work include the following: 1) a complete structural analysis of the deposit host sequence and structural influences on the geometry of the ore lenses and distribution of metals; 2) a 3-D reconstruction of the volcanic architecture and hydrothermal alteration system; and 3) the integration of all available data and information to complete a genetic model of the deposit, including the timing and processes of Au enrichment.

ACKNOWLEDGEMENTS

The authors thank HudBay Minerals Inc. and its personnel for the opportunity to study the Lalor deposit, permission to publish, continued support, and constructive discussions. Our research at Lalor is funded by the Geological Survey of Canada (GSC) through the Targeted Geoscience Initiative 4 program (TGI-4), and by HudBay Minerals Inc. A. Bailes, D. Tinkham, H. Gibson, B. Lafrance, M. Engelbert, J. Lam, V. Friesen, and A. Galley are thanked for their collaboration and for sharing their knowledge of the Snow Lake camp. S. Pehrsson is thanked for her review of a previous version of the manuscript. Thanks to J. Peter for his reviews and editorial handling.

REFERENCES

Bailes, A.H., 2008. Geological setting of the Lalor and Photo Lake VMS deposits; HudBay Internal Report, Bailes Geoscience, 45 p.

Bailes, A. and Galley, A., 1996. Setting of Paleoproterozoic volcanic-hosted massive base metal sulphide deposits, Snow Lake, *In:* EXTECH 1: a multidisciplinary approach to massive sulphide research in the Rusty Lake–Snow Lake greenstone gelts, Manitoba, (ed.) G. Bonham-Carter, A.G. Galley, and G.E.M. Hall; Geological Survey of Canada, Bulletin 426, p. 105–138.

Bailes, A.H. and Galley, A.G., 1999. Evolution of the Paleoproterozoic Snow Lake arc assemblage and geodynamic setting for associated volcanic-hosted massive sulphide deposits, Flin Flon Belt, Manitoba, Canada; Canadian Journal of Earth Sciences, v. 36, p. 1789–1805.

Bailes, A. H., Rubingh, K., Gagné, S., Taylor, C., Galley, A., Bernauer, S., and Simms, D., 2013. Volcanological and structural setting of Paleoproterozoic VMS and gold deposits at Snow Lake, Manitoba; Geological Association of Canada-Mineralogical Association of Canada, Joint Annual Meeting, Winnipeg, Manitoba, May 22–24, 2013, Field Trip Guidebook, Manitoba Innovation, Energy and Mines, Manitoba Geological Survey, 63 p.

Caté, A., Mercier-Langevin, P., Ross, P.-S., Duff, S., Hannington, M., Dubé, B., and Gagné, S., 2013. The Paleoproterozoic Lalor VMS deposit, Snow Lake, Manitoba: preliminary observations on the nature and architecture of the gold- and base metal-rich ore and alteration zones; Geological Survey of Canada, Open File 7483, 19 p.

Caté, A., Mercier-Langevin, P., Ross, P.-S., Duff, S., Hannington, M., Gagné, S., and Dubé, B., 2014a. Insight on the chemostratigraphy of the volcanic and intrusive rocks of the Lalor auriferous VMS deposit host succession, Snow Lake,

Manitoba; Geological Survey of Canada, Current Research 2014-6, 19 p.

Caté, A., Mercier-Langevin, P., Ross, P.-S., and Simms, D., 2014b. Structural controls on geometry and ore distribution in the Lalor volcanogenic massive-sulphide deposit, Snow Lake, west-central Manitoba (part of NTS 63K16): preliminary results from underground mapping, *In:* Report of Activities 2014; Manitoba Mineral Resources, Manitoba Geological Survey, p. 104–115.

Caté, A., Mercier-Langevin, P., Ross, P.-S., Duff, S., Hannington, M., Dubé, B., and Gagné, S., 2014c. Deciphering the multiple hydrothermal, metasomatic and structural events responsible for the formation and post-depositional evolution of the Paleoproterozoic Lalor auriferous VMS deposit, Snow Lake, Manitoba, *In:* Program with Abstracts; Geological Association of Canada-Mineralogical Association of Canada Annual Meeting, Fredericton, May 20–22, 2014, p. 52–53.

Caté, A., Mercier-Langevin, P., Ross, P.-S., Simms, D., Duff, S., and Dubé, B., 2014d. Structural controls on the Lalor VMS deposit geometry and ore distribution - preliminary results, *In:* Program with Abstracts; Manitoba Mining and Minerals Convention 2014, Winnipeg.

David, J., Bailes, A.H., and Machado, N., 1996. Evolution of the Snow Lake portion of the Palaeoproterozoic Flin Flon and Kisseynew belts, Trans-Hudson Orogen, Manitoba, Canada; Precambrian Research, v. 80, p. 107–124.

Duff, S., Caté, A., Hannington, M., Mercier-Langevin, P., and Ross, P.-S., 2013. Major ore types of the Lalor deposit, Snow Lake, Manitoba, *In:* Program with Abstracts; Geological Society of America Meeting, v. 45, no 7, p. 806.

Duff, S., Hannington, M.D., Caté, A., Mercier-Langevin, P., and Kjarsgaard, I.M., 2015. Major ore types of the Paleoproterozoic Lalor auriferous volcanogenic massive sulphide deposit, Snow Lake, Manitoba, *In:* Targeted Geoscience Initiative 4: Contributions to the Understanding of Volcanogenic Massive Sulphide Deposit Genesis and Exploration Methods Development, (ed.) J.M. Peter and P. Mercier-Langevin; Geological Survey of Canada, Open File 7853, p. 147–170.

Engelbert, M.S., Friesen, V., Gibson, H., and Lafrance, B., 2014. Volcanic reconstruction of the productive VMS ore interval in the Paleoproterozoic Chisel sequence, Snow Lake, Manitoba, *In:* Program with Abstracts; Geological Association of Canada-Mineralogical Association of Canada Annual Meeting, Fredericton, May 20-22, 2014, p. 83–84.

Franklin, J.M., 1993. Volcanic-associated massive sulphide deposits, *In:* Mineral Deposit Modeling, (ed.) R.V. Kirkham, W.D. Sinclair, R.I. Thorpe, and J.M. Duke; Geological Association of Canada Special Paper 40, p. 315–334.

Frost, B.R., Mavrogenes, J.A., and Tomkins, A.G., 2002. Partial melting of sulfide ore deposits during medium- and high-grade metamorphism; Canadian Mineralogist, v. 40, p. 1–18.

Galley, A.G., Bailes, A.H., and Kitzler, G., 1993. Geological setting and hydrothermal evolution of the Chisel Lake and North Chisel Zn-Pb-Cu-Ag-Au massive sulfide deposits, Snow Lake, Manitoba; Exploration and Mining Geology, v. 2, p. 271–295.

Galley, A.G., Syme, R., and Bailes, A.H., 2007. Metallogeny of the Paleoproterozoic Flin Flon Belt, Manitoba and Saskatchewan, in Mineral Deposits of Canada: A Synthesis of Major Deposit Types, District Metallogeny, the Evolution of Geological Provinces, and Exploration Methods, (ed.) W.D. Goodfellow; Geological Association of Canada, Mineral Deposits Division, Special Publication 5, p. 509–531.

Gifkins, C., Herrmann, W., and Large, R.R., 2005. Altered volcanic rocks: A guide to description and interpretation; Hobart, Tasmania, Australia, Centre for Ore Deposit Research, University of Tasmania, 275 p.

HudBay Minerals Inc. , 2014, Lalor operation webpage, http://www.hudbayminerals.com/English/Our-Business/Operations/Lalor/default.aspx .

Kelly, W.C. and Clark, B.R., 1975. Sulfide deformation studies; III, Experimental deformation of chalcopyrite to 2,000 bars and 500 degrees C; Economic Geology, v. 70, p. 431–453.

Kraus, J. and Williams, P.F., 1999. Structural development of the Snow Lake Allochthon and its role in the evolution of the southeastern Trans-Hudson Orogen in Manitoba, central Canada; Canadian Journal of Earth Sciences, v. 36, p. 1881–1899.

Large, R.R., Gemmell, J.B., Paulick, H., and Huston, D.L., 2001. The alteration box plot: a simple approach to understanding the relationship between alteration mineralogy and lithogeochemistry associated with volcanic-hosted massive sulfide deposits; Economic Geology, v. 96, p. 957–971.

Martin, P., 1966. Structural analysis of Chisel Lake orebody; Canadian Mining & Metallurgical Bulletin, v. 69, p. 208–214.

McNicoll, V., Goutier, J., Dubé, B., Mercier-Langevin, P., Ross, P.-S., Dion, C., Monecke, T., Legault, M., Percival, J., and Gibson, H., 2014. U-Pb geochronology of the Blake River Group, Abitibi greenstone belt, Quebec, and implications for base metal exploration; Economic Geology, v. 109, p. 27–59.

Menard, T. and Gordon, T.M., 1997. Metamorphic P-T paths from the eastern Flin Flon belt and Kisseynew domain, Snow Lake, Manitoba; Canadian Mineralogist, v. 35, p. 1093–1115.

Mercier-Langevin, P., Hannington, M.D., Dubé, B., and Bécu, V., 2011. The gold content of volcanogenic massive sulfide deposits; Mineralium Deposita, v. 46, p. 509–539.

Mercier-Langevin, P., Caté, A., and Ross, P.-S., 2014. Whole-rock oxygen isotope mapping, Lalor auriferous VMS deposit footwall alteration zones, Snow Lake, west-central Manitoba (NTS 63K16), *In:* Report of Activities 2014; Manitoba Mineral Resources, Manitoba Geological Survey, p. 94–103.

Pearce, J.A., 1996. A user's guide to basalt discrimination diagrams, *In:* Trace Element Geochemistry of Volcanic Rocks: Applications for Massive Sulphide Exploration, (ed) D.A. Wyman; Geological Association of Canada, Short Course Notes, p. 79–113.

Ross, P.-S. and Bédard, J.H., 2009. Magmatic affinity of modern and ancient subalkaline volcanic rocks determined from trace-element discriminant diagrams; Canadian Journal of Earth Sciences, v. 46, p. 823–839.

Tinkham, D.K., 2013. A model for metamorphic devolatilization in the Lalor deposit alteration system, Snow Lake, MB, *In:* Program with Abstracts; Geological Association of Canada-Mineralogical Association of Canada Annual Meeting, Winnipeg, May 22–24, 2013, p. 187.

Tomkins, A.G., 2007. Three mechanisms of ore re-mobilisation during amphibolite facies metamorphism at the Montauban Zn-Pb-Au-Ag deposit; Mineralium Deposita, v. 42, p. 627–637.

Tomkins, A.G., Pattison, D.R.M., and Frost, B.R., 2006. On the initiation of metamorphic sulfide anatexis; Journal of Petrology, v. 48, p. 511–535.

Winchester, J.A. and Floyd, P.A., 1977. Geochemical discrimination of different magma series and their differentiation products using immobile elements; Chemical Geology, v. 20, p. 325–343.

GEOLOGICAL SURVEY OF CANADA
OPEN FILE 7853

Targeted Geoscience Initiative 4: Contributions to the Understanding of Volcanogenic Massive Sulphide Deposit Genesis and Exploration Methods Development

Major ore types of the Paleoproterozoic Lalor auriferous volcanogenic massive sulphide deposit, Snow Lake, Manitoba

Shamus Duff[1], Mark D. Hannington[1], Antoine Caté[2], Patrick Mercier-Langevin[3], and Ingrid M. Kjarsgaard[4]

[1]University of Ottawa, Ottawa, Ontario
[2]Institut national de la recherche scientifique, Québec, Quebec
[3]Geological Survey of Canada, Québec, Quebec
[4]Consulting Mineralogist, Ottawa, Ontario

2015

Recommended citation

Duff, S., Hannington, M.D., Caté, A., Mercier-Langevin, and Kjarsgaard, I.M., 2015. Major ore types of the Paleoproterozoic Lalor auriferous volcanogenic massive sulphide deposit, Snow Lake, Manitoba, *In:* Targeted Geoscience Initiative 4: Contributions to the Understanding of Volcanogenic Massive Sulphide Deposit Genesis and Exploration Methods Development, (ed.) J.M. Peter and P. Mercier-Langevin; Geological Survey of Canada, Open File 7853, p. 147–170.

Publications in this series have not been edited; they are released as submitted by the author.

Contribution to the Geological Survey of Canada's Targeted Geoscience Initiative 4 (TGI-4) Program (2010–2015)

TABLE OF CONTENTS

Figures

Tables

Major ore types of the Paleoproterozoic Lalor auriferous volcanogenic massive sulphide deposit, Snow Lake, Manitoba

Shamus Duff[1,*], Mark D. Hannington[1†], Antoine Caté[2], Patrick Mercier-Langevin[3], and Ingrid M. Kjarsgaard[4]

[1]Department of Earth Sciences, University of Ottawa, Ottawa, Ontario K1N 6N5
[1]Institut national de la recherche scientifique, 490 rue de la Couronne, Québec, Quebec G1K 9A9
[2]Geological Survey of Canada, 490 rue de la Couronne, Québec, Quebec G1K 9A9
[4]Consulting Mineralogist, 15 Scotia Place, Ottawa, Ontario K1S 0W2
*Corresponding author's e-mail: sduff088@uottawa.ca
†Corresponding author's e-mail: mark.hannington@uottawa.ca

ABSTRACT

The Lalor deposit is a newly discovered Paleoproterozoic volcanogenic massive sulphide (VMS) deposit located at the east end of the Flin Flon-Snow Lake belt, within the Snow Lake arc assemblage. Lalor is the largest of 11 VMS deposits in the Snow Lake arc assemblage, with combined resources and reserves of 25.3 Mt and average grades of 2.9 g/t Au, 25 g/t Ag, 5 wt% Zn, and 0.79 wt% Cu, including 8.8 Mt at 4.6 g/t Au. Lalor and all other deposits in the Snow Lake arc assemblage have been affected by intense polyphase deformation and amphibolite facies metamorphism. As a result, both the original hydrothermal alteration assemblages and the ore mineral assemblages have been completely recrystallized. However, a variety of different ore types have been preserved, allowing the partial reconstruction of the hydrothermal system, including massive Fe-Zn sulphide lenses, discordant Cu-Au stringer zones, and distinctive precious metal-rich Au-Ag-Pb-Cu zones. The different ore types occur in a series of stratigraphically and structurally "stacked" ore lenses that partly overlap but still largely preserve the original architecture of the deposit.

The ore is distributed in 12 discrete lenses or zones of mineralization that are interpreted to be the result of several distinct and overlapping hydrothermal events. Type 1 Fe-Zn massive sulphide ore is the most common ore type in 6 ore lenses and consists of massive coarse-grained pyrite and sphalerite with trace galena in dominantly quartz-muscovite±kyanite-biotite schist (K-alteration association). Type 2 Cu-Au mineralization consists of semi-massive and stockwork chalcopyrite and pyrrhotite in garnetiferous quartz-biotite±staurolite-amphibole-cordierite gneisses (footwall Mg-Fe alteration association). Despite extensive recrystallization and local remobilization, these two ore types are interpreted to represent the (metamorphosed) low- and high-temperature ore assemblages, respectively, of a typical volcanogenic massive sulphide deposit. Type 3 Au-Ag-Pb-Cu-rich ore consists of stringer and disseminated sulphides and sulphosalts mainly hosted in chlorite-carbonate-actinolite schist (Mg-Ca and Ca alteration associations). Galena is an important indicator of Au mineralization and occurs in this ore type as fine-grained blebs in a matrix of chlorite, dolomite, calcite, anthophyllite, Ca-plagioclase, and calc-silicates (epidote, grossular, diopside, Ca-amphibole ± scapolite). Where abundant, the galena is associated with chalcopyrite, pyrite, and pyrrhotite, and with minor to trace sphalerite, Ag-Sb-Pb sulphosalts, electrum, and native gold. Type 4 low-sulphide ore contains ≤10 vol% disseminated pyrite in quartz-biotite-anthophyllite gneiss, with minor chlorite, staurolite, and coarse almandine garnet, and has variable Au grades. The sulphides and sulphosalts in ore types 3 and 4 are interpreted to be metamorphically remobilized from pre-existing disseminated mineralization.

The hydrothermal system developed during two main episodes of seafloor volcanism. Type 1 massive sulphide in the 10 and 11 lenses and in the 20, 30, 31, and 40 lenses were formed at the paleoseafloor. These lenses are underlain by Type 2 Cu-Au stockwork mineralization (27 Lens) and originally conformable zones of Type 3 Au-Ag-Pb mineralization (21, 24, 25, 26, and 28 lenses). The large Cu-Au stockwork zone (27 Lens) may have been the main feeder of the deposit and is partly continuous with disseminated Au-Ag-Pb-Cu galena-sulphosalts-chalcopyrite mineralization below the 20 Lens. The Au-Ag-Pb-Cu mineralization is thought to have formed in the subseafloor from late-stage, lower temperature hydrothermal fluids (approximately <300°C). In this model, significant Au was introduced first by high-temperature (>300°C) fluids responsible for the Type 2 Cu-Au mineralization and then by lower temperature (possibly boiling) hydrothermal fluids responsible for Type 3 Ag-Au-Pb-Cu mineralization. Although all the ore types are extensively recrystallized and partly remobilized, their distribution strongly supports primary hydrothermal

Duff, S., Hannington, M.D., Caté, A., Mercier-Langevin, and Kjarsgaard, I.M., 2015. Major ore types of the Paleoproterozoic Lalor auriferous volcanogenic massive sulphide deposit, Snow Lake, Manitoba, *In:* Targeted Geoscience Initiative 4: Contributions to the Understanding of Volcanogenic Massive Sulphide Deposit Genesis and Exploration Methods Development, (ed.) J.M. Peter and P. Mercier-Langevin; Geological Survey of Canada, Open File 7853, p. 147–170.

Au enrichment at Lalor. The lead isotopic compositions of the ore galena show no evidence of post-magmatic disturbance, which would be expected if Au had been introduced during deformation and metamorphism (e.g. as in the nearby New Britannia orogenic Au deposit), and the Au-rich assemblages are very similar to those that commonly occur in unmetamorphosed Au-rich volcanogenic massive sulphide deposits.

INTRODUCTION

The Lalor volcanogenic massive sulphide (VMS) deposit is located in Snow Lake, Manitoba, 200 km east of the Flin Flon and 777 deposits. The Snow Lake camp has been a prolific producer of base metals and Au since 1949, with more than 10 past-producing VMS deposits (Table 1) as well as the closed New Britannia (formerly Nor Acme) orogenic Au mine. Lalor is the largest VMS deposit to have been put into production in Snow Lake and the only currently operating mine in the area. The combined resources and reserves total 25.3 Mt with grades of 2.9 g/t Au, 25 g/t Ag, 5 wt% Zn and 0.79 wt% Cu (HudBay Minerals Inc., 2014), including 8.8 Mt at 4.6 g/t Au, making it the largest and richest VMS deposit of the Snow Lake camp (Mercier-Langevin et al., 2014). The Au grades are among the highest of any deposit in the Flin Flon-Snow Lake belt, rivalling those of the nearby Chisel North and Photo Lake auriferous VMS deposits (e.g. Galley et al., 2007). This paper describes the main ore lenses of the Lalor deposit and the spatial and paragenetic relationships of the different ore types, with the aim of better constraining the Au-enrichment processes and their relative timing.

REGIONAL AND DEPOSIT GEOLOGY

The 10 past-producing VMS mines in the Snow Lake district (Rod, Stall, Anderson, Ghost, Chisel, Chisel North, Photo Lake, Osborne Lake, Reed Lake, and Spruce Point) and the currently operating Lalor Mine are located in the Snow Lake arc assemblage (SLA; Fig. 1). The Lalor deposit is in the lower portion of the Chisel sequence (termed Lower Chisel subsequence), together with the Chisel, Lost, and Ghost Zn-Cu deposits and the Photo Lake auriferous VMS deposit (Fig. 2; Bailes and Galley, 1999; Bailes, 2009; Bailes et al., 2013; Caté et al., 2014; Engelbert et al., 2014a,b). The Lower Chisel subsequence consists of bimodal mafic and felsic volcanic rocks, dominated by mafic volcaniclastic rocks and aphyric basalt and the Powderhouse dacite unit. These rocks are overlain by the Threesomes basalt (Galley et al., 2007), which marks the transition between the lower and upper parts of the Chisel sequence (Bailes and Galley, 1996; Engelbert, et al., 2014a,b). The Chisel and Chisel North deposits are spatially associated with rhyolite domes, located close to the contact between the Upper and Lower Chisel subsequences (Galley et al., 1993; Bailes and Galley, 1996; Bailes, 2009). The Anderson sequence, which underlies the Chisel sequence and hosts the Stall, Rod, and Anderson deposits, consists dominantly of aphyric basalt and small felsic centres. In contrast to the deposits of the Chisel sequence, which are dominantly Zn-Cu deposits, the deposits of the Anderson sequence are distinctly Cu-rich (Bailes et al., 2013).

Table 1. Grades and tonnage of current and past-producing volcanogenic massive sulphide deposits of Snow Lake (after Bailes et al., 2013).

Mine	Tonnes	Au (g/t)	Ag (g/t)	Cu (wt%)	Zn (wt%)
Chisel Sequence					
Lalor Zn-Cu	18100000	0.64	25.24	0.64	8.97
Lalor Cu-Au	5400000	4.7	30.6	0.47	0.46
Chisel	7153532	1.76	44.76	0.54	10.6
Chisel North	2606212	0.58	21.43	0.21	9.49
Ghost and Lost	581438	1.2	39.09	1.34	8.6
Photo Lake	689885	4.9	29.38	4.58	6.35
Anderson Sequence					
Stall	6381129	1.41	12.34	4.41	0.5
Rod	735219	1.71	16.11	6.63	2.9
Anderson	2510000	0.62	7.54	3.4	0.1
Other					
Schist Lake	1846656	1.3	37.03	4.3	7.27
Osborne	2807471	0.27	4.11	3.14	1.5
Spruce Point	1865095	1.68	19.54	2.06	2.4
Reed Lake	2720000	0.62	7.63	4.5	0.89

The Snow Lake arc assemblage is affected by at least four episodes of deformation associated with the Trans-Hudson orogeny (Kraus and Williams, 1999). The D_1 and D_2 events produced tight, isoclinal, south-verging folds, shallowly dipping thrusts, and the main foliation (Kraus and Williams, 1999; Bailes et al., 2013). These structures are refolded by north-north-east-trending F_3 folds and an associated S_3 crenulation cleavage (Martin, 1966; Kraus and Williams, 1999). The F_4 folds with east-trending axes locally overprint F_3 folds (Kraus and Williams, 1999). In the Lalor deposit, $D_{1\text{-}2}$ and D_3 structures largely control the geometry of the ore lenses (Caté et al., 2014a). Volcanic units in the host succession are generally oriented parallel to the main $S_{1\text{-}2}$ foliation and dip to the northeast (Caté et al., 2014a). The hanging-wall rocks are part of a separate volcanic succession in structural contact with the Lalor volcanic succession (Caté et al., 2014b) that dips steeply toward the northeast (Bailes, 2008, 2011).

The ore lenses of the Lalor deposit are located in the uppermost section of a volcanic succession that has

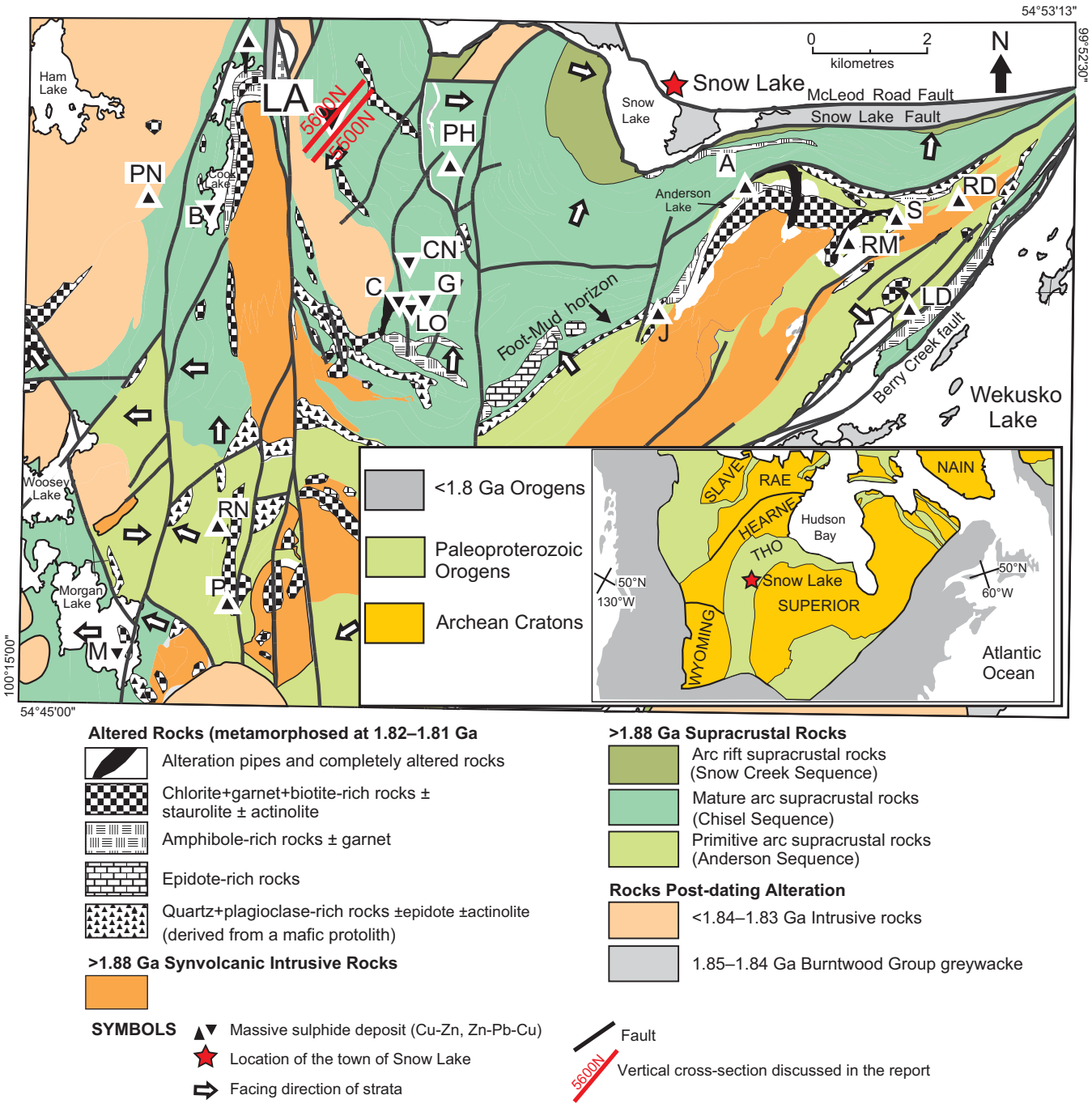

Figure 1. Simplified geological map of the Snow Lake area (from Galley et al., 2007), showing major alteration zones and volcanogenic massive sulphide deposits, including the Lalor deposit (LA). Other deposits: A = Anderson; B = Bomber zone; C = Chisel Lake; CN = Chisel North; G = Ghost; J = Joannie zone; LO = Lost; LD = Linda zone; M = Morgan Lake zone; P = Pot Lake zone; PH = Photo Lake; PN = Pen zone; RD = Rod; RM = Ram zone; RN = Raindrop zone; S = Stall Lake. The location of the Snow Lake area in North America is shown in the inset map.

been intensely hydrothermally altered (Lalor volcanic succession: Caté et al., 2014b). The hydrothermal alteration was metamorphosed to amphibolite facies during D_{1-2}, with syn- to late-D_2 peak conditions estimated at ~5 kbar and temperatures up to 550°C (Zaleski et al., 1991; Menard and Gordon, 1997; Lam et al., 2013, 2014; Tinkham, 2013). The metamorphic mineral assemblages have been correlated with whole-rock lithogeochemistry and define 5 distinct chemical associations (K-rich, K-Fe-Mg, Mg-Fe, Mg-Ca, and Ca) described by Caté et al. (2013a,b, 2015).

SAMPLING AND ANALYTICAL METHODS

In June through August 2012, 11 exploration drillholes along section 5600 N were logged and sampled in detail (Fig. 3). The drill core was logged in the interval

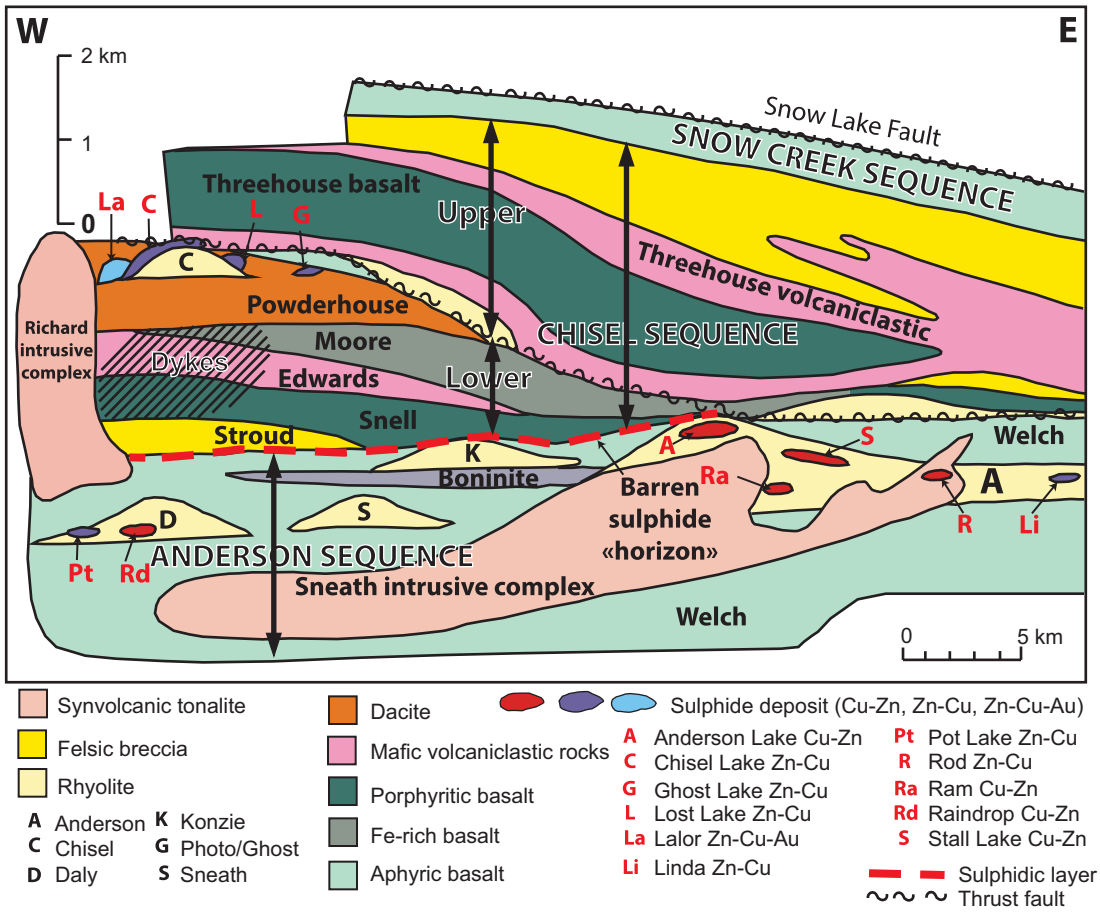

Figure 2. Schematic cross-section through the Snow Lake arc assemblage (Bailes et al., 2013, modified from Bailes and Galley, 1999), showing the positions of the Lalor, Chisel, Lost, and Ghost Zn-Cu deposits and the Photo Lake Au-rich volcanogenic massive sulphide deposit in the upper portion of the Chisel Sequence.

starting 50 m above the first sign of significant mineralization to the end of the hole. Samples were collected wherever strong mineralization was intersected, with the aim of encompassing the entire deposit and obtaining representative samples of all the different ore types. An additional 10 exploration holes were logged along section 5300 N. All logging and sampling was completed between May and August 2013. During this time, the mine opened and was in a pre-production phase, allowing the opportunity to map and sample underground in 5 areas between 795 and 865 m below surface. Results of the underground mapping and sampling are presented in Caté et al. (2014a, 2015).

Seventy drill-core samples were selected for detailed petrographic study and chemical analysis, including major metals, oxides, and trace elements. Splits of each sample were crushed using a steel jaw crusher (in order to increase Au content and minimize cross-contamination), then pulverized in a Cr-steel mill, both at the University of Ottawa. Pulverized samples were analyzed at Activation Laboratories in Ancaster, Ontario. SiO_2, Al_2O_3, Fe_2O_3, MnO, MgO, CaO, Na_2O, K_2O, TiO_2, P_2O_5, Sc, Be, V, Sr, and Ba were analyzed by peroxide fusion followed by dissolution and inductively couple plasma optical emission spectrometry (FUS-ICPOES). Silver, As, Bi, Ce, Co, Cr, Cu, Dy, Er, Eu, Ga, Gd, Ge, Hf, Ho, In, La, Lu, Mo, Nb, Nd, Ni, Pb, Pr, Rb, Sb, Sm, Sn, Tb, Tm, Ta, Tl, Th, U, W, Y, Yb, and Zr were analyzed by fusion followed by ICP mass spectrometry (FUS-ICPMS). Silver, Cd, Co, Cr, Cu, In, Li, Mn, Mo, Ni, Pb, and Zn were analyzed by 4-acid total dissolution followed by ICP mass spectrometry (TD-ICPMS). Tellurium, Se, As, Bi, and Sb were analyzed by hydride generation and ICPMS, and Hg was analyzed on a flow injection mercury system (Hg-FIMS). Gold and Ag were analyzed by fire assay with a graphite-furnace atomic absorption finish. Fluorine was analyzed by specific ion electrode, and B was analyzed by prompt gamma neutron activation analysis (PGNAA). Total C, S, and CO_2 were analyzed by combustion and infrared detection (IR). Loss on ignition was also determined by combustion. FeO was determined by titration. The full analytical data, including detections limits and reproducibility are included in the M.Sc. thesis of S. Duff (in prep.).

Petrographic descriptions of the main ore types were supplemented by microanalysis of representative ore minerals, and gangue by wavelength dispersive X-ray

a)

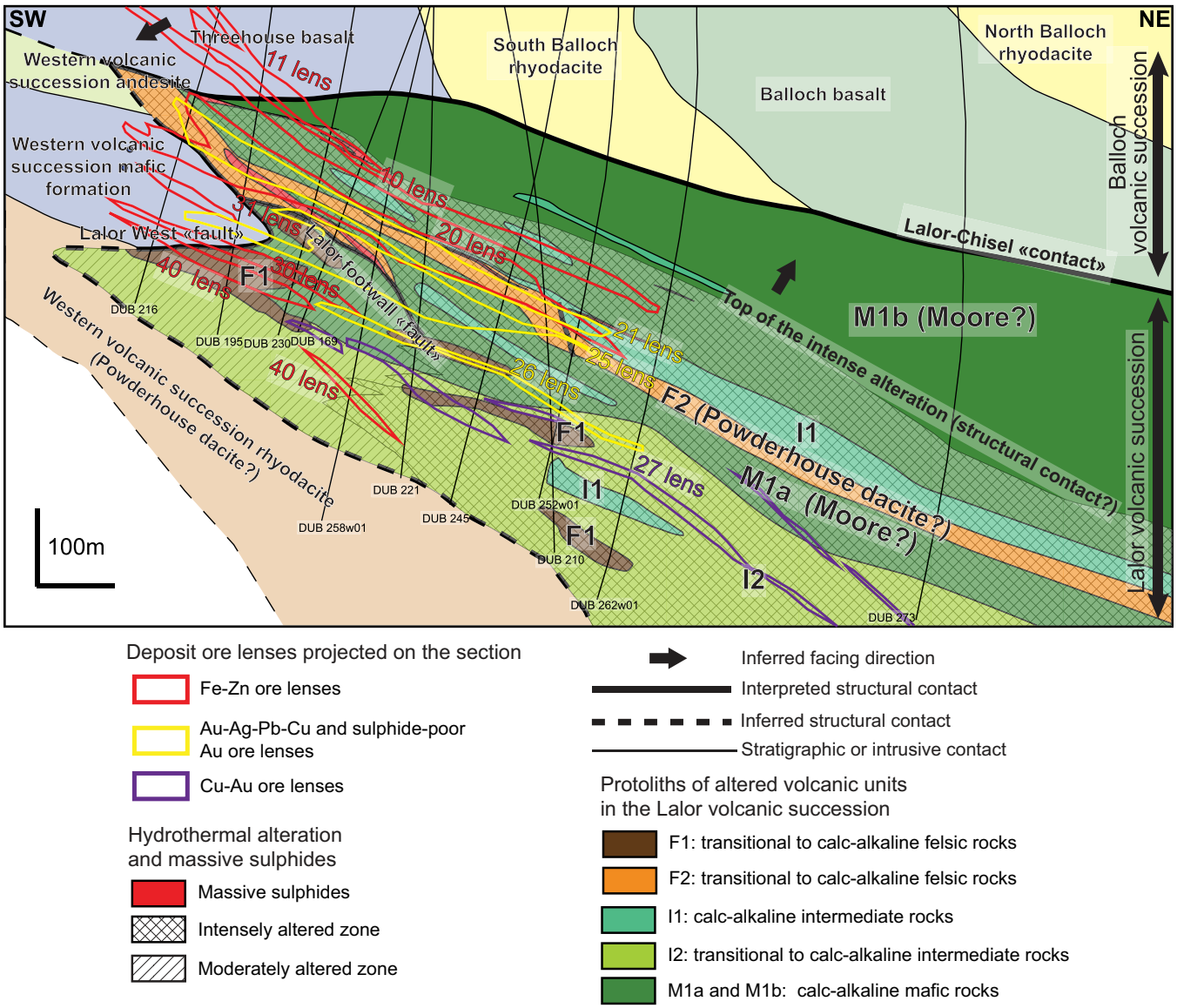

Figure 3. Schematic cross-section of the Lalor deposit at 5600 N (looking northwest) from Caté et al. (2014). The approximate locations of the main Fe-Zn massive sulphide, Au-Ag-Pb-rich ore zones, and Au-Cu zones discussed in the text are shown. 10 Lens is projected from section 5500 N. Inferred lithologies are from Caté et al. (2014) and (Bailes, 2008).

analysis (WDX) using a four-spectrometer Camebax MBX electron microprobe at the Earth Sciences Department of Carleton University, Ottawa. Sulphur isotope analyses were made on selected mineral separates of pyrite, chalcopyrite, pyrrhotite, sphalerite, and galena at the University of Ottawa's G.G. Hatch Stable Isotope Laboratory. Lead isotope ratios of galena were determined at Carleton University's Isotope Geochemistry and Geochronology Center (IGGC).

DISTRIBUTION OF THE ORE LENSES

Unlike other deposits in the Snow Lake camp, the ore at Lalor is distributed among many different lenses. The currently defined resource has been divided into 12 ore lenses. Assay data for the main lenses considered in this study are shown in Table 2. Some of the ore lenses (main massive sulphide lenses 10, 11, 20, 30, 31, and 40) are conformable with the host stratigraphy (dipping ~30°) and are stacked. The longest dimensions of most of these lenses strike northwest-southeast; however, the 20 Lens, in the middle of the succession, strikes north-south, possibly indicating an intersecting fault control. Although the 6 main massive sulphide lenses are stacked, Bailes (2011) and Caté et al. (2014, 2015) suggest that there are fewer primary ore horizons, and numerous thrust faults and/or folds are likely responsible for the dismemberment and "stacking" of multiple sulphide zones. They recognized only two paleoseafloor horizons, one containing the 10 and 11 lenses and the other hosting the 20, 30, 31, and 40 lenses (Bailes et al., 2013; Caté et al., 2014a,b). The lithogeochemically distinct rock types that host the

Table 2. Average ore grades of the different lenses discussed in the text (from Hudbay Minerals Inc.).

Lens	Ore Type	Au (g/t)	Ag (g/t)	Cu (wt%)	Zn (wt%)	Pb (wt%)	Fe (wt%)
Fe-Zn							
10	Type 1	2.12	23.58	0.79	11.48	0.25	25.28
11	Type 1	0.21	17.1	0.26	12.13	0.06	27.88
20	Type 1	2.49	31.16	0.91	8.37	0.32	19.59
31	Type 1	2.67	30.33	0.24	5.86	0.45	18.55
30	Type 1	1.67	28.25	0.3	5.36	0.56	17.06
40	Type 1	2. 11	36.2	0.49	7.99	0.92	15.42
Au-Cu							
27	Type 2	8.38	22.63	4.45	0.29	0.02	8.63
Au-Ag-Pb							
21	Type 3	6.98	41.02	0.91	2.07	0.27	7.7
24	Type 3	7.13	32.13	0.3	1.42	0.4	4.74
25	Type 3	6.33	31.16	0.31	0.83	0.28	4.33
26	Type 3	6.31	38.07	0.67	0.48	0.38	6.42
28	Type 3	4.66	21.17	0.49	0.57	0.06	4.88

massive sulphide lenses confirm that they formed during separate volcanic episodes (Caté et al., 2014b, 2015). Discordant stockwork mineralization is spatially associated with the upper lenses (10 and 11) but has not been recognized in association with the lower lenses. Substantial Au enrichment is most closely associated with discordant Cu-Au stockwork mineralization in the 27 Lens and with broadly conformable disseminated Au-Ag-Pb-Cu mineralization in the 21, 24, 25, 26, and 28 lenses. The largest zone of Au-Ag-Pb-Cu mineralization is in the footwall of the 20 massive sulphide lens and is underlain by the discordant Cu-Au stockwork mineralization of the 27 Lens. Brief descriptions of the main massive sulphide ore lenses and their different host rocks are given below.

10 and 11 Lenses

The 10 and 11 lenses are structurally and stratigraphically the highest ore zones in the Lalor volcanic sequence. The 10 Lens consists of massive and semi-massive pyrite and sphalerite within quartz-muscovite-pyrite schist (K-alteration association). Chloritic zones with stringer chalcopyrite mineralization occur at the base of the 10 Lens. In most places, the contact between the hanging-wall rocks and the massive sulphides is sharp; locally there is a narrow transition from semi-massive pyrite-sphalerite into quartz-muscovite-pyrite schist. Wall rocks immediately above the 10 and 11 lenses are strongly pyritized, with abundant muscovite and kyanite. Locally, kyanite comprises up to 25 vol.% of the rock as porphyroblasts up to 2 cm in size.

The contact between the massive sulphides and the underlying chloritic schist is generally gradational, with increasing chlorite and chalcopyrite content and decreasing pyrite and sphalerite in the footwall. Massive chlorite is common in the ore zones. Volcanic rocks in the footwall contain abundant quartz, biotite, and chlorite, with coarse Mg-Fe amphibole (anthophyllite), kyanite, staurolite, and garnet porphyroblasts (K-Mg-Fe and Mg-Fe alteration association). Garnet is most commonly almandine garnet, which can vary from centimetre-sized up to massive 10 cm porphyroblasts. Although Cu-rich stockwork mineralization is well developed beneath the 10 Lens, the 11 Lens lacks a stringer zone and is thought to be a structurally dislocated portion of the 10 Lens.

20 Lens

The 20 Lens also consists of massive and semi-massive pyrite and sphalerite, but the hydrothermal alteration zoning in the immediate host rocks is more complex, owing to the presence of several different parent lithologies. In section 5300 N, the hanging wall is a quartz-biotite-muscovite-kyanite assemblage (K-alteration association), similar to the hanging wall of the 10 and 11 lenses and weakly altered intermediate rocks. Further north (section 5600 N), the hanging wall is chlorite schist with abundant carbonate that is locally associated with Ca-rich (skarn-like) diopside, epidote, grossular, and actinolite-tremolite alteration. Bright orange Ca-rich grossular is locally present in this alteration style. The footwall is dominantly chlorite-carbonate schist, but kyanite, muscovite, garnet, staurolite, anthophyllite, and/or talc are also present, representing complex transitions between the K, K-Mg-Fe, Mg-Fe, Mg-Ca, and Ca associations.

30, 31, and 40 Lenses

The 30, 31, and 40 lenses consist of both massive and semi-massive sulphides, with carbonate, actinolite and chlorite gangue minerals. The hanging wall and footwall of the 30 and 31 lenses consist of alternating chlorite-carbonate and chlorite-actinolite/tremolite assemblages (Ca-Mg-alteration association: Caté et al., 2015). Coarse magnetite crystals are also present in the hanging wall. The 40 Lens is the deepest zone of massive sulphides in the mine but it is thought to have formed at the same stratigraphic horizon as the 30 and 31 lenses, owing to the presence of similar host rocks and alteration styles. Quartz, plagioclase, and biotite, with abundant garnet and minor anthophyllite, are dominant about 15 m below the ore zone and are considered to represent the metamorphic equivalent of moderately altered mafic, intermediate, and felsic volcanic rocks in the footwall of the lenses (Caté et al., 2014).

METAL ZONATION

The 10 Lens shows the expected VMS zonation, with

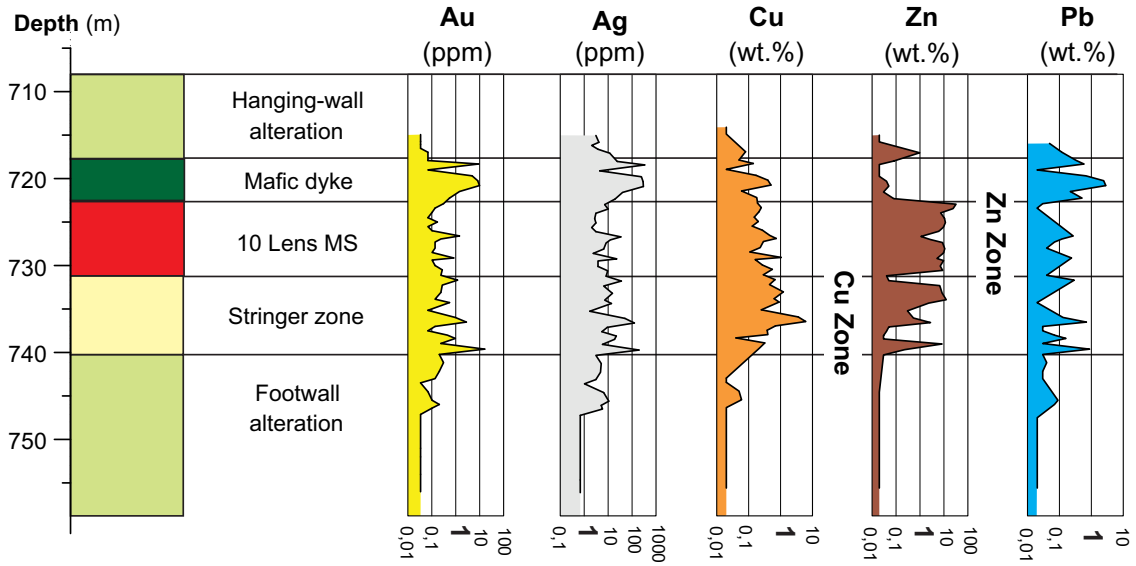

Figure 4. Composite graphic log of metal zonation in drillholes DUB174 and DUB239 through the 10 Lens massive sulphide zone, showing the expected volcanogenic massive sulphide zonation with Fe-Zn in the upper portion of the lens and then Cu-Au stringer mineralization at the base.

Fe-Zn in the upper portion of the lens and a discordant, although strongly transposed, Cu-Au stringer zone at the base (Fig. 4). The 20 Lens lacks a Cu-Au stringer zone but is underlain (and possibly partly overprinted) by disseminated Au-Ag-Pb-Cu-rich mineralization. A large portion of the Au-rich 21 Lens cuts the western part of the 20 Lens (on section 5600 N) and extends into the hanging wall. The 31 Lens is similarly cut by the Au-rich 25 Lens. For the most part, however, the Au-Ag-Pb-Cu-rich ore zones are broadly conformable. This conformable nature may indicate that heterogeneous permeability of the volcanic pile was a major control on mineralization. The large zone of semi-massive and stockwork-like chalcopyrite mineralization in the 27 Lens is stratigraphically the lowest occurrence of ore in the mine and may have been a central feeder zone for the entire deposit, in agreement with the high-temperature alteration in this part of the sequence (Caté et al., 2014; Mercier-Langevin et al., 2014). Although metamorphic remobilization of metals is apparent in all ore types, the scale of the remobilization is generally restricted to the ore lenses, with the large-scale metal zonation remaining intact (see also Gagné et al., 2007).

ORE TYPES OF THE LALOR DEPOSIT

Four main ore types have been identified among the different ore lenses (Table 3). Some can be compared to mineralization typical of unmetamorphosed VMS deposits, but others may be hybrid ore types related to hydrothermal overprinting and the effects of metamorphic recrystallization and remobilization.

Type 1 Fe-Zn Massive Sulphide

Fe-Zn-rich massive sulphide (Fig. 5a,b) is volumetrically the most abundant ore type and dominates in 6 of the 12 delineated ore lenses. The 10 and 11 Fe-Zn lenses are contained mostly within quartz-muscovite-pyrite rocks of the K-alteration association, and the 20, 30, 31, and 40 Fe-Zn lenses are mostly hosted by chlorite-carbonate-actinolite/tremolite schists of the Mg-Ca-alteration association (Caté et al., 2015). Disseminated pyrite is abundant in the quartz-muscovite-altered rocks (Fig. 5c). Although mostly intact bodies, slivers of the ore lenses, up to several metres across, occur in the adjacent wall rocks, displaced from the lenses by folding and transposition. Similarly, large enclaves of altered and foliated wall rocks are locally enclosed within massive sulphides (e.g. Bailes, 2011;

Figure 5 (opposite page). Photographs of representative ore types in NQ drill core (47.6 mm or 1-7/8 in diameter) from the Lalor deposit. **a)** Type 1 Fe-Zn-rich massive sulphide from 10 Lens (drillhole DUB174, 834.3–838.6 m), containing mostly euhedral pyrite with atoll structures in a matrix of Fe-rich sphalerite. **b)** Type 1 massive pyrite-sphalerite ore from 10 Lens (drillhole DUB205, 788.0–805.0 m). **c)** Disseminated pyrite in the foliations of a quartz-biotite schist from the hanging wall of the 31 Lens (drillhole DUB174, 872.0 m). **d)** Type 2 semi-massive chalcopyrite with pyrrhotite from the type locality in the 27 Lens (drillhole DUB263W05, 1270 m). **e)** Type 2 stockwork chalcopyrite mineralization with garnet porphyroblasts in a quartz-biotite matrix (Mg-Fe alteration association) from the 27 Lens (drillhole DUB263W05). **f)** Type 2 massive chalcopyrite with large garnet porphyroblasts from the 27 Lens (drillhole DUB262W05, 1271.3 m). **g)** Type 3 Au-Ag-Pb-Cu galena-sulphosalts-chalcopyrite ore in chlorite-carbonate-actinolite schist (Mg-Ca alteration association), typical of the 21, 24, and 25 lenses (drillhole DUB210, 1038.8 m). The fine-grained, steel grey matrix is galena. **h)** Type 4 low-sulphide ore with disseminated chalcopyrite-pyrrhotite-pyrite in quartz-chlorite-biotite schist (Mg-Fe alteration association) from the 25 Lens (drillhole DUB245; 995.8–1005.9 m).

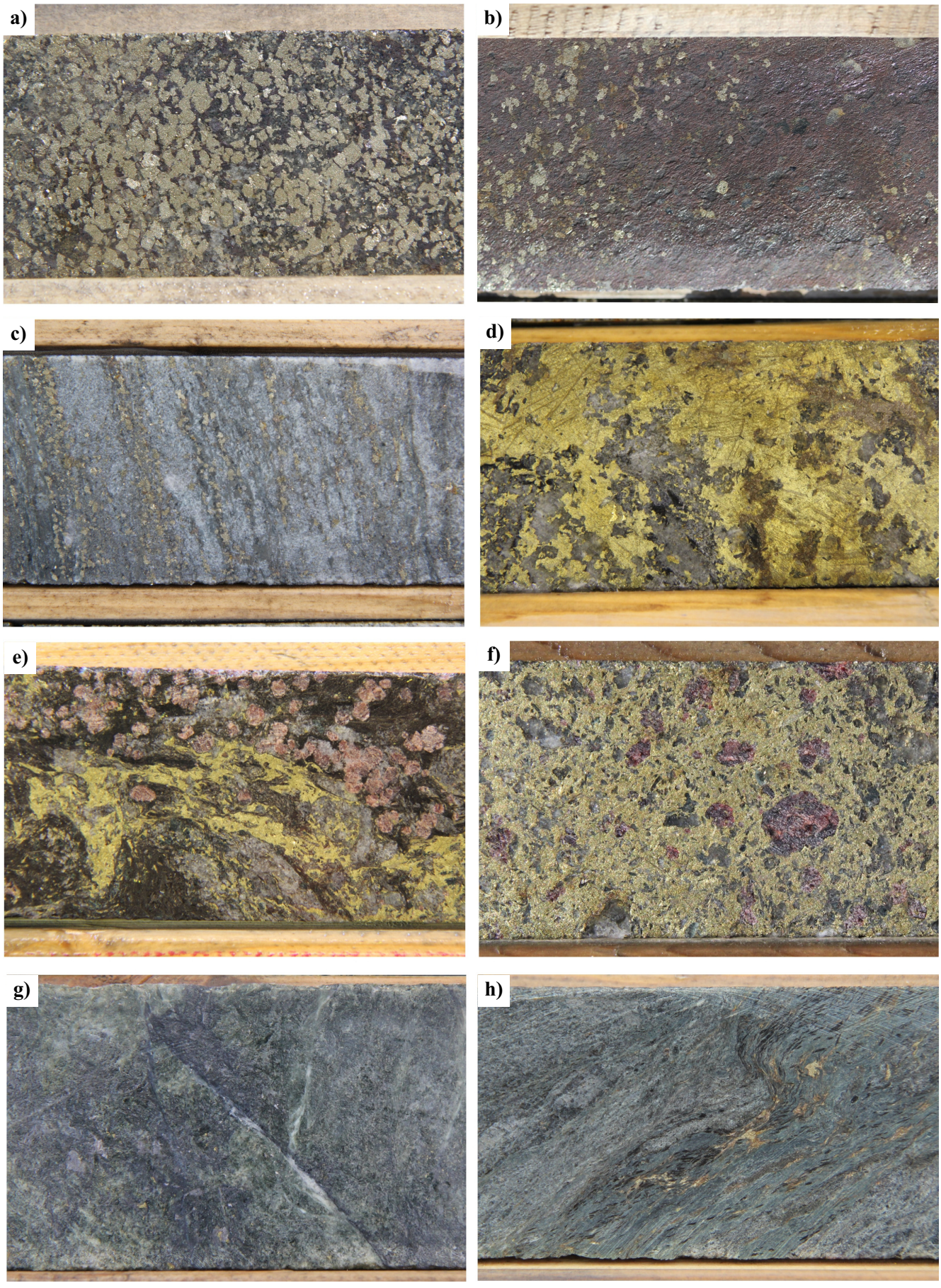
a)
b)
c)
d)
e)
f)
g)
h)

Table 3. Principal ore types of the Lalor volcanogenic massive sulphide deposit, Snow Lake.

Ore Type		Dominant Sulphides	Host Rock and Gangue Minerals
Type 1 (Fe-Zn)	Massive sulphides	Coarse-grained pyrite, sphalerite, ±pyrrhotite, ±chalcopyrite, ±galena	Quartz-muscovite schist
Type 2 (Au-Cu)	Semi-massive and stockwork	Semimassive and stringer chalcopyrite, ±pyrrhotite	Garnetiferous quartz-biotite schist and gneiss; large garnet porphyroblasts, ±cordietite, ±anthophyllite, ±staurolite
Type 3 (Au-Ag-Pb)	Chlorite-carbonate	Stringer and disseminated galena, ±sulphosalts, ±pyrite, ±sphalerite, ±chalcopyrite, ±pyrrhotite	Chlorite-carbonate schist; mainly dolomite and calc-silicates (epidote, grossular, diopside)
Type 4 (±Au)	Low-sulphide	Disseminated and stringer pyrite, ±chalcopyrite, ±pyrrhotite, ±sphalerite	Quartz-biotite-chlorite schist; ±almandine garnet, ±anthophyllite, ±staurolite

Caté et al., 2014a). The sulphide mineralogy is generally the same in all of the lenses and is dominated by pyrite and sphalerite (10–70 vol.%); pyrrhotite and chalcopyrite are minor minerals (less than 10 vol.%). Galena is rare but present in fractures and tension gashes within fold hinges and especially where several mafic intrusions cut the upper massive sulphide lenses (10 and 11). The mafic dykes are folded, boudinaged, and S_2-foliated, suggesting that they were intruded before the main D_2 deformation, and remobilized sulphides are common at their margins and in crosscutting fractures. A number of features clearly indicate the extent of recrystallization and annealing of the massive sulphides, including the presence of coarse-grained polycrystalline aggregates with well developed triple junctions, large pyrite porphyroblasts (up to 5 cm), and *durchbewegung* texture (see below).

Type 2 Cu-Au-Rich Semi-Massive and Stockwork Mineralization

The Cu- and Au-rich semi-massive and stockwork mineralization is hosted in garnetiferous chlorite schist of the Mg-Fe alteration association immediately beneath the 10 Lens, and at depth in intensely altered quartz- and biotite-bearing rocks. Semi-massive (10–60 vol.%) chalcopyrite occurs in the immediate stratigraphic footwall of the 10 Lens, and disseminated and stringer mineralization (<10 vol.% chalcopyrite) grades outward into the surrounding wall rock. Masses of pyrrhotite are present locally within the chalcopyrite (Fig. 5d). In contrast, the strongly transposed, stockwork-like Cu-Au mineralization in the 27 Lens, much deeper in the footwall, is not physically connected to massive sulphide ore higher up in the Lalor volcanic succession. The semi-massive chalcopyrite-pyrrhotite ore typically contains abundant quartz and biotite, and large (0.5–5 cm) garnet porphyroblasts that are commonly surrounded by networks of remobilized chalcopyrite (Fig. 5e,f). Quartz flooding and veins of quartz with ankerite are also common. The adjacent wall rocks, which consist of the deep footwall, transposed high-temperature Mg-Fe alteration association (Mercier-Langevin et al., 2014; Caté et al., 2015), commonly contain quartz, cordierite, and anthophyllite with minor chlorite, and locally porphyroblasts of staurolite and garnet. The anthophyllite forms arborescent growths up to 5 cm in length, and the cordierite occurs as royal blue massive aggregates.

Type 3 Au-Ag-Pb-Cu-Rich Ore

The main precious metal-rich ore consists mostly of disseminated sulphides and sulphosalts comprising up to 5 vol.% galena (Fig. 5g) and 2 vol.% chalcopyrite. The nature of the host rock varies but garnet- and amphibole-bearing rocks of the Mg-Fe chemical alteration association and chlorite-actinolite and Fe-dolomite-calcite schist of the Mg-Ca and Ca association (e.g. footwall of the 20 Lens) are the most common host. Pyrite, sphalerite, chalcopyrite, and pyrrhotite are minor components that commonly occur as isolated grains in the cleavages of chlorite and in low-pressure zones between porphyroblasts of garnet.

Figure 6 (opposite page). Photomicrographs of representative ore textures in the main ore types of the Lalor deposit. **a)** Type 1 Fe-Zn massive sulphide with a large, fractured poikiloblastic pyrite grain infilled by pyrrhotite and chalcopyrite, in a matrix of dark grey sphalerite (drillhole DUB195, 824.3 m, reflected plane polarized light (PPL), field of view (FOV)=4.4 mm). **b)** Type 1 Fe-Zn massive sulphide with large poikiloblastic pyrite euehdra in a matrix of massive sphalerite (drillhole DUB195, 823.2 m, transmitted light, FOV=4.4 mm). **c)** Disseminated pyrite, chalcopyrite, and arsenopyrite rimming quartz inclusions in massive sphalerite. A gold grain is adjacent to chalcopyrite at the rim of a rounded quartz inclusion (drillhole DUB210, 1045.0 m, reflected PPL, FOV=1 mm). **d)** Close-up of Type 2 semi-massive Cu-Au ore in drill core showing chalcopyrite occurring as rims on, and inclusions in, large (1 cm) garnet porphyroblasts (drillhole DUB262W05, 1271.3 m). **e)** Typical poikiloblastic garnet with inclusions of pyrite, pyrrhotite, and chalcopyrite (drillhole DUB262W01, 980.5 m, reflected PPL, FOV=1 mm). **f)** Typical fine-grained disseminated galena in quartz (drillhole DUB210, 1045.0 m, reflected PPL, FOV=1.1 cm). **g)** Pyrite and pyrrhotite in cleavages within quartz-chlorite-biotite hosting Type 2 Cu-Au ore (drillhole DUB258W01, 946.5 m, reflected PPL, FOV=4.4 mm). h) Typical texture of sulphides in cleavages within quartz-muscovite-garnet schist (drillhole DUB205, 815.2 m, transmitted light, FOV=4.4 mm).

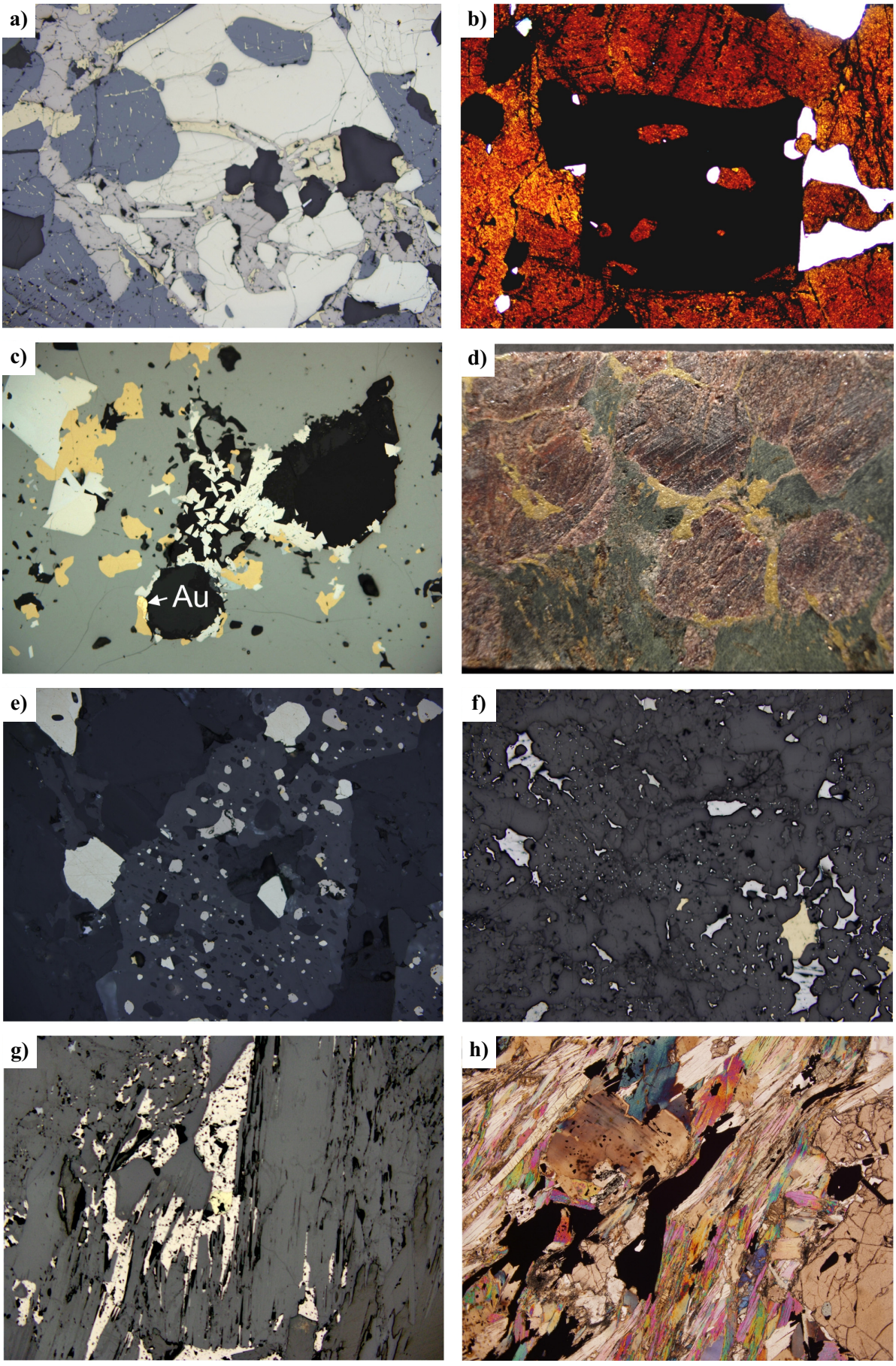
a)
b)
c)
Au
d)
e)
f)
g)
h)

This style of mineralization is typically isolated from the main massive sulphide lenses and is best developed in the 21, 24, 25 West, 26 and 28 lenses. In general, the galena is a strong prognostic indicator of Au grade in all of these lenses. The chlorite-carbonate-actinolite rocks locally include skarn-like assemblages with a variety of calc-silicates (epidote, grossular, diopside ± scapolite), corresponding to the Mg-Ca and Ca alteration associations of Caté et al. (2015).

Type 4 Low-Sulphide Quartz-Pyrite Mineralization

Low-sulphide quartz-pyrite ore consists of quartz-biotite-anthophyllite rock with a distinctive gneissic or schistose texture. This ore type has locally high Au grades. Sulphide contents do not exceed 10 vol.% and generally do not correlate with Au grade. Pyrite is dominant, but chalcopyrite, sphalerite, and pyrrhotite are present locally in low-pressure zones between cleavages of the major phyllosilicate minerals and adjacent to porphyroblasts (Fig. 5h). Staurolite and anthophyllite are also present locally. Type 4 mineralization is spatially associated with Au-Ag-Pb-Cu-rich galena-sulphosalts-chalcopyrite ore in several lenses (e.g. in the 21, 24, and 25 lenses) and occurs in the same broad zones of mineralization and locally grades into Au-Ag-Pb-Cu-rich ore over distances of a few metres.

ORE MINERALOGY AND MINERAL CHEMISTRY

Pyrite

In the massive sulphide lenses, pyrite occurs as coarse-grained polycrystalline aggregates, in 2–5 cm patches with intergranular sphalerite. Elsewhere, pyrite occurs as isolated porphyroblasts in a homogenous sphalerite matrix. In many places, pyrite porphyroblasts show evidence of brittle deformation with fractures filled by sphalerite and other sulphides (Fig. 6a,b). In other places, pyrite and sphalerite are clearly segregated into discontinuous gneissic bands. Classic durchbewegung texture is common, in which hard (6.0–6.5), brittle pyrite and locally quartz nodules show evidence of rotation in a flowing matrix of softer (ductile) sphalerite (Fig. 7; Craig and Simpson, 1991). All analyzed pyrite is nearly stoichiometric FeS_2. However, some pyrite contains up to 2 wt% Co, especially where intergrown with pyrrhotite. Some pyrite also contains up to 0.1 wt% Ni and up to 1 wt% As (Table 4).

Sphalerite

Sphalerite in the massive sulphide lenses is coarsely crystalline "blackjack", with high Fe contents (Table 4). Where it is most abundant, sphalerite is commonly associated with Fe-rich carbonate. Coarse-grained polycrystalline aggregates with curved or straight grain boundaries are most common, but locally the sphalerite occurs in homogenous masses, typically with chalcopyrite inclusions distributed in a gridded network (e.g. chalcopyrite disease: Barton and Bethke, 1987) (Fig. 6a) or more commonly remobilized to grain boundaries (Fig. 6c). The average Fe content of sphalerite is 7.65 wt% (more than 15 mol.% FeS: Table 4) and is very homogeneous throughout most of the deposit. Cd contents are generally low (<5 wt%, average 2.3 wt%). Hg is present in detectable abundances but never exceeds 0.10 wt%. In the 40 Lens, the sphalerite is orange, indicating much lower Fe contents, which contrasts with the blackjack sphalerite in the rest of the deposit and may possibly be a result of metamorphic reactions.

Figure 7. Photograph of classic *durchbewegung* texture (Craig and Simpson, 1991) in type 1 Fe-Zn-rich massive sulphide ore (DUB195, 809.7 m). The texture shows rounded nodules of hard pyrite and quartz nodules in a matrix of softer sphalerite. NQ drill core (47.6 mm or 1-7/8 in diameter).

Chalcopyrite, Bornite, and Cubanite

Disseminated chalcopyrite is present as isolated blebs and anhedral masses in the massive sulphide ores, and these generally increase in abundance toward the bottoms of the lenses. In the Cu-Au stockwork zones, chalcopyrite occurs as discrete stringers within the main foliation of the altered host rocks, rimming large garnet porphyroblasts (Fig. 6d), and disseminated in the cleavages of the major gangue minerals. The chalcopyrite is nearly stoichiometric $CuFeS_2$ throughout the deposit (Table 4), although several grains of Ag-bearing chalcopyrite (up to 4 wt% Ag) were identified in association with Ag-sulphosalts. Traces of cubanite are present as exsolution lamellae in the chalcopyrite, typically as thin peach-coloured flames and locally as distinct crystallographically controlled bands intersecting at 60 and 120°. Bornite also occurs locally as inclusions in chalcopyrite and rarely with galena, electrum, and sulphosalts in Type 3 Au-Ag-Pb-Cu-rich ore.

Pyrrhotite

Pyrrhotite is present in the massive sulphide ores, com-

Table 4. Electron microprobe analyses of selected ore minerals of the Lalor massive sulphide deposit (average, minimum, and maximum values for n samples).

Mineral	(n)	S	Fe	Co	Ni	Cu	Zn	Ga	As	Se	Ag	Cd	In	Sn	Sb	Te	Au	Hg	Pb	Bi	Total
Major and Minor Minerals																					
Pyrite	27	53.7	47.29	0.27	0.02	0.01	0.02	0.01	0.11	0.02	0.02	0.02	0.01	0.01	<0.01	0.01	0.03	0.03	<0.01	0.12	101.71
FeS_2	min	52.23	45.61	<0.01	<0.01	<0.01	<0.01	<0.01	<0.01	<0.01	<0.01	<0.01	<0.01	<0.01	<0.01	<0.01	<0.01	<0.01	<0.01	<0.01	100.54
	max	55.18	48.07	2.08	0.12	0.09	0.09	0.07	1.4	0.05	0.09	0.07	0.04	0.05	<0.01	0.08	0.1	0.14	0.09	0.21	103.5
Pyrrhotite	30	38.8	60.97	0.01	0.02	0.02	0.02	0.02	0.01	0.02	0.02	0.01	<0.01	0.01	<0.01	0.01	0.03	0.01	0.06	0.09	100.13
FeS	min	37.39	59.9	<0.01	<0.01	<0.01	<0.01	<0.01	<0.01	<0.01	<0.01	<0.01	<0.01	<0.01	<0.01	<0.01	<0.01	<0.01	<0.01	<0.01	98.94
	max	40	62	0.05	0.13	0.14	0.09	0.09	0.05	0.09	0.11	0.07	0.05	0.05	<0.01	0.04	0.14	0.09	0.47	0.23	101.54
Sphalerite	19	32.24	7.65	0.01	0.01	0.54	55.97	0.18	0.01	0.02	0.01	2.32	<0.01	0.01	0.01	<0.01	0.04	0.02	0.05	0.07	99.17
ZnS	min	31.56	3.85	<0.01	<0.01	<0.01	52	0.04	<0.01	<0.01	<0.01	0.02	<0.01	<0.01	<0.01	<0.01	<0.01	<0.01	<0.01	<0.01	96.77
	max	32.82	9.24	0.03	0.07	3.57	60.14	0.32	0.03	0.06	0.06	5.1	0.05	0.06	0.07	0.01	0.16	0.09	0.35	0.17	100.94
Chalcopyrite	13	34.34	30.56	0.01	0.01	34.41	0.05	0.01	0.01	0.03	0.04	0.03	<0.01	0.01	0.01	0.01	0.02	0.01	0.09	0.07	99.72
$CuFeS_2$	min	33.91	29.84	<0.01	<0.01	34.04	<0.01	<0.01	<0.01	<0.01	<0.01	<0.01	<0.01	<0.01	<0.01	<0.01	<0.01	<0.01	<0.01	<0.01	98.21
	max	34.74	30.88	0.03	0.03	34.88	0.15	0.03	0.04	0.07	0.26	0.07	0.01	0.03	0.15	0.03	0.08	0.11	0.29	0.24	100.44
Cubanite	6	34.85	41.06	<0.01	0.02	23.3	<0.01	0.02	<0.01	0.02	0.09	0.01	0.01	0.01	<0.01	0.01	0.04	0.01	0.11	0.12	99.67
$CuFe_2S_3$	min	34.43	40.51	<0.01	<0.01	23.11	<0.01	<0.01	<0.01	<0.01	<0.01	<0.01	<0.01	<0.01	<0.01	<0.01	<0.01	<0.01	<0.01	0.07	98.4
	max	35.42	41.39	0.01	0.06	23.49	0.01	0.05	0.01	0.05	0.26	0.03	0.04	0.02	<0.01	0.04	0.23	0.04	0.38	0.2	100.51
Arsenopyrite	8	21.68	35.97	0.02	0.01	0.18	0.04	<0.01	42.63	0.27	0.02	0.01	<0.01	0.01	0.25	0.1	0.04	0.02	0.05	0.05	101.35
FeAsS	min	20.13	34.67	<0.01	<0.01	<0.01	0.01	<0.01	39.15	0.22	<0.01	<0.01	<0.01	<0.01	<0.01	0.01	<0.01	<0.01	<0.01	<0.01	98.97
	max	24.61	37.4	0.05	0.02	0.62	0.14	<0.01	45.47	0.31	0.06	0.07	0.03	0.04	1.73	0.23	0.11	0.11	0.19	0.14	101.98
Galena	12	13.59	0.03	0.01	<0.01	0.05	0.04	0.01	<0.01	0.38	0.05	0.04	<0.01	0.01	0.05	0.04	0.02	<0.01	85.3	0.06	99.71
PbS	min	13.19	<0.01	<0.01	<0.01	0.01	<0.01	<0.01	<0.01	0.05	<0.01	<0.01	<0.01	<0.01	<0.01	<0.01	<0.01	<0.01	84.49	<0.01	98.92
	max	13.92	0.18	0.03	0.01	0.18	0.1	0.04	0.03	0.6	0.22	0.13	0.03	0.04	0.15	0.12	0.09	0.04	86.03	0.3	100.66
Gold	7	0.06	0.79	0.01	0.01	0.09	<0.01	0.17	0.02	<0.01	22.99	0.01	<0.01	0.3	0.01	0.03	73.94	2.67	0.01	0.02	101.13
(Au,Ag)	min	<0.01	0.07	<0.01	<0.01	<0.01	<0.01	<0.01	<0.01	<0.01	12.1	<0.01	<0.01	<0.01	<0.01	<0.01	63.22	<0.01	<0.01	<0.01	100.26
	max	0.12	2.66	0.02	0.03	0.21	<0.01	0.61	0.07	0.01	29.19	0.08	<0.01	1.32	0.07	0.07	87.52	7.95	0.04	0.17	101.98
Electrum	11	0.05	0.17	0.01	0.01	0.11	0.02	<0.01	0.03	0.01	50.85	0.06	<0.01	0.13	0.62	0.09	43.83	3.88	0.05	0.01	99.92
(Au,Ag)	min	<0.01	<0.01	<0.01	<0.01	<0.01	<0.01	<0.01	<0.01	<0.01	40.21	<0.01	<0.01	<0.01	<0.01	0.06	16.86	0.09	<0.01	<0.01	98.21
	max	0.19	0.39	0.04	0.03	0.33	0.2	<0.01	0.28	0.02	78.55	0.3	<0.01	0.97	2.68	0.16	54.53	7.49	0.28	0.16	101.59
Tetrahedrite	7	25.53	6.38	<0.01	<0.01	37.77	0.76	<0.01	7.24	0.09	3.68	0.07	<0.01	0.06	19.17	<0.01	0.01	<0.01	0.01	0.05	100.85
$(Cu,Ag)_{12}(Sb,As)_4S_{13}$	min	24.38	6.01	<0.01	<0.01	34.19	0.32	<0.01	1.13	0.04	1.44	<0.01	<0.01	0.02	15.34	<0.01	<0.01	<0.01	<0.01	<0.01	99.62
	max	26.41	6.77	0.01	0.02	40.16	1.22	0.01	9.96	0.13	6.94	0.15	0.01	0.13	27.3	<0.01	0.05	0.01	0.08	0.15	101.78
Freibergite	13	22.6	5.73	0.01	0.01	23.04	0.67	<0.01	1.66	0.03	20.54	0.42	<0.01	0.07	24.86	<0.01	0.02	<0.01	0.07	0.04	99.77
$(Ag,Cu)_{12}(Sb,As)_4S_{13}$	min	18.58	5.05	<0.01	<0.01	12.85	0.25	<0.01	0.03	<0.01	12.39	0.12	<0.01	<0.01	14.26	<0.01	<0.01	<0.01	<0.01	<0.01	98.01
	max	24.99	7.22	0.04	0.04	30.34	1.16	<0.01	10.05	0.22	36.65	1.08	<0.01	0.12	28.18	<0.01	0.06	<0.01	0.35	0.15	101.22

Table 4 continued.

Mineral	(n)	S	Fe	Co	Ni	Cu	Zn	Ga	As	Se	Ag	Cd	In	Sn	Sb	Te	Au	Hg	Pb	Bi	Total
Bournonite (As)	9	19.85	0.05	0.01	0.01	13.03	0.03	0.01	1.76	0.27	0.02	0.03	0.01	0.11	22.66	0.04	<0.01	<0.01	41.94	0.09	99.92
$PbCuSbS_3$	min	19.31	<0.01	<0.01	<0.01	12.52	<0.01	<0.01	0.09	0.11	<0.01	<0.01	<0.01	0.07	18.22	<0.01	<0.01	<0.01	41.29	<0.01	99.07
	max	20.32	0.2	0.03	0.05	13.61	0.1	0.05	4.78	0.43	0.07	0.1	0.03	0.14	25.13	0.14	0.01	<0.01	42.43	0.17	101.07
Boulangerite (As)	4	18.3	0.04	0.01	<0.01	0.05	0.02	<0.01	0.47	0.17	0.18	0.07	<0.01	0.12	25.13	<0.01	0.03	<0.01	54.23	0.09	98.92
$Pb_5Sb_4S_{11}$	min	18.2	<0.01	<0.01	<0.01	<0.01	<0.01	<0.01	0.02	<0.01	<0.01	<0.01	<0.01	0.09	24.27	<0.01	<0.01	<0.01	53.6	<0.01	98.32
	max	18.45	0.14	0.01	<0.01	0.2	0.06	<0.01	1.74	0.32	0.69	0.18	<0.01	0.15	26	<0.01	0.11	<0.01	54.85	0.27	99.18
Allargentum	4	2	0.02	0.01	<0.01	0.08	<0.01	<0.01	0.05	0.01	75.02	0.3	<0.01	0.01	17.99	0.05	4.65	0.13	0.07	0.02	100.4
$Ag_{1-x}Sb_x$	min	0.88	<0.01	<0.01	<0.01	<0.01	<0.01	<0.01	<0.01	<0.01	73.24	0.25	<0.01	<0.01	13.91	<0.01	1.76	<0.01	<0.01	<0.01	99.11
	max	3.19	0.04	0.02	<0.01	0.2	<0.01	<0.01	0.08	0.02	77.17	0.34	<0.01	0.03	20.11	0.1	7.35	0.35	0.14	0.05	102.1
Trace Minerals																					
Ag-Chalcopyrite $CuFeS_2$	2	32.45	28.96	<0.01	<0.01	32.19	0.03	0.05	0.03	0.03	3.71	0.02	<0.01	<0.01	<0.01	0.01	0.04	<0.01	0.19	0.05	97.75
Galena (Se) Pb(S,Se)	3	12.51	0.53	0.02	<0.01	0.01	0.04	0.01	<0.01	2.45	0.06	0.02	<0.01	0.09	0.03	0.04	0.04	<0.01	83.89	<0.01	99.75
Cobaltite CoAsS	1	19.96	4.97	29.46	0.46	<0.01	<0.01	<0.01	43.32	0.3	<0.01	<0.01	<0.01	0.05	1.07	<0.01	0.04	<0.01	0.1	0.14	99.86
Gudmundite FeSbS	2	15.14	26.78	<0.01	0.16	0.05	<0.01	0.05	0.27	0.01	0.01	<0.01	<0.01	0.25	58.5	0.09	0.03	<0.01	0.08	0.01	101.42
Meneghinite $Pb_{13}CuSb_7S_{24}$	2	17.86	<0.01	0.01	0.01	1.29	0.03	<0.01	0.06	0.18	0.05	<0.01	<0.01	0.06	19.77	0.01	0.02	<0.01	61.35	0.07	100.77
Sterryite $Ag_2Pb_{10}(Sb,As)_{12}S_{29}$	2	18.94	0.08	0.01	<0.01	0.36	0.07	0.02	0.11	0.19	3.62	<0.01	<0.01	0.15	26.86	<0.01	0.07	<0.01	49.69	0.02	100.19
Ag-Pentlandite $(Ag,Fe,Ni)_9S_8$	1	31.88	38.15	0.08	15.72	1.7	<0.01	<0.01	0.04	0.03	12.64	<0.01	<0.01	<0.01	<0.01	0.03	<0.01	<0.01	<0.01	0.05	100.31
Benleonardite $Ag_8(Sb,As)Te_2S_3$	1	6.07	0.04	<0.01	0.01	<0.01	<0.01	<0.01	0.01	0.39	63.3	0.23	<0.01	0.05	7.38	23.6	0.01	<0.01	<0.01	0.1	101.2
Stützite(?) Ag_5Te_3	1	1.23	1.8	<0.01	<0.01	0.15	0.03	<0.01	<0.01	0.02	57.83	0.28	<0.01	0.68	<0.01	31.76	0.06	0.1	1.31	<0.01	95.25

monly as rims around pyrite or in pressure shadows. It is always closely associated with chalcopyrite, especially in the Type 2 semi-massive and stockwork chalcopyrite ore. Locally pyrrhotite is also present in late quartz veins, commonly with gahnite. Like pyrite, the pyrrhotite is essentially stoichiometric FeS (Table 4). One euhedral grain of Ag-pentlandite $(Ag,Fe,Ni)_9S_8$ was identified intergrown with pyrrhotite and cubanite.

Galena

Galena is most abundant in Type 3 Au-Ag-Pb-Cu-rich ore. It is a minor (<5 vol.%) component of the massive sulphide ores where it occurs as coarse-grained aggregates in the 10 and 11 lenses and as finer grained disseminations in the lower lenses (30, 31, 40). It occurs most commonly as anhedral to subhedral masses at grain boundaries of pyrite and sphalerite (Fig. 6f). However, (remobilized) galena also occurs as coarse cubes up to 1 cm in size in some late quartz veins. In the Au-Ag-Pb-Cu ore, fine-grained galena occurs within the mineral cleavages of the host chlorite-carbonate-actinolite schist, where it is commonly associated with microscopic grains of electrum and sulphosalts. Galena is rare in the low-sulphide Au-rich zones (Type 4), but where present shows the same general paragenesis with electrum and sulphosalts. Galena contains up to 4 wt% Se but is generally Ag-poor (<0.2 wt%) and Te-poor (<0.1 wt%) (Table 4).

Pb-Sb-Sulphosalts

Numerous complex sulphosalts have been identified in the Type 3 Au-Ag-Pb-rich ore, together with galena, chalcopyrite, and electrum. These include tetrahedrite $[(Cu,Fe)_{12}Sb_4S_{13}]$, bournonite $[PbCuSbS_3]$, boulangerite $[Pb_5Sb_4S_{11}]$, and meneghinite $[Pb_{13}CuSb_7S_{24}]$. These minerals typically occur as fine-grained, complex intergrowths with galena and, less commonly, with chalcopyrite, freibergite (see below), and gold (Fig. 6c). The sulphosalts contain minor As (up to 4 wt%) , Se (up to 0.4 wt%), and Sn (up to 0.2 wt%) (Table 4).

Ag-Sulphosalts

The major Ag minerals, other than electrum, are Ag-bearing tetrahedrite, freibergite $[(Ag,Cu,Fe)_{12}(Sb,As)_4S_{13}]$, allargentum $[Ag_{1-x}Sb_x]$, and sterryite $[Ag_2Pb_{10}(Sb,As)_{12}S_{29}]$. They occur mainly as Ag-rich inclusions in galena and less commonly as intergrowths with chalcopyrite. Silver-bearing tetrahedrite (Table 4) contains 1 to 7 wt% Ag, freibergite contains up to 37 wt% Ag, and some grains are notably tarnished. Lam et al. (2014) also identified aurostibite $(AuSb_2)$, but this mineral was not found in the present study.

Ag-Bearing Telluride Minerals

Two Ag-bearing telluride minerals were identified by microprobe (Table 4). They are a Te-rich Ag-sulphide, possibly benleonardite $[Ag_8(Sb,As)Te_2S_3]$, intergrown with electrum, and a hessite-like mineral, possibly stutzite $[Ag_{5-x}Te_3]$, intergrown with chalcopyrite and sphalerite. Lam et al. (2014) also identified hessite $[Ag_2Te]$ and altaite [PbTe], but we did not encounter these minerals.

Gold and Electrum

The main Au-bearing mineral in Type 2 Au-Cu mineralization and Type 3 Au-Ag-Pb-rich ore is electrum. Electrum commonly occurs at the grain boundaries and in microfractures of larger grains of galena, commonly together with various Sb- and Ag-bearing sulphosalts, as inclusions in pyrite or chalcopyrite, and rimming quartz inclusions in the sulphides. The size of the electrum grain is up to 0.1 mm, but much smaller grains are common. Both gold (<30 wt% Ag) and electrum (40–80 wt% Ag) compositions were obtained, but the Au:Ag ratio is variable and averages approximately 2:1 (Table 4). Significant Hg (average 3.41 wt%) and traces of Sb (0.38 wt%) are also present. Both gold and electrum are Hg-rich, although gold contains only 2.5 wt% Hg (average of 7 analyses) and electrum commonly contains 6–7 wt% Hg. Gold was not detected by microprobe in any of the other ore minerals.

Other Trace Minerals

Arsenopyrite [FeAsS], cobaltite [CoAsS], and gudmundite [FeSbS] were found in a number of different ore types. Fine-grained, euhedral arsenopyrite is locally associated in the massive sulphides with tetrahedrite, galena, and electrum (Fig. 6c). Arsenopyrite contains up to 0.3 wt% Se but is otherwise free of trace elements (Table 4). Cobaltite and gudmundite occur together with pyrrhotite and chalcopyrite, and both contain up to 0.5 wt% Ni. Trace Bi occurs in some pyrite, pyrrhotite, and chalcopyrite grains (average 0.12 wt%; maximum 0.23 wt%), perhaps as micro-inclusions of Bi minerals.

ORE GEOCHEMISTRY

Table 5 lists the average bulk geochemical compositions of the different ore types determined for the 70 samples analyzed in this study. The samples of massive sulphide ore average 11.7 wt% Fe and 12.3 wt% Zn, corresponding to 25 wt% FeS_2 and 18 wt% ZnS. Zinc shows a strong correlation with Cd (r = 0.97), Hg (r = 0.61), In (r = 0.56), and Sb (r = 0.48). Fe shows a positive correlation with Co (r = 0.41) and Ni (r = 0.48), but not with Zn. The pyrite-rich ores and sphalerite-rich ores clearly represent geochemically distinct

Table 5. Average bulk compositions of selected ore types of the Lalor volcanogenic massive sulphide deposit.

Element	Unit	Massive Sulphide	Semi-Massive Chalcopyrite	Chlorite Carbonate	Low-Sulphide High-Au
		n = 26	n = 9	n = 26	n = 10
SiO_2	%	19.63	57.67	39.71	46.94
Al_2O_3		5.08	8.52	7.25	9.17
Fe_2O_3		13.25	2.08	2.9	4.32
FeO		15.1	13.4	8	14.1
MgO		3.3	7.48	9.94	8.23
MnO		0.2	0.12	0.25	0.29
CaO		3.05	1.81	10.52	1.45
Na_2O		0.16	0.07	0.08	0.11
K_2O		0.32	0.3	0.16	0.41
TiO_2		0.19	0.25	0.15	0.31
P_2O_5		0.06	0.16	0.06	0.16
CO_2		0.78	0.11	3.45	0.25
Total C		0.23	0.04	0.98	0.08
Total S		25.7	6.11	7.87	7.08
LOI		0.52	0.07	2.21	0.17
Cu		2.37	1.42	1.06	4.13
Zn		12.32	0.42	4.57	1.88
Pb		0.15	0.04	0.84	0.04
Au	ppm	10.5	44	147	11.4
Ag		51	124	365	66.4
As		356	102	38	57.5
Sb		93	2.2	8.6	2.4
Cd		307	17.1	107	49.2
Hg		83.12	1.01	14.84	5.53
Tl		0.21	0.2	0.74	0.15
Sn		14	3	9	16
In		0.6	0.2	0.2	0.4
W		26	2.4	1.1	4.4
Ga		10	11	12	14
Ge		1.6	0.8	1.2	1.1
Co		96	88	38	70
Ni		20	9	6	15
Se		122	74	121	77
Bi		1.2	0.4	5.8	2.8
Te		14	65.2	63.8	20.8
Mo		5	2	3	4
V		54	63	22	179
U		1.75	0.78	1.29	0.92
Th		1.1	1.67	1.41	2.1
Ba		37	37	31	78
Sr		30	12	38	16
Cs		0.1	0.2	0.1	0.2
F		250	860	510	600
B		1	2	1	<1
Be		<1	<1	<1	<1
Li		9	22	8	11
Hf		0.6	1	1.3	1.1
Ta		0.13	0.15	0.15	0.15
Zr		24	38	44	45
Nb		2.2	3.3	3.1	3.4
Sc		10	14	9	24
Y		5	10.5	16.7	11.5
∑REE		42.4	67.3	85.5	95.8

assemblages, despite their occurrence together in the massive sulphide lenses.

Copper, which is present mainly in the semi-massive chalcopyrite ore, shows a moderately strong correlation with Se (r = 0.48) and As (r = 0.63), and to a lesser extent with Sn (r = 0.39) and In (r = 0.27). Tin and In are common trace constituents of Cu-rich ores in other VMS deposits, typically in the chalcopyrite-like minerals stannite and roquesite, but these were not identified in the present study.

Gold shows the strongest correlation with Ag (r = 0.98) and Te (r = 0.80), but the precious metals are distributed bimodally, with equally high contents in the Pb-rich ores and Au-Cu ores, so the statistical correlations with Pb and Cu in the bulk ore are weak. Although galena is the most common visual prognostic indicator for precious-metal enrichment in the chlorite-carbonate-actinolite-altered zones, Pb has a very poor correlation with Au and Ag at the hand-specimen scale. The strong correlation of Ag with Au reflects the high Ag content of the electrum and the association of electrum with Ag-rich sulphosalts, especially in the precious metal-rich chlorite-carbonate-actinolite-altered zones. The correlation with Te suggests the presence of an unidentified Au-bearing telluride.

Principal components analysis confirms that the bulk geochemical compositions of the ores include a significant mafic volcanic component (TiO_2, Al_2O_3, Na_2O, P_2O_5, Sc, Th, Y, Cr, V), a felsic element component (Al_2O_3, Hf, Nb, Ta, Zr, and light rare earth elements), a phyllosilicate component (K_2O, Al_2O_3, Ba, Cs, Li, F, and Ga), a chloritic component (MgO, Al_2O_3, TiO_2, Mn), and a carbonate or calc-silicate component (CO_2, CaO, MgO, MnO, and Sr). CaO and CO_2 contents strongly correlate with Pb in the precious metal-rich Au-Ag-Pb-Cu-rich ores hosted in chlorite-carbonate-actinolite altered rocks, as well as with U, Th, Y, and heavy rare earth elements. The latter may reflect an association with secondary minerals (e.g. xenotime) that are the product of metamorphic remobilization. CaO is also weakly correlated with Sr, Mn, and MgO (present in dolomite but also in co-existing chlorite, actinolite, and tremolite).

SULPHUR AND LEAD ISOTOPES

Sulphur isotope compositions of pyrite, sphalerite, pyrrhotite, and chalcopyrite show a limited range from $\delta^{34}S$ 0.41 to 2.84 ‰ with no significant difference between minerals (Table 6). This narrow range is typical of sulphides that have been extensively recrystallized during metamorphism (e.g. Shanks 2001; Fig. 8). Although it has been shown that many sulphide minerals can retain their isotopic compositions through metamorphism (e.g. Corriveau and Spry, 2014), it is common for highly metamorphosed massive sulphide

Table 6. Sulphur isotope compositions of ore minerals from the Lalor massive sulphide deposit.

Sample	Lens	Ore Type	$\delta^{34}S$ (‰)	Mineral
517-Py	10	1	2.58	pyrite
518-Py	10	1	2.22	pyrite
521-Py	10	1	2.27	pyrite
545-Py	10	1	1.65	pyrite
632-Py	10	1	2.61	pyrite
635-Py	10	1	2.84	pyrite
637-Py	10	1	2.06	pyrite
643-Py	10	1	1.87	pyrite
651-Py	10	1	1.88	pyrite
666-Py	10	1	1.29	pyrite
545-Sp	10	1	0.93	sphalerite
667-Sp	10	1	0.41	sphalerite
664-Cp	10	1	1.36	chalcopyrite
516-Po	10	1	1.41	pyrrhotite
651-Po	10	1	1.83	pyrrhotite
664-Po	10	1	1.17	pyrrhotite
549-Cp	10	3	1.03	chalcopyrite
658-Py	10	3	0.85	pyrite
665-Cp	10	4	1.08	chalcopyrite
665-Po	10	4	1.22	pyrrhotite
536-Py	21	1	1.51	pyrite
595-Py	21	1	2.59	pyrite
596-Py	21	1	1.86	pyrite
536-Sp	21	1	1.72	sphalerite
559-Py	21	3	2.4	pyrite
611-Py	21	3	2.45	pyrite
559-Sp	21	3	1.6	sphalerite
598-Py	21/20	1	1.8	pyrite
599-Py	21/20	1	2.19	pyrite
598-Sp	21/20	1	1.36	sphalerite
618-Py	21/25	1	2.13	pyrite
608-Py	21/20	3	2.2	pyrite
619-Py	25	N/A	2.79	pyrite
562-Py	25	1	2.33	pyrite
587-Py	25	1-3	1.52	pyrite
524-Py	25	3	2.66	pyrite
586-Py	25	3	2.42	pyrite
575-Py	25/26	3	0.56	pyrite
538-Cp	27	2	2.34	chalcopyrite
539-Cp	27	2	1.84	chalcopyrite
540-Py	27	2	1.28	pyrite
578-Py	27	2	1.68	pyrite
538-Po	27	2	2.27	pyrrhotite
603-Cp	N/A	2	1.4	chalcopyrite
631-Py	N/A	2	1.96	pyrite
628-Cp	N/A	4	2.45	chalcopyrite
628-Py	N/A	4	2.3	pyrite
581-Py	Vein	N/A	0.96	pyrite
586-Sp	N/A	N/A	2.07	sphalerite

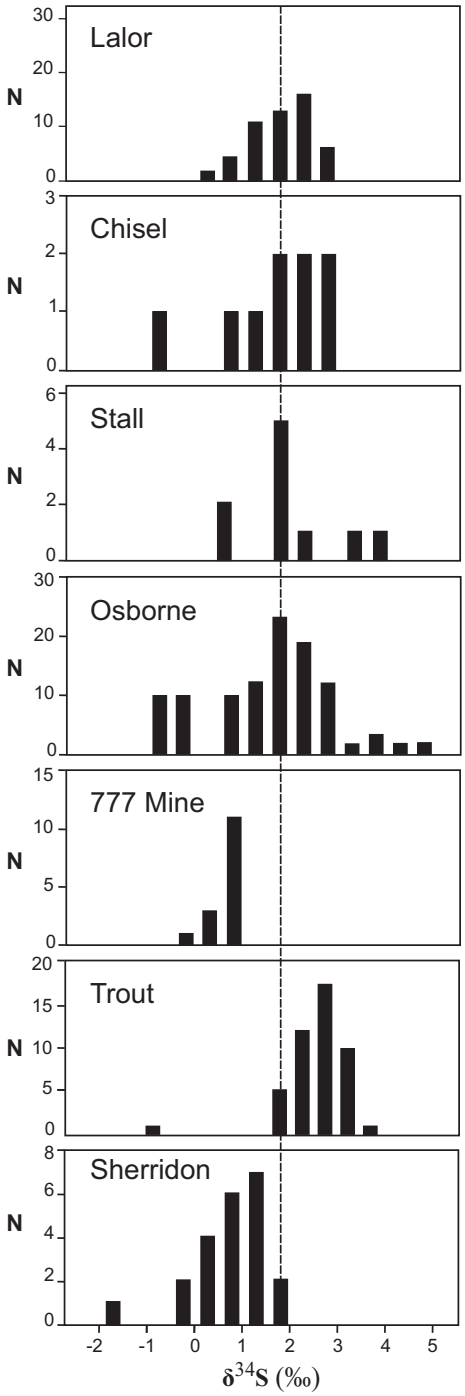

Figure 8. Histogram of sulphur isotope data from the Lalor massive sulphide deposit (Table 7), comparing the average value for Lalor sulphides (dashed line) with the distribution of $\delta^{34}S$ values for Chisel Lake and Stall in the Snow Lake camp (J.M. Franklin, unpublished data) and for the 777 Mine and Trout Lake Mine in Flin Flon (Polito et al., 2007). Data for the Sherridon sediment-hosted massive sulphide deposit are from (Sangster, 1972, 1978). Sulfide $\delta^{34}S$ values for Lalor range from 0.4 to 2.8 per mil (average +1.8 per mil), similar to all other Paleoproterozoic volcanogenic massive sulphide deposits in the region. Somewhat more variable compositions are evident at 777 and Trout Lake, at Osborne Lake northeast of Snow Lake, and at Sherridon; the lower $\delta^{34}S$ values at Sherridon may reflect the influence of reduced sedimentary rocks in the mine sequence.

Table 7. Pb isotope ratios of galena from different ore types of the Lalor massive sulphide deposit.

Sample	Description	Location (Ore Type)	$^{206}Pb/^{204}Pb$	$^{207}Pb/^{204}Pb$	$^{208}Pb/^{204}Pb$
SD-524	Euhedral grains with minor pyrite and pyrrhotite in a matrix of quartz and chlorite (DUB252W01, 1016.8 m)	25 Lens (Type 3)	15.403	15.12	34.899
SD-581	12 cm thick vein of pyrrhotite, pyrite, and galena with minor chalcopyrite in quartz- biotite-actinolite/ tremolite-garnet (DUB258W01, 803.7 m)	N/A (vein)	15.402	15.128	34.892
SD-611	Vein of sphalerite and galena with minor chalcopyrite in quartz-muscovite-gahnite-biotite (DUB169, 900.5 m)	21 Lens (Type 3)	15.399	15.113	34.888
SD-652	Coarse pyrite and sphalerite with lesser galena in actinolite-tremolite and epidote (DUB211, 909.2 m)	10 Lens (Type 3)	15.398	15.125	34.898
SD-654	Coarse pyrite and galena with interstitial sphalerite in carbonate (DUB174, 877.8 m)	31 Lens (Type 1)	15.396	15.122	34.885
SD-655	Galena adjacent to quartz vein in a massive pyrite (underground, 825 mL)	10 Lens (N/A)	15.394	15.116	34.868
SD-662	Thick (50 cm) galena vein cutting stringer zone sulphides (underground, 810 mL)	10 Lens (vein)	15.396	15.122	34.891
SD-663	Quartz vein with galena concentrated in a fold hinge (underground, 865 mL)	20 Lens (vein)	15.412	15.132	34.936

deposits to have a very narrow range of values, reflecting probable loss of light sulphur during recrystallization (Crowe, 1994; Cook and Hoefs, 1997). In contrast, shear zone-hosted orogenic gold deposits in the Flin Flon-Snow Lake belt have generally higher $\delta^{34}S$ values (2.8 to 5.5‰: Fedorowich et al., 1991; Ansdell and Kyser, 2006), consistent with hydrothermal fluids in the shear zones interacting with a wide range of Proterozoic metamorphic and igneous rocks. The data also contrast with the $\delta^{34}S$ values of barren sulphide occurrences in rocks of similar age and metamorphic grade but outside the Flin Flon-Snow Lake belt (e.g. Polito et al., 2007).

Lead isotope ratios were measured on 6 galena separates from the Au-Ag-Pb-Cu mineralization associated with chlorite-carbonate-altered rocks and 3 galena separates from the massive sulphides in the 10 and 11 lenses (Table 7). All samples exhibit a tight cluster of $^{206}Pb/^{204}Pb$, $^{207}Pb/^{204}Pb$, and $^{208}Pb/^{204}Pb$ ratios, averaging 15.400, 15.122, and 34.895, respectively, with no difference between the ore types. These data compare closely to the Pb-isotope ratios of galena separates from Chisel and Chisel North (15.432, 15.161, and 35.058: Thorpe, 2008) at low $^{206}Pb/^{204}Pb$ and $^{207}Pb/^{204}Pb$ (Fig. 9). The similarity of Pb isotope compositions of galena in the Au-Ag-Pb-Cu galena-sulphosalts-chalcopyrite mineralization and in the massive sulphides strongly suggests a common Pb source and negates a late-stage post-magmatic event as the origin of the Au-Ag-Pb-Cu mineralization. A post-magmatic event would have been expected to introduce distinctly different and likely more radiogenic Pb (cf. Sangster, 1972, 1978; Thorpe, 2008), similar to that in the nearby New Britannia (Nor Acme), Rex, Herb

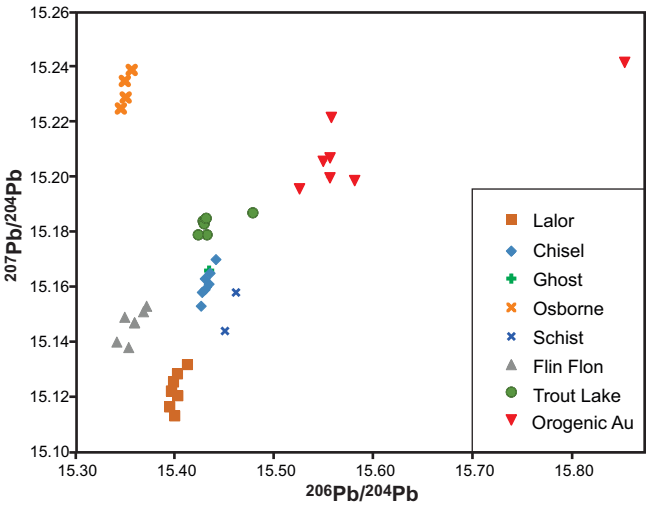

Figure 9. Bivariate plot of $^{207}Pb/^{204}Pb$ versus $^{206}Pb/^{204}Pb$ ratios for galena from selected volcanogenic massive sulphide (VMS) deposits and orogenic Au deposits in the Flin Flon-Snow Lake belt. Data are from Thorpe (2008) and J.M. Franklin (unpublished). The samples were collected by D. Sangster, J.M. Franklin, A. Galley, M. Fedikow, and R. Healy, and the analyses were performed in a number of different laboratories, including at the University of Alberta (G.L. Cumming, 1982), Geospec Consultants Limited, and at the Geological Survey of Canada. Data for late post-magmatic mineralization are from orogenic Au deposits: Nor Acme (New Britannia), Bingo, Ferro, Herb lake, Rex Mine, and Threehouse. Data for Lalor are from this study. The Pb isotopic compositions of galena from Lalor are the least radiogenic of the VMS deposits in the region, but generally fall on a Pb-isotope linear array including the Lalor, Ghost, and Chisel deposits. Galena lead isotope signatures for the younger, orogenic Au deposits of the Snow Lake camp (Nor Acme-New Britannia, Rex, Herb Lake, Bingo, and Ferro) form a distinctly separate secondary array.

Lake, Bingo, and Ferro Au deposits of the Snow Lake camp (Fig. 9).

Lalor ore galena is the least radiogenic of the VMS deposits in the region but generally falls on the Pb-isotope linear array of the Flin Flon-Snow Lake mineral belt (cf. Sangster 1972, 1978). The linear array of data on the Pb-Pb plot is similar to that inferred for crust-mantle mixing in other Precambrian greenstone terranes (e.g. Thorpe, 1999) and reflects contributions of both older crustal components and mantle sources. The most radiogenic end-members represent the signatures of material derived from the crust.

SUMMARY AND CONCLUSIONS

Four major ore types are recognized in the 12 ore lenses at Lalor, including Fe-Zn-rich massive sulphides, Au-Cu rich semi-massive and stockwork-like chalcopyrite in chloritic rocks (dominated by chlorite-biotite-staurolite-anthophyllite-cordierite ± kyanite/sillimanite), Au-Ag-Pb-Cu disseminated sulphides and sulphosalts in chlorite-carbonate-actinolite (dominated by chlorite-calcite ± diopside ± epidote ± talc), and pyritic quartz-biotite rock. In the Fe-Zn-rich massive sulphides, Au is interstitial to pyrite and sphalerite in coarsely recrystallized polycrystalline aggregates, commonly with sulphosalts and chalcopyrite. In semi-massive and stockwork-like Cu-Au mineralization Au is closely associated with chalcopyrite, and in chlorite-carbonate-actinolite ± calc-silicate rocks Au is associated with disseminated polymetallic sulphides, especially galena, and related Ag-Sb-Pb-sulphosalts.

All ores have been extensively recrystallized during syn-D_2 amphibolite-facies metamorphism. The stoichiometric compositions of the major Cu-Fe-sulphides (pyrite, pyrrhotite, chalcopyrite), the very uniform composition of sphalerite, the low trace-element contents in galena, and the abundance of minor and trace sulphosalts and other minerals are typical of massive sulphide ores that have been extensively recrystallized (e.g. Chen and Petruk, 1980; Petruk and Schnarr, 1981; Craig and Vokes, 1993; Petruk and Wilson, 1993; Huston et al., 1995). In such ores, trace elements in the major ore minerals are expelled during recrystallization to form minor phases that commonly occur at the margins of the grains or at triple-junction contacts. The presence of mercurian gold probably reflects the loss of Hg from primary sphalerite during metamorphism and its collection by electrum (cf. Healy and Petruk, 1988), a major source of Hg in all of the deposits of the belt (e.g. Healy and Petruk, 1990). Certain minerals, such as tetrahedrite, retain their high Ag contents despite the metamorphism. In some metamorphosed ore deposits, pyrite decomposition liberates sulphur that may play a role in remobilization of Au (e.g. as $Au(HS)_2^-$ in metamorphic hydrothermal fluids derived from dehydration reactions), and high fS_2 conditions caused by pyrite breakdown have been documented at several highly metamorphosed massive sulphide deposits, such as Osborne Lake, Montauban, and Geco (Bristol and Froese, 1989; Tomkins et al., 2006; Tomkins 2007). However, strong buffering by iron silicates or oxides may limit this process, and the uniformly high FeS contents of sphalerite at Lalor suggest that fS_2 remained low during metamorphism (e.g. Craig and Vokes, 1993). Thus, although soft and ductile minerals like galena, various sulphosalts, electrum, and gold were mechanically remobilized into fractures and cleavages, metamorphic reactions that might have dissolved (and transported) Au likely did not occur.

The ore lenses also preserve an apparent primary metal enrichment. Zn-rich massive sulphide ores are Cd-, Hg-, Sb-, and As-rich, whereas the Cu-rich semi-massive sulphide and stockwork ores (normalized to 100% sulphides) are enriched in Co, Ni, Mo, Se, Te, ±Bi. The Pb-rich ores are enriched in Au, Ag, As, Se, and Te compared to the other ore types. In general, Au shows a generally poor correlation with all other trace elements, except Ag. As in other deposits of the Chisel Sequence, high Au grades occur in both Cu- and Zn-rich ores in different lenses, and this most likely reflects primary differences in the conditions of Au mineralization (e.g. including both high-temperature Cu-Au mineralization and lower temperature Zn-Au mineralization (Huston, 2000).

The unusual stratigraphic position of the Pb-rich ores relative to the other ore lenses at Lalor raises the possibility that they are not part of the VMS system but were emplaced during a much later metamorphic event. However, the tight clustering of the Pb-isotope data along the Flin Flon-Snow Lake linear array suggests that the Pb and the closely associated Au were cogenetic with the massive sulphides. As noted by Sangster (1978), the fact that the galena from the various VMS deposits cluster and do not lie on secondary isochrons, like the Au deposits, suggests that the Pb (and by inference other metals) in each deposit have a discrete uniform composition and do not show any multi-stage post-magmatic history. The presence of "low-temperature" disseminated galena-rich ores stratigraphically below the main massive sulphide lenses suggests that they formed as a late-stage synvolcanic hydrothermal overprint, possibly in response to subseafloor boiling. Galley et al. (1993) and Gibson et al. (2014) similarly interpret the Chisel, Lost, and Ghost deposits as having formed within a shallow marine basin in which boiling of the hydrothermal fluid likely occurred, and Engelbert et al. (2014b) proposes boiling as the probable mechanism of formation of the high-grade Au ores at Photo Lake. Such low-temperature, disseminated-style ore assemblages at Lalor are

Table 8. Trace element contents of different ore types from Lalor (normalized to 100% sulphides) compared to Snow Lake mineral concentrates.

Deposit	Concentrate/ Ore	(n)	Cu	Fe	Zn	Pb	Au	Ag	As	Sb	Co	Se	Ni	Cd	Mo	Te	Bi	Hg	Tl	Ga	In	Sn
			wt.%				ppm															
Lalor	Fe-Zn	23	5.08	17	24.9	0.34	4.39	110	768	181	208	273	48	648	11	30	1	180	0.3	19	2	24
Lalor	Cu-Au	6	29.1	20.4	7.93	0.19	86.15	362	91	15	342	533	77	219	18	142	15	24	0.8	65	3	75
Lalor	Au-Ag-Pb	15	7.69	13.3	24.4	10.1	38.21	563	314	38	294	778	41	625	17	140	8	82	0.9	88	2	80
Lalor	Low-sulphide	5	16	15	3.16	0.49	66.61	401	464	3	901	824	90	155	16	117	4	12	0.5	64	2	23
Snow Lake	Cu concentrate	3	19.5	34.6	2.16	0.03	5.91	93	655	367	381	225	21	57	29	63	29	16	0.6	12	30	16
Stall/Rod	Cu Concentrate	3	19.6	34.4	1.36	0.02	6.16	37	472	49	297	255	16	40	22	52	41	10	0.2	7	29	12
Chisel	Cu Concentrate	3	19.7	22.2	9.73	6.21	21	1800	2042	3379	38	293	24	250	28	46	55	73	4.7	5	9	26
Snow Lake	Zn Concentrate	3	0.71	9.61	53.7	0.02	0.52	30	353	78	17	116	<10	1300	2	4	2	120	0.5	11	8	9
Chisel	Zn Concentrate	4	0.22	8.42	54.5	0.2	0.22	27	585	56	20	83	10	1300	2	3	2	120	0.4	10	6	8
Chisel	Pb Concentrate	3	1.21	6.86	6.29	61.4	8.03	956	2229	8436	8	589	24	120	8	120	200	130	26	2	1	6

Lalor data are calculated from samples in Table 5, after normalizing to 100% metals+Fe+S. Type 1 includes only samples with Me+Fe+S >30 wt%; Au, Ag, and Te concentrations in the calculations were cut-off at 30 ppm Au, 300 ppm Ag, and 150 ppm Te. Data for mill concentrates from other Snow Lake deposits are from Hannington and Jonasson, 1986, unpublished data.

also much more sensitive to metamorphism and remobilization, perhaps explaining why part of the Au-Ag-Pb-Cu ore is spatially associated with highly strained rocks, brittle amphibolitic assemblages, and weakly altered mafic dykes (Caté et al., 2015).

The ores at Lalor are geochemically and mineralogically similar to the other deposits of the Chisel Sequence (Chisel, Chisel North, Lost, and Ghost). Gold is significantly enriched in all of the deposits compared to the Anderson Sequence (Stall, Rod, and Anderson). Silver, As, Cd, Hg, and Sn contents (normalized to 100% sulphides) are also higher than in typical Snow Lake concentrates (M. Hannington and I. Jonasson, unpublished; Table 8). Notably, the Co, Se, Ni, and Te abundances in the Lalor ore-related minerals are significantly higher than those in the Chisel ores. Trace Co and Ni occur in pyrrhotite and pyrite, and cobaltite, gudmundite, and Se-bearing arsenopyrite are present in the massive sulphides. These differences may reflect the dominantly mafic host rocks and the lack of rhyolite at Lalor compared to Chisel. The most Au-rich deposits of the Chisel Sequence show a close association with felsic volcanic rocks and local rhyolite domes (Galley et al., 1993; Gibson et al., 2014). Similarly, the Au-rich Photo Lake deposit has been interpreted to occur within a thick section of coherent rhyolite (Engelbert et al., 2014a). Although the Lalor deposit is thought to be situated at a similar stratigraphic position as Chisel and Chisel North (Bailes et al., 2013), detailed studies suggest some differences between the footwall successions (Bailes et al., 2013; Caté et al., 2013a,b, 2015), including a minor proportion of felsic volcanic rocks in the Lalor volcanic (footwall) succession. Moreover, mafic magmatism was clearly ongoing during the mineralizing event at Lalor, as evidenced by the presence of dykes with compositions similar to the Threehouse basalt. These observations indicate that Au enrichment in the camp is not limited to deposits that have mainly rhyolite in the immediate footwall.

ACKNOWLEDGEMENTS

We thank Hudbay Minerals Inc. and the Manitoba Geological Survey, in particular, A. Bailes, S. Bernauer, C. Böhm, S. Gagné, B. Janser, J. Levers, D. Simms, T. Schwartz and C. Taylor, who provided access to the mine and core and insightful discussions on the Lalor deposit. H. Gibson, B. Lafrance, D. Tinkham, J. Lam, and M. Englebert of the Laurentian University Snow Lake research group shared knowledge of the Snow Lake district and VMS systems. The senior author was funded jointly by Hudbay Minerals and by the Geological Survey of Canada through the RAP program. We thank Jan Peter for reviews and editorial handling.

REFERENCES

Ansdell, K.M. and Kyser, K.T., 2006. Mesothermal gold mineralization in a Proterozoic greenstone belt, western Flin Flon Domain, Saskatchewan, Canada; Economic Geology, v. 87, p. 1496–1524.

Bailes, A.H., 2008. Geological setting of the Lalor and Photo Lake VMS deposits; Hudbay Internal Report, Bailes Geoscience, 45 p.

Bailes, A.H., 2009. Geological and Geochemical Investigation of Altered Rocks Hosting the Lalor VMS Deposit; Unpublished Report for HudBay Minerals Inc., 96 p.

Bailes A.H., 2011. A review of structural features associated with VMS deposits in the Chisel-Lalor-Photo lakes area; Unpublished Report for HudBay Minerals Inc., 31 p.

Bailes, A.H. and Galley, A.G., 1996. Setting of Paleoproterozoic volcanic-hosted massive sulphide deposits, Snow Lake, *In:* EXTECH I: A Multidisciplinary Approach to Massive Sulphide Research in the Rusty Lake and Snow Lake Greenstone Belts, Manitoba, (ed.) G.F. Bonham-Carter, A.G. Galley and G.E.M. Hall; Geological Survey of Canada, Bulletin 426, p.105–138.

Bailes, A.H. and Galley, A.G., 1999. Evolution of the Paleoproterozoic Snow Lake arc assemblage and geodynamic setting for associated volcanic-hosted massive sulphide deposits, Flin

Flon Belt, Manitoba, Canada; Canadian Journal of Earth Sciences, v. 36, no. 11, p. 1789–1805. doi:10.1139/e98-111

Bailes, A., Rubingh, K., Gagné, S., Taylor, C., Galley, A., Bernaeur, S., and Simms, D., 2013. Volcanological and structural setting of Paleoproterozoic VMS and Gold deposits at Snow Lake, Manitoba; Geological Association of Canada–Mineralogical Association of Canada Joint Annual Meeting, Winnipeg, Manitoba, May 2013, Field Trip Guidebook FT-A2, Manitoba Innovation, Energy and Mines, Manitoba Geological Survey Open File OF2013-3, 63 p.

Barton, P.B. and Bethke, P.M. Jr., 1987. Chalcopyrite disease in sphalerite: Pathology and epidemiology; American Mineralogist, v. 72, p. 451–467.

Bristol, C.C. and Froese, E., 1989. Highly metamorphosed altered rocks associated with the Osborne Lake volcanogenic massive sulfide deposit, Snow Lake area, Manitoba; Canadian Mineralogist, v. 27, p. 593–600.

Caté, A., Mercier-Langevin, P., Ross, P.-S., Duff, S., Hannington, M.D., Dubé, B., and Gagné, S., 2015. Geology and Au enrichment processes at the Paleoproterozoic Lalor auriferous volcanogenic massive sulphide deposit, Snow Lake, Manitoba, *In:* Targeted Geoscience Initiative 4: Contributions to the Understanding of Volcanogenic Massive Sulphide Deposit Genesis and Exploration Methods Development, (ed.) J.M. Peter and P. Mercier-Langevin; Geological Survey of Canada, Open File 7853, p. 131–145.

Caté, A., Mercier-Langevin, P., Ross, P.-S., Duff, S., Hannington, M., Dubé, B., and Gagné, S., 2013a. The Paleoproterozoic Lalor VMS deposit, Snow Lake, Manitoba: preliminary observations on the nature and architecture of the gold- and base metal-rich ore and alteration zones; Geological Survey of Canada, Open File 7483, 19 p.

Caté, A., Mercier-Langevin, P., Ross, P.-S., Duff, S., Hannington, M., Dubé, B., and Gagné, S., 2013b. Preliminary observations on the geological environment of the Paleoproterozoic auriferous volcanogenic massive sulphide deposit of Lalor, Snow Lake, Manitoba; Geological Survey of Canada, Open File 7372, 13 p.

Caté, A., Mercier-Langevin, P., Ross, P.-S., and Simms, D., 2014a. GS-8 Structural controls on geometry and ore distribution in the Lalor auriferous VMS deposit, Snow Lake, west-central Manitoba (part of NTS 63K16): preliminary results from underground mapping, *In:* Report of Activities 2014; Manitoba Mineral Resources, Manitoba Geological Survey, p. 104–115.

Caté, A., Mercier-Langevin, P., Ross, P.-S., Duff, S., Hannington, M., Gagné, S., and Dubé, 2014b. Insights on the chemostratigraphy of the volcanic and intrusive rocks of the Lalor auriferous volcanogenic massive-sulphide deposit host succession, Snow Lake, Manitoba; Geological Survey of Canada, Current Research 2014-6, 20 p.

Chen, T.T. and Petruk, W., 1980. Mineralogy and characteristics that affect recoveries of metals and trace elements from the ore at Heath Steele Mines, New Brunswick; Canadian Institute of Mining and Metallurgy Bulletin v. 73, p. 167–178.

Cook, N.J. and Hoefs, J., 1997. Sulphur isotope characteristics of metamorphosed Cu-(Zn) volcanogenic massive sulfide deposits in the Norwegian Caledonides; Chemical Geology, v. 135, p. 307–324.

Corriveau, L. and Spry, P.G., 2014. Metamorphosed hydrothermal ore deposits, *In:* Geochemistry of Mineral Resources, Treatise on Geochemistry, (ed.) S.D. Scott; Elsevier, New York, v. 12.

Craig, J.R., Vokes, F.M., and Simpson, C., 1991. Rotational fabrics in pyrite from Ducktown, Tennessee; Economic Geology, v. 86, p. 1737–1746.

Craig, J.R. and Vokes, F.M., 1993. The metamorphism of pyrite and pyritic ores: an overview; Mineralogical Magazine, v. 57, p. 3–18.

Crowe D.E., 1994. Preservation of original hydrothermal $\delta^{34}S$ values in greenschist to upper amphibolite volcanogenic massive sulfide deposits; Geology, v. 22, p. 873–876.

Engelbert, M.S., Friesen, V., Gibson, H., and Lafrance, B., 2014a. Volcanic reconstruction of the productive VMS ore interval in the Paleoproterozoic Chisel sequence, Snow Lake, Manitoba, *In:* Program with Abstracts; Geological Association of Canada–Mineralogical Association of Canada Joint Annual Meeting, Fredericton, May 22–22, 2014, p. 83–84.

Engelbert, M.S., Gibson, H.L., and Lafrance, B., 2014b. Geologic Setting, Mineralogy, and Geochemistry of the Paleoproterozoic Photo Lake VMS Deposit, Snow Lake, Manitoba; PDAC-SEG Student Minerals Colloquium, March 3, (poster presentation).

Fedorowich, J., Stauffer, M., and Kerrich, R., 1991. Structural setting and fluid characteristics of the Proterozoic Tartan Lake gold deposit, Trans-Hudson Orogen, northern Manitoba; Economic Geology, v. 86, p. 1434–1467.

Gagné, S., Beaumont-Smith, C.J., Williams-Jones, A.E., and Hynes, A., 2007. Investigation of a Pb-Ag-Au–rich hanging-wall in lens 4 of the Chisel North mine, Snow Lake, Manitoba (NTS 63K16): preliminary results, *In:* Report of Activities 2007; Manitoba Science, Technology, Energy and Mines, Manitoba Geological Survey, p. 43–50.

Galley, A.G., Syme, R., and Bailes, A.H., 2007. Metallogeny of the Paleoproterozoic Flin Flon Belt, Manitoba and Saskatchewan, *In:* Mineral Deposits of Canada: A Synthesis of Major Deposit Types, District Metallogeny, the Evolution of Geological Provinces, and Exploration Methods, (ed.) W.D. Goodfellow; Geological Association of Canada, Mineral Deposits Division, Special Publication 5, p. 509–531.

Galley, A.G., Bailes, A.H., and Kitzler, G., 1993. Geological setting and hydrothermal evolution of the Chisel Lake and North Chisel Zn–Pb–Cu–Ag–Au massive sulphide deposits, Snow Lake, Manitoba; Exploration and Mining Geology, v. 2, p. 271–295.

Gibson, H., Engelbert, M.S., Lafrance, B., Friesen, V., DeWolfe, M., Tinkham, D.K., and Bailes, A.H., 2014. Reconstruction of the ore interval and environment for the Paleoproterozoic Lost and Ghost Lake VMS deposits, Snow Lake, Manitoba; *In:* Program with Abstracts; Geological Association of Canada-Mineralogical Association of Canada Joint Annual Meeting, Fredericton, May 22–22, 2014, p. 102.

Healy, R.E. and Petruk, W., 1988. Mineralogical characteristics that affect metal recoveries from Cu, Zn, Pb and Ag ores of Manitoba: An Investigation of the mineralogy of the Trout Lake deposit; Canada Centre for Minerals and Energy Technology, Investigative Report IR 88-61, 181 p.

Healy, R.E. and Petruk W., 1990. Petrology of Au-Ag-Hg alloys and 'invisible' gold in the Trout Lake massive sulfide deposit, Flin Flon, Manitoba; Canadian Mineralogist, v. 28, p.189–206.

HudBay Minerals Inc., 2014, Lalor operation webpage, http://www.hudbayminerals.com/English/OurBusiness/Operations/Lalor/default.aspx

Huston, D.L., Sie, S.H., Suter, G.F., Cooke, D.R., and Both, R.A., 1995. Trace elements in sulfide minerals from eastern Australian volcanic-hosted massive sulfide deposits: Part I. Proton microprobe analyses of pyrite, chalcopyrite, and sphalerite, and Part II. Selenium levels in pyrite: comparison with $\delta^{34}S$ values and implications for the source of sulfur in volcanogenic hydrothermal systems; Economic Geology, v. 90, p. 1167–1196.

Huston, D.L., 2000. Gold in volcanic-hosted massive sulfide deposits: distribution, genesis, and exploration, *In:* Gold in 2000, (ed.) S.G. Hagemann and P.E. Brown; Reviews in Economic Geology, v. 13, p. 400–426.

Kraus, J. and Williams, P.F., 1999. Structural development of the Snow Lake allochthon and its role in the evolution of the southeastern Trans-Hudson Orogen in Manitoba, central Canada; Canadian Journal of Earth Sciences, v. 36, p. 1881–1899.

Lam, J., Tinkham, D.K., and Gibson, H., 2013. Identification of metamorphic assemblages and textures associated with gold mineralization at the Lalor deposit, Snow Lake, Manitoba, *In:* Program with Abstracts; Geological Association of Canada–Mineralogical Association of Canada Joint Annual Meeting, Winnipeg, May 22–24, 2013, p. 127.

Lam, J., Tinkham, D.K., and Gibson, H., 2014. Characterization of gold occurrences with respect to metamorphism at the Lalor deposit, Snow Lake, Manitoba, *In:* Program with Abstracts; Geological Association of Canada–Mineralogical Association of Canada Joint Annual Meeting, Fredericton, May 22–22, 2014, p. 150–151.

Martin, P., 1966. Structural analysis of Chisel Lake orebody; Canadian Mining and Metallurgical Bulletin, v. 69, p. 208–214.

Menard, T. and Gordon, T.M., 1997. Metamorphic P-T paths from the eastern Flin Flon belt and Kisseynew domain, Snow Lake, Manitoba; Canadian Mineralogist, v. 35, p. 1093–1115.

Mercier-Langevin, P., Caté, A., and Ross, P.-S., 2014. GS-7 Whole-rock oxygen-isotope mapping of the footwall alteration zones at the Lalor auriferous VMS deposit, Snow Lake, west-central Manitoba (NTS 63K16), *In:* Report of Activities 2014; Manitoba Mineral Resources, Manitoba Geological Survey, p. 94–103.

Petruk, W. and Schnarr, J.R., 1981. An evaluation of the recovery of free and unliberated mineral grains, metals and trace elements in the concentrator of Brunswick Mining and Smelting Corp. Ltd.; Canadian Institute of Mining and Metallurgical Bulletin, v. 74, p. 132–159.

Petruk, W. and Wilson, J.M., 1993. Silver and gold in some Canadian volcanogenic base metal deposits, *In:* Proceedings, (ed.) Maurice, Y.T.; 8th Quadrennial IAGOD Symposium, Schweizerbart'sche, Stuttgart, p. 105–117.

Polito P., Kyser, K., Lawie, D., Cook, S., and Oates, C., 2007. Application of sulphur isotopes to discriminate Cu-Zn VHMS mineralization from barren Fe sulphide mineralization in the greenschist to granulite facies Flin-Flon - Snow Lake - Hargrave River region; Geochemistry, Exploration, Analysis, Environment, v. 7, p. 129–138.

Sangster D.F., 1972. Isotopic Studies of Ore-Leads in the Hanson Lake - Flin Flon - Snow Lake Mineral Belt, Saskatchewan and Manitoba; Canadian Journal of Earth Sciences, v. 9, p. 500–513.

Sangster, D.F., 1978. Isotopic studies of ore-leads of the circum-Kisseynew volcanic belt of Manitoba and Saskatchewan; Canadian Journal of Earth Sciences, v. 15, p. 1112–1121.

Shanks, W.C., 2001. Stable Isotopes in Seafloor Hydrothermal Systems: Vent fluids, hydrothermal deposits, hydrothermal alteration, and microbial processes; Reviews in Mineralogy and Geochemistry, v. 43, p. 468–525.

Tinkham, D.K., 2013. A model for metamorphic devolatilization in the Lalor deposit alteration system, Snow Lake, Manitoba, *In:* Program with Abstracts; Geological Association of Canada–Mineralogical Association of Canada Joint Annual Meeting, Winnipeg, May 22–24, 2013, p. 187.

Thorpe, R.I., 1999. The lead isotope linear array for volcanogenic massive sulfide deposits of the Abitibi and Wawa subprovinces, Canadian Shield, *In:* The Giant Kidd Creek Volcanogenic Massive Sulfide Deposit, Western Abitibi Subprovince, Canada, (ed.) M.D. Hannington and C.T. Barrie; Society of Economic Geologisst, Monograph 10, p. 555– 576.

Thorpe, R.I., 2008. Release of lead isotope data in 4 databases: Canadian, western Superior, foreign, and whole rock and feldspar; Geological Survey of Canada, Open File Report 5664, 42 p.

Tomkins, A.G., 2007. Three mechanisms of ore re-mobilisation during amphibolite facies metamorphism at the Montauban Zn-Pb-Au-Ag deposit; Mineralium Deposita, v. 42, p. 627–637.

Tomkins, A.G., Frost, R.B., and Pattison, D.R.M., 2006. Arsenopyrite melting during metamorphism of sulfide ore deposits; Canadian Mineralogist, v. 44, p. 1045–1062.

Zaleski, E., Froese, E., and Gordon, T. M., 1991. Metamorphic petrology of Fe-Zn-Mg-Al alteration at the Linda volcanogenic massive sulfide deposit, Snow Lake, Manitoba; Canadian Mineralogist, v. 29, p. 995–1017.

GEOLOGICAL SURVEY OF CANADA
OPEN FILE 7853

Targeted Geoscience Initiative 4: Contributions to the Understanding of Volcanogenic Massive Sulphide Deposit Genesis and Exploration Methods Development

Geological and geochemical characteristics of the Waconichi Formation east of the Lemoine auriferous volcanogenic massive sulphide deposit, Abitibi greenstone belt, Quebec

Alexandre R. Boulerice[1], Pierre-Simon Ross[1], and Patrick Mercier-Langevin[2]

[1]Institut national de la recherche scientifique, Québec, Quebec
[2]Commission géologique du Canada, Québec, Quebec

2015

This publication is available for free download through GEOSCAN (http://geoscan.nrcan.gc.ca/)

Recommended citation

Boulerice, A.R., Ross, P.-S., and Mercier-Langevin, P., 2015. Geological and geochemical characteristics of the Waconichi Formation east of the Lemoine auriferous volcanogenic massive sulphide deposit, Abitibi greenstone belt, Quebec, *In:* Targeted Geoscience Initiative 4: Contributions to the Understanding of Volcanogenic Massive Sulphide Deposit Genesis and Exploration Methods Development, (ed.) J.M. Peter and P. Mercier-Langevin; Geological Survey of Canada, Open File 7853, p. 171–182.

Publications in this series have not been edited; they are released as submitted by the author.

Contribution to the Geological Survey of Canada's Targeted Geoscience Initiative 4 (TGI-4) Program (2010–2015)

TABLE OF CONTENTS

Geological and geochemical characteristics of the Waconichi Formation east of the Lemoine auriferous volcanogenic massive sulphide deposit, Abitibi greenstone belt, Quebec

Alexandre R. Boulerice[1]*, Pierre-Simon Ross[1]†, and Patrick Mercier-Langevin[2]

[1]Institut national de la recherche scientifique, 490 rue de la Couronne, Québec, Quebec, G1K 9A9
[2]Ressources Naturelles Canada, Commission géologique du Canada, 490 rue de la Couronne, Québec, Quebec, G1K 9A9
*Corresponding authors' e-mail: alexandre.boulerice@ete.inrs.ca
†Corresponding authors' e-mail: pierre-simon.ross@ete.inrs.ca

ABSTRACT

The Lemoine Mine exploited a small but exceptionally rich auriferous volcanogenic massive sulphide body (0.76 Mt of ore grading 4.6 g/t Au). The deposit was located in the Lower Lemoine Member of the Waconichi Formation, in the Chibougamau area of the Archean Abitibi greenstone belt. The Lower Lemoine Member, which is mostly of tholeiitic magmatic affinity, is overlain by the Upper Lemoine Member comprising transitional basalt and transitional to calc-alkaline rhyolite. Field mapping, geochemical analyses, and detailed core logging of every accessible drillhole in the study area, east of the former mine, has helped to define the Lower Lemoine Member subunits and identify their mode of emplacement. The Lower Lemoine Member is composed of multiple extrusive subunits: from the bottom of the volcanic stratigraphy, the Alpha Rhyolite followed by the Lemoine Rhyolite, the Lemoine Dacite, the Lemoine Andesite, and the Hanging-wall Quartz and Feldspar Porphyry. A second, later, component of the Alpha Rhyolite intrudes the Lemoine Rhyolite locally. The Marelle Quartz and Feldspar Porphyry and the Coco Lake Rhyolite represent subvolcanic intrusions that form concordant sills at multiple stratigraphic levels in the Lower Lemoine Member. Preliminary results also indicate the potential presence and general location of previously unrecognized volcanic vents northeast of the Lemoine deposit, which may have been the site of paleohydrothermal fluid up-flow and may host additional mineralization. The precise location of the volcanic vents is the topic of ongoing work and will have implications for exploration for volcanogenic massive sulphides in the area and in similar settings elsewhere. Moreover, our work indicates that the Lemoine auriferous volcanogenic massive sulphide deposit is hosted in a felsic-dominated volcanic sequence comprising a significant portion of shallow intrusive rocks, defining a major thermal corridor over a large synvolcanic intrusion; conditions that may have contributed in forming such a base- and precious-metal-rich deposit.

INTRODUCTION

Situated in the northeastern portion of the Abitibi greenstone belt (Fig. 1), south of Chibougamau, the Lemoine auriferous volcanogenic massive sulphide (VMS) deposit was Canada's second-richest VMS deposit in terms of net smelter return, after Eskay Creek in British Columbia, and the sixth worldwide (Lafrance and Brisson, 2006). The Lemoine Mine has produced a total of 0.76 Mt of ore grading 4.6 g/t Au, 4.2% Cu, 9.5% Zn, and 83 g/t Ag (Mercier-Langevin et al., 2014) and is the only VMS deposit in the Chibougamau district that has been mined. According to the criteria established by Mercier-Langevin et al. (2011), the Lemoine deposit classifies as an auriferous VMS deposit due to its elevated Au grade but low tonnage. Its discovery in 1973 generated VMS exploration activity in the Chibougamau region, but so far the unmined Scott Lake deposit (including the Selco prospect: Saunders and Allard, 1990; Salmon and McDonough, 2011), with total inferred resources of 5.4 Mt of rock grading 1.2 wt% Cu, 4.2 wt% Zn, 0.2 g/t Au, and 34 g/t Ag, is the only additional potentially economic VMS deposit in the district. Both deposits are hosted by felsic tholeiitic members of the Waconichi Formation (Daignault and Allard, 1990; Leclerc et al., 2012), known as the Lemoine and Scott members, respectively. The paucity of other known significant VMS deposits, despite favourable geology in the Chibougamau area (Leclerc et al., 2012), and knowing that VMS deposits usually occurs in clusters (Sangster, 1980), justifies further exploration.

The Lemoine deposit is situated in the western part of the ca. 2728 Ma (Mortensen, 1993) Lower Lemoine Member (Leclerc et al., 2011) (Fig. 2a). The Lower

Boulerice, A.R., Ross, P.-S., and Mercier-Langevin, P., 2015. Geological and geochemical characteristics of the Waconichi Formation east of the Lemoine auriferous volcanogenic massive sulphide deposit, Abitibi greenstone belt, Quebec, *In:* Targeted Geoscience Initiative 4: Contributions to the Understanding of Volcanogenic Massive Sulphide Deposit Genesis and Exploration Methods Development, (ed.) J.M. Peter and P. Mercier-Langevin; Geological Survey of Canada, Open File 7853, p. 171–182.

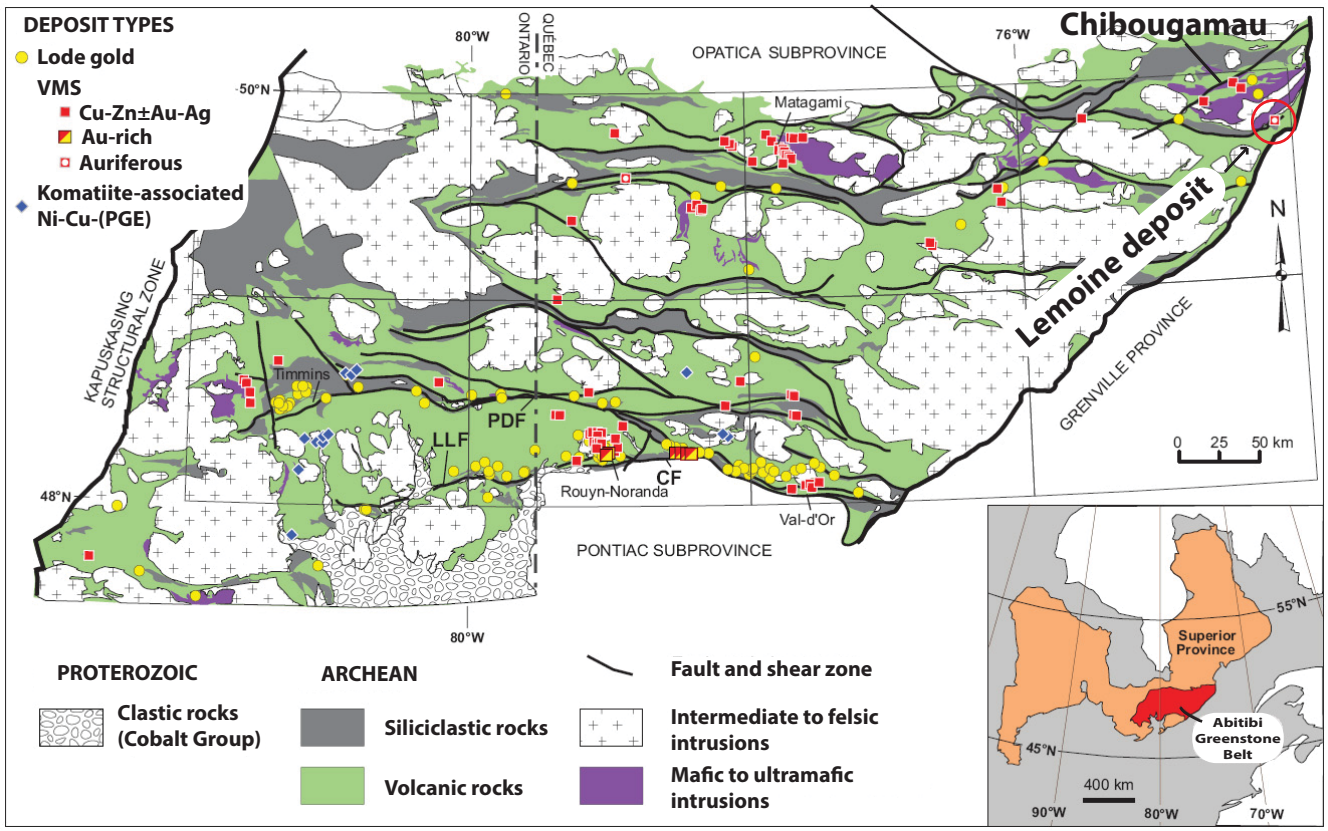

Figure 1. Map of the Abitibi greenstone belt highlighting the Chibougamau camp and the Lemoine deposit. Also shown are significant lode gold, VMS, and Ni-Cu-(PGE) deposits. Modified from Mercier-Langevin et al. (2014).

Lemoine Member is bordered to the north by the Fe-Ti-V-hosting synvolcanic (Mortensen, 1993) Doré Lake Complex and to the south by the Upper Lemoine Member, formerly known as the Gilman Formation (Daigneault and Allard, 1990; Leclerc, 2011) (Fig. 2). Extensive VMS exploration has been undertaken in prospective rocks in the vicinity of the Lemoine deposit and to a lesser extent in the eastern part of the Lower Lemoine Member. However, the geology in the east is somewhat different from that in the Lemoine deposit area, and a better understanding of the volcanic architecture in this prospective area would provide a framework for future exploration. This report presents an overview of the completed work thus far as part of an M.Sc. project at the Institut National de la Recherche Scientifique (INRS) by the first author.

Previous Work

Lafrance and Brisson (2006) summarized knowledge of the Lemoine Member and compiled a detailed geological map covering the mine area and the eastern part of the Lower Lemoine Member. They also reported several synvolcanic faults within the area (Fig. 2). Mercier-Langevin et al. (2014) characterized the various deformed and metamorphosed alteration assemblages associated with the Lemoine deposit, the spatial distributions of these assemblages, and presented a more detailed geochemical analysis of Lower Lemoine Member units in the former mine area. Ross et al. (2014) logged the physical, chemical, and mineralogical properties of drill core from five drillholes located both east and west of the former Lemoine Mine.

Objectives

The main objectives of this study of the eastern sector of the Lower Lemoine Member are (1) better geochemically and texturally define subunits within the Lower Lemoine Member; (2) determine the emplacement processes associated with each subunit; (3) provide a model for the volcanic architecture of the Lower Lemoine Member; and (4) characterize the alteration assemblages and provide an understanding of their spatial distribution in relation to the volcanic architecture, with the aim that this information can be used to vector toward VMS mineralization in the study area and in similar settings elsewhere.

Methodology

Over the course of two field seasons, 145 outcrops were visited, six were mapped in detail at decimetre-scale and 18 drillholes totalling 13,500 metres, were logged. Some 283 samples were collected for lithogeo-

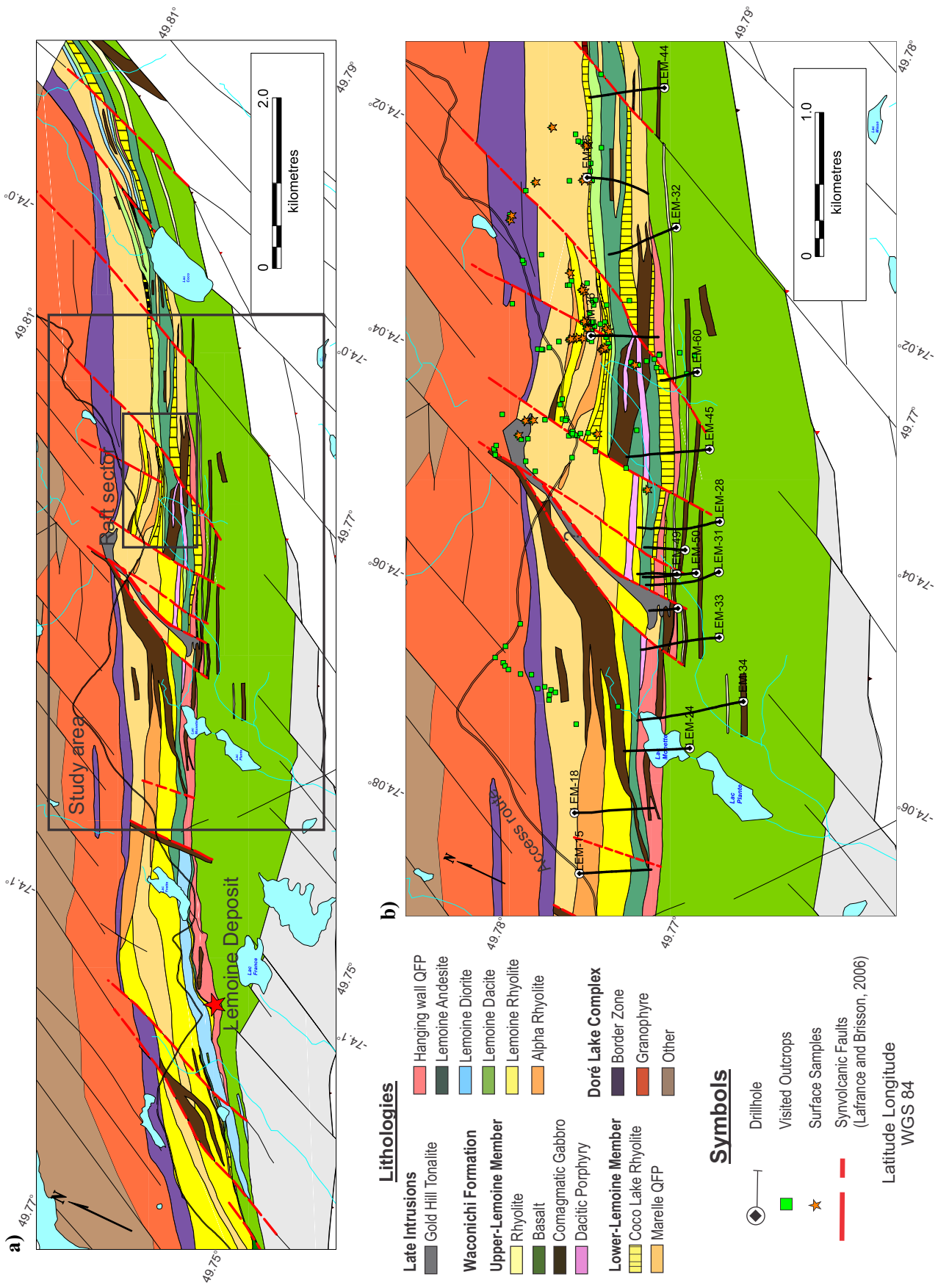

Figure 2. a) Map showing the extent of the Lemoine Member on the south limb of the Chibougamau anticline. **b)** Map of the study area on the Lemoine Property showing all studied drillholes as well as studied outcrops and field samples. Both maps show the most current modifications based on the initial map from Lafrance and Brisson (2006).

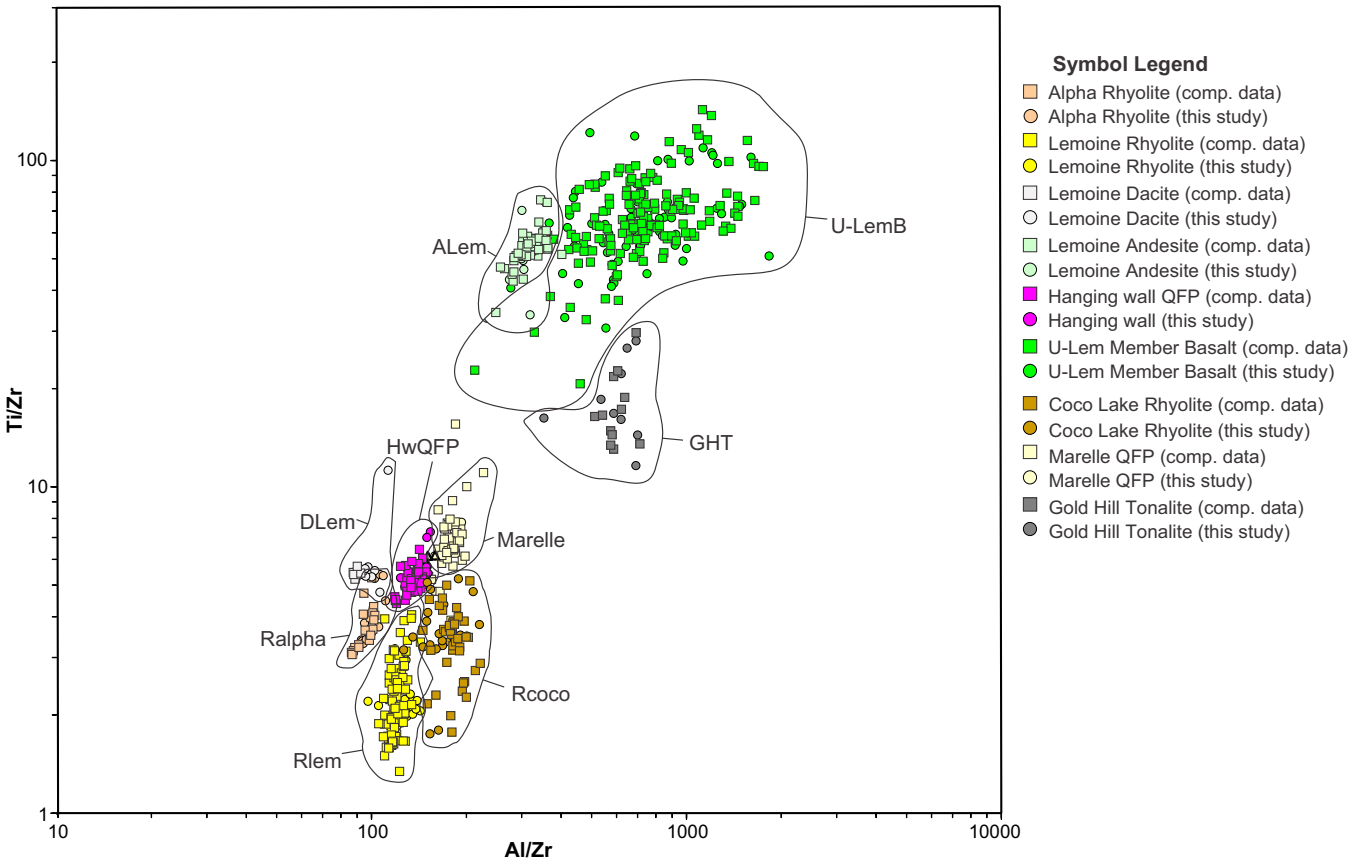

Figure 3. Plot of Ti/Zr versus Al/Zr discrimination diagram. Data represented by circles are from this study. Data represented by squares are compiled from Mercier-Langevin et al. (2014) and from Lafrance and Brisson (2006). Note: comp. = compilation.

chemistry (major and trace elements) and thin sections; 660 additional geochemical analyses were already available from company work in the study area. Bulk geochemical data were first used to discriminate the Lower Lemoine Member subunits from one another and gain a better understanding of their geochemical relationships. Immobile element ratios (e.g. MacLean and Barrett, 1993) were used to discriminate between rocks of similar mineralogical composition and textures. Volcanic textures and lithofacies (e.g. McPhie et al., 1993) helped to elucidate volcanic emplacement modes. Petrographic observations supported identification of macroscopic features and helped to characterize the different alterations assemblages present throughout the study area.

RESULTS

Lower Lemoine Member — Extrusive Units

In the study area, the Lower Lemoine Member contains numerous extrusive units that stratigraphically young towards the southeast. The following sections describe these subunits from the northwest to the southeast (see Fig. 2b), with an emphasis on macroscopic observations, bulk rock geochemistry, and facies identification.

Alpha Rhyolite (RAlpha)

The Alpha Rhyolite (previously the "High-Zr Marelle QFP", Lafrance and Brisson, 2006; Mercier-Langevin et al., 2014) is present in two places in the study area.

Figure 4 opposite. Photographs of selected drill-core samples and intervals. **a)** Fragmental zone ("frag") from 144.53 to 144.70 m in drillhole LEM-15, defined by elongated dark fragments in a lighter sericite altered groundmass within a lobe facies of the Alpha Rhyolite. Fragments are moderately chloritized with a strongly sericitized matrix. **b)** The coherent and spherulitic Alpha Rhyolite on outcrop 13-ARB-019 with the typical "leopard-rock" appearance. **c)** Flow banding in a Lemoine Rhyolite lobe defined by bands of Fe-carbonate, drillhole LEM-18, 350 m. **d)** Fragmental zone ("frag") in the Lemoine Rhyolite, drillhole LEM-18, 406.03 to 406.18 m, defined by dark grey fragments in a lighter grey finer grained groundmass. Fragments sometimes contain an iron-carbonate core (Fe-carb). **e)** Strongly deformed lapilli in the Lemoine Dacite, drillhole LEM-25, 356.9 m. **f)** Pyrrhotite (Po) and pyrite (Py) mineralization within amygdules in the Lemoine Andesite, drillhole LEM-49, 404 m. **g)** Marelle QFP in drillhole LEM-44, 355.5 m. Note the abundant quartz (bluish) and feldspar (milky white) phenocrysts. **h)** Gold Hill Tonalite (GHT) with coarse crystalline texture in contact with the Lemoine Andesite (ALem) in drillhole LEM-28, 387.7 m.

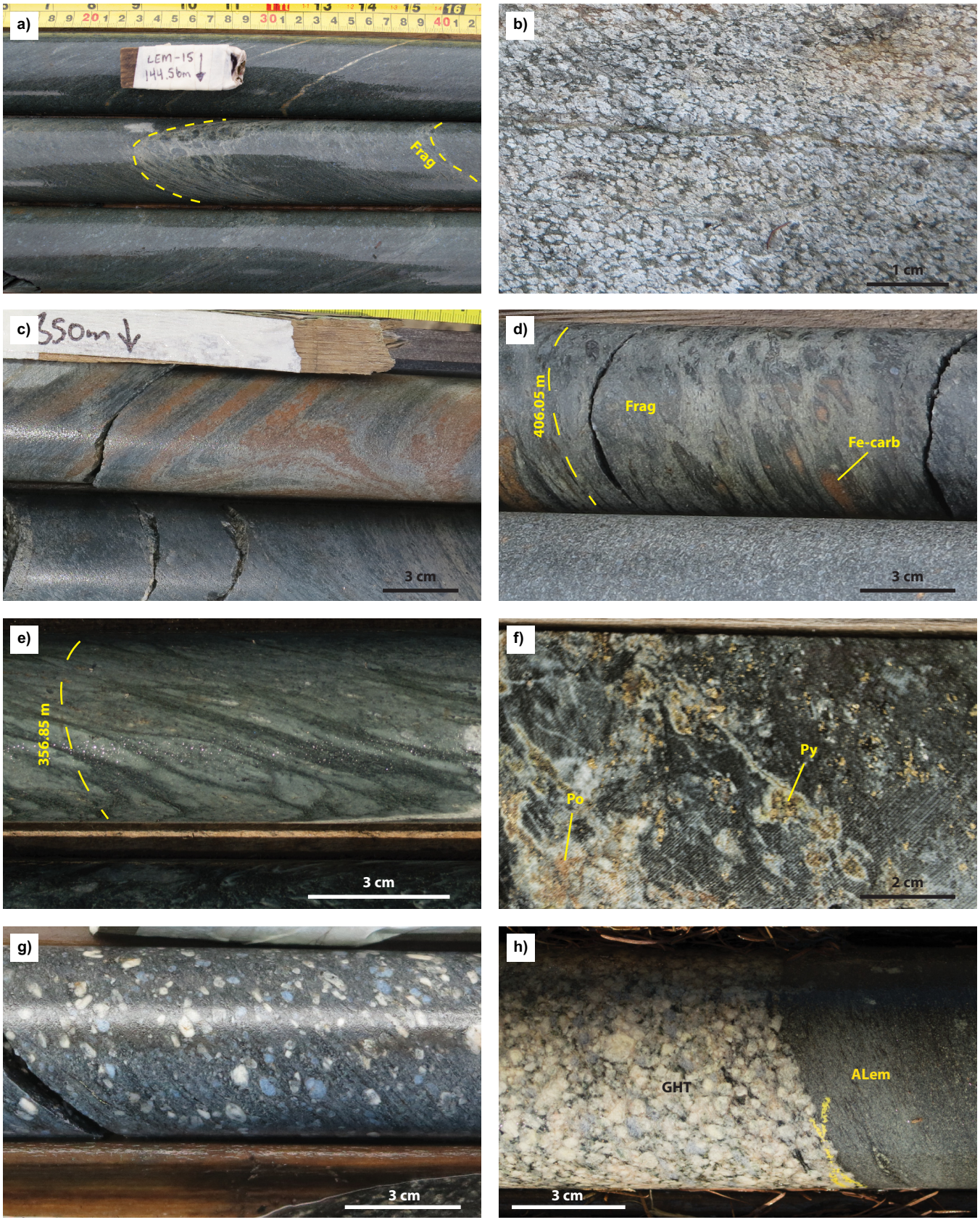
a)
LEM-15
144.56m
Frag
b)
1 cm
c)
3 cm
d)
406.05 m
Frag
Fe-carb
3 cm
e)
356.85 m
3 cm
f)
Py
Po
2 cm
g)
3 cm
h)
GHT
ALem
3 cm

In the southwest, where it is only found in drill core (LEM-15, LEM-18) and does not crop out, it is the oldest extrusive unit and borders the Doré Lake Complex, emplaced prior to formation of the Lemoine Rhyolite. The Alpha Rhyolite is also present in the Raft sector (Fig. 2), where it outcrops. There, it is underlain by the intrusive Marelle QFP (see Fig. 2) and overlain by the extrusive Lemoine Rhyolite. In the Raft sector the Alpha Rhyolite is interpreted to be intrusive.

The Alpha Rhyolite contains 3 to 7 vol.% resorbed quartz phenocrysts (1–3 mm), and locally also contains 1 to 5 vol.% feldspar phenocrysts (1–3 mm), all in a fine groundmass. It is texturally similar to other quartz and feldspar porphyritic (QFP) units in the Lower Lemoine Member (e.g. Marelle QFP and Hanging-wall QFP - see below). The Alpha Rhyolite is of tholeiitic to transitional chemical affinity and is distinguishable from all other Lemoine subunits in a plot of Ti/Zr-Al/Zr ratios (Ti/Zr averages 4.0 and Al/Zr averages 100, Fig. 3). Also the Alpha Rhyolite has less pronounced negative Nb and Ta anomalies (not shown) with an average $[La/Lu]_N$ (McDonough and Sun, 1995) of 1.4, indicating a flatter REE pattern than the Marelle QFP (average $[La/Lu]_N = 3.0$).

The southwest occurrence of the Alpha Rhyolite contains coherent ("massive"), lobate, and hyaloclastite facies; amygdules are locally preserved. The proportions of the facies are compatible with a lobe-hyaloclastite lava-flow architecture (cf. Gibson et al., 1999; Fig. 4a). Within the study area, values for Ishikawa alteration index ($AI = 100(K_2O+MgO)/(K_2O+MgO+Na_2O+CaO)$) (Ishikawa, 1976) and chlorite-carbonate-pyrite index ($CCPI = 100(MgO+FeO)/(MgO+FeO+Na_2O+K_2O)$) (Large et al., 2001) alteration indices (not shown) are highest in the Alpha Rhyolite, largely in samples from drillholes LEM-15 and LEM-18 (Fig. 2b).

In the Raft sector, the Alpha Rhyolite is coherent and a coarse "leopard-like" spherulitic texture is omnipresent (Fig. 4b) with up to 1 cm-wide, locally coalescing spherules. The overall map pattern, stratigraphic relationships, uniformly coherent textures, and the presence of an angular enclave of Lemoine Rhyolite within the Alpha Rhyolite suggests that the Alpha Rhyolite is intrusive in the Raft sector. It represents a second pulse of magma of Alpha Rhyolite composition, rich in quartz phenocrysts (up to 15 vol.% in drillhole LEM-36), emplaced after both the extrusive Alpha Rhyolite in the southwest and the overlying Lemoine Rhyolite.

Lemoine Rhyolite (RLem)

The Lemoine Rhyolite, which is the immediate footwall of the Lemoine deposit (Donahue, 1982; Mercier-Langevin et al., 2014), extends 10 km along strike from southwest of the former mine site to the Raft sector in the northeast. It reaches a thickness of ~200 m near the Lemoine deposit (Mercier-Langevin et al., 2014) and thins systematically to the northeast (Fig. 2a). This subunit is tholeiitic (Figs. 5, 6), with average Ti/Zr and Al/Zr ratios of 2.1 and 126, respectively (Fig. 3). The Lemoine Rhyolite varies in colour from light to dark grey-green, depending on the abundance of chlorite alteration. The subunit contains 1–5 vol.%, 1–3 mm euhedral blue quartz phenocrysts surrounded by a milky quartz corona in an aphanitic groundmass.

The Lemoine Rhyolite has substantial coherent portions with massive to flow-banded lobes (Fig. 4c), spherulitic (Fig. 4b), or amygdular zones (quartz and Fe-carbonate-filled amygdules), and lesser fragmental

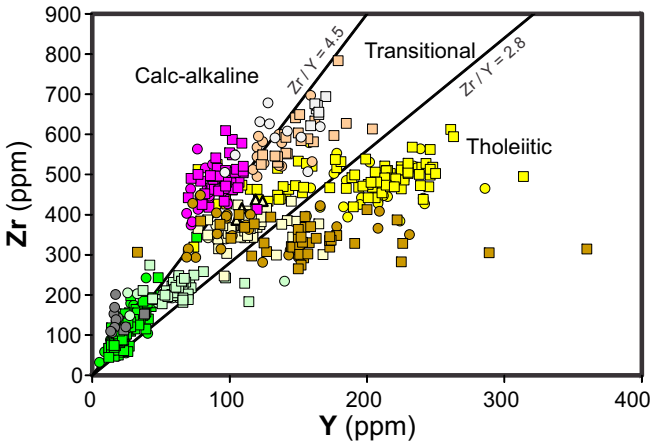

Figure 5. Zr versus Y plot of tholeiitic versus calc-alkaline magmatic affinity. Fields from Ross and Bédard (2009). Data from this study, from Mercier-Langevin et al. (2014) and from Lafrance and Brisson (2006). Symbol legend can be found on Figure 3.

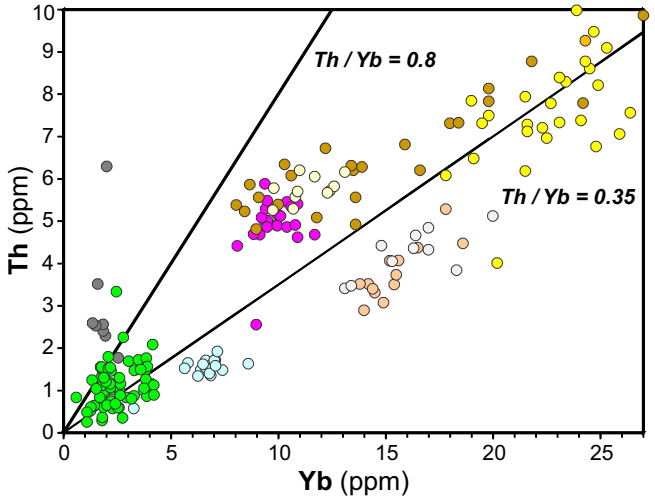

Figure 6. Th versus Yb plot of tholeiitic versus calc-alkaline magmatic affinity. Fields from Ross and Bédard (2009). Data shown are from this study, from Mercier-Langevin et al. (2014), and from Lafrance and Brisson (2006). Symbol legend can be found on Figure 3.

portions (e.g. hyaloclastite: Fig. 4d). Two major phases are present in the Lemoine Mine area (Mercier-Langevin et al., 2014) and a similar architecture is present in the study area. The first phase has a lobe-hyaloclastite flow-style basal component and an upper fragmental zone composed of lapilli-size fragments. The second phase is a mostly massive flow that is intruded by the Coco Lake Rhyolite in the Raft sector. Alteration indices are highest in drillholes LEM-15 and -18 in the southwest part of the study area, as well as in drillhole LEM-36, just south of the Raft sector (Fig. 2b).

Lemoine Dacite (DLem)

The Lemoine Dacite is a ≤60 m-thick, laterally continuous unit that is only present in the northeast part of the study area, extending between drillhole LEM-52 and the edge of the study area in the northeast (Fig. 2b). Geochemically, the Lemoine Dacite has average Al/Zr and Ti/Zr ratios of 99 and 6.0 (Fig. 3), respectively, distinguishing it from the Alpha Rhyolite. The Lemoine Dacite is transitional to calc-alkaline with an average Zr/Y ratio of 4.5 (Fig. 5). This unit does not outcrop well in the study area and is only present in drill core, where it is grey-green to dark grey-green, aphanitic, and ranges from massive to mostly fragmental and spherulitic. There is a systematic spatial variation in fragment size from 2 to 3 cm-wide fragments in drillhole LEM-25 (Fig. 4e) to millimetre-scale fragments in drillhole LEM-52, which is situated in the southwest part of the study area (Fig. 2b). Except for some chloritic alteration of the tuff matrix and late carbonate veining, the Lemoine Dacite is only weakly altered.

Lemoine Andesite (ALem)

The Lemoine Andesite forms a ≤200 m-thick lava unit that extends from east of the Lemoine Mine to the northeast termination of the Lower Lemoine Member (Fig. 2). It is differentiated from the Upper Lemoine Member basalt by being tholeiitic with an average Th/Yb ratio of 0.26 (Fig. 6). The Lemoine Andesite also has flatter REE patterns with an average $[La/Lu]_N$ of 1.6 (Upper Lemoine Member basalt averages $[La/Lu]_N = 3.6$). The Lemoine Andesite is black to dark grey-green with local amygdaloidal zones that contain 1–5 vol.%, 1–3 mm blue quartz amygdules. Light green patches of agglomerated epidotized plagioclase phenocrysts are irregularly present throughout the unit. Some 1–3 mm euhedral garnet porphyroblasts occur in narrow bands in drillhole LEM-49, between 325 and 328 m. The Lemoine Andesite is composed predominantly of massive and pillowed flows; the pillows are separated by thin (<10 cm) layers of hyaloclastite. The Lemoine Andesite contains one tuffaceous zone in the middle and a second one at the top of the subunit. The middle tuffaceous zone, composed of centimetre-scale interbedded chert and biotite-rich tuff, only occurs in the eastern part of the study area, and its thickness cannot properly be constrained as it is always in contact with an intrusion (e.g. drillhole LEM-44 at 491 m). The top tuffaceous layer is thickest in drillhole LEM-15, where it forms a 3 m-thick laminated siliceous tuff interbedded with thin centimetre-scale beds of lapilli-size hyaloclastite. The same top tuffaceous unit in drillhole LEM-31E is only 32 cm thick. The Lemoine Andesite is commonly strongly chloritic due to metamorphism to upper-greenschist facies, but alteration indices are strongest near drillholes LEM-49 and -33, where pyrite and pyrrhotite mineralization is associated with amygdules (Fig. 4f).

Hanging-Wall Quartz and Feldspar Porphyry (HwQFP)

The Hanging-wall QFP conformably overlies the Lemoine Andesite in the northeast part of the Lower Lemoine Member and sits directly on top of the Lemoine Rhyolite in the mine area, where it forms the immediate hanging-wall to VMS mineralization (Mercier-Langevin et al., 2014). It is a laterally extensive unit up to 175 m thick near the former mine site and pinches out progressively to the northeast. It is readily identified by its stratigraphic position, its transitional to calc-alkaline magmatic affinity, and lower Al/Zr ratios than the other QFPs (Fig. 3). This unit is quartz- and feldspar-phyric with similar size and abundance of quartz (3–7 vol.%, 1–4 mm) and feldspar (5–8 vol.%, 1–4 mm) phenocrysts to the Coco Lake Rhyolite and the Marelle QFP. Both coherent and fragmental facies have been documented (Lafrance and Brisson, 2006), but the emplacement mode of this subunit has not been studied in detail. Iron-carbonate amygdules, up to 5 cm across, are present in the Hanging-wall QFP in the western part of the study area, but are less abundant elsewhere. A tuffaceous layer situated at the top of the HwQFP in drillhole LEM-31 is composed of five 10–15 cm-thick, normally graded beds of lapilli-tuff to tuff in contact with the Coco Lake Rhyolite.

Upper Lemoine Member — Extrusive Units

The Upper Lemoine Member (previously known as the Gilman Formation) conformably overlies the Lower Lemoine Member. It is composed mostly of basaltic flows with lesser gabbro, rhyolitic massive flows, and a few chert layers.

Upper Lemoine Member Basalt (BuLem)

This unit forms the bulk of the Upper Lemoine Member volcanic package in the study area and is laterally continuous. It is geochemically variable but is distinct from the Lemoine Andesite based on its differ-

ent stratigraphic position and its transitional to calc-alkaline magmatic affinity (Figs. 5, 6). The Upper Lemoine Basalt is composed essentially of massive and pillow facies. Texturally, the basalt is mostly aphanitic, with local areas containing up to 10 vol.% acicular amphibole crystals. The unit also locally contains 3–6 vol.% quartz-carbonate amygdules within pillows.

Upper Lemoine Member Rhyolite (RuLem)

Thin massive aphanitic rhyolite layers are intercalated with the basaltic flows, but they comprise only a minute part of the Upper Lemoine Member. Geochemical analyses indicate the calc-alkaline nature of this subunit (average Zr/Y = 5.2), and this feature, together with its position higher up in the volcanic stratigraphy, provide the basis for its identification.

Intrusions

Marelle Quartz and Feldspar Porphyry (QFP)

The Marelle QFP is a laterally extensive subunit that extends from southwest of the Lemoine Mine to beyond the study area to the east (Fig. 2). In the study area it occurs at multiple positions in the volcanic stratigraphy, but the thickest sill borders the Doré Lake Complex. The Marelle QFP is up to 350 m thick in some locations, making it the thickest subunit in the Lower Lemoine Member. The Marelle QFP crops out in multiple locations because of its great thickness, coherent texture, felsic composition, and relative minor alteration. Contacts with other units are sharp.

The Marelle QFP exhibits an average Ti/Zr ratio of 6.8 and an average Al/Zr ratio of 178, but with variable Al/Zr ratios (see Fig. 3). Texturally, the Marelle QFP contains 10–25 vol.%, 4–7 mm sub- to euheudral zoned blue quartz phenocrysts and 10–20 vol.% subeuhedral to euhedral poikiolitic plagioclase crystals in an aphanitic groundmass (Fig. 6g). Petrographically the groundmass is composed predominantly of 20–50 µm quartz and feldspar, making this groundmass coarser than that of other QFP subunits.

Coco Lake Rhyolite (RCoco)

The Coco Lake Rhyolite (previously "Upper Lemoine Rhyolite", Lafrance and Brisson, 2006; Mercier-Langevin et al., 2014) is a subvolcanic intrusive subunit present as a laterally continuous sill and dyke complex that occurs at multiple stratigraphic levels in and above the Lower Lemoine Member. The Coco Lake Rhyolite is present only in the northeast part of the Lemoine Member, mostly in and around the Raft sector. It is a quartz- and feldspar-phyric subunit with 7–10 vol.% blue quartz and 3–5 vol.% plagioclase phenocrysts. Intrusions of Coco Lake Rhyolite occur within the Lemoine Rhyolite, immediately below the Lemoine Dacite, above the Lemoine Andesite and above the HwQFP.

This subunit is difficult to distinguish visually from other QFP subunits in the Lower Lemoine Member because of subtle variations in phenocrysts populations and similar shapes and sizes thereof. Geochemically it has a tholeiitic magmatic affinity (Figs. 5, 6) and has a distinctively lower Ti/Zr ratio (average of 3.7) and a lower Al/Zr ratio (average of 169) than the Marelle QFP. The Coco Lake Rhyolite is consistently coherent throughout the study area and has sharp contact relationships with surrounding subunits. The subunit is likely subvolcanic, as it occurs at multiple stratigraphic levels, is coherent, and has sharp contacts with surrounding subunits. Where it is situated between the HwQFP and the Lemoine Andesite, it is responsible for the discontinuity of the chert horizon.

Gold Hill Tonalite (TGH)

The Gold Hill Tonalite is present in the lower part of the volcanic stratigraphy, immediately west of the Raft sector, where it is in contact with multiple subunits, ranging from the Lemoine Rhyolite to the Lemoine Andesite (Fig. 4h). Geochemically it occupies a specific area of moderate Al/Zr and high Ti/Zr by which it is readily distinguished from other lithologies (Fig. 3). Also, the Gold Hill Tonalite is strongly calc-alkaline (Figs. 5, 6) with a steep REE pattern (average $[La/Lu]_N$ = 5.8). It is pink and is phaneritic with abundant plagioclase (70 vol.%), moderate quartz (25 vol.%), and minor potassium feldspar (5 vol.%). One outcrop sample is geochemically identical to a drill-core sample, but the outcrop lacks the porphyritic to almost crystalline texture present in drill core. Contact relationships are sharp (Fig. 4h), and surrounding rocks are commonly highly magnetic up to 20 m away from the contact. The Gold Hill Tonalite is weakly altered relative to the volcanic rocks of the Lower Lemoine Member.

DISCUSSION

Volcanic Model

Our data indicate that the base of the Lower Lemoine Member is composed locally of extrusive Alpha Rhyolite, which was emplaced in one or more lobe-hyaloclastite flow(s). Based on the laterally restricted nature of this subunit, the volcanic centre is most likely situated in the western part of the study area.

A more sustained volcanic episode was necessary to produce the lava flows associated with the laterally extensive Lemoine Rhyolite. The emplacement of the Lemoine Rhyolite can be divided into two stages, as identified by Mercier-Langevin et al. (2014): coherent rhyolite at the base with overlying lobes and hyaloclastite. Based on lateral thickness variations, we suggest that the effusive centre for the Lemoine Rhyolite is situated to the west of the study area.

Overlying the Lemoine Rhyolite, but only present in the eastern part of the study area, is the Lemoine Dacite. The Lemoine Dacite also extends outside the study area to the east and thus more work is needed to pinpoint the location of the effusive centre. However, at depth this subunit becomes consistently thinner, suggesting that the volcanic vent was situated above present day erosion levels.

The Lemoine Andesite consists of massive flows and pillowed flows. It can be subdivided into at least two flows or flow packages based of the presence of a chert layer mid-level within its stratigraphy, and which marks a hiatus in volcanism. A second chert layer is located at the top of the subunit. The presence of sulphide mineralization in amygdules suggests that hydrothermal fluids were circulating within the Lemoine Andesite. Based on thickness variations, it is plausible that the Lemoine Andesite vent is located in the study area.

The HwQFP represents the last episode of volcanism associated with the Lower Lemoine Member. Lobes with flow banding present on an outcrop west of the study area confirm the extrusive nature of this subunit. Based on thickness variations alone, the HwQFP may share the same volcanic vent as the Lemoine Rhyolite west of the study area, but confirmation based on volcanic facies variations is needed. The HwQFP marks a change in magmatic affinity relative to the underlying subunits, which may indicate a change in the tectonic environment or different petrogenetic conditions; however, subsequent felsic intrusions in the Lower Lemoine Member revert to tholeiitic to transitional affinities. Above the HwQFP, the Upper Lemoine Basalt and Rhyolite become more transitional to calc-alkaline magmatic in affinity. Upper Lemoine Basalt was emplaced as massive and pillowed flows. However, the extrusive nature of the Upper Lemoine Rhyolite is unclear, as it only occurs as coherent rocks that forms thin discontinuous bands within the Upper Lemoine Basalt.

Intrusions

The timing of the multiple subvolcanic intrusions within the Lower Lemoine Member is not completely resolved. The Marelle QFP occurs at the stratigraphic base, within the Lemoine Andesite, and in contact with the Upper Lemoine Basalt in the northeast part of the property. The Coco Lake Rhyolite is also present at similar stratigraphic positions. Together, these observations suggest that the intrusions are younger than at least some Upper Lemoine Basalt (and therefore all extrusive subunits in the Lower Lemoine Member). However, it has not been established which of the two intrusive QFPs, Marelle or Coco Lake, is the youngest.

The strong calc-alkaline magmatic affinity of the Gold Hill Tonalite and the distinct magnetite alteration in the adjacent host rocks suggests it post-dates the Marelle QFP and the Coco Lake Rhyolite. It is possible that the GHT is linked with a phase of the ca. 2718–2712 Ma Chibougamau Pluton.

The results of this study indicate that the Lower Lemoine Member, which hosts the Lemoine auriferous VMS deposit, consists of a relatively thick, felsic-dominated sequence that comprises a significant portion of shallow intrusive rocks that are coeval and cogenetic with the effusive rocks. This sequence is intruded at its base by the large synvolcanic Doré Lake Complex (Mortensen, 1993; Leclerc et al., 2012; Mercier-Langevin et al., 2014). This setting indicates the development of a major thermal corridor in that area and we speculate that these conditions may have contributed in forming such a base- and precious-metal-rich deposit, as suggested by the analysis of Singer et al. (2011), who observe higher average copper and gold grades in VMS deposits that are associated with syn-VMS mineralization intrusions.

IMPLICATIONS FOR EXPLORATION

The results presented herein provide an improved volcanological, textural, geochemical, and mineralogical characterization of all subunits present within the Lower Lemoine Member, and provide key stratigraphic relationships and the overall volcanic architecture of the Lower Lemoine Member. This sets the framework for future exploration by highlighting volcanic subunits and marker horizons that can be followed and used to vector toward concealed mineralization in subsequent drillholes laterally and at depth on the property. Understanding emplacement processes of the Lower Lemoine Member subunits will help optimize exploration by providing an improved geological model and, perhaps, new exploration targets. The spatial distribution of the metamorphosed, synvolcanic hydrothermal alteration can be mapped, and the classic AI alteration index of Ishikawa et al. (1976) appears to be a robust vectoring tool. Although determination of the locations of the paleo-volcanic vents is still in progress, these vents are commonly spatially associated with synvolcanic fissures and faults. Such fissures and faults are zones of increased cross-stratal permeability along which high-temperature, VMS-mineralizing hydrothermal fluids can have been channelized (e.g. Gibson et al., 1999; Franklin et al., 2005). The information provided above, although preliminary, can be used to develop potential new targets for exploration.

FUTURE WORK

Additional work is underway by the authors of this paper to better understand the volcanic architecture of

the Lower Lemoine Member, including (1) quantitative facies-variation analysis within each extrusive subunit in the Lower Lemoine Member; (2) precise U-Pb zircon geochronology to help understand the volcanic and intrusive evolution of the Lemoine Member; (3) characterization of alteration assemblages in the study area and comparisons with work done in the Lemoine deposit vicinity (Mercier-Langevin et al., 2014) to help define exploration vectors in the study area; and (4) testing the inferred synvolcanic nature of the north-northeast–south-southwest (NNE–SSW) faults in the study area identified by Lafrance and Brisson (2006) remains to be examined.

ACKNOWLEDGEMENTS

We thank Cogitore Resources Inc., National Science and Engineering Council (NSERC) and the Geological Survey of Canada (TGI-4 program) for supporting the project financially. Discussions with Tony Brisson, François Leclerc, Francis Lefebvre, Sylvain Lépine, and Gérald Riverin on the geology of the Chibougamau area have been very helpful. We thank Cogitore Resources for the authorization to publish. Thanks to Jan Peter and Steve Piercey for their careful review of the manuscript.

REFERENCES

Daigneault, R. and Allard, G.O., 1990. Le Complexe du Lac Doré et son environnement géologique (région de Chibougamau - sous-province de l'Abitibi); Ministère de l'Énergie, des Mines et des Ressources du Québec, Report MM 89-03, 275 p.

Donahue, J.C., 1982. The Geology and Petrochemistry of the Patino-Lemoine Deposit and its Host Rocks, Lemoine Township, Québec; M.Sc. thesis, University of Georgia, Athens, Georgia, 275 p.

Franklin, J., Gibson, H., Jonasson, I., and Galley, A., 2005. Volcanogenic massive sulfide deposits, *In:* 100th Anniversary Volume, (ed..) J.W. Hedenquist, J.F.H. Thompson, R.J. Goldfarb, and J.P. Richards; Society of Economic Geologists, Littleton, Colorado, p. 523–560.

Gibson, H.L., Morton, R.L., and Hudak, G.J., 1999. Submarine volcanic processes, deposits and environments favorable for the location of volcanic-associated massive sulfide deposits; Reviews in Economic Geology, v. 8, p. 13–51.

Ishikawa, Y., Sawaguchi, T., Iwaya, S., and Horiuchi, M., 1976. Delineation of prospecting targets for Kuroko deposits based on modes of volcanism of underlying dacite and alteration haloes; Mining Geology, v. 26, p. 105–117.

Lafrance, B. and Brisson, T., 2006. Rapport sur le programme de forage 2005, projet Lemoine, Woodruff Capital Management Inc.; Ministère de l'Énergie et des Ressources Naturelles du Québec, Report GM 62564, 36 p.

Large, R.R., Gemmell, J.B., Paulick, H., and Huston, D.L., 2001. The alteration box plot: A simple approach to understanding the relationship between alteration mineralogy and lithogeochemistry associated with volcanic-hosted massive sulfide deposit; Economic Geology, v. 96, p. 957–971.

Leclerc, F., Bédard, J.H., Harris, L.B., McNicoll, V.J., Goulet, N., Roy, P., and Houle, P., 2011, Tholeiitic to calc-alkaline cyclic volcanism in the Roy Group, Chibougamau area, Abitibi Greenstone Belt— revised stratigraphy and implications for VHMS exploration; Canadian Journal of Earth Sciences, v. 48, p. 661-694.

Leclerc, F., Harris, L.B., Bédard, J.H., Van Breemen, O., and Goulet, N., 2012. Structural and stratigraphic controls on magmatic, volcanogenic, and shear zone-hosted mineralization in the Chapais-Chibougamau mining camp, northeastern Abitibi, Canada; Economic Geology, v. 107, p. 963–969.

MacLean, W. and Barrett, T., 1993. Lithogeochemical techniques using immobile elements; Journal of Geochemical Exploration, v. 48, p. 109–133.

McDonough, W. F., and Sun, S.-S., 1995, The composition of the Earth; Chemical Geology, v. 120, p. 223-253.

McPhie, J., Doyle, M., and Allen, R., 1993. Volcanic Textures: A Guide to the Interpretation of Textures in Volcanic Rocks; Centre for Ore Deposit and Exploration Studies, University of Tasmania, 196 p.

Mercier-Langevin, P., Hannington, M.D., Dubé, B., and Bécu, V., 2011. The gold content of volcanogenic massive sulfide deposits; Mineralium Deposita, v. 46, p. 509–539.

Mercier-Langevin, P., Lafrance, B., Bécu, V., Dubé, B., Kjarsgaard, I., and Guha, J., 2014. The Lemoine auriferous volcanogenic massive sulfide deposit, Chibougamau Camp, Abitibi greenstone belt, Quebec, Canada: geology and genesis; Economic Geology, v. 109, p. 231–269.

Mortensen, J. K., 1993. U-Pb geochronology of the eastern Abitibi Subprovince. Part 1: Chibougamau - Matagami - Joutel region; Canadian Journal of Earth Sciences, v. 30, p. 11–28.

Ross, P.-S. and Bédard, J.H., 2009. Magmatic affinity of modern and ancient subalkaline volcanic rocks determined from trace-element discriminant diagrams; Canadian Journal of Earth Sciences, v. 46, p. 823–839.

Ross, P.S., Bourke, A., Leclerc, F., and Boulerice, A.R., 2014. Analyse multiparamétrique à haute résolution de carottes de forage dans la région de Chibougamau 2012-2014, rapport final; Ministère de l'Énergie et des Ressources naturelles du Québec, in press.

Salmon, B. and McDonough, B., 2011. Technical report on the mineral resource estimate of the Scott Lake project, northern Québec, Canada, Roscoe Postle Associates Inc; Internal Report to Cogitore Resources, 102 p.

Sangster, D., 1980. Quantitative characteristics of volcanogenic massive sulphide deposits I; Canadian Institute of Mining and Metallurgy Bulletin, v. 73, p. 74–81.

Saunders, J.A. and Allard, G.O., 1990. The Scott Lake deposit: a contact-metamorphosed volcanogenic massive sulfide deposit, Chibougamau area, Quebec; Canadian Journal of Earth Sciences, v. 27, p. 180–186.

Singer, D.A., Berger, V.I., and Mosier, D.L., 2011. Effects of intrusions on grades and contents of gold and other metals in volcanogenic massive sulfide deposits; Ore Geology Reviews, v. 39, p. 116–118.

GEOLOGICAL SURVEY OF CANADA
OPEN FILE 7853

Targeted Geoscience Initiative 4: Contributions to the Understanding of Volcanogenic Massive Sulphide Deposit Genesis and Exploration Methods Development

Mineralogical, sulphur, and lead isotopic study of the Lemarchant Zn-Pb-Cu-Ag-Au-VMS deposit: Implications for precious-metal enrichment processes in the VMS environment

Shannon B. Gill[1], Stephen J. Piercey[1], Daniel Layton-Matthews[2], Graham D. Layne[1], and Glenn Piercey[3]

[1]Memorial University of Newfoundland, St. John's, Newfoundland and Labrador
[2]Queen's University, Kingston, Ontario
[3]MicroAnalysis Facility, CREAIT Network, Memorial University of Newfoundland, St. John's, Newfoundland and Labrador

2015

Recommended citation

Gill, S.B., Piercey, S.J., Layton-Matthews, D., Layne, G.D., and Piercey, G., 2015. Mineralogical, sulphur, and lead isotopic study of the Lemarchant Zn-Pb-Cu-Ag-Au-VMS deposit: Implications for precious-metal enrichment processes in the VMS environment, *In:* Targeted Geoscience Initiative 4: Contributions to the Understanding of Volcanogenic Massive Sulphide Deposit Genesis and Exploration Methods Development, (ed.) J.M. Peter and P. Mercier-Langevin; Geological Survey of Canada, Open File 7853, p. 183–195.

TABLE OF CONTENTS

Mineralogical, sulphur, and lead isotopic study of the Lemarchant Zn-Pb-Cu-Ag-Au-VMS deposit: Implications for precious-metal enrichment processes in the VMS environment

Shannon B. Gill[1]*, Stephen J. Piercey[1]†, Daniel Layton-Matthews[2], Graham D. Layne[1], and Glenn Piercey[3]

[1]Department of Earth Sciences, Memorial University of Newfoundland, St. John's, Newfoundland and Labrador A1B 3X5
[2]Department of Geological Sciences and Geological Engineering, Queen's University, Kingston, Ontario K7L 3N6
[3]MicroAnalysis Facility, CREAIT Network, Memorial University of Newfoundland, St. John's, Newfoundland and Labrador A1B 3X5
*Corresponding author's e-mail: s.gill@mun.ca
†Corresponding author's e-mail: spiercey@mun.ca

ABSTRACT

The Lemarchant deposit is a Cambrian volcanogenic massive sulphide (VMS) deposit located in the Central Mobile Belt of the Newfoundland Appalachians. Unlike other polymetallic VMS deposits in the bimodal felsic Tally Pond group, Lemarchant is enriched in precious metals. The deposit is composed of contrasting styles of sulphide mineralization, and formed in three discrete stages: *Stage 1:* barite-rich, low-temperature (<250ºC) VMS mineralization; *Stage 2:* 150 to 250ºC intermediate- to high-sulphidation epithermal-style mineralization; and *Stage 3*: polymetallic, high-temperature (>300ºC) VMS mineralization. Sulphur isotopes suggest that S is derived from three sources: thermochemically reduced seawater sulphate, leached igneous basement rock, and magmatic SO_2. Lead isotopes indicate that Pb is primarily derived from evolved crustal material, with some input from juvenile volcanic rock (i.e. arc-rift). Precious metals associated with epithermal-style mineralization are consistent with a magmatic contribution to the hydrothermal fluid. Precious metals were precipitated from intermittently boiled fluids, at relatively shallow (<1500 m) water depth.

INTRODUCTION

Although volcanogenic massive sulphide (VMS) deposits with precious metal enrichment have been studied globally (e.g. Huston, 2000; Dubé et al., 2007; Mercier-Langevin et al., 2011), precious metal-bearing VMS deposits in the Newfoundland Appalachians are not well-documented and the cause(s) of enrichment in these deposits is poorly understood. The source(s) of precious metals, the environmental and physiochemical conditions that persist during the formation of a VMS deposit can all influence the degree to which a deposit is enriched in metal, including Au and Ag (Poulsen and Hannington, 1995; Hannington et al., 1999; Huston, 2000; Dubé et al., 2007). The Central Mobile Belt in Newfoundland hosts a large number of VMS deposits, including past and presently producing mines, and non-producing deposits and prospects that range from Cu-rich to polymetallic (Swinden and Kean, 1988; Piercey and Hinchey, 2012); a number of these deposits are also precious metal-enriched (e.g. Santaguida and Hannington, 1993, 1996; Pilote and Piercey, 2013; Pilote et al., 2014; Brueckner et al., 2014). The Zn-Pb-Cu-Ag-Au Lemarchant VMS deposit is located in the Tally Pond volcanic belt, together with the currently producing (yet precious metal-poor) Duck Pond and Boundary VMS deposits (Evans and Kean, 2002; McNicoll et al., 2010; Piercey et al., 2014). Lemarchant contains well-preserved sulphide mineral textures and presents an ideal subject for investigating mechanisms of precious metal enrichment in Newfoundland VMS deposits.

The Lemarchant deposit was discovered in 1983, and contains an indicated mineral resource of 1.24 million tonnes grading 5.38 wt% Zn, 0.58 wt% Cu, 1.19 wt% Pb, 1.01 g/t Au, and 59.17 g/t Ag and an inferred mineral resource of 1.34 million tonnes grading 3.70 wt% Zn, 0.41 wt% Cu, 0.86 wt% Pb, 1.00 g/t Au, and 50.41 g/t Ag (Fraser et al., 2012). Herein, we present detailed petrographic and in situ trace and isotope mineral chemical data for the Lemarchant deposit collected using a combination of scanning electron microscopy (SEM), electron microprobe (EMPA), laser ablation

Gill, S.B., Piercey, S.J., Layton-Matthews, D., Layne, G.D., and Piercey, G., 2015. Mineralogical, sulphur, and lead isotopic study of the Lemarchant Zn-Pb-Cu-Ag-Au-VMS deposit: Implications for precious-metal enrichment processes in the VMS environment, *In:* Targeted Geoscience Initiative 4: Contributions to the Understanding of Volcanogenic Massive Sulphide Deposit Genesis and Exploration Methods Development, (ed.) J.M. Peter and P. Mercier-Langevin; Geological Survey of Canada, Open File 7853, p. 183–195.

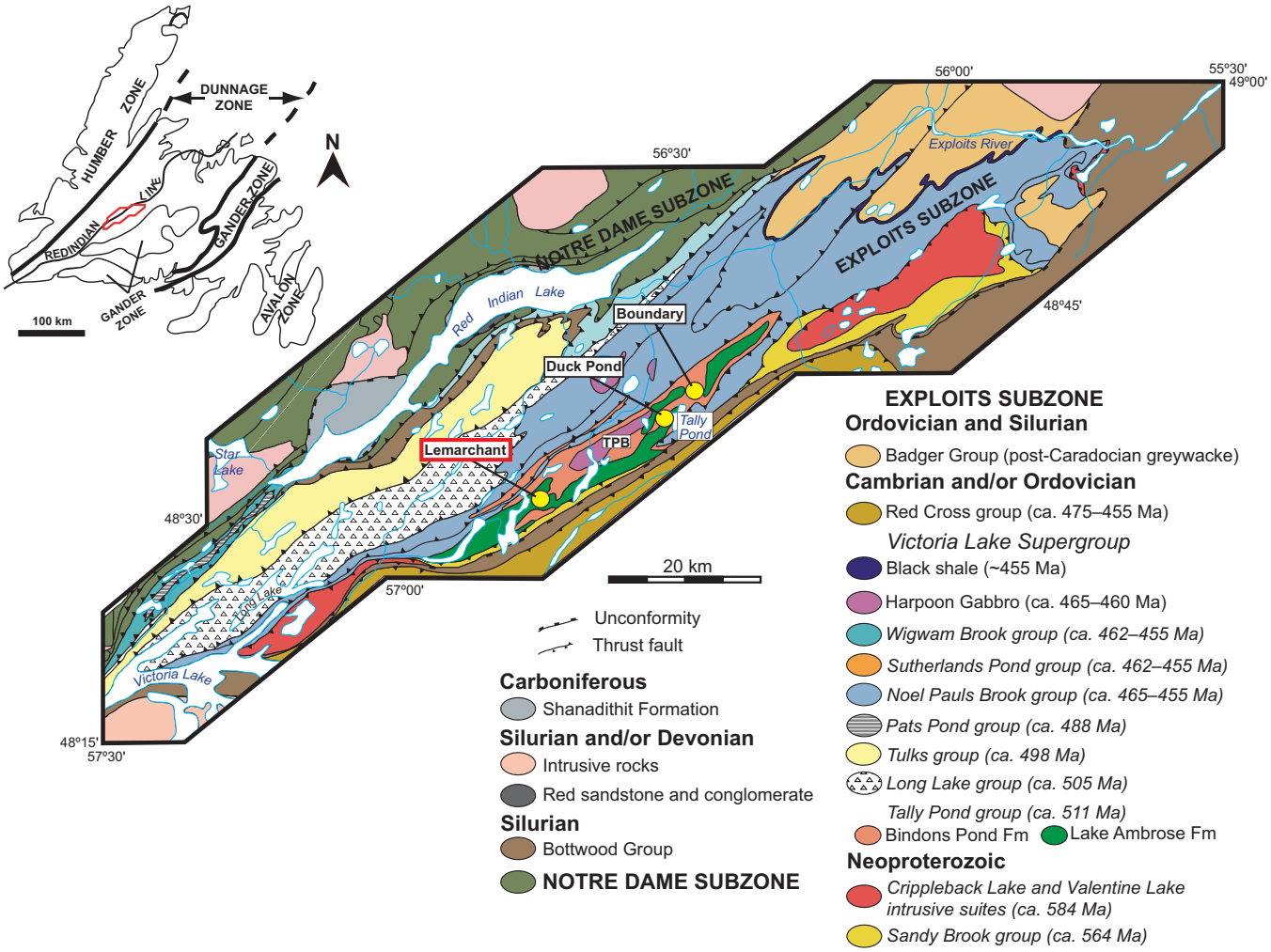

Figure 1. Geological map of the volcanic sequences comprising the Exploits subzone, eastern Dunnage Zone. The Tally Pond volcanic belt (TPB) is host to the Lemarchant VMS deposit (in red), Duck Pond and Boundary VMS deposits. Modified from Rogers et al. (2006), McNicoll et al. (2010), and Piercey and Hinchey (2012). Inset map (Williams, 1979) outlines the 4 tectonostratigraphic zones of the Newfoundland Appalachians; map area of Exploits subzone is outlined in red.

inductively coupled plasma (LA-ICP-MS), and secondary ion mass spectrometry (SIMS). The goal of this project is to provide a model for the mineralogical and metallogenic evolution of the Zn-Pb-Cu-Ag-Au Lemarchant deposit. We present here a summary of the work completed to date, and a genetic model for the Lemarchant deposit (and similar deposits elsewhere) that explains the enrichment of precious metals in VMS deposits.

GEOLOGICAL SETTING

Most VMS deposits in the Newfoundland Appalachians are situated within the Dunnage Zone, the central tectonostratigraphic zone of the Newfoundland Appalachians. The Dunnage Zone hosts a suture zone (Red Indian Line, Fig. 1 inset) between volcanic arc sequences of Laurentian and Gondwanan affinity that merged during the Silurian closure of the Iapetus Ocean (Williams, 1979; van Staal et al., 1998; van Staal and Barr, 2012). The eastern, peri-Gondwanan portion of the Dunnage Zone, the Exploits subzone, consists of a series of nascent to mature volcanic arc rocks that include the Victoria Lake Supergroup (Fig. 1; Rogers et al., 2006; Zagorevski et al., 2007). The oldest sequence in the Victoria Lake Supergroup is the 513–509 Ma Cambrian Tally Pond group (Pollock, 2004; Rogers et al., 2006; McNicoll et al., 2010), which is composed of the mafic volcanic-dominated Lake Ambrose formation and the felsic volcanic-dominated Bindons Pond formation (Dunning et al., 1991; Evans and Kean, 2002; Squires and Moore, 2004; Rogers et al., 2006).

The volcanic rocks hosting VMS mineralization in the Tally Pond group are predominantly felsic (Fig. 2a; McNicoll et al., 2010); the Lemarchant VMS deposit, in particular, has been well preserved despite regional greenschist facies metamorphism, folding, and local normal and thrust faulting (Squires and Moore, 2004; Copeland et al., 2008a,b; Fraser et al., 2012). Footwall

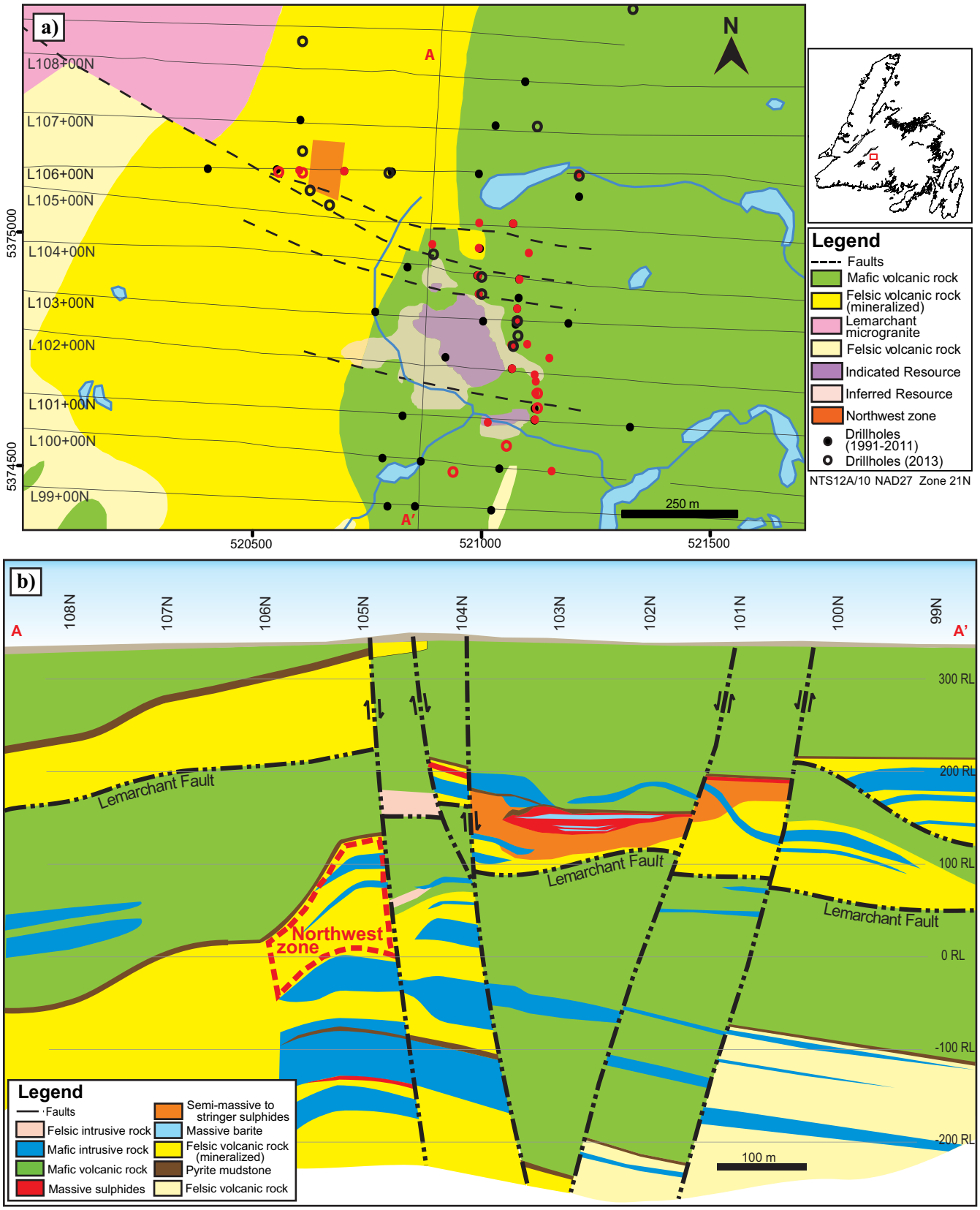

Figure 2. Geology of the Lemarchant deposit. **a)** Surface geology map of Lemarchant deposit. Red drillholes were logged for this project, and section A-A' is marked in red. Map location is approximated in inset map of Newfoundland (Williams et al., 1979). **b)** Idealized north-south cross-section of the Lemarchant deposit, looking east. Modified from Fraser et al. (2012).

host rocks at Lemarchant consist of calc-alkaline aphyric rhyolite breccias and flows that are interbedded with tuff breccias and lapilli tuffs containing devitrified volcanic glass shards (hyaloclastite). Hanging wall rocks consist of basalt and basaltic andesite flows and pillow flows that are variably intercalated with pyritic to graphitic mudstone that has a significant exhalative (chemical sedimentary) component (Lode et al., 2014; Fig. 2b). Two types of mafic dykes, a synvolcanic, pyroxene-porphyritic type and an undeformed gabbroic type, as well as an undeformed felsic dyke, crosscut the Lemarchant host rock and mineralization (Copeland et al., 2008a,b; Fraser et al., 2012). Thrust faulting at Lemarchant has resulted in local repetition of the volcanic stratigraphy (Fig. 2b).

Hydrothermal alteration is manifested by quartz-sericite±chlorite-albite in the footwall host rock, and by weak quartz-chlorite±epidote in the hanging wall (Copeland et al., 2008a,b). Synvolcanic mafic dykes contain rare fuchsite. Late carbonate alteration, consisting of calcite, ankerite, and dolomite, is present in all lithologies, and crosscutting quartz-carbonate veinlets are common throughout the deposit.

Table 1. Ore-related minerals present in the Lemarchant deposit, with mineral formulas (where applicable), in order of decreasing relative abundance.

Mineral phase	Formula
Barite	$BaSO_4$
Sphalerite	(Zn,Fe)S
Pyrite	FeS_2
Galena	PbS
Chalcopyrite	$CuFeS_2$
Tetrahedrite group minerals	$(Cu,Ag)_{10}(Fe,Zn)_2(As,Sb)_4S_{13}$
Bornite	Cu_5FeS_4
Marcasite	FeS_2
Stromeyerite	AgCuS
Colusite group minerals	$Cu_{26}V_2(As,Ge,Sb,Sn)_6S_{32}$
Pyrrhotite	$Fe_{1-x}S$
Arsenopyrite	FeAsS
Covellite	CuS
Electrum	(Au,Ag)
Bournonite	$PbCuSbS_3$
Polybasite	$[(Ag,Cu)_6(Sb,As)_2S_7][Ag_9CuS_4]$
Miargyrite	$AgSbS_2$
Silver telluride	-----
Sulvanite	$Cu_3(V,Fe)S_4$
Reinerite	$(Cu,Fe)_{22}(Ge_{4-x}As_x)Fe_8S_{32}$
Nickel sulphide	-----

SULPHIDE MINERALOGY

The elongate Lemarchant deposit is (at ~200 m depth) 350 m long, <20 m thick, and strikes north-northwest (Fig. 2). The upper stratigraphic stratiform zone contains abundant barite mineralization and is dominated by Zn-Pb sulphides, whereas the lower stratigraphic stringer zone is mostly composed of Cu-rich sulphides. However, the Lemarchant thrust fault (Fig. 2b) has truncated the stringer zone and translocated a portion of the deposit to the northwest (Fig. 2a). The main sulphide minerals are sphalerite, pyrite, galena, and chalcopyrite (see Table 1). Minor sulphide and sulphosalt minerals include the tetrahedrite group minerals, bornite, marcasite, stromeyerite, colusite group minerals, pyrrhotite and arsenopyrite. Trace minerals include electrum, covellite, bournonite, polybasite, miargyrite, sulvanite, and reinerite, as well as unknown silver tellurides and nickel sulphides.

There are five types of mineralization, based on sulphide mineral textures and crosscutting relationships. The type 1 mineral assemblage is composed of semi-massive granular barite-white to honey sphalerite-colloform pyrite-galena±chalcopyrite-tetrahedrite group minerals (Fig. 3a–c). Type 2A and type 2B mineral assemblages crosscut the type 1 mineral assemblage; type 2A mineralization consists of bornite-galena-chalcopyrite±stromeyerite-covellite-NiS stringers (Fig. 3d, e), and type 2B mineralization contains disseminated

Figure 3 opposite. Drillcore photographs, reflected and transmitted light thin section photomicrographs and back-scatter electron (BSE) images of the type mineral assemblages at Lemarchant. *Type 1:* **a)** Granular barite with semi-massive white sphalerite, pyrite, and galena in drillcore (drillhole LM11-64 at 218.8 m depth). **b)** White sphalerite with chalcopyrite disease in transmitted light (sample CNF29959 in drillhole LM11-59 at 207.7 m). **c)** Colloform pyrite with sphalerite and galena in reflected light (sample CNF29960 in drillhole LM11-59 at 216 m). *Type 2A:* **d)** Bornite-galena-chalcopyrite stringers crosscutting type 1 mineralization in drillcore (drillhole LM11-62 at 259.6 m). **e)** Chalcopyrite infilling fractures in bornite, with galena and diagenetic covellite in reflected light (sample CNF14279 in drillhole LM08-33 at 230.8 m). *Type 2B:* **f)** Recrystallized fine-grained pyrite with growth zones of higher As, visible only in back-scatter electron (BSE) image (lighter grey bands; sample CNF25134 in drillhole LM11-56 at 158.7 m). **g)** Coarse barite-dark grey tetrahedrite-galena-white sphalerite stringers crosscutting type 1 mineralization in drillcore (drillhole LM11-52 at 212.3 m). **h)** Myrmekitic intergrowth of galena-colusite-sphalerite in reflected light (sample CNF14279 in drillhole LM08-33 at 230.8 m). **i)** Electrum associated with galena and massive tetrahedrite in reflected light (sample CNF25121 in drillhole LM11-52 at 212.3 m). **j)** Zoned tetrahedrite-tennantite crystal, highlighting increase in silver content and visible in BSE image (lighter grey bands; sample CNF14293 in drillhole LM11-65 at 161.75 m). *Type 3:* **k)** Massive red sphalerite-euhedral pyrite-galena in drillcore (drillhole LM11-65 at 158.7 m). **l)** Subhedral pyrite atoll with chalcopyrite-galena-sphalerite in reflected light (sample CNF14290 in drillhole LM11-65 at 158.7 m). **m)** Massive red sphalerite with scalloped galena in transmitted light (sample CNF29959 from drillhole LM11-59 at 207.72 m). *Type 4:* **n)** Chalcopyrite-pyrite stringers in rhyolite breccia in drillcore (drillhole LM07-14 at 207.4 m). **o)** Subhedral and euhedral atoll pyrite-chalcopyrite stringers with sphalerite in reflected light (sample CNF29971 in drillhole LM11-63 at 224.7 m). Abbreviations: Ag-Trt = silver-rich tetrahedrite; Ant = anatase; Bn = bornite; Brt = barite; Ccp = chalcopyrite; Col = colusite; Cv = covellite; Elec = electrum; Gn = galena; Py = pyrite; Sp = sphalerite; Tnn = tennantite; Trt = tetrahedrite.

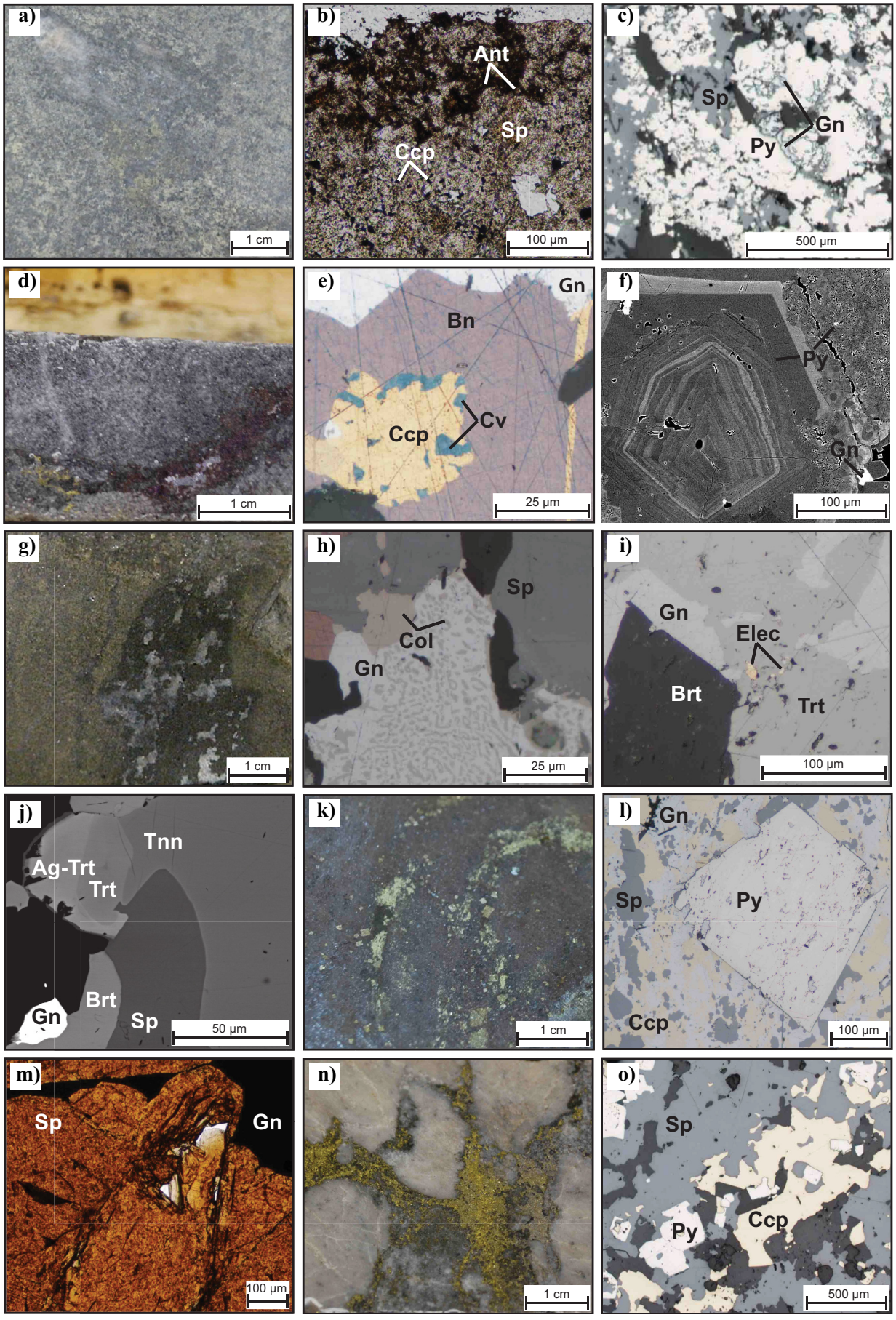
a)
1 cm
b)
Ant
Sp
Ccp
100 µm
c)
Sp
Gn
Py
500 µm
d)
1 cm
e)
Gn
Bn
Cv
Ccp
25 µm
f)
Py
Gn
100 µm
g)
1 cm
h)
Sp
Col
Gn
25 µm
i)
Gn
Elec
Brt
Trt
100 µm
j)
Tnn
Ag-Trt
Trt
Brt
Gn
Sp
50 µm
k)
1 cm
l)
Gn
Sp
Py
Ccp
100 µm
m)
Sp
Gn
100 µm
n)
1 cm
o)
Sp
Py
Ccp
500 µm

tetrahedrite group minerals-galena-bladed barite-white sphalerite-recrystallized pyrite±electrum-colusite group minerals-Ag-tetrahedrite-polybasite-miargyrite-bournonite-AgTe (Fig. 3f–j). Type 3 massive honey-brown to red sphalerite-subhedral to euhedral pyrite-galena-chalcopyrite± pyrrhotite-arsenopyrite overprints the type 1 assemblage in the uppermost portion of the stratiform zone (Fig. 3k–m). The type 4 mineral assemblage occurs in the stringer zone as chalcopyrite-euhedral pyrite± orange sphalerite-galena stringers (Fig. 3n, o).

MINERAL CHEMISTRY

Samples of representative mineral species and sulphide textures were analyzed using a scanning electron microprobe (SEM) equipped with an energy dispersive X-ray (EDX) detector, and quantitative compositions of sulphide and sulphosalt phases (see Table 1) were obtained by wavelength dispersive spectroscopy (WDS) using electron microprobe analysis (EMPA). Elemental precision for major elements is <1% (1σ); minor element (<1 wt%) precision is lower, with detection limits between 100–500 ppm (3σ). Semi-quantitative determinations of trace elements in sulphide and sulphosalt grains >50 μm were obtained via laser ablation inductively-coupled plasma mass spectrometry (LA-ICP-MS), on a 193 nm Excimer laser and quadropole mass spectrometer following the methods outlined by Longerich et al. (1996) and Eggins et al. (1998). Internal calibration was performed using USGS standards (to R >0.95) and compared to recommended values for the external standard (less than 20% error for trace elements <10 ppm).

Minor and Trace Element Geochemistry

Microprobe results reveal variations in minor element and precious metal contents in sphalerite, pyrite, tetrahedrite group minerals, bornite, and electrum phases. Iron contents of sphalerite range from below detection limit to 8.4 wt% (7.4 mol%), and correspond to variations in sphalerite colour—white to honey sphalerite (Fig. 3b) from type 1, 2A, and 2B assemblages contains Fe <2.6 wt% (<2.3 mol%), whereas honey brown to red sphalerite (Fig. 3m) from the type 3 and 4 assemblages has 2.7–8.4 wt% Fe (2.4–7.4 mol%) (Fig. 4). Arsenic contents in zoned pyrite (Fig. 3f) range up to 3.6 wt%. Tetrahedrite group minerals range from end-member tennantite to end-member tetrahedrite, and Ag is positively correlated with Sb, which is consistent with the fractional crystallization model of Hackbarth and Petersen (1984) and Huston et al. (1996) for tetrahedrite. Silver-tetrahedrite (i.e. friebergite) is distinct from tetrahedrite and is significantly enriched in Ag (15–28 wt%; see Fig. 3j). Silver also occurs in stromeyerite, electrum, polybasite, miargyrite, and

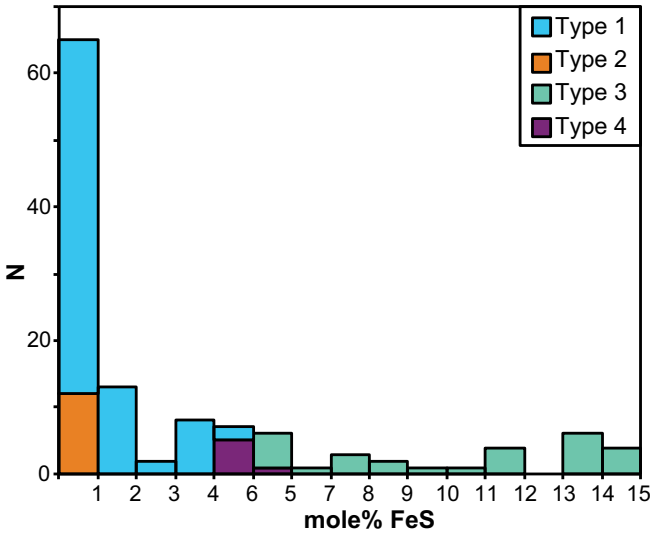

Figure 4. Compositional variation in iron contents (mol% FeS) of sphalerite from sphalerite-bearing mineral assemblages in the Lemarchant deposit (data from electron microprobe analyses).

AgTe, and in trace amounts in bornite (<1.5 wt%). Gold occurs primarily in electrum, which is predominant in the centre of the deposit as Au-rich electrum (Au:Ag > 0.7). Ag-bearing minerals and Ag-rich electrum (Au:Ag = 0.4 to 0.7) are more abundant toward the edges of mineralization.

Laser ablation ICP-MS analyses reveal distinct variations in trace element contents between the five type mineral assemblages (e.g. Au, Bi, In, Sn; Fig. 5). The type 1 mineral assemblage is enriched in As, Mo, and Tl relative to the other mineral assemblages. The type 2A mineral assemblage is enriched in Ag, Ge, and Sn, and the type 2B mineral assemblage is enriched in V, In, Au, and Sb; both assemblages contain elevated Bi, Cr, Co, In, Ni, and Ti. The type 3 assemblage is also enriched in Ni. The type 4 assemblage has low trace element contents relative to the other assemblages, with the exception of Sn.

ISOTOPE GEOCHEMISTRY

Offcuts from thin sections analyzed by SEM, EMPA, and LA-ICP-MS were mounted in epoxy and gold-coated for in situ isotope analyses by secondary ion mass spectrometry. Grains with unblemished spots >10 μm were chosen (where possible) in galena, pyrite, and chalcopyrite that were representative of the five types of mineralization. Precision, based on an internal galena standard for radiogenic isotope ratios ($^{204}Pb/^{206}Pb$, $^{207}Pb/^{206}Pb$, and $^{208}Pb/^{206}Pb$), is better than 0.05–0.10% (1σ). Repeated analyses on galena standards indicate accuracy is better than 0.10–0.15% (1σ). Internal precision of $\delta^{34}S$ analyses on pyrite, galena, and chalcopyrite standards is ±0.3‰ (1σ), and accuracy of repeated standard analyses is better than

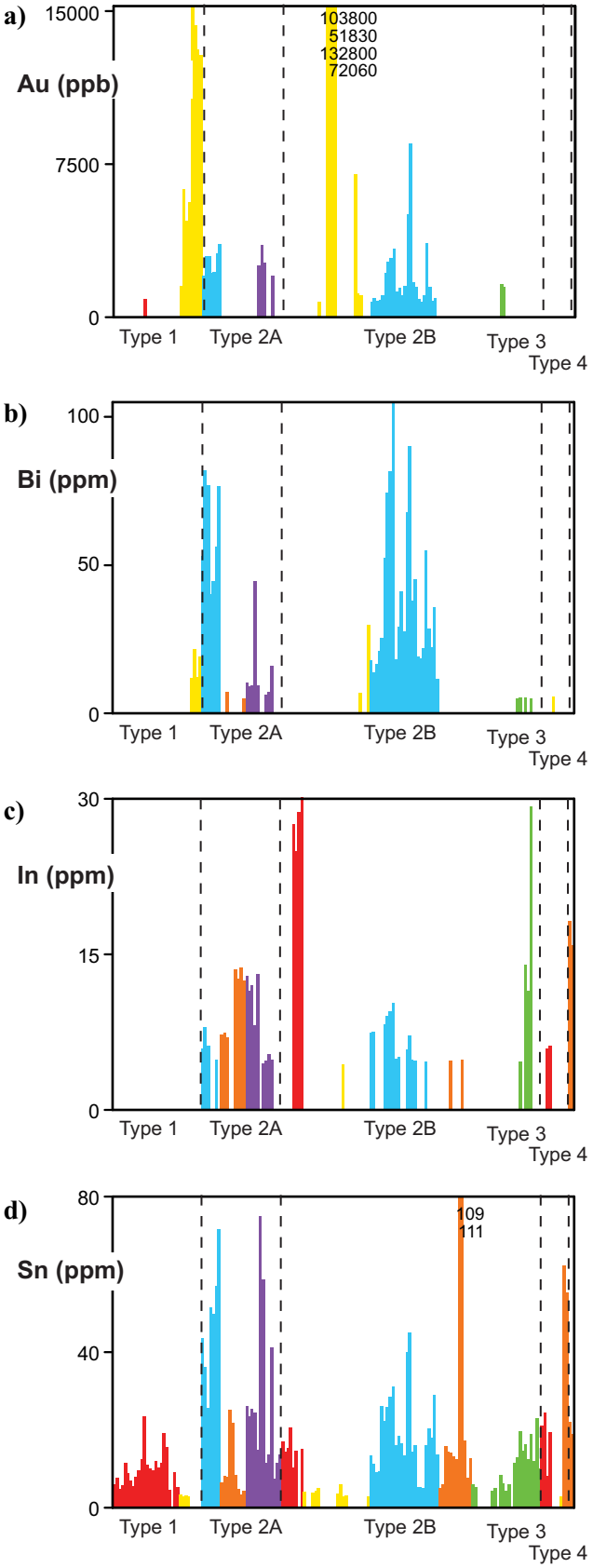

Figure 5. Trace element variations in sphalerite (red), pyrite (yellow), chalcopyrite (orange), galena (blue), tetrahedrite (green), and bornite (purple) from the five types of mineralization at the Lemarchant deposit.

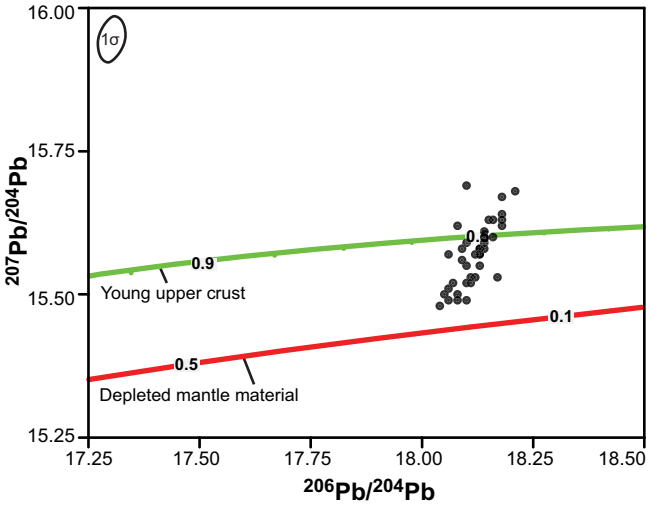

Figure 6. $^{207}Pb/^{204}Pb$ versus $^{206}Pb/^{204}Pb$ plot of galena from the Lemarchant deposit. Error ellipse for average standard deviation (1σ) does not include outlying values. Young upper crust and depleted mantle material growth curves from Kramers and Tolstikhin (1997).

±0.35–0.45‰ (1σ).

Lead Isotope Geochemistry

Lead isotope compositions of galena from Lemarchant form a linear array on a $^{207}Pb/^{204}Pb$ versus $^{206}Pb/^{204}Pb$ plot (Fig. 6; n=42). Model ages and μ values calculated using the two-stage growth model of Stacey and Kramers (1975) give Pb-Pb ages that are much younger than Cambrian (509–513 Ma, as determined by U-Pb dating of the Lemarchant host rocks; Pollock, 2004; Rogers et al., 2006; McNicoll et al., 2010) and an average μ of 9.63. These μ values are very similar to the μ value for young upper crust at 500 Ma (μ=9.66; Kramers and Tolstikhin, 1997), which is consistent with the volcanic and intrusive Neoproterozoic basement rock that has a dominant continental arc signature (εNdt<0; Rogers et al., 2006; McNicoll et al., 2010) and immediately underlies the Tally Pond group. However, the spread of data, which lie mostly below the young upper crust growth curve (Fig. 6), suggest that an additional source with low-μ values (i.e. juvenile Pb from mafic rocks of the lower Neoproterozoic basement or Lake Ambrose formation; Rogers et al., 2006; McNicoll et al., 2010) must have contributed to the Pb isotope signature at Lemarchant.

Sulphur Isotope Geochemistry

Sulphur isotope compositions of Lemarchant sulphides reveal a relatively wide range of $\delta^{34}S$ values between -6.4 and +15.1‰ (avg. +5.0 ± 3.3 ‰, n = 119). Sulphur isotope values ~0‰ occur in type 2A pyrite (+1.4 ± 2.2‰), type 2B galena (+4.4 ± 4‰), and type 3 galena (+4.5 ± 6.6‰), whereas the highest $\delta^{34}S$ values are from galena in the type 3 (<+15.1‰) and type 4 (+7.2 ± 4.2‰) assemblages (Fig. 7).

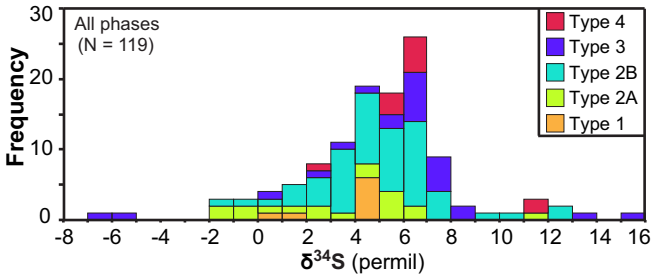

Figure 7. Frequency distribution of $\delta^{34}S$ values for all analyzed sulphides (pyrite, galena, and chalcopyrite) from the 5 mineral assemblage types at the Lemarchant deposit.

SUMMARY

The Lemarchant VMS deposit is composed of contrasting styles of mineralization, which were deposited in three discrete paragenetic stages (Fig. 8). The type 1 mineral assemblage was deposited during stage 1 of paragenesis and contains fine-grained barite and fine-grained polymetallic sulphides, such as low-Fe sphalerite and colloform pyrite that are indicative of transport by low-temperature (200-300ºC), oxidized hydrothermal fluids (Large, 1977; Barton and Skinner, 1979; Ohmoto et al., 1983; Pisutha-Arnond and Ohmoto, 1983; Ohmoto, 1996). The type 1 assemblage was crosscut by the type 2A and 2B mineral assemblages during stage 2 paragenesis, which contain low-Fe sphalerite and abundant sulphosalts, precious metals, and precious metal-bearing sulphides atypical of polymetallic VMS deposits (c.f. Hannington and Scott, 1989; Sillitoe et al., 1996; Dubé et al., 2007); rather, the type 2A and 2B assemblages resemble an intermediate- to high-sulphidation epithermal suite of minerals that were deposited from low-temperature (150–250ºC), oxidized, near neutral (pH ~5) hydrothermal fluids with high sulphur activity (Scott and Barnes, 1971; Czamanske, 1974; Barton and Skinner, 1979; Pisutha-Arnond and Ohmoto, 1983; Hannington and Scott, 1989; Huston and Large, 1989). Paragenetic stage 3 resulted in the overprinting of type 1, 2A, and 2B assemblages in the stratiform zone by the type 3 assemblage, and the formation of a stringer sulphide zone with the type 4 assemblage. The high-Fe sphalerite, high Cu-content, and lack of precious and trace metals in the type 3 and 4 assemblages suggests that these polymetallic, Kuroko-style VMS assemblages were deposited from higher temperature (>300ºC), less oxidized hydrothermal fluids with low sulphur activity (Scott and Barnes, 1971; Barton and Skinner, 1979; Eldridge et al., 1983; Pisutha-Arnond and Ohmoto, 1983; Ohmoto, 1996).

The intermediate- to high-sulphidation epithermal suite of minerals (i.e. tetrahedrite group minerals, bornite, colusite group minerals, electrum, covellite) and epithermal trace element suite (i.e. Au, As, Bi, Co, Cr, In, Mo, Ni, Sb, Se, Te) that characterize the type 2A and 2B assemblages suggest that direct contribution of magmatic fluid to the hydrothermal fluid occurred during the formation of the Lemarchant deposit (Hedenquist and Lowenstern, 1994; Poulsen and Hannington, 1995; White and Hedenquist, 1995;

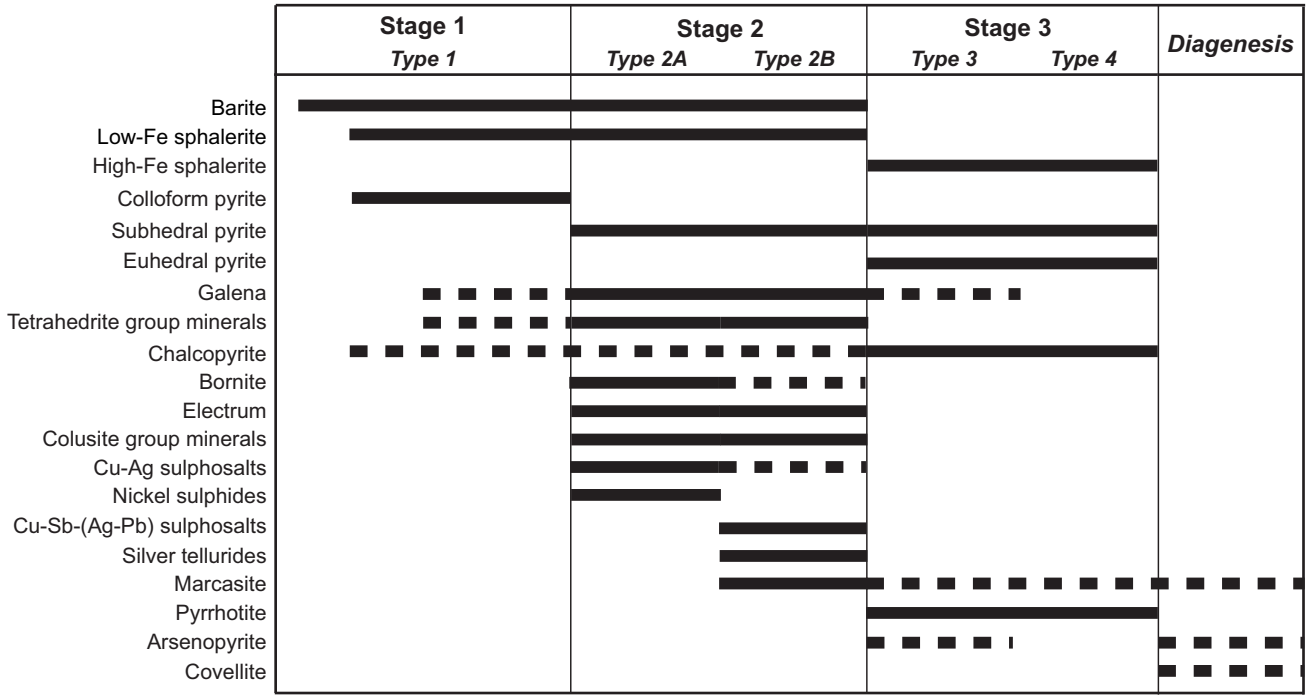

Figure 8. Paragenetic diagram for the three main stages of deposition of the Lemarchant deposit. Dashed lines indicate intermittent deposition of mineral phase.

Lydon, 1996; Sillitoe et al., 1996; Hannington et al., 1999). Magmatic fluids are consistent with the presence of anomalous Au in the deposit, which would have been efficiently transported by the low-temperature, highly oxidized, near neutral and S-rich fluids of stage 1 and 2 paragenesis (Hannington and Scott, 1989; Huston and Large, 1989; Lydon, 1996). Further evidence for a magmatic contribution to the hydrothermal fluid comes from the S isotope signature of the Lemarchant sulphides (Fig. 7; Gill, 2015). Positive $\delta^{34}S$ values (>4‰) indicate that some S at Lemarchant was derived from thermochemical sulphate reduction (TSR; Sakai and Dickson, 1978; Ohmoto and Rye, 1979; Shanks, 2001; Seal, 2006); however, $\delta^{34}S$ values of ~0 suggest that leaching of igneous basement rock and/or magmatic fluids also contributed to the overall S isotope signature at Lemarchant (Sakai et al., 1984; Ueda and Sakai, 1984; Huston, 1999; Franklin et al., 2005). The epithermal mineral and trace element suite, abundance of precious metals, and oxidized state of the type 1, 2A, and 2B assemblages are consistent with a magmatic contribution of S (in the form of SO_2; Ohmoto and Rye, 1979; Seal, 2006) during paragenetic stages 1 and 2. The more 'normal' VMS mineralization of the type 3 and 4 assemblages indicate that magmatic fluids were not as prevalent during paragenetic stage 3, so the very low $\delta^{34}S$ values of the type 3 assemblage must be attributed to leaching of igneous rocks.

Precious metal enrichment of the Lemarchant deposit occurred during stage 2 paragenesis, with transport and precipitation from low-temperature, oxidized, near neutral and S-rich fluids. The association of electrum, bladed barite, and euhedral albite in the type 2B assemblage provides further evidence that Au and Ag were precipitated from hydrothermal fluids that intermittently boiled at or very near the seafloor (Sillitoe et al., 1996; Huston et al., 2000; Dubé et al., 2007; Hannington and Monecke, 2009). Boiling of low-temperature fluids at the seafloor requires that Lemarchant formed in relatively shallow water (<1500 m depth) during Au-Ag deposition (Bischoff and Rosenbauer, 1984; Butterfield et al., 1990; Hannington et al., 1999; Hannington and Monecke, 2009; Monecke et al., 2014). However, the Cu-rich, high-temperature mineral assemblages deposited during paragenetic stage 3 show no evidence for boiling. Furthermore, fluid temperatures >250ºC require confining pressures at >1500 m depth to suppress boiling (and concomitant precious metal deposition), suggesting deposition of the type 3 and 4 assemblages occurred at depths greater than 1500 m (Bischoff and Rosenbauer, 1984; Butterfield et al., 1990; Hannington et al., 1995; Hannington et al., 2005). A change in water depth during deposition of mineralization is consistent with the rifted arc environment in which Lemarchant formed (Fig. 6; Squires and Moore, 2004; Copeland et al., 2008a,b; McNicoll et al., 2010; Monecke et al., 2014; Piercey et al., 2014), where extension of the arc during deposit formation resulted in greater depths of water for the latter stages of mineralization.

Lemarchant is a precious-metal-bearing VMS deposit that contains polymetallic, Kuroko-style mineralization, and intermediate- to high-sulphidation epithermal-style mineralization that is atypical of 'normal' VMS systems that lack precious metal enrichment. Precious metals were likely derived directly from a magmatic fluid; however, precipitation and concentration of Au occurred during boiling of the hydrothermal fluid, which could have occurred only at shallow depths. The precious metal deposition at Lemarchant likely occurred in an extensional tectonic environment, consistent with the rifted arc setting.

ACKNOWLEDGEMENTS

Funding for this project primarily came from the GSC TGI-4 Program and the Research Affiliate Program of NRCan. This research is also supported by grants to Dr. Stephen J. Piercey, including an NSERC Discovery Grant and the NSERC-Altius Industrial Research Chair in Mineral Deposits supported by NSERC, Altius Resources Inc., and the Research and Development Corporation of Newfoundland and Labrador. Access to the Lemarchant drill core, core logs, and assay database were provided by the Canadian Zinc Corporation. Many thanks to Stefanie Lode, Christine Divine, Diane Fost, Michael Schaeffer, David Grant, Brian Joy, and Mike Gadd for their technological help and interpretive guidance. The authors thank Jan Peter and Patrick Mercier-Langevin for reviews and editorial handling.

REFERENCES

Barton Jr, P. and Skinner, B., 1979. Sulphide mineral stabilities, *In:* Geochemistry of Hydrothermal Ore Deposits, 2nd Edition, (ed.) H.L. Barnes; John Wiley & Sons, p. 278–403.

Bischoff, J.L. and Rosenbauer, R.J., 1984. The critical point and two-phase boundary of seawater, 200–500ºC; Earth and Planetary Science Letters, v. 68, p. 172–180.

Brueckner, S.M., Piercey, S.J., Sylvester, P.J., Maloney, S., and Pilgrim, L., 2014. Evidence for syngenetic precious metal enrichment in an Appalachian volcanogenic massive sulfide system: the 1806 zone, Ming mine, Newfoundland, Canada; Economic Geology, v. 109, 1611–1642.

Butterfield, D.A., Massoth, G.J., McDuff, R.E., Lupton, J.E., and Lilley, M.D., 1990. Geochemistry of hydrothermal fluids from Axial Seamount hydrothermal emissions study vent field, Juan de Fuca Ridge: Subseafloor boiling and subsequent fluid-rock interaction; Journal of Geophysical Research: Solid Earth, v. 95, p. 12895–12921.

Copeland, D.A., Toole, R.M.S., and Piercey, S.J., 2008a. Assessment report on diamond drilling and soil sampling, License 8183M (10th Year) and 9569M (5th Year) South Tally Pond property, Rogerson Lake area, Newfoundland and Labrador, NTS 12A/10 and 12A/07; Newfoundland and

Labrador Geological Survey, Assessment Report, 956 p. [for Paragon Minerals and Altius Minerals].

Copeland, D.A., McClenaghan, S.M., and Piercey, S.J., 2008b. Ninth year assessment report on diamond drilling, lithogeochemistry, pulse EM surveying and linecutting on license 8183M, South Tally Pond Property, Rogerson Lake area, Newfoundland and Labrador NTS 12A/10 and 12A/07. Newfoundland and Labrador Geological Survey, Assessment Report, 91 p. [for Paragon Minerals and Altius Minerals].

Czamanske, G.K., 1974. The FeS content of sphalerite along the chalcopyrite-pyrite-bornite sulphur fugacity buffer; Economic Geology, v. 69, p. 1328–1334.

Dubé, B., Gosselin, P., Mercier-Langevin, P., Hannington, M., and Galley, A., 2007. Gold-rich volcanogenic massive sulphide deposits, *In:* Mineral Deposits of Canada: A Synthesis of Major Deposit Types, District Metallogeny, the Evolution of Geological Provinces, and Exploration Methods, (ed.) W.D. Goodfellow; Geological Association of Canada, Mineral Deposits Division, Special Publication, v. 5, p. 75–94.

Dunning, G.R., Swinden, H.S., Kean, B.F., Evans, D.T.W., and Jenner, G.A., 1991. A Cambrian island arc in Iapetus; geochronology and geochemistry of the Lake Ambrose volcanic belt, Newfoundland Appalachians; Geological Magazine, v. 128, p. 1–17.

Eggins, S., Rudnick, R., and McDonough, W., 1998. The composition of peridotites and their minerals: a laser-ablation ICP–MS study; Earth and Planetary Science Letters, v. 154, p. 53–71.

Eldridge, C.S., Barton, P.B., Jr., and Ohmoto, H., 1983. Mineral textures and their bearing on formation of the Kuroko orebodies, *In:* The Kuroko and Related Volcanogenic Massive Sulfide Deposits, (ed..) H. Ohmoto and B.J. Skinner; Economic Geology, Monograph 5, p. 241–281.

Evans, D., and Kean, B., 2002. The Victoria Lake Supergroup, central Newfoundland – its definition, setting and volcanogenic massive sulphide mineralization; Newfoundland Department of Mines and Energy, Geological Survey, Open File NFLD/2790, 68 p.

Franklin, J., Gibson, H., Jonasson, I., and Galley, A., 2005. Volcanogenic massive sulphides, *In:* Economic Geology100th Anniversary Volume, (ed.) J.W. Hedenquist, J.F.H. Thompson, R.J. Goldfarb, and J.P. Richards; Society of Economic Geologists, Littleton, Colorado, p. 523–560.

Fraser, D., Giroux, G.H., Copeland, D.A., and Devine, C.A., 2012. Technical Report and Resource Minerals Estimate on the Lemarchant Deposit, South Tally Pond VMS Project, Central Newfoundland, Canada; NI 43-101 Technical Report prepared for Paragon Minerals Corporation, 132 p.

Gill, S.B., 2015. Mineralogy, Metal-Zoning, and Genesis of the Cambrian Zn-Pb-Cu-Ag-Au Lemarchant Volcanogenic Massive Sulfide (VMS) Deposit; M.Sc. thesis, Memorial University, St. John's, Newfoundland, 154 p.

Hackbarth, C.J. and Petersen, U., 1984. A fractional crystallization model for the deposition of argentian tetrahedrite; Economic Geology, v. 79, p. 448–460.

Hannington, M.D. and Scott, S.D., 1989. Sulfidation equilibria as guides to gold mineralization in volcanogenic massive sulfides: evidence from sulfide mineralogy and the composition of sphalerite; Economic Geology, v. 84, p. 1978–1995.

Hannington, M.D., Jonasson, I.R., Herzig, P.M., and Petersen, S., 1995. Physical and chemical processes of seafloor mineralization at mid-ocean ridges; *In:* Seafloor Hydrothermal Systems: Physical, Chemical, Biological, and Geological Interactions (ed.) S.E. Humphris, R.A. Zierenberg, L.S. Mullineaux, and R.E. Thomson; Geophysical Monograph, v. 91, p. 115–157.

Hannington, M.D., Poulsen, K.H., Thompson, J.F.H., and Sillitoe, R.H., 1999. Volcanogenic gold in the massive sulfide environment; Reviews in Economic Geology, v. 8, p. 325–356.

Hannington, M.D., de Ronde, C.D., and Petersen, S., 2005. Seafloor tectonics and submarine hydrothermal systems, *In:* Economic Geology 100th Anniversary Volume, (ed.) J.W. Hedenquist, J.F.H. Thompson, R.J. Goldfarb, and J.P. Richards; Society of Economic Geologists, Littleton, Colorado, p. 111–141.

Hannington, M.D., and Monecke, T., 2009. Modern submarine hydrothermal systems - A global perspective on distribution, size and tectonic settings, *In:* Submarine Volcanism and Mineralization: Modern through Ancient, (ed.) B. Cousens and S.J. Piercey; Geological Association of Canada, Mineral Deposits Division, Short Course Notes, v. 19, p. 91–146.

Hedenquist, J.W. and Lowenstern, J.B., 1994. The role of magmas in the formation of hydrothermal ore deposits; Nature, v. 370, p. 519–527.

Huston, D.L., 1999. Stable isotopes and their significance for understanding the genesis of volcanic-hosted massive sulphide deposits: a review; Reviews in Economic Geology, v. 8, p. 157–179.

Huston, D.L., 2000. Gold in volcanic-hosted massive sulphide deposits; distribution, genesis, and exploration; Reviews in Economic Geology, v. 13, p. 401–426.

Huston, D.L. and Large, R.R., 1989. A chemical model for the concentration of gold in volcanogenic massive sulphide deposits; Ore Geology Reviews, v. 4, p. 171–200.

Huston, D.L., Jablonski, W., and Sie, S., 1996. The distribution and mineral hosts of silver in eastern Australian volcanogenic massive sulphide deposits; The Canadian Mineralogist, v. 34, p. 529–546.

Kramers, J.D. and Tolstikhin, I.N., 1997. Two terrestrial lead isotope paradoxes, forward transport modeling, core formation and the history of the continental crust; Chemical Geology, v. 139, p. 75–110.

Large, R.R., 1977. Chemical evolution and zonation of massive sulphide deposits in volcanic terrains; Economic Geology, v. 72, p. 549-572.

Lode, S., Piercey, S. J., Devine, C. A., Layne, G. D., Piercey, G., and Hewa, L., 2014. Lithogeochemistry and sulphur isotopic composition of hydrothermal mudstones associated with the Lemarchant volcanogenic massive sulphide (VMS) deposit, Tally Pond Belt, Central Newfoundland, *In:* Abstracts; Geological Association of Canada, Newfoundland Spring Technical Meeting, v. 40, p. 20.

Longerich, H.P., Jackson, S.E., and Gunther, D., 1996. Inter-laboratory note: Laser ablation inductively coupled plasma mass spectrometric transient signal data acquisition and analyte concentration calculation; Journal of Analytical Atomic Spectrometry, v. 11, p. 899–904.

Lydon, J.W., 1996. Characteristics of volcanogenic massive sulphide deposits; interpretations in terms of hydrothermal convection systems and magmatic hydrothermal systems; Boletin Geologico y Minero, v. 107, p. 215–264.

Ohmoto, H. and Rye, R., 1979. Isotopes of sulphur and carbon, *In:* Geochemistry of Hydrothermal Ore Deposits, 2nd Edition, (ed.) H.L. Barnes; John Wiley & Sons, p. 509–567.

Ohmoto, H., Mizukami, M., Drummond, S., Eldridge, C., Pisutha-Arnond, V., and Lenagh, T., 1983. Chemical processes of Kuroko formation, *In:* The Kuroko and Related Volcanogenic Massive Sulfide Deposits, (ed.) H. Ohmoto and B.J. Skinner; Economic Geology, Monograph 5, p. 570–604.

Ohmoto, H., 1996. Formation of volcanogenic massive sulphide deposits; the Kuroko perspective; Ore Geology Reviews, v. 10, p. 135–177.

McNicoll, V., Squires, G., Kerr, A., and Moore, P., 2010. The Duck Pond and Boundary Cu-Zn deposits, Newfoundland; new insights into the ages of host rocks and the timing of VHMS mineralization; Canadian Journal of Earth Sciences, v. 47, p. 1481–1506.

Mercier-Langevin, P., Hannington, M., Dubé, B., and Bécu, V., 2011. The gold content of volcanogenic massive sulphide deposits; Mineralium Deposita, v. 46, p. 509–539.

Monecke, T., Petersen, S., and Hannington, M.D., 2014. Constraints on water depth of massive sulfide formation: evidence from modern seafloor hydrothermal systems in arc-related settings; Economic Geology, v. 109, p. 2079–2101.

Piercey, S.J. and Hinchey, J., 2012. Volcanogenic massive sulphide (VMS) deposits of the Central Mineral Belt, Newfoundland; Geological Association of Canada–Mineralogical Association of Canada Joint Annual Meeting, Field Trip Guidebook B, Newfoundland and Labrador Department of Natural Resources, Geological Survey, Open File NFLD/3173, 56 p.

Piercey, S.J., Squires, G.C., and Brace, T.D., 2014. Lithostratigraphic, hydrothermal, and tectonic setting of the Boundary volcanogenic massive sulphide deposit, Newfoundland Appalachians, Canada: Formation by subseafloor replacement in a Cambrian rifted arc; Economic Geology, v. 109, p. 661–687.

Pilote, J-L., Piercey, S.J., and Mercier-Langevin, P., 2014. Stratigraphy and hydrothermal alteration of the Ming Cu-Au volcanogenic massive-sulphide deposit, Baie Verte Peninsula, Newfoundland; Geological Survey of Canada, Current Research 2014-7, 18 p.

Pilote, J-L. and Piercey, S.J., 2013. Detailed volcano-stratigraphic relationships of the 1807 zone of the Cu-Au Ming volcanogenic massive sulphide (VMS) deposit, Baie Verte Peninsula, northern Newfoundland; Geological Survey of Canada, Current Research 2013-20, 17 p. doi: 10.4095/293128

Pisutha-Arnond, V. and Ohmoto, H., 1983. Thermal history, and chemical and isotopic compositions of the ore-forming fluids responsible for the Kuroko massive sulphide deposits in the Hokuroku District of Japan, *In:* The Kuroko and Related Volcanogenic Massive Sulfide Deposits, (ed.) H. Ohmoto and B.J. Skinner; Economic Geology, Monograph 5, p. 523–558.

Pollock, J., 2004. Geology and paleotectonic history of the Tally Pond Group, Dunnage zone, Newfoundland Appalachians: An integrated geochemical, geochronological, metallogenic and isotopic study of a Cambrian island arc along the Peri-Gondwanan margin of Iapetus; M.Sc. thesis, Memorial University, St. John's, Newfoundland, 420 p.

Poulsen, K.H. and Hannington, M.D., 1995. Volcanic-associated massive sulphide gold, *In:* Geology of Canada No. 8: Geology of Canadian Mineral Deposit Types, (ed.) O.R. Eckstrand, W.D. Sinclair, and R.I. Thorpe; Geological Society of America, Decade of North American Geology (DNAG), Part 1, p. 183–196.

Rogers, N., van Staal, C.R., McNicoll, V., Pollock, J., Zagorevski, A., and Whalen, J., 2006. Neoproterozoic and Cambrian arc magmatism along the eastern margin of the Victoria Lake Supergroup: A remnant of Ganderian basement in central Newfoundland?; Precambrian Research, v. 147, p. 320–341.

Sakai, H. and Dickson, F., 1978. Experimental determination of the rate and equilibrium fractionation factors of sulphur isotope exchange between sulphate and sulphide in slightly acid solutions at 300ºC and 1000 bars; Earth and Planetary Science Letters, v. 39, p. 151–161.

Sakai, H., Des Marais, D., Ueda, A., and Moore, J., 1984. Concentrations and isotope ratios of carbon, nitrogen and sulphur in ocean-floor basalts; Geochimica et Cosmochimica Acta, v. 48, p. 2433–2441.

Santaguida, F. and Hannington, M., 1993. Preliminary results on gold mineralization in volcanogenic massive sulphide deposits, central Newfoundland, *In:* Current Research, (ed..) C.P.G. Pereira, D.G. Walsh, and R.F. Blackwood; Government of Newfoundland and Labrador, Department of Mines and Energy, Geological Survey Branch, Report 93-01, p. 373–381.

Santaguida, F. and Hannington, M., 1996. Characteristics of gold mineralization in volcanogenic massive sulphide deposits of the Notre Dame Bay area, central Newfoundland; Canadian Journal of Earth Sciences, v. 33, p. 316–334.

Scott, S. and Barnes, H., 1971. Sphalerite geothermometry and geobarometry; Economic Geology, v. 66, p. 653–669.

Seal, R.R., 2006. Sulphur isotope geochemistry of sulphide minerals; Reviews in Mineralogy and Geochemistry, v. 61, p. 633–677.

Shanks, W., 2001. Stable isotopes in seafloor hydrothermal systems: vent fluids, hydrothermal deposits, hydrothermal alteration, and microbial processes; Reviews in Mineralogy and Geochemistry, v. 43, p. 469–525.

Sillitoe, R.H., Hannington, M.D., and Thompson, J.F.H., 1996. High sulfidation deposits in the volcanogenic massive sulfide environment; Economic Geology, v. 91, p. 204–212.

Squires, G. and Moore, P., 2004. Volcanogenic massive sulphide environments of the Tally Pond Volcanics and adjacent area: Geological, lithogeochemical and geochronological results, *In:* Current Research; Newfoundland and Labrador Department of Natural Resources, Geological Survey, Report 04-1, p. 63–91.

Stacey, J.S. and Kramers, J., 1975. Approximation of terrestrial lead isotope evolution by a two-stage model; Earth and Planetary Science Letters, v. 26, p. 207–221.

Swinden, H. and Kean, B., 1988. The volcanogenic sulphide districts of central Newfoundland: A guidebook and reference manual for volcanogenic sulphide deposits in the Early Paleozoic oceanic volcanic terranes of central Newfoundland; Geological Association of Canada, Mineral Deposits Division, p. 2–27.

Ueda, A. and Sakai, H., 1984. Sulphur isotope study of Quaternary volcanic rocks from the Japanese Islands Arc; Geochimica et Cosmochimica Acta, v. 48, p. 1837–1848.

van Staal, C.R., Dewey, J.F., Niocaill, C.M., and McKerrow, W.S., 1998. The Cambrian-Silurian tectonic evolution of the northern Appalachians and British Caledonides: History of a complex, west and southwest Pacific-type segment of Iapetus; Geological Society, London, Special Publications, v. 143, p. 197–242. doi:10.1144/GSL.SP.1998.143.01.17

van Staal, C. and Barr, S., 2012. Lithospheric architecture and tectonic evolution of the Canadian Appalachians and associated Atlantic margin, Chapter 2 *In:* Tectonic Styles in Canada Revisited: the LITHOPROBE perspective, (ed.) J.A. Percival, F.A. Cook, and R.M. Clowes; Geological Association of Canada, Special Paper 49, p. 41–95.

White, N.C. and Hedenquist, J.W., 1995. Epithermal gold deposits: styles, characteristics and exploration; Society of Economic Geologists newsletter, v. 23, p. 9–13.

Williams, H., 1979. Appalachian orogen in Canada; Canadian Journal of Earth Sciences, v. 16, p. 792–807.

Zagorevski, A., Van Staal, C.R., McNicoll, V., and Rogers, N., 2007. Upper Cambrian to upper Ordovician peri-Gondwanan island arc activity in the Victoria Lake Supergroup, Central Newfoundland: tectonic development of the northern Ganderian margin; American Journal of Science, v. 307, p. 339–370.

GEOLOGICAL SURVEY OF CANADA
OPEN FILE 7853

Targeted Geoscience Initiative 4: Contributions to the Understanding of Volcanogenic Massive Sulphide Deposit Genesis and Exploration Methods Development

Volcanic architecture and alteration assemblages of the Ming Cu-Au-(Zn-Ag) VMS deposit, Baie Verte, Newfoundland and Labrador: Implications for Au-enrichment processes and exploration

Jean-Luc Pilote[1], Stephen J. Piercey[1], and Patrick Mercier-Langevin[2]

[1]Memorial University of Newfoundland, St. John's, Newfoundland and Labrador
[2]Geological Survey of Canada, Québec, Quebec

2015

This publication is available for free download through GEOSCAN (http://geoscan.nrcan.gc.ca/)

Recommended citation

Pilote, J.-L., Piercey, S.J., and Mercier-Langevin, P., 2015. Volcanic architecture and alteration assemblages of the Ming Cu-Au-(Zn-Ag) VMS deposit, Baie Verte, Newfoundland and Labrador: Implications for Au-enrichment processes and exploration, *In:* Targeted Geoscience Initiative 4: Contributions to the Understanding of Volcanogenic Massive Sulphide Deposit Genesis and Exploration Methods Development, (ed.) J.M. Peter and P. Mercier-Langevin; Geological Survey of Canada, Open File 7853, p. 197–210.

Publications in this series have not been edited; they are released as submitted by the author.

Contribution to the Geological Survey of Canada's Targeted Geoscience Initiative 4 (TGI-4) Program (2010–2015)

TABLE OF CONTENTS

Volcanic architecture and alteration assemblages of the Ming Cu-Au-(Zn-Ag) VMS deposit, Baie Verte, Newfoundland and Labrador: Implications for Au-enrichment processes and exploration

Jean-Luc Pilote[1], Stephen J. Piercey[1]*, and Patrick Mercier-Langevin[2]

[1]Department of Earth Sciences, Memorial University of Newfoundland, St. John's, Newfoundland and Labrador A1B 3X5
[2]Geological Survey of Canada, 490 rue de la Couronne, Québec, Quebec G1K 9A9
*Corresponding author's e-mail: spiercey@mun.ca

ABSTRACT

The Ming deposit is hosted in Cambro-Ordovician intermediate to felsic rocks underlain by ca. 490 Ma ophiolite slivers of boninitic composition. The deposit consists of five elongated semi-massive to massive sulphide lenses that plunge 30º to the northeast and occur in the uppermost part of a calc-alkalic intermediate to felsic volcanic succession. The immediate hanging wall varies from mafic volcanic breccia to magnetite-rich volcanogenic siltstone. Three generations of mafic to intermediate intrusive rocks are present in the deposit; they each have distinctive lithogeochemical signatures and are interpreted to be genetically related to the mafic rocks of the cover sequence.

The Ming deposit has seven distinct alteration mineral assemblages (from proximal to distal from mineralization): quartz-pyrite, quartz-calcite-garnet, sericite-green mica-sulphide, sericite-quartz-pyrite, chlorite-amphibole-quartz, chlorite-sericite-quartz-sulphide, and chlorite-stringer zone assemblages. A chalcopyrite-pyrrhotite-pyrite stringer zone associated with the chlorite-stringer zone assemblage occurs 50–100 m stratigraphically below the Ming North and Ming South lenses, at what was the site of high-temperature fluid discharge from a hydrothermal system. The spatial and temporal geological relationships between the stratigraphic package, alteration styles, mineralization, and deformation strongly support a syngenetic origin for mineralization and Au-enrichment.

INTRODUCTION

The Ming deposit is a Au-Ag-bearing volcanogenic massive sulphide (VMS) deposit located in the Baie Verte Peninsula in northern Newfoundland, which is part of the Notre-Dame subzone of the Canadian Appalachian orogen (Fig. 1). The deposit is part of a group of four past and currently producing precious metal-rich VMS deposits that collectively are known as the consolidated Rambler and Ming mining camp (herein referred to as the Rambler camp). The Rambler camp deposits are hosted by the ca. 489–487 Ma upper Pacquet Complex, part of the Baie Verte Oceanic Tract (Fig. 2; van Staal and Barr, 2012; van Staal et al., 2013). The Ming deposit consists of five Cu-Au-Zn-Ag-rich, semi-massive to massive pyrite-rich lenses, veins, and stringer zones located within variously sericite-chlorite-quartz-altered intermediate to felsic volcanic rocks with a large proportion of volcaniclastic rocks. These zones are, from the northwest to the southeast, the 1807, 1806, Ming North, Ming South, and Lower Footwall zones (Fig. 3). The current combined past production, reserves, and measured, indicated, and inferred resources at Ming are estimated at 35.44 Mt grading 1.56 wt% Cu, 0.1 wt% Zn, 2.6 g/t Ag, and 0.42 g/t Au (Rambler Metals and Mining, press releases, January 27, 2014 and November 27, 2014). The base and precious metal contents vary among these zones (Fig. 4) with the highest Au grades in the 1806 zone (measured resources of 267,000 tonnes at 0.56 wt% Cu, 1.31 wt% Zn, 32.15 g/t Ag, and 4.31 g/t Au), which puts it into the subclass of "auriferous" VMS deposits (Poulsen and Hannington, 1995; Poulsen et al., 2000; Mercier-Langevin et al., 2011; Brueckner et al., 2014a).

The timing and mode of Au-Ag introduction in ancient VMS deposits in general, including Ming, is debated due to modifications to the primary features through superimposed deformation and metamorphism (e.g. Mercier-Langevin et al., 2015); this lack of agreement has hampered the improvement of exploration models. In this study, we describe the geology of the Ming deposit and recently discovered precious metal-rich zones, the hydrothermal alteration, and the geochemical composition of the host rocks in order to con-

Pilote, J.-L., Piercey, S.J., and Mercier-Langevin, P., 2015. Volcanic architecture and alteration assemblages of the Ming Cu-Au-(Zn-Ag) VMS deposit, Baie Verte, Newfoundland and Labrador: Implications for Au-enrichment processes and exploration, *In:* Targeted Geoscience Initiative 4: Contributions to the Understanding of Volcanogenic Massive Deposit Sulphide Genesis and Exploration Methods Development, (ed.) J.M. Peter and P. Mercier-Langevin; Geological Survey of Canada, Open File 7853, p. 197–210.

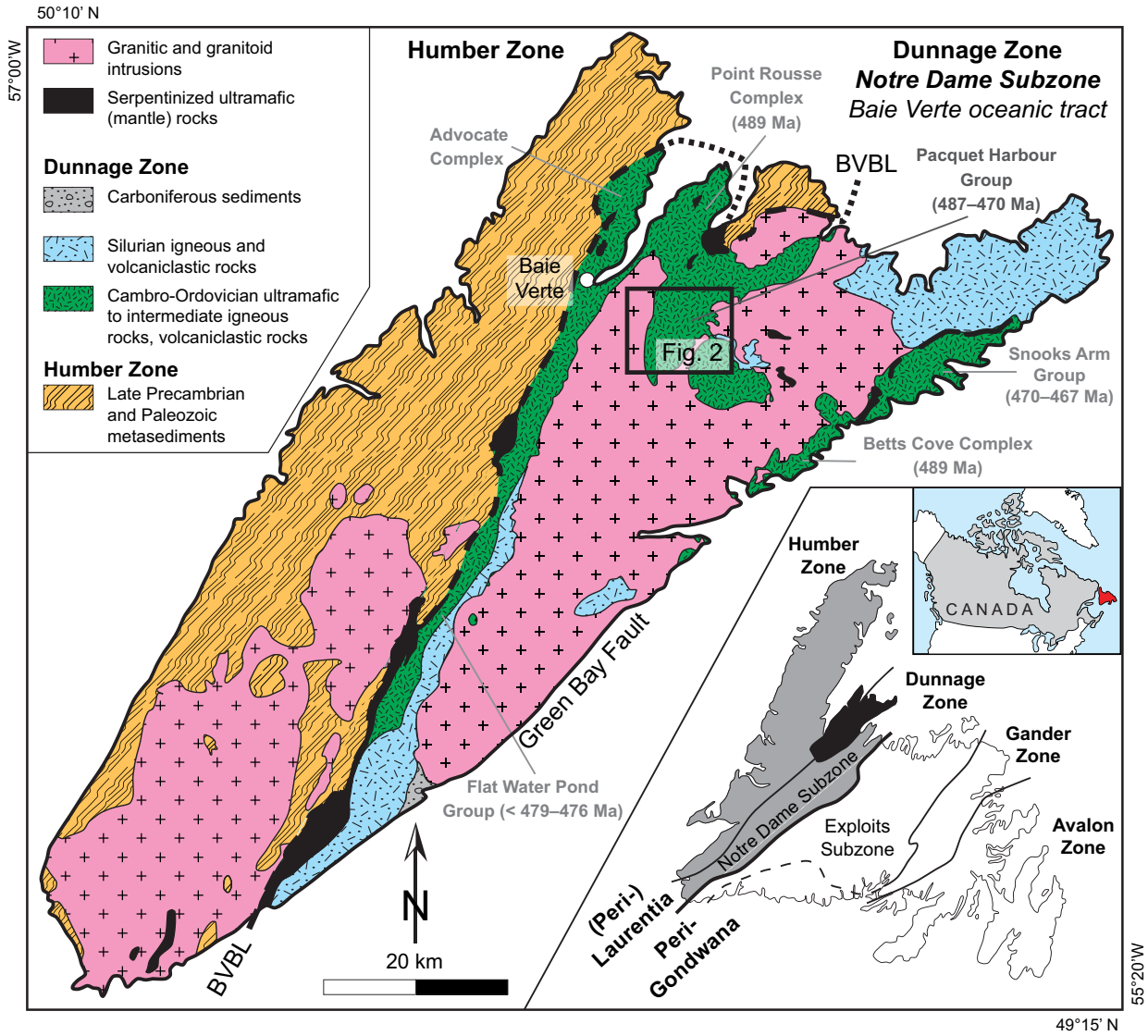

Figure 1. Simplified geological map of the Baie Verte Peninsula (modified from Skulski et al., 2010) showing the (peri-) Laurentian (inset: in grey) and (peri-)Gondwanan tectonostratigraphic zones that form the Appalachian orogenic belt in Newfoundland (Williams, 1979). Abbreviation: BVBL = Baie Verte-Brompton Line.

strain the timing and processes of precious metal-enrichment to develop improved genetic and exploration models.

REGIONAL GEOLOGY

The Ming deposit is hosted by intermediate to felsic rocks of the informally named Rambler Rhyolite formation (Skulski et al., 2010), which consists of a 6 km-wide and 2.5 km-thick folded dome-shaped sequence of quartz-phyric rhyodacite, felsic tuff and tuff breccia, striking northwest and dipping 30º (Fig. 3; Hibbard, 1983; Castonguay et al., 2009). Rhyolite immediately stratigraphically below the nearby Rambler Main deposit yielded a U-Pb zircon age of 487 ± 4 Ma (Fig. 2; Skulski et al., 2010). Stratigraphically below the Rambler Rhyolite formation is low-Ti boninite intercalated with thin (<50 m) beds of felsic tuff and rhyodacite flows (Hibbard, 1983; Piercey et al., 1997; Skulski et al., 2010) of the Betts Head Formation (Skulski et al., 2010), which hosts the Big Rambler Pond (Fig. 2) and the Tilt Cove and Betts Cove VMS deposits (Fig. 1). Stratigraphically overlying the Betts Head Formation are intermediate Ti boninite, island arc tholeiitic pillow basalt, breccia, and minor felsic tuff, which are part of the Mount Misery Formation (Skulski et al., 2010). The upper part of this sequence is structurally repeated in the hanging wall of the Rambler Brook Fault (Fig. 2; Castonguay et al., 2009) where it hosts the Rambler Rhyolite formation and the massive sulphide lenses of the Ming deposit. The Rambler Rhyolite formation is locally overlain by thin lenses of basalt of island-arc affinity that are chemically similar to those of the Mount Misery Formation (Skulski et al., 2010). The latter are overlain by the ca. 479–467 Ma

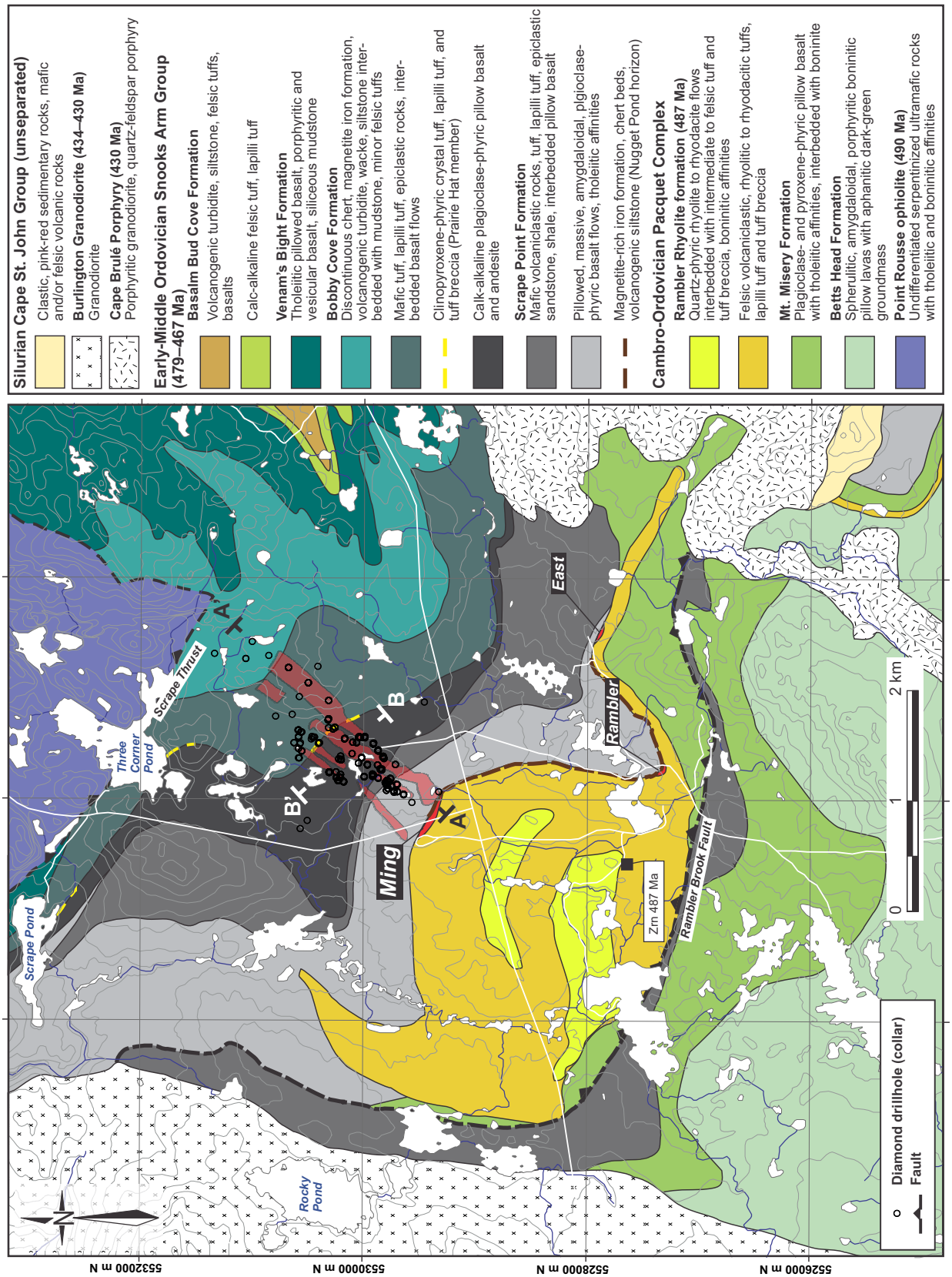

Figure 2. Geological map of the study area, Baie Verte Peninsula, with Ming VMS orebodies projected to surface and shown in light red. Datum is UTM 21N NAD 83. Map compiled and modified from Tuach and Kennedy (1978), Hibbard (1983), Castonguay et al. (2009), Pilgrim (2009), and Skulski et al. (2010). Ages are from Cawood et al. (1993), Castonguay et al. (2009), and Skulski et al. (2010).

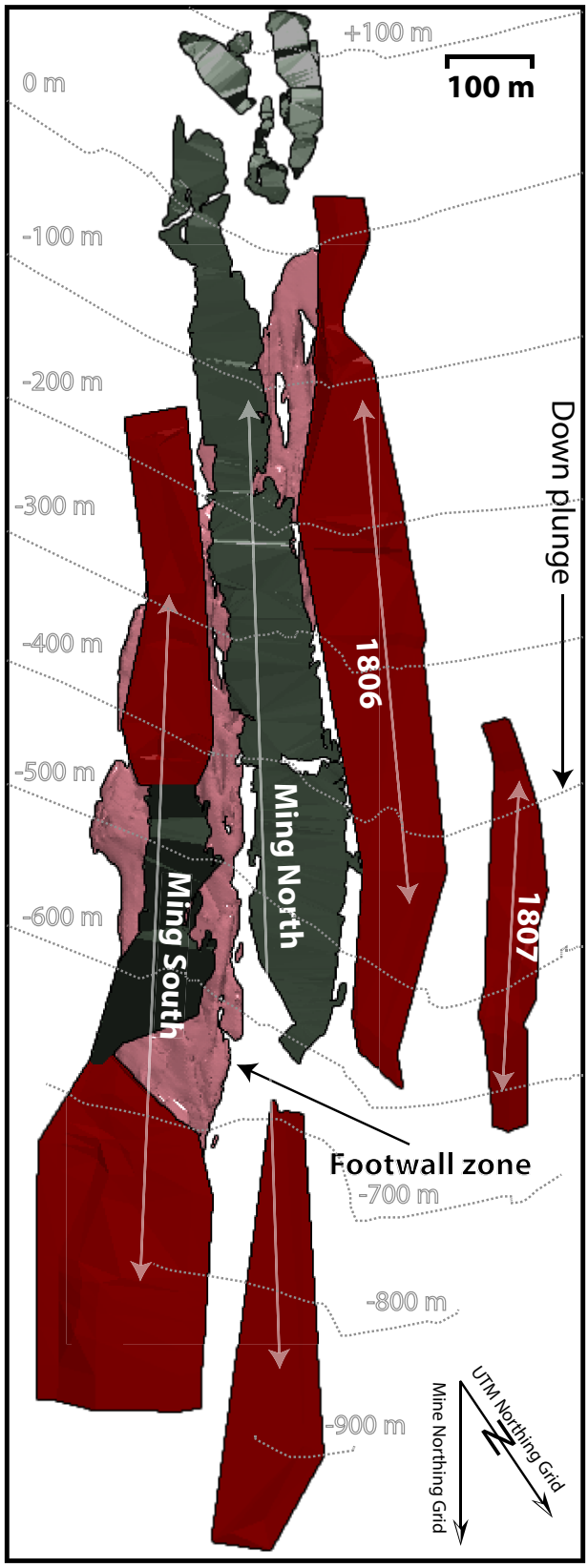

Figure 3. Plan view of a 3-D model of the Ming orebodies projected to surface (0 m). The surface of wireframes in red represent orebodies currently in production or those that will be mined, whereas those in grey were mined in the past. Mine north is 34° east of UTM north. Model modified from Pilgrim (2009).

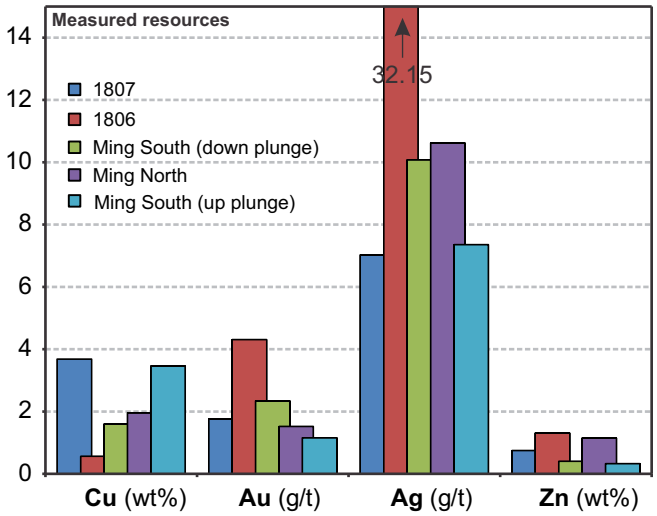

Figure 4. Measured resources of Cu (wt%), Au (g/t), Ag (g/t), and Zn (wt%) for the 1807, 1806, Ming South (down and up plunge), and Ming North zones. Data from Pilgrim (2009).

Snooks Arm Group, which is the cover sequence to the Pacquet Complex. The base of the Snooks Arm Group consists of a thin (<1 m) sequence of chert, magnetite-rich mudstone to siltstone, and sandstone (Nugget Pond horizon). This sequence is laterally extensive and is present throughout the Baie Verte Peninsula (Skulski et al., 2010). Overlying this unit are thin (<1 m) to thick (>100 m) alternating sequences of volcaniclastic monomictic to polymictic conglomerate, epiclastic wacke, iron formation, high-Ti tholeiitic to calc-alkaline basalt, and mafic to felsic volcaniclastic rocks (Hibbard, 1983; Skulski et al., 2010).

DEPOSIT GEOLOGY

The stratigraphic footwall of the deposit is composed of three main volcanic and volcaniclastic units (classified following the nomenclature of White and Houghton, 2006).

The lower part of the stratigraphic footwall at Ming (Fig. 5) is dominated by quartz-phyric rhyodacite (Fig. 6a), with minor intercalated beds of fine rhyodacitic tuff to coarse lapilli tuff (unit 1.1). This unit has a minimum thickness of 150 m and has gradational to sharp contacts with the flows. The rhyodacite is massive with up to 15 vol.% quartz phenocrysts (≤5 mm in size). Overlying unit 1.1 is a sequence predominantly composed of volcaniclastic rocks (unit 1.2) that range from a dominantly fine tuff in the southeast (Ming South zone) to a tuff breccia in the northwest (1807 zone) (Fig. 6b, c). Unit 1.2 is ~100 m thick and consists of several volcaniclastic sequences with subrounded and intermediate tuffaceous fragments that are elongated due to deformation. Quartz porphyroclasts occur both in the matrix and the latter fragments with similar abundance to rocks of unit 1.1. Units 1.1 and 1.2 contain discordant sulphide stringer veins, such as the

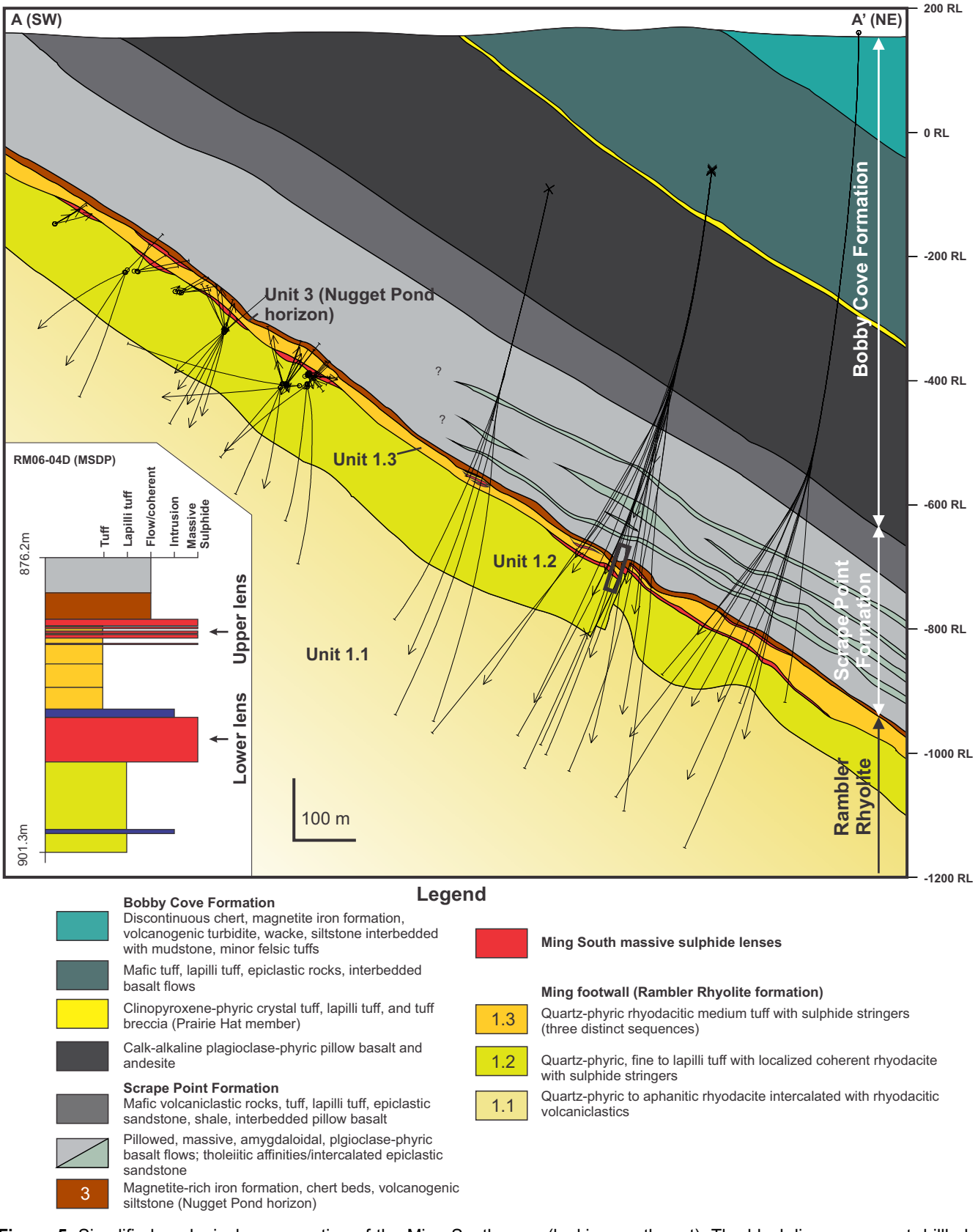

Figure 5. Simplified geological cross-section of the Ming South zone (looking southwest). The black lines represent drillhole traces from which the geology was interpreted. The dykes were omitted to simplify the map. Units 1.1, 1.2, 1.3, and 2 are described in the text. The inset shows the stratigraphy close to the mineralization from a representative drillhole (location indicated by the black box). Unit names are from Skulski et al. (2010). The Ming North, 1806, and 1807 lenses have not been depicted as they occur northwest of this cross-section.

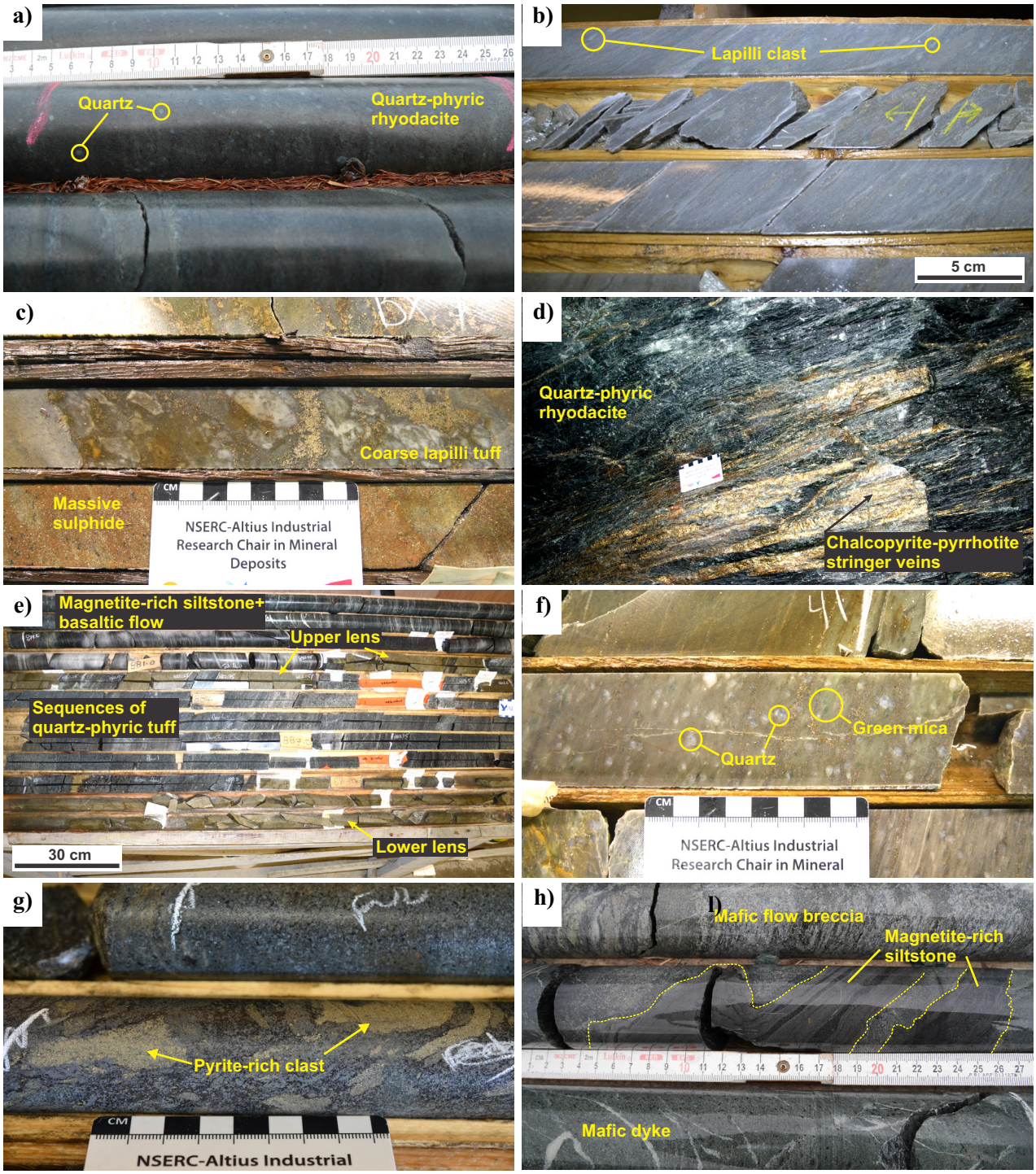

Figure 6. Representative and selected underground and drillcore photographs of the rock units that comprise the Ming footwall. **a)** Coherent quartz-phyric rhyodacite from the Ming North footwall (unit 1.1; DDH RM09-22, 612.5 m depth). Scale is in cm. **b)** Rhyodacitic tuff to lapilli tuff typical of the Ming South zone footwall (unit 1.2; DDH RM04-04, 1036.5 m depth). **c)** Coarse lapilli tuff with the matrix replaced by sulphides from immediately below the 1806 massive sulphide lens (unit 1.2; DDH RMUG08-140; 40.5 m depth). Scale is in cm. **d)** Transposed sulphide (chalcopyrite+pyrrhotite) stringer veins cutting a quartz-phyric rhyodacite in the Lower Footwall zone (1450 level). Scale is in cm. **e)** Drillcore intersection showing the upper and lower sulphide lenses of the Ming South zone, separated by quartz-phyric tuff beds. The upper lens is overlain by magnetite-rich siltstone and basalt (unit 1.3; DDH RM06-04D, starting at 876.2 m depth). **f)** Quartz-bearing rhyodacitic tuff with minor green mica, which is representative of unit 1.3, between the lower and upper sulphide lenses of the Ming South zone (DDH RMUG08-25, 42.5 m depth). **g)** Polymictic mafic tuff breccia with up to 20 vol.% pyrite-rich clasts. This unit occurs above the 1806 and 1807 zones (unit 2; DDH RMUG13-205, 34 m depth). Scale is in cm. **h)** Folded magnetite-rich siltstone bed part of the Nugget Pond horizon (unit 3), overlain by a mafic flow breccia. This unit is extensive and occurs at or near the contact with the Ming deposit (DDH RM09-22, 40 m depth). Scale is in cm. Abbreviation: DDH = diamond drillhole

Table 1. Characteristics of the alteration assemblages in the Ming deposit.

Mineralogical assemblage	Main minerals (vol %)	Associated minerals (minor and traces)	Distribution
1. Quartz-pyrite	Quartz (≤90%), pyrite (≤10%)	Green mica	Immediately above and below the massive sulphide of the 1806 and 1807 zones
2. Quartz-calcite-garnet	Quartz (≤40%), Calcite (≤20%), garnet (≤40%)	Epidote (≤10%)	1807 zone to a maximum depth of 10 m
3. Sericite-green mica-pyrite	Sericite (≤40%), green mica (≤30%), pyrite (≤20%), quartz (≤10%)	Biotite, garnet, magnetite, chalcopyrite, sphalerite, galena, electrum, sulfosalts, tellurides	In all zones to a depth of 30 m
4. Sericite-quartz-pyrite	Sericite (≤45%), quartz (≤40%), pyrite (≤5%)	Sphalerite, biotite, epidote, ilmenite, rutile, and chlorite	1806, Ming North, Ming South to a maximum depth of 50 m
5. Chlorite-actinolite-quartz	Chlorite (≤40%), actinolite (≤20%), quartz (≤20%)	Epidote (≤10%), biotite (≤10%)	Sporadically throughout all zones but mainly 1806, Ming North and Ming South
6. Chlorite-sericite-quartz-sulphide	Chlorite (≤45%), sericite (≤45%), quartz (≤10%)	Biotite, epidote, apatite, pyrite, chalcopyrite, pyrrhotite	Below Ming South and Ming North at a minimum depth of 50 m
7. Chlorite-stringer zone	Chlorite (≤45%), quartz (≤45%)	Biotite, epidote, actinolite, titanite, apatite, zircon, epidote, chalcopyrite, pyrrhotite, pyrite, Bi-telluride	Below Ming South and Ming North at a minimum depth of 50 m

Lower Footwall zone (Fig. 6d), and stratiform to discordant semi-massive to massive sulphides. The semi-massive to massive sulphide lenses have a maximum thickness of 11 m (average ~4 m) consisting of >30 metal-bearing minerals (Brueckner et al., 2014b) and quartz gangue, with the most common sulphides being pyrite, chalcopyrite, pyrrhotite, and sphalerite.

The Ming South zone contains two stratabound and stratiform massive sulphide lenses separated by three ≤10 m-thick discrete beds of rhyodacitic tuff (unit 1.3; Fig. 6e). The tuff beds are quartz-bearing (Fig. 6f), light to dark grey, and are cut by chalcopyrite-pyrite-quartz stringer veins (<2 vol. % of the rock). The upper and lower sulphide lenses in the Ming South zone have different mineral assemblages; the lower lens has chalcopyrite, sphalerite, and galena, whereas the upper lens has pyrite and chalcopyrite. The grades in the lower lens average 3.58 wt% Cu and 4.8 g/t Au, and the upper lens averages 0.78 wt% Cu and 1.2 g/t Au (averaged sulphide assays from five diamond drillholes; RM06-04c, d, e, g, and RM05-09, L. Pilgrim, unpublished data, 2015), in agreement with the dominant sulphide mineralogy.

The massive sulphides in the 1806 and 1807 zones are immediately stratigraphically overlain by a dark grey mafic tuff breccia with sulphide clasts (unit 2; Fig. 6g). The matrix is fine-grained and biotite-rich that contains fragments of medium-grained pyrite-quartz clasts, quartz-altered aphanitic felsic volcanic clasts, and epidote-altered mafic volcanic clasts. The fragments are subrounded, elongated, and up to 5 cm in length. Unit 2 is overlain by the regionally extensive magnetite-rich siltstone (unit 3; Fig. 6h).

Three generations of mafic to intermediate sills and dykes have intruded the deposit, and they crosscut all styles of mineralization. Each dyke generation has a distinctive lithogeochemical signature (Pilote et al., 2014). The dykes have similar geochemical affinities as the rocks of the Snooks Arm Group (J.-L. Pilote, unpublished data, 2014) and are cogenetic with them.

The Baie Verte Peninsula was affected by three phases of regional deformation, but only the last two are recognized at Ming. In the deposit, the D_2 deformation is defined by an east-west-striking cleavage to a penetrative schistosity (S_2) that is axial-planar to megascopic east-trending open to tight F_2 folds, with strong L > S fabrics. The north-dipping, south-directed Rambler Brook Fault and Scrape Thrust (Fig. 2) are interpreted to be D_2 structures (Castonguay et al., 2009). The D_3 deformation is characterized by open, upright cross folds with axial planes trending north-northeast. The elongated morphology of the orebodies (Fig. 2 and 3) is in large part due to the S_2 stretching (L_2) and superimposed effect of D_3 deformation (Castonguay et al., 2009).

HYDROTHERMAL ALTERATION ASSEMBLAGES

The Ming stratigraphic footwall rocks contain seven alteration assemblages that have distinctive mineralogies and relative abundances of key minerals (Table 1),

with a strong lateral and vertical alteration zonation. Immediately above and below the 1806 and 1807 zone massive sulphide lenses, the rocks have grey quartz-pyrite alteration (Fig. 7a), with samples containing up to 92 wt% SiO_2 (J.-L. Pilote, unpublished data, 2014).

The footwall of the 1807 zone contains a distinct salmon-pink quartz-calcite-Mn-rich garnet alteration assemblage that extends up to 10 m stratigraphically below the massive sulphides (Fig. 7b and 8). This mineral assemblage comprises fine-grained (≤100 μm) polygonal quartz and idioblastic garnet. This alteration overprints a sericite-quartz-altered, quartz-bearing, medium-grained felsic tuff (unit 1.2).

A sericite-green mica-sulphide assemblage occurs in all zones within 30 m of the massive sulphide lenses (Fig. 7c). This alteration assemblage is cut by discordant stringers of pyrite-chalcopyrite-sphalerite-galena with trace electrum, sulphosalts, and tellurides (up to 10 vol.%). This assemblage also contains trace euhedral magnetite and syn-D_2 garnet and biotite porphyroblasts. Green mica is more abundant in the Au-rich 1806 zone (≤30 vol.%) than in the other zones (≤5 vol.%). Preliminary lithogeochemical analyses indicate that green mica-bearing rocks have a higher Cr content (~1600 ppm) than the surrounding sericite-rich rock (~100 ppm) (J.-L. Pilote, unpublished data, 2014).

Sericite-quartz-pyrite alteration is present in the 1806, Ming North, and Ming South zones up to ~50 m stratigraphically below the massive sulphide lenses (Fig. 7d). The assemblage is dominated by sericite, quartz, and disseminated anhedral pyrite with minor sphalerite, biotite, epidote, ilmenite, rutile, and chlorite. Sphalerite, pyrite, and ilmenite form thin (≤1 mm) discontinuous bands within this assemblage, whereas epidote, rutile, and biotite form hypidiomorphic porphyroblasts.

A chlorite-amphibole-quartz assemblage occurs in places throughout the footwall in all zones within 50 m stratigraphically below the massive sulphides (Fig. 7e). This assemblage predominantly occurs in volcaniclastic rocks and is composed of chlorite, actinolite, and quartz with subordinate epidote and biotite. The biotite and actinolite grains are porphyroblastic and actinolite is paragenetically later than biotite.

Below the Ming North and Ming South zones, a chlorite-sericite-quartz-sulphide alteration assemblage occurs mostly in the volcaniclastic rocks and is proximal to the chlorite-stringer zone assemblage (see below). This assemblage also contains minor biotite, epidote, and apatite. This assemblage also includes ≤5 mm-wide bands of fine-grained sericite and quartz veins that cut the chlorite-quartz-sulphide assemblage (Fig. 7f, g), and these bands themselves are cut by discordant <1 cm-wide pyrite, chalcopyrite, and pyrrhotite stringer veins.

Lastly, a pervasive chlorite-stringer zone alteration assemblage occurs 50 to 100 m stratigraphically below the Ming South and Ming North zones. This assemblage hosts the Lower Footwall stringer zone and is composed predominantly of chalcopyrite, pyrrhotite, pyrite, Bi-tellurides, chlorite, quartz, minor biotite, epidote, actinolite, titanite, apatite, and zircon (Fig. 7h). The sulphide minerals and Bi-tellurides form centimetre-scale stringer veins that are discordant and transposed into S_2.

DISCUSSION

Deposit Architecture and Preliminary Genetic Model

The nature and style of the ore and alteration of VMS deposits are partly controlled by the volcanic architecture of the host succession (Gibson et al., 1999). The Ming deposit is hosted by massive rhyodacitic and intercalated volcaniclastic rocks that grade upward into predominantly rhyodacitic volcaniclastic rocks where semi-massive to massive sulphide lenses occur. The vertical transition from unit 1.1 to 1.2 may reflect the evolution from a subaqueous flow-dome complex to an eruptive volcaniclastic succession, common for shallow marine environments and the setting of numerous VMS deposits (e.g. Allen et al., 1996; Franklin et al., 2005; Gibson, 2005; Ross and Mercier-Langevin, 2014). The lack of sedimentary rocks and/or laminated tuff in the footwall rocks (units 1.1 and 1.2) may be due to rapid emplacement and formation of the flow-dome complex.

The mineralization in the 1807, 1806, Ming North and Ming South (lower lens) zones are immediately stratigraphically underlain by a distinctive rhyodacitic fine tuff to lapilli tuff unit, suggesting that all sulphide zones formed contemporaneously. In the southeastern part of the deposit, a younger succession of intermediate tuff beds and pyrite-rich massive sulphides (upper lens) were deposited above sulphide lenses (Ming South and possibly Ming North), whereas in the northwestern part of the deposit, a sulphide-rich volcanic breccia succession was formed, possibly coeval with the deposition of unit 1.3. The occurrence of a sulphide-rich volcanic breccia succession may indicate either that flow-breccia or talus-breccia deposits formed on top, or at the margin, of the flow-dome complex, or it reflects the presence of a depression controlled by synvolcanic faulting.

Mineralization at Ming is hosted predominantly in volcaniclastic rocks, close to a flow-dome complex. This volcanic architecture is likely due to permeability contrasts between the coherent and volcaniclastic rocks (Pilote et al., 2014). The spatial distribution of the alteration assemblages (Fig. 8) reflects these lithofacies changes. The lithofacies changes together with the

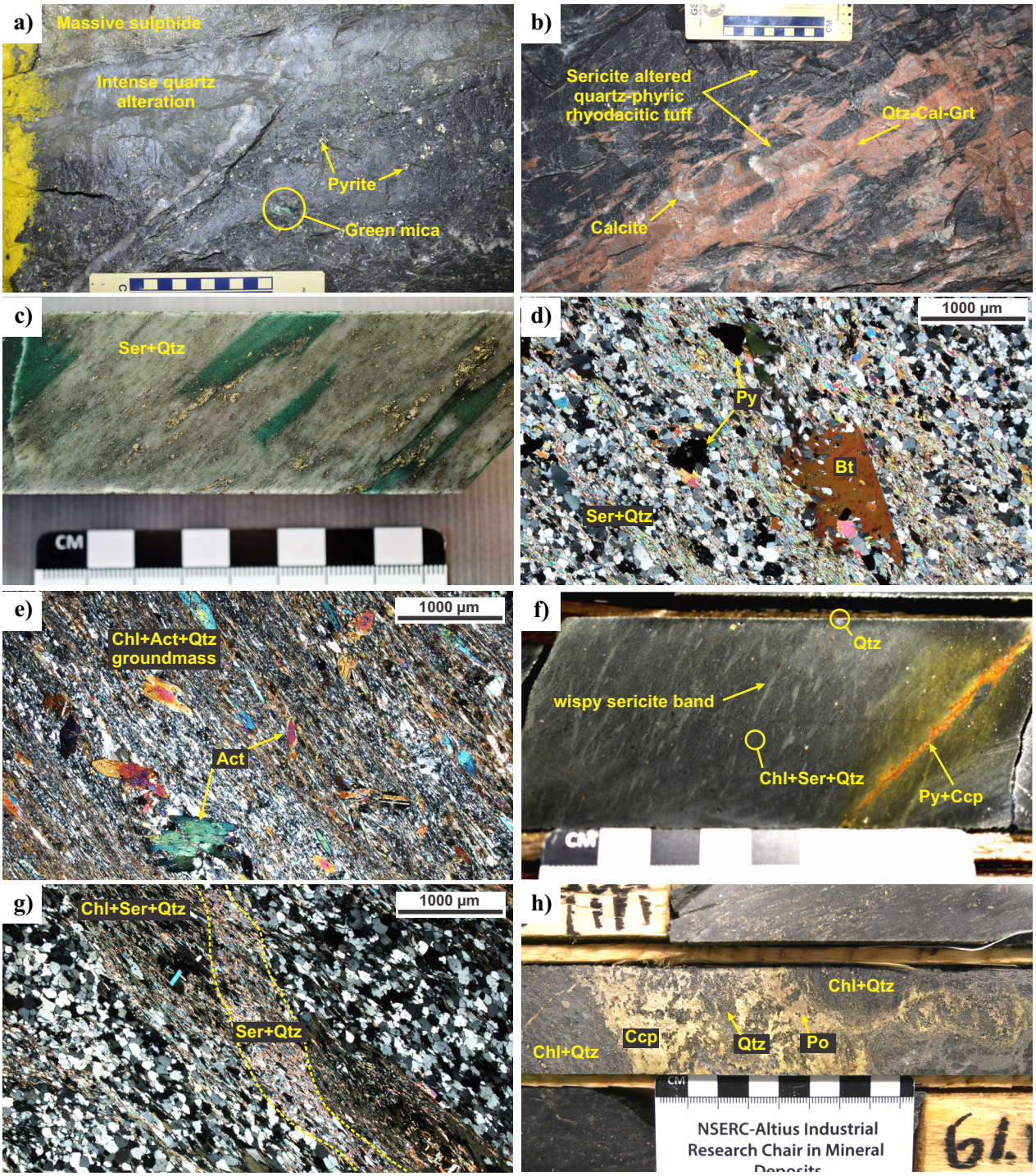

Figure 7. Representative and selected underground and drillcore photographs and photomicrographs of the different alteration styles that characterize the Ming footwall rocks. **a)** View looking south in level 329 (1807 zone) of the silica-pyrite alteration overprinting the weakly sericitized ±green mica rhyodacitic tuff. **b)** View looking southwest of a Mn-altered (Mn-garnet, quartz, and calcite) quartz-phyric rhyodacitic tuff underlying the massive sulphide (level 481, 1807 zone). **c)** Drillcore showing intense sericite-green mica-pyrite alteration in the 1806 zone (DDH RMUG14-261, 28.6 m depth). **d)** Photomicrograph illustrating the close relationship between quartz, sericite, disseminated pyrite, and biotite porphyroblasts in the sericite-quartz-pyrite alteration assemblage (sample 60553; DDH RM05-08, 1054 m depth). **e)** A fine-grained groundmass composed of chlorite-actinolite-quartz with randomly oriented actinolite porphyroblasts (sample 62515; DDH RM07-18, 729 m depth). **f)** Wispy sericite bands cutting an intense chlorite-sericite-quartz-altered quartz-phyric rhyodacite. These are in turn cut by a pyrite-chalcopyrite stringer vein (DDH RM05-08, 1275 m depth). **g)** A photomicrograph of (f) showing the relationship between the chlorite-sericite-quartz alteration assemblage cut by a later vein of sericite-quartz. **h)** Intense chlorite alteration cut by discordant chalcopyrite-pyrrhotite-quartz-rich veins, which is representative of the chlorite-stringer zone alteration assemblage (DDH RMUG14-250, 59.5 m depth). Abbreviations: Act = actinolite, Bt = biotite, Cal = calcite, Ccp = chalcopyrite, Chl = chlorite, Grt = garnet, Po = pyrrhotite, Py = pyrite, Qtz = quartz, Ser = sericite.

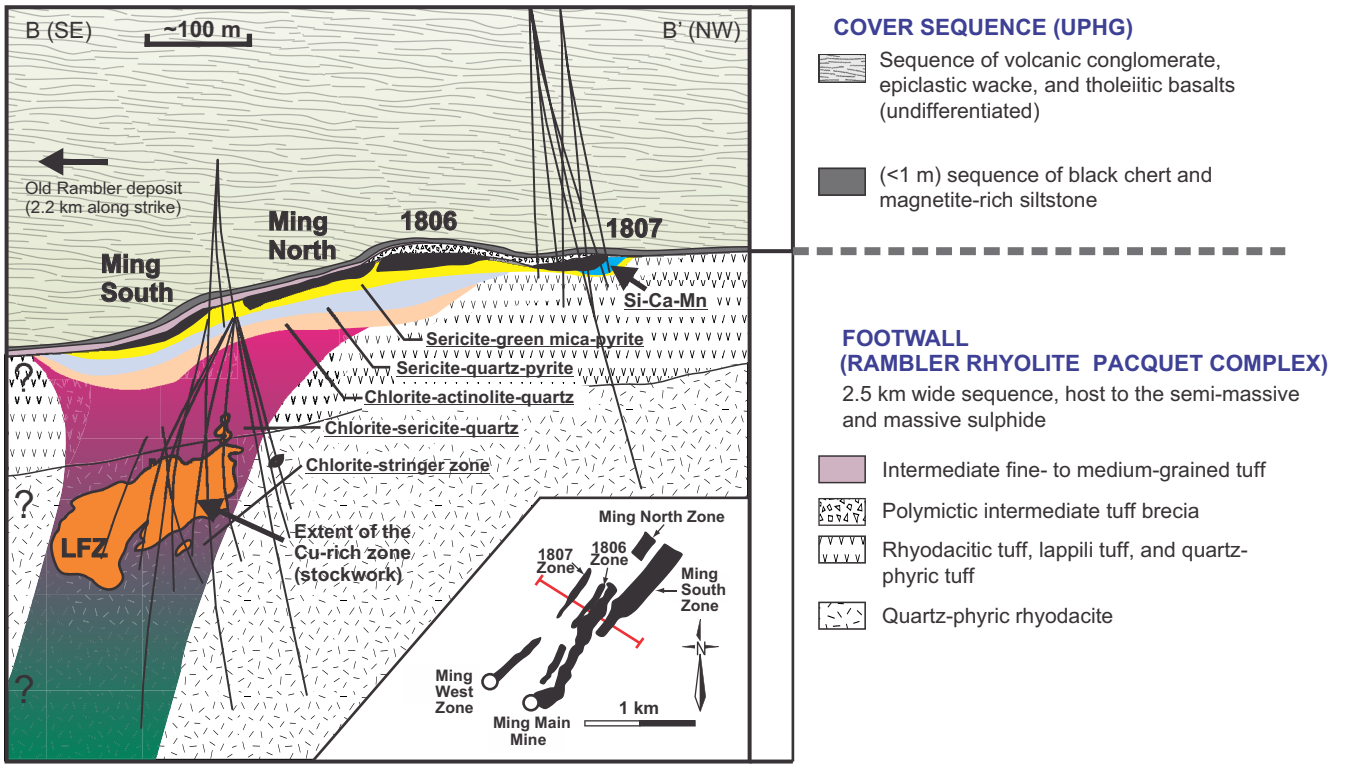

Figure 8. Simplified geological cross-section (looking southwest) of the Ming deposit. The distribution of the alteration assemblages (described in more detail in the text) was defined using petrographic, hyperspectral, and geochemical analyses (J.-L. Pilote, unpublished data, 2014) from numerous diamond drillholes (black lines) and underground mapping.

hydrothermal fluid conditions (i.e. temperature, pressure, pH, fO_2, and fS_2) were likely controlled by emplacement into relatively shallow water. The pervasive chlorite-stringer zone alteration assemblage that occurs adjacent to, and subparallel with, the Ming North and Ming South zones, and the discordant chalcopyrite-pyrite stringer veins indicate high-temperature fluid-rock interaction and ore deposition (>300ºC; e.g. Lydon, 1988; Ohmoto, 1996) in the Lower Footwall zone. No such alteration occurs stratigraphically below the 1806 and 1807 zones, indicating that these zones were formed from lower temperature fluids at potentially distal parts of the hydrothermal system (Fig. 8; Brueckner et al., 2014a). Within 50 m of massive sulphides, the alteration mineral assemblage is dominated by sericite and quartz, which is consistent with lower temperature alteration (Fig. 8; e.g. Lydon, 1988).

Timing of Mineralization and Gold Enrichment

Determining the timing of Au introduction into Au-enriched VMS (and modern seafloor massive sulphide) deposits is key to formulating and refining exploration models for such deposits and understanding their genesis. At Ming, multiple lines of evidence suggest Au-enrichment was synvolcanic: 1) the multiple stratabound massive sulphide lenses occur at the same stratigraphic position (i.e. at the top of units 1.2 and 1.3), which reflects a stratigraphic control, thus favouring a syngenetic model of mineralization; 2) mafic to intermediate feeder dykes to the hanging-wall Snooks Arm Group crosscut the massive sulphides (Pilote and Piercey, 2013; Pilote et al., 2014). These dykes and rocks of the Snooks Arm Group postdate mineralization, are deformed, and are unmineralized, indicating that Au-enrichment was likely not due to a later structural and metamorphic overprint, as these post-mineralization rocks should display Au-enrichment as well if this were the case; 3) despite deposit-scale variations in Au and Ag contents, Au and Ag are almost exclusively confined to the massive sulphides, and only locally has Au remobilization into hosting volcanic rocks been documented (e.g. 1807 zone; Pilote et al., 2014). The massive sulphides and rocks above and below them are deformed with crosscutting structures that extend outside the deposit. These structures contain no Au, and this, together with the evidence presented in (2) above, suggests that the precious metals originated in the primary ore and were not introduced by a later orogenic overprint; and 4) the Au-enriched 1806 zone and parts of the 1807 and Ming South zones are enveloped by the synvolcanic sericite-green mica-sulphide alteration assemblage. Green mica is present in some VMS systems (e.g. Que River and Hellyer: Gemmell and Fulton, 2001; LaRonde-Penna: Dubé et al., 2007). Although the evidence is circumstantial, the close asso-

ciation between Au-enriched ore and green mica alteration in the 1806 zone at Ming may represent a key indicator to Au-rich mineralization. The relationship of this green mica alteration with the Au-enrichment process(es) at Ming is currently under investigation.

The Au-enrichment at Ming may originate from direct magmatic hydrothermal fluids containing Ag and Au. Based on the presence of abundant sulphosalts, including Ag-bearing tennantite-tetrahedrite, stannite, boulangerite, and loellingite, and precious metal-rich phases (tellurides, miargyrite, pyrargyrite, mercurian stephanite, unnamed AgCuFeS phase, Ag-Hg ± Au alloys), Brueckner et al. (2014a) concluded that the mineralization is of an intermediate-sulphidation type in which magmatic hydrothermal fluids containing volatiles and Au were introduced by magmatic degassing of a large rhyodacitic flow-dome complex in the immediate footwall to the deposit; this model is similar to that proposed at the LaRonde Penna deposit, Quebec (Mercier-Langevin et al., 2007).

IMPLICATIONS FOR EXPLORATION

Numerous geological field criteria from the Ming deposit can be used to determine proximity to mineralization, and these may be useful in exploring for precious metal-rich VMS deposits elsewhere. Key criteria include (1) the presence of altered rhyodacitic rocks; (2) proximal to ore, alteration assemblages are typified by sericite-green mica-pyrite and sericite-quartz-pyrite, and peripheral to mineralization, alteration is quartz-calcite-garnet; (3) intense chlorite-stringer zone alteration occurs stratigraphically below and distal to some of the massive sulphide lenses — these lenses are commonly Cu-rich and Au-Ag-poor (e.g. Ming and East Mine deposits). It is also notable that there is a spatial "gap" between the chlorite-stringer zone alteration assemblage and the massive sulphide lenses. The Au-rich 1806 zone, and parts of the Ming South and 1807 zones, do not have associated advanced argillic alteration typical of other Au-rich VMS deposits (e.g. Bousquet 2-Dumagami; Dubé et al., 2014) They do, however, contain alteration assemblages similar to those in intermediate sulphidation VMS deposits (e.g. Eskay Creek: Roth et al., 1999). Characteristic ore minerals, such as tellurides and sulphosalts, can also be used as pathfinders for Au-enriched mineralization.

No major structural breaks have been identified southeast of the Ming deposit and there has been limited surface or subsurface exploration outside of the immediate deposit area; therefore, the prospectivity of the area outside of the immediate deposits remains high. It is now recognized that the Ming, Rambler Main, and East deposits are located at the top of the Rambler Rhyolite, at the contact with the overlying rocks of the Snooks Arm Group (Castonguay et al., 2009; Skulski et al., 2010). At or near (≤5 m from massive sulphide mineralization) this contact is an iron-rich sedimentary rock (Nugget Pond horizon) that serves as a regional "favourable" horizon and is a focus for exploration in the Rambler camp.

FUTURE WORK

Ongoing research on the Ming deposit focuses on the characterization of the petrogenesis and geochronology of the host rocks. Element mobility due to hydrothermal alteration will be characterized using lithogeochemical and optical reflectance spectroscopy on altered and unaltered host-rock samples. Structural relationships will be established using detailed underground mapping to determine the deformation history of the deposit and controls on the geometry and distribution of the ore.

ACKNOWLEDGEMENTS

This study was funded by the Targeted Geoscience Initiative (TGI-4) program of Natural Resources Canada. We sincerely thank Rambler Metals and Mining PLC (particularly L. Pilgrim and P. Legrow) for underground access and providing data. This research has also been financially supported by a Natural Sciences and Engineering Research Council of Canada (NSERC) Discovery Grant, by the NSERC-Altius Industrial Research Chair in Mineral Deposits supported by NSERC, Altius Resources Inc., and by the Research and Development Corporation of Newfoundland and Labrador. Thanks to P.-S. Ross and J.M. Peter for their careful reviews of this manuscript.

REFERENCES

Allen, R.L., Weihed, P., and Svenson, S.-A., 1996. Setting of Zn-Cu-Au-Ag massive sulfide deposits in the evolution and facies architecture of a 1.9 Ga marine volcanic arc, Skellefte District, Sweden; Economic Geology, v. 91, p. 1022–1053.

Brueckner, S.M., Piercey, S.J., Sylvester, P.J., Maloney, S., and Pilgrim, L., 2014a. Evidence for syngenetic precious metal enrichment in an Appalachian volcanogenic massive sulfide system: The 1806 zone, Ming mine, Newfoundland, Canada; Economic Geology, v. 109, p. 1611–1642.

Brueckner, S., Piercey, S., Layne, G., Piercey, G., and Sylvester, P., 2014b. Variations of sulphur isotope signatures in sulphides from the metamorphosed Ming Cu(-Au) volcanogenic massive sulphide deposit, Newfoundland Appalachians, Canada; Mineralium Deposita. doi: 10.1007/s00126-014-0567-7.

Castonguay, S., Skulski, T., van Staal, C., and Currie, M., 2009. New insights on the structural geology of the Pacquet Harbour group and Point Rousse complex, Baie Verte peninsula, Newfoundland, *In:* Current Research; Newfoundland and Labrador Department of Natural Resources, Geological Survey, Report 09-1, p. 147–158.

Cawood, P.A., van Gool, J.A.M., and Dunning, G.R., 1993. Silurian age for movement on the Baie Verte Line: Implications for accretionary tectonics in the Northern Appalachians, *In:* Abstract with Programs; Geological Society of America, v. 25, p. A422.

Dubé, B., Mercier-Langevin, P., Hannington, M.D., Lafrance, B., Gosselin, G., and Gosselin, P., 2007. The LaRonde Penna world-class Au-rich volcanogenic massive sulfide deposit, Abitibi, Quebec: mineralogy and geochemistry of alteration and implications for genesis and exploration; Economic Geology, v. 102, p. 633–666.

Dubé, B., Mercier-Langevin, P., Kjarsgaard, I., Hannington, M., Bécu, V., Côté, J., Moorhead, J., Legault, M., and Bédard, N., 2014. The Bousquet 2-Dumagami world-class Archean Au-rich volcanogenic massive sulfide deposit, Abitibi, Quebec: Metamorphosed submarine advanced argillic alteration footprint and genesis; Economic Geology, v. 109, p. 121–166.

Franklin, J.M., Gibson, H.L., Jonasson, I.R., and Galley, A.G., 2005. Volcanogenic massive sulfide deposits, *In:* Economic Geology 100th Anniversary Volume, (ed.) J.W. Hedenquist, J.F.H. Thompson, R.J. Goldfarb, and J.P. Richards; Society of Economic Geologists, Littleton, Colorado, p. 523–560.

Gemmell, J.B. and Fulton, R., 2001. Geology, genesis, and exploration implications of the footwall and hanging-wall alteration associated with the Hellyer volcanic-hosted massive sulfide deposit, Tasmania, Australia; Economic Geology, v. 96, p. 1003–1035.

Gibson, H.L., 2005. Volcano-Hosted Ore Deposits, *In:* Volcanoes and the Environment, (ed.) G.G.J. Ernst; Cambridge University Press, New York, New York, p. 333–386.

Gibson, H., Morton, R.L., and Hudak, G.J., 1999. Submarine volcanic processes, deposits, and environments favorable for the location of volcanic-associated massive sulfide deposits; Reviews in Economic Geology, v. 8, p. 13–51.

Hibbard, L.J., 1983. Geology of the Baie Verte Peninsula, Newfoundland; Department of Mines and Energy, Government of Newfoundland and Labrador, Memoir 2, 279 p.

Lydon, J.W., 1988. Volcanogenic massive sulphide deposits Part 2: Genetic models; Geoscience Canada, v. 15, p. 43–65.

Mercier-Langevin, P., Dubé, B., Hannington, M.D., Richer-Laflèche, M., and Gosselin, G., 2007. The LaRonde Penna Au-Rich volcanogenic massive sulfide deposit, Abitibi greenstone belt, Quebec: Part II. Lithogeochemistry and paleotectonic setting; Economic Geology, v. 102, p. 611–631.

Mercier-Langevin, P., Hannington, M.D., Dubé, B., and Bécu, V., 2011. The gold content of volcanogenic massive sulfide deposits; Mineralium Deposita, v. 46, p. 509–539.

Mercier-Langevin, P., Hannington, M.D., Dubé, B., Piercey, S.J., Peter, J.M., and Pehrsson, S.J., 2015. Precious metal enrichment processes in volcanogenic massive sulphide deposits — A summary of key features, with an emphasis on TIGI-4 research contributions, *In:* Targeted Geoscience Initiative 4: Contributions to the Understanding of Volcanogenic Massive Sulphide Deposit Genesis and Exploration Methods Development, (ed.) J.M. Peter and P. Mercier-Langevin; Geological Survey of Canada, Open File 7853, p. 117–130.

Ohmoto, H., 1996. Formation of volcanogenic massive sulfide deposits: The Kuroko perspective; Ore Geology Reviews, v. 10, p. 135–177.

Piercey, S.J., Jenner, G.A., and Wilton, D.H.C., 1997. The stratigraphy and geochemistry of the southern Pacquet Harbour Group, Baie Verte Peninsula, Newfoundland: Implications for mineral exploration, *In:* Current Research, (ed.) C.P.G. Pereira and D.G. Walsh; Newfoundland and Labrador Department of Mines and Energy, p. 119–139.

Pilgrim, L., 2009. Mineral Resource Estimate for the Ming Mine, Newfoundland, Canada; Rambler Metals and Mining Canada Ltd., unpublished technical report, p. 114.

Pilote, J.-L. and Piercey, S.J., 2013. Volcanostratigraphy of the 1807 zone of the Ming Cu-Au volcanogenic massive-sulphide deposit, Baie Verte Peninsula, northern Newfoundland; Geological Survey of Canada, Current Research 2013-20, 13 p. doi:10.4095/293128

Pilote, J.-L., Piercey, S.J., and Mercier-Langevin, P., 2014. Stratigraphy and hydrothermal alteration of the Ming Cu-Au volcanogenic massive-sulphide deposit, Baie Verte Peninsula, Newfoundland; Geological Survey of Canada, Current Research 2014-7, 18 p. doi:10.4095/295145

Poulsen, K.H. and Hannington, M.D., 1995. Volcanic-associated massive sulphide gold, *In:* Geology of Canadian Mineral Deposit Types, (ed.) O.R. Eckstrand, W.D. Sinclair, and R.I. Thorpe; Geological Survey of Canada, Geology of Canada Series no. 8, p. 183–196. doi:10.4095/207944

Poulsen, K.H., Robert, F., and Dubé, B., 2000. Geological Classification of Canadian Gold Deposits; Geological Survey of Canada, Bulletin 540, 113 p.

Ross, P.-S. and Mercier-Langevin, P., 2014. Igneous rock associations 14. The volcanic setting of VMS and SMS deposits: a review; Geoscience Canada, v. 41, p. 365–377.

Roth, T., Thompson, J.F.H., and Sillitoe, R.H., 1999. The precious metal-rich Eskay Creek deposit, northwestern British Columbia; Reviews in Economic Geology, v. 8, p. 357–373.

Skulski, T., Castonguay, S., McNicoll, V., van Staal, C., Kidd, W., Rogers, N., Morris, W., Ugalde, H., Slavinski, H., Spicer, W., Moussallam, Y., and Kerr, I., 2010. Tectonostratigraphy of the Baie Verte oceanic tract and its ophiolite cover sequence on the Baie Verte Peninsula, *In:* Current Research; Newfoundland and Labrador Department of Natural Resources, Geological Survey, Report 10-1, p. 315–335.

Tuach, J. and Kennedy, M.J., 1978. The geologic setting of the Ming and other sulfide deposits, consolidated Rambler mines, Northeast Newfoundland; Economic Geology, v. 73, p. 192–206.

van Staal, C.R. and Barr, S.M., 2012. Lithospheric architecture and tectonic evolution of the Canadian Appalachians and associated Atlantic margin, *In:* Tectonic Styles in Canada: The LITHOPROBE Perspective, (ed.) J.A. Percival, F.A. Cook, and R.M. Clowes; Geological Association of Canada, Special Paper 49, p. 41–96.

van Staal, C.R., Chew, D.M., Zagorevski, A., McNicoll, V., Hibbard, J., Skulski, T., Escayola, M.P., Castonguay, S., and Sylvester, P.J., 2013. Evidence of Late Ediacaran hyperextension of the Laurentian Iapetan margin in the Birchy Complex, Baie Verte Peninsula, Northwest Newfoundland: Implications for the opening of Iapetus, formation of Peri-Laurentian microcontinents and Taconic – Grampian orogenesis; Geoscience Canada, v. 40, p. 94–117.

White, J.D.L. and Houghton, B.F., 2006. Primary volcaniclastic rocks; Geology, v. 34, p. 677–680.

Williams, H., 1979. Appalachian orogen in Canada; Canadian Journal of Earth Sciences, v. 16, p. 792–807.